

Front Page

Certificate by supervisor

Declaration

Acknowledgements

Dedication

Abstract

Chapter 1

Introduction

solving a given model Hamiltonian H for a system of interacting electrons arises from the presence of multiple

Chapter 2

Methods

2.1 The Unitary Renormalisation Group Method

The URG method was introduced and formalised in refs. [1–4]. This section is adapted from those references and expanded wherever required.

2.2 Formalism

2.2.1 Description of the problem

We are given a Hamiltonian \mathcal{H} which is not completely diagonal in the occupation number basis of the electrons, \hat{n}_k : $[\mathcal{H}, \hat{n}_k] \neq 0$. k labels any set of quantum numbers depending on the system. For spin-less Fermions it can be the momentum of the particle, while for spin-full Fermions it can be the set of momentum and spin. There are terms that scatter electrons from one quantum number k to another quantum number k' .

We take a general Hamiltonian,

$$\mathcal{H} = H_e \hat{n}_{q\beta} + H_h (1 - \hat{n}_{q\beta}) + c_{q\beta}^\dagger T + T^\dagger c_{q\beta} \quad (2.1)$$

Formally, we can decompose the entire Hamiltonian in the subspace of the electron we want to decouple ($q\beta$).

$$\mathcal{H} = \begin{pmatrix} |1\rangle & |0\rangle \\ H_1 & T \\ T^\dagger & H_0 \end{pmatrix} \quad (2.2)$$

The basis in which this matrix is written is $\{|1\rangle, |0\rangle\}$ where $|i\rangle$ is the set of all states where $\hat{n}_{q\beta} = i$. The aim of one step of the URG is to find a unitary transformation U such that the new Hamiltonian $U\mathcal{H}U^\dagger$ is diagonal in this already-chosen basis.

$$\tilde{\mathcal{H}} \equiv U\mathcal{H}U^\dagger = \begin{pmatrix} |1\rangle & |0\rangle \\ \tilde{H}_1 & 0 \\ 0 & \tilde{H}_0 \end{pmatrix} \quad (2.3)$$

U_q is defined by

$$\tilde{\mathcal{H}} = U_q \mathcal{H} U_q^\dagger \text{ such that } [\tilde{\mathcal{H}}, n_q] = 0 \quad (2.4)$$

It is clear that U is the diagonalizing matrix for \mathcal{H} . Hence we can frame this problem as an eigenvalue equation as well. Let $|\psi_1\rangle, |\psi_0\rangle$ be the basis in which the original Hamiltonian \mathcal{H} has no off-diagonal terms corresponding to $q\beta$. Hence, we can write

$$\mathcal{H} |\psi_i\rangle = \tilde{H}_i |\psi_i\rangle, i \in \{0, 1\} \quad (2.5)$$

Since $|\psi_i\rangle$ is the set of eigenstates of \mathcal{H} and $|i\rangle$ is the set of eigenstates in which $U\mathcal{H}U^\dagger$ has no off-diagonal terms corresponding to $q\beta$, we can relate $|\psi_i\rangle$ and $|i\rangle$ by the same transformation : $|\psi_i\rangle = U^\dagger |i\rangle$. We can expand the state $|\psi_i\rangle$ in the subspace of $q\beta$:

$$|\psi_i\rangle = \sum_{j=0,1} |j\rangle \langle j| |\psi_i\rangle \equiv |1\rangle |\phi_1^i\rangle + |0\rangle |\phi_0^i\rangle \quad (2.6)$$

where $|\phi_j^i\rangle = \langle j| |\psi_i\rangle$. If we substitute the expansion 2.2 into the eigenvalue equation 2.5, we get

$$\left[H_e \hat{n}_{q\beta} + H_h (1 - \hat{n}_{q\beta}) + c_{q\beta}^\dagger T + T^\dagger c_{q\beta} \right] |\psi_i\rangle = \tilde{H}_i |\psi_i\rangle \quad (2.7)$$

The diagonal parts $H_e = \text{tr}[\mathcal{H} \hat{n}_{q\beta}]$ and $H_h = \text{tr}[\mathcal{H} (1 - \hat{n}_{q\beta})]$ can be separated into a purely diagonal part \mathcal{H}^d that contains the single-particle energies and the multi-particle correlation energies or Hartree-like contributions, and an off-diagonal part \mathcal{H}^i that scatters between the remaining degrees of freedom $k\sigma \neq q\beta$. That is,

$$H_e \hat{n}_{q\beta} + H_h (1 - \hat{n}_{q\beta}) = \mathcal{H}^d + \mathcal{H}^i$$

This gives

$$\left[c_{q\beta}^\dagger T + T^\dagger c_{q\beta} \right] |\psi_i\rangle = (\tilde{H}_i - \mathcal{H}^i - \mathcal{H}^d) |\psi_i\rangle \quad (2.8)$$

2.2.2 Obtaining the decoupling transformation

We now define a new operator $\hat{\omega}_i = \tilde{H}_i - \mathcal{H}^i$, such that

$$\left[c_{q\beta}^\dagger T + T^\dagger c_{q\beta} \right] |\psi_i\rangle = (\hat{\omega}_i - \mathcal{H}^d) |\psi_i\rangle \quad (2.9)$$

From the definition of $\hat{\omega}_i$, we can see that it is Hermitian and has no term that scatters in the subspace of $q\beta$, so it is diagonal in $q\beta$ and we can expand it as $\hat{\omega}_i = \hat{\omega}_i^1 \hat{n}_{q\beta} + \hat{\omega}_i^0 (1 - \hat{n}_{q\beta})$. Using the expansion 2.6, we can write

$$\hat{\omega}_i |\psi_i\rangle = \hat{\omega}_i^1 |1\rangle |\phi_1^i\rangle + \hat{\omega}_i^0 |0\rangle |\phi_0^i\rangle \quad (2.10)$$

Since the only requirement on $|\psi_i\rangle$ is that it diagonalize the Hamiltonian in the subspace of $q\beta$, there is freedom in the choice of this state. We can exploit this freedom and choose the $|\phi_0^i\rangle$ to be an eigenstates of $\hat{\omega}_i^{1,0}$ corresponding to real eigenvalues $\omega_i^{1,0}$:

$$\left[\mathcal{H}^d + c_{q\beta}^\dagger T + T^\dagger c_{q\beta} \right] |\psi_i(\omega_i)\rangle = (\omega_i^1 - \mathcal{H}^d) |1\rangle |\phi_1^i\rangle + (\omega_i^0 - \mathcal{H}^d) |0\rangle |\phi_0^i\rangle \quad (2.11)$$

If we now substitute the expansion 2.6 and gather the terms that result in $\hat{n}_{q\beta} = 1$, we get

$$c_{q\beta}^\dagger T |0\rangle |\phi_0^i\rangle = (\omega_i^1 - \mathcal{H}^d) |1\rangle |\phi_1^i\rangle \quad (2.12)$$

Similarly, gathering the terms that result in $\hat{n}_{q\beta} = 0$ gives

$$T^\dagger c_{q\beta} |1\rangle |\phi_1^i\rangle = (\omega_i^0 - \mathcal{H}^d) |0\rangle |\phi_0^i\rangle \quad (2.13)$$

We now define two many-particle transition operators:

$$\begin{aligned} \eta^\dagger(\omega_i^1) &= \frac{1}{\omega_i^1 - \mathcal{H}^d} c_{q\beta}^\dagger T \equiv G_1 c_{q\beta}^\dagger T \\ \eta(\omega_i^0) &= \frac{1}{\omega_i^0 - \mathcal{H}^d} T^\dagger c_{q\beta} \equiv G_0 T^\dagger c_{q\beta} \end{aligned} \quad (2.14)$$

where G_j is the propagator $\frac{1}{\omega_i^j - \mathcal{H}^d}$. We can write this compactly as

$$\eta(\hat{\omega}) = GT^\dagger c_{q\beta} = \frac{1}{\hat{\omega}_i - \mathcal{H}^d} T^\dagger c_{q\beta} \quad (2.15)$$

where $\hat{\omega}_i = \omega_i^0(1 - \hat{n}_{q\beta}) + \omega_i^1 \hat{n}_{q\beta} = \begin{pmatrix} \omega_i^1 & \\ & \omega_i^0 \end{pmatrix}$ is a 2x2 matrix and $\mathcal{H}^d = \mathcal{H}_0^d(1 - \hat{n}_{q\beta}) + \mathcal{H}_1^d \hat{n}_{q\beta}$ and $G = (\hat{\omega} - \mathcal{H}^d)^{-1}$. It is easy to check that this reproduces the previous forms of η_0 and η_1^\dagger . We will later find that it is important to demand that these two be Hermitian conjugates of each other; that constraint is imposed on the denominators:

$$\eta^\dagger(\omega_i^0) = \eta^\dagger(\omega_i^1) \implies \frac{1}{\omega_i^1 - \mathcal{H}^d} c_{q\beta}^\dagger T = c_{q\beta}^\dagger T \frac{1}{\omega_i^0 - \mathcal{H}^d} \quad (2.16)$$

Henceforth we will assume that this constraint has been imposed.

In terms of these operators, eq. 2.13 becomes

$$|1\rangle |\phi_1^i\rangle = \eta^\dagger |0\rangle |\phi_0^i\rangle, \quad |0\rangle |\phi_0^i\rangle = \eta |1\rangle |\phi_1^i\rangle \quad (2.17)$$

These allow us to write

$$|\psi_1\rangle = |1\rangle |\phi_1^i\rangle + |0\rangle |\phi_0^i\rangle = (1 + \eta) |1\rangle |\phi_1^i\rangle, \quad |\psi_0\rangle = (1 + \eta^\dagger) |0\rangle |\phi_0^i\rangle \quad (2.18)$$

Recalling that $|\psi_i\rangle = U^\dagger |i\rangle$, we can read off the required transformation:

$$U_1 = 1 + \eta \quad (2.19)$$

2.2.3 Properties of the many-body transition operators

The operators η have some important properties. First is the Fermionic nature:

$$\eta^2 = \eta^{\dagger 2} = 0 \quad [c^{\dagger 2} = c^2 = 0] \quad (2.20)$$

Second is:

$$\begin{aligned} |1\rangle |\phi_1^i\rangle &= \eta^\dagger |0\rangle |\phi_0^i\rangle = \eta^\dagger \eta |1\rangle |\phi_1^i\rangle \implies \eta^\dagger \eta = \hat{n}_{q\beta} \\ |0\rangle |\phi_0^i\rangle &= \eta |1\rangle |\phi_1^i\rangle = \eta \eta^\dagger |\phi_0^i\rangle \implies \eta \eta^\dagger = 1 - \hat{n}_{q\beta} \end{aligned} \quad (2.21)$$

and hence the anticommutator

$$\implies \{\eta, \eta^\dagger\} = 1 \quad (2.22)$$

Note that the three equations in 2.21 work only when applied on the eigenstate $|\psi_i\rangle$ and not any arbitrary state.

$$\begin{aligned} \eta^\dagger \eta |\psi_i\rangle &= |1\rangle |\phi_1^i\rangle = \hat{n}_{q\beta} |\psi_i\rangle \\ \eta \eta^\dagger |\psi_i\rangle &= |0\rangle |\phi_0^i\rangle = (1 - \hat{n}_{q\beta}) |\psi_i\rangle \\ \{\eta^\dagger, \eta\} |\psi_i\rangle &= |\psi_i\rangle \end{aligned}$$

2.2.4 Form of the unitary operators

Although we have found the correct similarity transformations U_i (eqs. 2.19), we need to convert them into a unitary transformation. Say we are trying to rotate the eigenstate $|\psi_1\rangle$ into the state $|1\rangle$. We can then work with the transformation

$$U_1 = 1 + \eta \quad (2.23)$$

In this form, this transformation is not unitary. It can however be written in an exponential form:

$$U_1 = e^\eta \quad (2.24)$$

using the fact that $\eta^2 = 0$. It is shown in ref. [5] that corresponding to a similarity transformation e^ω , there exists a unitary transformation e^G where

$$G = \tanh^{-1}(\omega - \omega^\dagger) \quad (2.25)$$

Applying that to the problem at hand gives

$$U_1^\dagger = \exp\{\tanh^{-1}(\eta - \eta^\dagger)\} \quad (2.26)$$

Let $x = \tanh y$. Then,

$$x = \frac{e^{2y} + 1}{e^{2y} - 1} \implies y = \frac{1}{2} \log \frac{1+x}{1-x} \implies e^y = e^{\tanh^{-1} x} = \sqrt{\frac{1+x}{1-x}} \quad (2.27)$$

Therefore,

$$\exp\{\tanh^{-1}(\eta - \eta^\dagger)\} = \frac{1 + \eta - \eta^\dagger}{\sqrt{(1 + \eta^\dagger - \eta)(1 - \eta^\dagger + \eta)}} = \frac{1 + \eta - \eta^\dagger}{\sqrt{1 + \{\eta, \eta^\dagger\}}} = \frac{1}{\sqrt{2}} (1 + \eta - \eta^\dagger) \quad (2.28)$$

The *unitary* operator that transforms the entangled eigenstate $|\psi_1\rangle$ to the state $|1\rangle$ is thus

$$U_1 = \frac{1}{\sqrt{2}} (1 + \eta^\dagger - \eta) \quad (2.29)$$

It can also be written as $\exp\left\{\frac{\pi}{4}(\eta^\dagger - \eta)\right\}$ because

$$\begin{aligned}\exp\left\{\frac{\pi}{4}(\eta^\dagger - \eta)\right\} &= 1 + (\eta^\dagger - \eta) \frac{\pi}{4} + \frac{1}{2!} (\eta^\dagger - \eta)^2 \left(\frac{\pi}{4}\right)^2 + \frac{1}{3!} (\eta^\dagger - \eta)^3 \left(\frac{\pi}{4}\right)^3 + \dots \\ &= 1 + (\eta^\dagger - \eta) \frac{\pi}{4} - \frac{1}{2!} \left(\frac{\pi}{4}\right)^2 - \frac{1}{3!} (\eta^\dagger - \eta) \left(\frac{\pi}{4}\right)^3 + \frac{1}{4!} \left(\frac{\pi}{4}\right)^4 + \dots \\ &= \cos \frac{\pi}{4} + (\eta^\dagger - \eta) \sin \frac{\pi}{4} \\ &= \frac{1}{\sqrt{2}} (1 + \eta^\dagger - \eta)\end{aligned}\tag{2.30}$$

There we used

$$(\eta^\dagger - \eta)^2 = \eta^{\dagger 2} + \eta^2 - \{\eta^\dagger, \eta\} = -1 \quad [\because \eta^2 = \eta^{\dagger 2} = 0]\tag{2.31}$$

and hence

$$(\eta^\dagger - \eta)^3 = -1 (\eta^\dagger - \eta)\tag{2.32}$$

and so on.

2.2.5 Effective Hamiltonian

We can now compute the form of the effective Hamiltonian that comes about when we apply U_1 - that is - when we rotate one exact eigenstate $|\psi_1\rangle$ into the occupied Fock space basis $|1\rangle$. From eq. 2.29,

$$\begin{aligned}U_1 \mathcal{H} U_1^\dagger &= \frac{1}{2} (1 + \eta^\dagger - \eta) \mathcal{H} (1 + \eta - \eta^\dagger) \\ &= \frac{1}{2} (1 + \eta^\dagger - \eta) (\mathcal{H} + \mathcal{H}\eta - \mathcal{H}\eta^\dagger) \\ &= \frac{1}{2} (\mathcal{H} + \mathcal{H}\eta - \mathcal{H}\eta^\dagger + \eta^\dagger \mathcal{H} + \eta^\dagger \mathcal{H}\eta - \eta^\dagger \mathcal{H}\eta^\dagger - \eta \mathcal{H} - \eta \mathcal{H}\eta + \eta \mathcal{H}\eta^\dagger) \\ &= \frac{1}{2} (\mathcal{H}^d + \mathcal{H}^i + \mathcal{H}^I + \mathcal{H}\eta - \mathcal{H}\eta^\dagger + \eta^\dagger \mathcal{H} + \eta^\dagger \mathcal{H}\eta - \eta^\dagger \mathcal{H}\eta^\dagger - \eta \mathcal{H} - \eta \mathcal{H}\eta + \eta \mathcal{H}\eta^\dagger) \\ &= \frac{1}{2} (\mathcal{H}^d + \mathcal{H}^i + \mathcal{H}^I + [\eta^\dagger - \eta, \mathcal{H}] + \eta^\dagger \mathcal{H}\eta - \eta^\dagger \mathcal{H}\eta^\dagger - \eta \mathcal{H}\eta + \eta \mathcal{H}\eta^\dagger)\end{aligned}\tag{2.33}$$

In the last two lines, we expanded the Hamiltonian into the three parts \mathcal{H}^d , \mathcal{H}^i and a third piece $\mathcal{H}^I \equiv c_{q\beta}^\dagger T + T^\dagger c_{q\beta}$.

For reasons that will become apparent, we will split the terms into two groups:

$$\tilde{\mathcal{H}} = \frac{1}{2} \left(\underbrace{\mathcal{H}^d + \mathcal{H}^i + [\eta^\dagger - \eta, \mathcal{H}] + \eta^\dagger \mathcal{H}\eta + \eta \mathcal{H}\eta^\dagger}_{\text{group 1}} + \overbrace{\mathcal{H}^I - \eta^\dagger \mathcal{H}\eta^\dagger - \eta \mathcal{H}\eta}^{\text{group 2}} \right)\tag{2.34}$$

Group 2 can be easily shown to be 0. Note that terms that have two η or two η^\dagger sandwiching a \mathcal{H} can only be nonzero if the intervening \mathcal{H} has an odd number of creation or destruction operators.

$$\eta \mathcal{H}\eta = \eta c_q^\dagger T \eta\tag{2.35}$$

and

$$\eta^\dagger \mathcal{H} \eta^\dagger = \eta^\dagger T^\dagger c_q \eta^\dagger \quad (2.36)$$

Group 2 becomes

$$\text{group 2} = \mathcal{H}^I - \eta^\dagger T^\dagger c_q \eta^\dagger - \eta c_q^\dagger T \eta = c_q^\dagger T + T^\dagger c_q - \eta^\dagger T^\dagger c_q \eta^\dagger - \eta c_q^\dagger T \eta \quad (2.37)$$

To simplify this, we use the relation

$$\begin{aligned} \eta c_q^\dagger T \eta &= \frac{1}{\omega_i^0 - \mathcal{H}^d} T^\dagger c_q c_q^\dagger T \eta \\ &= T^\dagger c_q \frac{1}{\omega_i^1 - \mathcal{H}^d} c_q^\dagger T \eta \quad [\text{eq. 2.16}] \\ &= T^\dagger c_q \eta^\dagger \eta \quad [\text{eq. 2.15}] \\ &= T^\dagger c_q \hat{n}_q \quad [\text{eq. 2.21}] \end{aligned} \quad (2.38)$$

which gives

$$\eta c_q^\dagger T \eta = T^\dagger c_q \quad (2.39)$$

Taking the Hermitian conjugate of eq. 2.39 gives

$$\eta^\dagger T^\dagger c_q \eta^\dagger = c_q^\dagger T \quad (2.40)$$

Substituting the expressions 2.39 and 2.40 into the expression for group 2, 2.37, shows that it vanishes. This leaves us only with group 1:

$$\tilde{\mathcal{H}} = \frac{1}{2} \left(\mathcal{H}^d + \mathcal{H}^i + \underbrace{\eta^\dagger \mathcal{H} \eta + \eta \mathcal{H} \eta^\dagger}_{\text{group A}} + \underbrace{[\eta^\dagger - \eta, \mathcal{H}]}_{\text{group B}} \right) \quad (2.41)$$

Group A simplifies in the following way. First note that $\eta^\dagger \mathcal{H}^I \eta = \eta^\dagger \mathcal{H}^I \eta = 0$ must be 0 because it will involve consecutive $c_{q\beta}$ or consecutive $c_{q\beta}^\dagger$. We are therefore left with the diagonal part of \mathcal{H} , which is $H_e \hat{n}_{q\beta} + H_h (1 - \hat{n}_{q\beta})$.

$$\eta^\dagger [H_e \hat{n}_{q\beta} + H_h (1 - \hat{n}_{q\beta})] \eta + \eta [H_e \hat{n}_{q\beta} + H_h (1 - \hat{n}_{q\beta})] \eta^\dagger = \eta^\dagger H_h \eta + \eta H_e \eta^\dagger \quad (2.42)$$

This can be shown to be equal to the diagonal part:

$$\text{group A} = \eta^\dagger H_h \eta + \eta H_e \eta^\dagger = H_e \hat{n}_{q\beta} + H_h (1 - \hat{n}_{q\beta}) = \mathcal{H}^d + \mathcal{H}^i \quad (2.43)$$

It can also be shown that

$$\text{group B} = [\eta^\dagger - \eta, \mathcal{H}] = 2 [c_{q\beta}^\dagger T, \eta] \quad (2.44)$$

Putting it all together,

$$\tilde{\mathcal{H}} = \mathcal{H}^d + \mathcal{H}^i + [c_{q\beta}^\dagger T, \eta] \quad (2.45)$$

The renormalizing in the Hamiltonian is

$$\Delta \mathcal{H} = \tilde{\mathcal{H}} - \mathcal{H}^d - \mathcal{H}^i = [c_{q\beta}^\dagger T, \eta] \quad (2.46)$$

Because of eq. 2.44, it can also be written as

$$\Delta\mathcal{H} = \frac{1}{2} [\eta^\dagger - \eta, \mathcal{H}_X] = \frac{1}{2} [\eta^\dagger - \eta, \mathcal{H}] \quad (2.47)$$

This form will be useful later when we make the connection with one-shot Schrieffer-Wolff transformation and CUT RG.

To check that the renormalised Hamiltonian indeed commutes with $\hat{n}_{q\beta}$,

$$\begin{aligned} [\tilde{\mathcal{H}}, \hat{n}_{q\beta}] &= \left[\left[c_{q\beta}^\dagger T, \eta \right], \hat{n}_{q\beta} \right] = \left[c_{q\beta}^\dagger T \eta, \hat{n}_{q\beta} \right] - \left[\eta c_{q\beta}^\dagger T, \hat{n}_{q\beta} \right] \\ &= c_{q\beta}^\dagger T \eta \hat{n}_{q\beta} - \hat{n}_{q\beta} c_{q\beta}^\dagger T \eta \quad \left[\text{2nd } [.] \text{ is 0, } \because c_{q\beta}^\dagger \hat{n}_{q\beta} = \hat{n}_{q\beta} \eta = 0 \right] \\ &= c_{q\beta}^\dagger T \eta - c_{q\beta}^\dagger T \eta = 0 \end{aligned} \quad (2.48)$$

2.2.6 Fixed point condition

Within the URG, it is a prescription that the fixed point is reached when the denominator of the RG equation vanishes. This is equivalent to either $\omega_i^1 = \mathcal{H}_1^d$ or $\omega_i^0 = \mathcal{H}_0^d$. This shows that at the fixed point, one of the eigenvalues of $\hat{\omega}_i$ matches the corresponding eigenvalue of the diagonal blocks. This also leads to the vanishing of the off-diagonal block, because eqs. 2.12 and 2.13 gives

$$c_{q\beta}^\dagger T |0\rangle |\phi_0^i\rangle = (\omega_i^1 - \mathcal{H}_1^d) |1\rangle |\phi_1^i\rangle = 0 \implies c_{q\beta}^\dagger T = 0 \quad (2.49)$$

2.2.7 Multiple off-diagonal terms

There is a subtle assumption in the definitions eq. 2.14. In order for η to be the Hermitian conjugate of η^\dagger , \mathcal{H}_d cannot have any information that relates to the structure of T . To see why, say the total off-diagonal term is composed of two parts: $T = T_1 + T_2$.

$$\begin{aligned} \eta &= \frac{1}{\omega_0 - \mathcal{H}_d} (T_1^\dagger + T_2^\dagger) c = \left[\frac{1}{\omega^0 - E_1^0} T_1^\dagger c + \frac{1}{\omega^0 - E_2^0} T_2^\dagger c \right] \\ \eta^\dagger &= \frac{1}{\omega^1 - \mathcal{H}_d} c^\dagger (T_1 + T_2) = \left[\frac{1}{\omega^1 - E_1^1} c^\dagger T_1 + \frac{1}{\omega^1 - E_2^1} c^\dagger T_2 \right] \end{aligned} \quad (2.50)$$

where $\mathcal{H}_d T_i^\dagger c = E_i^0 T_i^\dagger c$ and $\mathcal{H}_d c^\dagger T_i = E_i^1 c^\dagger T_i$. We can now see that in order for $\eta = (\eta^\dagger)^\dagger$ to hold, two conditions must be met:

$$\omega^0 - E_1^0 = \omega^1 - E_1^1, \quad \omega^0 - E_2^0 = \omega^1 - E_2^1 \quad (2.51)$$

This will not hold generally. The correct solution is to realize that each such off-diagonal term T_i will come with its own quantum fluctuation scale ω_i .

$$\begin{aligned} \eta &= \sum_i \frac{1}{\omega_i^0 - E_i^0} T_i^\dagger c \\ \eta^\dagger &= \sum_i \frac{1}{\omega_i^1 - E_i^1} c^\dagger T_i \end{aligned} \quad (2.52)$$

If we now impose the condition that $\eta = (\eta^\dagger)^\dagger$, we get the relations

$$\omega_i^0 - \omega_i^1 = E_i^0 - E_i^1 \quad (2.53)$$

and so

$$\eta^\dagger - \eta = \sum_i \frac{1}{\omega_i^0 - E_i^0} (c^\dagger T_i - T_i^\dagger c) \quad (2.54)$$

The expression for the renormalization will not be just $[c^\dagger T, \eta]$ in this case. That form will be non-Hermitian. The correct form is obtained from the more general form $[\eta^\dagger - \eta, \mathcal{H}_X]$:

$$\begin{aligned} \Delta\mathcal{H} &= \frac{1}{2} [\eta^\dagger - \eta, c^\dagger T + T^\dagger c] = \frac{1}{2} \sum_{ij} \frac{1}{\omega_i^0 - E_i^0} [c^\dagger T_i - T_i^\dagger c, c^\dagger T_j + T_j^\dagger c] \\ &= \frac{1}{2} \sum_{ij} \frac{1}{\omega_i^0 - E_i^0} [\hat{n} (T_i T_j^\dagger + T_j T_i^\dagger) - (1 - \hat{n}) (T_i^\dagger T_j + T_j^\dagger T_i)] \\ &= \frac{1}{2} \sum_{ij} \left(\frac{1}{\omega_i^0 - E_i^0} + \frac{1}{\omega_j^0 - E_j^0} \right) [\hat{n} T_i T_j^\dagger - (1 - \hat{n}) T_i^\dagger T_j] \end{aligned} \quad (2.55)$$

2.2.8 Equivalence of the two unitaries and preservation of partial trace

In the subsection 2.2.4, we determined the form of the operator U_1 that unitarily decouples the node $q\beta$ from the other degrees of freedom. Eq. 2.29 was derived by reading off the transformation of $|1\rangle$ to $|\psi_1\rangle$, the first equation in 2.18. We could easily have chosen the other equation in the same equation set,

$$|\psi_0\rangle = (1 + \eta^\dagger) |0\rangle |\phi_0^i\rangle$$

which gives a similarity transformation $1 + \eta^\dagger$ and hence a unitary

$$U_0 = \frac{1}{\sqrt{2}} (1 + \eta - \eta^\dagger) \quad (2.56)$$

This η will however be different from the η in eq. 2.29. The reason is, in order to get U_1 , we must start from the eigenvalue equation $\mathcal{H}|\psi_1\rangle = \tilde{H}_1|\psi_1\rangle$. This means that the corresponding $\hat{\omega}$ will be defined as $\hat{\omega}_1 = \tilde{H}_1 - \mathcal{H}^i$. On the other hand, in order to get U_0 we must start with $\mathcal{H}|\psi_0\rangle = \tilde{H}_0|\psi_0\rangle$, and hence this $\hat{\omega}$ will be $\hat{\omega}_0 = \tilde{H}_0 - \mathcal{H}^i$. This difference in the $\hat{\omega}$ will define two different sets of η :

$$\begin{aligned} \text{Starting from } |\psi_1\rangle: \eta_1 &= \frac{1}{\omega_1^0 - \mathcal{H}^d} T^\dagger c_{q\beta} \quad \text{and } \eta_1^\dagger = \frac{1}{\omega_1^1 - \mathcal{H}^d} T^\dagger c_{q\beta} \\ \text{Starting from } |\psi_0\rangle: \eta_0 &= \frac{1}{\omega_0^0 - \mathcal{H}^d} T^\dagger c_{q\beta} \quad \text{and } \eta_0^\dagger = \frac{1}{\omega_0^1 - \mathcal{H}^d} T^\dagger c_{q\beta} \end{aligned} \quad (2.57)$$

The ω_j^i eigenvalues have both upper and lower indices. The upper index i signifies which eigenstate it relates to - $\omega_j|i\rangle = \omega_j^i|i\rangle$. The lower index refers to the exact eigenstate we started with - starting with $\mathcal{H}|\psi_j\rangle = \tilde{H}_j|\psi_j\rangle$ leads to ω_j . The two unitaries are

$$\begin{aligned} U_1 &= \frac{1}{\sqrt{2}} (1 + \eta_1^\dagger - \eta_1) \\ U_0 &= \frac{1}{\sqrt{2}} (1 + \eta_0 - \eta_0^\dagger) \end{aligned} \quad (2.58)$$

Since the two unitaries should give the same effective Hamiltonian, we require $U_1 = U_0$. That requires $\eta_1 = -\eta_0$. Comparing the expressions of the η s, we get

$$\omega_1^0 - \mathcal{H}_0^d = -(\omega_0^0 - \mathcal{H}_0^d) \quad (2.59)$$

This is the constraint that ensures that both unitaries give the same effective Hamiltonian. The condition $\eta_1 + \eta_0 = 0$, when expressed without resolving $\hat{\omega}$ into its eigenvalues can also be shown to be a statement of the preservation of the partial trace under the RG flow.

$$\begin{aligned} \eta_1 &= \frac{1}{\tilde{H}_1 - \mathcal{H}^i - \mathcal{H}^d} T^\dagger c_{q\beta}, \quad \eta_0 = \frac{1}{\tilde{H}_0 - \mathcal{H}^i - \mathcal{H}^d} T^\dagger c_{q\beta} \\ \implies \eta_1 + \eta_0 &= \left[\frac{1}{\tilde{H}_1 - \mathcal{H}^i - \mathcal{H}^d} + \frac{1}{\tilde{H}_0 - \mathcal{H}^i - \mathcal{H}^d} \right] T^\dagger c_{q\beta} = 0 \\ \implies \tilde{H}_1 - \mathcal{H}^i - \mathcal{H}^d &= -[\tilde{H}_0 - \mathcal{H}^i - \mathcal{H}^d] \\ \implies \tilde{H}_1 + \tilde{H}_0 &= 2\mathcal{H}_0 \end{aligned} \quad (2.60)$$

$\mathcal{H}_0 = \mathcal{H}^i + \mathcal{H}^d$ is the total diagonal part of the bare model. To match the dimensions, we must take $\tilde{H}_1 = E_1 \otimes I$ and similarly $\tilde{H}_0 = E_0 \otimes I$, where the rotated Hamiltonian is

$$\tilde{H} = \begin{pmatrix} E_1 & 0 \\ 0 & E_0 \end{pmatrix} \quad (2.61)$$

Therefore, the trace of the rotated Hamiltonian is $t_{\text{new}} = E_1 + E_0$. The trace of the LHS in the final equation of 2.60 is $\text{tr}(\tilde{H}_1 + \tilde{H}_0) = \text{tr}(E_1 \otimes I + E_0 \otimes I) = 2(E_1 + E_0) = 2t_{\text{new}}$. The trace of the RHS in final equation of 2.60 is $2 \times \text{tr}(\mathcal{H}_0) = 2t_{\text{old}}$ where $t_{\text{old}} = \text{tr}(\mathcal{H}_0)$ is the trace of the old Hamiltonian. Equating the LHS and RHS gives $t_{\text{new}} = t_{\text{old}}$.

2.2.9 Complete generator for the unitary transformation

Given some operator O_0 , we can generate a family of unitarily-connected operators O_j using a unitary operator $U(t)$:

$$O_j = U_j O(0) U_j^\dagger, \quad j = 1, 2, \dots \quad (2.62)$$

The discrete change equation for O_j can be represented in the form of a commutator:

$$\Delta O_j \equiv O_{j+1} - O_j = [O_j, S_j] \quad (2.63)$$

where

$$S_j = U_j \Delta U_j^\dagger. \quad (2.64)$$

Note that because $\Delta(U_j U_j^\dagger) = 0$, we have $(\Delta U_j) U_j^\dagger = -U_j (\Delta U_j^\dagger)$ and so S_j is anti-Hermitian. To verify that eq. 2.62 is indeed the solution of eq. 2.63, we differentiate eq. 2.62:

$$O_{j+1} - O_j = \Delta U_j O(0) U_j^\dagger + U_j O(0) \Delta U_j^\dagger = \Delta U_j U_j^\dagger O_j + O_j U_j \Delta U_j^\dagger = [O_j, S_j] \quad (2.65)$$

This shows that given a family of operators eq. 2.62 connected through U_j , we can obtain a generator S_j that defines the flow equation of O_j .

Since the URG is unitary, we should be able to obtain such a generator for it as well. From the expression of the unitary transformation of URG:

$$U_j = \frac{1}{\sqrt{2}} (1 + \eta_j^\dagger - \eta_j) \quad (2.66)$$

From the definition of the generator S_j , we then get

$$S_j = \frac{1}{2} (1 + \eta_j^\dagger - \eta_j) (\eta_{j+1} - \eta_{j+1}^\dagger - \eta_j + \eta_j^\dagger) \quad (2.67)$$

The operators η_j and its hermitean conjugate can be thought of as angular momentum creation and annihilation operators acting on the 2×2 Hilbert space of the occupied and vacant states $|1\rangle |\phi_1\rangle, |0\rangle |\phi_0\rangle$:

$$\eta_j |1\rangle |\phi_1\rangle = |0\rangle |\phi_0\rangle, \quad \eta_j |0\rangle |\phi_0\rangle = 0, \quad \eta_j^\dagger |0\rangle |\phi_0\rangle = |1\rangle |\phi_1\rangle, \quad \eta_j^\dagger |1\rangle |\phi_1\rangle = 0, \quad (2.68)$$

$$(2.69)$$

To check whether they have the correct algebra, we design the three spin operators $S^i, i = \{x, y, z\}$.

$$\begin{aligned} S^x &= \frac{1}{2} (S^+ + S^-) = \frac{1}{2} (\eta_j^\dagger + \eta_j) \\ S^y &= \frac{1}{2i} (S^+ - S^-) = \frac{1}{2i} (\eta_j^\dagger - \eta_j) \\ S^z &= \hat{n} - \frac{1}{2} \end{aligned} \quad (2.70)$$

The commutation relations give

$$\begin{aligned} [S^x, S^y] &= \frac{1}{4i} [\eta_j^\dagger + \eta_j, \eta_j^\dagger - \eta_j] = \frac{1}{2i} [\eta_j, \eta_j^\dagger] = \frac{1}{2i} (1 - \hat{n} - \hat{n}) = \frac{-1}{i} \left(\hat{n} - \frac{1}{2} \right) = iS^z \\ [S^y, S^z] &= \frac{1}{2i} [\eta_j^\dagger - \eta_j, \hat{n} - \frac{1}{2}] = \frac{1}{2i} [-\eta_j \hat{n} - \hat{n} \eta_j^\dagger] = \frac{1}{2i} (-\eta_j - \eta_j^\dagger) = \frac{i}{2} (\eta_j^\dagger + \eta_j) = iS^x \\ [S^z, S^x] &= \frac{1}{2} \left[\hat{n} - \frac{1}{2}, \eta_j^\dagger + \eta_j \right] = \frac{1}{2} [\hat{n} \eta_j^\dagger - \eta_j \hat{n}] = \frac{1}{2} (\eta_j^\dagger - \eta_j) = i \frac{1}{2i} (\eta_j^\dagger - \eta_j) = iS^y \end{aligned} \quad (2.71)$$

These operators therefore satisfy the commutation algebra of angular momentum operators $[S^i, S^j] = i\epsilon^{ijk} S^k$.

2.2.10 A note on the various quantum fluctuation scales ω_i^j

At a particular step of the URG, there are two quantum fluctuation energy scales associated with each sector. If we rotate $|\psi_1\rangle$ to $|1\rangle$ (particle/occupied sector), the corresponding unitary will be a function of $\omega_1^{0,1}$. If we, on the other hand, rotate $|\psi_0\rangle$ to $|0\rangle$ (hole/unoccupied sector), the unitary will be a function of $\omega_0^{0,1}$. The superscript j signifies whether this particular ω_i^j is an eigenvalue corresponding to $|1, \phi_i\rangle$ or $|0, \phi_i\rangle$. ω_i^0 occurs in the many-body transition operator η , because η is preceded by c and hence it picks out the eigenstate $|0, \phi_i\rangle$. On the other hand, ω_i^1 occurs in the many-body transition operator η^\dagger , because that is preceded by c^\dagger . This constrains these two values, because we must have $\eta(\omega_i^0) = (\eta^\dagger(\omega_i^1))^\dagger$ (eq. 2.16), for each value of i , giving us two constraints in total. The subscript i

signifies whether ω_i^j is a part of the particle sector unitary $U_1(\omega_1^j)$ or the hole sector unitary $U_0(\omega_0^j)$. As mentioned in the previous section, since both ways are equivalent, we must have $U_1 = U_0$ which leads to the constraints $\eta(\omega_0^j) = -\eta(\omega_1^j)$. All the independent constraints are listed below.

$$\begin{aligned}\omega_1^0 - \omega_1^1 &= \mathcal{H}_d^0 - \mathcal{H}_d^1 \\ \omega_0^0 - \omega_0^1 &= \mathcal{H}_d^0 - \mathcal{H}_d^1 \\ \omega_1^0 + \omega_0^0 &= 2\mathcal{H}_d^0\end{aligned}\tag{2.72}$$

The first two come from $\eta(\omega_i^0) = (\eta^\dagger(\omega_i^1))^\dagger$ while the last comes from $\eta(\omega_0^j) = -\eta(\omega_1^j)$. These are the only independent relations. Other relations like the one between ω_1^0 and ω_0^1 can be derived from these. This means that we have four ω and three constraints, such that each step of the URG is characterized by just a single independent quantum fluctuation scale.

2.3 Prescription

Given a Hamiltonian

$$\mathcal{H} = \mathcal{H}_1 + \mathcal{H}_0 + c^\dagger T + T^\dagger c\tag{2.73}$$

the goal is to look at the renormalization of the various couplings in the Hamiltonian as we decouple high energy electron states. Typically we have a shell of electrons at some energy D . During the process, we make one simplification. We assume that there is only one electron on that shell at a time, say with quantum numbers q, σ , and calculate the renormalization of the various couplings due to this electron. We then sum the momentum q over the shell and the spin β , and this gives the total renormalization due to decoupling the entire shell.

From eq. 2.45, the first two terms in the rotated Hamiltonian are just the diagonal parts of the bare Hamiltonian; they are unchanged in that part. The renormalization comes from the third term. For one electron $q\beta$ on the shell, the renormalization is

$$\Delta\mathcal{H} = \left[c_{q\beta}^\dagger \text{Tr}(\mathcal{H}c_{q\beta}), \eta \right] = c_{q\beta}^\dagger \text{Tr}(\mathcal{H}c_{q\beta}) \eta - \eta c_{q\beta}^\dagger \text{Tr}(\mathcal{H}c_{q\beta})\tag{2.74}$$

Since this assumes we have obtained this from U_1 , it is fair to tag the η with a suitable label:

$$\Delta\mathcal{H} = c_{q\beta}^\dagger \text{Tr}(\mathcal{H}c_{q\beta}) \eta_1 - \eta_1 c_{q\beta}^\dagger \text{Tr}(\mathcal{H}c_{q\beta})\tag{2.75}$$

It is clear that the first term takes into account virtual excitations that start from a filled state ($\hat{n}_{q\beta} = 1$ initially) - such a term is said to be a part of the *particle sector*.

$$\Delta_1\mathcal{H} = c_{q\beta}^\dagger \text{Tr}(\mathcal{H}c_{q\beta}) \eta_1\tag{2.76}$$

The second term, on the other hand, considers excitations that start from an empty state. They constitute the *hole sector*.

$$\Delta_0\mathcal{H} = -\eta_1 c_{q\beta}^\dagger \text{Tr}(\mathcal{H}c_{q\beta})\tag{2.77}$$

To write the total renormalization in a particle-hole symmetric form, we can use the relation $\eta_0 = -\eta_1$, such that both the terms will now come with a positive sign:

$$\Delta\mathcal{H} = c_{q\beta}^\dagger \text{Tr}(\mathcal{H}c_{q\beta}) \eta_1 + \eta_0 c_{q\beta}^\dagger \text{Tr}(\mathcal{H}c_{q\beta})\tag{2.78}$$

We can make one more manipulation: using eq. 2.16, we get

$$\Delta\mathcal{H} = c_{q\beta}^\dagger \text{Tr}(\mathcal{H}c_{q\beta}) \eta_1 + \text{Tr}(c_{q\beta}^\dagger \mathcal{H}) c_{q\beta} \eta_0^\dagger \quad (2.79)$$

This form of the total renormalization is identical to the one we use in the "Poor Man's scaling"-type of renormalization that was used to get the scaling equations in the Kondo and Anderson models [6,7]. Writing down the forms of η and η^\dagger explicitly, we get

$$\Delta\mathcal{H} = c_{q\beta}^\dagger \text{Tr}(\mathcal{H}c_{q\beta}) \frac{1}{\omega_1^0 - \mathcal{H}_0^d} \text{Tr}(c_{q\beta}^\dagger \mathcal{H}) c_{q\beta} + \text{Tr}(c_{q\beta}^\dagger \mathcal{H}) c_{q\beta} \frac{1}{\omega_0^1 - \mathcal{H}_1^d} c_{q\beta}^\dagger \text{Tr}(\mathcal{H}c_{q\beta}) \quad (2.80)$$

The renormalization due to the entire shell is obtained by summing over all states on the shell.

$$\Delta\mathcal{H} = \sum_{q\beta} \left[c_{q\beta}^\dagger \text{Tr}(\mathcal{H}c_{q\beta}) \frac{1}{\omega_1^0 - \mathcal{H}_0^d} \text{Tr}(c_{q\beta}^\dagger \mathcal{H}) c_{q\beta} + \text{Tr}(c_{q\beta}^\dagger \mathcal{H}) c_{q\beta} \frac{1}{\omega_0^1 - \mathcal{H}_1^d} c_{q\beta}^\dagger \text{Tr}(\mathcal{H}c_{q\beta}) \right] \quad (2.81)$$

These equations will now need to be simplified. For example, in the particle sector, we can set $\hat{n}_{q\beta} = 0$ in the numerator, because there is no such excitation in the initial state. Similarly, in the hole sector, we can set $\hat{n}_{q\beta} = 1$ because that state was occupied in the initial state. Another simplification we typically employ is that $\mathcal{H}_{0,1}^d$ will, in general, have the energies of all the electrons. But we consider only the energy of the on-shell electrons in the denominator. After integrating out these electrons, we can rearrange the remaining operators to determine which term in the Hamiltonian it renormalizes and what is the renormalization.

At first sight, one might think that we must evaluate lots of traces to obtain the terms in $\Delta\mathcal{H}$. A little thought reveals that the terms in the numerator are simply the off-diagonal terms in the Hamiltonian; $\text{Tr}(c_{q\beta}^\dagger \mathcal{H}) c_{q\beta}$ is the off-diagonal term that has $c_{q\beta}$ in it, and $c_{q\beta}^\dagger \text{Tr}(\mathcal{H}c_{q\beta})$ is the off-diagonal term that has $c_{q\beta}^\dagger$ in it. \mathcal{H}^D is just the diagonal part of the Hamiltonian.

2.4 URG analysis of the star graph model

The star graph problem has already been analyzed using URG and an extensive study of its entanglement properties has already been carried out, in ref. [?]. Here we focus on just deriving the RG equations. The system consists of N spin-like degrees of freedom (labeled 1 through N) individually talking to a spin at the center (labeled 0). Each spin i ($\in [0, N]$) has an on-site energy ϵ_i . The coupling strength between 0 and i ($\in [1, N]$) is J_i . We choose the on-site energies such that $\epsilon_{i+1} > \epsilon_i, i \in [N-1, 1]$. In this way, ϵ_1 is the infrared limit and ϵ_N is the ultraviolet limit.

$$\mathcal{H} = \epsilon_0 S_0^z + \sum_{i=1}^N \left[\epsilon_i S_i^z + J_i \vec{S}_0 \cdot \vec{S}_i \right] \quad (2.82)$$

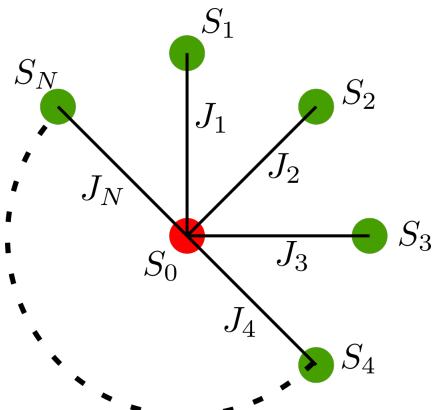


Figure 2.2: Star Graph model

By converting the last term into S^z and S^\pm , we can write the Hamiltonian as

$$\mathcal{H} = \epsilon_0 S_0^z + \sum_{i=1}^N \left[\epsilon_i S_i^z + J_i \left(S_0^z S_i^z + \frac{1}{2} (S_0^+ S_i^- + S_0^- S_i^+) \right) \right] \quad (2.83)$$

2.4.1 Calculation of Renormalization

The RG involves decoupling the nodes N through 1, and looking at the resultant renormalization in ϵ_i and J_i . As a simplification, we will ignore the lower nodes in the denominator and keep only the node currently being decoupled, ie node N . Since node 0 is connected to node N , we will keep node 0 in the denominator as well. Making this simplification gives

$$\mathcal{H}^D = \epsilon_0 S_0^z + \epsilon_N S_N^z + J_N S_0^z S_N^z \quad (2.84)$$

The off-diagonal part in the subspace of the node N is

$$\mathcal{H}_X = S_N^+ T + T^\dagger S_N^- = \frac{1}{2} J_N (S_N^+ S_0^- + S_N^- S_0^+) \quad (2.85)$$

The renormalization on doing one step of the URG is given by

$$\begin{aligned} \Delta \mathcal{H} &= S_N^+ T \frac{1}{\omega_0^1 - \mathcal{H}^D} T^\dagger S_N^- + T^\dagger S_N^- \frac{1}{\omega_1^0 - \mathcal{H}^D} S_N^+ T \\ &= \frac{J_N^2}{4} S_N^+ S_0^- \frac{1}{\omega_0^1 - \epsilon_0 S_0^z - \epsilon_N S_N^z - J_N S_0^z S_N^z} S_0^+ S_N^- + \frac{J_N^2}{4} S_0^+ S_N^- \frac{1}{\omega_1^0 - \epsilon_0 S_0^z - \epsilon_N S_N^z - J_N S_0^z S_N^z} S_N^+ S_0^- \end{aligned} \quad (2.86)$$

There, N refers to the spin being decoupled. The first Greens function has S_0^+ and S_N^- in front of it, so we substitute $S_0^z = \frac{1}{2}$, $S_N^z = -\frac{1}{2}$ in that Greens function. For the other Greens function we do the opposite.

$$\Delta \mathcal{H} = \frac{J_N^2}{4} S_N^+ S_0^- \frac{1}{\omega_1^0 - \frac{1}{2}\epsilon_0 + \frac{1}{2}\epsilon_N + \frac{1}{4}J_N} S_0^+ S_N^- + \frac{J_N^2}{4} S_0^+ S_N^- \frac{1}{\omega_0^1 + \frac{1}{2}\epsilon_0 - \frac{1}{2}\epsilon_N + \frac{1}{4}J_N} S_N^+ S_0^- \quad (2.87)$$

To relate ω_1^0 and ω_0^1 , we use eq. 2.72:

$$\omega_1^0 + \omega_0^1 = \mathcal{H}_0^D + \mathcal{H}_1^D = -\frac{1}{2} J_N \implies \omega_1^0 \equiv \omega, \quad \omega_0^1 \equiv \omega' = -\frac{1}{2} J_N - \omega \quad (2.88)$$

So, the renormalization becomes

$$\Delta \mathcal{H} = \frac{J_N^2}{4} \frac{1}{\omega - \frac{1}{2}\epsilon_0 + \frac{1}{2}\epsilon_N + \frac{1}{4}J_N} (S_N^+ S_0^- S_0^+ S_N^- - S_0^+ S_N^- S_N^+ S_0^-) = \frac{J_N^2}{4} \frac{1}{\omega - \frac{1}{2}\epsilon_0 + \frac{1}{2}\epsilon_N + \frac{1}{4}J_N} (S_N^z - S_0^z) \quad (2.89)$$

There we used $S^+ S^- = \frac{1}{2} + S^z$ and $S^- S^+ = \frac{1}{2} - S^z$.

We can now read off the renormalizations in ϵ_N and ϵ_0 .

$$\begin{aligned} \Delta \epsilon_N &= \frac{1}{4} J_N^2 \frac{1}{\omega - \frac{1}{2}\epsilon_0 + \frac{1}{2}\epsilon_N + \frac{1}{4}J_N} \\ \Delta \epsilon_0 &= -\frac{1}{4} J_N^2 \frac{1}{\omega - \frac{1}{2}\epsilon_0 + \frac{1}{2}\epsilon_N + \frac{1}{4}J_N} \end{aligned} \quad (2.90)$$

2.4.2 Nature of flows

We are interested in looking at the renormalization of the central node energy ϵ_0 , upon removing the nodes N through 1. We will hence concentrate on the second RG equation. We first make some simplifying assumptions: $J_i = J$, $\epsilon_i = \epsilon$ for all $i \in \{1, N\}$.

$$\Delta\epsilon_0 = -\frac{1}{4}J^2 \frac{1}{\omega - \frac{1}{2}\epsilon_0 + \frac{1}{2}\epsilon + \frac{1}{4}J} \quad (2.91)$$

Define $\tilde{\omega} = \omega + \frac{1}{2}\epsilon + \frac{1}{4}J$.

$$\Delta\epsilon_0 = -\frac{1}{4}J^2 \frac{1}{\tilde{\omega} - \frac{1}{2}\epsilon_0} \quad (2.92)$$

Our goal here is to look for a fixed-point condition such that the denominator vanishes at some point of the RG. If we start with a bare of ϵ_0 such that $\tilde{\omega} - \frac{1}{2}\epsilon_0 > 0$, the denominator will be positive and the RG equation will be irrelevant. This means that ϵ_0 will keep on decreasing, and the denominator will keep on becoming more and more positive, meaning there cannot be a fixed point in this situation.

If, on other hand, we start with a bare of ϵ_0 such that $\tilde{\omega} - \frac{1}{2}\epsilon_0 < 0$, the denominator will be negative and the RG equation will be relevant. This means that ϵ_0 will keep on increasing, and the denominator will keep on becoming more and more negative, meaning there cannot be a fixed point in this situation either. These situations are depicted in figure 2.3.

Since we cannot find a fixed point, we will use a different ω . Instead of ω_1^0 , we will use ω_1^1 . From eq. 2.72, we have

$$\omega_1^0 - \omega_1^1 = \mathcal{H}_0^D - \mathcal{H}_1^D = \epsilon_0 - \epsilon_N = \epsilon_0 - \epsilon \quad (2.93)$$

Defining $\omega_1^1 = \omega'$ and substituting this in eq. 2.91 gives

$$\Delta\epsilon_0 = -\frac{1}{4}J^2 \frac{1}{\omega' - \frac{1}{2}\epsilon + \frac{1}{2}\epsilon_0 + \frac{1}{4}J} \quad (2.94)$$

We again define $-\tilde{\omega} = \omega' - \frac{1}{2}\epsilon + \frac{1}{4}J$.

$$\Delta\epsilon_0 = \frac{1}{4}J^2 \frac{1}{\tilde{\omega} - \frac{1}{2}\epsilon_0} \quad (2.95)$$

We now repeat the exercise of determining the relevance of the flows under various regime. If we start with a bare ϵ_0 such that $\tilde{\omega} + \frac{1}{2}\epsilon_0 > 0$, then the denominator is positive so the renormalization will be irrelevant. ϵ_0 will decrease until we reach $\tilde{\omega} + \frac{1}{2}\epsilon_0 = 0$. This will be a fixed point. However, if we start with a bare ϵ_0 such that $\tilde{\omega} + \frac{1}{2}\epsilon_0 < 0$, then the denominator is negative so the renormalization will be relevant. ϵ_0 will increase until we reach $\tilde{\omega} + \frac{1}{2}\epsilon_0 = 0$. This will again be a fixed point. This new situation is depicted in right panel of figure 2.3.

2.4.3 Effective Hamiltonians

If $\tilde{\omega}$ and ϵ_0 are of the same sign at the bare level, then it is easy to see that since the fixed point is defined by $\tilde{\omega} = \frac{1}{2}\epsilon_0^*$ (* denotes value at fixed point), the effective Hamiltonian at the fixed point will be

$$\mathcal{H}^* = 2\tilde{\omega}S_0^z + \epsilon \sum_i S_i^z + J \sum_i \vec{S}_i \cdot \vec{S}_0, \quad \text{if } \tilde{\omega}\epsilon_0 > 0 \quad (2.96)$$

If, at the bare level, ϵ_0 and $\tilde{\omega}$ are of opposite signs, then ϵ_0 would undergo a change in sign at some point as it flows towards $\tilde{\omega}$. Since we do not expect a coupling to change sign under RG, we will restrict it to 0 in such cases.

$$\mathcal{H}^* = \epsilon \sum_i S_i^z + J \sum_i \vec{S}_i \cdot \vec{S}_0, \quad \text{if } \tilde{\omega}\epsilon_0 < 0 \quad (2.97)$$

Things get much more simpler if we assume the onsite energies of the surrounding nodes are zero.

$$\begin{aligned} \mathcal{H}^* &= 2\tilde{\omega}S_0^z + J \sum_i \vec{S}_i \cdot \vec{S}_0, & \text{if } \tilde{\omega}\epsilon_0 > 0 \\ \mathcal{H}^* &= J \sum_i \vec{S}_i \cdot \vec{S}_0, & \text{if } \tilde{\omega}\epsilon_0 < 0 \end{aligned} \quad (2.98)$$

2.4.4 Fixed points

The fixed points are obtained numerically by solving the RG equation. As mentioned before, there are two types of solutions: The first kind is those in which ϵ_0 and $\tilde{\omega}$ are of the same sign, and the former flows to the latter without crossing the 0 axis. These flows are shown (obtained numerically) in fig. 2.4. The second kind are those where the two couplings have different signs, and so ϵ_0 flows to 0. These are shown in fig. 2.5.

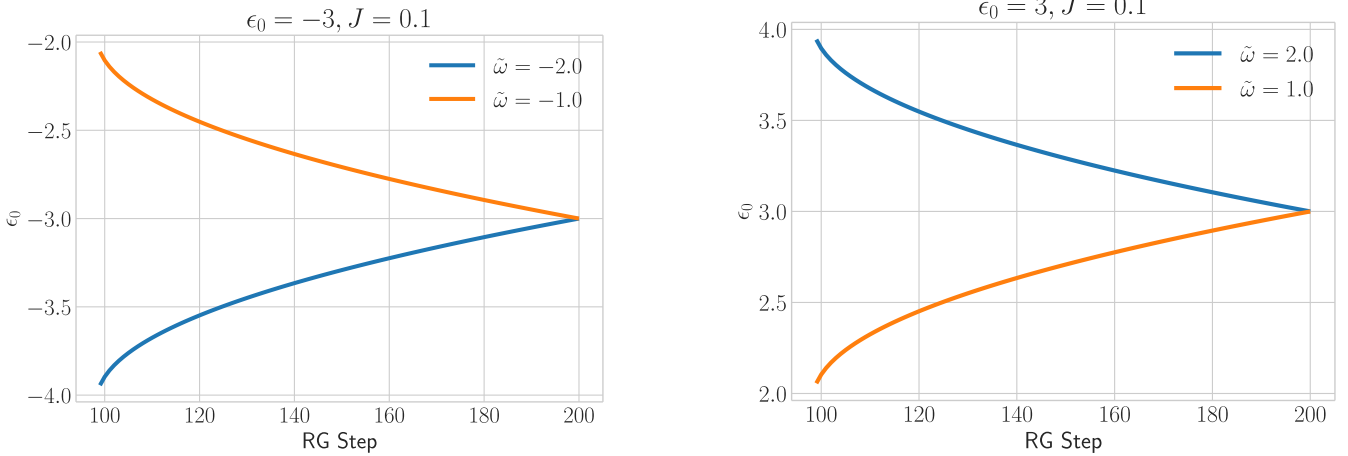


Figure 2.4: Flows where ϵ_0 and $\tilde{\omega}$ have same sign. The left and right panels show flows starting from negative and positive values respectively. The two plots in each panel correspond to different values of $\tilde{\omega}$, one greater than the bare ϵ_0 , the other less than that. The fixed point value is $2\tilde{\omega}$.

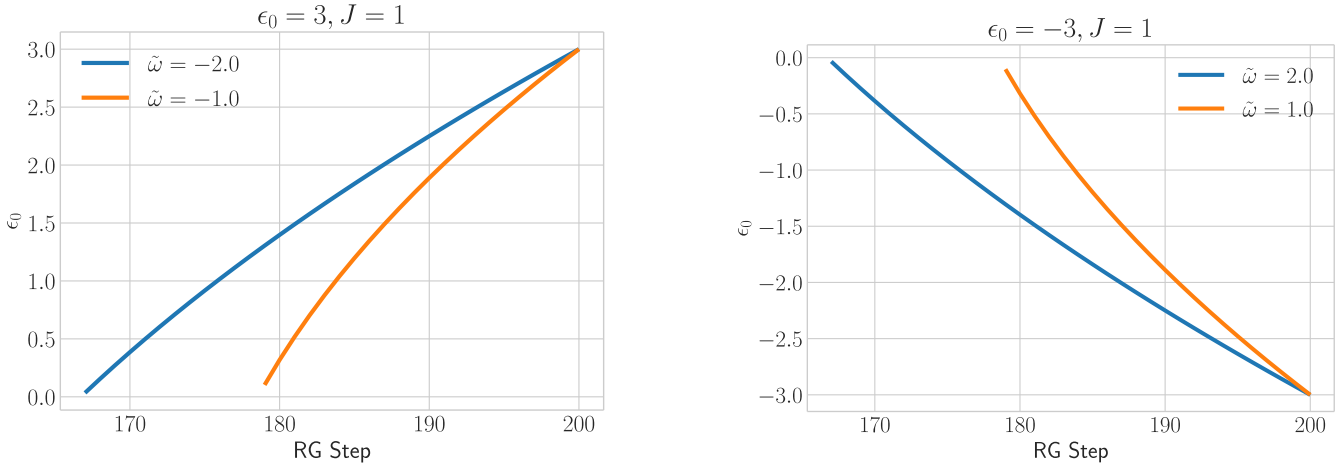


Figure 2.5: Flows where ϵ_0 and $\tilde{\omega}$ have opposite sign. The left and right panels show flows starting from negative and positive values respectively. The two plots in each panel correspond to different values of $\tilde{\omega}$, one greater than the bare ϵ_0 , the other less than that. The fixed point value is 0.

2.5 Poor man's scaling (PMS)

2.5.1 Formalism

We first describe the formalism of the poor man's scaling (PMS) method, first formulated by Anderson [6]. The problem is defined as

$$\mathcal{H} |\Psi\rangle = E |\Psi\rangle \quad (2.99)$$

\mathcal{H} is the total Hamiltonian and $|\Psi\rangle$ and E are the exact eigenstate and eigenvalue of \mathcal{H} . We imagine a separation of the total Hilbert space into two set of states, and we call these two states $|0\rangle$ and $|1\rangle$. This separation depends on which scattering term we want to kill by this transformation. For example, in the URG, we typically select a particular electron $q\beta$ and then kill the scattering terms that change the number of this state. In that case, $|0\rangle$ will refer to the set of states $\{|\hat{n}_{q\beta} = 0\rangle \otimes |\phi_0\rangle\}$ and $|1\rangle$ will refer to the set of states $\{|\hat{n}_{q\beta} = 1\rangle \otimes |\phi_1\rangle\}$. $|\phi_{0,1}\rangle$ refer to the states of all the other electrons. As another example, if we wanted to separate the charge-Kondo and the spin-Kondo from the SIAM, we would want to kill the terms that scatter between the spin-full subspace $\hat{n}_d = 1$ to the spin-less subspace $\hat{n}_d = 0, 2$. These two will then be the $|0\rangle$ and $|1\rangle$ sets.

Keeping this separation in mind, the exact eigenstate $|\Psi\rangle$ can be split as

$$|\Psi\rangle = \sum_i |\phi_0^i\rangle + \sum_i |\phi_1^i\rangle \quad (2.100)$$

The Hamiltonian can also be split as

$$\mathcal{H} = H_0 + V_+ + V_- \quad (2.101)$$

H_0 does not scatter between $\{|0\rangle\}$ and $\{|1\rangle\}$. It contains the diagonal parts as well as scatterings inside the subspaces. V_\pm scatter between the subspaces:

$$\begin{aligned} V_+ \{ |0\rangle \} &\mapsto \{ |1\rangle \}, \quad V_+ |1\rangle \rightarrow 0 \\ V_- \{ |1\rangle \} &\mapsto \{ |0\rangle \}, \quad V_- |0\rangle \rightarrow 0 \end{aligned} \quad (2.102)$$

The Schrodinger equation can thus be split into

$$\begin{aligned} H_0 \sum_i |\phi_0^i\rangle + V_- \sum_i |\phi_1^i\rangle &= E \sum_i |\phi_0^i\rangle \\ H_0 \sum_i |\phi_1^i\rangle + V_+ \sum_i |\phi_0^i\rangle &= E \sum_i |\phi_1^i\rangle \end{aligned} \quad (2.103)$$

Eliminating $\sum_i |\phi_1^i\rangle$ gives

$$H_0 \sum_i |\phi_0^i\rangle + V_- \frac{1}{E_1 - H_0} V_+ \sum_i |\phi_0^i\rangle = E \sum_i |\phi_0^i\rangle \quad (2.104)$$

The effective Hamiltonian in this subspace is therefore

$$\tilde{\mathcal{H}}_0 = H_0 + V_- \frac{1}{E - H_0} V_+ \quad (2.105)$$

Similarly, eliminating $\sum_i |\phi_0^i\rangle$ gives the effective Hamiltonian in the other subspace,

$$\tilde{\mathcal{H}}_1 = H_0 + V_+ \frac{1}{E - H_0} V_- \quad (2.106)$$

The total effective Hamiltonian that does not scatter between the two subspaces is

$$\tilde{\mathcal{H}}(E) = H_0 + \underbrace{V_- \frac{1}{E - H_0} V_+ + V_+ \frac{1}{E - H_0} V_-}_{\text{renormalization}} \quad (2.107)$$

This is of course a function of whatever exact energy eigenvalue we chose, E . Different choices will give different effective Hamiltonians. The renormalization will now be written in terms of the matrix elements. Since the entire \mathcal{H}_X must be Hermitian, we must have $V_- = V_+^\dagger \equiv V$.

$$\Delta\mathcal{H}(E) = V \frac{1}{E - H_0} V^\dagger + V^\dagger \frac{1}{E - H_0} V \quad (2.108)$$

Now take the first term and insert complete bases on both sides of V and V^\dagger .

$$V \frac{1}{E - H_0} V^\dagger = \sum_{ijk} |\phi_0^i\rangle \langle \phi_0^i| V |\phi_1^j\rangle \langle \phi_1^j| \frac{1}{E - H_0} |\phi_1^j\rangle \langle \phi_1^j| V^\dagger |\phi_0^k\rangle \langle \phi_0^k| = \sum_{ijk} |\phi_0^i\rangle V_{ij} \langle \phi_1^j| \frac{1}{E - H_0} |\phi_1^j\rangle V_{kj}^\dagger \langle \phi_0^k| \quad (2.109)$$

where we defined $\langle \phi_0^i | V | \phi_1^j \rangle = V_{ij}$. We now approximate H_0 by keeping just the diagonal part, and allowing the balance to redefine E into ω . Then, $(E - H_0) |\phi_{0,1}^j\rangle \equiv (\omega_{0,1} - E_{0,1}^j) |\phi_{0,1}^j\rangle$. That gives

$$V \frac{1}{E - H_0} V^\dagger = \sum_{ijk} |\phi_0^i\rangle \langle \phi_0^k| \frac{V_{ij} V_{kj}^\dagger}{\omega_1 - E_1^j} \quad (2.110)$$

The second term similarly gives

$$V^\dagger \frac{1}{E - H_0} V = \sum_{ijk} |\phi_1^i\rangle \langle \phi_1^k| \frac{V_{ji}^\dagger V_{jk}}{\omega_0 - E_0^j} \quad (2.111)$$

The total renormalization becomes

$$\Delta\mathcal{H}(E) = \sum_{ijk} \left(\frac{1}{\omega_1 - E_1^j} |\phi_0^i\rangle \langle \phi_0^k| V_{ij} V_{kj}^\dagger + \frac{1}{\omega_0 - E_0^j} |\phi_1^i\rangle \langle \phi_1^k| V_{ji}^\dagger V_{jk} \right) \quad (2.112)$$

This is a general expression that would work irrespective of whether you are decoupling multiple electrons or a single electron. However, the ω are unknown and we need some prescription for replacing them. Since the E is the eigenstate of the initial state on which the scattering terms act, it makes sense to replace them with the initial state energy.

$$\Delta\mathcal{H}(E) = \sum_{ijk} \left(\frac{1}{E_0^k - E_1^j} |\phi_0^i\rangle \langle \phi_0^k| V_{ij} V_{kj}^\dagger + \frac{1}{E_1^k - E_0^j} |\phi_1^i\rangle \langle \phi_1^k| V_{ji}^\dagger V_{jk} \right) \quad (2.113)$$

However, closer inspection reveals that this choice makes the renormalization non-Hermitian. So the correct choice is to keep both the initial and final energies.

$$\begin{aligned} \Delta\mathcal{H} &= \frac{1}{2} \sum_{ijk} \frac{1}{\omega_1 - E_1^j} \left(|\phi_0^i\rangle \langle \phi_0^k| V_{ij} V_{kj}^\dagger + |\phi_0^k\rangle \langle \phi_0^i| V_{kj} V_{ij}^\dagger \right) + \frac{1}{2} \sum_{ijk} \frac{1}{\omega_0 - E_0^j} \left(|\phi_1^i\rangle \langle \phi_1^k| V_{ji}^\dagger V_{jk} + |\phi_1^k\rangle \langle \phi_1^i| V_{jk}^\dagger V_{ji} \right) \\ &= \frac{1}{2} \sum_{ijk} \left(\frac{1}{E_0^k - E_1^j} |\phi_0^i\rangle \langle \phi_0^k| V_{ij} V_{kj}^\dagger + \frac{1}{E_0^k - E_1^j} |\phi_0^k\rangle \langle \phi_0^i| V_{kj} V_{ij}^\dagger \right) + \frac{1}{2} \sum_{ijk} \left(\frac{1}{E_1^k - E_0^j} |\phi_1^i\rangle \langle \phi_1^k| V_{ji}^\dagger V_{jk} \right. \\ &\quad \left. + \frac{1}{E_1^k - E_0^j} |\phi_1^k\rangle \langle \phi_1^i| V_{jk}^\dagger V_{ji} \right) \end{aligned} \quad (2.114)$$

Therefore,

$$\Delta\mathcal{H} = \frac{1}{2} \sum_{ijk} \left(\frac{1}{E_0^k - E_1^j} + \frac{1}{E_0^i - E_1^j} \right) |\phi_0^i\rangle \langle \phi_0^k| V_{ij} V_{kj}^\dagger + \frac{1}{2} \sum_{ijk} \left(\frac{1}{E_1^k - E_0^j} + \frac{1}{E_1^i - E_0^j} \right) |\phi_1^i\rangle \langle \phi_1^k| V_{ji}^\dagger V_{jk} \quad (2.115)$$

In summary, the prescription of replacing all ω with the initial state energy will be correct only if the initial and final states are the same. This happens when we are decoupling a single-electron state - then the total renormalization is of the form $c^\dagger T^\dagger c$ such that we start from an initial state, scatter to an intermediate state and then go back to the initial state so that the final state is the same as the initial state. However, if we are using PMS to decouple states in one-shot, each subspace will have multiple states and there might be terms where we do not end up at the initial state we started with. Then the correct prescription would be to use the mean of the initial and final state denominators.

One might wonder how we can generate higher order terms in this method. Eq. 2.115, as it stands, has only $\mathcal{O}(V^2)$ terms. The higher order terms were actually dropped when we replaced H_0 with its diagonal part in eq. 2.110. To see the higher order term, we do not drop the off-diagonal part in the denominator, but split the total H_0 into a diagonal and an off-diagonal part: $H_0 = H_d + X$. Note that X is off-diagonal in the subspace of the states that have not been decoupled yet but will be decoupled later. They represent scattering between the lower energy states. X is still diagonal with respect to the states that we are decoupling presently. The total effective Hamiltonian becomes

$$\tilde{\mathcal{H}}(E) = H_0 + V \frac{1}{G_0(E)^{-1} - X} V^\dagger + V^\dagger \frac{1}{G_0(E)^{-1} - X} V \quad (2.116)$$

where $G_0(E)^{-1} = E - H_d$ is the inverse of the non-interacting Greens function. To allow computation, we can expand the denominator in powers of $XG_0(E)^{-1}$:

$$\begin{aligned}\Delta H \equiv \tilde{\mathcal{H}}(E) - H_0 &= VG_0(E) [1 + XG_0(E) + XG_0(E)XG_0(E) + \dots] V^\dagger + V^\dagger \frac{1}{G_0(E)^{-1} - X} V \\ &= \underbrace{VG_0(E)V^\dagger + V^\dagger G_0(E)V}_{\text{two vertex or one loop correction}} + \underbrace{VG_0(E)XG_0(E)V^\dagger + V^\dagger G_0(E)XG_0(E)V}_{\text{three vertex or two loop correction}} \\ &\quad + \text{higher loop corrections}\end{aligned}\tag{2.117}$$

2.5.2 PMS third order equations for symmetric multi-channel Kondo model

To get a clear idea of what the various terms in eq. 2.117 mean, we will calculate the multi-channel Kondo model RG equations up to third order. The model is

$$H = \sum_{k\sigma,\gamma} \epsilon_{k\sigma}^{(\gamma)} c_{k\sigma}^\dagger c_{k\sigma}^{(\gamma)} + \sum_{k\alpha,k'\alpha',\gamma,a} J^a S_d^a \sigma_{\alpha\alpha'}^a c_{k\alpha}^{(\gamma)\dagger} c_{k'\alpha'}^{(\gamma)}\tag{2.118}$$

a goes over x, y, z and represents the directions. S_d^a therefore represents the spin operators for the impurity along the x, y and z directions. The labels $k\alpha$ and $k'\alpha'$ sum over the conduction electrons, while the index γ represents the channel. We will first calculate the second order terms. The virtual particle term is

$$VG_0(E)V^\dagger = \sum_{k,k',\alpha,\alpha',q,\beta,\gamma,a,b} c_{q\beta}^{(\gamma)\dagger} c_{k\alpha}^{(\gamma)} S_d^a \sigma_{\beta\alpha}^a \frac{J^a J^b}{E - H_d} c_{k'\alpha'}^{(\gamma)\dagger} c_{q\beta}^{(\gamma)} S_d^b \sigma_{\alpha'\beta}^b\tag{2.119}$$

The label q sums over the momentum states being decoupled ($|\epsilon_q| \in [D - |\delta D|, D]$). The labels k, k' , on the other hand, sum over the momentum states that are not being decoupled, so they lie in the complimentary range. The denominator of the Greens function is the excitation energy $\epsilon_q - \epsilon_{k'}$. We will now simplify the term.

$$\begin{aligned}VG_0(E)V^\dagger &= \sum_{k,k',\alpha,\alpha',q,\beta,\gamma,a,b} \frac{J^a J^b}{\epsilon_q - \epsilon_{k'}} S_d^a \sigma_{\beta\alpha}^a S_d^b \sigma_{\alpha'\beta}^b c_{q\beta}^{(\gamma)\dagger} c_{k\alpha}^{(\gamma)} c_{k'\alpha'}^{(\gamma)\dagger} c_{q\beta}^{(\gamma)} \\ &= \sum_{k,k',\alpha,\alpha',\beta,\gamma,a,b} \frac{J^a J^b}{\epsilon_q - \epsilon_{k'}} S_d^a \sigma_{\beta\alpha}^a S_d^b \sigma_{\alpha'\beta}^b c_{k\alpha}^{(\gamma)\dagger} c_{k'\alpha'}^{(\gamma)\dagger} \sum_q \hat{n}_{q\beta}^{(\gamma)} \\ &= \sum_{k,k',\alpha,\alpha',\beta,\gamma,a,b} S_d^a \sigma_{\beta\alpha}^a S_d^b \sigma_{\alpha'\beta}^b c_{k\alpha}^{(\gamma)\dagger} c_{k'\alpha'}^{(\gamma)\dagger} \int_{-D}^{-D+|\delta D|} d\epsilon \rho(\epsilon) \frac{J^a J^b \hat{n}^{(\gamma)}(\epsilon)_\beta}{\epsilon_q - \epsilon_{k'}} \\ &= \sum_{k,k',\alpha,\alpha',\beta,\gamma,a,b} S_d^a \sigma_{\beta\alpha}^a S_d^b \sigma_{\alpha'\beta}^b c_{k\alpha}^{(\gamma)\dagger} c_{k'\alpha'}^{(\gamma)\dagger} \frac{J^a J^b \rho(0)|\delta D|}{-D} \quad [\hat{n}(\epsilon) = \theta(-\epsilon), |\epsilon_{k'}| \ll D] \\ &= \sum_{\alpha,\alpha',a,b} S_d^a S_d^b (\sigma^b \sigma^a)_{\alpha',\alpha} \sum_{k,k',\gamma} c_{k\alpha}^{(\gamma)} c_{k'\alpha'}^{(\gamma)\dagger} \frac{J^a J^b \rho(0)|\delta D|}{-D} \\ &= \sum_{\alpha,\alpha',a,b} \left(\frac{1}{4} \delta_{ab} + \frac{i}{2} \sum_c \epsilon^{abc} S_d^c \right) \left(\delta_{ab} + i \sum_c \epsilon^{bac} \sigma^c \right) \sum_{\alpha',\alpha} \sum_{k,k',\gamma} c_{k\alpha}^{(\gamma)} c_{k'\alpha'}^{(\gamma)\dagger} \frac{J^a J^b \rho(0)|\delta D|}{-D}\end{aligned}\tag{2.120}$$

The spin part can now be simplified:

$$\begin{aligned} \sum_{a,b} J^a J^b \left(\frac{1}{4} \delta_{ab} + \frac{i}{2} \sum_c \epsilon^{abc} S_d^c \right) \left(\delta_{ab} + i \sum_c \epsilon^{bac} \sigma^c \right)_{\alpha',\alpha} &= \frac{\sum_a J^{a2}}{4} \delta_{\alpha,\alpha'} + \frac{1}{2} \sum_{a,b,c,c'} J^a J^b \epsilon^{abc} \epsilon^{abc'} S_d^c (\sigma^c)_{\alpha'\alpha} \\ &= \frac{\sum_a J^{a2}}{4} \delta_{\alpha,\alpha'} + \frac{1}{2} \sum_c S_d^c \sigma_{\alpha'\alpha}^c \left(\sum_{\substack{a,b, \\ a \neq b}} J^a J^b - 2 J^c \sum_{\substack{a \\ a \neq c}} J^a \right) \end{aligned} \quad (2.121)$$

The constant part renormalizes a potential scattering, so we drop that part. The renormalization from the other part is

$$\begin{aligned} &\sum_{\alpha,\alpha',c} S_d^c \sigma_{\alpha'\alpha}^c \sum_{k,k',\gamma} c_{k\alpha}^{(\gamma)} c_{k'\alpha'}^{(\gamma)} \frac{\frac{1}{2} \left(\sum_{\substack{a,b, \\ a \neq b}} J^a J^b - 2 J^c \sum_{\substack{a \\ a \neq c}} J^a \right) \rho(0) |\delta D|}{-D} \\ &= \sum_{\alpha,\alpha',c} S_d^c \sigma_{\alpha'\alpha}^c \sum_{k,k',\gamma} c_{k'\alpha'}^{(\gamma)} \frac{\frac{1}{2} \left(\sum_{\substack{a,b, \\ a \neq b}} J^a J^b - 2 J^c \sum_{\substack{a \\ a \neq c}} J^a \right) \rho(0) |\delta D|}{D} \end{aligned} \quad (2.122)$$

The virtual hole term $V^\dagger G_0(E) V$ gives the same contribution. The total renormalization at second order is therefore

$$\delta J^c = \frac{\left(\sum_{\substack{a,b, \\ a \neq b}} J^a J^b - 2 J^c \sum_{\substack{a \\ a \neq c}} J^a \right) \rho(0) |\delta D|}{D} = \frac{2 J^{c+1} J^{c-1} \rho(0) |\delta D|}{D} \quad (2.123)$$

where $\{c-1, c, c+1\}$ is a cyclic permutation of $\{x, y, z\}$. This reveals that the anisotropic Kondo coupling RG equations have a cyclic form:

$$\delta J^x = \frac{2 J^y J^z \rho(0) |\delta D|}{D} \quad (2.124)$$

Cyclic permutations of the labels x, y, z produce the other equations. From here on, we will assume $J^a = J$ for simplicity. This gives, at second order,

$$\delta J = \frac{2 J^2 \rho(0) |\delta D|}{D} \quad (2.125)$$

We now consider the third order term. The virtual hole three vertex term, $V^\dagger G_0(E) X G_0(E) V$, is of the form

$$J^3 \sum_{\substack{q,k_1,k_2,k,k', \\ \alpha,\alpha',\alpha_1,\alpha_2,\beta, \\ \gamma_1,\gamma_2}} c_{q\beta}^{(\gamma_1)\dagger} c_{k\alpha}^{(\gamma_1)} \vec{S}_d \cdot \vec{\sigma}_{\beta\alpha} \frac{1}{E - H_d} c_{k_1\alpha_1}^{(\gamma_2)\dagger} c_{k_2\alpha_2}^{(\gamma_2)} \vec{S}_d \cdot \vec{\sigma}_{\alpha_1\alpha_2} \frac{1}{E - H_d} c_{k'\alpha'}^{(\gamma_1)\dagger} c_{q\beta}^{(\gamma_1)} \vec{S}_d \cdot \vec{\sigma}_{\alpha'\beta} \quad (2.126)$$

The other term among the two third order terms is the virtual particle term. The labels q, k, k', k_1, k_2 run over the momentum states, $\alpha, \alpha', \alpha_1, \alpha_2, \beta$ run over the spin indices and γ_1, γ_2 run over the channel indices. q, β are the labels of the momentum states that are being decoupled. $|\epsilon_q|$ therefore lies in the range $[D, D - \delta D]$. The rest of the labels $(k, \alpha), (k_1, \alpha_1), (k_2, \alpha_2)$ lie in the compliment range and represent electrons that are not being decoupled at this step.

The denominator of the right-most Greens function measures the energy difference between the initial state and the state reached after the first excitation. This difference is $\epsilon_q - \epsilon_{k'}$. Similarly, the second Greens function has the energy difference between the initial state and the one obtained after two subsequent excitations. This difference is $\epsilon_q - \epsilon_{k'} + \epsilon_{k_2} - \epsilon_{k_1}$. With this substitution, we get

$$V^\dagger G_0(E) X G_0(E) V = J^3 \sum_{\substack{q, k_1, k_2, k, k', \\ \alpha, \alpha', \alpha_1, \alpha_2, \beta \\ \gamma_1, \gamma_2}} \frac{c_{q\beta}^{(\gamma_1)\dagger} c_{k\alpha}^{(\gamma_1)} \vec{S}_d \cdot \vec{\sigma}_{\beta\alpha} c_{k_1\alpha_1}^{(\gamma_2)\dagger} c_{k_2\alpha_2}^{(\gamma_2)} \vec{S}_d \cdot \vec{\sigma}_{\alpha_1\alpha_2} c_{k'\alpha'}^{(\gamma_1)\dagger} c_{q\beta}^{(\gamma_1)} \vec{S}_d \cdot \vec{\sigma}_{\alpha\beta}}{(\epsilon_q - \epsilon_{k'} + \epsilon_{k_2} - \epsilon_{k_1})(\epsilon_q - \epsilon_{k'})} \quad (2.127)$$

The sum over q can be performed in the usual manner.

$$\begin{aligned} \sum_q \frac{c_{q\beta}^\dagger c_{q\beta}}{(\epsilon_q - \epsilon_{k'} + \epsilon_{k_2} - \epsilon_{k_1})(\epsilon_q - \epsilon_{k'})} &= \int_{-D}^{-D+|\delta D|} \frac{d\epsilon \rho(\epsilon) \hat{n}(\epsilon)}{(\epsilon - \epsilon_{k'} + \epsilon_{k_2} - \epsilon_{k_1})(\epsilon - \epsilon_{k'})} \\ &= \frac{\rho(0)|\delta D|}{(D + \epsilon_{k'} - \epsilon_{k_2} + \epsilon_{k_1})(D + \epsilon_{k'})} \end{aligned} \quad (2.128)$$

where we have taken $\rho(\epsilon) = \rho(0)$, $\hat{n}(\epsilon) = \theta(-\epsilon)$ and $\epsilon_q \simeq -D$.

For the next step, note that $\vec{S}_d \cdot \vec{\sigma}_{x,y} = \sum_a S_d^a \sigma_{x,y}^a$. Substituting this into $V^\dagger G_0(E) X G_0(E) V$ gives

$$\sum_{\gamma_1, \gamma_2} \sum_{k_1, k_2, k, k'} \sum_{\alpha, \alpha', \alpha_1, \alpha_2, \beta} \sum_{a, b, c} \frac{J^3 \rho(0) |\delta D|}{(D + \epsilon_{k'} - \epsilon_{k_2} + \epsilon_{k_1})(D + \epsilon_{k'})} S_d^a \sigma_{\beta\alpha}^a S_d^b \sigma_{\alpha_1\alpha_2}^b S_d^c \sigma_{\alpha'\beta}^c c_{k_1\alpha_1}^{(\gamma_1)\dagger} c_{k_2\alpha_2}^{(\gamma_2)\dagger} c_{k'\alpha'}^{(\gamma_1)\dagger} \quad (2.129)$$

Now, note that all not all combinations of the momenta will renormalize the $\vec{S}_d \cdot \vec{s}$ term of the Hamiltonian. In order for such a term to come out, the four remaining momenta must be contracted to two. The first set of terms that satisfy this requirement is given by the condition $k'\alpha' = k\alpha$. The renormalization from this subset of terms is

$$\begin{aligned} &\sum_{\gamma_1, \gamma_2} \sum_{k_1, k_2, k} \sum_{\alpha, \alpha_1, \alpha_2, \beta} \sum_{a, b, c} \frac{J^3 \rho(0) |\delta D|}{(D + \epsilon_k - \epsilon_{k_2} + \epsilon_{k_1})(D + \epsilon_k)} S_d^a \sigma_{\beta\alpha}^a S_d^b \sigma_{\alpha_1\alpha_2}^b S_d^c \sigma_{\alpha\beta}^c c_{k_1\alpha_1}^{(\gamma_2)\dagger} c_{k_2\alpha_2}^{(\gamma_2)\dagger} c_{k\alpha}^{(\gamma_1)\dagger} c_{k\alpha}^{(\gamma_1)\dagger} \\ &= \sum_{\gamma_2} \sum_{k_1, k_2} \sum_{\alpha, \alpha_1, \alpha_2, \beta} \sum_{a, b, c} J^3 \rho(0) |\delta D| S_d^a \sigma_{\beta\alpha}^a S_d^b \sigma_{\alpha_1\alpha_2}^b S_d^c \sigma_{\alpha\beta}^c c_{k_1\alpha_1}^{(\gamma_2)\dagger} c_{k_2\alpha_2}^{(\gamma_2)\dagger} \sum_{\gamma_1} \int_0^{D-|\delta D|} \frac{d\epsilon \rho(\epsilon)}{(D + \epsilon - \epsilon_{k_2} + \epsilon_{k_1})(D + \epsilon)} \\ &\simeq \sum_{\gamma_2} \sum_{k_1, k_2} \sum_{\alpha, \alpha_1, \alpha_2, \beta} \sum_{a, b, c} J^3 \rho(0) |\delta D| S_d^a \sigma_{\beta\alpha}^a S_d^b \sigma_{\alpha_1\alpha_2}^b S_d^c \sigma_{\alpha\beta}^c c_{k_1\alpha_1}^{(\gamma_2)\dagger} c_{k_2\alpha_2}^{(\gamma_2)\dagger} \sum_{\gamma_1} \int_0^{D-|\delta D|} \frac{d\epsilon \rho(\epsilon)}{(D + \epsilon)^2} \\ &= \frac{K \rho^2(0) J^3 |\delta D|}{2D} \sum_{\alpha, \beta} \sum_{a, c, b} \sum_{\alpha_1, \alpha_2} S_d^a S_d^b S_d^c \sigma_{\beta\alpha}^a \sigma_{\alpha_1\alpha_2}^b \sigma_{\alpha\beta}^c \sum_{k_1, k_2, \gamma_2} c_{k_1\alpha_1}^{(\gamma_2)\dagger} c_{k_2\alpha_2}^{(\gamma_2)\dagger}. \end{aligned} \quad (2.130)$$

$K = \sum_{\gamma_1}$ is the total number of channels. The other set of terms is given by the condition $k_1\alpha_1 = k_2\alpha_2$. The renormalization from these terms can be calculated similarly:

$$\begin{aligned} &\sum_{\gamma_1, \gamma_2} \sum_{k_1, k, k'} \sum_{\alpha, \alpha', \alpha_1, \beta} \sum_{a, b, c} \frac{J^3 \rho(0) |\delta D|}{(D + \epsilon_{k'})^2} S_d^a \sigma_{\beta\alpha}^a S_d^b \sigma_{\alpha_1\alpha_1}^b S_d^c \sigma_{\alpha'\beta}^c c_{k\alpha}^{(\gamma_1)\dagger} c_{k_1\alpha_1}^{(\gamma_2)\dagger} c_{k_1\alpha_1}^{(\gamma_1)\dagger} c_{k'\alpha'}^{(\gamma_1)\dagger} \\ &= \sum_{\gamma_1} \sum_{k, k'} \sum_{\alpha, \alpha', \beta} \sum_{a, b, c} \frac{J^3 \rho(0) |\delta D|}{(D + \epsilon_{k'})^2} S_d^a \sigma_{\beta\alpha}^a S_d^b \text{Trace}(\sigma^b) S_d^c \sigma_{\alpha'\beta}^c c_{k\alpha}^{(\gamma_1)\dagger} \sum_{\gamma_2} \left[\int_{-D+|\delta D|}^0 d\epsilon \rho(\epsilon) \right] c_{k'\alpha'}^{(\gamma_1)\dagger} \\ &= 0 \end{aligned} \quad (2.131)$$

The spin products can be simplified using the identity

$$\sum_{\alpha\beta} \sigma_{\beta\alpha}^a \sigma_{\alpha\beta}^c = \text{Trace} [\sigma^a \sigma^c] = 2\delta_{ac} . \quad (2.132)$$

Using this identity, we get

$$V^\dagger G_0(E) X G_0(E) V = \frac{K\rho^2(0)J^3|\delta D|}{D} \sum_{a,b} \sum_{\alpha_1,\alpha_2} S_d^a S_d^b S_d^a \sigma_{\alpha_1\alpha_2}^b \sum_{k_1,k_2,\gamma_2} c_{k_1\alpha_1}^{(\gamma_2)\dagger} c_{k_2\alpha_2}^{(\gamma_2)} \quad (2.133)$$

The products of the impurity spin operators can now be simplified:

$$\sum_a S_d^a S_d^b S_d^a = \sum_a \left[S_d^b S_d^a + i \sum_c \epsilon^{abc} S_d^c \right] S_d^a = \frac{3}{4} S_d^b + i \sum_{a,c} \epsilon^{abc} S_d^c S_d^a = \frac{3}{4} S_d^b + \frac{1}{2} i^2 \sum_{a,c,e} \epsilon^{abc} \epsilon^{aec} S_d^e = -\frac{1}{4} S_d^b \quad (2.134)$$

Substituting this result in the renormalization gives

$$\begin{aligned} V^\dagger G_0(E) X G_0(E) V &= -\frac{K\rho(0)^2 J^3 |\delta D|}{4D} \sum_{k_1,k_2,\alpha_1,\alpha_2,b,\gamma_2} S_d^b \sigma_{\alpha_1\alpha_2}^b c_{k_1\alpha_1}^{(\gamma_2)\dagger} c_{k_2\alpha_2}^{(\gamma_2)} \\ &= -\frac{K\rho(0)^2 J^3 |\delta D|}{4D} \sum_{k_1\alpha_1,k_2\alpha_2,\gamma_2} \vec{S}_d \cdot \vec{\sigma}_{\alpha_1\alpha_2} c_{k_1\alpha_1}^{(\gamma_2)\dagger} c_{k_2\alpha_2}^{(\gamma_2)} \end{aligned} \quad (2.135)$$

The other term (virtual particle term) gives an equal contribution. The total renormalization is

$$\delta J = \frac{2J^2\rho(0)|\delta D|}{D} \left(1 - \frac{K\rho(0)J}{4} \right) \quad (2.136)$$

2.5.3 PMS in the language of the URG - obtaining the η operators

To make a better connection with URG, we next show how the PMS formalism works out for a single-electron decoupling. The corresponding problem can be phrased in the following manner. We want to decouple one electron at momentum q from the full Hamiltonian. We can split the exact wavefunction as

$$|\Psi\rangle = |\Psi_0\rangle + |\Psi_1\rangle \quad (2.137)$$

where $|\Psi_0\rangle = (1 - \hat{n}_q) |\Psi^N\rangle$ is that part of the wavefunction where the state q is occupied. $|\Psi_1^N\rangle = \hat{n}_q |\Psi\rangle$ is that part of the wavefunction where the state q is occupied. We can also split the Hamiltonian as

$$\mathcal{H} = \mathcal{H}^d + V_0 + V_+ + V_- \quad (2.138)$$

\mathcal{H}^d is the diagonal part; it has the purely energy terms as well as self-energies that may arise from the diagonal parts of interactions; V_0 is the purely off-diagonal term that does not change \hat{n}_q ; it is the scattering *inside* the low energy subspace. V_+ and V_- are the purely off-diagonal terms that *do* change \hat{n}_q ; V_+ takes you from $\hat{n}_q = 0$ to $\hat{n}_q = 1$ and V_- does the opposite.

Substituting eqs. 2.138 and 2.137 in eq. 2.99 gives

$$(\mathcal{H}^d + V_0 + V_+ + V_-) (|\Psi_0\rangle + |\Psi_1\rangle) = E (|\Psi_0\rangle + |\Psi_1\rangle) \quad (2.139)$$

Gathering the kets with $\hat{n}_q = 0, 1$ gives

$$\begin{aligned} (\mathcal{H}_0^d + V_0) |\Psi_0\rangle + V_- |\Psi_1\rangle &= E |\Psi_0\rangle \\ (\mathcal{H}_1^d + V_0) |\Psi_1\rangle + V_+ |\Psi_0\rangle &= E |\Psi_1\rangle \end{aligned} \quad (2.140)$$

The second equation can be written as

$$|\Psi_1\rangle = \eta^\dagger |\Psi_0\rangle \quad (2.141)$$

where

$$(\eta^\dagger)_{\text{PMS}} = \frac{1}{E - \mathcal{H}_1^d - V_0} V_+ \quad (2.142)$$

Substituting this in the first equation gives

$$(\mathcal{H}_0^d + V_0 + V_- \eta^\dagger) |\Psi_0\rangle = E |\Psi_0\rangle \quad (2.143)$$

This new Hamiltonian,

$$\tilde{\mathcal{H}}_0 = \mathcal{H}_0^d + V_0 + V_- \eta^\dagger \quad (2.144)$$

has the high energy mode removed; the scattering terms start from the low energy subspace and end at the low energy subspace as well. The renormalization in the low energy subspace scatterings is

$$\Delta V_0 = V_- \eta^\dagger \quad (2.145)$$

If we eliminate $|\Psi_0\rangle$ instead of $|\Psi_1\rangle$, we get the renormalized equation in the high energy subspace:

$$|\Psi_0\rangle = \eta |\Psi_1\rangle \quad (2.146)$$

where

$$(\eta)_{\text{PMS}} = \frac{1}{E - \mathcal{H}_0^d - V_0} V_- \quad (2.147)$$

, so

$$(\mathcal{H}_1^d + V_0 + V_+ \eta) |\Psi_1\rangle = E |\Psi_1\rangle \quad (2.148)$$

The renormalized Hamiltonian in the high energy subspace is thus

$$\tilde{\mathcal{H}}_1 = \mathcal{H}_1^d + V_0 + V_+ \eta \quad (2.149)$$

If we want to keep both the high energy and low energy parts of the Hamiltonian, the new Hamiltonian is

$$\begin{aligned} \tilde{\mathcal{H}} &= \tilde{\mathcal{H}}_1 \hat{n} + \tilde{\mathcal{H}}_0 (1 - \hat{n}) \\ &= \mathcal{H}_0^d + \mathcal{H}_1^d + V_0 + V_+ \eta + V_- \eta^\dagger \end{aligned} \quad (2.150)$$

The total renormalization is

$$(\Delta \mathcal{H})_{\text{PMS}} = V_+ (\eta)_{\text{PMS}} + V_- (\eta^\dagger)_{\text{PMS}} \quad (2.151)$$

It can be shown that if we define a unitary operator $U = 1 - \eta + \eta^\dagger$, the transformed Hamiltonian $U \mathcal{H} U^\dagger$ is the same as eq. 2.150. This, along with the properties of η , have been shown in section ???. The important feature of eq. 2.150 is that there is no term in the transformed Hamiltonian which scatters between $|\Psi_0\rangle$ and $|\Psi_1\rangle$ - the two subspaces have been truly decoupled.

$$[U \mathcal{H} U^\dagger, n_q] = 0 \quad (2.152)$$

We can write down the renormalized Schrodinger equation in the low energy subspace, from eq. 2.143,

$$\tilde{\mathcal{H}}_0 |\Psi_0\rangle = E |\Psi_0\rangle \quad (2.153)$$

and again repeat the entire process. $\tilde{\mathcal{H}}_0$ now takes the place of \mathcal{H} and $|\Psi_0\rangle$ takes the place of $|\Psi\rangle$ in eq. 2.99.

The expression for URG is obtained in an almost identical way. The only difference is that instead of starting with the exact eigenpair $(E, |\Psi\rangle)$, we start with a more general pair $(\tilde{\mathcal{H}}, |\Phi\rangle)$ where $|\Phi\rangle$ is not necessarily an exact eigenstate of \mathcal{H} . It is defined by \mathcal{H}' , which is in turn defined as $\hat{n}_q \mathcal{H}' (1 - \hat{n}_q) = 0$. $|\Phi\rangle$ is then defined by

$$\mathcal{H} |\Phi\rangle = \mathcal{H}' |\Phi\rangle \quad (2.154)$$

This definition of \mathcal{H}' is the very minimum that we must have in order to fulfill our goal (decouple q).

The operators η and its conjugate change accordingly:

$$\begin{aligned} (\eta)_{\text{URG}} &= \frac{1}{\tilde{\mathcal{H}} - \mathcal{H}_0^d - V_0} V_- \\ &= \frac{1}{\hat{\omega} - \mathcal{H}_1^d} V_- \end{aligned} \quad (2.155)$$

where $\hat{\omega} \equiv \mathcal{H}' - V_0$ now embodies the quantum fluctuations inherent in the Hamiltonian through the scattering term V_0 . Similarly,

$$(\eta^\dagger)_{\text{URG}} = \frac{1}{\hat{\omega} - \mathcal{H}_1^d} V_+ \quad (2.156)$$

The renormalization is again

$$(\Delta\mathcal{H})_{\text{URG}} = V_+ (\eta)_{\text{URG}} + V_- (\eta^\dagger)_{\text{URG}} \quad (2.157)$$

This again allows us to write down a unitary operator that decouples the entangled state:

$$U = 1 - \eta + \eta^\dagger, [\hat{n}_q, U \mathcal{H} U^\dagger] = 0 \quad (2.158)$$

where $\tilde{\mathcal{H}} = U^\dagger \mathcal{H} U$. We can now write down a new problem in this decoupled space with the rotated items and attempt to decouple another electron q' . We will again choose some general eigenpair $(\mathcal{H}', |\Phi\rangle)$ such that $\tilde{\mathcal{H}} |\Phi\rangle = \mathcal{H}' |\Phi\rangle$ and $[\mathcal{H}', \hat{n}_{q'}] = 0$.

Summarizing, the general Hamiltonian is not diagonal in the Fock space basis. URG, in order to proceed, selects one non-Fock basis of states $|\Phi\rangle$ such that q is decoupled in that Hamiltonian. Since there can be lots of such basis, there is a freedom in this choice. With this basis in mind, URG then finds a unitary operator which when operated on the Hamiltonian takes us to the form in which it is diagonal in the Fock space basis. Note that this form is a function of the chosen $|\Phi\rangle$. We then select the second degree of freedom and repeat the process. What PMS does is, it exploits the freedom of choice and selects the exact eigenstate $|\Psi\rangle$ of the Hamiltonian as the non-Fock basis $|\Phi\rangle$. Doing that returns a rotated Hamiltonian which is diagonal in q , and is a function of the chosen state, same as URG. The conclusion is that depending on which state we choose as our diagonal non-Fock basis, URG and PMS will cause flows along different lines in general.

As the couplings flow, V_0 will also flow, leading to a flow of $\hat{\omega}$. Just at the fixed point, the denominator of URG vanishes, giving the equation

$$(\hat{\omega} - \mathcal{H}_1^d) V_+ |\Psi_0\rangle \text{ or } (\hat{\omega} - \mathcal{H}_1^d) V_- |\Psi_1\rangle \quad (2.159)$$

This means that one of the eigenvalues of $\hat{\omega}$ matches with the eigenvalue of the diagonal part \mathcal{H}^d , either in the occupied sector (\mathcal{H}_1^d) or unoccupied sector (\mathcal{H}_1^u). Since the eigenvalues are unchanged during the unitary renormalization, this implies that ω takes up one of the eigenvalues of the whole Hamiltonian \mathcal{H} . This will correspond to the fixed point obtained from PMS if we had started PMS with that eigenvalue.

In short, while the PMS flow is parametrised by one of the exact energy eigenvalues E , the URG flow is parametrised by a non-trivial operator $\hat{\omega}$ which incorporates both a diagonal part and an off-diagonal part and itself flows under the URG. At the fixed point, the off-diagonal part cancels out and the $\hat{\omega}$ finally flows to one of the energy eigenvalues and the URG fixed point matches with one of the PMS fixed points.

2.5.4 PMS for the single impurity Anderson model

To demonstrate the implementation, we can look at a specific model. For the SIAM,

$$\mathcal{H} = \sum_{k\sigma} \left(\epsilon_k \tau_{k\sigma} + V c_{k\sigma}^\dagger c_{d\sigma} + \text{h.c.} \right) \quad (2.160)$$

where $\tau = \hat{n} - \frac{1}{2}$. We want to decouple the state $q\beta$ from the rest of the electrons. We have $H_0 = \epsilon_d \hat{n}_d + U \hat{n}_{d\uparrow} \hat{n}_{d\downarrow} + \sum_{k\sigma} \epsilon_k \hat{n}_{k\sigma}$, $V_0 = \sum_{k < q, \sigma} c_{k\sigma}^\dagger c_{d\sigma} + \text{h.c.}$, $V_+ = V c_{q\beta}^\dagger c_{d\beta}$ and $V_- = V c_{d\beta}^\dagger c_{q\beta}$. The renormalization in particle sector

$$\Delta V_0 = c_{d\beta}^\dagger c_{q\beta} \frac{1}{(E - V_0) - \hat{\mathcal{H}}_0^d} c_{q\beta}^\dagger c_{d\beta} \quad (2.161)$$

The intermediate energy (at the propagator) is

$$\hat{\mathcal{H}}_0^d = \sum_{k,\sigma} \epsilon_k \tau_{k\sigma} + \epsilon_d \hat{n}_{d\bar{\beta}} \quad (2.162)$$

This is because the $c_{d\beta}$ at the right of the propagator ensures that we must have $\hat{n}_{d\beta} = 0$ at the propagator.

$$\Delta V_0 = c_{d\beta}^\dagger c_{q\beta} \frac{1}{(E - V_0) - \sum_{k,\sigma} \epsilon_k \tau_{k\sigma} - \epsilon_d \hat{n}_{d\bar{\beta}}} c_{q\beta}^\dagger c_{d\beta} \quad (2.163)$$

Since E is the exact eigenvalue, we do not have an expression for it. Instead, we approximate $E - V_0$ by substituting it with the current diagonal part corresponding to the initial state on which this entire term will act. The intial state is characterized by $\hat{n}_{q\beta} = 0$ and $\hat{n}_{d\beta} = 1$, so

$$E - V_0 = \sum_{k < q, \sigma} \epsilon_k \tau_{k\sigma} - \frac{1}{2} \epsilon_q + \epsilon_d + (\epsilon_d + U) \hat{n}_{d\bar{\beta}} \quad (2.164)$$

The $-\frac{1}{2} \epsilon_q$ comes from substituting $\hat{n}_{q\beta} = 0$ in $\epsilon_q \tau_{q\beta}$.

Substituting this in ΔV_0 gives

$$\begin{aligned} \Delta V_0 &= c_{d\beta}^\dagger c_{q\beta} \frac{1}{-\frac{1}{2} \epsilon_q - \epsilon_q \tau_{q\beta} + \epsilon_d + U \hat{n}_{d\bar{\beta}}} c_{q\beta}^\dagger c_{d\beta} = c_{d\beta}^\dagger c_{q\beta} \frac{1}{-\epsilon_q + \epsilon_d + U \hat{n}_{d\bar{\beta}}} c_{q\beta}^\dagger c_{d\beta} = c_{d\beta}^\dagger c_{q\beta} c_{q\beta}^\dagger c_{d\beta} \frac{1}{-\epsilon_q + \epsilon_d + U \hat{n}_{d\bar{\beta}}} \\ &= -c_{d\beta}^\dagger c_{q\beta} c_{q\beta}^\dagger c_{d\beta} \frac{1}{\epsilon_q - \epsilon_d - U \hat{n}_{d\bar{\beta}}} = (1 - \hat{n}_{q\beta}) \left(\frac{-\hat{n}_{d\beta} \hat{n}_{d\bar{\beta}}}{\epsilon_q - \epsilon_d - U} + \frac{-\hat{n}_{d\beta} (1 - \hat{n}_{d\bar{\beta}})}{\epsilon_q - \epsilon_d} \right) \end{aligned} \quad (2.165)$$

On the second line, we substituted $\tau_{q\beta} = \frac{1}{2}$ in the denominator, which is ensured by the $c_{q\beta}^\dagger$ to the right of the propagator. The first term renormalizes the energy of the doublon state and the second term renormalizes that of the singly-occupied state:

$$\Delta E_2 = \frac{-1}{\epsilon_q - \epsilon_d - U}, \quad \Delta E_1 = \frac{-1}{\epsilon_q - \epsilon_d} \quad (2.166)$$

The renormalization in the hole sector is

$$\Delta V_0 = c_{q\beta}^\dagger c_{d\beta} \frac{1}{(E - V_0) - \hat{\mathcal{H}}_0^d} c_{d\beta}^\dagger c_{q\beta} = c_{q\beta}^\dagger c_{d\beta} \frac{1}{(E - V_0) - \sum_{k,\sigma} \epsilon_k \tau_{k\sigma} - \epsilon_d - (\epsilon_d + U) \hat{n}_{d\bar{\beta}}} c_{d\beta}^\dagger c_{q\beta} \quad (2.167)$$

This time we substitute

$$E - V_0 = \sum_{k < q, \sigma} \epsilon_k \tau_{k\sigma} + \tau_{q\beta} \epsilon_q^- + \epsilon_d \hat{n}_{d\bar{\beta}} = \sum_{k < q, \sigma} \epsilon_k \tau_{k\sigma} + \frac{1}{2} \epsilon_q^- + \epsilon_d \hat{n}_{d\bar{\beta}} \quad (2.168)$$

In the last step we put $\tau_{q\beta} = \frac{1}{2}$ because the state is occupied in the initial configuration. Note that since the electron $q\beta$ was occupied in the initial state, the energy ϵ_q^- in this sector must be opposite to that of the particle sector, ϵ_q . Hence $\epsilon_q^- = -\epsilon_q$, which gives

$$\begin{aligned} \Delta V_0 = c_{q\beta}^\dagger c_{d\beta} \frac{1}{-\frac{1}{2} \epsilon_q - \epsilon_q^- \tau_{q\beta} - \epsilon_d - U \hat{n}_{d\bar{\beta}}} c_{d\beta}^\dagger c_{q\beta} &= c_{q\beta}^\dagger c_{d\beta} c_{d\beta}^\dagger c_{q\beta} \frac{1}{-\epsilon_q - \epsilon_d - U \hat{n}_{d\bar{\beta}}} = \hat{n}_{q\beta} \left(\frac{-(1 - \hat{n}_{d\beta}) \hat{n}_{d\bar{\beta}}}{\epsilon_q + \epsilon_d + U} \right. \\ &\quad \left. - \frac{(1 - \hat{n}_{d\beta})(1 - \hat{n}_{d\bar{\beta}})}{\epsilon_q + \epsilon_d} \right) \end{aligned} \quad (2.169)$$

In the second line, we put $\epsilon_q^- = -\epsilon_q$ and $\tau_{q\beta} = -\frac{1}{2}$. The first term renormalizes the singly-occupied state while the second term renormalizes the holon state. Combining with the particle sector results, the total renormalization in all the three impurity states (holon, single and doublon) are

$$\begin{aligned} \Delta E_0 &= -\frac{1}{\epsilon_q + \epsilon_d} \\ \Delta E_1 &= -\frac{1}{\epsilon_q + \epsilon_d + U} - \frac{1}{\epsilon_q - \epsilon_d} \\ \Delta E_2 &= -\frac{1}{\epsilon_q - \epsilon_d - U} \end{aligned} \quad (2.170)$$

These results are also obtained in ref. [8]. The complete process is depicted in fig. 2.7.

Some conclusions:

- The *only* difference in the formalism of PMS and URG is that while PMS uses the exact energy eigenvalue E to parameterise the flow, URG uses a general intermediate decoupled Hamiltonian to do the same. Since the E is also, technically, an intermediate decoupled Hamiltonian (it is the final Hamiltonian), PMS can be seen as an URG but with a specific choice for the parameter.
- In practise, PMS replaces $E - V_0$ with the diagonal part of the initial state at the current step of the RG. We are talking about the energy of the initial state, not the intermediate state. This is because, from eq. 2.99, E is the energy of the initial state on which V_\pm act.

- The ideal solution would have been to substitute the exact energy and the total scattering term V , but since we do not know E and keeping the V would make the thing untractable, we use our current best guess (renormalised diagonal part). As the RG flows, both E_j and V flow, such that at the fixed point, V becomes zero (scattering terms get removed) and E_j morphs into the exact E .
- In practise, URG replaces the $\hat{\omega}$ with a guess for the final energy E . This however ignores the renormalization of $\hat{\omega}$. A better approach would be to replace it with E_j , following PMS. That would act like the one-particle renormalization of $\hat{\omega}$.
- PMS usually drops any diagonal component of the scattering from the denominator. For example, in the PMS of the Kondo model by Anderson [6] or that of the anisotropic power law Kondo model by Chenge et.al [9], they do not keep the term $J_z S_d^z s^z$ in the denominator although it is number(spin) conserving. Such terms are kept in the denominator of the URG though. It must be mentioned however that ref. [10] *does* bring a diagonal charge-charge interaction in the denominator in the PMS of the extended Anderson model.

2.6 Schrieffer-Wolff transformation (SWT)

2.6.1 Formalism

We have a general Hamiltonian

$$\mathcal{H} = \mathcal{H}_0 + \mathcal{H}_X \quad (2.171)$$

\mathcal{H}_0 is diagonal w.r.t a particular degree of freedom. V is off-diagonal w.r.t that same degree of freedom. Let S be an *anti-Hermitian* and *off-diagonal* operator. $U = e^S$ is then a unitary transformation.

$$\begin{aligned} U\mathcal{H}U^\dagger &= e^S (\mathcal{H}_0 + \mathcal{H}_X) e^{-S} \\ &= (\cosh(S) + \sinh(S)) (\mathcal{H}_0 + \mathcal{H}_X) (\cosh(S) - \sinh(S)) \\ &= H_1 + H_2 \end{aligned} \quad (2.172)$$

where H_1 is diagonal and H_2 is off-diagonal.

$$\begin{aligned} H_1 &= \cosh(S) \mathcal{H}_0 \cosh(S) - \sinh(S) \mathcal{H}_0 \sinh(S) - \cosh(S) \mathcal{H}_X \sinh(S) \\ &\quad + \sinh(S) \mathcal{H}_X \cosh(S) \\ H_2 &= -\cosh(S) \mathcal{H}_0 \sinh(S) + \sinh(S) \mathcal{H}_0 \cosh(S) + \cosh(S) \mathcal{H}_X \cosh(S) \\ &\quad - \sinh(S) \mathcal{H}_X \sinh(S) \end{aligned} \quad (2.173)$$

The decoupling condition is $H_2 = 0$.

For small S , we have $\sinh S \sim S$ and $\cosh S \sim 1 + \frac{1}{2}S^2$. Therefore, the off-diagonal part, up to second order, is

$$H_2 = -\mathcal{H}_0 S + S \mathcal{H}_0 + \mathcal{H}_X + O(S^3) = [S, \mathcal{H}_0] + \mathcal{H}_X \quad (2.174)$$

The second order decoupling condition is thus

$$[S, \mathcal{H}_0] = -\mathcal{H}_X \quad (2.175)$$

The effective Hamiltonian is what remains, H_1 . That becomes, at second order,

$$\begin{aligned}
H_1 &= \left(1 + \frac{1}{2}S^2\right) \mathcal{H}_0 \left(1 + \frac{1}{2}S^2\right) - S\mathcal{H}_0 S - \left(1 + \frac{1}{2}S^2\right) \mathcal{H}_X S + S\mathcal{H}_X \left(1 + \frac{1}{2}S^2\right) \\
&= \mathcal{H}_0 + \frac{1}{2}\{S^2, \mathcal{H}_0\} - S\mathcal{H}_0 S - \mathcal{H}_X S + S\mathcal{H}_X + O(S^3) \\
&= \mathcal{H}_0 + \frac{1}{2}S [S, \mathcal{H}_0] - \frac{1}{2}[S, \mathcal{H}_0] S + [S, \mathcal{H}_X] + O(S^3) \\
&= \mathcal{H}_0 + \frac{1}{2}[S, [S, \mathcal{H}_0]] + [S, \mathcal{H}_X] + O(S^3) \\
&= \mathcal{H}_0 + \frac{1}{2}[S, -\mathcal{H}_X] + [S, \mathcal{H}_X] + O(S^3) \\
&= \mathcal{H}_0 + \frac{1}{2}[S, \mathcal{H}_X] + O(S^3)
\end{aligned} \tag{2.176}$$

Avoiding the perturbative route, we can take $S = \frac{\pi}{4}(\eta^\dagger - \eta)$, where η and its conjugate are non-perturbative and Fermionic - they satisfy $\eta^2 = \eta^{\dagger 2} = 0$ and $\{\eta, \eta^\dagger\} = 1$. We can then write

$$\begin{aligned}
e^S &= \exp \left\{ \frac{\pi}{4} (\eta^\dagger - \eta) \right\} \\
&= 1 + (\eta^\dagger - \eta) \frac{\pi}{4} + \frac{1}{2!} (\eta^\dagger - \eta)^2 \left(\frac{\pi}{4}\right)^2 + \frac{1}{3!} (\eta^\dagger - \eta)^3 \left(\frac{\pi}{4}\right)^3 + \dots \\
&= 1 + (\eta^\dagger - \eta) \frac{\pi}{4} - \frac{1}{2!} \left(\frac{\pi}{4}\right)^2 - \frac{1}{3!} (\eta^\dagger - \eta) \left(\frac{\pi}{4}\right)^3 + \frac{1}{4!} \left(\frac{\pi}{4}\right)^4 + \dots \\
&= \cos \frac{\pi}{4} + (\eta^\dagger - \eta) \sin \frac{\pi}{4} \\
&= \frac{1}{\sqrt{2}} (1 + \eta^\dagger - \eta)
\end{aligned} \tag{2.177}$$

There we used

$$(\eta^\dagger - \eta)^2 = \eta^{\dagger 2} + \eta^2 - \{\eta^\dagger, \eta\} = -1 \quad \left[\because \eta^2 = \eta^{\dagger 2} = 0 \right] \tag{2.178}$$

and hence

$$(\eta^\dagger - \eta)^3 = -1 (\eta^\dagger - \eta) \tag{2.179}$$

and so on. This simplification allows us to write

$$\cosh S = \frac{1}{2} [e^S + e^{-S}] = \frac{1}{2\sqrt{2}} (1 + \eta^\dagger - \eta + 1 - \eta^\dagger + \eta) = \frac{1}{\sqrt{2}} \tag{2.180}$$

and

$$\sinh S = \frac{1}{2} [e^S - e^{-S}] = \frac{1}{2\sqrt{2}} (1 + \eta^\dagger - \eta - 1 + \eta^\dagger - \eta) = \frac{1}{\sqrt{2}} (\eta^\dagger - \eta) \tag{2.181}$$

The off-diagonal part now becomes

$$H_2 = \frac{1}{2} (\mathcal{H}_X - \eta^\dagger \mathcal{H}_X \eta^\dagger - \eta \mathcal{H}_X \eta + [\eta^\dagger - \eta, \mathcal{H}_0]) \tag{2.182}$$

The vanishing of this quantity is now the decoupling condition, and is also given in eq 16 of ref. [1].

	renormalization	decoupling condition
SWT	$\frac{1}{2} [S, \mathcal{H}_X]$	$[S, \mathcal{H}_0] = -\mathcal{H}_X$
URG	$\frac{2}{\pi} [S, \mathcal{H}_X]$	$[S, \mathcal{H}_0] = -\frac{\pi}{4} \mathcal{H}_X + \frac{4}{\pi} S \mathcal{H}_X S$

Table 2.1: Comparison of perturbative and non-perturbative canonical transformations

To look for a decoupling condition similar to eq. 2.175, we can re-express the cosh and sinh in eq. 2.180 in terms of S , by substituting $\eta^\dagger - \eta = \frac{4}{\pi} S$:

$$\cosh S = \frac{1}{\sqrt{2}}, \text{ and } \sinh S = \frac{4}{\sqrt{2}\pi} S \quad (2.183)$$

That gives

$$H_2 = \frac{1}{2} \left(\frac{4}{\pi} [S, \mathcal{H}_0] + \mathcal{H}_X - \frac{16}{\pi^2} S \mathcal{H}_X S \right) \quad (2.184)$$

The decoupling condition becomes

$$[S, \mathcal{H}_0] = -\frac{\pi}{4} \mathcal{H}_X + \frac{4}{\pi} S \mathcal{H}_X S \quad (2.185)$$

This can be compared to the second order condition: $[S, \mathcal{H}_0] = -\mathcal{H}_X$. We can also write the effective Hamiltonian for this non-perturbative case.

$$U \mathcal{H} U^\dagger = H_1 = \frac{1}{2} \mathcal{H}_0 - \frac{4}{\pi^2} S \mathcal{H}_0 S + \frac{2}{\pi} [S, \mathcal{H}_X] \quad (2.186)$$

The differences between the perturbative and non-perturbative ways are summarized in table 2.1. There appear to be two differences between these decoupling conditions: (a) a pre-factor of $\frac{\pi}{4}$ for the first term on the right hand side, and (b) the altogether new second term on the right hand side. Both are outcomes of the non-perturbative nature of URG. This offers evidence that the physics captured by the effective Hamiltonian (and its associated low-energy many-particle Hilbert space) obtained from URG lies well beyond that obtained from SWT. Further, it shows that the SWT can only be justified as an expansion in a small parameter (say, $\frac{1}{U}$) in the Anderson impurity problem), followed by a truncation of the BCH expansion and a projection onto a particular low-energy subspace. The truncation and projection are adopted simultaneously, and appear to impose the limit of $U = \infty$ by hand. The URG flow never attains such a limit, thus suggesting that there exists a lot of interesting physics that could potentially be lost in the SWT procedure. Further, the projection finally applied within SWT means that we can never recover what is thrown away. This is again not the case with URG.

2.6.2 Obtaining renormalization via Schrieffer-Wolff transformation - comparison with "poor man's scaling" and URG

Similar to the situation in Poor Man's scaling, one can visualize two set of states and let $\mathcal{H}_X = V_+ + V_-$ be the scattering that connects them and hence the one we want to kill. Let S be of the form

$$S = \sum_{ij} [s |\phi_1^i\rangle \langle \phi_0^j| - s^\dagger |\phi_0^j\rangle \langle \phi_1^i|] \quad (2.187)$$

This form is of course chosen to make S anti-Hermitian and off-diagonal. The part s can be determined from the decoupling condition:

$$-\mathcal{H}_X = [S, H_0] = SH_0 - H_0S \quad (2.188)$$

Multiplying with $\langle \phi_0^a |$ and $|\phi_1^b \rangle$ from the left and right respectively gives

$$-\langle \phi_0^a | V + V^\dagger |\phi_1^b \rangle = \langle \phi_0^a | SH_0 - H_0S |\phi_1^b \rangle \quad (2.189)$$

Since V^\dagger acts on $|0\rangle$, it will not affect the LHS. Also, $\langle \phi_0^a | V |\phi_1^b \rangle = V_{ab}$. If we now consider only the diagonal part of H_0 , we can write $H_0(|\phi_0^a\rangle, |\phi_1^b\rangle) = (E_{0,a} |\phi_0^a\rangle, E_{1,b} |\phi_1^b\rangle)$. We then get

$$\begin{aligned} -V_{ab} &= \langle \phi_0^a | \sum_i [S |\phi_1^i\rangle \langle \phi_1^i| H_0 - H_0 |\phi_0^i\rangle \langle \phi_0^i| S] |\phi_1^b \rangle = \sum_i [S_{ai} E_1^i \delta_{bi} - E_0^i \delta_{ai} S_{ib}] = S_{ab} E_1^b - E_0^a S_{ab} \\ \implies S_{ab} &= \frac{V_{ab}}{E_0^a - E_1^b} \end{aligned} \quad (2.190)$$

where we defined $\langle \phi_0^x | S |\phi_1^y \rangle = S_{xy}$. The total generator is

$$S = \sum_{ij} \left[S_{ij} |\phi_0^i\rangle \langle \phi_1^j| - S_{ij}^\dagger |\phi_1^j\rangle \langle \phi_0^i| \right] = \sum_{ij} \frac{1}{E_0^i - E_1^j} \left[V_{ij} |\phi_0^i\rangle \langle \phi_1^j| - V_{ij}^\dagger |\phi_1^j\rangle \langle \phi_0^i| \right] \quad (2.191)$$

The renormalization is thus

$$\begin{aligned} \Delta\mathcal{H} &= \frac{1}{2} [S, \mathcal{H}_X] \\ &= \frac{1}{2} \sum_{ij,kl} \left[\frac{1}{E_0^i - E_1^j} \left(V_{ij} |\phi_0^i\rangle \langle \phi_1^j| - V_{ij}^\dagger |\phi_1^j\rangle \langle \phi_0^i| \right), V_{kl} |\phi_0^k\rangle \langle \phi_1^l| + V_{kl}^\dagger |\phi_1^l\rangle \langle \phi_0^k| \right] \\ &= \frac{1}{2} \sum_{ij,kl} \left[\frac{1}{E_0^i - E_1^j} \left(V_{ij} V_{kl}^\dagger |\phi_0^i\rangle \langle \phi_0^k| \delta_{jl} - V_{ij}^\dagger V_{kl} |\phi_1^j\rangle \langle \phi_1^l| \delta_{ik} \right. \right. \\ &\quad \left. \left. - V_{kl}^\dagger V_{ij} |\phi_1^l\rangle \langle \phi_1^j| \delta_{ki} + V_{kl} V_{ij}^\dagger |\phi_0^k\rangle \langle \phi_0^i| \delta_{lj} \right) \right] \\ &= \frac{1}{2} \sum_{ijk} \left[\left(\frac{1}{E_0^i - E_1^j} + \frac{1}{E_0^k - E_1^l} \right) V_{ij} V_{kj}^\dagger |\phi_0^i\rangle \langle \phi_0^k| - \left(\frac{1}{E_0^i - E_1^j} + \frac{1}{E_0^k - E_1^l} \right) V_{ij}^\dagger V_{ik} |\phi_1^j\rangle \langle \phi_1^k| \right] \end{aligned} \quad (2.192)$$

This is the same as the PMS result eq. 2.115. It is easy to see that since this transformation is unitary, it has zero trace so as to preserve the trace of the Hamiltonian:

$$\text{Tr} [\mathcal{H}] = \sum_l (\langle \phi_0^l | + \langle \phi_1^l |) \Delta\mathcal{H} (|\phi_0^l\rangle + |\phi_1^l\rangle) = \frac{1}{2} \sum_{jl} \frac{2}{E_0^l - E_1^j} V_{lj} V_{lj}^\dagger - \frac{1}{2} \sum_{ji} \frac{2}{E_0^i - E_1^l} V_{il}^\dagger V_{il} = 0 \quad (2.193)$$

We can also make a comparison to the renormalization obtained from URG.

$$\Delta\mathcal{H} = \frac{1}{2} [\eta^\dagger - \eta, \mathcal{H}] \quad (2.194)$$

where

$$\begin{aligned}
\eta &= \frac{1}{\omega - \mathcal{H}^d} \sum_{ij} V_{ij} |\phi_0^i\rangle \langle \phi_1^j| = \sum_{ij} \frac{1}{\omega_1^j - E_0^i} V_{ij} |\phi_0^i\rangle \langle \phi_1^j| \\
\implies \eta^\dagger &= \sum_{ij} \frac{1}{\omega_1^j - E_0^i} V_{ij}^\dagger |\phi_1^j\rangle \langle \phi_0^i| \\
\implies \eta^\dagger - \eta &= \sum_{ij} \frac{1}{\omega_1^j - E_0^i} \left(V_{ij}^\dagger |\phi_1^j\rangle \langle \phi_0^i| - V_{ij} |\phi_0^i\rangle \langle \phi_1^j| \right)
\end{aligned} \tag{2.195}$$

This can be thought of as the generator for the unitary transformations of URG. Comparing with the generator S of eq. 2.191, the prescription to go from URG to SWT is to replace $\omega_1^j \rightarrow E_1^j$. Doing a similar calculation gives

$$\Delta \mathcal{H}_{URG} = \frac{1}{2} \sum_{ijk} \left[\left(\frac{1}{E_0^i - \omega_1^j} + \frac{1}{E_0^k - \omega_1^j} \right) V_{ij} V_{kj}^\dagger |\phi_0^i\rangle \langle \phi_0^k| - \left(\frac{1}{E_0^i - \omega_1^j} + \frac{1}{E_0^i - \omega_1^k} \right) V_{ij}^\dagger V_{ik} |\phi_1^j\rangle \langle \phi_1^k| \right] \tag{2.196}$$

2.7 A comparison of URG, SWT and PMS on the Anderson model

The SWT for the single-impurity Anderson model is briefly sketched below. In order to decouple a state $q\beta$ from the SIAM ($\epsilon_q > 0$), we take an ansatz $S = (A + B\hat{n}_{d\bar{\beta}})(c_{q\beta}^\dagger c_{d\beta} - \text{h.c.})$. Plugging this into the decoupling condition gives

$$-\epsilon_q (A + B\hat{n}_{d\bar{\beta}}) + \epsilon_d (A + B\hat{n}_{d\bar{\beta}}) + U (A + B) \hat{n}_{d\bar{\beta}} = -V \tag{2.197}$$

which gives

$$S = V \left[\frac{1 - \hat{n}_{d\bar{\beta}}}{\epsilon_q - \epsilon_d} + \frac{\hat{n}_{d\bar{\beta}}}{\epsilon_q - \epsilon_d - U} \right] (c_{q\beta}^\dagger c_{d\beta} - \text{h.c.}) \tag{2.198}$$

The remaining diagonal part constitutes the effective Hamiltonian.

$$\begin{aligned}
U\mathcal{H}U^\dagger &= H_1 = \mathcal{H}_0 + \frac{1}{2} \{ \mathcal{H}_0, S^2 \} - S\mathcal{H}_0 S + [S, \mathcal{H}_X] \\
&= \mathcal{H}_0 + \frac{1}{2} [[\mathcal{H}_0, S], S] + [S, \mathcal{H}_X] \\
&= \mathcal{H}_0 + \frac{1}{2} [\mathcal{H}_X, S] + [S, \mathcal{H}_X] \\
&= \mathcal{H}_0 + \frac{1}{2} [S, \mathcal{H}_X]
\end{aligned} \tag{2.199}$$

For the SIAM (and noting that we are decoupling $q\beta$), the two parts are

$$\begin{aligned}
\mathcal{H}_0 &= \sum_{k\sigma} \epsilon_k \hat{n}_{k\sigma} + \epsilon_d \hat{n}_d + U \hat{n}_{d\uparrow} \hat{n}_{d\downarrow} + \sum_{k\sigma \neq q\beta} (c_{k\sigma}^\dagger c_{d\sigma} + \text{h.c.}) \\
\mathcal{H}_X &= c_{q\beta}^\dagger c_{d\beta} + \text{h.c.}
\end{aligned} \tag{2.200}$$

The renormalization in the effective Hamiltonian from decoupling a high energy particle state is thus

$$\begin{aligned} \frac{1}{2} [S, \mathcal{H}_X] \Big|_{\hat{n}_{q\beta}=0} &= |V|^2 \left[\frac{1 - \hat{n}_{d\bar{\beta}}}{\epsilon_q - \epsilon_d} + \frac{\hat{n}_{d\bar{\beta}}}{\epsilon_q - \epsilon_d - U} \right] [\hat{n}_{q\beta} (1 - \hat{n}_{d\beta}) - \hat{n}_{d\beta} (1 - \hat{n}_{q\beta})] \Big|_{\hat{n}_{q\beta}=0} \\ &= -\hat{n}_{d\beta} |V|^2 \left[\frac{1 - \hat{n}_{d\bar{\beta}}}{\epsilon_q - \epsilon_d} + \frac{\hat{n}_{d\bar{\beta}}}{\epsilon_q - \epsilon_d - U} \right] \end{aligned} \quad (2.201)$$

In the last step, we put $\hat{n}_{q\beta} = 0$ because previously we assumed $\epsilon_q > 0$ and high energy virtual excitations above the Fermi surface must necessarily be vacant in the initial state (at $T = 0$). We can obtain the renormalization from decoupling a high energy *hole* state directly from this expression, just by choosing $\hat{n}_{q\beta} = 1$ and setting $\epsilon_q \rightarrow -\epsilon_q$.

$$\frac{1}{2} [S, \mathcal{H}_X] \Big|_{\hat{n}_{q\beta}=1} = -(1 - \hat{n}_{d\beta}) |V|^2 \left[\frac{1 - \hat{n}_{d\bar{\beta}}}{\epsilon_q + \epsilon_d} + \frac{\hat{n}_{d\bar{\beta}}}{\epsilon_q + \epsilon_d + U} \right] \quad (2.202)$$

These two results - the renormalization in the particle and hole sectors - is identical to the result obtained from PMS of the SIAM [7, 11]. The renormalizations in the various energy levels of the impurity can be read off now, after summing over all states in the interval we are decoupling.

$$\begin{aligned} \Delta E_2 &= -2 \sum_q \frac{|V_q|^2}{\epsilon_q - \epsilon_d - U} \\ \Delta E_1 &= - \sum_q \frac{|V_q|^2}{\epsilon_q - \epsilon_d} - \sum_q \frac{|V_q|^2}{\epsilon_q + \epsilon_d + U} \\ \Delta E_0 &= -2 \sum_q \frac{|V_q|^2}{\epsilon_q + \epsilon_d} \end{aligned} \quad (2.203)$$

This can be compared with the URG result, eq. ??,

$$\begin{aligned} \Delta E_2 &= 2 \sum_q \frac{|V_q|^2}{\omega - \frac{1}{2}\epsilon_q + \epsilon_d + U} \\ \Delta E_1 &= \sum_q \frac{|V_q|^2}{\omega - \frac{1}{2}\epsilon_q - \epsilon_d - U} + \sum_q \frac{|V_q|^2}{\omega - \frac{1}{2}\epsilon_q + \epsilon_d} \\ \Delta E_0 &= 2 \sum_q \frac{|V_q|^2}{\omega - \frac{1}{2}\epsilon_q - \epsilon_d} \end{aligned} \quad (2.204)$$

We can transform the URG result to the SWT result if we ignore the effect of the quantum fluctuations in ω (arising from the presence of the off-diagonal term \mathcal{H}^i) and replace it with the renormalised diagonal value of $-\frac{1}{2}\epsilon_q$. This means that SWT tracks the effect of the off-diagonal terms only in the numerator. Of course, all this assumes we are doing an iterative SWT instead of a one-shot SWT; the latter is the conventional way. A second difference is that URG has a Green's function like structure in the renormalization such that a fixed point is reached when the diagonal part \mathcal{H}^d matches one of the eigenvalues of ω (see 2.2.6). SWT does not have such a fixed point structure.

Another point to note is that decoupling a single electron does not generate all the charge-charge or spin-spin interactions that come out when one performs a one-shot SWT. This implies that such

terms are a result of decoupling the non-local interactions of the impurity (it is talking to all the mobile electrons), and cannot be generated when we remove just the local interactions of the mobile electrons. Instead, if one performs a URG in which we non-perturbatively kill the 2-point vertices in the SIAM, such 4-point vertices are generated. This is shown in the next subsection.

2.8 Deriving the Kondo model from the Anderson model via a one-shot URG

Here we will show how we can obtain the spin-spin interaction of the Kondo model by performing a one-shot URG on the SIAM. This should justify that the action of performing an SWT is analogous to decoupling the whole band via URG. There are three departures from the conventional way of doing URG (or PMS).

- We will be severing the connections of the impurity with all the mobile electrons in one-shot, and not iteratively.
- We will have to trivialize the quantum fluctuation operator $\hat{\omega}$ by replacing it with the diagonal part of the initial state energy.

Since we are decoupling the whole band, the off-diagonal part that we want to remove is

$$\mathcal{H}^I = \sum_{k\sigma} \left[V_k c_{k\sigma}^\dagger c_{d\sigma} + \text{h.c.} \right] \quad (2.205)$$

The diagonal part is the rest of the Hamiltonian.

$$\mathcal{H}^d = \sum_{k\sigma} \epsilon_k \hat{n}_{k\sigma} + \epsilon_d \hat{n}_d + U \hat{n}_{d\uparrow} \hat{n}_{d\downarrow} = \sum_{k\sigma} \epsilon_k \tau_{k\sigma} + \epsilon_d \hat{n}_d + U \hat{n}_{d\uparrow} \hat{n}_{d\downarrow} \quad (2.206)$$

Following eq. 2.47, the renormalization is

$$\Delta\mathcal{H} = \frac{1}{2} [\eta^\dagger - \eta, \mathcal{H}_X] \quad (2.207)$$

The transition operator η is

$$\begin{aligned} \eta &= \frac{1}{\omega - \mathcal{H}^d} \sum_{k\sigma} V_k^* c_{d\sigma}^\dagger c_{k\sigma} = \sum_{k\sigma} \frac{1}{\omega + \frac{1}{2}\epsilon_k - \epsilon_d - (\epsilon_d + U) \hat{n}_{d\bar{\sigma}}} V_k^* c_{d\sigma}^\dagger c_{k\sigma} \\ &= \sum_{k\sigma} \left[\frac{\hat{n}_{d\bar{\sigma}}}{\omega_1 + \frac{1}{2}\epsilon_k - 2\epsilon_d - U} + \frac{1 - \hat{n}_{d\bar{\sigma}}}{\omega_0 + \frac{1}{2}\epsilon_k - \epsilon_d} \right] V_k^* c_{d\sigma}^\dagger c_{k\sigma} = \sum_{k\sigma} \left[\frac{\hat{n}_{d\bar{\sigma}}}{E_k^1} + \frac{1 - \hat{n}_{d\bar{\sigma}}}{E_k^0} \right] V_k^* c_{d\sigma}^\dagger c_{k\sigma} \end{aligned} \quad (2.208)$$

where $E_k^1 = \omega_1 + \frac{1}{2}\epsilon_k - 2\epsilon_d - U$ and $E_k^0 = \omega_0 + \frac{1}{2}\epsilon_k - \epsilon_d$. The total generator is therefore

$$\eta^\dagger - \eta = \sum_{k\sigma} \left[\frac{\hat{n}_{d\bar{\sigma}}}{E_k^1} + \frac{1 - \hat{n}_{d\bar{\sigma}}}{E_k^0} \right] (V_k c_{k\sigma}^\dagger c_{d\sigma} - V_k^* c_{d\sigma}^\dagger c_{k\sigma}) \quad (2.209)$$

The renormalization is

$$\Delta\mathcal{H}(\omega_1, \omega_0) = \frac{1}{2} \sum_{kq\sigma\alpha} \left[\left(\frac{\hat{n}_{d\bar{\sigma}}}{E_k^1} + \frac{1 - \hat{n}_{d\bar{\sigma}}}{E_k^0} \right) \left(V_k c_{k\sigma}^\dagger c_{d\sigma} - V_k^* c_{d\sigma}^\dagger c_{k\sigma} \right), V_q c_{q\alpha}^\dagger c_{d\alpha} + V_q^* c_{d\alpha}^\dagger c_{q\alpha} \right] \quad (2.210)$$

The summation has two parts, $\Delta_{1,2}$ - one where $\sigma = \alpha$ and another where $\sigma = \bar{\alpha}$. The first part Δ_1 gives

$$\begin{aligned} \Delta_1 &= \frac{1}{2} \sum_{kq\sigma=\alpha} \left[\left(\frac{\hat{n}_{d\bar{\sigma}}}{E_k^1} + \frac{1 - \hat{n}_{d\bar{\sigma}}}{E_k^0} \right) \left(V_k c_{k\sigma}^\dagger c_{d\sigma} - V_k^* c_{d\sigma}^\dagger c_{k\sigma} \right), V_q c_{q\sigma}^\dagger c_{d\sigma} + V_q^* c_{d\sigma}^\dagger c_{q\sigma} \right] \\ &= \frac{1}{2} \sum_{kq\sigma} \left(\frac{\hat{n}_{d\bar{\sigma}}}{E_k^1} + \frac{1 - \hat{n}_{d\bar{\sigma}}}{E_k^0} \right) \left[V_k c_{k\sigma}^\dagger c_{d\sigma} - V_k^* c_{d\sigma}^\dagger c_{k\sigma}, V_q c_{q\sigma}^\dagger c_{d\sigma} + V_q^* c_{d\sigma}^\dagger c_{q\sigma} \right] \\ &= \frac{1}{2} \sum_{kq\sigma} \left(\frac{\hat{n}_{d\bar{\sigma}}}{E_k^1} + \frac{1 - \hat{n}_{d\bar{\sigma}}}{E_k^0} \right) \left\{ V_k V_q^* \left[c_{k\sigma}^\dagger c_{d\sigma}, V_q^* c_{d\sigma}^\dagger c_{q\sigma} \right] - V_k^* V_q \left[c_{d\sigma}^\dagger c_{k\sigma}, c_{q\sigma}^\dagger c_{d\sigma} \right] \right\} \\ &= \frac{1}{2} \sum_{kq\sigma} \left(\frac{\hat{n}_{d\bar{\sigma}}}{E_k^1} + \frac{1 - \hat{n}_{d\bar{\sigma}}}{E_k^0} \right) \left\{ V_k V_q^* \left[c_{k\sigma}^\dagger c_{d\sigma}, V_q^* c_{d\sigma}^\dagger c_{q\sigma} \right] + V_k^* V_q \left[c_{q\sigma}^\dagger c_{d\sigma}, c_{d\sigma}^\dagger c_{k\sigma} \right] \right\} \\ &= \frac{1}{2} \sum_{kq\sigma} \left[\hat{n}_{d\bar{\sigma}} \left(\frac{1}{E_k^1} + \frac{1}{E_q^1} \right) + (1 - \hat{n}_{d\bar{\sigma}}) \left(\frac{1}{E_k^0} + \frac{1}{E_q^0} \right) \right] V_k V_q^* \left[c_{k\sigma}^\dagger c_{d\sigma}, c_{d\sigma}^\dagger c_{q\sigma} \right] \\ &= \sum_{kq\sigma} \left[\frac{1}{2} V_k V_q^* \left(\frac{1}{E_k^0} + \frac{1}{E_q^0} \right) + \hat{n}_{d\bar{\sigma}} \frac{1}{2} V_k V_q^* \left(\frac{1}{E_k^1} + \frac{1}{E_q^1} - \frac{1}{E_k^0} - \frac{1}{E_q^0} \right) \right] \left(c_{k\sigma}^\dagger c_{q\sigma} - c_{d\sigma}^\dagger c_{d\sigma} \delta_{kq} \right) \end{aligned} \quad (2.211)$$

We can now define two new energy scales:

$$W_{kq} = \frac{1}{2} V_k V_q^* \left(\frac{1}{E_k^0} + \frac{1}{E_q^0} \right), \quad J_{kq} = \frac{1}{2} V_k V_q^* \left(\frac{1}{E_k^1} + \frac{1}{E_q^1} - \frac{1}{E_k^0} - \frac{1}{E_q^0} \right) \quad (2.212)$$

The renormalization Δ_1 becomes

$$\begin{aligned} \Delta_1 &= \sum_{kq\sigma} [W_{kq} + \hat{n}_{d\bar{\sigma}} J_{kq}] \left(c_{k\sigma}^\dagger c_{q\sigma} - c_{d\sigma}^\dagger c_{d\sigma} \delta_{kq} \right) \\ &= \sum_{kq\sigma} [W_{kq} + \hat{n}_{d\bar{\sigma}} J_{kq}] c_{k\sigma}^\dagger c_{q\sigma} - \sum_{k\sigma} [W_{kk} + \hat{n}_{d\bar{\sigma}} J_{kk}] \hat{n}_{d\sigma} \\ &= \sum_{kq\sigma} \left[W_{kq} + \frac{1}{2} \hat{n}_d J_{kq} \right] c_{k\sigma}^\dagger c_{q\sigma} - \sum_{kq\sigma} \sigma J_{kq} S_d^z c_{k\sigma}^\dagger c_{q\sigma} - \sum_{k\sigma} [W_{kk} + \hat{n}_{d\bar{\sigma}} J_{kk}] \hat{n}_{d\sigma} \end{aligned} \quad (2.213)$$

There we exchanged $\hat{n}_{d\bar{\sigma}}$ for S_d^z and \hat{n}_d , in the first term, by using the definitions $\hat{n}_{d\sigma} + \hat{n}_{d\bar{\sigma}} = \hat{n}_{d\sigma}$ and $\hat{n}_{d\sigma} - \hat{n}_{d\bar{\sigma}} = 2\sigma S_d^z$.

The second term in the summation comes from the choice $\sigma = \bar{\alpha}$.

$$\begin{aligned}
\Delta_2 &= \frac{1}{2} \sum_{kq\bar{\sigma}=\alpha} \left[\left(\frac{\hat{n}_{d\bar{\sigma}}}{E_k^1} + \frac{1 - \hat{n}_{d\bar{\sigma}}}{E_k^0} \right) \left(V_k c_{k\sigma}^\dagger c_{d\sigma} - V_k^* c_{d\sigma}^\dagger c_{k\sigma} \right), V_q c_{q\bar{\sigma}}^\dagger c_{d\bar{\sigma}} + V_q^* c_{d\bar{\sigma}}^\dagger c_{q\bar{\sigma}} \right] \\
&= \frac{1}{2} \sum_{kq\sigma} \left(V_k c_{k\sigma}^\dagger c_{d\sigma} - V_k^* c_{d\sigma}^\dagger c_{k\sigma} \right) \left[\frac{\hat{n}_{d\bar{\sigma}}}{E_k^1} + \frac{1 - \hat{n}_{d\bar{\sigma}}}{E_k^0}, V_q c_{q\bar{\sigma}}^\dagger c_{d\bar{\sigma}} + V_q^* c_{d\bar{\sigma}}^\dagger c_{q\bar{\sigma}} \right] \\
&= \frac{1}{2} \sum_{kq\sigma} \left(V_k c_{k\sigma}^\dagger c_{d\sigma} - V_k^* c_{d\sigma}^\dagger c_{k\sigma} \right) \left(V_q^* c_{d\bar{\sigma}}^\dagger c_{q\bar{\sigma}} - V_q c_{q\bar{\sigma}}^\dagger c_{d\bar{\sigma}} \right) \left(\frac{1}{E_k^1} - \frac{1}{E_k^0} \right) \\
&= \frac{1}{2} \sum_{kq\sigma} \left(V_k V_q^* c_{k\sigma}^\dagger c_{d\sigma} c_{d\bar{\sigma}}^\dagger c_{q\bar{\sigma}} - V_k V_q c_{k\sigma}^\dagger c_{d\sigma} c_{q\bar{\sigma}}^\dagger c_{d\bar{\sigma}} - V_k^* V_q^* c_{d\sigma}^\dagger c_{k\sigma} c_{d\bar{\sigma}}^\dagger c_{q\bar{\sigma}} + V_k^* V_q c_{d\sigma}^\dagger c_{k\sigma} c_{q\bar{\sigma}}^\dagger c_{d\bar{\sigma}} \right) \\
&\quad \times \left(\frac{1}{E_k^1} - \frac{1}{E_k^0} \right)
\end{aligned} \tag{2.214}$$

We now use the following trick to combine the first and fourth terms:

$$\begin{aligned}
&\frac{1}{2} \sum_{kq\sigma} \left(V_k V_q^* c_{k\sigma}^\dagger c_{d\sigma} c_{d\bar{\sigma}}^\dagger c_{q\bar{\sigma}} + V_k^* V_q c_{d\sigma}^\dagger c_{k\sigma} c_{q\bar{\sigma}}^\dagger c_{d\bar{\sigma}} \right) \times \left(\frac{1}{E_k^1} - \frac{1}{E_k^0} \right) \\
&= \frac{1}{2} \sum_{kq\sigma} V_k V_q^* c_{k\sigma}^\dagger c_{d\sigma} c_{d\bar{\sigma}}^\dagger c_{q\bar{\sigma}} \left(\frac{1}{E_k^1} - \frac{1}{E_k^0} \right) + \frac{1}{2} \sum_{kq\sigma} V_k^* V_q c_{d\sigma}^\dagger c_{k\sigma} c_{q\bar{\sigma}}^\dagger c_{d\bar{\sigma}} \left(\frac{1}{E_k^1} - \frac{1}{E_k^0} \right) \\
&= \frac{1}{2} \sum_{kq\sigma} V_k V_q^* c_{k\sigma}^\dagger c_{d\sigma} c_{d\bar{\sigma}}^\dagger c_{q\bar{\sigma}} \left(\frac{1}{E_k^1} - \frac{1}{E_k^0} \right) + \frac{1}{2} \sum_{qk\sigma} V_q^* V_k c_{d\bar{\sigma}}^\dagger c_{q\bar{\sigma}} c_{k\sigma}^\dagger c_{d\sigma} \left(\frac{1}{E_q^1} - \frac{1}{E_q^0} \right) \\
&= - \sum_{kq\sigma} J_{kq} c_{k\sigma}^\dagger c_{q\bar{\sigma}} c_{d\bar{\sigma}}^\dagger c_{d\sigma}
\end{aligned} \tag{2.215}$$

In the penultimate step, we interchanged the dummy indices k and q and changed $\sigma \leftrightarrow \bar{\sigma}$ in the second term.

Similarly, for the second term, we get

$$\begin{aligned}
& \frac{1}{2} \sum_{kq\sigma} V_k V_q c_{k\sigma}^\dagger c_{d\sigma} c_{q\bar{\sigma}}^\dagger c_{d\bar{\sigma}} \left(\frac{1}{E_k^1} - \frac{1}{E_k^0} \right) \\
&= \frac{1}{4} \sum_{kq\sigma} \left[V_k V_q \left(\frac{1}{E_k^1} - \frac{1}{E_k^0} \right) c_{k\sigma}^\dagger c_{d\sigma} c_{q\bar{\sigma}}^\dagger c_{d\bar{\sigma}} + \underbrace{V_k V_q \left(\frac{1}{E_k^1} - \frac{1}{E_k^0} \right) c_{k\bar{\sigma}}^\dagger c_{d\bar{\sigma}} c_{q\sigma}^\dagger c_{d\sigma}}_{\sigma \leftrightarrow \bar{\sigma}} \right] \\
&= \frac{1}{4} \sum_{kq\sigma} \left[V_k V_q \left(\frac{1}{E_k^1} - \frac{1}{E_k^0} \right) c_{k\sigma}^\dagger c_{d\sigma} c_{q\bar{\sigma}}^\dagger c_{d\bar{\sigma}} + \underbrace{V_q V_k \left(\frac{1}{E_q^1} - \frac{1}{E_q^0} \right) c_{q\bar{\sigma}}^\dagger c_{d\bar{\sigma}} c_{k\sigma}^\dagger c_{d\sigma}}_{k \leftrightarrow q} \right] \\
&= \sum_{kq\sigma} V_k V_q \frac{1}{4} \left(\frac{1}{E_k^1} - \frac{1}{E_k^0} + \frac{1}{E_q^1} - \frac{1}{E_q^0} \right) c_{k\sigma}^\dagger c_{d\sigma} c_{q\bar{\sigma}}^\dagger c_{d\bar{\sigma}} \\
&= \frac{1}{2} \sum_{kq\sigma} K_{kq} c_{k\sigma}^\dagger c_{d\sigma} c_{q\bar{\sigma}}^\dagger c_{d\bar{\sigma}}
\end{aligned}$$

where K_{kq} is yet another energy scale.

$$K_{kq} = \frac{1}{2} V_k V_q \left(\frac{1}{E_k^1} - \frac{1}{E_k^0} + \frac{1}{E_q^1} - \frac{1}{E_q^0} \right) \quad (2.216)$$

The third term gives

$$\frac{1}{2} \sum_{kq\sigma} V_k^* V_q^* c_{d\sigma}^\dagger c_{k\sigma} c_{d\bar{\sigma}}^\dagger c_{q\bar{\sigma}} \left(\frac{1}{E_k^1} - \frac{1}{E_k^0} \right) = \sum_{kq\sigma} K_{kq} c_{d\sigma}^\dagger c_{k\sigma} c_{d\bar{\sigma}}^\dagger c_{q\bar{\sigma}} \quad (2.217)$$

The total renormalization can thus be written as

$$\begin{aligned}
\Delta \mathcal{H}(\omega_1, \omega_0) &= - \sum_{k\sigma} [W_{kk} + \hat{n}_{d\bar{\sigma}} J_{kk}] \hat{n}_{d\sigma} && [\text{renormalization in } \epsilon_d, U] \\
&+ \sum_{kq\sigma} \left[W_{kq} + \frac{1}{2} \hat{n}_d J_{kq} \right] c_{k\sigma}^\dagger c_{q\sigma} && [\text{potential scattering}] \\
&- \sum_{kq\sigma} J_{kq} \left[S_d^z \sigma c_{k\sigma}^\dagger c_{q\sigma} + \sum_{kq\sigma} J_{kq} c_{k\sigma}^\dagger c_{q\bar{\sigma}} c_{d\bar{\sigma}}^\dagger c_{d\sigma} \right] && [\text{spin Kondo}] \\
&+ \sum_{kq\sigma} K_{kq} c_{k\sigma}^\dagger c_{d\sigma} c_{q\bar{\sigma}}^\dagger c_{d\bar{\sigma}} + \text{h.c.} && [\text{charge Kondo}]
\end{aligned} \quad (2.218)$$

Note that this renormalization is in a particular eigendirection of the total quantum fluctuation operator $\hat{\omega}$. In other words, the single perturbative J_{kq} has been replaced with 2^N scales, each with its own value

of ω . This is where the complexity has been transferred in going from the second-order SWT to the non-perturbative URG. The new energy scales are thus the non-perturbative variants of the ones generated in SWT.

$$\begin{aligned}
W_{kq}^{SWT} &= \frac{1}{2} V_k V_q^* \left(\frac{1}{\epsilon_k - \epsilon_d} + \frac{1}{\epsilon_q - \epsilon_d} \right) \\
J_{kq}^{SWT} &= \frac{1}{2} V_k V_q^* \left(\frac{1}{\epsilon_k - \epsilon_d - U} + \frac{1}{\epsilon_q - \epsilon_d - U} - \frac{1}{\epsilon_k - \epsilon_d} - \frac{1}{\epsilon_q - \epsilon_d} \right) \\
W_{kq}^{URG}(\omega) &= \frac{1}{2} V_k V_q^* \left(\frac{1}{\omega_0 + \frac{1}{2}\epsilon_k - \epsilon_d} + \frac{1}{\omega_0 + \frac{1}{2}\epsilon_q - \epsilon_d} \right) \\
J_{kq}^{URG}(\omega) &= \frac{1}{2} V_k V_q^* \left(\frac{1}{\omega_1 + \epsilon_k - \epsilon_d - U} + \frac{1}{\omega_1 + \epsilon_q - \epsilon_d - U} - \frac{1}{\omega_0 + \epsilon_k - \epsilon_d} - \frac{1}{\omega_0 + \epsilon_q - \epsilon_d} \right)
\end{aligned} \tag{2.219}$$

To recover the SWT scales from the URG ones, we have to substitute each ω_i by the energy of the initial state to which it corresponds. From eq. 2.208, we note that ω_1 refers to the initial state in which $\hat{n}_{k\sigma} = \hat{n}_{d\bar{\sigma}} = 1 - \hat{n}_{d\sigma} = 1$. Therefore, $\omega_1 = \frac{1}{2}\epsilon_k + \epsilon_d$. Similarly, ω_0 refers to the initial state in which $\hat{n}_{k\sigma} = 1 - \hat{n}_{d\bar{\sigma}} = 1 - \hat{n}_{d\sigma} = 1$. Therefore, $\omega_0 = \frac{1}{2}\epsilon_k$. Substituting these into the URG energy scales gives back the SWT scales.

2.9 Continuous unitary transformation RG

2.9.1 Formalism

The following equation generates a family of unitary Hamiltonians.

$$\frac{d\mathcal{H}(l)}{dl} = [\mathcal{H}, \eta(l)] \tag{2.220}$$

To prove the unitarity [12], we construct the unitary operator $U(l)$ that connects the Hamiltonians $\mathcal{H}(l)$ and $\mathcal{H}(l=0)$. Let $\mathcal{H}(l) = U(l)\mathcal{H}(l=0)U^\dagger(l)$, where $U(l)$ is defined by

$$\eta(l) = \frac{dU}{dl}U^\dagger = -U\frac{dU^\dagger}{dl} \quad \left[UU^\dagger = 1 \implies \frac{d(UU^\dagger)}{dl} = 0 \right] \tag{2.221}$$

This will give

$$\begin{aligned}
\frac{d\mathcal{H}(l)}{dl} &= \frac{dU}{dl}\mathcal{H}(0)U^\dagger(l) + U\mathcal{H}(0)\frac{dU^\dagger}{dl} \\
&= \frac{dU}{dl}U^\dagger\mathcal{H}(l) + \mathcal{H}(l)U\frac{dU(l)^\dagger}{dl} \\
&= \eta(l)\mathcal{H}(l) - \mathcal{H}(l)\eta(l) \\
&= [\eta(l), \mathcal{H}(l)]
\end{aligned} \tag{2.222}$$

This proves that the family of Hamiltonians $\mathcal{H}(l)$ satisfy the flow equation eq. 2.220. $\eta(l)$ is referred to as the generator of the flow equation. It is chosen so as to reduce the off-diagonal part of the Hamiltonian, either progressively or in one shot. In Schrieffer-Wolff transformation, the transformation is one-shot,

and the η there is the S that sits on top of the exponential in the unitary transformation. In URG, the generator to decouple one electron $q\beta$ is $\eta_{q\beta}^\dagger - \eta_{q\beta}$.

In Continuous unitary transformation (CUT) RG [13], we progressively block-diagonalize the Hamiltonian by removing off-diagonal terms that are farthest from the diagonal, through infinitesimal unitary transformations. The change is described as a flow against the parameter l . The canonical choice of the generator is $\eta(l) = [\mathcal{H}_d, \mathcal{H}_X]$, where \mathcal{H}_d is the diagonal part of the Hamiltonian and $\mathcal{H}_X = \mathcal{H} - \mathcal{H}_d$ is the off-diagonal part of the Hamiltonian. Therefore,

$$\frac{d\mathcal{H}}{dl} = [[\mathcal{H}_d(l), \mathcal{H}_X(l)], \mathcal{H}(l)] \quad (2.223)$$

To see how this choice of the generator results in a decay of the off-diagonal terms, we can consider a simple 2-particle Hamiltonian:

$$\mathcal{H} = \sum_i \epsilon_i \hat{n}_i + \sum_{i \neq j} g_{ij} c_i^\dagger c_j \quad (2.224)$$

where $g_{ij}^* = g_j i$. The canonical generator then turns out to be

$$\eta = \left[\sum_i \epsilon_i \hat{n}_i, \sum_{j \neq k} g_{jk} c_j^\dagger c_k \right] = \sum_{k \neq i} \epsilon_i \left[g_{ik} c_i^\dagger c_k - g_{ki} c_k^\dagger c_i \right] = \sum_{k \neq i} g_{ik} c_i^\dagger c_k (\epsilon_i - \epsilon_k) \quad (2.225)$$

and the renormalization in the Hamiltonian is

$$\frac{d\mathcal{H}}{dl} = [\eta, \mathcal{H}] = \left[\sum_{k \neq i} g_{ik} c_i^\dagger c_k (\epsilon_i - \epsilon_k), \sum_i \epsilon_i \hat{n}_i + \sum_{i \neq j} g_{ij} c_i^\dagger c_j \right] \quad (2.226)$$

The first commutator gives

$$-\sum_{i \neq k} g_{ik} (\epsilon_i - \epsilon_k)^2 c_i^\dagger c_k \quad (2.227)$$

The second commutator gives

$$\sum_{\substack{k \neq i \\ j}} \left[g_{kj} g_{ik} (\epsilon_i - \epsilon_k) c_i^\dagger c_j + g_{ji} g_{ik} (\epsilon_k - \epsilon_i) c_j^\dagger c_k \right] = \sum_{\substack{k \neq i \\ j}} g_{ik} g_{kj} (\epsilon_i + \epsilon_j - 2\epsilon_k) c_i^\dagger c_j \quad (2.228)$$

The total renormalization is

$$\frac{d\mathcal{H}}{dl} = -\sum_{i \neq j} g_{ij} (\epsilon_i - \epsilon_j)^2 c_i^\dagger c_j + \sum_{\substack{k \neq i \\ j}} g_{ik} g_{kj} (\epsilon_i + \epsilon_j - 2\epsilon_k) c_i^\dagger c_j \quad (2.229)$$

The couplings renormalize as

$$\begin{aligned} \frac{d\epsilon_i}{dl} &= \sum_{k \neq i} 2|g_{ik}|^2 (\epsilon_i - \epsilon_k) \\ \frac{dg_{ij}}{dl} &= -g_{ij} (\epsilon_i - \epsilon_j)^2 + \sum_{k \neq i} g_{ik} g_{kj} (\epsilon_i + \epsilon_j - 2\epsilon_k) \end{aligned} \quad (2.230)$$

To see the decay of the off-diagonal terms, first we will relate the off-diagonal flow to the diagonal flow using the invariance of the trace under a unitary transformation:

$$0 = \frac{d\text{Tr}(\mathcal{H})^2}{dl} = \frac{d\text{Tr}(\mathcal{H})^2}{dl} = \sum_i \frac{d\epsilon_i^2}{dl} + \sum_{i \neq j} \frac{d|g_{ij}|^2}{dl} \implies \sum_{i \neq j} \frac{d|g_{ij}|^2}{dl} = - \sum_i \frac{d\epsilon_i^2}{dl} \quad (2.231)$$

From the flow equation, we can see that

$$\sum_i \frac{d\epsilon_i^2}{dl} = 2 \sum_{i \neq k} \epsilon_i \frac{d\epsilon_i}{dl} = 2 \sum_i |g_{ik}|^2 (\epsilon_i - \epsilon_k)^2 \geq 0 \quad (2.232)$$

Therefore,

$$\sum_{i \neq j} \frac{d|g_{ij}|^2}{dl} \leq 0 \quad (2.233)$$

This implies that at $l \rightarrow \infty$, the only off-diagonal terms that survive are those with g_{ij} that scatter between degenerate states, that is, those with $\epsilon_i - \epsilon_j = 0$.

2.9.2 CUT-RG for the Fröhlick Hamiltonian

To get a feel for the method, we will apply it on the Fröhlick Hamiltonian to remove the electron-phonon coupling term.

$$\mathcal{H} = \mathcal{H}_d + \mathcal{H}_X \quad (2.234)$$

where \mathcal{H}_X is the electron-phonon coupling term

$$\sum_{kq} g_q b_{-q}^\dagger c_{k+q,\sigma}^\dagger c_{k\sigma} + \text{h.c.} \quad (2.235)$$

and-1 $\mathcal{H}_d = \sum_{k\sigma} \epsilon_k \hat{n}_{k\sigma} + \sum_q \hbar\omega_q b_q^\dagger b_q$ is the kinetic energy of the electron and phonons. We assume time-reversal invariance such that $\omega_q = \omega_{-q}$. We choose

$$\eta(l) = [\mathcal{H}_d, \mathcal{H}] = [\mathcal{H}_d, \mathcal{H}_X] \quad (2.236)$$

It is easy to compute the commutators.

$$\begin{aligned} \left[\sum_{k\sigma} \epsilon_k \hat{n}_{k\sigma}, \sum_{kq\sigma} b_{-q}^\dagger c_{k+q,\sigma}^\dagger c_{k\sigma} \right] &= \sum_{kq\sigma} g_q (\epsilon_{k+q} - \epsilon_k) g_q b_{-q}^\dagger c_{k+q,\sigma}^\dagger c_{k\sigma} \\ \left[\sum_q \hbar\omega_q b_q^\dagger b_q, \sum_{kq} g_q b_{-q}^\dagger c_{k+q,\sigma}^\dagger c_{k\sigma} \right] &= \sum_{kq} g_q \hbar\omega_q b_{-q}^\dagger c_{k+q,\sigma}^\dagger c_{k\sigma} \end{aligned} \quad (2.237)$$

Therefore,

$$\eta = \sum_{kq\sigma} g_q (\epsilon_{k+q} - \epsilon_k + \hbar\omega_q) b_{-q}^\dagger c_{k+q,\sigma}^\dagger c_{k\sigma} - \text{h.c.} \quad (2.238)$$

We define $\xi \equiv \epsilon_{k+q} - \epsilon_k + \hbar\omega_q$. The renormalization in the total Hamiltonian becomes

$$\frac{d\mathcal{H}}{dl} = [\eta, \mathcal{H}] \quad (2.239)$$

The flow equation for the electron-phonon coupling is

$$\frac{dg_q}{dl} = -\xi^2 g_q \implies g_q(l) = g_q(0) \exp\{-\xi^2 l\} \quad (2.240)$$

A new electron-electron coupling $V_{kk'q} c_{k+q}^\dagger c_{k'-q}^\dagger c_{k'} c_k$ is also generated. For the Cooper channel ($k' = -k$), the flow equation is

$$V_{k,-k,q}(\infty) = V_{k,-k,-q}(0) - \frac{g_q^2 \omega_q}{\omega_q^2 + (\epsilon_{k+q} - \epsilon_k)^2} \quad (2.241)$$

Off-diagonal terms that connect larger energy differences ξ decay the fastest.

2.9.3 Deriving CUT RG from URG

We will now see that the renormalization in URG can also be put into a similar form. From eq. 2.47, we can write the URG renormalization in the diagonal part as

$$\Delta\mathcal{H}^0 = \frac{1}{2} [\eta^\dagger - \eta, \mathcal{H}] \quad (2.242)$$

where $\mathcal{H}^0 = \mathcal{H}^d + \mathcal{H}^i$. The URG generator can be recast (starting from the definitions of η , eqs. 2.14) as

$$\begin{aligned} \eta^\dagger - \eta &= G_1 c^\dagger T - G_0 T^\dagger c \\ &= \frac{1}{\omega_1 - \omega_0} [G_1 (\omega_1 - \omega_0) c^\dagger T - G_0 (\omega_1 - \omega_0) T^\dagger c] \\ &= \frac{1}{\omega_1 - \omega_0} [G_1 \omega_1 c^\dagger T - c^\dagger T \omega_0 G_0 - T^\dagger c \omega_1 G_1 + G_0 \omega_0 T^\dagger c] \end{aligned} \quad (2.243)$$

In the last step, we changed the second and fourth terms using the constraints $G_1 c^\dagger T = c^\dagger T G_0$ and $G_0 T^\dagger c = T^\dagger c G_1$, eq. 2.16. We now add and subtract $G_1 G_1^{-1} c^\dagger T = c^\dagger T$ and $G_0 G_0^{-1} T^\dagger c = T^\dagger c$ for each term.

$$\begin{aligned} \eta^\dagger - \eta &= \frac{1}{\omega_1 - \omega_0} [G_1 (\omega_1 - G_1^{-1}) c^\dagger T + c^\dagger T - c^\dagger T (\omega_0 - G_0^{-1}) G_0 - c^\dagger T \\ &\quad - T^\dagger c (\omega_1 - G_1^{-1}) G_1 - T^\dagger c + G_0 (\omega_0 - G_0^{-1}) T^\dagger c + T^\dagger c] \\ &= \frac{1}{\omega_1 - \omega_0} [G_1 (\omega_1 - G_1^{-1}) c^\dagger T - c^\dagger T (\omega_0 - G_0^{-1}) G_0 \\ &\quad - T^\dagger c (\omega_1 - G_1^{-1}) G_1 + G_0 (\omega_0 - G_0^{-1}) T^\dagger c] \end{aligned} \quad (2.244)$$

In the last step, the extra $c^\dagger T$ and $T^\dagger c$ terms canceled out. In the second and third terms, we can bring the Greens function closer to the operators $c^\dagger T$ and $T^\dagger c$ because $(\omega_j - G_j^{-1}) G_j = G_j (\omega_j - G_j^{-1})$:

$$\begin{aligned} \eta^\dagger - \eta &= \frac{1}{\omega_1 - \omega_0} [G_1 (\omega_1 - G_1^{-1}) c^\dagger T - c^\dagger T G_0 (\omega_0 - G_0^{-1}) \\ &\quad - T^\dagger c G_1 (\omega_1 - G_1^{-1}) + G_0 (\omega_0 - G_0^{-1}) T^\dagger c] \\ &= \frac{1}{\omega_1 - \omega_0} [G_1 (\omega_1 - G_1^{-1}) c^\dagger T - G_1 c^\dagger T (\omega_0 - G_0^{-1}) \\ &\quad - G_0 T^\dagger c (\omega_1 - G_1^{-1}) + G_0 (\omega_0 - G_0^{-1}) T^\dagger c] \end{aligned} \quad (2.245)$$

In the last step, we again used the constraint $G_1 c^\dagger T = c^\dagger T G_0$ and its partner. From the definition of the Green's function $G = (\omega - \mathcal{H}^d)^{-1}$, we can write $\omega_j - G_j^{-1} = \mathcal{H}_j^d$. Therefore,

$$\begin{aligned}\eta^\dagger - \eta &= \frac{1}{\omega_1 - \omega_0} [G_1 \mathcal{H}_1^d c^\dagger T - G_1 c^\dagger T \mathcal{H}_0^d - G_0 T^\dagger c \mathcal{H}_1^d + G_0 \mathcal{H}_0^d T^\dagger c] \\ &= \frac{1}{\omega_1 - \omega_0} [G \mathcal{H}^d c^\dagger T - G c^\dagger T \mathcal{H}^d - G T^\dagger c \mathcal{H}^d + G \mathcal{H}^d T^\dagger c] \\ &= \frac{1}{\omega_1 - \omega_0} G [\mathcal{H}^d, c^\dagger T + T^\dagger c]\end{aligned}\quad (2.246)$$

where $\mathcal{H}^d = \mathcal{H}_1^d \hat{n} + \mathcal{H}_0^d (1 - \hat{n})$ and $G = G_1 \hat{n} + G_0 (1 - \hat{n}) = (\hat{\omega} - \mathcal{H}^d)^{-1}$. For URG, the relevant off-diagonal part of the Hamiltonian for the current node is $\mathcal{H}^I = c^\dagger T + T^\dagger c$. Therefore,

$$\eta^\dagger - \eta = \frac{1}{\omega_1 - \omega_0} G [\mathcal{H}^d, \mathcal{H}^I] = \left[\mathcal{H}^d, \frac{1}{\omega_1 - \omega_0} G \mathcal{H}^I \right] \quad (2.247)$$

The last equality comes about because both G and \mathcal{H}^d are completely diagonal and hence commute. The renormalization in the Hamiltonian under URG, which is a function of both the quantum fluctuation scale ω and the running bandwidth D , can thus be written as

$$\Delta \mathcal{H}(\omega, D) = \left[[\mathcal{H}^d, \tilde{\mathcal{H}}^I], \mathcal{H} \right] - \mathcal{H}_X \quad (2.248)$$

The most obvious difference with the CUT version is the presence of the off-diagonal piece $-\mathcal{H}_X$. This is a result of the philosophical difference between URG and CUT-RG - while CUT-RG gradually suppresses the off-diagonal matrix elements, URG makes the off-diagonal components in each 2×2 block vanish completely. We can instead look at the renormalization in the diagonal part of the Hamiltonian under URG:

$$\Delta \mathcal{H}^0(\omega, D) = \left[[\mathcal{H}^d, \tilde{\mathcal{H}}^I], \mathcal{H} \right] \quad (2.249)$$

where $\tilde{\mathcal{H}}^I = \frac{1}{\omega_1 - \omega_0} G \mathcal{H}^I$. This can be compared to the analogous equation for CUT (eq. 2.223),

$$\Delta \mathcal{H}(\lambda) = \Delta \lambda [[\mathcal{H}_d, \mathcal{H}_X], \mathcal{H}] \quad (2.250)$$

Leaving aside the obvious differences in the philosophies (the presence of ω in URG or the fact that while URG decouples as a flow in the bandwidth, CUT uses a general parameter λ or the algorithmic difference that while URG decouples one specific node, CUT tries to make the Hamiltonian band-diagonal), the major physical difference is the presence of the total Green's function in the URG equation. It must be noted that while CUT employs the entire off-diagonal part in \mathcal{H}_X , the \mathcal{H}^I of URG contains only those parts that are off-diagonal with respect to the node being decoupled at this step.

To bring the URG form closer to CUT, we can make some approximations.

$$G = (\hat{\omega} - \mathcal{H}^d)^{-1} \approx -(\mathcal{H}^d)^{-1} \quad (2.251)$$

where we assumed that the quantum fluctuations are small and can be ignored w.r.t the diagonal contribution \mathcal{H}^d . This gives

$$\frac{\Delta \mathcal{H}^0(\omega, D)}{[\mathcal{H}_1^d (\omega_0 - \omega_1)]^{-1}} = [[\mathcal{H}^d, \mathcal{H}^I], \mathcal{H}] \quad (2.252)$$

We can thus make the connection,

$$\Delta\lambda \sim [\mathcal{H}_1^d(\omega_0 - \omega_1)]^{-1} \quad (2.253)$$

Note that in going from eq. 2.249 to the simplified form eq. 2.252, we had to drop all quantum fluctuations in the denominator and we lose the fixed point structure in the process. This results in the distinction that while URG can reach a fixed point theory in a finite number of steps, CUT cannot do so.

2.10 Comparison of the Canonical Transformations

We have considered three canonical transformations in this section: the Poor Man's scaling (PMS), the Schrieffer-Wolff transformation (SWT) and the continuous unitary transformation renormalization group (CUT-RG). PMS and SWT are more or less identical; they differ in the context in which they are used. PMS is used when there is an entire spectrum of energies in the model, ranging from a low energy limit to a high energy; it is then employed to decouple the highest energy modes in an iterative fashion. SWT is used when the Hamiltonian can be split into one high and one low energy part, and we need to decouple these two modes. It is clear when seen from this perspective that SWT is like a one-shot PMS; it decouples the UV from the IR in one step, compared to the iterative approach of PMS. However, as has been shown in the previous subsections, both PMS and SWT can be formalized in an identical fashion, so that one can be switched for the other in both contexts.

Now that we have established that PMS and SWT are formally identical, we can relate them to URG. URG is similar in philosophy to PMS in the fact that URG also successively decouples high energy modes from the low energy ones. The difference is that URG takes care of the quantum fluctuations, at least in principle, by introducing a new set of energy scales ω . These ω then parameterise the RG flows of URG, compared to the single RG flow of PMS. Since SWT is formally the same as PMS, these is also a comparison between SWT and URG. Both PMS and SWT trivialize the quantum fluctuation scales of URG by replacing it with the bare energy values.

CUT-RG is philosophically different from the other transformations. Its goal is to gradually reduce the contributions of the off-diagonal terms by making them decay along a certain scale l . Off-diagonal terms that connect states with large energy differences decay faster. In this sense, there is no sequential dropping out of off-diagonal terms; all off-diagonal terms disappear at $l = \infty$. In this sense, it is like a continuous version of SWT. While SWT strives to remove an entire off-diagonal term in one-shot, CUT RG does this gradually by introducing a scale l . This separation of scales is absent in SWT. It does exist in URG and PMS, albeit in a different fashion. There, the separation comes in when we decouple single electron states starting from the Brillouin zone boundary Λ_N and come down to the Fermi surface Λ_0 . Each Λ provides a natural energy scale for separating the high and low energy physics.

If one integrates the continuum generator η over all the scales, one should recover something analogous to the SWT generator. This generator is however necessarily perturbative in the off-diagonal term, since by definition η will only be of first order in \mathcal{H}_X . This is in contrast to the non-perturbative generators in URG and, at least in principle, PMS. This non-perturbative form is encapsulated in the presence of a second completely different set of energy scales ω (or E in PMS). This second energy scale is absent in CUT RG because it takes care of at most the second order term.

Another point to note is that since SWT keeps the entire off-diagonal piece in the generator, new terms will almost certainly be generated at every step, and they have to be truncated. This is not the case with URG or PMS, because in those methods, we decouple just a single-electron at each step,

and so those electrons become integrals of motion at that step, leading to their removal from the off-diagonal piece, and very often the Hamiltonian retains the same form as the bare model. This makes the philosophy of URG and PMS easier to work with. Tied to this is the fact that CUT RG often takes a certain type of interaction in the generator part, and not the entire off-diagonal piece. Hence, at the limit of the flow parameter going to ∞ , the chosen off-diagonal piece goes to zero but the remaining off-diagonal pieces still remain. As a result, the Hamiltonian is almost block diagonal at this stage. On the other hand, URG progressively decouples single electrons, meaning all scattering terms corresponding to that electron vanish at each step.

One last thing to note is that URG, being unitarily implemented with a well-defined generator, does not accommodate for spontaneous symmetry breaking (SSB). In order to see SSB, the symmetry-breaking term has to be added to the bare model explicitly; if this term grows under the RG, then the ground state will be symmetry-broken. CUT RG, however, does allow for SSB through the idea that the generator is not uniquely defined. If the generator commutes with a particular symmetry, then the family of Hamiltonians will also have the symmetry [12]. However, if the generator is replaced by something that is normal ordered w.r.t a particular expectation value, then the CUT RG flow will usually be towards either the symmetry-preserved state or the symmetry-broken state, depending on whichever is stable [14].

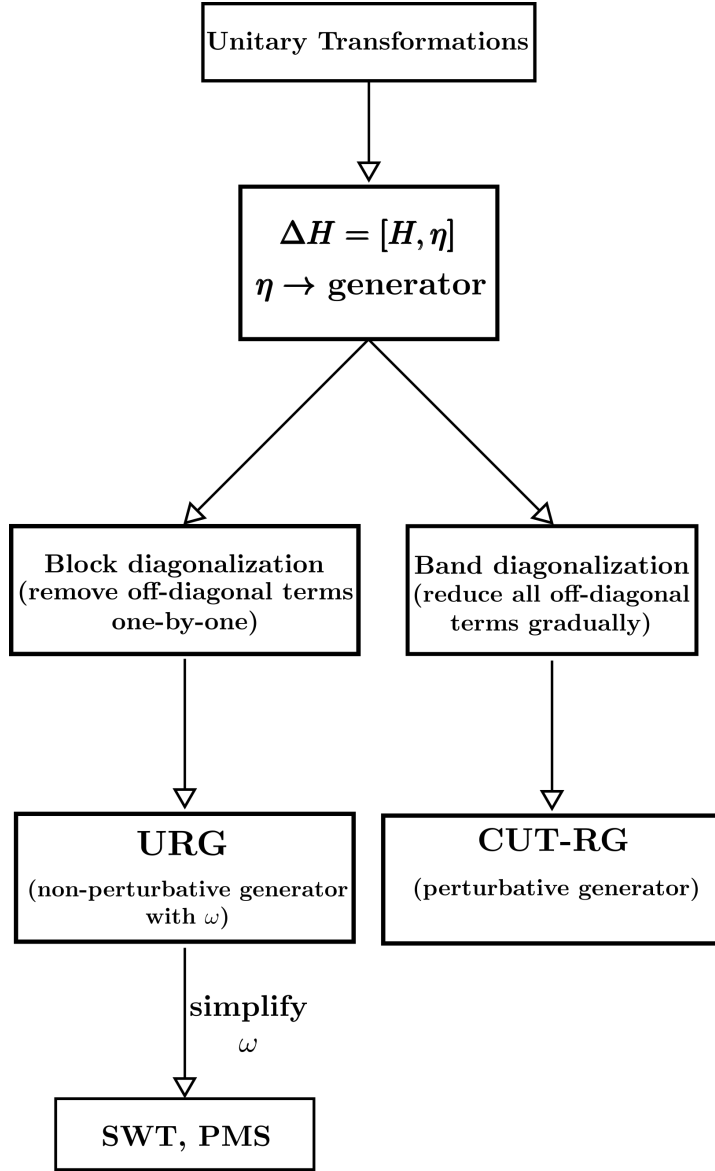


Figure 2.8: Comparison of the various unitary transformations and their relationships to each other.

2.11 Iterative Diagonalisation of Quantum Impurity Models

The broad idea is the following. We have a Hamiltonian describing an interacting set of states (in real or momentum space). We can express the total Hamiltonian in an incremental fashion: $H = \sum_i H_i$, where H_{i+1} involves more number of states than H_i . For example, a tight-binding model can be written in that form, with the definition $H_i = c_{i+1}^\dagger c_i + \text{h.c.}$. The iterative diagonalisation method obtains the low-energy spectrum of this problem in the following manner: We first diagonalise the Hamiltonian H for a smaller value of i , small enough such that this can be done exactly. We then truncate the spectrum to a predefined size, and rotate all existing operators to this truncated basis, including the Hamiltonian H . We then consider the "bonding Hamiltonian" ΔH between the existing sites and the new sites, and rotate the same into the truncated basis. Adding the previous rotated Hamiltonian H and the rotated

increment Hamiltonian ΔH gives us a truncated but effective Hamiltonian for the increased number of sites. We again diagonalise this, and again retain only a fixed number of states in the spectrum. We keep repeating this until we reach the required number of sites.

2.12 Structure of Hamiltonian and Operators

2.12.1 Jordan-Wigner Matrix Representation of Fermionic Operators

For a single qubit, the creation/annihilation matrices are

$$c = \begin{pmatrix} 0 & 1 \\ 0 & 0 \end{pmatrix}, c^\dagger = \begin{pmatrix} 0 & 0 \\ 1 & 0 \end{pmatrix}, \quad (2.254)$$

given the convention that $|1\rangle = (0 \ 1)$ is the occupied state. For a many-body system, these must be replaced with field operators that have the canonical fermionic algebra. For a system of N 1-particle levels, this can be accomplished through a *Jordan-Wigner*-like transformation

$$c_j = (\otimes_1^j \sigma_z) \otimes c \otimes (\otimes_1^{N-j} \mathbb{I}), j \in [0, N-1], \quad (2.255)$$

where $\sigma_z = \begin{pmatrix} 1 & 0 \\ 0 & -1 \end{pmatrix}$ and $\mathbb{I} = \begin{pmatrix} 1 & 0 \\ 0 & 1 \end{pmatrix}$. For example, for spinless electrons on a three-site lattice, we can have three fermionic operators: c_1, c_2 , and c_3 . Following the above expression, their matrices are

$$c_1 = c \otimes \mathbb{I} \otimes \mathbb{I} = \begin{bmatrix} 0 & 0 & 1 & 0 & 0 & 0 & 0 & 0 \\ 0 & 0 & 0 & 1 & 0 & 0 & 0 & 0 \\ 0 & 0 & 0 & 0 & 0 & 0 & 0 & 0 \\ 0 & 0 & 0 & 0 & 0 & 0 & 0 & 0 \\ 0 & 0 & 0 & 0 & 0 & 0 & -1 & 0 \\ 0 & 0 & 0 & 0 & 0 & 0 & 0 & -1 \\ 0 & 0 & 0 & 0 & 0 & 0 & 0 & 0 \\ 0 & 0 & 0 & 0 & 0 & 0 & 0 & 0 \end{bmatrix},$$

$$c_2 = \sigma \otimes c \otimes \mathbb{I} = \begin{bmatrix} 0 & 0 & 1 & 0 & 0 & 0 & 0 & 0 \\ 0 & 0 & 0 & 1 & 0 & 0 & 0 & 0 \\ 0 & 0 & 0 & 0 & 0 & 0 & 0 & 0 \\ 0 & 0 & 0 & 0 & 0 & 0 & 0 & 0 \\ 0 & 0 & 0 & 0 & 0 & 0 & -1 & 0 \\ 0 & 0 & 0 & 0 & 0 & 0 & 0 & -1 \\ 0 & 0 & 0 & 0 & 0 & 0 & 0 & 0 \\ 0 & 0 & 0 & 0 & 0 & 0 & 0 & 0 \end{bmatrix},$$

$$c_3 = \sigma \otimes \sigma \otimes c = \begin{bmatrix} 0 & 1 & 0 & 0 & 0 & 0 & 0 & 0 \\ 0 & 0 & 0 & 0 & 0 & 0 & 0 & 0 \\ 0 & 0 & 0 & -1 & 0 & 0 & 0 & 0 \\ 0 & 0 & 0 & 0 & 0 & 0 & 0 & 0 \\ 0 & 0 & 0 & 0 & 0 & -1 & 0 & 0 \\ 0 & 0 & 0 & 0 & 0 & 0 & 0 & 0 \\ 0 & 0 & 0 & 0 & 0 & 0 & 0 & 1 \\ 0 & 0 & 0 & 0 & 0 & 0 & 0 & 0 \end{bmatrix},$$

For later use, we define the *antisymmetriser matrix* $S(j)$ and identity matrix $\mathbb{I}(j)$,

$$\begin{aligned} S(j) &= \otimes_1^j \sigma_z = \sigma_z \otimes \dots j \text{ times } \dots \otimes \sigma_z, \\ \mathbb{I}(j) &= \otimes_1^{N-j} \mathbb{I} = \mathbb{I} \otimes \dots j \text{ times } \dots \otimes \mathbb{I}, \end{aligned} \tag{2.256}$$

to express the fermionic representation compactly:

$$c_j = S(j) \otimes c \otimes \mathbb{I}(N-j). \tag{2.257}$$

2.12.2 Structure of Hamiltonian

We consider a general impurity model, of L number of sites (excluding the impurity site):

$$H_{\text{sys}}(L) = H_{\text{imp}} + H_{\text{imp-bath}} + -t \sum_{\sigma,j=1}^{L-1} \left(c_{j,\sigma}^\dagger c_{j+1,\sigma} + \text{h.c.} \right), \tag{2.258}$$

where H_{imp} is the Hamiltonian for the decoupled impurity site and $H_{\text{imp-bath}}$ is the impurity-bath coupling. Such a system has $2L + 2$ single-particle levels in the full system (2 spin levels for each of the $L + 1$ sites).

Iteration scheme (the initial number of states is L_0):

$$\begin{aligned} H_0(L_0) &= H_{\text{sys}}(L_0), \\ H_{r+1}(L_0) &= H_r(L_0) + \Delta H_r(L_0), \quad r \geq 0, \\ \Delta H_r(L_0) &= -t \sum_{\sigma} \left(c_{L_0+r,\sigma}^{\dagger} c_{L_0+r+1,\sigma} + \text{h.c.} \right). \end{aligned} \tag{2.259}$$

H_0 is the initial Hamiltonian, consisting of L_0 lattice sites in the bath, $H_{r+1}(L_0)$ is the Hamiltonian after $r + 1$ iterations having started with L_0 sites, and $\Delta H_r(L_0)$ is the increment term that gets added to $H_r(L_0)$ during the $(r + 1)^{\text{th}}$ iteration to give rise to $H_{r+1}(L_0)$.

2.13 The Algorithm

2.13.1 Iterative Diagonalization

Let the starting Hamiltonian be $H_0(L_0)$, consisting of L_0 single-particle levels (hence a Hilbert space dimension of 2^{L_0}). We start with a single-particle computational basis and construct the L_0 fermionic operators c_1, c_2, \dots, c_{L_0} in this basis, using eq. 2.257. We also keep track of a large antisymmetriser matrix $S(L_0)$ that will be used to attach new sites when we expand the system. Let M_s be the maximum number of eigenstates we retain in the spectrum at any given step. The value of M_s should be chosen so that a $M_s \times M_s$ matrix can be diagonalised in reasonable time.

- S1. Construct the complete Hamiltonian matrix H_0 in our present basis using the field operators $\{c_j\}$. Diagonalise the Hamiltonian (of size $D_0 \times D_0$) and obtain the eigenvalues E_n and eigenstates X_n . Each X_n is a column vector of size D_0 .
- S2. Retain at most M_s number of eigenstates, preferring the ones with lower energy. The reduced basis for this rotated truncated subspace is constructed by stacking the column vectors X_n horizontally:

$$R = [X_1 X_2 \dots X_{M_s}]_{D_0 \times M_s}. \tag{2.260}$$

This matrix also acts as the transformation to rotate and truncate all operators from the old basis into the new one.

- S3. We rotate our Hamiltonian H_0 , our fermionic operators $\{c_j\}$ and the large antisymmetrizer matrix $S(L_0)$ into the new reduced basis, using the transformation $\mathcal{O} \rightarrow R^{\dagger} \mathcal{O} R$.
- S4. We now need to expand our system by adding the increment Hamiltonian ΔH_0 . Let the number of new 1-particle levels in ΔH_0 be L_{Δ} . These new levels will be indexed as $L_0 + 1, \dots, L_0 + L_{\Delta}$. We need to define antisymmetrized fermionic operators for the new sites:

$$\begin{aligned} c_{L_0+1} &= c \otimes \mathbb{I}(2^{L_{\Delta}-1}), \\ c_{L_0+2} &= \sigma_z \otimes c \otimes \mathbb{I}(2^{L_{\Delta}-2}), \\ &\dots \\ c_{L_0+L_{\Delta}} &= (\otimes_1^{L_{\Delta}-1} \sigma) \otimes c. \end{aligned} \tag{2.261}$$

These have to be calculated in the local computational basis (of size $2^{L_{\Delta}}$) of the new levels.

- S5. Combining the new sites with the old sites leads to a combined Hilbert space dimension of $(M_s + 2^{L_\Delta}) \times (M_s + 2^{L_\Delta})$. To allow all operators to act on the enlarged Hilbert space, we expand both sets of operators:

$$\begin{aligned} c_j &= S(L_0) \otimes c_j; \quad j = L_0 + 1, \dots, L_\Delta, \\ c_j &= c_j \otimes \mathbb{I}(2^{L_\Delta}); \quad j = 1, 2, \dots, L_0, \\ H_0 &\rightarrow H_0 \otimes \mathbb{I}(2^{L_\Delta}), \\ S(L_1) &= S(L_0) \otimes \mathbb{I}(2^{L_\Delta}). \end{aligned} \tag{2.262}$$

where $\mathbb{I}(2^{L_\Delta})$ is an identity matrix of dimension $2^{L_\Delta} \times 2^{L_\Delta}$. Note that the operators in the last three equations are the rotated ones (following Step 3).

- S6. Using the transformed operators $c_{L_0+1}, \dots, c_{L_0+L_\Delta}$ for the new sites, construct the difference Hamiltonian matrix ΔH_0 and hence the updated Hamiltonian $H_1 = H_0 + \Delta H_0$ for the next step. Repeat the process starting from step 2 with the new Hamiltonian H_1 , the new operators c_j and the new matrix $S(L_1)$ replacing the old counterparts.

2.13.2 Static Correlations

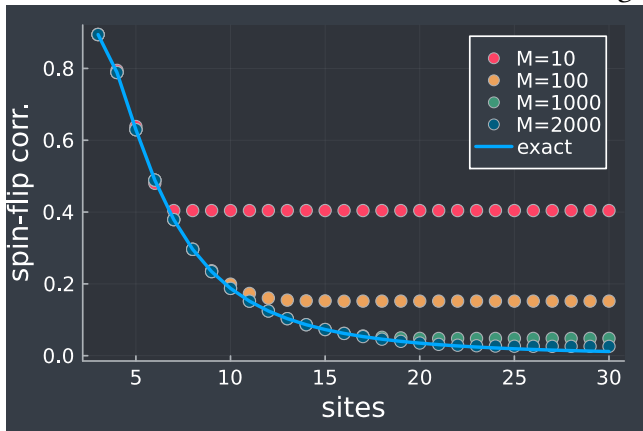
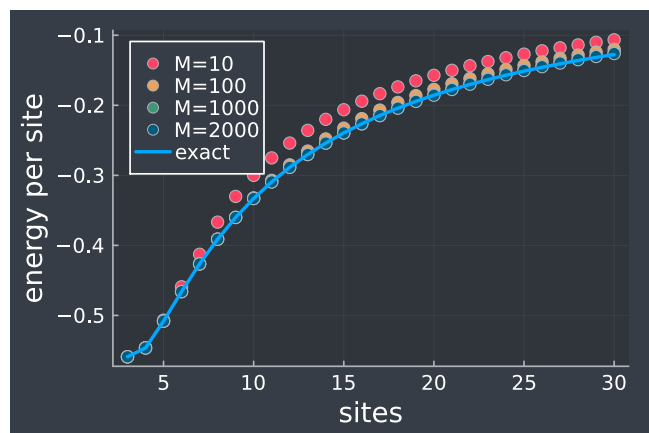
We are in general interested in n -point correlations of the form $\langle \mathcal{O}_1 \mathcal{O}_2 \dots \mathcal{O}_n \rangle$, where \mathcal{O}_i are operators that act on 1-particle Hilbert spaces. Let the earliest step of the iterative diagonalisation procedure at which all these operators have entered the system be r . At this step r , construct the correlation operator $\mathcal{O}_1 \mathcal{O}_2 \dots \mathcal{O}_n$ using the fermionic matrices c_j at that step (recall that these matrices will be highly rotated versions of the matrices we started with). Having constructed the operator O , we expand and rotate it after the completion of every future step: $O_{n+1} = (R_n^\dagger O_n R_n) \otimes \mathbb{I}(2^{L_\Delta})$, where R_n is the rotation matrix for the n^{th} step. The last step n^* of the iterative diagonalisation consists of only a diagonalisation and no expansion, resulting in a final set of eigenstates $\{X_i\}$. The form of the correlation operator in this basis is $O_{n^*} = R_{n^*-1}^\dagger O_{n^*-1} R_{n^*}$. The expectation value can now be calculated using the matrix O_{n^*} and the ground state of $\{X_i\}$.

2.14 Examples and Benchmarks

2.14.1 Single-Impurity Anderson Model

The single-impurity Anderson model at half-filling is obtained by setting $H_{\text{imp}} = -\frac{U}{2} (n_{d\uparrow} - n_{d\downarrow})^2$ and $H_{\text{imp-bath}} = -V \sum_\sigma (c_{d\sigma}^\dagger c_{0\sigma} + \text{h.c.})$ in eq. 2.258. We studied this model using the above approach to benchmark the ground state energy and spin-flip correlation $\langle \frac{1}{2} S_d^+ S_0^- + \text{h.c.} \rangle$ against exact diagonalization (ED). In order to extend the ED to a larger number of sites, we restricted ourselves to just the $N = 2$ sector, N being the total occupancy. We find very good agreement for $M_s \sim$

1000 and above. These results are shown in Fig. ??.



occupied
component

particle
fluctua

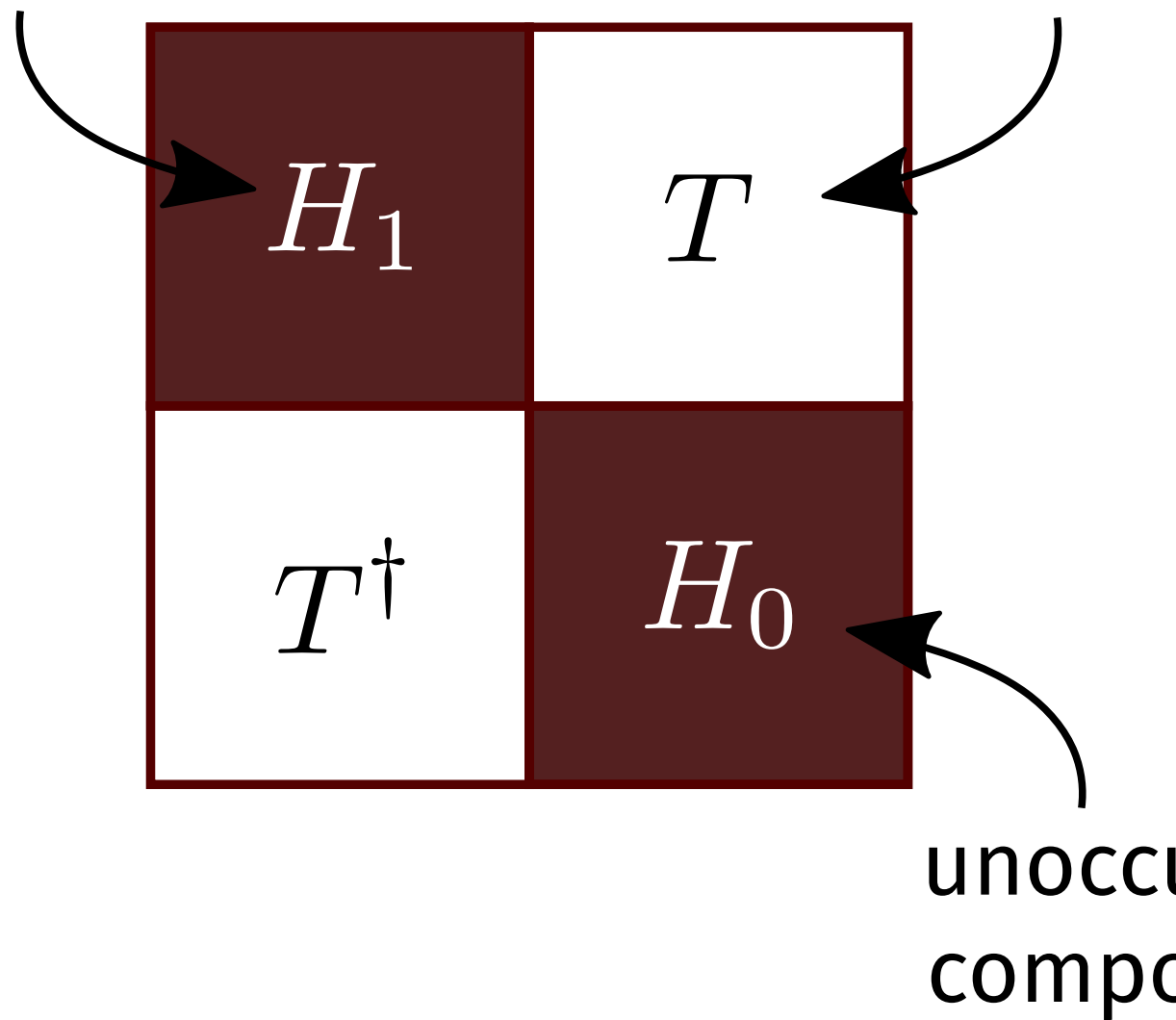




Figure 2.3: Left: RG flow for the two cases. The green line is the distance between the bare values of the two couplings, and hence also the magnitude of the denominator. The red arrow denotes the direction in which ϵ_0 will flow. Upward flow is increase. In both cases, the flow is such that the distance between the two quantities (and hence the magnitude of the denominator) increases. The RG fixed point occurs when the magnitude of the denominator goes to 0. This happens if the distance vanishes. Since the distance necessarily increases, we cannot get a fixed point in this way. Right: RG flow for the two cases with the new $-\tilde{\omega} = \omega' - \frac{1}{2}\epsilon + \frac{1}{4}J$. Now we can see that in both cases, the flow is such that the distance (green dotted line) between the couplings decreases. A fixed point is reached when this distance vanishes.

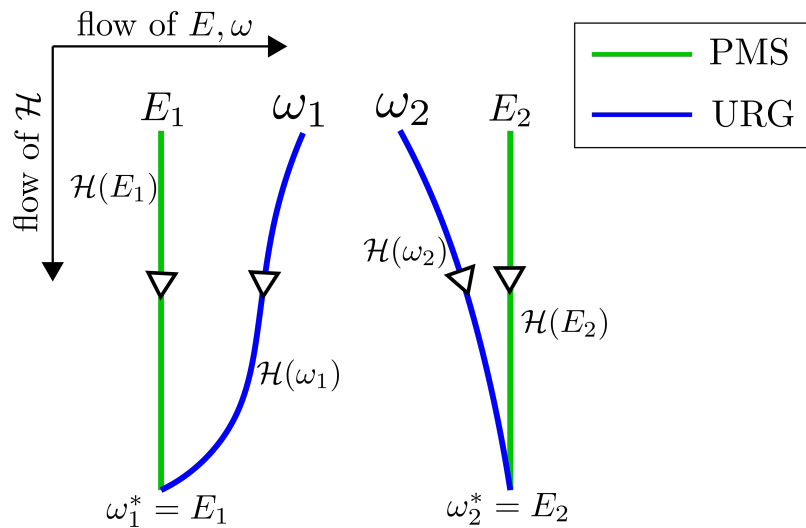


Figure 2.6: Flows of PMS(green) and URG(blue)

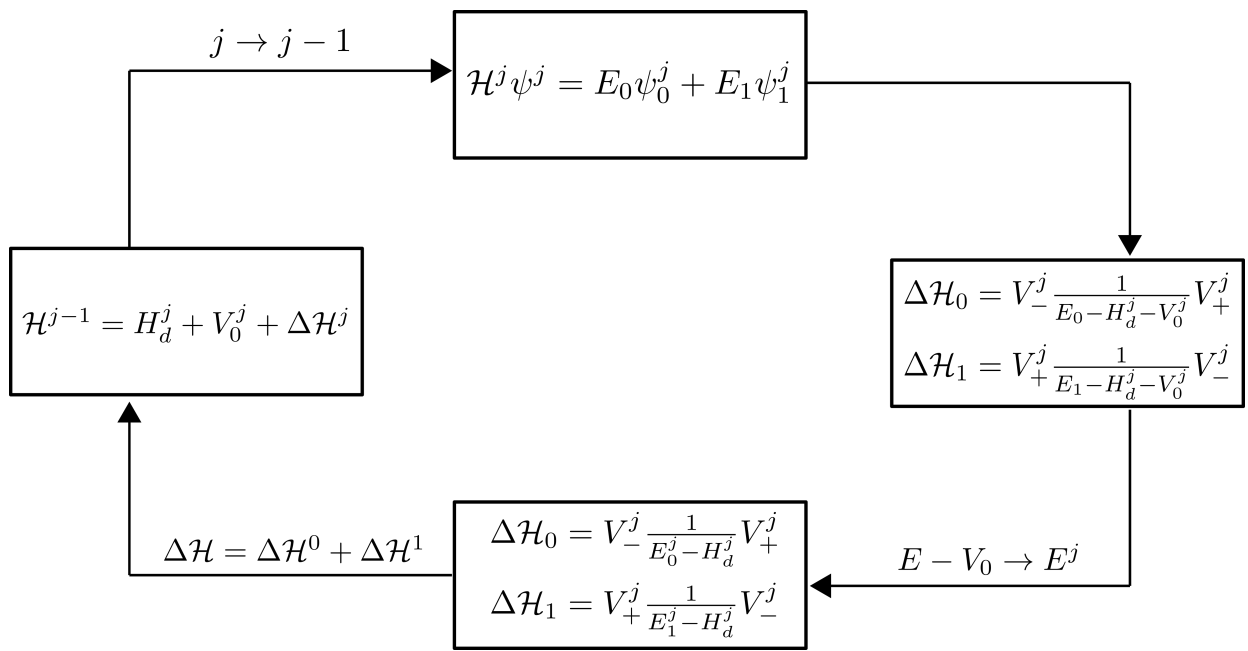


Figure 2.7: Flow chart of "Poor Man's" scaling algorithm

Chapter 3

Entanglement RG

3.1 Introduction

The present millennium has seen a rapid surge in the use of quantum entanglement towards the study of quantum and condensed matter systems [15–20]. By tracking quantum correlations among particles across both small and large distances, entanglement measures offer valuable insights into the nature of the ground state and low-energy excitations. This, for example, allows us to distinguish strongly-correlated topologically ordered states characterised by long-ranged entanglement (in the form of a sub-leading topological term in their entanglement entropy [21–24]) from weakly-interacting topologically trivial phases that have short-ranged area-law entanglement [17, 25, 26].

More pertinent to the present work is the entanglement of non-interacting relativistic fermionic systems. Such phases are known to emerge in several condensed matter systems [27], appearing at the surfaces of three-dimensional topological insulators [28–31], quasi-2D organic materials [32–34] and in artificial quantum simulators such as cold atom gases, molecular and microwave crystals [35–41]. Massless critical systems (or conformal field theories (CFTs)) differ from gapped systems due to the fact that their entanglement satisfies a modified area law; in one spatial dimension, the entanglement entropy (S) of a single subsystem of length l scales as $S \sim \frac{c}{3} \ln l$ [42–46], where c is the conformal central charge of the CFT. This violation arises from the non-local nature of the gapless quantum fluctuations that lie proximate to the $d - 1$ -dimensional Fermi surface of a quantum critical fermionic system in d spatial dimensions. For massive fermions, an entropic c –function (spatial derivative of the entanglement entropy) can be expressed in the form of differential equations that need to be solved numerically [47–50].

Unlike topologically ordered phases, there is no geometry-independent topological term in the entanglement entropy of free fermionic systems [51, 52]. It is, however, possible to generate such a term even here by placing the system on a multiply connected manifold such as a cylinder, and inserting a magnetic flux through the cylinder [51, 53–56]. It has been shown that if there are ϕ number of electronic flux quanta piercing the system, an additional term is generated in the entanglement entropy of a subsystem of massless Dirac fermions of sufficiently large length (as defined in Ref. [51]) with the form $\frac{1}{6} \ln |2 \sin \frac{\phi}{2}|$ [51, 54]. Further, there is evidence from numerical computations on discrete models that such a term is a signature of the specific field theory and encodes universality [56–58].

The notion of entanglement also plays a key role in the context of holographic duality, which posits that there exists a duality relation between a quantum field theory in d –spatial dimensions and a gravity theory in $d + 1$ –spatial dimensions [59–65]. It is widely believed that the additional dimension can

be visualised as a renormalisation group flow that starts from the (almost) critical field theory on the boundary and extends into the bulk [66–75]. The most popular realisation of the holographic principle is the AdS/CFT correspondence that links a conformal field theory with a theory of quantum gravity through a strong-weak duality relation [76–83]. This has led to new insights in various areas of high energy and condensed matter physics, such as the viscosity of the quark-gluon plasma [84], the response functions of the Bose-Hubbard model [85, 86], and the phenomenology of non-Fermi liquids [87–90], holographic superconductors [91–96], striped phases [97–99] and holographic Fermi liquids [100–104].

Conversely, the holographic principle also implies that studying the boundary conformal theory can provide insights into the nature of the bulk quantum gravity theory. This requires constructing the emergent dimension from first principles by investigating the RG flow of the (often strongly coupled) quantum field theory, and has proved to be considerably more difficult. Nevertheless, there exist some examples of constructive attempts towards a bulk gravity theory, including [1, 2, 105–112]. These include the momentum-shell renormalisation approach of Refs. [107, 108, 113, 114], the multi-scale entanglement renormalisation ansatz (MERA) approach of Refs. [109–112, 115], the exact holographic mapping (EHM) [116, 117], the Wilsonian RG-based approach of Ki-Seok Kim [118–120] and the unitary renormalisation group (URG) approach [1, 2, 121].

Questions on entanglement and holography become particularly interesting in systems of critical fermions. As mentioned earlier, such systems differ from bosonic and gapped systems through the presence of longer-ranged entanglement that follows a modified area-law [46, 122] as well as topological features arising from the incompressibility of the Fermi volume [123, 124]. Fermi surface gapping phase transitions in such systems are often driven by changes in topological quantum numbers and the nature of the inter-particle entanglement [1, 2, 125]. Constructing a framework for fermionic criticality is therefore an active area of research with consequences for important systems such as unconventional superconductors, strange metals and heavy fermions [3, 4, 126, 127]. Still less is known about the holographic implications of such systems. We extend this body of work by providing an explicit demonstration of the holographic principle in the form of a simple and tractable exact holographic mapping (EHM) for a free fermion system with and without a mass gap. Our program yields analytic relations between the RG flow parameters and their dual bulk quantities such as distances and curvature. This also allows us to study the consequences of a critical Fermi surface (lying precisely at the quantum phase transition) on the nature of the holographic space.

We first briefly describe the strategy employed in the present work. (i) We perform a set of scaling transformations T_j (corresponding to a step index j) on the set of k -states in the Hilbert space of our system of fermions, and we show that the renormalisation of entanglement measures along the sequence of Hamiltonians $T_j^\dagger H_j T_j$ constitutes an emergent additional spatial dimension. (ii) By employing the mutual information between multiple subsets of the Hilbert space, we define a measure of distance that is used to obtain holographic relations between boundary and bulk quantities. Additional results are obtained upon further analysis of the entanglement and these holographic relations. The approach presented in this work is similar in spirit to other renormalisation group approaches that apply decoupling transformations on the Hamiltonian, such as the continuous unitary transformation (CUT) RG [14, 128–130], the strong-disorder RG [131, 132] and the spectrum-bifurcation RG [133]. As the system we consider is non-interacting, the scaling transformations implemented in this work do not lead to the decoupling of states, and only result in the coarse-graining of the system in momentum space, through non-local transformations.

The manuscript is structured in the following manner. Sec. 3.2 describes the system we work with and defines certain physical ideas and measures of entanglement that are employed in later sections.

In Sec. 3.3, we define the scaling transformations mentioned earlier, and discuss its implications on the scaling of entanglement in the system under study. In Sections 3.4, 3.5 and 3.6, we probe the holographic nature of the entanglement, unveiling an emergent spatial dimension in the process and obtain several characteristics of this emergent geometry. Section 3.7 discusses the consequences of a critical Fermi surface on the holographic space, and how the emergent curvature can be linked to a convergence parameter associated with the RG flows. In Section 3.9, we probe the topological aspects of the entanglement, and discuss its implications for the system at hand. We conclude with a discussion of our results in Sec. 3.10 and point out some open questions.

Summary of our main results

For the convenience of the reader, we present below a summary of the main results obtained by us.

1. Quantum information measures (such as entanglement entropy and multipartite information) reveal a hierarchical structure in the nature of entanglement within the system. We relate geometric parameters like distance and curvature of the holographic dimension to an RG beta function of the mass gap, providing thereby an explicit analytic manifestation of the holographic principle. We show that a change in the boundedness of the space corresponds to a change in certain topological winding numbers.
2. We go on to argue that this topological transition and the underlying critical Fermi surface coincides with the formation of a quantum wormhole geometry that connects the UV and the IR of the emergent dimension. The additional (conformal) symmetry at the transition links the emergent metric and the stress-energy tensor.
3. We show that the geometry-independent part of the entanglement is invariant under appropriate scaling transformations for a system of fixed number density, and is related to the Luttinger volume of the gapless fermionic system. In the presence of a strong transverse magnetic field, the topological Luttinger volume in the metallic state transforms into the Chern number \mathcal{C} of the insulating integer quantum Hall state.

3.2 Preliminaries and definitions

3.2.1 The system

In this work, we focus on the case of Dirac fermions in two spatial dimensions described by the Lagrangian (in natural units $\hbar = c = 1$) $\mathcal{L} = \int dx dy \bar{\psi}(x, y, t) (i\gamma^\mu \partial_\mu - m) \psi(x, y, t)$. The system is placed on a 2-torus of dimensions $L_x \times L_y$ with periodic boundary conditions, such that $\psi(x, y, t) = \psi(x + L_x, y, t) = \psi(x, y + L_y, t)$. Entanglement measures will be calculated in the presence of a gauge field A that transforms the Lagrangian by shifting the momenta: $i\partial_\mu \rightarrow i\partial_\mu + eA$. We choose the vector potential A such that, in any particular setup, it couples to just one component of the momentum (say, the x -component). This results in $\phi = eAL_x/2\pi$ units of flux quantum threading the torus in the y -direction. One of our goals is to express the Luttinger volume V_L in terms of multi-partite measures of entanglement $(I_{\{\mathcal{A}_i\}}^g(\phi))$ between multiple subsystems $\{\mathcal{A}_i, i = 1, 2, \dots, g\}$ [136], in the presence of the flux ϕ . The precise definition of I^g and the method of choosing the subsystems will be given later. In order to calculate $I_{\{\mathcal{A}_i\}}^g$, however, we find it convenient to take the thin torus limit: $(L_y/L_x) \rightarrow \infty$,

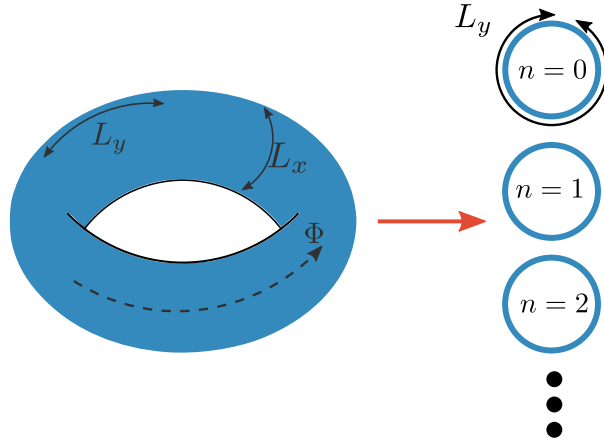


Figure 3.1: The model on the left consists of a system of non-interacting electrons placed on a torus with a flux threading through it. The model on the right consists of a sum of $1 + 1$ -dimensional systems, each consisting of massive electrons placed on a ring; the $1 + 1$ -D systems are decoupled from each other. The mass arises from the flux. These two models can be shown to be equivalent to each other [51, 54, 134, 135].

keeping l/L_y fixed. Importantly, this operation does not affect quantities such as V_L as long as we keep the number density unchanged.

In order to calculate entanglement measures, we will express the $2 + 1$ -dimensional system as a sum of an infinite number of massive $1 + 1$ -dimensional systems [51, 54, 134, 135]. In the presence of a gauge field $\vec{A} = A\hat{x}$, the complete Lagrangian (in natural units) is

$$\mathcal{L} = \int dx dy \bar{\psi}(x, y) [\gamma^\mu (i\partial_\mu + eA_\mu) - m] \psi(x, y), \quad (3.1)$$

where $A_\mu = A\delta_{\mu,x}$ and $\phi = eAL_x/2\pi$. The integral ranges over the surface area of the torus, and the time dependence of the fields has been suppressed. Due to the periodic boundary conditions (PBCs) in the x -direction, the momenta k_x are quantised: $k_x^n = \frac{2\pi n}{L_x}$, $n \in \mathbb{Z}$. We then expand the fields $\psi(x, y)$ in these momenta:

$$\psi(x, y) = \sum_{n=-\infty}^{\infty} e^{ik_x^n x} \psi(k_x^n, y). \quad (3.2)$$

In terms of these dual fields, the Lagrangian can be shown to be equivalent to a tower of massive $1 + 1$ -dimensional fermions (see Fig. 3.1). Details are provided in Appendix 3.10:

$$\mathcal{L} = \sum_{k_x^n} \int dy \bar{\psi}(k_x^n, y) (i\gamma^\mu \partial_\mu - M(n, \phi)) \psi(k_x^n, y), \quad (3.3)$$

with an effective mass $M_{n,\phi}$ given by

$$M_{n,\phi} = \sqrt{m^2 + (k_x^n + eA)^2} = \sqrt{m^2 + \frac{4\pi^2}{L_x^2} (n + \phi)^2}. \quad (3.4)$$

This decoupling ensures that the various modes $n \in \mathbb{Z}$ are disentangled from one another, such that the total density matrix ρ_{2D} of the $2 + 1$ -dimensional system can be written as a product of the density

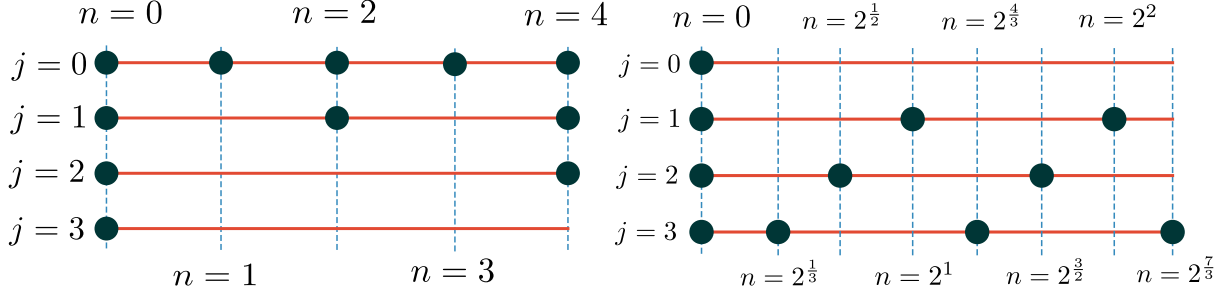


Figure 3.2: Visual depiction of the subsets $\mathcal{A}_z(j)$ employed by us in this work, for $z = 1$ and $z = -1$. As j is changed by 1, the spacing between the modes in the subset increases by a factor of 2^{j^z} . *Top:* $z = 1$. The initial subset $\mathcal{A}_z(0)$ has k -states at the modes $n = 0, 1, 2, 3, 4$. Upon changing j by 1, the new subset obtained has double the spacing between the modes ($2^{j^z} = 1/2^j$) of the previous number of modes. That is, if $j = 0$ has 0, 1, 2, 3, 4, then $j = 1$ has 0, 2, 4, $j = 2$ has 0, 4 and $j = 3$ has 0. *Bottom:* $z = -1$. In this case, the number of modes get double at each state ($2^{-i^z} = 2^i$). We start with k -modes present only at $n = 0$, but the scaling transformations lead to $j = 1$ having the modes 0, 4, $j = 2$ having 0, 2, 4, and so on.

matrices ρ_{1D}^n for each of the modes:

$$\rho_{2D} = \prod_{n=-\infty}^{\infty} \rho_{1D}^n. \quad (3.5)$$

We will focus primarily on the case of massless $2 + 1$ -dimensional electrons by setting $m = 0$, such that the effective mass is given by $M_{n,\phi} = \frac{2\pi}{L_x}|n + \phi|$. Certain results will, however, be generalised to the case of massive fermions ($m \neq 0$). While the massless case corresponds to the gapless excitations of a Fermi liquid or those at the surface of a topological insulator, the massive case corresponds to gapped or insulating states of matter, e.g., the Bogoliubov-de Gennes quasiparticles above an s -wave superconducting gap. Massive Dirac fermions have also been observed experimentally in several materials like ultrathin films [137], topological insulating crystals [138] and van der Waals heterostructures [139]. They are also emergent at low-energies, for instance, in fermionic nonlinear σ -models [140], and can also be realised near the IR fixed point of the kagome Heisenberg quantum antiferromagnets placed in an external magnetic field along the z -direction [141].

3.2.2 Entanglement measures

We will work with two measures of entanglement discussed below. Given the density matrix $\rho = |\Psi\rangle\langle\Psi|$ for the ground state $|\Psi\rangle$ of the complete system, the entanglement entropy (EE) of a set of subsystems $\{\mathcal{A}_i, i = 1, 2, \dots, g\}$ with the rest of the system is given by:

$$S_{\{\mathcal{A}_i\}} = -\text{Tr} [\rho_{\{\mathcal{A}_i\}} \ln \rho_{\{\mathcal{A}_i\}}]; \quad \rho_{\{\mathcal{A}_i\}} = \text{Tr}_{\{\mathcal{A}_i\}} [\rho]. \quad (3.6)$$

$\text{Tr} [\cdot]$ is the trace operation over all degrees of freedom, while $\text{Tr}_{\{\mathcal{A}_i\}} [\cdot]$ is the partial trace over only the states corresponding to the set of subsystems $\{\mathcal{A}_i\}$. $\rho_{\{\mathcal{A}_i\}}$ is referred to as the reduced density matrix for the rest of the system (complement of the set $\{\mathcal{A}_i\}$). Using EE, one can define the mutual information $I(\{\mathcal{A}_i\} : \{\mathcal{B}_i\})$ between two subsystems A and B :

$$I_2(\{\mathcal{A}_i\} : \{\mathcal{B}_i\}) = S(\{\mathcal{A}_i\}) + S(\{\mathcal{B}_i\}) - S(\{\mathcal{A}_i\} \cup \{\mathcal{B}_i\}), \quad (3.7)$$

where $S(\{\mathcal{A}_i\} \cup \{\mathcal{B}_i\})$ is the EE of $\{\mathcal{A}_i\} \cup \{\mathcal{B}_i\}$ with the rest. Higher order measures of information among N subsystems can also be defined similarly (see, e.g., [136]). Such multi-partite measures of quantum information convey the degree of correlations present within the system - the presence of N -particle correlations ensures all information measures up to the N -partite information will be non-zero.

One final object of interest in this context is the entanglement Hamiltonian $\mathcal{H}(\{\mathcal{A}_i\})$ for a subsystem $\{\mathcal{A}_i\}$, defined through the relation [142, 143]

$$\rho_{\{\mathcal{A}_i\}} = \frac{e^{-\mathcal{H}(\{\mathcal{A}_i\})}}{\text{Tr}(e^{-\mathcal{H}(\{\mathcal{A}_i\})})}. \quad (3.8)$$

The entanglement Hamiltonian is essentially the spectrum of the reduced density matrix, and contains additional information on the nature of correlations beyond the entanglement entropy. For the system we are considering (described in the previous subsection), the total reduced density matrix can be decomposed into decoupled 1D modes (eq. (3.5)). This implies that the total entanglement Hamiltonian is simply a sum of the individual Hamiltonians for the 1D modes:

$$\rho_{2D} = \prod_{n=-\infty}^{\infty} \rho_{1D}^n \sim \prod_{n=-\infty}^{\infty} e^{-\mathcal{H}_{1D}^n(\{\mathcal{A}_i\})} = e^{-\mathcal{H}_{2D}(\{\mathcal{A}_i\})}, \quad (3.9)$$

where $\mathcal{H}_{2D} = \sum_n \mathcal{H}_{1D}^n$.

3.2.3 Luttinger volume

The Luttinger volume V_L is defined as the number of \vec{k} -space points inside the Fermi surface [144, 145] :

$$V_L = \int_{G_{\vec{k}}(\omega=0)>0} \frac{1}{(2\pi)^d} d\vec{k} = \int_0^{k_F} \frac{1}{(2\pi)^d} d\vec{k}. \quad (3.10)$$

The integral (referred to as Luttinger's integral) runs over all \vec{k} -space points where the $\omega = 0$ Greens function is positive, and the Fermi momentum k_F is defined as the set of points in \vec{k} -space where $G_{\vec{k}}(\omega = 0)$ changes sign. Luttinger's integral can be shown to be topological in nature [123, 124], promoting Luttinger's volume to the status of a topological invariant that characterises the system. For systems with long-lived excitations close to the Fermi surface, V_L is equal to the average number density of electrons in the system, leading to Luttinger's theorem [144–146]. For systems with gapped excitations in the momentum window $k \leq k^*$ above the ground state, the violation ΔV_L of Luttinger's theorem can be quantified through a count of the bound states [1]:

$$\Delta V_L = \int_0^{k_F} \frac{1}{(2\pi)^d} d\vec{k} - \int_{k^*}^{k_F} \frac{1}{(2\pi)^d} d\vec{k} = \int_0^{k^*} \frac{1}{(2\pi)^d} d\vec{k} \quad (3.11)$$

3.3 Entanglement hierarchy in mixed momentum and real space

Before beginning our calculations of entanglement measures, we define the subsystem(s) whose entanglement we want to obtain. The subsystems we will use in this work are of the following kind:

$$\mathcal{A}_z(i) = \tilde{A}_z(i) \times A_z(i), \quad (3.12)$$

where i takes integral values starting from zero, z can take all integral values apart from 0 and \times represents the Cartesian product between the set of real space points $\tilde{A}_z(i) = \{0 \leq y \leq l\}$ and the set of momentum space points

$$A_z(i) = \left\{ k_x^n \right\}; k_x^n = \frac{2\pi}{L_x} n; \max(\{k_x^n\}) = \frac{2\pi N}{L_x}; \\ n \in \{-N, -N + t_z(i), \dots, -t_z(i), 0, t_z(i), N\}; t_z(i) = 2^{i^z}, \quad (3.13)$$

and where $t_z(i) = 2^{i^z}$ is the difference between consecutive values of n . The subset $A_z(i)$ is therefore a region in mixed momentum and real spaces, spanned by the variables k_x and y respectively. In y -space, the region is of length l and bounded by the points $y = 0$ and $y = l$. In k_x -space, $A_z(i)$ comprises the points $\left\{ 0, \pm 2^{i^z} \frac{2\pi}{L_x}, \pm 2^{i^z} \frac{4\pi}{L_x}, \dots \right\}$ such that $|k_x| \leq \frac{2\pi N}{L_x}$. For example, for the case of $z = 1$ and N being a multiple of 4, we have

$$A_1(0) = \left[-\frac{2\pi}{L_x} N, -\frac{2\pi}{L_x} (N-1), \dots, -\frac{2\pi}{L_x} 2, -\frac{2\pi}{L_x} 1, 0, \frac{2\pi}{L_x} 1, \frac{2\pi}{L_x} 2, \dots, \frac{2\pi}{L_x} (N-1), \frac{2\pi}{L_x} N \right], \\ A_1(1) = \left[-\frac{2\pi}{L_x} N, -\frac{2\pi}{L_x} (N-2), \dots, -\frac{2\pi}{L_x} 4, -\frac{2\pi}{L_x} 2, 0, \frac{2\pi}{L_x} 2, \frac{2\pi}{L_x} 4, \dots, \frac{2\pi}{L_x} (N-2), \frac{2\pi}{L_x} N \right], \\ A_1(2) = \left[-\frac{2\pi}{L_x} N, -\frac{2\pi}{L_x} (N-4), \dots, -\frac{2\pi}{L_x} 8, -\frac{2\pi}{L_x} 4, 0, \frac{2\pi}{L_x} 4, \frac{2\pi}{L_x} 8, \dots, \frac{2\pi}{L_x} (N-4), \frac{2\pi}{L_x} N \right]. \quad (3.14)$$

Note that N represents the edge of the Brillouin zone, and will be sent to infinity when we calculate quantities in the continuum limit. In Fig. 3.2, we have shown two such families of subsets $A_z(0), A_z(1), A_z(2), A_z(3)$ for $z = 1$ and $z = -1$.

We note here that the transformations for $z < 0$ correspond to increasing the density (fine-graining) of k_x -states by adding more momentum states while keeping the bounds fixed. This involves reducing the interval in k_x -space, and hence equivalent to increasing the system size L_x . This is similar to methods such as numerical renormalisation group treatment of the Kondo problem [147] where an increasing number of states are added to the system at increasingly larger distances from the impurity site, such that the system asymptotically goes to the thermodynamic limit. The other case of $z > 0$ is, on the contrary, a decimation process in k_x -space, and equivalent to reducing the system size. Indeed, it will be shown later that the sequence of Hamiltonians generated in the process (for both positive and negative z) are related to one other by renormalisation group transformations.

Within a given set $A_z(i)$, the distance between adjacent k -space points is $\frac{2\pi}{L_x} t_z(i)$ where $t_z(i) = 2^{i^z}$. Choosing $i = 0$ keeps the set of k_x -space points unchanged, such that we recover the entire Lagrangian of eq. (3.1) in the x -direction for system size L_x , while the y -direction is constrained to length l . This means that $A_z(0)$ is just an annulus that wraps around the x -direction of the torus and extends to a length l longitudinally in the y -direction (shown in Fig. 3.3). Along with the period $t_z(i)$, one can also define the fraction of maximum points present in the set $A_z(i)$ as

$$f_z(i) = 1/t_z(i) = 2^{-i^z}. \quad (3.15)$$

For example, for $z > 0$, $f_z(i) = 2^{-i^z}$ expresses the fact that in going from the set at $j = 0$ to the set at $j = i$, the number of elements in the set is scaled down by a factor of 2^{i^z} (see Fig. 3.4).

We now define the shorthand notation $S_z(i)(\phi) \equiv S_{A_z(i)}(\phi)$ to denote the EE of the subsystem $A_z(i)$ in the presence of the Aharonov-Bohm flux ϕ . In order to calculate $S_z(i)$, we start with $i = 0$. As

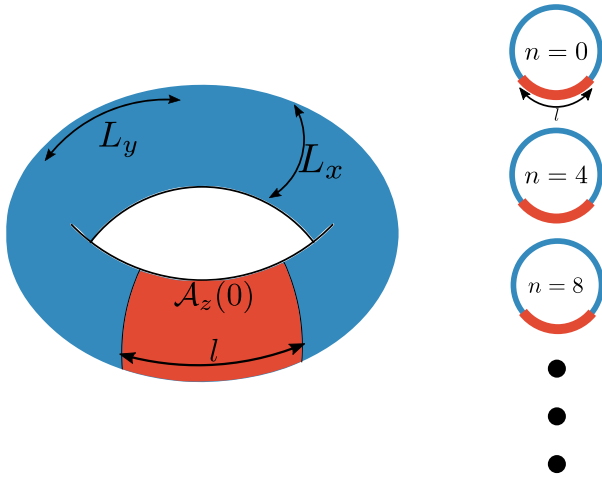


Figure 3.3: *Top:* Depiction of the subset $\mathcal{A}_z(i)$ for the choice $i = 0$. Setting $i = 0$ leads to unchanged length L_x along x and the constraint $0 \leq y \leq l$ in the y -direction. This creates an annulus (red region) of height l and circumference L_x .

Bottom: Typical k -modes present in the subset $\mathcal{A}_z(i)$ for $z = 1$ and $i = 2$. This is because, if $i = 0$ has the modes $n = 0, 1, 2, 3, 4, \dots$, increasing i by 2 increases the spacing between the modes to $2^{2z} = 4$, so that the mode just after $n = 0$ is $n = 4$, and the one following that is $n = 8$, and so on.

mentioned earlier, this is essentially the EE between an annulus of length l and the rest of the 2-torus. Since the density matrices are in product, the total EE is just a sum of the EE arising from each mode:

$$S_{\mathcal{A}_z(0)}(\phi) \equiv S_z(0)(\phi) = \lim_{N \rightarrow \infty} \sum_{n=-N}^N S_{\tilde{\mathcal{A}}_z(0)}^n, \quad (3.16)$$

where $\tilde{\mathcal{A}}_z(0)$ acts as a projection of the annulus on the $k_x - y$ plane, and S^n indicates that the EE is calculated for the n^{th} mode. Each massive fermionic mode has a correlation length-scale $\xi_n = 1/M_{n,\phi}$. We choose l to be much larger than the largest correlation length: $l \gg \max(\{\xi_n, \forall n\})$. Using the expression for ϕ and the quantisation of the momenta k_x^n , this condition can be expressed as

$$l \gg \frac{L_x}{2\pi} \times \max \left(\left\{ \frac{1}{|n + \phi|} \right\} \right) = \frac{L_x}{2\pi \{\phi\}}, \quad (3.17)$$

where $\{\phi\} = \phi - \lfloor \phi \rfloor$ is the fractional part of the flux ϕ in units of the flux quantum. Since we are in the thin torus limit, L_x must remain finite, and the maximum correlation can diverge only if $\{\phi\} = 0$. We ensure that l is larger than the correlation lengths by choosing ϕ to be necessarily non-integral, as this guarantees that the correlation lengths remain finite. Then, the EE of the annulus is given by [51, 54]

$$S_z(0)(\phi) = c \left[\alpha \frac{L_x}{\epsilon} - \ln |2 \sin(\pi \phi)| \right], \quad (3.18)$$

where c is the conformal central charge and ϵ is a UV cutoff; c is $1/3$ for a Dirac fermion. The computation of $S_z(0)(\phi)$ uses the EE $S_{\tilde{\mathcal{A}}_z(0)}^n$ of a 1-D chain of fermions with a mass $M_{n,\phi}$ [45, 148]: $S_{\tilde{\mathcal{A}}_z(0)}^n = c \ln \frac{L_x}{2\pi\epsilon} - c \ln |n + \phi|$. On summing over n and regularising the UV cutoff, the first term of eq.(3.18)

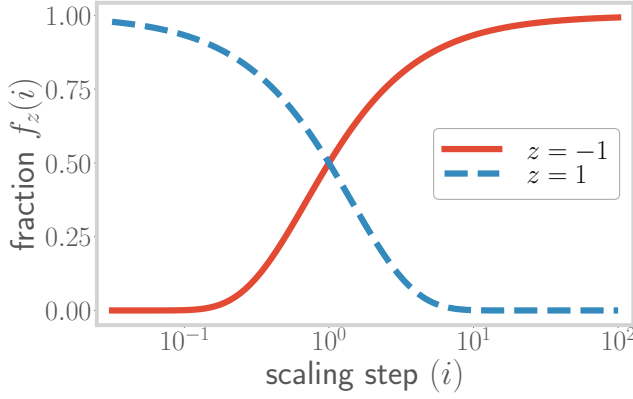


Figure 3.4: A plot of the fraction of states remaining upon performing i number of transformations on the starting Hamiltonian. Obtained by plotting the expression $f = 2^{-iz}$, for a range of i , and for two values of z (red and blue). This fraction decreases for $z > 0$ (blue curve), and increases for $z < 0$ (red curve).

produces the leading area-law term of $S_0(\phi)$ [51]:

$$\sum_{n=-\infty}^{\infty} c \ln \frac{L_x}{2\pi\epsilon} \rightarrow c\alpha \frac{L_x}{\epsilon}, \quad (3.19)$$

where α is a cutoff-dependent non-universal constant. The flux-dependent term in $S_{A_z(0)}^n$ leads to the sub-leading term of $S_z(0)(\phi)$, and requires a regularisation using the Hurwitz zeta function [51]:

$$\begin{aligned} \sum_{n=-\infty}^{\infty} \ln |n + \phi| &= \sum_{n=-\infty}^{\infty} [\ln |n + \phi| + \ln |n + (1 - \phi)|] \\ &= -\frac{\partial \zeta(\phi)}{\partial \phi} - \frac{\partial \zeta(1 - \phi)}{\partial \phi}, \end{aligned} \quad (3.20)$$

where $\zeta(\phi) = \sum_{n=-\infty}^{\infty} (n + \phi)^{-1}$ is the Hurwitz zeta function. The derivative converges to $\frac{\partial \zeta(\phi)}{\partial \phi} = \ln \Gamma(\phi) - \frac{1}{2} \ln 2\pi$, as long as the zero mode $n + \phi = 0$ is excluded from the summation. The latter condition is guaranteed as we have chosen ϕ to be a non-integer. Γ is the Gamma function, satisfying $\Gamma(\phi)\Gamma(1 - \phi) = \pi / \sin(\pi\phi)$. Substituting the derivative gives [51, 54, 58]

$$\sum_{n=-\infty}^{\infty} \ln |n + \phi| = \ln 2\pi - \ln [\Gamma(\phi)\Gamma(1 - \phi)] = \ln |2 \sin(\pi\phi)|. \quad (3.21)$$

For a general $\mathcal{A}_z(i)$, there are certain modifications to the expression in eq. (3.18). For the first term in eq.(3.18), we have

$$\begin{aligned} \lim_{N \rightarrow \infty} \sum_{\substack{n=-N, \\ -N+tz(i), \dots}}^N c \ln \frac{L_x}{2\pi\epsilon} &= \lim_{N \rightarrow \infty} \sum_{\substack{n'=-\frac{N}{tz(i)}, \\ -\frac{N}{tz(i)}+1, \dots}}^{\frac{tz(i)}{N}} c \ln \frac{L_x}{2\pi\epsilon} \\ &= t_z^{-1}(i) \lim_{N \rightarrow \infty} \sum_{n=-N}^N c \ln \frac{L_x}{2\pi\epsilon} \rightarrow cf_z(i) \frac{\alpha L_x}{\epsilon}. \end{aligned} \quad (3.22)$$

Similarly, for the second term, we have

$$\begin{aligned}
& \lim_{N \rightarrow \infty} \sum_{\substack{n=-N, \\ -N+t_z(i), \dots}}^N \ln |n + \phi| \\
&= \lim_{N \rightarrow \infty} \sum_{\substack{n'=-\frac{N}{t_z(i)}, \\ -\frac{N}{t_z(i)}+1, \dots}}^{\frac{N}{t_z(i)}} \ln |n't_z(i) + \phi| \\
&= \lim_{N \rightarrow \infty} \sum_{\substack{n'=-\frac{N}{t_z(i)}, \\ -\frac{N}{t_z(i)}+1, \dots}}^{\frac{N}{t_z(i)}} \ln (f_z(i)|n' + f_z(i)\phi|) \\
&= \sum_{n'=-\infty}^{\infty} \ln |n' + f_z(i)\phi| ,
\end{aligned} \tag{3.23}$$

where we have assumed that $t_z(i)$ is finite, and dropped the constant part $\ln f_z(i)$ (which can be absorbed into the UV cutoff ϵ in eq. (3.22)). Following eq. (3.21), this gives

$$\lim_{N \rightarrow \infty} \sum_{\substack{n=-N, \\ -N+t_z(i), \dots}}^N \ln |n + \phi| = \ln |2 \sin (\pi f_z(i)\phi)| . \tag{3.24}$$

Combining both parts, we obtain the expression for the EE that will be employed in what lies ahead:

$$S_z(i)(\phi) = c f_z(i) \frac{\alpha L_x}{\epsilon} - c \ln |2 \sin (\pi f_z(i)\phi)| . \tag{3.25}$$

It is evident from the expression in eq. (3.25) that, as modes are added into the subsystem, the L_x -dependent geometric part of the EE increases, leading to a *hierarchical structure* in the entanglement. A similar result was previously shown to hold for geometric measures of entanglement of quantum-mechanical systems with eigenstates such as the W and GHZ states and their symmetric superpositions [149]. The variation of the geometric part with the subsystem index j is shown in Fig. 3.4.

The above-mentioned hierarchy in entanglement measures leads to an interesting property for the entanglement: the combined entanglement entropy of any number of systems $\{\mathcal{A}_z(i)\}$ is equal to the entanglement entropy of the most dense system among them. For $z > 0$, the sets become smaller as the RG index increases, while for $z < 0$, the sets become larger as the RG index increases. Thus, we may write

$$S_{\{\mathcal{A}_z(i)\}} = \theta(z) S_{\min\{i\}, z} + \theta(-z) S_{\max\{i\}, z} , \tag{3.26}$$

The mutual information $I^2(i, j)$ between the systems at two RG steps i and j can then be computed:

$$\begin{aligned}
I^2(i, j) &\equiv S_z(i) + S_{j,z} - S_{i \cup j, z} \\
&= \theta(-z) S_{\min(i,j), z} + \theta(z) S_{\max(i,j), z} .
\end{aligned} \tag{3.27}$$

In light of this subsystem-based hierarchical structure, we can also consider the g -partite information $I_{\{\mathcal{A}_z(i)\}}^g$ among g sets $\{\mathcal{A}_z(i)\}$. I^g is defined as [136]

$$I_{\{\mathcal{A}_z(i)\}}^g = \sum_{r=1}^g (-1)^{r+1} \sum_{\substack{\beta \in \mathcal{P}(\{\mathcal{A}_z(i)\}) \\ |\beta|=r}} S_\beta , \quad (3.28)$$

where $\mathcal{P}(\{\mathcal{A}_z(i)\})$ is the power set of $\{\mathcal{A}_z(i)\}$, and $|\beta| = r$ indicates that the sum is carried out only over those sets β that have r number of elements in them. For example, for $g = 3$, we have

$$\begin{aligned} I^3 = & S_{\mathcal{A}_z(0)} + S_{\mathcal{A}_z(1)} + S_{\mathcal{A}_z(2)} - S_{\mathcal{A}_z(0) \cup \mathcal{A}_z(1)} \\ & - S_{\mathcal{A}_z(1) \cup \mathcal{A}_z(2)} - S_{\mathcal{A}_z(2) \cup \mathcal{A}_z(0)} + S_{\mathcal{A}_z(0) \cup \mathcal{A}_z(1) \cup \mathcal{A}_z(2)} . \end{aligned} \quad (3.29)$$

For our choice of subsystems, the g -partite information can be shown to be equal to the EE of the *intersection set* of the concerned g -sets (details in Appendix 3.10). For the case of $z > 0$, this takes the form

$$I_{\{\mathcal{A}_z(i)\}}^g(\phi) = S_g(\phi) = c f_{g,z} \alpha \frac{L_x}{\epsilon} - c \ln |2 \sin(\pi f_{g,z} \phi)| . \quad (3.30)$$

Since the g -partite information is simply the EE of the g^{th} subsystem, the hierarchy in the EE can thus be seen to lead to multiple levels of correlation in the system, corresponding to an increasing number of parties entering the set.

Finally, we note that the geometric (L_x -dependent) part of the EE in eq. (3.25), as well as any of the information measures I^g (eq. (3.30)), has the same form even if we start with a non-zero mass $m > 0$ [51]. This ensures that the above observations regarding the hierarchical structure of the entanglement hold even for gapped electronic systems.

3.4 EHM, the Ryu-Takayanagi bound and holographic inequalities

As we will now show, the approach laid out above to the creation of subsystems amounts essentially to performing a sequence of renormalisation group (RG) transformations on the momentum modes of the Hamiltonian in the x -direction. We consider here the general case of massive Dirac electrons $M_{n,\phi} = \sqrt{m^2 + \frac{\pi^2}{L_x^2} (n + \phi)^2}$. Further, we define the superset $\mathcal{A}_z^{(0)}$ of k_x -states: $\mathcal{A}_z^{(0)} = \bigcup_{i=0}^{\infty} \mathcal{A}_z(i)$, such that all k_x -states that can appear at any point of the sequence $\{\mathcal{A}_z(i); i = 0, 1, 2, \dots\}$ are present within it. This superset can now be used to define a parent Hamiltonian $H(0)$ that consists of all the modes in the x -direction:

$$H(0) = \sum_{k_x \in \mathcal{A}_z^{(0)}} H(k_x) , \quad (3.31)$$

where $H(k_x)$ is the Hamiltonian for a massive Dirac fermion that extends over a length L_y in the single spatial dimension, and having mass $M_{n,\phi}$. The Hamiltonian at any given step of the RG is then obtained by projecting onto appropriate sets of momenta. The set of momentum at step j is given by $\mathcal{A}_{j,z} = \frac{2\pi}{L_x} \times \{0, \pm t_z(j), \pm, 2t_z(j), \dots\}$ with $t_z(j) = 2^{j^z}$. The projector onto this set is given by

$$\begin{aligned} P_{j,z} = & \sum_{k_x^1=0,1} \sum_{k_x^2=0,1} \dots \sum_{k_x^N=0,1} |\hat{n}_{k_x^1} \hat{n}_{k_x^2} \dots\rangle \langle \hat{n}_{k_x^1} \hat{n}_{k_x^2} \dots| , \\ & k_x^j \in \mathcal{A}_{j,z} , \end{aligned} \quad (3.32)$$

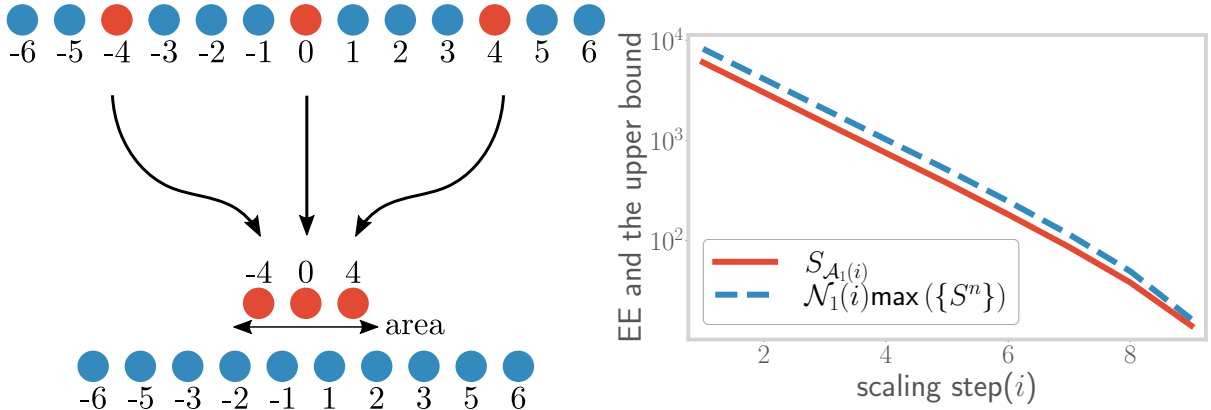


Figure 3.5: *Top:* Modes forming the subsystem $\mathcal{A}_z(i)$ (red circles) form the boundary between $\mathcal{A}_z(i)$ and its complement (blue circles). *Bottom:* Scaling of the subsystem entanglement entropy (red), and its upper bound (blue), as the RG transformations are performed (denoted by increasing index i). The bound is saturated at large i .

and the Hamiltonian at the corresponding step is then obtained as

$$H_z(i) = P_z(i) H(0) P_z(i) . \quad (3.33)$$

In this formulation of the RG, the index i represents the RG step, while the parameter z indicates the *strength of the scaling* mechanism: for $z > 0$, a higher value of z means that the states of the Hamiltonian become rarer as the index i increases, while for $z < 0$, the states become denser with increasing i . Importantly, we will see subsequently that the parameter z corresponds also to the anomalous dimension of the coupling that leads to a spectral gap in the electronic dispersion, dictating its growth or decay under RG evolution (eq.(3.44)).

Since this is a free theory, the k -modes are decoupled, and the projection operation preserves the spectrum of the remaining degrees of freedom. The renormalised Hamiltonian (eq. (3.33)) can then be said to constitute an exact holographic mapping (EHM) [116, 117] in the direction of the RG transformations. It is also pertinent to note that the sequence of transformations in eq. (3.33) can be thought of as a simple and specific example of a unitary renormalisation group (URG) procedure [1, 2] that first disentangles and then projects out a certain set of degrees of freedom. Because the operation is unitary, the URG preserves the spectrum in the process. In the present case, the disentanglement operation is unity. The URG has already been shown to lead to a holographic renormalisation of the Hilbert space geometry which can be seen through the evolution of the Fubini-Study metric under the URG transformations [1]. Our approach differs from MERA implementations like those in refs. [150, 151] in the fact that while those are involve a real space renormalisation scheme, we perform our scaling transformations in momentum space.

More evidence for the holographic nature of the construction comes from the fact that the entanglement entropy for both the massless and massive cases satisfy the bound provided by the Ryu-Takayanagi proposal that relates the entanglement of a conformal field theory (CFT) with the geometry of its gravity dual [82, 83]:

$$S_{\mathcal{A}_z(i)} \leq \mathcal{N}_z(i) \max(\{S^n\}) . \quad (3.34)$$

In the above constraint, $\max(\{S^n\})$ is the maximum single entropy of all the modes n residing in $\mathcal{A}_z(i)$, and \mathcal{N} is the area of the minimal surface that separates the subsystem $\mathcal{A}_z(i)$ from the rest. In order to see how this is satisfied in the presence case, we note that since the subsystem $\mathcal{A}_z(i)$ is interspersed among the rest of the system (see left panel of Fig. 3.5), the minimal surface is as large as the subsystem itself. The area of this surface is therefore given by the number of modes in $\mathcal{A}_z(i)$. Using this information, the right hand side of eq. (3.34) can be written as

$$\mathcal{N}_z(i)\max(\{S^n\}) = \max(\{S^n\}) N f_z(i) = \max(\{S^n\}) \sum_{n \in \mathcal{A}_z(i)} . \quad (3.35)$$

Following eq. (3.5), the left hand side of eq. (3.34) can, on the other hand, be written as

$$S_{\mathcal{A}_z(i)} = \sum_{n' \in \mathcal{A}_z(i)} S^{n'} \leq \sum_{n' \in \mathcal{A}_z(i)} \max(\{S^n\}) . \quad (3.36)$$

Comparing eqs. (3.35) and (3.36), we recover the Ryu-Takayanagi condition of eq. (3.34). The scaling of both the left and right hand sides of eq. (3.34) has been shown in the right panel of Fig. 3.5.

Entanglement measures like entanglement entropy and mutual information (associated with disjoint intervals) have been shown to satisfy a number of inequalities in quantum field theories with gravity duals. We now consider some of them here, and show that the theory considered by us here also satisfies these inequalities. One such constraint is the monogamy of mutual information, which says that for three disjoint regions A_1, A_2 and A_3 , we must have $I_2(A_1 : A_2) + I_2(A_1 : A_3) \leq I_2(A_1 : A_2 \cup A_3)$, where $I_2(A_1 : A_2) = S(A_1) + S(A_2) - S(A_1 \cup A_2)$ [152]. For this, we consider three disjoint regions, all of the kind depicted in the left panel of fig. 3.3, but at different positions $y_i \in [l_i, l_i + L], i = 1, 2, 3$. We assume that the distance $l_i - l_{i+1}$ between adjacent regions is much larger than the correlation length. Calabrese and Cardy have shown that the total entanglement entropy of the union of such disjoint regions is obtained by multiplying the entanglement entropy of any one region with the number of disjoint intervals. Putting all this together, we get

$$\begin{aligned} S(A_1) &= S(A_2) = S(A_3), \\ S(A_1 \cup A_2) &= S(A_1 \cup A_3) = 2S(A_1), \\ S(A_1 \cup A_2 \cup A_3) &= 3S(A_1), \end{aligned} \quad (3.37)$$

leading to the above inequality being satisfied:

$$I_2(A_1 : A_2) + I_2(A_1 : A_3) - I_2(A_1 : A_2 \cup A_3) = 0 . \quad (3.38)$$

We next consider a cyclic family of inequalities in terms of conditional entropies, introduced and proved in Ref. [153]: $\sum_{i=1}^{2k+1} S(A_i | A_{i+1} \dots A_{i+k}) \geq S(A_1 \dots A_{2k+1})$, where $S(A_i | A_j) = S(A_i \cup A_j) - S(A_j)$. Using the results of eq. (3.37), we get $\sum_{i=1}^{2k+1} S(A_i | A_{i+1} \dots A_{i+k}) = \sum_{i=1}^{2k+1} S(A_i) = (2k+1)S(A_1)$ and $S(A_1 \dots A_{2k+1}) = (2k+1)S(A_1)$, leading to $\sum_{i=1}^{2k+1} S(A_i | A_{i+1} \dots A_{i+k}) = S(A_1 \dots A_{2k+1})$, which also satisfies the inequality. In both cases, we find that the inequality is satisfied by saturating the bound; this is a consequence of the fact that the intervals are separated by distances larger than the correlation length and the total entanglement entropies are simply a sum of the individual entropies.

3.5 Holographic geometry of the RG flow

3.5.1 RG evolution as the emergent dimension

To obtain a more specific description of the RG flow as the emergence of a geometric space, we introduce a measure of distance. For this, we will employ another bipartite measure of entanglement - the mutual information I^2 , as defined in eq. (3.7), due to its non-negative nature. We focus on the massless case $m = 0$ for the time-being. Inspired by Refs. [117, 126, 154, 155], we adopt the following definition for distance:

$$d_z(i, j) \equiv \ln \frac{I_{\max}^2}{I_z^2(i : j)} , \quad (3.39)$$

where $I_z^2(i : j) \equiv I^2(\mathcal{A}_z(i), \mathcal{A}_{j,z})$ is the mutual information between the two mentioned sets, and I_{\max}^2 is the mutual information between two maximally entangled systems. Accordingly, $d_z(j)$ is zero (i.e., the mutual information is maximum) at $j = 0$ if $z > 0$ and $j = \infty$ if $z < 0$, and this distance increases (decreases) with the decrease (increase) in the mutual information as the scaling transformations are performed.

We compute the distance between the points i and j to obtain the scaling of the distance $d_z(j)$. We assume $i < j$ without loss of generality. At each step, we tune the flux ϕ so as to remove the flux-dependent part from the EE. Following eq. (3.27), the mutual information is of the form $\theta(-z)S_i + \theta(z)S_j$, such that the distance is given by

$$\begin{aligned} d_z(i, j) &= \theta(-z) \ln \frac{S_{\max}}{S_z(i)} + \theta(z) \ln \frac{S_{\max}}{S_{j,z}} \\ &= \theta(z)j^z \ln 2 + \theta(-z)i^z \ln 2 . \end{aligned} \quad (3.40)$$

For $z > 0$, the distance increases as j increases (keeping i fixed), as the k -space points are made more coarse-grained under the RG transformations. On the other hand, for $z < 0$, the distance decreases as i is increased (keeping j fixed). The rate of increase or decrease depends on the value of z . This scaling of the distance is shown in the left panel of Fig. 3.6.

At any given RG step j , we define two subsystems \mathcal{B}_j^1 and \mathcal{B}_j^2 . The first subsystem \mathcal{B}_j^1 is the entire set of states $\mathcal{A}_{j,z}$ available at the j^{th} RG step, while the second subsystem \mathcal{B}_j^2 is the set comprising those modes that remain to be considered at the next RG step if $z > 0$, and the set comprising only the modes that were present in the previous step for $z < 0$. This scheme is shown in the right panel of Fig. 3.6. The mutual information between these two sets defines a measure of distance y_j at the j^{th} RG step:

$$y_z(j) \equiv \ln \frac{I_{\max}^2}{I_z^2(\mathcal{B}_j^1 : \mathcal{B}_j^2)} = \begin{cases} (j+1)^z \ln 2 , & z > 0 , \\ (j-1)^z \ln 2 , & z < 0 . \end{cases} \quad (3.41)$$

The distance along the RG direction ($x_z(j)$) is, on the other hand, defined as the distance between the current RG step and the one with the maximum entanglement entropy:

$$x_z(j) \equiv \theta(z)d(0, j) + \theta(-z)d(j, \infty) = j^z \ln 2 , \quad (3.42)$$

where $d(i, j)$ was defined in eq. (3.39).

The connection of the x - and y -distances to the RG can be made manifest by relating them to the RG beta function. As we have seen above, even though we are working with massless Dirac fermions

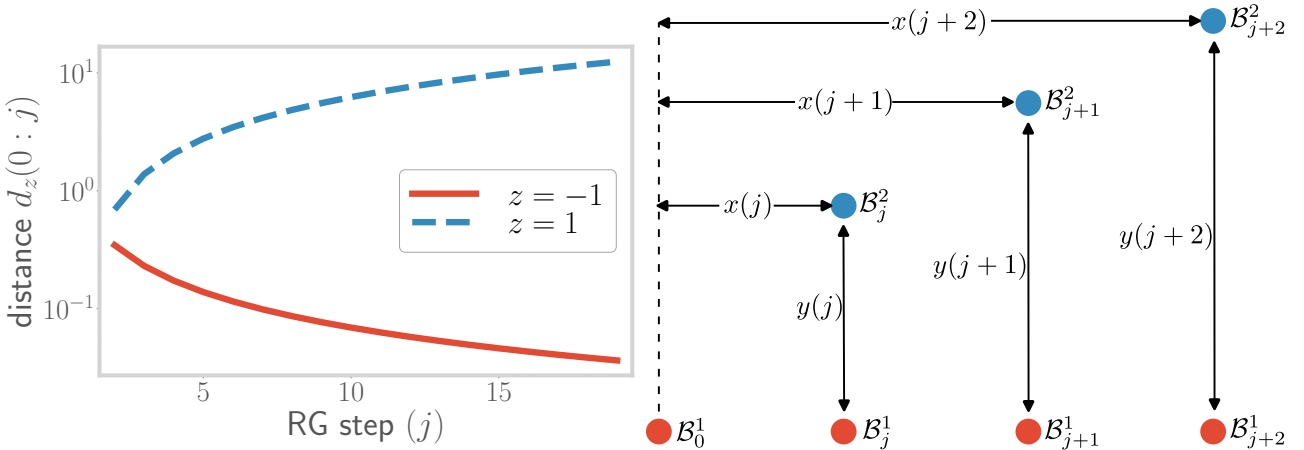


Figure 3.6: *Top:* Variation of the information distance $d_z(0:j)$ (defined along the RG direction) under the scaling transformations. Obtained by plotting the expression for the distance, as a function of the number of transformations j , for two values of z . For $z = 1$ (blue curve), the distance between two extreme points increases, showing a decrease in entanglement. For $z = -1$ (red curve), the distance decreases, showing an increase in entanglement. *Bottom:* Geometry of subsystems used for calculating the emergent curvature. The red blobs represent the subsystems generated along the emergent direction, through the scaling transformations: $\mathcal{A}_{\in j} \rightarrow \mathcal{B}_{j+1}$. The blue blobs represent subsystems generated within the $1 + 1$ -dimensional field theory, transverse to the emergent direction.

($m = 0$), the Aharonov-Bohm flux and the dimensional reduction into $1 + 1$ -dimensional modes generate an effective mass $M_{n,\phi} = \frac{2\pi}{L_x}(n + \phi)$ for $n > 0$. At a specific RG step j , the n^{th} mode is given by $t_z(j) \times n$ on account of the RG transformations in k_x -space. With these points in mind, we define a coupling $g_z(j)$ that acts as a measure of the gap in the single-particle spectrum

$$g_z(j) \equiv \ln \frac{M_{n+1,\phi}(j) - M_{n,\phi}(j)}{2\pi/L_x} = \ln t_z(j) = j^z \ln 2. \quad (3.43)$$

The RG beta-function for the coupling $g_z(j)$ can then be written as

$$\beta_z(j) \equiv \frac{\Delta \log g_z}{\Delta j} = \log \frac{g_z(j+1)}{g_z(j)} = z \ln \left(1 + \frac{1}{j}\right), \quad (3.44)$$

where we have substituted $\Delta j = 1$. The beta function is positive for $z > 0$, indicating that the coupling $g_z(j)$ is RG-relevant in this regime (left panel of Fig. 3.7). On the other hand, the beta function is negative for $z < 0$, leading to irrelevant RG flows in this regime. The RG beta-function $\beta_z(j)$ itself decreases monotonically as j increases under the RG transformations (see Fig. 3.7): for a finite z , a fixed point is reached at $j \rightarrow \infty$ where the beta function goes to zero.

As we will now see, the flow of the RG beta functions can be related to the extremisation of a potential defined in the space of Hamiltonians. This potential is a function of the mutual information $I_z^2(0:j)$:

$$\beta_z(j) = -\Delta \left[\ln \left(\ln \frac{I_z^2(0:j)}{I_{\max}^2} \right) \right]. \quad (3.45)$$

The potential given within the square brackets above corresponds to an RG monotone whose fixed point corresponds with the fixed point of the RG. For relevant flows, the above equation ensures that the func-

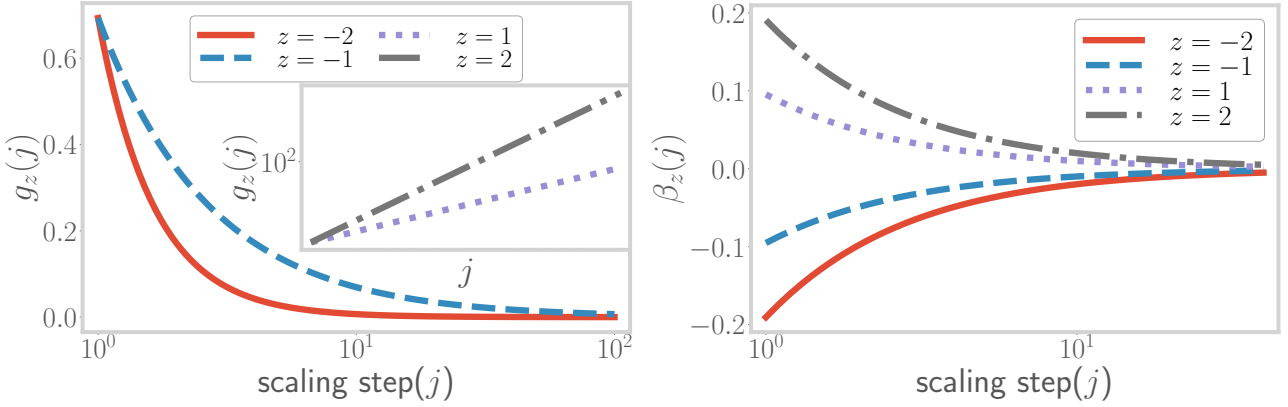


Figure 3.7: *Top:* Depiction of the RG flow of the coupling $g_z(j)$. For $z < 0$ (blue and red curves), the coupling is RG-irrelevant and shows a decrease as j is increased. For $z > 0$ (gray and violet curves), the coupling is RG-relevant and shows an increase as j is increased. *Bottom:* Variation of RG beta function $\beta_z(j)$ for the coupling $g_z(j)$, as a function of step index j . For all values of z , the beta function converges to 0 as $j \rightarrow \infty$, indicating a fixed point of the coupling g .

tion $\ln \left(\ln \frac{I_z^2(0:j)}{I_{\max}^2} \right)$ is always minimised under the RG flow, with the consequence that the trajectories ultimately lead to minimisation of the mutual information. This indicates that the relevance of the mass coupling leads in turn to the decrease of the correlation length and hence a lowering of entanglement between points that are separated in real space. On the other hand, for irrelevant flows, the above-mentioned function is maximised, implying that the RG trajectories now maximise the entanglement. This reflects the fact that the decreasing mass leads to increased correlation lengths and an approach towards criticality.

Given eqs.(3.41), (3.42) and (3.45), we can relate the distances x and y to the beta function β_z :

$$x_z = \left(e^{\frac{\beta_z}{z}} - 1 \right)^{-z} \ln 2 , \quad (3.46)$$

$$y_z = \begin{cases} x_z e^{\beta} & z > 0 , \\ x_z \left(2 - e^{\frac{\beta}{z}} \right)^z & z < 0 . \end{cases} \quad (3.47)$$

The contrasting behaviour of the beta function depending on the sign of z indicates that it tracks the effective number of degrees of freedom that contribute to the entanglement (eq. (3.25)) at any given RG step. Indeed, we find that the effective number of degrees of freedom is the effective c -function (or central charge) $\tilde{c}_z(j)$ of the theory, taking the form $\tilde{c}_z(j) = f_z(i)c$. The beta function is thus related to the c -function as

$$\beta_z = \Delta \left[\ln \left(\ln \frac{c}{\tilde{c}_z(j)} \right) \right] . \quad (3.48)$$

For RG relevant flows, the c -function is found to diminish from the free fermion central charge $c = 1/3$, reaching the value of zero at the fixed point (where only the central $n = 0$ mode remains and the rest have been removed because of the large mass gap). The non-negative, non-increasing nature of the c -function, and its flow towards its minimum at the fixed point, leads to speculate that eq.(3.48) can be thought of as a holographic counterpart of Zamalodchikov's c -theorem [67,156–158]. For RG irrelevant flows, the behaviour is reversed. The flow of the c -function is shown in the left panel of Fig. 3.8.

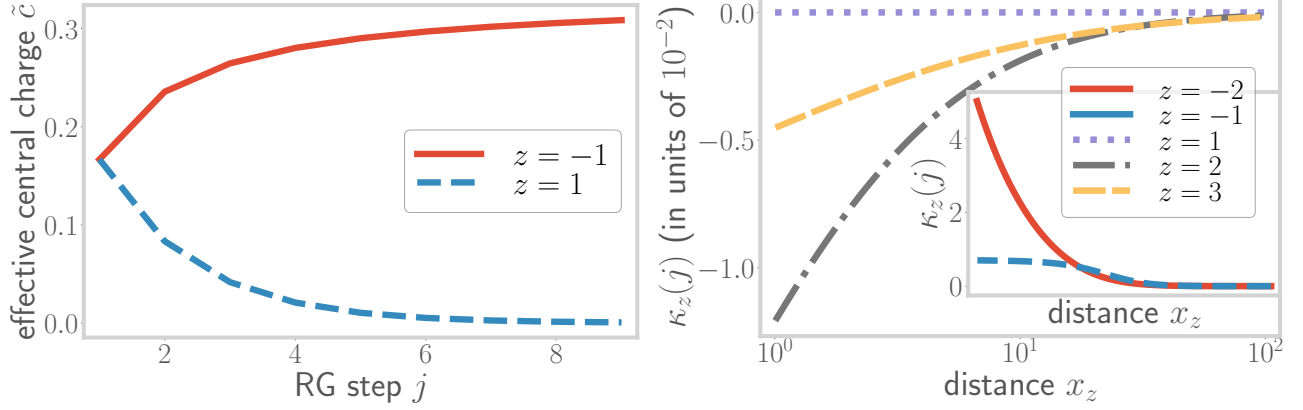


Figure 3.8: *Top:* Variation of the effective central charge defined in eq. (3.48), under the RG transformations for relevant ($z = 1$, blue curve) and irrelevant ($z = -1$, red curve) flows. In the former case, the central charge starts from the fermionic gapless value of $1/3$ and vanishes towards the fixed point, indicating the flow to a gapped massive phase. In the latter case, it starts from the gapped value of 0 , and increases to $1/3$ at the fixed point, indicating the flow to a gapless phase. *Bottom:* Variation of the curvature $\kappa_z(j)$ along the RG for multiple values of z . $z = 1$ leads to a flat space with zero curvature, while $z > 1$ and $z < 1$ (inset) lead to negative and positive curvature respectively.

3.5.2 Embedding the emergent dimension on a metric space

We have shown above that the renormalisation group flow of the Hamiltonian leads to the emergence of an additional direction, quantified by the parameter x_j . This will now be used to construct a metric, in the following way. We already know that the scaling transformations lead to a graph of theories that are connected via edges that represent the mutual information between any two theories. As a result, this ‘‘information graph’’ can be mapped on to a new ‘‘distance graph’’ where the edges now represent the distance between the theories at the nodes. Finally, these distances can be used to define a metric for the distance graph: the metric between any two nodes will be the distance along the shortest path between these two nodes. This approach as well as some of the terminology are inherited from reference [159].

The RG flow can be represented as an ‘‘information graph’’ $G(V, E)$, where the systems \mathcal{B}_j^1 (defined above eq. (3.41)) constitute the set of vertices $V = \{V_j\}$ and the mutual information $I_z^2(j : j')$ between the systems \mathcal{B}_j^1 and $\mathcal{B}_{j'}^1$ constitute the edges E_{ij} between the vertices. This information graph is characterised by an adjacency matrix whose elements are defined by the mutual information edge weights $I_z^2(j : j')$ [160]. This graph structure is shown in Fig. (3.6), with the red spheres indicating the vertices. In order to define a metric space, we will map the graph G to another graph \mathcal{G} that has the same vertices as G , but whose edges are weighted according to a well-defined notion of distance.

A path \mathcal{P} in \mathcal{G} is defined as a sequence of m vertices: $\mathcal{P}(V_1, V_2, \dots, V_m)$. The distance along the path is defined as the sum of distances along every pair of consecutive vertices: $l(\mathcal{P}) = \sum_{i=1}^{m-1} d(V_i, V_{i+1})$, where $d(V_i, V_{i+1}) = d(i, i+1)$ (see eq. (3.39)). The geodesic between two points V_i and V_j is the path \mathcal{P} which minimises the distance $l(\mathcal{P})$, and the distance along the geodesic then defines the metric $\tilde{d}(V_i, V_j)$ between two vertices V_i and V_j [159, 160]:

$$\tilde{d}(V_i, V_j) = \min_{\mathcal{P}} \{l(\mathcal{P})\} = \min_{\mathcal{P}} \left\{ \sum_{i=1}^{m-1} d(V_i, V_{i+1}) \right\}, \quad (3.49)$$

where the minimisation is carried out over all possible connected paths $\{\mathcal{P}\}$ between V_i and V_j , and m is the total number of vertices in a particular connected path \mathcal{P}_m . Following the expression for the distance $d(i, j)$ obtained in eq. (3.40), the metric takes the form

$$\tilde{d}(V_i, V_j) = \theta(z)j^z \ln 2 + \theta(-z)i^z \ln 2, \quad (i < j), \quad (3.50)$$

where we have assumed $i < j$, without loss of generality.

Finally, the metric dimension of the emergent space can be determined by finding the set with the lowest possible cardinality that can resolve the metric space [159, 161]. In order for a set to resolve the metric space, we must have $d(i, a) = d(j, a) \implies i = j$ for all points a in the set and for any pair of points i and j in the metric space. In our case, the singleton set $\mathcal{R} = \{0\}$ can resolve the metric space for $z > 0$, as $d(i, 0) = d(j, 0) \implies i^z = j^z \implies i = j$. Similarly, the singleton set $\mathcal{R} = \{\infty\}$ resolves the metric space for $z < 0$. As a result, we conclude that our emergent metric space is one-dimensional in nature.

3.6 Curvature of the emergent space

Further insight on the spatial geometry of the RG flows can be obtained by looking at the curvature generated by the RG transformations. In the plane of the directions x and y generated by the RG flow, the curvature can be written using the ideas of analytic geometry as

$$\kappa_z(j) = \frac{v'_z(j)}{[1 + v_z(j)^2]^{\frac{3}{2}}}, \quad (3.51)$$

where

$$v_z(j) \equiv \frac{\Delta y_z(j)}{\Delta x_z(j)} = \frac{y_z(j+1) - y_z(j)}{x_z(j+1) - x_z(j)} \\ = \begin{cases} \frac{(j+2)^z - (j+1)^z}{(j+1)^z - j^z} & z > 0, \\ \frac{(j)^z - (j-1)^z}{(j+1)^z - j^z} & z < 0, \end{cases} \quad (3.52)$$

and

$$v'_z(j) \equiv \frac{v_z(j+1) - v_z(j)}{x_z(j+1) - x_z(j)}. \quad (3.53)$$

The curvature $\kappa_z(j)$ has been plotted against the RG step index j in right panel of Fig. 3.8. For $z = 1$, the first derivative $v_z(j)$ becomes unity, so the second derivative $v'_z(j)$ (and hence the curvature) vanishes, leading to a flat (Minkowski) space. For $z > 1$, the curvature becomes negative, while it is positive for $z < 0$. All the flows lead to an asymptotically flat space (i.e., the curvature vanishes) as $j \rightarrow \infty$.

The different signatures of the emergent curvatures can be attributed to the different ways in which the mass of the theory scales under the decimation procedure. For $z > 0$, the curvature defined in eq. (3.51) can be written in terms of the beta function:

$$\kappa_z(j) = \frac{[e^{\beta(j)} - 1]^{\frac{1}{2}} j^{-z}}{[e^{\beta(j)+\beta(j+1)} - 1]^{\frac{3}{2}}} \left[\frac{e^{\beta(j+2)} - 1}{1 - e^{-\beta(j+1)}} - \frac{e^{\beta(j+1)} - 1}{1 - e^{-\beta(j)}} \right]. \quad (3.54)$$

This equation relates directly a geometric quantity (i.e., the curvature) of the bulk emergent space with the RG beta function for the field theory on the boundary. From Fig. 3.7, as the beta functions flow towards zero, we see from eq. (3.54) that the first fraction inside the square brackets is the first to vanish, followed by the second fraction. The sequential vanishing of these two fractions prior to the vanishing of the denominator $e^{\beta(j)} - 1$ in eq.(3.54) leads to the asymptotic vanishing of the curvature towards the fixed point. Different choices of $z > 0$ can be thought to represent different relevant perturbations that drive the system towards *gapped fixed points*, leading to distinct curvatures of the bulk. By employing the relation $v_z(j) = \Delta S_{j+1,z}/\Delta S_{j,z}$, eq. (3.51) can also be cast in terms of the entanglement entropy $S_{j,z}$, $S_{j+1,z}$ and $S_{j+2,z}$. The resulting non-linear relationship between $\kappa_z(j)$ and $S_{j,z}$ obtained is, however, in contrast to the linear dependence obtained by Cao et al. [159] between entanglement perturbations on the Hilbert space and the curvature of the resultant holographic space.

3.6.1 Topological nature of the sign of curvature

We will now argue that the signature of the curvature κ corresponds to a topological quantum number, and that a change in the signature as z is tuned through 1 amounts to a topological translation. For this, we first point out (following eq. (3.51)) that the sign of the curvature is determined purely by the sign of $\gamma_z(j) \equiv 1 - v_z(j+1)/v_z(j)$ and $\alpha_z(j) = y_z(j+1) - y_z(j)$:

$$\begin{aligned} \kappa_z(j) &= \frac{v'_z(j)}{[1 + v_z(j)^2]^{\frac{3}{2}}} = -\frac{\alpha_z(j) \gamma_z(j)}{(\Delta x_z(j))^2 [1 + v_z(j)^2]^{\frac{3}{2}}} \\ &\implies \text{sign} [\kappa_z(j)] = -\text{sign} [\alpha_z(j)] \text{ sign} [\gamma_z(j)] . \end{aligned} \quad (3.55)$$

We now promote j to a continuous complex variable with the real part being greater than or equal to 1: $\text{Re}[j] \geq 1$. The quantities $\alpha_z(j)$ and $\gamma_z(j)$ can be written as

$$\alpha_z(j) = \begin{cases} [(j+2)^z - (j+1)^z] \log 2, & z > 0 \\ [j^z - (j-1)^z] \log 2, & z < 0 \end{cases}, \quad (3.56)$$

$$\gamma_z(j) = \begin{cases} 1 - \frac{[(j+3)^z - (j+2)^z][(j+1)^z - j^z]}{[(j+2)^z - (j+1)^z]^2}, & z > 0 \\ 1 - \frac{[(j+1)^z - j^z]^2}{[j^z - (j-1)^z][(j+2)^z - (j+1)^z]}, & z < 0 \end{cases}. \quad (3.57)$$

As shown in Fig.3.9(left panel), the function γ_z is positive and monotonically decreasing for $z > 1$ or $z \leq -1$, and vanishes identically for $z = 1$. On the other hand, $\alpha_z(j)$ is positive for $z > 1$, zero at $z = 1$ and negative for $z \leq -1$ (see Fig.3.9(right panel)). Combining this, we find that the sign of the curvature can be written as:

$$\text{sign} [\kappa_z] = \begin{cases} -1, & z \geq 1 \\ 1, & z \leq -1 \end{cases} = \begin{cases} -\text{sign} [\gamma_z(j)], & z \geq 1 \\ -\text{sign} [\alpha_z(j)], & z \leq -1 \end{cases}. \quad (3.58)$$

We start by considering the region $z \geq 1$. Since $z = 0$ is excluded by definition, the denominator is always non-zero. This indicates that $\gamma_z(j)$ is continuous and monotonically decreasing in this range: the maximum value of $\{\gamma_z(j), j \in [1, \infty]\}$ occurs at $j = 1$. Further, the maximum value $\gamma_z(1)$ increases with the value of z , ranging between $\gamma_2(2)$ at $z = 2$ and unity at $z \rightarrow \infty$. These two features are demonstrated in the left panel of Fig. 3.9, and imply that all curves $\{\gamma_z(j) : j\}$ will take values both

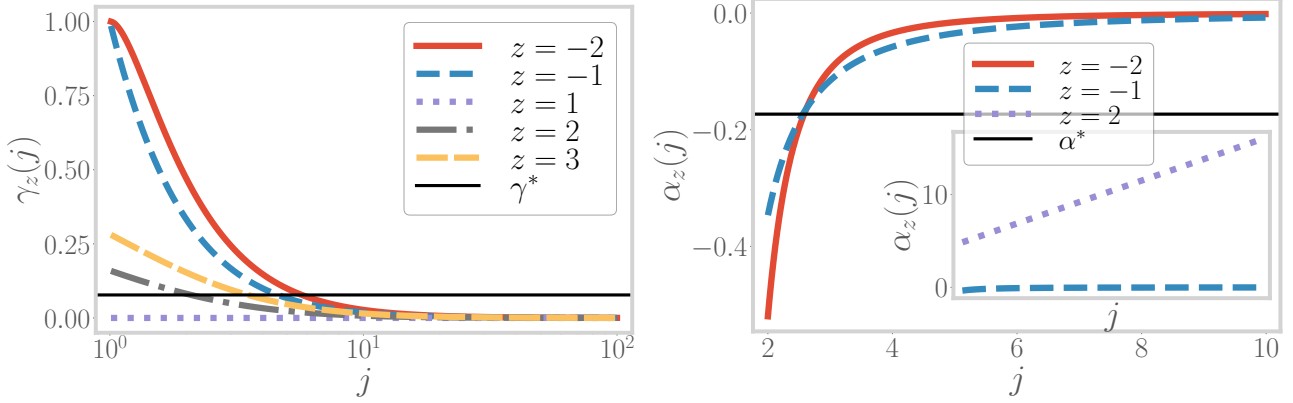


Figure 3.9: *Top*: Variation of γ_z along the RG for multiple values of $z > 0$. All trajectories for $z > 1$ intersect the line $y = \gamma^*$. *Bottom*: Variation of α_z along the RG for multiple values of $z < 0$. All trajectories intersect the line $y = \alpha^*$

greater than and less than the value $\gamma^* \equiv \gamma_2(2)$ (dotted line in left panel of Fig. 3.9). Thus, the plot shows that there always exists a real value j_z^* for any given integer value $z > 1$ such that $\gamma_z(j_z^*) = \gamma^* = \gamma_2(2)$. This is precisely what ceases to happen for $z = 1$, as that is the only curve in the left panel of Fig. 3.9 that does not pass through γ^* .

Indeed, the difference between the curvature for the $z = 1$ and $z > 1$ classes can be captured by expressing the presence of the solution j_z^* in the form of a winding number. For this, we use the fact that the sign of $\gamma_j(z)$ is given by the following integral:

$$\text{sign} [\gamma_z(j)] \Big|_{z \geq 1} = \frac{1}{2\pi i} \oint_C dj \frac{\partial}{\partial j} \ln [\gamma_z(j) - \gamma^*] , \quad (3.59)$$

where the contour C extends from $j = 1$ to $j = \infty$, and is shown in the left panel of Fig. 3.12. As the value of z is tuned from 2 to 1, the pole at j_z^* disappears and the integral reduces to zero. As shown in Fig. 3.10, the integral can thus be expressed as the winding number of the curve $\gamma_z(C(j))$ that counts the number of times the contour $\gamma_z(C)$ winds around the singularity at γ^* :

$$\text{sign} [\gamma_z(j)] = \frac{1}{2\pi i} \oint_C dj \frac{\partial(\gamma_z(j) - \gamma^*)}{\gamma_z(j) - \gamma^*} = \frac{1}{2\pi i} \oint_{\gamma_z(C)} \frac{d\gamma_z}{\gamma_z - \gamma^*} . \quad (3.60)$$

This is easily seen from the following argument. If we write a general complex variable y in the form $y = re^{i\theta}$ and consider a general contour C that starts from $r = r_0, \theta = 0$ and ends at $r = r_0, \theta = 2w\pi$ (such that the winding number of the curve is w), integrals of the form given above simplify and return the winding number itself:

$$\frac{1}{2\pi i} \oint_C \frac{dy}{y} = \frac{1}{2\pi i} \int_{r_0}^{r_0} \frac{dr}{r} + \frac{1}{2\pi} \int_0^{2w\pi} d\theta = w , \quad (3.61)$$

where we used $dy = y \left(\frac{dr}{r} + d\theta \right)$.

The winding numbers take integer values, and are topological in nature: they are robust against geometric deformations, and change only when the curve crosses the singularity at $\gamma = \gamma^*$. Thus, for

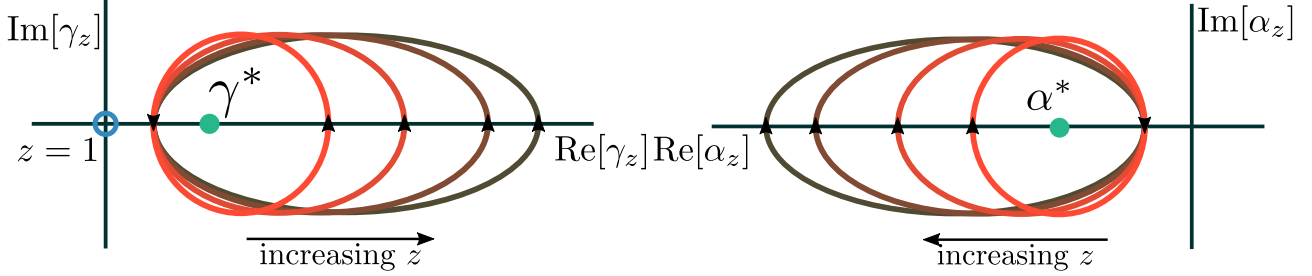


Figure 3.10: *Top:* Contours $\gamma_z(\mathcal{C})$ for multiple values of $z > 0$. As z increases, the contours extend in the positive $\text{Re}[\gamma_z]$ direction. *Bottom:* Contours $\alpha_z(\mathcal{C})$ for multiple values of $z > 0$. As z increases, the contours extend in the negative $\text{Re}[\gamma_z]$ direction.

$z > 1$, the contour $\gamma_z(\mathcal{C})$ encloses the singularity at γ^* exactly once, leading to a winding number of unity. As z is lowered towards $z = 2$, the contours becomes smaller such that, in order to go from $z = 2$ to $z = 1$, the contour has to be moved across the singularity. This constituting a change in the topology of the contour: for $z = 1$, the contour no longer encloses the pole and the winding number is zero. In fact, at $z = 1$, the contour itself (depicted in blue) is of vanishing radius because $\gamma_1(j)$ has a constant value of zero. To complete the connection, we use eq. (3.55) to relate this topological winding number to the sign of the curvature:

$$\left. \text{sign} [\kappa_z] \right|_{z \geq 1} = -\mathcal{W}_z(\gamma^*) , \quad (3.62)$$

where $\mathcal{W}_z(\gamma^*)$ is the winding number for $\gamma_z(\mathcal{C})$ around γ^* .

One can make a very similar argument for the case of $z \leq -1$. Here, as shown in the right panel of Fig. 3.21, the relevant quantity is $\alpha_z(j)$. For each curve α_z , the minimum value is at $j = 1$. For all z , this minimum starting value is largest for $z = -1$, and all subsequent curves $\alpha_z(j)$ start from even lower values. If we define a value $\alpha^* \equiv \alpha_z(j = 1)/2$, it is then clear that all curves $\alpha_z(j)$ will pass through the value α^* (dotted line in right panel of Fig. 3.21) at some value of j . This is very similar to the situation discussed just above for the case of $z \geq 1$ (with γ^* playing the role of α^*); we, therefore, employ the same technique here. Taking the same contour \mathcal{C} as defined above, we write the sign of α_z as the winding number of the curve $\alpha_z(\mathcal{C})$ around the point $\alpha_z = \alpha^*$

$$\left. \text{sign} [\alpha_z(j)] \right|_{z \leq -1} = -\mathcal{W}'_z(\alpha^*) = \frac{1}{2\pi i} \oint_{\alpha_z(\mathcal{C})} \frac{d\alpha_z}{\alpha_z - \alpha^*} . \quad (3.63)$$

For $z > 0$, α_z is positive, and the curve $\alpha_z(\mathcal{C})$ encloses points in the positive half of the real axis such that the winding number in the right panel of Fig. 3.10 is then zero. This indicates that the function $1 - 2\mathcal{W}'_z(\alpha^*)$ is unity for $z > 0$, leaving any other function in product with it unchanged. On the other hand, it is -1 for $z < 0$, returning the correct sign of $\alpha_z(j)$ in that range. Combining with eq. (3.62), the sign in the entire range can be expressed as

$$\text{sign} [\kappa_z] = \mathcal{W}_z(\gamma^*) \times [2\mathcal{W}'_z(\alpha^*) - 1] . \quad (3.64)$$

We can now summarise the topological nature of the sign of the curvature. For $z > 0$, the second winding number \mathcal{W}' is 0. As z varies from 2 to 1, the other winding number \mathcal{W} changes from 1 to 0, constituting the first topological change. In contrast, upon varying z from 1 to -1 , both winding

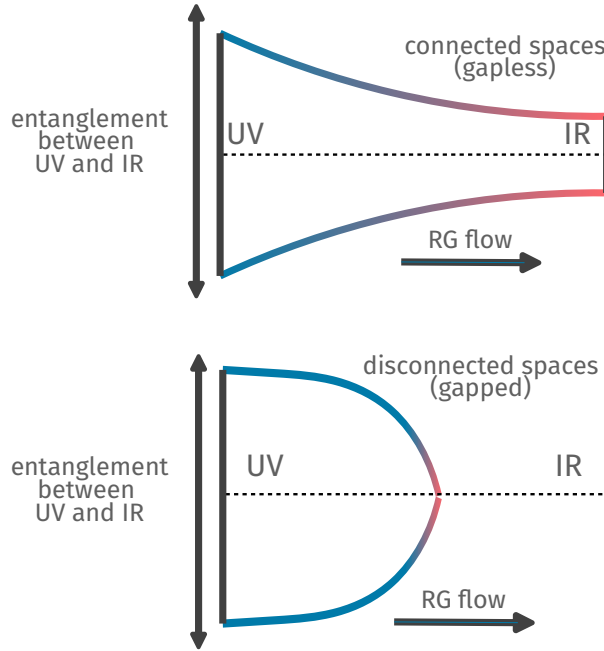


Figure 3.11: Schematic depiction of the emergent geometries in the cases of gapless (top) and gapped (bottom) RG flows. While the gapless RG flow involves a growth in the entanglement between the UV and IR spaces, the latter leads to the vanishing of UV-IR entanglement. This results in the emergence of connected and disconnected geometries, respectively.

numbers change: \mathcal{W} from 0 to 1, and \mathcal{W}' from 0 to 1. This constitutes the second topological change. Together, the two changes show that going from an open geometry (negative curvature) to a closed geometry (positive curvature) involves two topological transformations.

3.7 Entanglement Holography and Fermionic Criticality

3.7.1 Equivalence between a critical Fermi surface and a holographic wormhole

As mentioned previously under eq. (3.33), the quantity z corresponds to the anomalous dimension of the spectral gap g_z in the effective field theory: a change in the sign of z corresponds to a change in the nature of the RG flow from relevance to irrelevance and vice-versa. The holographic nature of the RG flow dictates that such a change arises by a variation in some quantity in the parent interacting theory from which the effective field theory of non-interacting Dirac fermions can be thought to have originated. Indeed, such a change in the RG relevance has drastic consequences: a relevant spectral distance g_z implies a gap in the excitations at the fixed point, while an irrelevant g_z indicates the presence of gapless excitations. The presence or absence of a gap in the low-energy excitations determines the topology of the electronic Fermi surface through the change of a topological invariant, the Luttinger volume of the system [1, 2, 123, 124, 144] (also see eq. (3.11)).

At the transition between the gapless (metallic) and gapped (insulating) states, the Fermi surface becomes critical, signalled by the vanishing lifetime of the gapless excitations close to it. Our formulation shows that such a gap-inducing transition and its associated quantum critical Fermi surface has consequences for the space generated along the RG flow. For the gapless case ($z < 0$), the degrees

of freedom in the UV and the IR have finite entanglement, indicating that they are part of the same connected holographic space (see Figs. 3.6 and 3.7), while for the gapped case ($z < 0$), the entanglement vanishes into the IR, leading to a decoupling of these two regions and their separation into disconnected spaces [154]. These two scenarios are shown schematically in Fig. 3.11. It is therefore tempting to conclude that at the transition between the gapped and gapless states, a *wormhole geometry* connects the UV and the IR via some minimal entanglement [154, 159]. Our results also suggest that the presence of such a wormhole would then coincide with two topological transitions, the first being the change in the sign of the curvature (as shown in the previous subsection), and the second being the change in the topological Luttinger volume of the underlying quantum field theory (as discussed in the previous paragraph). We end by noting that we have provided, in a later section of this work, additional support for the topological nature of Luttinger's volume and its connection to the holographically generated space by relating it to multipartite entanglement (see eq. (3.93)).

3.7.2 Connecting modular energy with the metric

The notion of an entanglement Hamiltonian was introduced in eq. (3.8). At the transition between the gapless (metallic) and gapped (insulating) states, the system becomes critical, and the Dirac electrons are described by a CFT. It turns out that for such a CFT, the entanglement Hamiltonian takes a particularly simple form. In this subsection, we will relate the emergent metric to the entanglement Hamiltonian obtained at the IR fixed point, focusing on the theory at the transition.

For a 1D CFT, the entanglement Hamiltonian corresponding to a partition of length l is given by [162, 163]

$$\mathcal{H}_{1\text{D}} = \frac{2\pi L}{c} \int_0^l dx \frac{L^2 - x^2}{2L^2} T_{00}(x) , \quad (3.65)$$

where $T_{\mu\nu}$ is the stress-energy tensor of the CFT and c is the speed of light. We have already shown in eq. (3.9) that the entanglement Hamiltonian for the 2D theory is simply a sum of the 1D counterparts, owing to the decoupling of 1D modes in the Lagrangian. Working in a region where T_{00} is approximately uniform, the 2D entanglement Hamiltonian can be expressed as

$$\mathcal{H}_{2\text{D}} \sim \sum_n \mathcal{H}_{1\text{D}} = \frac{2\pi L^2}{3c} \sum_n T_{00}^n , \quad (3.66)$$

where T_{00}^n is the average value of T_{00} within the partition for the CFT associated with the n^{th} mode.

In order to make the connection with the emergent geometry, we use the entanglement first law [164], which states that at first order, small variations ΔS of the entanglement entropy can be equated to the associated change in the expectation value of the entanglement Hamiltonian:

$$\Delta S(A) = \Delta I_2(A_0 : A) = \langle \Delta \mathcal{H} \rangle = \frac{2\pi L^2}{3c} \sum_n \langle T_{00}^n \rangle , \quad (3.67)$$

where $\langle \mathcal{H} \rangle = \text{Tr}(\rho \mathcal{H})$ is often referred to as the modular energy, and we have equated $\Delta S(A)$ and $\Delta I_2(A_0 : A)$ following eq. (3.27). Further, since the entanglement at the critical point is expected to be large, we can approximate the expression for the metric between points (i, j) obtained in subsection 3.5.2 as $\tilde{d}(i, j) = -\ln I^2(i : j)/I_{\max}^2 \simeq |I^2(i : j)/I_{\max}^2 - 1|$. Combining this equation with eq. (3.67)

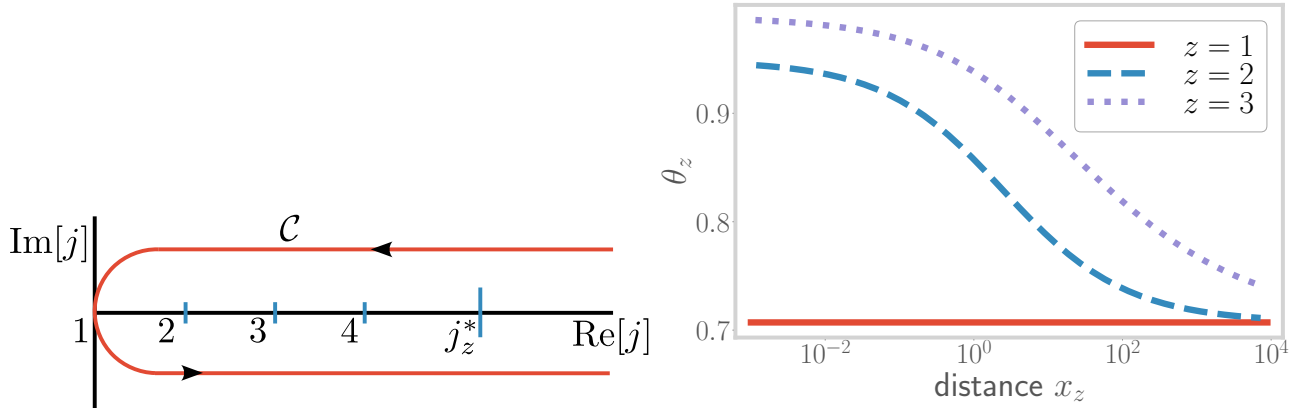


Figure 3.12: *Top:* The contour \mathcal{C} used in eq. (3.59). It extends across all values of j , and the integral counts the number of poles of the function $1/(\gamma - \gamma^*)$ encircled by the contour. *Bottom:* Evolution of expansion parameter θ_z with distance x_z , leading to the fixed point at $\theta_z^* = 1/\sqrt{2}$.

leads to the following interesting relation:

$$\Delta\tilde{d}(i, j) \simeq \frac{2\pi L^2}{3c} \sum_n \langle T_{00}^n \rangle . \quad (3.68)$$

The equation relates the change in a geometric measure (the emergent metric) with a mass/energy term. An analogous relation was obtained for states for which the entropy obeys an area law by Cao et al [159], connecting the spatial curvature and the stress tensor, ultimately leading to a semi-classical Einsteins field equation for gravity. Our formulation does not however lead to a relation involving the curvature, and we speculate that this is due to the violation of the area law in entanglement of fermionic critical systems. Instead, we show in the next section that the curvature in our formulation is related to the rate of convergence of the RG flows.

3.7.3 Kinematics of the RG flows

Further statements on the RG flow and the emergent holographic dimension can be made by studying quantities that can serve as candidates for the convergence parameter θ for the RG flows of g_z [165, 166]. We consider the following function as a candidate for the convergence parameter for the case of $z > 0$:

$$\theta_z(j) = \frac{1}{\sqrt{v_z^{-2} + 1}} = \left[1 + \left\{ \frac{1 - e^{-\beta_z(j)}}{e^{\beta_z(j+1)-1}} \right\}^2 \right]^{-\frac{1}{2}} . \quad (3.69)$$

The parameter θ_z has been plotted in Fig. 3.12, and the behaviour is observed to be very similar to that of the beta function shown in Fig. 3.7. Indeed, this similarity describes the holographic nature of the RG flow: the emergent geometry (as seen through θ_z) is dictated by the RG flow described by β .

The quantity θ can be interpreted as an estimate of the rate of change of area enclosed by a fixed number of RG trajectories. To see that this is the case, we note that by using $v_j = \Delta y / \Delta x$, the expansion parameter can be written as $\theta = \Delta y(j) / \sqrt{\Delta x^2 + \Delta y^2} \sim \Delta g(j+1) / \sqrt{\Delta x^2 + \Delta y^2}$. Considering RG flows for $g_z(j)$ corresponding to multiple z , the area enclosed by the curves is given by the maximum g_z ,

and Δg_z is then the change in the area under the RG transformation. The denominator $\sqrt{\Delta x^2 + \Delta y^2}$ is the distance covered in the emergent spacetime, rendering θ as the rate of change of the area.

The equation of motion for this expansion parameter can then be obtained as:

$$\frac{d\theta_z}{dx} = \frac{v_z^{-3}}{(1+v_z^{-2})^{\frac{3}{2}}} \frac{dv_z}{dx_j} = \kappa_z. \quad (3.70)$$

The simple form of this relation makes it clear that for relevant flows (corresponding to a negative curvature $\kappa_z < 0$), θ_z flows to a minimum. Following Fig. 3.8, this is accompanied by the minimisation of the c -function to zero. It is, therefore, tempting to conclude that eq. (3.70) for the spatial evolution of the convergence parameter θ is dual to eq. (3.48) that controls the flow of the c -function of the quantum theory along the RG flow.

3.8 Extension to the massive case

We will now generalise several of the main results obtained above to the case of two-dimensional electrons with a single-particle mass-gap $M_{n,\phi} = \sqrt{m^2 + \frac{4\pi^2}{L_x^2}(n+\phi)^2}$. Given that they depend only on the geometric part of the entanglement (which remains unchanged on introducing the mass $M_{n,\phi}$), the following set of key qualitative results and observations discussed earlier continue to hold for the case of a dispersion with a mass-gap:

- the hierarchical structure of the entanglement content (e.g., the area-law term in eqns.(3.25) and (3.28)) and the fact that the entanglement satisfies the Ryu-Takayanagi bound (right panel of Fig.3.5),
- the dependence of the emergent distances x and y on the RG flow (Fig.3.6, eqns.(3.40) and (3.41)), and the fact that the RG beta function tracks the central charge (Fig.3.8),
- various qualitative and quantitative properties of the curvature (e.g., eq.(3.51)), including the topological nature of its sign (eq.(3.64)), and
- the existence of a convergence parameter that is related to the RG flow, and the equation that governs the evolution of the convergence parameter (eq.(3.70)).

The functional forms of certain other results do, however, undergo changes. For instance, the coupling $g_z(j)$ is given by the (more general) expression

$$\begin{aligned} g_z(n, j) &= \ln \frac{M_{n+1,\phi}(j) - M_{n,\phi}(j)}{2\pi/L_x} \\ &= \ln \left[\sqrt{\tilde{m}^2 + (t_z(j)(n+1) + \phi)^2} - \sqrt{\tilde{m}^2 + (t_z(j)n + \phi)^2} \right], \end{aligned} \quad (3.71)$$

where $\tilde{m} = mL_x/2\pi$ is a dimensionless parameter. We will work with the coupling for the mode $n = 0$:

$$g_z(0, j) = \ln \left[\sqrt{\tilde{m}^2 + (t_z(j) + \phi)^2} - \sqrt{\tilde{m}^2 + \phi^2} \right]. \quad (3.72)$$

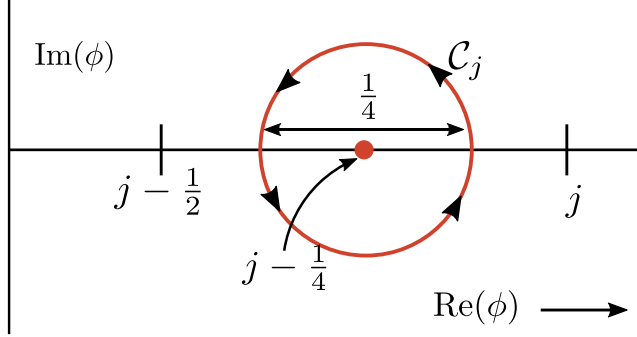


Figure 3.13: Contour \mathcal{C}_j used to integrate eq. (3.79). The contour is chosen so as to encircle the simple pole of $1/Q$ at $\phi = j - 1/4$.

In order to simplify the analysis, we work in the large mass limit $\frac{t_z + \phi}{2\tilde{m}} \rightarrow 0$. In this limit, upon expanding the square root and retaining only the lowest order term, we obtain

$$g_z(0, j) = \ln \frac{[t_z(j) + \phi]^2 - \phi^2}{2\tilde{m}}. \quad (3.73)$$

The RG beta function $\beta = \ln(g_z(j+1)/g_z(j))$ can, in the large mass limit, then be related to the emergent distances x and y in terms of the coupling $g_z(j)$:

$$x_z(j) = \ln t_z(j) = \ln \left[\sqrt{2\tilde{m} e^{g_z(0,j)} + \phi^2} - \phi \right], \quad (3.74)$$

$$y_z(j) = \begin{cases} \ln \left[\sqrt{2\tilde{m} e^{g_z(0,j+1)} + \phi^2} - \phi \right], & z > 0, \\ \ln \left[\sqrt{2\tilde{m} e^{g_z(0,j-1)} + \phi^2} - \phi \right], & z < 0. \end{cases} \quad (3.75)$$

The quantitative dependence of the c -function on the RG beta function can also be expressed more generally as

$$e^{\beta_z(j)} = \left[\ln \frac{\left(\frac{\tilde{c}(j+1)}{c} + \phi \right)^2 - \phi^2}{2\tilde{m}} \right] \left[\ln \frac{\left(\frac{\tilde{c}(j)}{c} + \phi \right)^2 - \phi^2}{2\tilde{m}} \right]^{-1}. \quad (3.76)$$

Quantities such as the curvature κ and the convergence parameter θ can similarly be expressed in terms of the coupling $g_z(j)$.

3.9 Topological content of the entanglement spectrum

3.9.1 Luttinger's volume as a winding number: the massless case

We will now show how to obtain Luttinger's volume (eq.(3.10)) from the g -partite information entanglement measure I^g of a system of massless 2D electrons. The flux-dependent part of the g -partite information I^g can be used to probe the k -space volume V_L within the Fermi surface. We define a

quantity $Q_g(\phi)$ that is periodic in the flux ϕ and independent of the geometry:

$$\begin{aligned} Q_g(\phi) &= f_{g,z} \left[\frac{1}{\sqrt{2}} - \frac{1}{2} e^{-\frac{1}{c} (I_{\{\mathcal{A}_z(i)\}}^g(\phi) - I_{\{\mathcal{A}_z(i)\}}^g(\phi^{(0)} f_{g,z}))} \right] \\ &= f_{g,z} \left[\frac{1}{\sqrt{2}} - |\sin(\pi\phi f_{g,z})| \right], \end{aligned} \quad (3.77)$$

where $\phi^{(0)} = \frac{1}{6}$ is the value at which the flux-dependent part of $S_0(\phi)$ vanishes. Further, from eq.(3.30), we have

$$I_{\{\mathcal{A}_z(i)\}}^g(\phi_g) - I_{\{\mathcal{A}_z(i)\}}^g(\phi_g^{(0)} f_{g,z}) = -c \ln(2|\sin(\pi\phi f_{g,z})|). \quad (3.78)$$

Note that the non-differentiability of $Q_g(\phi)$ at $\phi f_{g,z} = 0, 1, 2, \dots$ is not a concern as ϕ is chosen to be non-integral, ensuring that $\phi f_{g,z}$ is also non-integral.

In order to express the number N_L^x of positive k_x -states available inside the Fermi surface in the x -direction in terms of $Q_g(\phi)$, we need to establish a relation between the flux ϕ and the Fermi surface. The k_x -states of interest to us are given by $k_x^n = \frac{2\pi n}{L_x}, n \in \mathbb{Z}, 0 \leq k_x^n \leq k_x^F$, where k_x^F is the x -component of the Fermi momentum \vec{k}_F . Assuming the flux-free Hamiltonian has time-reversal symmetry, there should be an equal number of states with the opposite momenta. Let n^* be the integer for which $k_x^{n^*} \leq k_x^F$ and $k_x^{n^*+1} > k_x^F$. Since the flux couples to the k_x -states as $k_x^n \rightarrow k_x^n + eA = \frac{2\pi n + 2\pi\phi}{L_x}$, tuning ϕ by 1 leads to the entire spectrum of k_x -states being shifted by one quantum number: $k_x^n \rightarrow \frac{2\pi(n+1)}{L_x} = k_x^{n+1}$. This means that the state $k_x^{n^*}$ moves to $k_x^{n^*+1}$, and hence out of the Fermi volume by crossing k_x^F . This flow of the spectrum is shown in Fig. 3.15.

If we now connect the system to a particle reservoir with the chemical potential set to zero, any k_x -state that moves out of the Fermi volume becomes unoccupied. We continue tuning the flux to a value ϕ^* , where the system becomes entirely devoid of any particles. The number of k_x -states that are below k_x^F can then be said to be given by the number of times ϕ goes through an integer value while changing from 0^+ to $\phi^* + 0^+$. Since we do not set the flux to an integer value, we can equivalently count the number of times ϕ goes through, say, three-quarters of an integer $-j - \frac{1}{4} : j = 1, 2, \dots$ in changing from 0^+ to $\phi^* - 0^+$. We will now show that this count can be expressed in terms of Q_g . We begin by considering $Q_0(\phi) = \frac{1}{\sqrt{2}} - |\sin \pi\phi|$. At every three-quarter value of the flux, the quantity $\phi_j = j - \frac{1}{4} : j = 1, 2, \dots, |\sin \pi\phi_j|$ attains the value of $\sin \frac{\pi}{4} = \frac{1}{\sqrt{2}}$, such that $Q_0^{-1}(\phi)$ goes through a simple pole. Each such pole ϕ_j can be picked up via a complex integral around a contour \mathcal{C}_j that encloses the pole:

$$-f_j \frac{1}{2\sqrt{2}i} \oint_{\mathcal{C}_j} \frac{d\phi}{Q_0(\phi)} = 1, \quad (3.79)$$

where f_j is either $+1$ or -1 and is defined through the equation $|\sin(\pi(j - \frac{1}{4}))| = f_j \sin(\pi(j - \frac{1}{4}))$, and \mathcal{C}_j is a circle of diameter $1/4$ centered at $\phi = j - \frac{1}{4}$ (shown in Fig. 3.13). The evaluation of the integral eq.(3.79) is shown in Appendix 3.10. In order to drop the sign prefactor f_j , we reorient those contours for which f_j is $+1$, and such that they wind around in the clockwise direction. The contours are shown in the left panel of Fig. 3.14, and defined as

$$C_j(\phi) = \left\{ \phi : \phi = j - \frac{1}{4} + \frac{1}{8}e^{i\theta}, \theta \in [0, -2\pi f_j] \right\}, \quad (3.80)$$

such that they host a singularity at their center. With this redefinition of the contours, we have

$$\frac{1}{2\sqrt{2}i} \oint_{C_j} \frac{d\phi}{Q_0(\phi)} = 1 . \quad (3.81)$$

Counting the number of three-quarter values then reduces to counting the number of poles of Q_0^{-1} in the above-mentioned range $\phi \in (0, \phi^*)$. In this way, we can now express the count N_L^x in terms of Q_0 :

$$N_L^x = \frac{1}{2} \sum_{j=1}^{\phi^*} \frac{1}{2\sqrt{2}i} \oint_{C_j(\phi)} \frac{d\phi}{Q_0(\phi)} = \frac{1}{2\sqrt{2}} \sum_{j=1}^{\phi^*} \frac{1}{2i} \oint_{C_j(\phi)} \frac{d\phi}{Q_0(\phi)} . \quad (3.82)$$

The factor of half in eq.(3.82) is required as we want to count only the number of positive momentum states (and which is equal to the number of negative momentum states).

In going from $Q_0(\phi)$ to a general $Q_g(\phi)$, the only change required is to redefine $\phi \rightarrow \phi_g = f_{g,z}\phi$. This implies that while the states in k -space have become more coarse-grained, the flux ϕ has become more fine-tuned by the same scaling factor. This is a reflection of the overall conservation of particle number density: keeping the chemical potential fixed, the increased spacing between the k_x -states implies that a smaller number of particles are now occupying an equally smaller volume. As the number density is conserved, so is the Luttinger volume (eq.(3.10)), and this shows that our approach is consistent with the holographic Luttinger theorem [103]. Thus, given that $\phi_g^* = \phi^*$, the expression for N_L^x remains practically unchanged:

$$N_L^x = \frac{1}{2\sqrt{2}} \sum_{j=1}^{\phi^*} \frac{1}{2i} \oint_{C_j(f_{g,z}\phi)} \frac{d\phi_g}{\frac{1}{\sqrt{2}} - |\sin \pi \phi_g|} . \quad (3.83)$$

In order to rewrite N_L^x in terms of the flux ϕ , we start by making the substitution $\phi_g \rightarrow f_{g,z}\phi$:

$$N_L^x = \frac{1}{2\sqrt{2}} \sum_{j=1}^{\phi^*} \frac{1}{2i} \oint_{C_j(f_{g,z}\phi)} \frac{f_{g,z} d\phi}{\frac{1}{\sqrt{2}} - |\sin (\pi f_{g,z}\phi)|} . \quad (3.84)$$

In the above equation, we can recognise $\frac{f_{g,z}}{\frac{1}{\sqrt{2}} - |\sin (\pi f_{g,z}\phi)|}$ as $Q_g^{-1}(\phi)$. Also note that the contour can be written as

$$\mathcal{C}_j(f_{g,z}\phi) \equiv \mathcal{C}_j^g(\phi) = \left\{ \phi : \phi = t_{g,z} \left(j - \frac{1}{4} + \frac{e^{i\theta}}{8} \right), \theta \in [0, -2\pi f_j] \right\} . \quad (3.85)$$

These curves are again circles of radius $1/8$, but centered at $t_{g,z} \times (1 - \frac{1}{4})$, $t_{g,z} \times (2 - \frac{1}{4})$, $t_{g,z} \times (3 - \frac{1}{4})$ and so on. These are simply a generalisation of the curves defined in eq. (3.80); the curves for $t_{g,z} = 2$ are shown in the right panel of Fig. 3.14. Substituting this in eq.(3.84) gives

$$N_L^x = \frac{1}{2\sqrt{2}} \sum_{j=1}^{\phi^*} \frac{1}{2i} \oint_{\mathcal{C}_j^g(\phi)} \frac{d\phi}{Q_g} . \quad (3.86)$$

For a spatially isotropic system, the Fermi volume is given by

$$V_L = v_2 \times \pi (N_L^x)^2 = \frac{1}{2} \frac{\pi^3}{V} \left[\sum_{j=1}^{\phi^*} \frac{1}{2i} \oint_{\mathcal{C}_j^g(\phi)} \frac{d\phi}{Q_g(\phi)} \right]^2 , \quad (3.87)$$

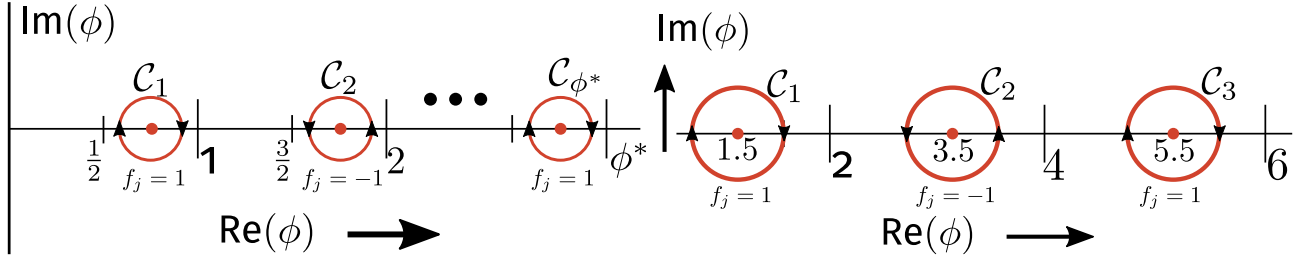


Figure 3.14: *Top:* Contours \mathcal{C}_j used to integrate over Q_0^{-1} in eq. (3.82). Tall vertical lines represent integer values of $\text{Re}(\phi)$. All contour start and end within two adjacent integer values. The final contour \mathcal{C}_{ϕ^*} ends just short of $\text{Re}(\phi) = \phi^*$. Note the alternating direction of the contours brought about by the alternation of f_j in going from $j = 1$ to $j = 2$, and so on. *Bottom:* Contours \mathcal{C}_j^g for $t_{g,z} = 2$, centered at $2(1 - \frac{1}{4})$, $2(2 - \frac{1}{4})$ and $2(3 - \frac{1}{4})$. Note the alternating directions of the contours.

where V is the real space volume of the system, and $v_d = (2\pi)^d/V$ is the volume of the smallest unit in k -space. For a generally anisotropic Fermi volume, each direction in the d -dimensional k -space can be completely specified by an angular coordinate θ with respect to some predefined coordinate system. For each direction $\hat{\theta}$, we can insert a gauge field $\vec{A} = A\hat{\theta}$ and take the thin torus limit in this direction, obtaining thereby the g -partite information $I^g(\phi_\theta)$ for length l in the direction perpendicular to $\hat{\theta}$. With the θ -dependent I^g , one can then define the quantity $Q_g(\phi_\theta)$ which counts the number of states N_L^θ in the direction $\hat{\theta}$ inside the Fermi volume. In this way, the total Fermi volume can be obtained by integrating over θ :

$$V_L = \frac{\pi^2}{4V} \int_0^{2\pi} d\theta \left[\sum_{j=1}^{\phi_\theta^*} \frac{1}{2\pi i} \oint_{\mathcal{C}_j^g(\phi)} \frac{d\phi}{Q_g(\phi)} \right]^2. \quad (3.88)$$

It is important to note that the quantity V_L is independent of the RG index g , and is thus identical in value for all g members of the hierarchy at the g th step of the coarse-graining process.

The topological nature of Luttinger volume can be made further manifest by expressing it in terms of winding numbers, following Ref. [124] for the case of interacting electrons. To do so, we point out that the integrand $Q_g^{-1}(\phi)$ can be written as a derivative:

$$\frac{1}{Q_g(\phi)} = \frac{\sqrt{2}}{\pi} \frac{\partial}{\partial \phi} \ln Y_j^g = \frac{\sqrt{2}}{\pi} \frac{1}{Y_j^g} \frac{\partial Y_j^g}{\partial \phi}, \quad (3.89)$$

where

$$\begin{aligned} Y_j^g(\phi) &\equiv \left[\frac{f_j \tan 3\pi/8 - \tan(\pi f_{g,z}\phi/2)}{\tan(\pi f_{g,z}\phi/2) - \tan(\pi/8)} \right]^{f_j} \\ &= \begin{cases} \frac{\tan 3\pi/8 - \tan(\pi f_{g,z}\phi/2)}{\tan(\pi f_{g,z}\phi/2) - \tan(\pi/8)}, & \text{when } j = \text{odd, and} \\ \frac{\tan(\pi f_{g,z}\phi/2) + \tan(\pi/8)}{-\tan 3\pi/8 - \tan(\pi f_{g,z}\phi/2)}, & \text{when } j = \text{even.} \end{cases} \end{aligned} \quad (3.90)$$

Substituting this into the expression for 2-dimensional isotropic Luttinger volume in eq. (3.87), we obtain

$$V_L = \frac{\pi^3}{V} \left[\sum_{j=1}^{\phi^*} \frac{1}{2\pi i} \oint_{Y_j^g(\mathcal{C}_j^g)} \frac{dY_j^g}{Y_j^g} \right]^2. \quad (3.91)$$

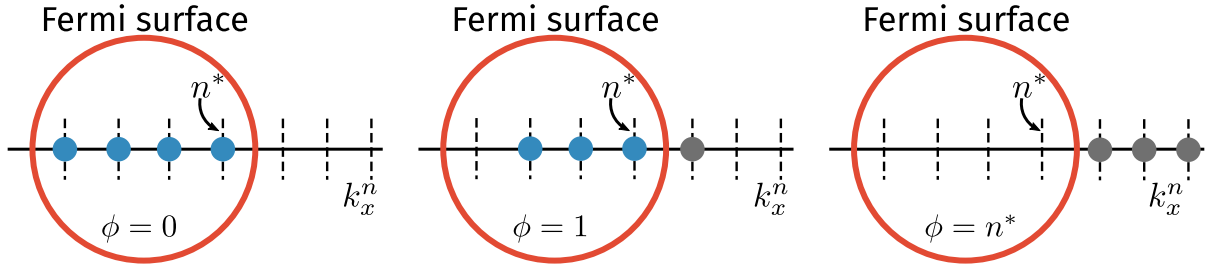


Figure 3.15: Spectral flow of the states within the Fermi volume. The red curve represents the Fermi surface. Upon tuning the flux ϕ , the k -space states (indicated in the form of dotted lines along the k_x -axis) are shifted towards the Fermi surface. The blue circles represent electrons with momenta below k_F , and are part of the ground state. On the other hand, the grey circles represent particles with momenta above k_F : they have moved out of the system, and into the reservoir connected to it (see discussion in main text). Each time ϕ changes by 1, the state nearest to the Fermi surface moves out of the Fermi volume. Tuning ϕ by n^* empties the entire Fermi volume.

As before, the specific integral in the above expression is a winding number that counts the number of times the contour $Y_j^g(\mathcal{C}_j^g)$ winds around the singularity at $Y_j^g = 0$. Note that these are the same singularities that exist at the centers of the contours \mathcal{C}_j^g and that are picked up in, for example, eq. (3.79). To demonstrate this, we point out that the centers of the contours are given by $\phi = t_{g,z}(j - \frac{1}{4})$, $j = 1, 2, \dots, \phi^*$. At these values, we have

$$\tan\left(\frac{\pi f_{g,z}\phi}{2}\right) = \tan\left(\frac{\pi j}{2} - \frac{\pi}{8}\right) = \begin{cases} \tan\frac{3\pi}{8}, j = 1, 3, \dots \\ -\tan\frac{\pi}{8}, j = 2, 4, \dots \end{cases} \quad (3.92)$$

Comparing with eq. (3.90), we can see that the numerators of Y_g^j are zero at these values of ϕ for both even and odd values of j . This leads to $Y_g^j = 0$, and hence a singularity in $\frac{dY_g^j}{Y_g^j}$. These values of the flux are therefore the common singularities that are picked up by the poles of $Q_g^{-1}(\phi)$ as well as the winding numbers.

We now define w_g^j as the winding number for the curve $Y_g^j(\mathcal{C}_j^g)$ around $Y_g^j = 0$, and $\mathcal{W}(\phi^*) = \sum_{j=1}^{\phi^*} w_g^j$ as the total winding number for all the curves $\{Y_g^j(\mathcal{C}_j), j = 1, 2, \dots\}$. Then, the isotropic Fermi volume takes the compact form

$$V_L = \frac{\pi^3}{V} \mathcal{W}(\phi^*)^2. \quad (3.93)$$

3.9.2 A relation between the quantum hall Chern numbers and Luttinger's volume

Interestingly, the above method employed in using entanglement measures to extract the Luttinger volume can also be applied (with suitable modifications) to an integer quantum hall system (generated upon placing the system in a strong transverse magnetic field) to obtain the number of filled Landau levels (a Chern number). To begin, we imagine a system of free non-relativistic electrons in a cylinder geometry (fig. 3.16), and placed in a magnetic field $\nabla \times \vec{A} = \vec{B}$ that points radially outwards. The field \vec{B} generates Φ flux quanta through the surface of the cylinder. An Aharonov-Bohm flux $\vec{A}' = -2\pi\phi/L_x \hat{x}$ is also placed in the x -direction (i.e., along the circumference of the cylinder). We divide the cylinder

into two subsystems A and B (fig. 3.16), such that tuning the dimensionless flux ϕ by 1 transfers a charge equal to the first Chern number, from A to B . The translation invariance in the x -direction ensures that the momentum k_x are good quantum numbers; for each value of k_x , we can define the matrix elements of the single-particle correlation matrix $G(k_y)$ for the subsystem A as [167, 168]

$$G_{ij}^A(k_x) = \langle \psi_{\text{gs}} | c_{k_x,i}^\dagger c_{k_x,j} | \psi_{\text{gs}} \rangle , \quad (3.94)$$

where $|\psi_{\text{gs}}\rangle$ is the ground state and i, j represent the degrees of freedom other than k_x . The total matrix G^A is constructed by joining the smaller blocks $G^A(k_x)$. As ϕ is varied, the variation of the trace of the flux-dependent matrix $G^A(\phi)$ is linear in the flux ϕ : $\text{Tr}[G^A(\phi)] - \text{Tr}[G^A(0)] = -\frac{1}{e}\sigma_H\phi$. This implies that as long as there are extended states at sufficiently small energies, we will have spectral flow that can be captured through the integral:

$$-\frac{\sigma_H}{2\pi ie} \int_{\mathcal{C}_H} \frac{d\phi}{\text{Tr}[G^A(\phi)] - \text{Tr}[G^A(0)]} , \quad (3.95)$$

where \mathcal{C}_H is a circle of radius $1/2$ in the complex plane centered at $\phi = 0$. This integral is zero if there is no spectral flow, i.e., the effect of the gauge field can be removed by a gauge transformation and the trace is insensitive to the flux. In order to count the number of filled Landau levels (essentially, the filling factor ν), we can now vary the flux quanta Φ (due to \vec{B}) so as to change the filling from ν to 0:

$$\nu = -\frac{\sigma_H}{2\pi ie} \sum_{\Phi'=\Phi}^{\Phi^{\max}} \int_{\mathcal{C}_H} \frac{d\phi}{\text{Tr}[G_{\Phi'}^A(\phi)] - \text{Tr}[G_{\Phi'}^A(0)]} . \quad (3.96)$$

The subscript Φ' on G^A indicates that the correlations depend on the variable magnetic field \vec{B}' . The upper limit Φ^{\max} is given by the lowest value of the magnetic field \vec{B}' for which only one Landau level is filled. The magnetic field is varied such that exactly an integer number of Landau levels are filled at any given value. Importantly, the filling factor ν is known to be a Chern number $\mathcal{C}(\Phi)$ [24, 169].

We can also relate eq. (3.96) to the entanglement of the system by introducing the entanglement spectrum [18, 142], which refers to the set of eigenvalues $\{\lambda_\chi^A(k_x)\}$ of the reduced density matrix $\rho^A(k_x)$ for subsystem A corresponding to the momentum mode k_x in the x -direction and χ is a particular configuration of the degrees of freedom $\{i\}$ in the y -direction. We have the relation [168]

$$\lambda_\chi^A(k_x) = \text{Det} [P_\chi G^A(k_x) (1 - P_\chi) G^A(k_x)] , \quad (3.97)$$

where P_χ is an operator that projects on to the subset of states $\{j\}$ in $\{i\}$ that are occupied in the configuration χ . This relation between G^A and the eigenvalues λ then leads to the same conclusion as in the case without the magnetic field: the pole structure of the entanglement spectrum encodes the topological information of the system revealed in eq.(3.96). In the case of zero magnetic field, the topological quantity revealed from the pole structure was a winding number (\mathcal{W}), while in the present case it is a Chern number.

Finally, we reveal the connection between the winding numbers \mathcal{W} in the metallic case and the Chern numbers in the integer quantum Hall system. The degeneracy of each Landau level is equal to the number of flux quanta Φ generated by the magnetic field B . Since the total number of particles in the system is fixed, the electronic states of the filled Fermi sea that form the Luttinger volume (in the absence of the external B-field) are redistributed into the Landau levels with the appropriate degeneracy

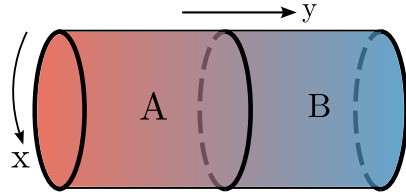


Figure 3.16: Cylindrical geometry for the integer quantum Hall system, with a magnetic field \vec{B} pointing radially outwards through the surface of the cylinder. An Aharonov-Bohm vector potential acts in the x -direction (i.e., along the circumference). The entanglement is calculated between the subsystem A and its complement B .

as a strong transverse magnetic field is turned on. Thus, we have the constraint that the total number of occupied states $\mathcal{C} \times \Phi$ in the quantum hall system (\mathcal{C} being the Chern number and equal to the number of filled Landau levels) must be equal to $\pi (N_L^x)^2$, the total number of occupied states in the metallic system. Combining eqs. 3.86 and 3.93 with this discussion then allows us to relate \mathcal{C} to the winding number $\mathcal{W}(\phi^*)$:

$$\mathcal{C} \times \Phi = \left\lfloor \frac{\pi}{4} \mathcal{W}(\phi^*)^2 \right\rfloor = \frac{V_L}{v_2}, \quad (3.98)$$

where $v_2 = 4\pi^2/V$ is the volume of the k -space unit cell (defined below eq. (3.86)) and $\lfloor \cdot \rfloor$ is the floor function and returns the largest integer less than or equal to the argument.

3.10 Conclusions and Outlook

In summary, we have shown that considering the renormalisation group flows of the spectral gap coupling of a system of non-interacting electrons in $2 + 1$ -dimensional theory leads to hierarchical arrangement of the entanglement with scale, and that the geometrical part of the entanglement can be described as the emergence of an additional spatial dimension, leading to holographic expressions for geometric parameters like distance and curvature. We show that changing the boundedness of the holographic space involves a topological transition with the Fermi surface of the boundary theory turning critical, and involves the generation of a geometric wormhole between the UV and IR degrees of freedom. For the massless case, the presence of an Aharonov-Bohm flux generates a geometry-independent term in the entanglement entropy which can be linked to the Luttinger volume of the gapless fermionic system. By placing the system of $2 + 1$ dimensional electrons in a strong magnetic field, we argue that the Chern number topological invariant for the ground states of the integer quantum Hall ground system are constrained by the value of the Luttinger volume in the underlying metallic system (i.e., prior to the insertion of the field).

How robust are our conclusions towards the inclusion of electronic correlations? Given the adiabatic continuity that links Fermi liquids to the non-interacting Fermi gas, i.e., the preservation of the k -space quantum numbers under adiabatic inclusion of (screened) inter-particle interactions, we expect our results to be equally valid for the many-particle entanglement of the excitations described by the fixed point effective theory for the Fermi liquid. This also suggests that our results for the wormhole geometry and the stress-energy tensor relation at the critical Fermi surface apply very generally to phase transitions that destabilise and gap out the Fermi surface. Specifically, this has profound implications for metal-insulator transitions driven by strong correlations. Non-Fermi liquids are, however, not

adiabatically continuous to the Fermi gas. Thus, it should be interesting to adapt our approach to the study of interacting models of electrons that lead to gapless non-Fermi liquids (including those that are known to appear at quantum critical points related to the breakdown of a Fermi liquid). For instance, Ref. [170] reports that the second Renyi entropy of a thin k -space shell proximate to the Fermi surface is related to the quasiparticle residue; how would this change in a non-Fermi liquid? It also appears interesting to identify the effects of electronic correlations on various aspects of the emergent space. The renormalisation group techniques applied in Refs. [170–174] could also be worth investigating towards answering these questions.

It is interesting to note that our results point towards a broader similarity between the gapless fermionic systems considered here and gapped topologically ordered quantum liquids. Recall that the latter are known to possess a ground state degeneracy that is dependent on the topological nature of the interacting electronic system, leading to a subsystem entanglement entropy that has a geometry-independent subleading piece (S_{topo}) referred to as the topological entanglement entropy. It was shown by some of us recently [136] that for a collection of N subsystems (CSS) that form a closed annular structure, the n -partite quantum entanglement information measures I^n ($3 \leq n \leq N$) are a topological invariant equal to the product of S_{topo} and the Euler characteristic of the planar manifold on which the CSS is embedded. This appears to be analogous to our finding of the hierarchical sequence of quantities $\{Q_g\}$ defined at a particular RG step (and arising out of the topological flux-dependent piece of the entanglement entropy), all of whom encode the same Luttinger volume for the gapless systems we have studied (eq. (3.88)). Further, the robustness of the n -partite information I^n against small deformations of the CSS in a topologically ordered system can be compared to the invariance of N_L^x to small deformations of the contours C_1, C_2, \dots (see right panel of Fig. 3.14). It appears tempting to speculate on a possible universal origin underlying these similarities (see also [174] for a recent investigation of the entanglement properties of various quantum liquids).

Our results lead to a number of interesting questions. Firstly, the convergence parameter θ is reminiscent of the expansion rate of congruence flows on Riemannian manifolds in the context of the Raychaudhuri equation [165]. While the evolution equation for θ (eq. (3.70)) obtained by us is not of the same form (as there is no time variable, neither is there a θ^2 term in the expansion rate), we do expect such an equation to hold for an appropriately defined expansion parameter [166, 175]. This likely requires the introduction of temporal dynamics of the emergent spatial dimension, and lies well beyond the purview of the present work. Secondly, it remains to be seen how the geometry-independent part of the entanglement behaves in the presence of a mass ($m > 0$) for the Dirac fermions: a spectral gap is expected to have consequences for Luttinger's theorem [1] (see also eq.(3.11)), as well as for the many-particle entanglement. For instance, Ref. [170] reports that the second Renyi entropy shows the signatures of the condensation of Cooper pairs in the BCS problem.

Finally, we would like to point out an interesting conclusion that emerges from our analysis. As observed by us, the system considered here shows a hierarchy of multipartite entanglement measures beyond just the mutual information. Further, we have shown that the mutual information leads to the emergence of the holographic dimension. However, whether the higher-party measures also have a holographic interpretation remains an open question. We note that studies of the time-variation of tripartite information during an equilibrium process after the injection of energy suggest that it remains negative throughout the process [176–178], indicating that care must be taken in defining geometric measures using it. Nevertheless, our study raises the possibility of obtaining a generalisation of the gauge-gravity duality from the perspective of many-particle entanglement. We speculate that the higher order information measures will lead to a modification of the universal entanglement Hamiltonian.

nian obtained at criticality. Further, that these modifications can be visualised as a *hypergraph*: just as a graph contains edges that connect any two nodes, a hypergraph contains *hyperedges* that can connect more than two nodes. The eigenvalues $\epsilon^{(n)}$ (with $n > 2$) of the entanglement Hamiltonian would act as hyperedges connecting the degrees of freedom $\{i, j, \dots\}$. We leave an investigation of these aspects to future works.

Appendix A: Reduction of the $2 + 1$ -D system to a tower of $1 + 1$ -D massive modes

In the absence of the gauge field, the Lagrangian for $2 + 1$ -dimensional massive non-interacting relativistic electrons (in natural units) is

$$\mathcal{L} = \int dx dy \bar{\psi}(x, y) [i\gamma^\mu \partial_\mu - m] \psi(x, y). \quad (3.99)$$

The integral ranges over the area of the torus on which the electrons reside, and the time dependence of the fields has been suppressed. Each component $\psi^a, a = 0, 1, 2, 3$, of the Dirac spinor $\psi = (\psi^0 \quad \psi^1 \quad \psi^2 \quad \psi^3)$ satisfies the Dirac equation

$$[i\gamma^\mu \partial_\mu - m] \psi^a(x, y) = 0, \quad (3.100)$$

which is equivalent to the form

$$\int dx \bar{\psi}^a(x, y) [i\partial^\nu \gamma_\nu + m] [i\gamma^\mu \partial_\mu - m] \psi^a(x, y) = 0. \quad (3.101)$$

Due to the periodic boundary conditions (PBCs) in the x -direction, the momenta k_x are quantised: $k_x^n = \frac{2\pi n}{L_x}, n \in \mathbb{Z}$. We expand the fields $\psi^a(x, y)$ in these momenta:

$$\psi^a(x, y) = \sum_{n=-\infty}^{\infty} e^{ik_x^n x} \psi^a(k_x^n, y). \quad (3.102)$$

Writing the Dirac equation in terms of the dual fields $\psi^a(k_x^n, y)$ gives

$$\begin{aligned} \sum_{m,n} (\bar{\psi}^a(k_x^m, y) e^{-ik_x^m x}) [i\partial^\nu \gamma_\nu + m] [i\gamma^\mu \partial_\mu - m] \times \\ (e^{ik_x^n x} \psi^a(k_x^n, y)) = 0, \end{aligned} \quad (3.103)$$

where

$$[i\gamma^\mu \partial_\mu - m] (e^{ik_x^n x} \psi^a) = e^{ik_x^n x} [i\gamma^\mu \partial_\mu - (\gamma^x k_x^n + m)] \psi^a. \quad (3.104)$$

Similarly,

$$\begin{aligned} (\bar{\psi}^a(k_x^m, y) e^{-ik_x^m x}) [i\partial^\nu \gamma_\nu + m] \\ = [[i\gamma^\nu \partial_\nu + m] (e^{ik_x^m x} \gamma_0 \psi^a)]^\dagger \\ = \bar{\psi}^a e^{-ik_x^m x} [i\partial^\nu \gamma_\nu - (\gamma^x k_x^m - m)]. \end{aligned} \quad (3.105)$$

Substituting these into the equation eq.(3.103) gives

$$\sum_n \int dy \bar{\psi}^a(k_x^n, y) [\partial_\mu \partial^\mu + k_x^{n2} + m^2] \psi^a(k_x^n, y) = 0, \quad (3.106)$$

where we have used $\int dx e^{ix(k_x^m - k_x^n)} = \delta_{m,n}$.

Appendix B: Evaluation of the multi-partite information

We define the multipartite information among g sets $\{\mathcal{A}_z(i)\}$ as [136]

$$I_{\{\mathcal{A}_z(i)\}}^g = \sum_{r=1}^g (-1)^{r-1} \sum_{\beta \in \mathcal{P}(\{\mathcal{A}_z(i)\})}^{|\beta|=r} S_\beta , \quad (3.107)$$

where $\mathcal{P}(\{\mathcal{A}_z(i)\})$ is the power set of $\{\mathcal{A}_z(i)\}$, and $|\beta| = r$ implies that we sum only over those sets β that have r number of elements in them. We will first evaluate the internal sum σ_r over the set β for a general r :

$$\sigma_r = \sum_{\beta \in \mathcal{P}(\{\mathcal{A}_z(i)\})}^{|\beta|=r} S_\beta . \quad (3.108)$$

For this, we first note that following eq. (3.26), the entanglement entropy (EE) of the union of a given sequence of sets $\{i\}$ is given by the EE of the set with the highest (lowest) index for a positive (negative) z . As a result, the EE S_β for the set β is simply $S_\beta = \theta(z)S_{\min(\beta)} + \theta(-z)S_{\max(\beta)}$. If $n_j^{(r,+)} (n_j^{(r,-)})$ is the number of sets of cardinality r that have the element $\mathcal{A}_{j,z}$ as the element with the smallest (largest) index j , the internal sum can be written as

$$\sigma_r = \sum_{j=1}^{g-(r-1)} \theta(z)n_j^{(r,+)} S_{j,z} + \sum_{j=r}^g \theta(-z)n_j^{(r,-)} S_{j,z} . \quad (3.109)$$

The number $n_j^{(r,+)}$ corresponds to the number of ways one can pick $r-1$ elements out of a set of $g-j$ elements: $n_j^{(r,+)} = \binom{g-j}{r-1}$. Similarly, $n_j^{(r,-)}$ corresponds to the number of ways one can pick $r-1$ elements out of a set of j elements: $n_j^{(r,-)} = \binom{j}{r-1}$. We can also extend the limits on the two summations by defining $\binom{n}{m} = 0$ for $n < m$. With these considerations, eq. (3.109) takes the form

$$\sigma_r = \sum_{j=1}^g \left[\theta(z) \binom{g-j}{r-1} + \theta(-z) \binom{j}{r-1} \right] S_{j,z} . \quad (3.110)$$

This can now be substituted into the full expression for the multipartite equation, giving

$$\begin{aligned} I_{\{\mathcal{A}_z(i)\}}^g &= \sum_{r=1}^g (-1)^{r-1} \sum_{j=1}^g \left[\theta(z) \binom{g-j}{r-1} + \theta(-z) \binom{j}{r-1} \right] S_{j,z} \\ &= \sum_{j=1}^g S_{j,z} \left[\theta(z) \sum_{r=0}^{g-j} (-1)^r \binom{g-j}{r} + \theta(-z) \sum_{r=0}^j (-1)^r \binom{j}{r} \right] . \end{aligned} \quad (3.111)$$

From the binomial theorem, we can now recognise each internal sum as over r as a polynomial expansion. That is, upon comparing with $(x-1)^n = \sum_{m=0}^n \binom{n}{m} (-1)^m x^{n-m}$, we obtain $\sum_{r=0}^{g-j} (-1)^r \binom{g-j}{r} = \lim_{x \rightarrow 1} (x-1)^{g-j} = \delta_{g,j}$. Similarly, the other sum evaluates to $\delta_{j,0}$. Substituting these into the expression

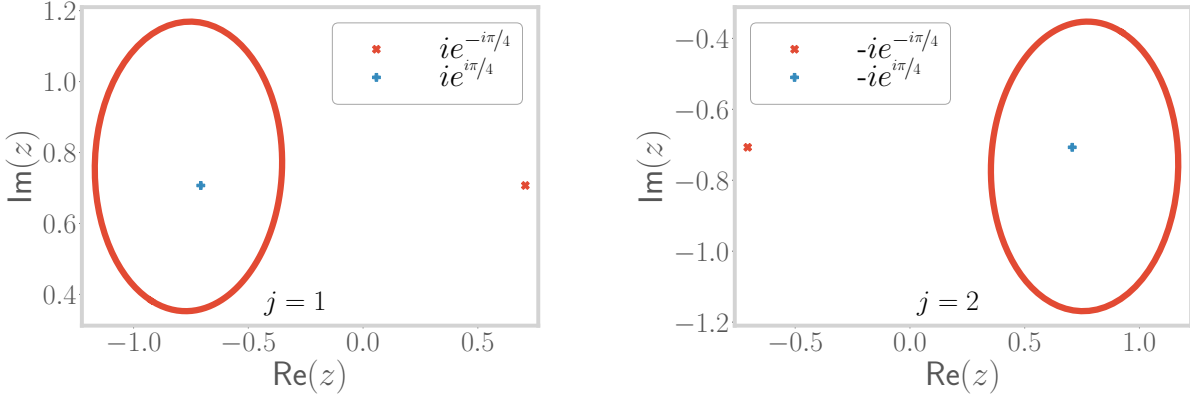


Figure 3.17: Contours $z(\mathcal{C}_j)$ for two values of j employed for evaluating the integral eq.(3.114), and the locations of the poles z_{\pm}^{\pm} . For each j , only one pole (shown in blue) contributes, as the other (shown in red) is not enclosed by the contour.

for $I_{\{\mathcal{A}_z(i)\}}^g$ gives

$$\begin{aligned} I_{\{\mathcal{A}_z(i)\}}^g &= \sum_{j=1}^g S_{j,z} [\theta(z)\delta_{g,j} + \theta(-z)\delta_{j,0}] \\ &= \theta(z)S_g + \theta(-z)S_0 . \end{aligned} \quad (3.112)$$

By noting that S_g and S_0 are, respectively, the EE of the intersection set of $\{\mathcal{S}_z(i)\}$, one can combine the two terms in the previous equation into

$$I_{\{\mathcal{A}_z(i)\}}^g = \theta(z)S_g + \theta(-z)S_0 = S_{\cap\{\mathcal{A}_z(i)\}} . \quad (3.113)$$

Appendix C: Evaluation of the contour integral that counts poles

We prove eq. (3.79) in this appendix. The integral in question is given by

$$\mathcal{I} = \oint_{\mathcal{C}_j} \frac{d\phi}{Q_0(\phi)} = \oint_{\mathcal{C}_j} \frac{d\phi}{\frac{1}{\sqrt{2}} - |\sin \pi\phi|} , \quad (3.114)$$

where \mathcal{C}_j is the contour shown in Fig. 3.13 and the variable ϕ is given by $\phi = \{\phi_j + \frac{1}{8}e^{i\theta} : \theta \in [0, 2\pi]\}$, where $\phi_j = j - \frac{1}{4}$ is the center of the contour. In order to evaluate the integral, we make a variable change: $z = e^{i\pi\phi}$, giving $dz = i\pi z d\phi$ and $\sin \pi\phi = \frac{1}{2i}(z - \frac{1}{z})$. Depending on the value of j , $\sin \pi\phi$ can be either positive or negative. We denote either case by a subscript \mathcal{I}_{\pm} corresponding to the contour \mathcal{C}_{\pm} , giving $|\sin(\pi\phi)| = \pm \sin(\pi\phi)$. Casting the integral in terms of z , we obtain

$$\mathcal{I}_{\pm} = \frac{1}{i\pi} \oint_{z(\mathcal{C}_{\pm})} \frac{dz/z}{\frac{1}{\sqrt{2}} \mp \frac{1}{2i}(z - \frac{1}{z})} = \oint_{z(\mathcal{C}_{\pm})} \frac{\mp \frac{2}{\pi} dz}{\left(z \mp \frac{i}{\sqrt{2}}\right)^2 - \frac{1}{2}} . \quad (3.115)$$

The integrand in \mathcal{I}_+ has two simple poles at $z_{+}^{\pm} = +ie^{\mp i\pi/4}$. Similarly, the integrand in \mathcal{I}_- has two simple poles at $z_{-}^{\pm} = -z_{+}^{\pm}$. We plot the contour and the two poles for two contours of opposite signature

in Fig. 3.17; it is clear that only the pole at z_{\pm}^+ contributes to the integral. Using the residue theorem, the integral evaluates to

$$\begin{aligned}\mathcal{I}_{\pm} &= \oint_{z(C_{\pm})} \frac{\mp \frac{2}{\pi} dz}{(z - z_{\pm}^+) (z - z_{\pm}^-)} \\ &= \mp \frac{2}{\pi} 2\pi i \lim_{z \rightarrow z_{\pm}^+} \frac{1}{z - z_{\pm}^-} \\ &= \mp 2\sqrt{2}i.\end{aligned}\tag{3.116}$$

This proves eq. (3.79).

Chapter 4

ESIAM

4.1 Introduction

The rich physics of metal-insulator transitions in strongly correlated systems has been an active subject of study for quite some time [179–181], yet much still remains to be understood. It involves diverse aspects such as spin and charge fluctuations, quasiparticle renormalisation effects, anomalous metallic phases and unconventional superconductivity, and has been studied using an equally diverse array of methods like mean-field theory, renormalisation group approaches, numerical techniques like exact diagonalisation, quantum Monte Carlo and dynamical mean-field theory, and many others. In particular, dynamical mean-field theory (DMFT) [182–190] obtains an exact solution of the Mott metal-insulator transition (MIT) for the 1/2-filled Hubbard model [191–195] on the Bethe lattice with infinite coordination number, in terms of an Anderson impurity model with a self-consistently determined bath obtained by requiring, in an iterative manner, that its local Greens function be equal to that of the impurity site. The above-mentioned transition can be captured by the local spectral function through (i) the continuous appearance of a Mott gap, followed by (ii) the sharpening and vanishing of the central Kondo resonance. These two features are often referred to, respectively, as the Mott-Hubbard [194] and Brinkman-Rice [195] scenarios of the Mott MIT. The exact nature of the solution arises from the fact that all non-local contributions to the lattice self-energy are observed to vanish upon taking the limit of an infinite coordination number for the lattice model. Thus, the simplification is that the dynamics of any local site on the lattice is determined completely by a quantum impurity problem [186, 196]. It must also be noted that this exact solution precludes any long-range order in the system, and corresponds to the case of a maximally frustrated Hubbard model involving long-range and frustrating inter-site hopping such that both the metallic and insulating phases remain paramagnetic [197]. Due to the exact and non-perturbative nature of the DMFT solution for the MIT in $d = \infty$, the method has been extended to models of strongly correlated electrons in finite spatial dimensions [188, 198, 199], as well as the study of the electronic properties of various correlated materials [189, 200, 201].

Despite this progress, a key aspect of the DMFT solution for the Hubbard model in $d = \infty$ remains to be understood. During the search for a self-consistent impurity model, the conduction bath is modified drastically in order to become correlated [202]. The numerical implementation of self-consistency, however, precludes a deeper understanding of the precise nature of the correlations present in the conduction bath of the impurity model, and its implications for the electron dynamics of the associated bulk lattice (Hubbard) model. Indeed, as we demonstrate below, our work paves the way for a more insightful exploration of the physics of the Mott Hubbard transition in strongly correlated electronic

systems. Further, it has considerable consequences for the development of functional quantum materials and next-generation quantum technologies. Below, we lay out the specific questions addressed by us, and summarise our results at the end of this section.

- i. Is there a minimal but effective quantum impurity model Hamiltonian that describes the Mott MIT of the $1/2$ -filled Hubbard model on the Bethe lattice in $d = \infty$? Finding such an impurity model would also reduce the considerable computational effort that is presently required in self-consistent approaches.
- ii. What are the fluctuations that destroy the metal and lead to the insulating phase? Can we obtain a universal theory for these competing tendencies?
- iii. The coexistence of metallic and insulating phases at $T = 0$ within DMFT shows that the insulating solution is present within the many-body spectrum of the metallic phase. Can an associated impurity model Hamiltonian display the emergence of the insulating state prior to the transition? Analytic insight of this kind is particularly important because approaching a coexistence region numerically is often fairly tricky.
- iv. Is it possible to obtain a low-energy theory for the local gapless excitations precisely at the MIT, where the metal is on the brink of destruction? How do these excitations compare with those of the local Fermi liquid, e.g., in terms of self-energies and two-particle correlation functions?

Obtaining answers to these questions would go a long way towards understanding the dominant fluctuations at the heart of the Mott transition and the physical processes that become important as one approaches it. It would also help in understanding the mechanism of DMFT's search for the self-consistent impurity model within the space of Anderson impurity models.

The essence of our approach is to model phenomenologically the lattice self-energy obtained from DMFT in the form of additional bath correlations within an extended Anderson impurity model. In addition to the usual on-site repulsion (U) and single-particle hybridisation (V) between the impurity and the conduction bath of the Anderson impurity model (eq. (4.1)), we introduce (i) an additional on-site correlation (U_b) on the bath site with which the impurity couples, and (ii) an antiferromagnetic Kondo coupling (J) between the impurity and the conduction bath (eq. (4.2)). We note that a similar impurity model-based approach was taken towards understanding the physics of the heavy fermions several years ago by Si and Kotliar [203, 204]. We postpone a comparison of our work with theirs to the discussions section. The rest of the work is structured as follows. Sec. (4.2.1) describes the extended model that we will study, and the unitary renormalisation group (URG) method that we employ to study it is presented in Sec. (4.2.2). In Sec. (4.3) and (4.4), we describe the phase diagram and various characteristics of the impurity phase transition. In Sec. (4.6), we use our extended model to explain various features of the coexistence region observed in DMFT. In Sec. (4.7), we describe the effect of the impurity on the low-lying excitations of the bath, near and at the transition. We conclude in Sec. (4.8) with some discussions and possible future directions. For the convenience of readers, we first present below a brief summary of our main results.

Summary of our main results

- *Presence of a local metal-insulator transition:* At a critical value of the parameter $r = -U_b/J$, the effective impurity model shows a transition from a Kondo screened phase into an unscreened

local moment phase. The quantum critical point (QCP) involves a degeneration of the Kondo singlet and the local moment states.

- *The physics of Kondo screening and local pairing drives the transition:* The transition involves the frustration of the Kondo screening of the impurity by enhanced local pairing fluctuations in the bath and can be described by a universal theory written in terms of J and U_b .
- *Emergence of insulating solutions in the metallic phase:* Our analysis reveals that at a certain value of the parameter r prior to the transition, the single-particle hybridisation parameter (V) turns irrelevant (in the RG sense), and this leads to the emergence of the local moment solutions within the many-particle spectrum through an excited state quantum phase transition (ESQPT).
- *Critical fluctuations and the coexistence region:* We observe the appearance of long-ranged quantum fluctuations extending into the conduction bath in the vicinity of both the ESQPT at $r = r_{c1}$ and QPT at $r = r_{c2}$. We believe that these are the likely origin of the critical fluctuations observed above the finite temperature second-order critical point in DMFT [197, 205]. The two-step process at $T = 0$ also provides a natural explanation for the coexistence of metallic and insulating features in the phase diagram, in the regime $r_{c1} < r < r_{c2}$.
- *Emergence of non-Fermi liquid excitations at the QCP:* Precisely at the QCP, the local Fermi liquid is replaced by a quasi-local non-Fermi liquid (NFL) that spans the impurity, zeroth and first sites of the conduction bath. The NFL results from a degeneracy between the local moment and singlet states and leads to (i) “Andreev scattering” of incoming states into orthogonal outgoing states, (ii) anomalous power-law behaviour in the self-energies and two-particle correlations with universal exponents, and (iii) a fractional entanglement entropy of the impurity.
- *Correlated Fermi liquid excitations in the Hubbard sidebands:* A many-body perturbation theoretic treatment of the Hubbard sidebands reveals that they are comprised of the holon-doublon excitations created by the hybridisation of the impurity site with the conduction bath. These excitations consist of decoupled local Fermi liquids for the holons and doublons at the lowest order, which, at higher orders, become coupled via correlated holon-doublon scattering between impurity and bath.

4.2 Model Hamiltonian and method

4.2.1 The extended Anderson impurity model

The single-impurity Anderson model (SIAM) [206, 207] consists of a single impurity site with local repulsive correlation U hybridising with a non-interacting fermionic conduction bath through a (momentum-independent) single-particle transfer whose coupling is V . For the case of a half-filled impurity site, the Hamiltonian of the SIAM is given by

$$\mathcal{H}_A = -\frac{U}{2} (\hat{n}_{d\uparrow} - \hat{n}_{d\downarrow})^2 + \sum_{\vec{k},\sigma} \epsilon_{\vec{k}} \tau_{\vec{k},\sigma} + V \sum_{\sigma} \left(c_{d\sigma}^\dagger c_{0\sigma} + \text{h.c.} \right), \quad (4.1)$$

where $\tau_{\vec{k},\sigma} \equiv c_{\vec{k},\sigma}^\dagger c_{\vec{k},\sigma} - 1/2$ indicate the occupancy of the single-particle momentum state $|\vec{k}\rangle$. Also, $c_{d\sigma}$ and $c_{0\sigma} = \sum_k c_{k\sigma}$ are the fermionic annihilation operators of spin σ for the impurity and conduction

bath site to which it couples (henceforth referred to as the *zeroth site*) respectively. The conduction bath is typically considered to possess a constant (i.e., energy-independent) density of states.

The SIAM (along with its $U \rightarrow \infty$ limit, the Kondo model) has been studied using several analytical and numerical techniques [6, 7, 11, 147, 208–219]. The general conclusion for the positive U case at $T = 0$ is that on the particle-hole symmetric (that is, half-filled) line, the impurity local moment is always screened by the conduction electrons (referred to as the Kondo cloud [220–231]). Enhanced spin-flip scattering at low-energies leads to the formation of a macroscopic singlet ground state and local Fermi liquid gapless excitations [232, 233]. In order to enhance the SIAM, we introduce two extra two-particle interaction terms into the Hamiltonian:

- a spin-exchange term $J\vec{S}_d \cdot \vec{S}_0$ between the impurity spin \vec{S}_d and the spin \vec{S}_0 of the zeroth site, and
- a local particle-hole symmetric correlation term $-U_b(\hat{n}_{0\uparrow} - \hat{n}_{0\downarrow})^2$ on the bath zeroth site.

With these additional terms, the Hamiltonian of the *extended single-impurity Anderson model* (henceforth referred to as the e-SIAM) is, at particle-hole symmetry, given by

$$\mathcal{H}_{\text{E-A}} = \mathcal{H}_{\text{A}} + J\vec{S}_d \cdot \vec{S}_0 - \frac{1}{2}U_b(\hat{n}_{0\uparrow} - \hat{n}_{0\downarrow})^2. \quad (4.2)$$

All the terms in the Hamiltonian have been depicted schematically in the left panel of Fig. (6.2). The additional interaction terms J and U_b enjoy particle-hole, SU(2)-spin and U(1)-charge symmetries. The e-SIAM Hamiltonian (eq. (4.2)) therefore preserves all the local symmetries of the half-filled Hubbard model on a lattice, and can potentially serve as an effective auxiliary quantum impurity model (with a correlated bath) describing the local physics of the latter.

4.2.2 The unitary renormalisation group method

In order to obtain the various low-energy phases of the e-SIAM, we perform a scaling analysis of the associated Hamiltonian (eq. (4.2)) using the recently developed unitary renormalisation group (URG) method [1, 2]. The method has been applied successfully on a wide variety of problems of correlated fermions [1–4, 141, 219, 234–236]. The method proceeds by resolving quantum fluctuations in high-energy degrees of freedom, leading to a low-energy Hamiltonian with renormalised couplings and new emergent degrees of freedom. Typically, for a system with Fermi energy ϵ_F and bandwidth D_0 , the sequence of isoenergetic shells $\{D_{(j)}\}, D_{(j)} \in [\epsilon_F, D_0]$ define the states whose quantum fluctuations we sequentially resolve. The momentum states lying on shells $D_{(j)}$ that are far away from the Fermi surface comprise the UV states, while those on shells near the Fermi surface comprise the IR states. This scheme is shown in the right panel of Fig. (6.2).

As a result of the URG transformations, the Hamiltonian $H_{(j)}$ at a given RG step j involves scattering processes between the k -states that have energies lower than $D_{(j+1)}$. The unitary transformation $U_{(j)}$ is then defined so as to remove the number fluctuations of the currently most energetic set of states $D_{(j)}$ [1, 2]:

$$H_{(j-1)} = U_{(j)} H_{(j)} U_{(j)}^\dagger, \text{ such that } [H_{(j-1)}, \hat{n}_j] = 0. \quad (4.3)$$

The eigenvalue of \hat{n}_j has, thus, been rendered an integral of motion (IOM) under the RG transformation.



Figure 4.1: *Left:* Schematic 1D representation of the extended SIAM Hamiltonian. The red sphere is the impurity site with on-site Hubbard term U . It is connected via two couplings V and J to the bath zeroth site (large blue sphere) that has its own on-site Hubbard term U_b . The small blue spheres make up the rest of the bath, connected through the single-particle hopping t . *Right:* High energy - low energy scheme defined and used in the URG method. The states away from the Fermi surface form the UV subspace and are decoupled first, leading to a Hamiltonian which is more block-diagonal and comprised of only the IR states near the Fermi surface.

The unitary transformations can be expressed in terms of a generator $\eta_{(j)}$ that has fermionic algebra [1, 2]:

$$U_{(j)} = \frac{1}{\sqrt{2}} \left(1 + \eta_{(j)} - \eta_{(j)}^\dagger \right), \quad \left\{ \eta_{(j)}, \eta_{(j)}^\dagger \right\} = 1, \quad (4.4)$$

where $\{\cdot\}$ is the anticommutator. The unitary operator $U_{(j)}$ that appears in Eq. (6.8) can be cast into the well-known general form $U = e^S, S = \frac{\pi}{4} (\eta_{(j)}^\dagger - \eta_{(j)})$ that a unitary operator can take, defined by an anti-Hermitian operator S . The generator $\eta_{(j)}$ is given by the expression [1, 2]

$$\eta_{(j)}^\dagger = \frac{1}{\hat{\omega}_{(j)} - \text{Tr}(H_{(j)} \hat{n}_j)} c_j^\dagger \text{Tr}(H_{(j)} c_j). \quad (4.5)$$

The operators $\eta_{(j)}, \eta_{(j)}^\dagger$ behave as the many-particle analogues of the single-particle field operators c_j, c_j^\dagger - they change the occupation number of the single-particle Fock space $|n_j\rangle$. The important operator $\hat{\omega}_{(j)}$ originates from the quantum fluctuations that exist in the problem because of the non-commutation of the kinetic energy terms and the interaction terms in the Hamiltonian:

$$\hat{\omega}_{(j)} = H_{(j-1)} - H_{(j)}^i. \quad (4.6)$$

$H_{(j)}^i$ is the part of $H_{(j)}$ that commutes with \hat{n}_j but does *not* commute with at least one \hat{n}_l for $l < j$. The RG flow continues up to energy D^* , where a fixed point is reached from the vanishing of the RG function. Detailed comparisons of the URG with other methods (e.g., the functional RG, spectrum bifurcation RG etc.) can be found in Refs. [1, 3]. More information on the unitary RG method is provided in Section 1 of the Supplementary Materials [237].

4.3 $T = 0$ scaling theory for the e-SIAM

4.3.1 URG equations for the e-SIAM

The derivation of the RG equations for the extended Anderson impurity model (e-SIAM) Hamiltonian is shown in Section 2 of the Supplementary Materials [237]. The bath coupling U_b is marginal. We provide

below the RG equations of the remaining couplings for a given quantum fluctuation scale ω :

$$\begin{aligned}\Delta U &= 4V^2 n_j \left(\frac{1}{d_1} - \frac{1}{d_0} \right) - n_j \frac{J^2}{d_2}, \\ \Delta V &= -\frac{3n_j V}{8} \left[J \left(\frac{1}{d_2} + \frac{1}{d_1} \right) + \frac{4U_b}{3} \sum_{i=1}^4 \frac{1}{d_i} \right], \\ \Delta J &= -\frac{n_j J (J + 4U_b)}{d_2},\end{aligned}\tag{4.7}$$

where the denominators d_i are given by

$$d_0 = \omega - \frac{D}{2} + \frac{U_b}{2} - \frac{U}{2}, \quad d_1 = \omega - \frac{D}{2} + \frac{U_b}{2} + \frac{U}{2} + \frac{J}{4},\tag{4.8}$$

$$d_2 = \omega - \frac{D}{2} + \frac{U_b}{2} + \frac{J}{4}, \quad d_3 = \omega - \frac{D}{2} + \frac{U_b}{2}.\tag{4.9}$$

The symbols used in the RG equations have the following meanings: ΔU represents the renormalisation of the coupling U in going from the j^{th} Hamiltonian to the $(j-1)^{\text{th}}$ Hamiltonian by decoupling the isoenergetic shell at energy $D_{(j)}$ (see right panel of Fig.(6.2)). n_j is the number of electronic states on the shell $D_{(j)}$. We note that the labels U_0, J_0, V_0 that appear in various figures (and elsewhere in the text) represent the bare values of the associated couplings U, J and V . The RG equations reduce, in the perturbative regime of the couplings U, V and J , to the well-known ‘‘poor man’s’’ scaling forms obtained for the SIAM [7] and the single-channel Kondo model [6] respectively.

The RG fixed point Hamiltonian describes the low-energy phase of the system. In general, if the RG fixed point is reached at an energy scale D^* , the fixed point Hamiltonian \mathcal{H}^* is obtained simply from the fixed point values of the couplings (and by noting that the states above D^* are now part of the IOMs):

$$\mathcal{H}^* = \sum_{\sigma, \vec{k}}^{| \epsilon_{\vec{k}} | < D^*} \epsilon_{\vec{k}} \tau_{\vec{k}, \sigma} + V^* \sum_{\sigma} \left(c_{d\sigma}^\dagger c_{0\sigma} + \text{h.c.} \right) + J^* \vec{S}_d \cdot \vec{S}_0 - \frac{1}{2} U^* (\hat{n}_{d\uparrow} - \hat{n}_{d\downarrow})^2 - \frac{1}{2} U_b (\hat{n}_{0\uparrow} - \hat{n}_{0\downarrow})^2.$$

The fixed point values of the couplings are obtained by solving the RG equations numerically.

4.3.2 Phase diagram

We will work in the low-energy regime where the quantum fluctuation scale ω is such that all the denominators are negative: $d_i < 0 \forall i$. Moreover, we constrain the impurity and local bath correlations (U and U_b respectively) through the relation $U_b = -U/10$. While the precise value of the factor of $1/10$ is unimportant, we have chosen a factor considerably smaller than 1 in order to demonstrate that an interesting body of results can be obtained with a value of $|U_b|$ that is much smaller than that of U . Further, the negative sign in the above relation is significant, as we shall see below that the MIT is obtained for the case of U_b being negative (i.e., attractive on-site correlations on the zeroth site of the bath). The relation between U_b and U is motivated on phenomenological grounds such that the MIT occurring in the bulk lattice model (obtained upon increasing the on-site Hubbard repulsion to large values) corresponds, in the auxiliary model mapping within DMFT, to the local MIT observed upon tuning the impurity correlation U (and the related bath correlation U_b) within the proposed effective

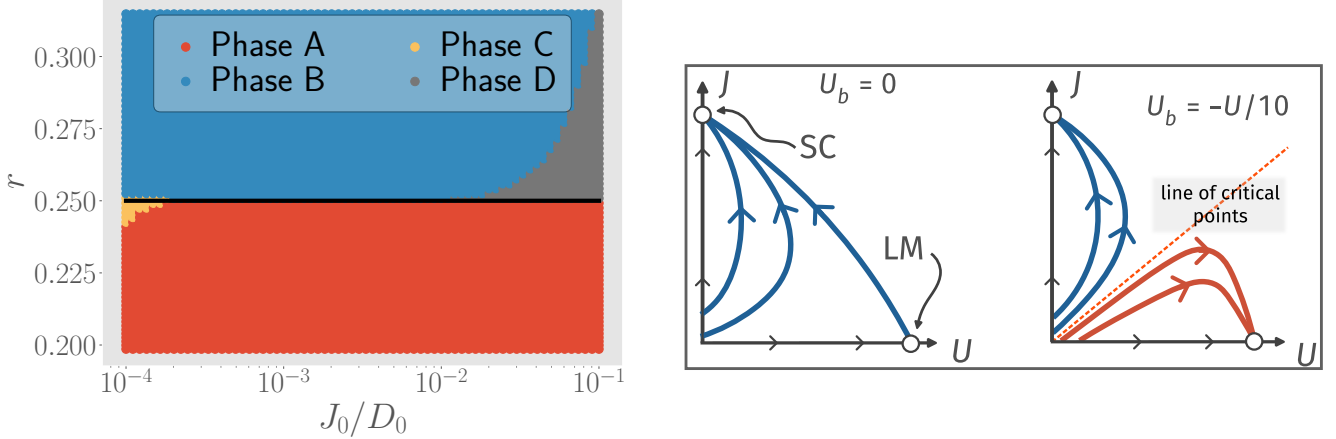


Figure 4.2: *Left:* Phase diagram of the e-SIAM, in the space of r and J_0/D_0 . U_b is set to $-U_0/10$. The various phases are described in the text. *Right:* Schematic nature of RG flows for $U_b = 0$ and $U_b = -U/10$. Blue curves represent RG flows towards the strong-coupling (SC) fixed point, while red curves represent RG flows towards the local moment (LM) fixed point.

impurity model Hamiltonian. The physical significance of attractive on-site correlations in the bath lies in providing a mechanism for the frustration of Kondo screening (in the RG equation for an antiferromagnetic Kondo coupling $J(> 0)$, eq. (4.70)) within an Anderson impurity coupled to a single channel of conduction electrons. We provide a detailed discussion of this point in the concluding section of our work.

Regime	Low-energy effective Hamiltonian	impurity ground-state
1. $0 < r < r_{c1}$	$K.E^* + V^* \sum_\sigma (c_{d\sigma}^\dagger c_{0\sigma} + h.c.) + J^* \vec{S}_d \cdot \vec{S}_0$	$\frac{1}{\sqrt{2}} (\uparrow_d\rangle \downarrow_0\rangle - \downarrow_d\rangle \uparrow_0\rangle + 2_d\rangle 0_0\rangle + 0_d\rangle 2_0\rangle)$
2. $r_{c1} < r < r_{c2}$	$K.E^* + J^* \vec{S}_d \cdot \vec{S}_0 - \frac{1}{2} U_b (\hat{n}_{0\uparrow} - \hat{n}_{0\downarrow})^2$	$\frac{1}{\sqrt{2}} (\uparrow_d\rangle \downarrow_0\rangle - \downarrow_d\rangle \uparrow_0\rangle)$
3. $r_{c2} < r$	$K.E^* - \frac{U^*}{2} (\hat{n}_{d\uparrow} - \hat{n}_{d\downarrow})^2 - \frac{U_b}{2} (\hat{n}_{0\uparrow} - \hat{n}_{0\downarrow})^2$	$\{ \uparrow_d\rangle, \downarrow_d\rangle\}$

Table 4.1: Effective Hamiltonians and ground-states of the three important parts of the phase diagram in Fig. (4.2). The ground-state is simplified to capture only the configuration of the impurity site and at most the bath zeroth site. $K.E.^*$ represents the kinetic energy of the conduction electron states residing within the fixed point window D^* .

The phase diagram is shown in the left panel of Fig. (4.2) in terms of the parameter $r = |U_b|/J$ (y-axis) and the ratio of the bare Kondo coupling (J_0) to the bare conduction bath bandwidth (D_0) (x-axis), we first define two important points in the space of couplings. These are values of the parameter r where there is a qualitative change in the nature of RG flows, and hence in the low-energy physics of the model

- $r = r_{c1} (= -(\frac{U_b}{J})_{c1} = \frac{3}{20} = (\frac{U}{10J})_{c1} > 0)$: At this point, the coupling V becomes irrelevant,
- $r = r_{c2} (= -(\frac{U_b}{J})_{c2} = \frac{1}{4} = (\frac{U}{10J})_{c2})$: At this point, the coupling J also turns irrelevant. Note that $r_{c2} > r_{c1}$.

We will use these two values of the parameter r as checkpoints around which we can describe the low-energy physics. There are three important parts in Fig. (4.2):

- red region, $0 < r < r_{c1}$: the $J - V$ model; V and J are both relevant, but U is irrelevant; spin and charge delocalisation on the impurity; spin-charge mixing in ground-state
- blue region, $r_{c1} < r < r_{c2}$: the $J - U_b$ model; J is relevant, but V and U are both irrelevant; charge localisation and spin delocalisation on the impurity; singlet ground-state
- violet region, $r_{c2} < r$: the $U - U_b$ model; U is relevant, but V and J are both irrelevant; spin and charge localisation on the impurity; local moment ground-state. This phase describes a local Mott insulator on the impurity site, characterised by vanishing local double occupancy in ground state (black curve in left panel of Fig. 4.4).

Typical RG flows that lead to these phases are shown in Fig. (4.3). We also note that the grey region shown in the top right corner of Fig.(4.2) corresponds to a model in which all three couplings (J , U and V) are RG irrelevant. We find, however, that this phase is an artefact of solving the RG equations for an impurity coupled to a finite-sized conduction bath, and it gradually disappears upon increasing the bath size.

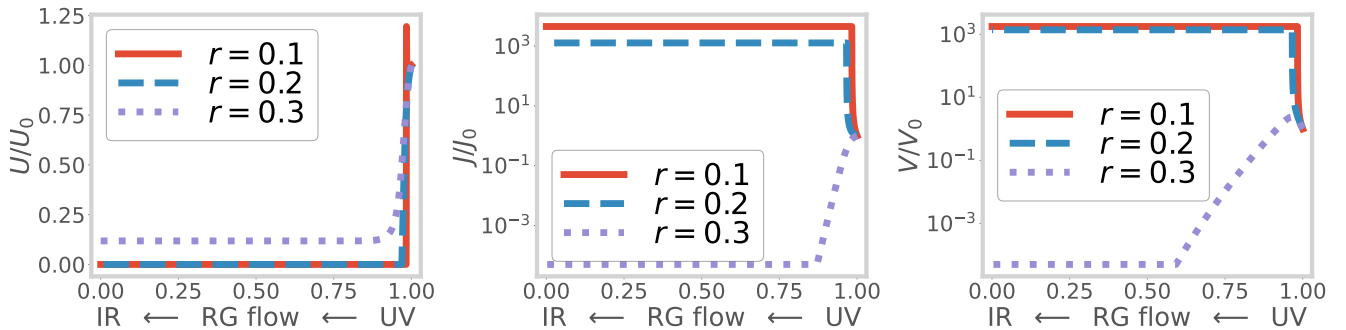


Figure 4.3: Variation of couplings U , V and J along the RG transformations, for three values of the transition-tuning ratio $r = -U_b/J_0$. The x-axis represents the distance of the running cutoff from the Fermi surface; the rightmost point is the first RG step (UV) and the leftmost point is the final RG step (IR). The red curves represent the flows for $r < r_{c1}$, where both V and J are relevant. The blue curves represent the RG flows for $r_{c1} < r < r_{c2}$, where J is relevant but V is irrelevant. The violet curves represent RG flows for $r > r_{c2}$, where both V and J are irrelevant but U flows to a finite value.

4.3.3 Phase transition at r_{c2}

The effective Hamiltonians and corresponding impurity ground-states for various phases have been listed in table (4.1). The variation in the ground state has been checked by numerically solving the fixed point Hamiltonian for various bare values of the couplings and is shown in the left panel of Fig. (4.4). A sharp change in the ground state from spin-singlet to local moment shows that the blue and violet phases are separated by an *impurity delocalisation-localisation transition* (black line in Fig. (4.2)). The transition occurs at finite values of the correlations: $r_{c2} = -(\frac{U_b}{J})_{c2} = \frac{1}{4} = (\frac{U}{10J})_{c2}$. This is a stark contrast from the standard SIAM, where the transition can happen only at on-site correlation $U \rightarrow \infty$.

Therefore, the presence of the critical point at finite values of the various couplings transforms the landscape of RG phase diagram shown schematically in the right panel of Fig. (4.2) (right panel): the RG flows split into two classes - those that flow towards the strong-coupling Kondo screened fixed point and those that flow towards the local moment fixed point.

By a simple rewriting of the RG equation for J (eq. (4.70)), the impurity transition can be seen to arise from a competition between the Kondo screening physics of J and the local pairing physics of U_b :

$$\Delta J = \frac{\overbrace{(J + 2U_b)^2 n_j}^{\text{usual Kondo physics}}}{|d_2|} - \frac{\overbrace{(2U_b)^2 n_j}^{\text{competing pairing physics}}}{|d_2|}, \quad (4.10)$$

where $d_2 = \omega - D/2 + U_b/2 + J/4$. The competition between the effective Kondo term $(J + 2U_b)^2$ and the competing pairing term $-4U_b^2$ leads to the presence of two stable phases - one that is Kondo screened and one that remains unscreened.

In the DMFT treatment of the 1/2-filled Hubbard model on the Bethe lattice in infinite dimensions, the vanishing of non-local contributions to the lattice self-energy means that the lattice Greens function can be computed self-consistently by solving a local quantum impurity problem [186]. In the rest of the work, we provide extensive evidence that the local transition observed in the e-SIAM is very similar to the Mott MIT observed in DMFT. We conclude thereby that the e-SIAM models faithfully the round-trip excursions of an electron on the Bethe lattice, and that the impurity phase transition observed in the e-SIAM offers a local description of the Mott MIT in the bulk Hubbard model. With this evidence in mind, we will henceforth refer to the transition at r_{c2} as a *local metal-insulator transition*.

4.3.4 The case of repulsive U_b

Henceforth, we will only consider the case of attractive U_b ($U_b > 0$), because that is the regime in which an impurity phase transition is realised at finite values of the couplings. However, before moving on, we will comment briefly on the effects of a repulsive U_b ($U_b > 0$). From the RG equation for J in eq. 4.70, we see that ΔJ is always positive for $U_b > 0$. Moreover, something similar happens in the RG equation for V , where the two terms in the square brackets now enforce each other (J and U_b now have the same sign). Together, they indicate that there will not be any Kondo destruction in the case of $U_b > 0$, and the only fixed points are the weak-coupling one ($J^* = 0$) and the strong coupling one ($J^* = \infty$); there is no local moment phase. This case is therefore adiabatically connected to the case of $U_b = 0$.

4.4 Descriptors of the local MIT

The present section gives more clarity on the nature of the impurity phase transition in the form of additional descriptors of the transition such as impurity spectral function and measures of entanglement, computed from the e-SIAM Hamiltonian. Throughout the rest of the work, we have set the value of the coupling V equal to the Kondo coupling J while generating the quantitative plots.

4.4.1 Evolution of the impurity spectral function

The impurity spectral function of the standard SIAM (eq. (4.1)) always displays a central peak at finite values of U (along with Hubbard sidebands at sufficiently large U), indicating the presence of gapless

local Fermi liquid excitations on the impurity site [147, 238, 239]. To demonstrate the impurity localisation transition, we compute the impurity local spectral function of the e-SIAM (eq. (4.2)). This involves numerically diagonalising the effective Hamiltonian at various energy scales along the RG flow and computing the spectral weight at a range of frequencies from UV to IR. We find that the spectral function (shown in the right panel of Fig. (4.4)) displays three notable features, in agreement with DMFT results [186]:

- The appearance of a *preformed gap* (flattening of spectral function between the central peak and sidebands) as r crosses r_{c1} ($= -\left(\frac{U_b}{J}\right)_{c1} = \frac{3}{20} = \left(\frac{U}{10J}\right)_{c1}$): The preformed optical gap simply indicates the separation of the spin (central peak) and charge (sidebands) degrees of freedom beyond r_{c1} . This separation is brought about by the irrelevance of V . We note that the consequences of an irrelevant hybridisation V can be accounted for in many-body perturbation theory, leading to “in-gap” processes within the optical gap of the impurity spectral function [240]. However, we expect that such contributions will be small, and cannot fill in the optical gap observed in Fig. 4.4 completely.
- The sharpening of the central peak, and concomitant increase in the preformed gap, as r is increased in the range $r_{c1} < r < r_{c2}$.
- The vanishing of the central peak and appearance of a *hard gap* as r crosses r_{c2} : The irrelevance of J beyond r_{c2} destroys the Kondo screening and localises the impurity moment. This involves the destabilisation of the singlet ground state, and the stabilisation of the local moment states in its place.

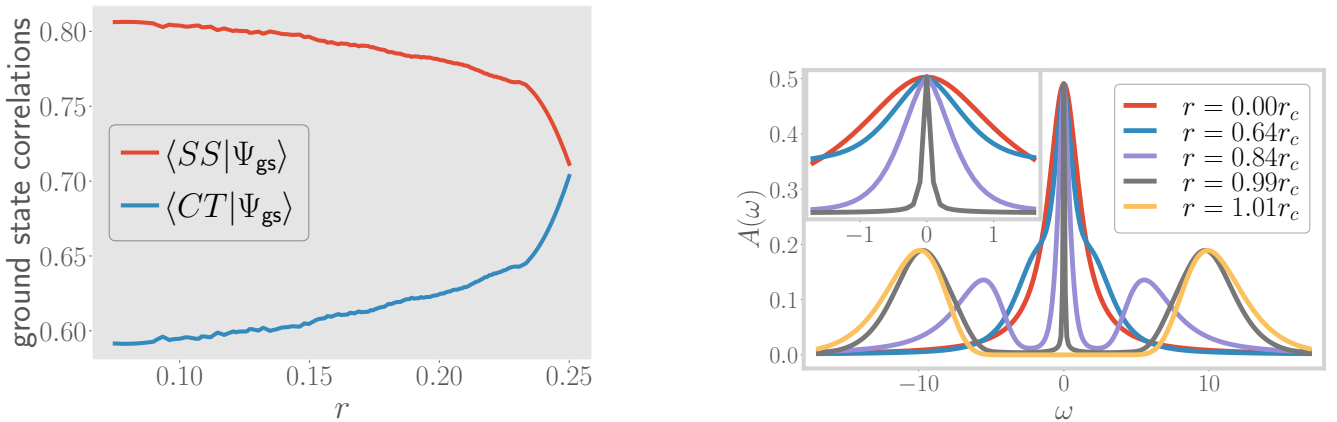


Figure 4.4: *Left:* Overlap of the RG fixed point ground state $|\Psi\rangle_{gs}$ with the spin-singlet state $|SS\rangle$, the zero charge member of the charge triplet states $|CT\rangle$ and the local moment states $|LM\rangle$, for all three regimes of the model. The black curve corresponds to the double occupancy on the impurity site and is observed to be strongly suppressed beyond r_{c1} . Beyond the critical point $r_{c2} = 0.25$, the overlaps with the entangled states vanish, indicating the transition to a decoupled local moment. *Right:* Variation of the impurity spectral function from $r = 0$ to $r > r_{c2}$. At small r , the central peak is broad, but at larger r , it sharpens, and the difference in spectral weight is used in creating the Hubbard sidebands. For $r > r_{c2}$, the central peak vanishes.

These features are also reflected in ground-state correlation measures like spin-flip and charge isospin-flip correlations (see left panel of Fig. (4.5)), which are defined as follows:

$$\frac{1}{2} (\langle S_i^+ S_j^- \rangle + \text{h.c.}) = \frac{1}{2} (\langle c_{i\uparrow}^\dagger c_{i\downarrow} c_{j\downarrow}^\dagger c_{j\uparrow} \rangle + \text{h.c.}) , \quad \frac{1}{2} (\langle C_i^+ C_j^- \rangle + \text{h.c.}) = \frac{1}{2} (\langle c_{i\uparrow}^\dagger c_{i\downarrow}^\dagger c_{j\downarrow} c_{j\uparrow} \rangle + \text{h.c.}) . \quad (4.11)$$

At small values of r , both the correlations are large as the ground-state has both spin and charge content (row 1 of table (4.1)). The subsequent decrease in the impurity-bath charge flip correlation (violet points of Fig. (4.5)), and the simultaneous increase in the impurity-bath spin-flip correlation (red points of Fig. (4.5)), can be attributed to the irrelevance of V at $r \simeq r_{c1}$ and the appearance of the preformed gap in the spectral function. Beyond r_{c2} , the spin-flip correlation sharply drops to zero due to the irrelevance of J . They are replaced by intra-bath correlations like the charge isospin-flip correlation between the zeroth site and the first site (blue points of Fig. (4.5)). Such intra-bath correlations are promoted by the bath on-site term U_b . The sudden change in the nature of the ground state, and resulting correlations, at r_{c2} indicates the presence of a quantum critical point whose nature will be analysed further in subsequent sections.

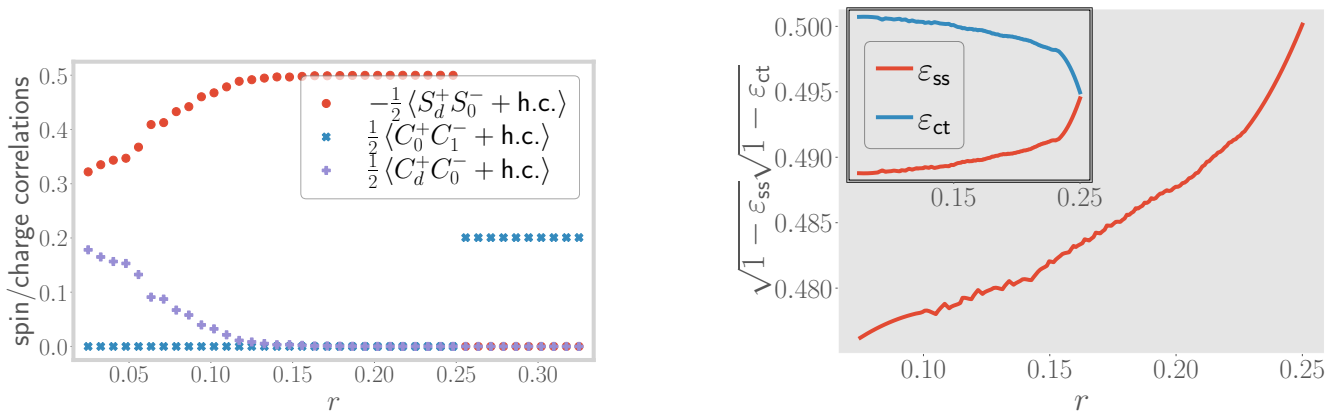


Figure 4.5: *Left:* Variation of impurity-bath spin-flip correlation (red) and charge isospin-flip correlation (violet), as well as intra-bath charge isospin-flip correlation (blue), from $r \sim 0$ to $r > r_{c2}$. The imp.-bath isospin correlation vanishes at r_{c1} , indicating the change in RG relevance of V . The imp.-bath spin correlation vanishes at r_{c2} , indicating the marginality of J at that point. The intra-bath correlation picks up after the transition, showing the decoupling of the impurity from the bath. *Right:* Variation of the geometric entanglement ε_{ss} (blue) w.r.t. the singlet state and that w.r.t the charge triplet zero state, ε_{ct} (red), with r . The former becomes maximum (unity) at r_{c1} , showing that the true ground state has no charge content. The latter discontinuously jumps to unity at r_{c2} , therefore acting as an order parameter for the transition.

4.4.2 Using entanglement to track correlations across the transition

We will now show that a certain measure of entanglement behaves as an order parameter for the transition. We can define a geometric measure of entanglement in terms of wavefunctions $|\psi_1\rangle$ and $|\psi_2\rangle$ [16, 241, 242]:

$$\varepsilon(\psi_1, \psi_2) = 1 - |\langle \psi_1 | \psi_2 \rangle|^2 . \quad (4.12)$$

From this definition, if $|\psi_1\rangle$ corresponds to a separable state, the entanglement content of the state $|\psi_2\rangle$ is small if its overlap with $|\psi_1\rangle$ is large. For brevity, we will use the notation $\varepsilon_{ss} \equiv \varepsilon\left(\psi_{ss}, \psi_{gs}^{(2)}\right)$, $\varepsilon_{ct} \equiv \varepsilon\left(\psi_{ct}, \psi_{gs}^{(2)}\right)$ to represent the geometric entanglement between the e-SIAM ground-state $|\psi_{gs}\rangle$ and the singlet state $|\psi_{ss}\rangle$ or the charge triplet zero state $|\psi_{ct}\rangle$. The latter two states are shown in Table (4.1). The entanglement measures ε_{ss} and ε_{ct} can be related to the impurity Greens function through the following equation (details can be found in Sec. 3 of the Supplementary Materials [237]):

$$G_d(\omega) = \sum_n \left[(1 - \varepsilon_{ss}) G_{\Phi_{ss}, \Phi_{ss}}(\omega, n) + (1 - \varepsilon_{ct}) G_{\Phi_{ct}, \Phi_{ct}}(\omega, n) \right. \\ \left. + 2\sqrt{(1 - \varepsilon_{ss})}\sqrt{(1 - \varepsilon_{ct})} G_{\Phi_{ss}, \Phi_{ct}}(\omega, n) \right], \quad (4.13)$$

where

$$G_{\psi_1, \psi_2}(\omega, n) = \frac{1}{2} \frac{\langle \psi_1 | c_{d\sigma} | \Psi_n \rangle \langle \Psi_n | c_{d\sigma}^\dagger | \psi_2 \rangle + \text{h.c.}}{\omega + E_{gs} - E_n} + \frac{1}{2} \frac{\langle \psi_1 | c_{d\sigma}^\dagger | \Psi_n \rangle \langle \Psi_n | c_{d\sigma} | \psi_2 \rangle + \text{h.c.}}{\omega - E_{gs} + E_n}. \quad (4.14)$$

This expression displays that the evolution of the impurity Greens function G_d with r (and related correlation functions shown in the left panel of Fig.(4.5)) is dependent on that of the entanglement measures ε_{ss} and ε_{ct} (shown in the right panel of Fig. (4.5)). Indeed, we find that the geometric entanglement ε_{ct} with the charge sector increases towards unity as the transition at r_{c2} is approached, and remains unity after the transition. A more sensitive measure is the singlet entanglement ε_{ss} : it initially decreases to zero at r_{c1} owing to the irrelevance of V , but rises discontinuously to unity at the transition and becomes equal to the charge entanglement in the local moment phase. Therefore, ε_{ss} acts as an order parameter for the local MIT at r_{c2} . We find that the cross-term $\sqrt{(1 - \varepsilon_{ss})}\sqrt{(1 - \varepsilon_{ct})}$ decreases monotonically to zero with increasing r (not shown), displaying a continual decrease in the mixing of the spin and charge sectors and the *immobilisation of the doublons and holons on the impurity site*.

In general, any one-particle or two-particle fluctuation $\langle O_1 O_2^\dagger \rangle$ that acts on the combined Hilbert space of the impurity and the zeroth site can be expressed in terms of these entanglement measures $\varepsilon_{ss}, \varepsilon_{ct}$. The detailed derivations and expressions are given in Section 3 of the Supplementary Materials [237]. As a demonstration, consider the spin-spin correlation $\langle S_d^+ S_0^- \rangle$ between the impurity and the zeroth site shown in the left panel of Fig. (4.5). The general expression given in Section 3 of the Supplementary Materials [237] is of the form

$$\langle S_d^+ S_0^- \rangle = (1 - \varepsilon_{ss}) \langle \Phi_{ss} | S_d^+ S_0^- | \Phi_{ss} \rangle + (1 - \varepsilon_{ct}) \langle \Phi_{ct} | S_d^+ S_0^- | \Phi_{ct} \rangle \\ + \sqrt{1 - \varepsilon_{ss}} \sqrt{1 - \varepsilon_{ct}} (\langle \Phi_{ss} | S_d^+ S_0^- | \Phi_{ct} \rangle + \langle \Phi_{ct} | S_d^+ S_0^- | \Phi_{ss} \rangle). \quad (4.15)$$

From the expression given, we find that only the singlet overlap is non-zero, such that $\langle S_d^+ S_0^- \rangle$ is directly proportional to the quantity $1 - \varepsilon_{ss}$. As the entanglement measure ε_{ss} increases towards the transition (right panel of Fig. (4.5)), the quantity $1 - \varepsilon_{ss}$ decreases, in turn leading to the decrease in the magnitude of the correlation observed in the left panel of Fig. (4.5). For another explicit connection between correlations and entanglement measures, we present relations between the quantum Fisher information (QFI) [243] and many-particle Greens functions in Section 3 of the Supplementary Materials [237]. There, we also plot the QFI for a number of two-particle operators as a function of r , notably the ones corresponding to the degree of compensation for the impurity ($\langle \vec{S}_d \cdot \vec{S}_0 \rangle$) and the impurity

magnetisation ($\langle S_d^z \rangle$). These two quantities (and hence the corresponding QFI) are important because they track the local MIT and act as order parameters for the transition, and the QFI corresponding to these two operators quantify the quantum fluctuations present in the system corresponding to these order parameters. We show in Sec. 3 of the Supplementary Materials that the two phases on either side of the transition are characterised by distinct values of this pair of QFI: while the QFI corresponding to the degree of compensation is zero in the Kondo screened phase, it becomes non-zero in the local moment phase, and the opposite is true for the QFI arising from the impurity magnetisation. The phase precisely at the transition is distinct from those on either side because it displays a non-zero value for both of the QFI. While it is expected that a critical point would show enhanced fluctuations of multiple kinds (giving rise to universality), it is enlightening to find that this is also reflected in a measure of many-particle entanglement.

4.5 Universal theory for the local metal-insulator transition

In order to identify the competing tendencies near the transition at r_{c2} , we will now obtain the minimal effective Hamiltonian that displays the same transition. This involves integrating out the degrees of freedom that do not affect the low-energy physics near r_{c2} . We note that, due to the irrelevance of V , there is no scattering between the spin and charge states on the impurity at low energies. Further, the impurity charge states $|0\rangle$ and $|\uparrow_d\downarrow_d\rangle$ have been pushed to the high energy Hubbard sidebands because of the large value of U close to r_{c2} . As a result, the impurity charge states can be safely decoupled from the spin states through a Schrieffer-Wolff transformation. Up to second order in V^2/U , this transformation accounts for the effects of U and V by generating an additional (Kondo) spin-exchange term $\delta J \left(\sim \frac{V^2}{U+U_b} \right)$, as well as an additional on-site correlation $\delta U_b \left(\sim \frac{2V^2}{U+U_b+J/2} - \frac{8V^2}{U-U_b} \right)$ on the zeroth site of the conduction bath. In this way, we obtain the following renormalised effective Hamiltonian:

$$H_{\text{MIT}} = \mathcal{J} \vec{S}_d \cdot \vec{S}_0 - \frac{1}{2} \mathcal{U}_b (\hat{n}_{0\uparrow} - \hat{n}_{0\downarrow})^2 + H_{\text{K.E.}}, \quad (4.16)$$

where $\mathcal{J} = J + \delta J$ is the renormalised s-d interaction and $\mathcal{U}_b = U_b + \delta U_b$ is the renormalised local correlation on the bath zeroth site. A schematic 1D construction of the effective Hamiltonian is shown in the left panel of Fig. (4.6). We note that a similar approach towards extracting an effective theory for the Mott MIT has been employed in the past ([244, 245]). However, those works essentially led to renormalised Kondo models that do not possess any frustration of the Kondo screening. Thus, they cannot display an impurity transition in the absence of the requirement of self-consistency and can describe only the physics of the metallic regime. Importantly, the effective $\mathcal{J} - \mathcal{U}_b$ model (eq. (4.16)) is consistent with the IR fixed point Hamiltonian obtained in the appropriate regime $r_{c1} < r < r_{c2}$ (row 2 of table (4.1)).

The RG equations for \mathcal{J} and \mathcal{U}_b of the simplified effective impurity model eq. (4.16) can be obtained by setting $U = V = 0$ in the RG equations (4.70):

$$\Delta \mathcal{J} = -\frac{n_j \mathcal{J} (\mathcal{J} + 4\mathcal{U}_b)}{d_2}, \quad \Delta \mathcal{U}_b = 0. \quad (4.17)$$

For $\mathcal{J} + 4\mathcal{U}_b > 0$, the Kondo coupling is relevant and the low-energy phase is a paramagnetic local Fermi liquid with gapless excitations. But for $\mathcal{J} + 4\mathcal{U}_b < 0$, the Kondo coupling becomes irrelevant and the ground state is a decoupled local moment that is isolated from the bath. Such an effective picture of

the transition can be understood if one notes that a straightforward way to destroy the Kondo screening is to inhibit the coordinated spin fluctuations between the impurity and the bath. Such frustration of Kondo screening is precisely the effect of the \mathcal{U}_b term: it promotes charge fluctuations on the bath site coupled directly to the impurity, reducing thereby the spectral weight for spin-flip scatterings between the impurity and bath.



Figure 4.6: *Left:* Schematic 1D construction of universal theory for the metal-insulator transition, obtained by integrating out the charge states of the impurity near the transition. *Right:* Zero bandwidth limit of the low-energy effective Hamiltonian for r between r_{c1} and r_{c2} (second row in table (4.1)). The bath is reduced to just a single degree of freedom - the zeroth site that is directly coupled to the impurity site.

Indeed, the local correlation \mathcal{U}_b encourages entanglement between the sites of the bath and makes the formation of the impurity-bath singlet difficult. In other words, the $\mathcal{J}-\mathcal{U}_b$ model displays the destabilisation of the singlet by redistributing the entanglement from the impurity+bath system to purely within the bath (see left panel of Fig. (4.7)). Given the simplicity of these arguments, our analysis makes the case that local pairing fluctuations of the bath in eq. (4.16) offer a universal mechanism by which to frustrate the Kondo effect and lead thereby to an impurity transition that is the local counterpart of the Mott MIT obtained by auxiliary model approaches such as DMFT. We note that similar conclusions were reached in Refs. [203, 204, 215] for the emergence of non-Fermi liquid phases at critical points in the mixed valence regime of the periodic Anderson model.

Further insight into the destabilisation of the singlet can be obtained from a zero-bandwidth approximation of the bath. Under such an approximation, the IR effective Hamiltonian obtained from the RG flow (row 2 of Fig. (4.1)) takes the form of a two-site model with modified couplings (shown in the right panel of Fig. (4.6)):

$$\tilde{\mathcal{J}} \vec{S}_d \cdot \vec{S}_0 - \frac{1}{2} \tilde{\mathcal{U}}_b (\hat{n}_{0\uparrow} - \hat{n}_{0\downarrow})^2 . \quad (4.18)$$

The spectrum of this model is shown in the right panel of Fig. (4.7). For $|\tilde{\mathcal{U}}_b|/\tilde{\mathcal{J}} < 3/2$, the singlet ground-state (red) is separated from the excited local moment states (blue) by a gap of $\frac{-3\tilde{\mathcal{J}}}{4} - \frac{\tilde{\mathcal{U}}_b}{2}$. As we tune r towards r_{c2} , $|\tilde{\mathcal{U}}_b|$ increases and the fixed point value $\tilde{\mathcal{J}}$ decreases, leading to an overall reduction in the gap. At the critical point, the gap closes and the states become degenerate at zero energy; this is the equivalent of the quantum critical point at r_{c2} of the full impurity model that was discussed earlier. We note that the vanishing of the energy of the metallic state was also observed by Brinkman and Rice from a Gutzwiller-type variational calculation of the Hubbard model at half-filling [195].

4.5.1 Local pairing and the destruction of Kondo screening

Very close to the transition at r_{c2} , we find signatures of the breakdown of the Kondo cloud in terms of decaying impurity-zeroth site correlations (blue curve in the left panel of Fig. (4.8)) and enhanced intra-bath correlations. Remarkably, we find an *increase in pairing correlations* between the bath zeroth

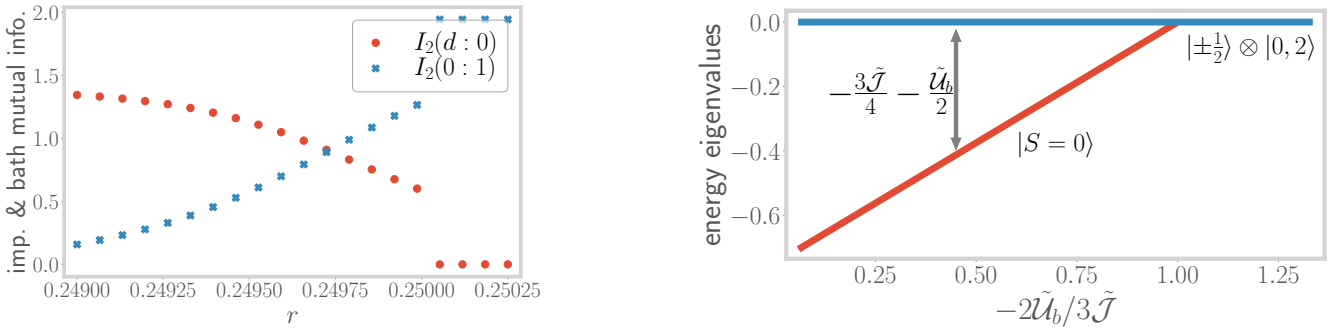


Figure 4.7: *Left:* Very close to the transition, the mutual information $I_2(d : 0)$ (red curve) between impurity and the zeroth site reduces, while that between the zeroth and the first site ($I_2(0 : 1)$, blue curve) increases, showing the redistribution of entanglement. *Right:* Spectrum of the zero bandwidth Hamiltonian of the right panel of Fig. (4.6). The blue line represents the local moment states at zero energy, while the red line represents the singlet state at an energy that continuously increases upon increasing r .

site and first site (red curve in the left panel of Fig. (4.8)). As discussed above, these are observed to be responsible for the destruction of the Kondo screening: spin and charge degrees of freedom are mutually exclusive, and the increased charge fluctuations on the bath zeroth site suppress the spin-flip scattering processes between the impurity and the zeroth site. We will show later that these fluctuations lead to the destruction of the local Fermi liquid excitations in our model, and replace them with non-Fermi local excitations in the neighbourhood of r_{c2} . We believe that the observed growth in non-local pairing correlations near the transition at r_{c2} is likely tied to a putative low-energy divergence of the local pairing susceptibility. A similar observation was made in Ref. [203] from an auxiliary model-based analysis of a hole-doped extended Hubbard model in infinite dimensions that is pertinent to the physics of the heavy fermions. Similar to the conclusions of Ref. [203], we expect the pairing fluctuations of the bath to become dominant upon tuning the e-SIAM away from half-filling, signalling an instability towards a superconducting state.

4.5.2 Emergent self-consistency in the e-SIAM

As is well-established, the DMFT self-consistency equation is equivalent to requiring that the impurity Greens function become equal to the local Greens function in the bath [186]. Such a condition is also used in the projective self-consistent technique of Moeller et al. [244] for the states within the central Kondo resonance. We will now show that our model displays a qualitatively similar emergent feature. To proceed, by employing a one-step URG transformation, we integrate out the impurity site from the rest of the fixed-point Hamiltonian of eq. (4.10). The details are shown in Sec. 4 of the Supplementary Materials [237]. The essential idea is similar to that of the Schrieffer-Wolff transformation: removing the impurity-bath couplings J and V generates an additional repulsive correlation δU_z^* on the zeroth site. The new low-energy model H_Z is therefore an Anderson impurity model with a net local correlation $U_z^* = \delta U_z^* + U_b$ on the zeroth site (which is now the “new impurity site”), and a single-particle hybridisation $V_z^* = -t$ coupling with a conduction bath formed by the remaining sites. This new impurity

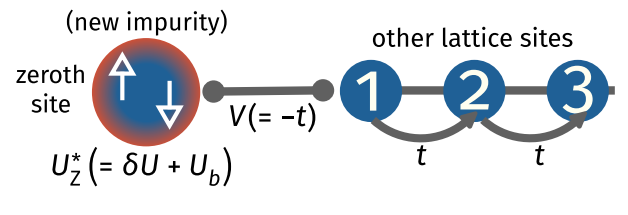
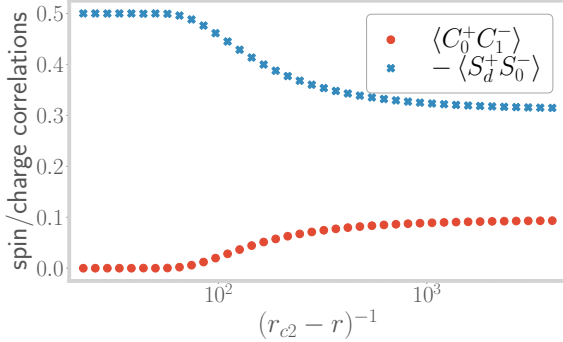


Figure 4.8: *Left:* Spin-flip correlation between the impurity and the bath (blue), and charge isospin-flip correlation between the bath zeroth and first sites (red), both as a function of the tuning parameter r , very close to the transition. The operators are defined as $S_i^+ = c_{i\uparrow}^\dagger c_{i\downarrow}$ and $C_i^+ = c_{i\uparrow}^\dagger c_{i\downarrow}^\dagger$. *Right:* New effective SIAM Hamiltonian generated upon integrating out the coupling between the impurity and the bath zeroth site. In the new SIAM, the zeroth site acts as the new impurity site with a renormalised on-site correlation $U_Z^* = U_b + \delta U_Z^*$.

model is depicted schematically in the right panel of Fig. (4.8).

$$H_Z^* = \underbrace{-\frac{1}{2}U_Z^*(\hat{n}_{0\uparrow} - \hat{n}_{0\downarrow})^2}_{\text{new impurity } = 0^{\text{th}} \text{ site}} + \underbrace{V_Z^*\sum_{\langle j,0 \rangle} (c_{0\sigma}^\dagger c_{j\sigma} + \text{h.c.})}_{\text{hopping between } 0^{\text{th}} \text{ site \& new bath}} + \underbrace{(-t)\sum_{\langle i,j \rangle} (c_{i\sigma}^\dagger c_{j\sigma} + \text{h.c.})}_{\text{K.E. of new bath}}. \quad (4.19)$$

Since, for $r < r_{c2}$, the model always flows to strong coupling at low energies, the largest energy scales are J^* and V^* . Using this, the effective correlation U_Z^* on the zeroth site can be expressed to leading order as

$$U_Z^* \simeq \frac{J^*}{4} \frac{1}{1 + 2\gamma} - V^* \frac{\gamma}{\gamma^2 - \frac{1}{4}}, \quad \text{where } \gamma \equiv V^*/J^*. \quad (4.20)$$

From $r = 0$ to $r = r_{c1}$, the factor γ decreases due to the gradual removal of single-particle hopping from the impurity site (irrelevance of V), leading to an increase in the correlation U_Z^* . This is simply a restatement of the fact that the scattering processes that create the central impurity resonance induce a repulsive correlation on the bath zeroth site. The fact that we end up with a standard SIAM on the zeroth site once the impurity site has been integrated out means that the spectral function of this new impurity will again go undergo a sharpening of the central peak (and the appearance of the Hubbard sidebands) upon increasing the parameter r of the original e-SIAM. This ensures that the impurity and zeroth site spectral functions look qualitatively similar up to r_{c1} . One can now repeat iteratively this process - decoupling the zeroth site generates a standard SIAM with a repulsive correlation on the first site, and so on. The fact that excursions starting from any point along the bath can be described by a positive U SIAM is, therefore, the emergent self-consistency in our model. Similar indications of a correlated spectral function on lattice sites far away from the impurity were also observed in Ref. [224] from finite- U slave boson calculations of the SIAM. Beyond r_{c1} , the irrelevance of V means that U_Z^* reduces to just $J^*/4$. As r is now increased towards r_{c2} , the correlation decreases because J is moving towards its critical point, indicating that the bath zeroth site is moving away from its local moment

regime. This is another reflection of the increase in pairing fluctuations of the bath, as well as the lowering of spin-flip fluctuations between the impurity and the bath.

For $r > r_{c2}$, the impurity site decouples from the bath in the impurity model. This impurity model can be promoted to a bulk model as follows. Recall that in the auxiliary model mapping, any lattice site \vec{r}_i of the bulk lattice can act as the impurity, and one can think of the impurity model with the impurity at \vec{r}_i as a representation of the excursion of an electron from any such site \vec{r}_i into the rest of the bath. When all such impurity models undergo the transition at $r = r_{c2}$ simultaneously, the result is the decoupling of all sites from their respective baths and a paramagnetic bulk insulator is obtained.

4.6 Coexistence of local metallic and insulating phases in the e-SIAM

The DMFT solution of the Hubbard model on the Bethe lattice exhibits a coexistence region of metallic and insulating solutions between two spinodal lines $U_{c1}(T)$ and $U_{c2}(T)$ [186], with the metallic solution having lower internal energy and the insulating solution being a metastable state at a higher energy [186, 244, 246–248]. The $T = 0$ transition is observed to be second order in nature and occurs through a merging of the metallic and insulating solutions at U_{c2} [244, 249]. On the other hand, at $T > 0$, the MIT happens along the first-order line $U_c(T)$ ($U_{c1} < U_c < U_{c2}$) where the free energies of the two solutions become equal, and the two spinodal lines merge into a second order critical point at a sufficiently high temperature T_c . We will now show that our Hamiltonian-based approach gives a clear zero temperature picture of various aspects that can lead to the emergence of the metal-insulator coexistence at $T > 0$.

4.6.1 Excited state quantum phase transition at r_{c1} : the Mott-Hubbard scenario

We have already discussed in detail the nature of the phase transition at r_{c2} : the zero-bandwidth picture provided (around eq. (4.18)) shows the merging of the metallic and insulating solutions at that point, enabling identification of r_{c2} with the $T = 0$ continuous phase transition observed at U_{c2} in the DMFT phase diagram. The focus of this subsection is the physics of the other important point r_{c1} . As has been mentioned before, this point marks the RG irrelevance of the single-particle hybridisation amplitude V , and leads to the exclusion of the charge states from the ground-state (see left panel of Fig. (4.4)). This exclusion means that there is now one fewer scattering channel by which the impurity electron can hybridise with the bath. In turn, this leads to a *partial localisation of the impurity*, and can be thought of as the first step towards the more complete localisation that occurs at r_{c2} .

Apart from the change in the ground state, the physics at r_{c1} also involves a phase transition in certain excited states of the spectrum. To expose this, we consider the following states in the zero-bandwidth spectrum of the impurity model given in eq. (4.2):

$$\begin{aligned} |1, \sigma, \pm\rangle &= \alpha_{\pm} |\sigma_d\rangle |0_0\rangle \mp \sqrt{1 - \alpha_{\pm}^2} |0_d\rangle |\sigma_0\rangle, \quad |3, \sigma, \pm\rangle = \alpha_{\pm} |\sigma_d\rangle |2_0\rangle \mp \sqrt{1 - \alpha_{\pm}^2} |2_d\rangle |\sigma_0\rangle, \\ E_+ &= -\frac{U_0}{4} + \sqrt{V_0^2 + \frac{U_0^2}{16}}, \quad E_- = -\frac{U_{\text{im}}}{4} - \sqrt{V_{\text{im}}^2 + \frac{U_{\text{im}}^2}{16}}, \\ \alpha_+(U_0, V_0) &= \frac{V_0}{\sqrt{V_0^2 + (E_+ + \frac{U_0}{2})^2}}, \quad \alpha_- = \frac{E_- + \frac{U_{\text{im}}}{2}}{\sqrt{V_{\text{im}}^2 + (E_- + \frac{U_{\text{im}}}{2})^2}}. \end{aligned} \tag{4.21}$$

where ($\sigma = \uparrow, \downarrow$) and E_{\pm} is the energy of the states $|1(3), \sigma, \pm\rangle$ and the subscripts d and 0 refer to the impurity and bath zeroth site respectively. The states $|1(3), \sigma, +\rangle$ are high-energy states, so their energy E_+ and coefficient α_+ involve the bare single-particle hybridisation V_0 and impurity on-site repulsion U_0 . On the other hand, the other states $|1(3), \sigma, -\rangle$ are closer to the IR energy scale and involve renormalised intermediate-scale couplings V_{im} and U_{im} . Both E_+ and E_- are four-fold degenerate because of the SU(2) spin ($\uparrow \leftrightarrow \downarrow$) and particle-hole ($|0\rangle \leftrightarrow |2\rangle$) symmetries. For example, the degenerate subspace corresponding to E_+ is the set of states $\{|1, \uparrow, +\rangle, |1, \downarrow, +\rangle, |3, \uparrow, +\rangle, |3, \downarrow, +\rangle\}$.

All these states are in general delocalised - they involve the impurity hybridising with the bath via V . At $r = r_{c1}$, however, the coupling V becomes irrelevant and $V_{\text{im}} \rightarrow 0$, so that the coefficient α_- of the low-energy state becomes unity beyond that point. The low-energy states $|1(3), \sigma, -\rangle$ thus become localised at r_{c1} and give rise to a set of excited and *degenerate local moment states*, i.e., $\alpha_- \rightarrow 0$ as $r \rightarrow r_{c1}$ leads to

$$|1(3), \sigma, -\rangle \rightarrow \begin{cases} |\uparrow_d\rangle |0_0\rangle, |\downarrow_d\rangle |0_0\rangle \\ |\uparrow_d\rangle |2_0\rangle, |\downarrow_d\rangle |2_0\rangle \end{cases}. \quad (4.22)$$

The other coefficient α_+ remains non-zero because, as mentioned earlier, V is non-zero in the UV scales of the RG flow. As a result, the high-energy states $|1(3), \sigma, +\rangle$ remain delocalised, and are separated from the localised states by an energy-scale

$$\lim_{r \rightarrow r_{c1}^-} (E_+ - E_-) \simeq \sqrt{V_0^2 + \left(\frac{U_0}{4}\right)^2} + \sqrt{V_{\text{im}}^2 + \left(\frac{U_{\text{im}}}{4}\right)^2} + \frac{U_{\text{im}} - U_0}{4}. \quad (4.23)$$

This is shown schematically in the left panel of Fig. (4.9), and corresponds to the preformed gap in the zero mode spectrum. The point r_{c1} therefore represents a *delocalisation-localisation excited state quantum phase transition* (ESQPT) where degenerate local moment states are emergent as excited states in the many-body spectrum. This localisation of the impurity at r_{c1} is shown in the form of excited state mutual information in the right panel of Fig. (4.9). This ESQPT acts as a precursor to the QPT at r_{c2} , where the local moment states become degenerate with the spin-singlet ground state. The local moment states are stabilised as ground states in the insulating phase for $r > r_{c2}$.

4.6.2 Theory for the charge excitations in the Hubbard sidebands

Beyond r_{c1} , excitations into the *local moment states* $|1, \sigma, -\rangle$ and $|3, \sigma, -\rangle$ reside at the edge of the central peak in the impurity spectral function (purple curve in the right panel of Fig.(4.4)) but provide no spectral weight due to the lack of electron mobility. This explains the development of a preformed gap in the impurity spectral function. That these local moment states have to reside at the edge of the central peak becomes clear when we note that as the width of the central peak shrinks continuously, the local moment states must also recede towards zero frequency and finally replace the zero frequency peak at $r = r_{c2}$ in order to give rise to the insulating local moment phase for $r > r_{c2}$. On the other hand, the *still-delocalised high-energy states* $|1, \sigma, +\rangle$ and $|3, \sigma, +\rangle$ are pushed into the Hubbard sidebands, and their hybridisation with the bath through V and t is responsible for the broadening of the sidebands.

This isolation of the delocalised states into the sidebands means that charge delocalisation processes are now excluded from the physics at low energies. As accessing the sidebands involves excitations at exorbitantly high energy scales, such processes can only happen virtually and involve very short

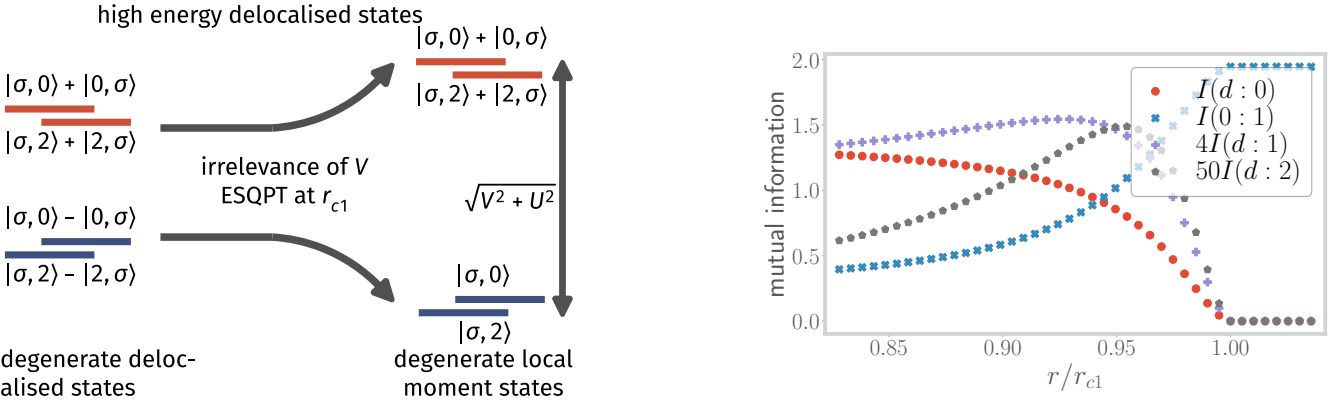


Figure 4.9: *Left:* Evolution of the excited states mentioned in Eqs. (4.21) as r is tuned through r_{c1} . The high-energy states (red) retain their impurity-bath coupling, while their low-energy counterparts (blue) become disentangled and form a degenerate set of local moment states. The high-energy states allow delocalisation into the bath and lead to the broad Hubbard sidebands. *Right:* Variation of mutual information (MI) between various parties, across the ESQPT at r_{c1} . The MI (red) between the impurity and the zeroth site vanishes at r_{c1} , showing the localisation of the impurity. The same between the bath zeroth site and the next site becomes maximum at r_{c1} . The MI between the impurity and the other sites (purple and gray) of the bath show an initial rise near r_{c1} , indicating that entanglement is becoming long-ranged near the ESQPT.

time scales. The central Kondo resonance observed at low energies, therefore, does not support any charge delocalisation, and metallic excitations propagate only through spin-flip scattering processes of the impurity. This reveals that the Mott insulator comes about through a local binding of doublons and holons [191, 250, 251]. Closely related to this is the Mott-Hubbard scenario of the MIT, which is equivalent to our observation of the appearance of an optical gap in the spectrum after r_{c1} .

The fact that the sidebands are broad indicates that there are gapless excitations propagating from the impurity site into the conduction bath, but whose energy lies outside the Mott gap. These can also be viewed as metallic excitations of the bath that are induced by the coupled impurity. In order to expose the nature of these excitations, we perform a calculation similar to the local Fermi liquid calculation of Nozières [238]. This involves considering the states at $\omega \sim \pm U/2$ as the ground-states of the Hubbard sidebands, and then computing how excitations into the bath renormalise the ground-state subspace. Up to the second order in the hopping strength t , the effective Hamiltonian for the excitations of the bath can be expressed as

$$H_{\text{eff}}^{(2)} = \frac{4t^2(1 - \alpha_+^2)}{E_+ - E_{\text{gs}}} C_{\text{tot}}^z C_1^z - t \sum_{i>0,\sigma} \left(c_{i\sigma}^\dagger c_{i+1\sigma} + \text{h.c.} \right), \quad (4.24)$$

where E_+ and α_+ have been defined in eq. (4.21), $C_i^z |2(0)\rangle = +(-)\frac{1}{2} |2(0)\rangle$ is the z-component of the charge isospin operator at a particular site i , and $\vec{C}_{\text{tot}} = \vec{C}_d + \vec{C}_0$ is the total isospin for the impurity and zeroth sites. $E_{\text{gs}} = U/2$ is the two-site energy of the ground-state subspace within the sideband. These excitations are of the local Fermi liquid kind - the absence of any isospin-flip scattering term promotes the independent delocalisation of the doublon and holon states into the bath. The second-order effective Hamiltonian can therefore be written as the sum of two decoupled parts corresponding to holon and doublon propagation respectively, and suggesting adiabatic continuity with the $U = 0$

Hubbard model [252].

However, fourth-order corrections lead to the appearance of scattering processes that convert holon and doublons into one another, resulting in the local Fermi liquid becoming correlated

$$H_{\text{eff}}^{(4)} = \frac{\gamma^4 \alpha_+^2 \beta^2}{(1 - \alpha_+^2)(E'_+ - E_{\text{gs}})} \left[-C_{\text{tot}}^z C_{\text{tot}}^2 C_1^z + \sqrt{2} \mathcal{P}_{\text{tot}}^4 (C_0^+ - C_d^+) C_1^- + \text{h.c.} \right], \quad (4.25)$$

where $E'_+ = \frac{U}{4} - \frac{3J}{8} + \sqrt{4V^2 + \left(\frac{U}{4} + \frac{3J}{8}\right)^2}$ is the energy of the state containing the charge isospin triplet zero, and $\beta = \frac{2V}{\sqrt{4V^2 + (U+3J/4)^2}}$. $\mathcal{P}_{\text{tot}}^4$ projects on to the $n_d + n_0 = 4$ subspace. The scattering processes in eq. (4.25) are clearly non-Fermi liquid in nature as they allow the inter-conversion of the charge isospin eigenstates, and therefore reduce the lifetime of the quasiparticle excitations of the local Fermi liquid obtained in eq. (4.25). Additional details pertaining to the calculation of this effective Hamiltonian are present in Sec. 5 of the Supplementary Materials [237].

4.6.3 Zero temperature origin of critical fluctuations above the second order point

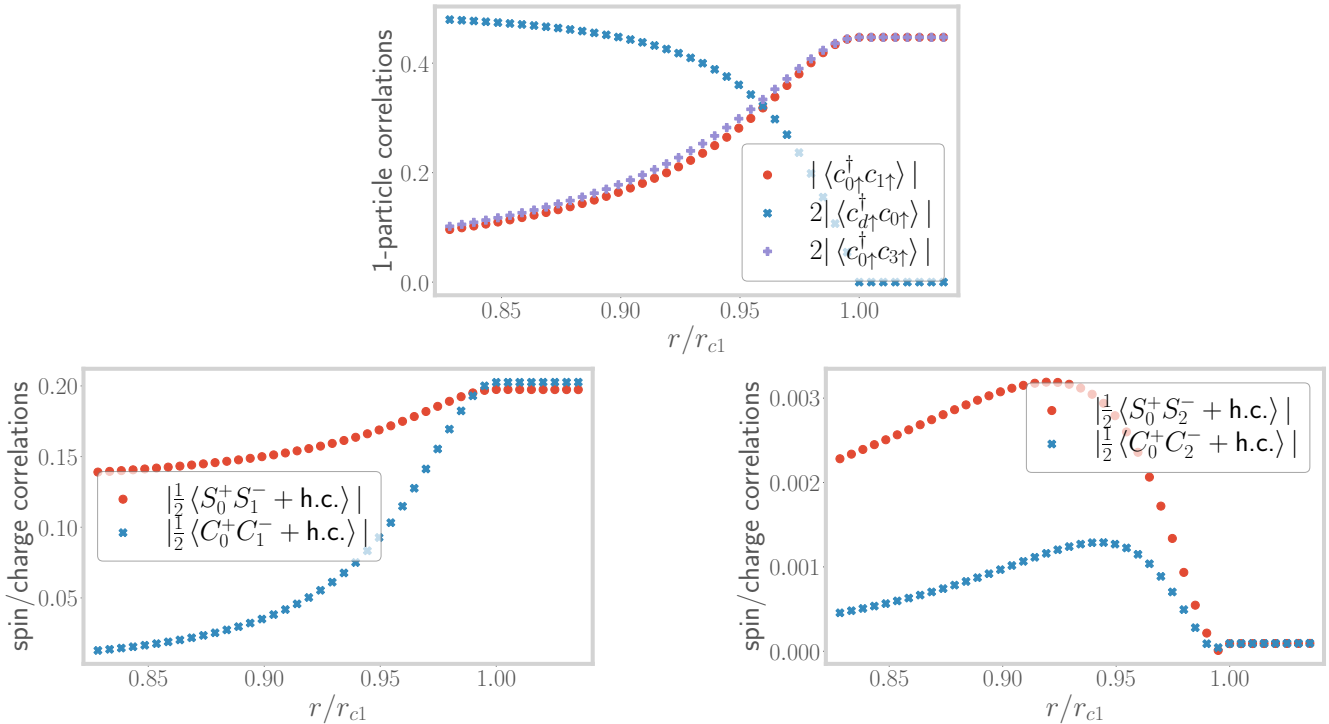


Figure 4.10: *Top:* Variation of the one particle correlations in the state $|1, \sigma, -\rangle$ between impurity and bath zeroth site (blue), as well as within the bath (red and violet). The former vanishes, depicting the excited state localisation transition at r_{c1} . *Left:* Variation of the spin-flip (red) and charge isospin-flip (blue) correlations between impurity and bath, close to r_{c1} . They both increase, indicating that the impurity is now less strongly coupled with the bath. *Right:* Variation of the spin-flip (red) and charge isospin-flip (blue) correlations between the zeroth and second sites of the bath, close to r_{c1} . Both show an initial increase, leading to the propagation of relatively long-range correlations into the bath.

Above the second order point $r_c(T_c)$, the DMFT phase diagram shows a rapid crossover from the paramagnetic metallic solution to the paramagnetic insulating solution [186, 253]. Remarkably, signatures of quantum critical scaling in this crossover region have been recently predicted from theoretical analyses [197, 205], as well as detected experimentally in transport measurements of several organic compounds [254, 255]. In Refs. [197, 205], this has been ascribed to the existence of a *hidden quantum criticality* in the maximally frustrated 1/2-filled Hubbard model on the Bethe lattice with infinite coordination number. In order to locate the zero temperature origin of these signatures of quantum criticality, we inspect carefully the quantum-mechanical fluctuations near the two important points r_{c1} and r_{c2} in our model.

Close to r_{c1} , we compute correlations in the state $|1, \sigma, -\rangle$. As shown in the top panel of Fig. (4.10), we find that while the one-particle correlation between the impurity and the bath vanishes, the same between the zeroth and first sites of the bath picks up. Importantly, these correlations extend beyond the immediate neighbourhood of the impurity. This is observed in, for example, the one-particle correlation between the zeroth site and the second site (purple curve in the top panel of Fig. (4.10)). Some other signatures of correlations in the bath are shown in Fig. (4.10): while the left panel displays increased spin-flip and charge isospin-flip correlations between the zeroth and first sites of the bath, a similar phenomenon is observed between the zeroth and second sites of the bath in the right panel. Our findings are consistent with the presence of scale-invariant solutions obtained from recent NRG-DMFT calculations [256] that correspond to the metastable insulating solutions in the coexistence region.

The growth of similar long-ranged correlations within the bath (and leading away from the immediate neighbourhood of the impurity) near r_{c2} as well. We recall that correlations between the impurity and the zeroth site are observed to decrease (see left panel of Fig.(4.5)). Instead, as shown in Fig. (4.11), non-trivial two-particle correlations arise between the impurity and bath zeroth sites with bath sites that are farther away. The spreading of the spin-spin correlations shown in the left panel of Fig. (4.11) indicates a “stretching” of the Kondo singlet state prior to its destruction. We will show later that these enhanced correlations also result in a diverging quasiparticle mass at r_{c2} , indicating a breakdown of the local Fermi liquid metal. Further, the right panel of Fig. (4.11) indicates that longer-ranged pairing correlations develop between the bath zeroth site and bath sites farther away upon approaching the transition.

In general, within the metallic phase and away from r_{c1} or r_{c2} , the impurity is strongly coupled to the bath zeroth site and the impurity-bath entanglement follows an area law characteristic of the local nature of the impurity problem. However, near the excited state and ground state transitions at r_{c1} or r_{c2} respectively, these results indicate a spreading of entanglement into the bath: more and more bath sites beyond the zeroth site get correlated with the impurity site as the ESQPT or the QCP is approached. This is corroborated in Fig. 3 of the Supplementary Materials [237]. This suggests a significant enhancement of the entanglement beyond the area law and is consistent with the critical quantum fluctuations observed in the various two-particle correlations.

The results of this subsection indicate that it might be possible to experimentally detect the signatures of such critical quantum fluctuations around the spinodals of the DMFT phase diagram even at $T > 0$. We note that signatures of second-order criticality have been indeed observed recently in vanadium sesquioxide, in the form of critical slowing down and critical opalescence [257]. It is, therefore, tempting to speculate that these signatures arise from the presence of critical quantum fluctuations.

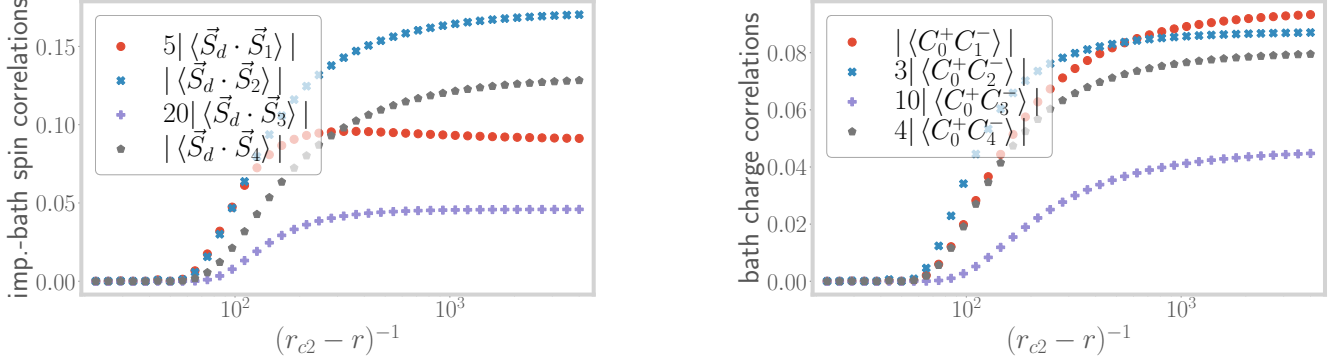


Figure 4.11: *Left:* Variation of the spin-spin correlations between the impurity and bath sites 1 through 4, close to r_{c2} . They show an increase, revealing the distribution of entanglement into the bath. *Right:* Variation of pairing correlations within the bath. These correlations show an increase, because of the weakening of the Kondo singlet.

4.7 Non-Fermi liquid signatures at the MIT

4.7.1 Death of the local Fermi liquid: the Brinkman-Rice scenario

The low-lying metallic excitations of the bath can be obtained by considering the singlet ground-state of the model (of energy $\sim -3\tilde{\mathcal{J}}/4$) in the metallic phase, and then studying the effect of an electron hopping term (with coupling t) between the singlet and the rest of the bath as a perturbation (see left panel of Fig. (4.12)). Such a strong-coupling expansion in powers of $t^2/\tilde{\mathcal{J}}$ leads to the usual local Fermi liquid effective Hamiltonian in the Kondo model [147, 219, 238, 258]:

$$H_{\text{LFL}} = \mathcal{F} \hat{n}_{1\uparrow} \hat{n}_{1\downarrow} + H_{\text{KE}}, \quad \mathcal{F} \sim t^4/\tilde{\mathcal{J}}^3, \quad (4.26)$$

where $\hat{n}_{1\sigma}$ are the number operators for the first site (site adjacent to the zeroth site of the conduction bath), H_{KE} is the kinetic energy arising from the nearest-neighbour hopping among all sites in the bath apart from the zeroth site, and \mathcal{F} is the local Fermi liquid correlation strength. The Kondo singlet (formed between the impurity spin and the bath zeroth site) has decoupled from the rest of the lattice, and eq. (4.26) describes the effective Hamiltonian for the rest of the bath beyond the zeroth site.

Following an identical approach, we find that the effective Hamiltonian for the low-lying excitations in the metallic phase is given by

$$H_{\text{LFL}} = \mathcal{F} [\hat{n}_{1\uparrow} \hat{n}_{1\downarrow} + (1 - \hat{n}_{1\uparrow})(1 - \hat{n}_{1\downarrow})] + H_{\text{KE}}, \quad \text{where } \mathcal{F} = \frac{2t^4}{\tilde{\mathcal{J}} (3\tilde{\mathcal{J}}/4 + \tilde{\mathcal{U}}_b)^2}. \quad (4.27)$$

We note that for our extended SIAM, the local Fermi liquid correlation \mathcal{F} diverges as the transition is approached at $3\tilde{\mathcal{J}}/4 + \tilde{\mathcal{U}}_b \rightarrow 0$. The divergence of \mathcal{F} leads to the divergence of the renormalised mass of the quasiparticles, and can also be obtained from a Gutzwiller variational calculation as shown by Brinkman and Rice [195]. This shows the breakdown of perturbation theory and is indicative of the fact that the ground state is about to change at the metal-insulator transition.

The death of the local Fermi liquid is also seen from the vanishing of the dynamically generated low-energy Kondo screening scale T_K . Towards obtaining T_K close to the transition, we follow the approach

used by Moeller et al. 1995 [244] and Held et al. 2013 [245]. Near the transition, they obtained a Kondo model from the SIAM by applying a Schrieffer-Wolff transition that removes the charge fluctuations of the impurity site and retains the physics of only the Kondo coupling J . This amounts to removing the side peaks from the impurity spectral function and focusing on the low-energy central peak (right panel of Fig. (4.12)). Held et al. then integrated the RG equation for this Kondo model by using a Lorentzian DOS $\rho(D)$ in the bath: $\rho(D) = \frac{\rho_0 \Gamma^2}{D^2 + \Gamma^2}$. This is motivated by the fact that the central peak



Figure 4.12: *Left:* Setup for obtaining the low-energy excitations above the strong-coupling ground state. The effects of the rest of the bath is included by treating the hopping between the zeroth site (blue sphere on the left) and the first site (sphere labelled 1) as a perturbation on top of the singlet ground state formed by the impurity (red sphere) and the zeroth site. *Right:* At r_{c1} , the Hubbard sidebands have become isolated from the central peak in the local spectral function because of the finite optical gap. Removing the UV excitations that couple the low-energy and high-energy bands then leads to a theory of the Kondo model with a Lorentzian DOS.

of the impurity spectral function is a Lorentzian, and the bath becomes equivalent to the impurity site under self-consistency.

We implement the same approach on the e-SIAM, such that the Schrieffer-Wolff transformation leads to a $J - U_b$ model with a Lorentzian electronic DOS in the bath. The expression of the Kondo temperature for such a system has been derived in Sec. 6 of the Supplementary Materials [237]. Very close to the transition, we have $r \rightarrow 0.25^-$, and the Kondo temperature is given by

$$T_K = \frac{D_0}{k_B} \exp \left[-\frac{\ln(r_{c2} - r)}{4U_b \rho_0} \right], \quad (4.28)$$

where $r_{c2} = 0.25$ and D_0 is the bare bandwidth. Note that the pre-factor of the logarithm is positive as U_b is negative: $-4U_b \rho_0 = |4U_b \rho_0|$. As we approach the transition, the parameter r takes the limit $r \rightarrow r_{c2}^-$, and the Kondo temperature scale vanishes:

$$\lim_{r \rightarrow r_{c2}^-} T_K = \frac{D_0}{k_B} \lim_{r \rightarrow r_{c2}^-} (r_{c2} - r)^{4|U_b \rho_0|} \rightarrow 0. \quad (4.29)$$

Following the renormalised perturbation theory approach of Hewson [8, 259], the imaginary part of the self-energy of the local Fermi liquid quasiparticles is given by

$$\text{Im} [\Sigma(\omega)] \sim \frac{\mathcal{F}^2 \omega^2}{D_0 T_K^2}, \quad (4.30)$$

while the quasiparticle residue is given by $Z \sim T_K$. The divergence of $\text{Im} [\Sigma(\omega)]$ at the transition and the vanishing of T_K and the quasiparticle residue are important indicators of the loss of the local Fermi liquid excitations and the breakdown of Kondo screening.

The vanishing of the Kondo temperature scale also leads to the divergence of thermodynamic quantities such as the impurity contribution to local spin susceptibility χ_{imp} and the specific heat coefficient γ_{imp} . As the low-energy theory is a local Fermi liquid, χ_{imp} and γ_{imp} retain their Fermi liquid forms but involve the highly renormalised Kondo temperature scale [147, 260]:

$$\begin{aligned}\chi_{\text{imp}} &= \frac{w}{4k_B T_K}, \quad \lim_{r \rightarrow r_{c2}^-} \chi_{\text{imp}} = \frac{w}{4k_B} (r_{c2} - r)^{-4|U_b\rho_0|}, \\ \gamma_{\text{imp}} &= \frac{\pi^2 k_B^2 w}{6T_K}, \quad \lim_{r \rightarrow r_{c2}^-} \gamma_{\text{imp}} = \frac{\pi^2 k_B^2 w}{6} (r_{c2} - r)^{-4|U_b\rho_0|},\end{aligned}\quad (4.31)$$

where $w \sim 0.4128$ is the Wilson number for the Kondo model [147, 219]. These results also show that the ratio of χ_{imp} and γ_{imp} , referred to as the Wilson ratio $R \equiv \frac{4\pi^2 k_B^2 \chi_{\text{imp}}}{3\gamma_{\text{imp}}}$, remains pinned at the single-channel Kondo value of $R_{\text{LFL}} = 2$ for $r \rightarrow r_{c2}^-$. This shows that the low-frequency Landau quasiparticles are able to survive until very close to the QCP. As we will show in the next subsection, the metallic excitations precisely at the QCP acquire non-Fermi liquid character and involve additional correlations between holons and doublons. These additional correlations are expected to lead to an enhancement of the Wilson ratio. Evidence for this can be found in the DMFT calculation of a local Wilson ratio very close to the Brinkman-Rice transition, $R_{\text{loc}} = 2.9 \pm 0.2$ [186].

4.7.2 Emergence of non-Fermi liquid excitations at the transition

In order to obtain an effective Hamiltonian for the excitations precisely at the critical point $r = 1/4$, we first note that the ground-state subspace of the zero bandwidth $J - U_b$ effective model (eq. (4.18)) becomes degenerate at this point:

$$\frac{1}{\sqrt{2}} (|\uparrow\rangle_d |\downarrow\rangle_0 - |\downarrow\rangle_d |\uparrow\rangle_0), \quad |\sigma\rangle_d |0\rangle_0, \quad |\sigma\rangle |2\rangle_0, \quad (\sigma = \uparrow, \downarrow), \quad (4.32)$$

with all the states lying at zero energy. Here, the first ket (with subscript d) represents the impurity spin configuration while the second ket (with subscript 0) represents the configuration of the bath zeroth site). We now diagonalise these states in the presence of the electron hopping t into the rest of the conduction bath, and obtain the effective Hamiltonian for the low-lying excitations mediated by t . This is described in detail in Sec. 7 of the Supplementary Materials [237]. We note that the ground state is four-fold degenerate at energy $-t$ in the presence of the hopping, and comprises the following states:

$$|N_{\text{tot}} = 2, S_{\text{tot}}^z = 0\rangle, \quad |N_{\text{tot}} = 4, S_{\text{tot}}^z = 0\rangle, \quad |N_{\text{tot}} = 3, S_{\text{tot}}^z = \frac{1}{2}\rangle, \quad |N_{\text{tot}} = 3, S_{\text{tot}}^z = -\frac{1}{2}\rangle, \quad (4.33)$$

where $N_{\text{tot}} = \hat{n}_d + \hat{n}_0 + \hat{n}_1$ and $S_{\text{tot}}^z = S_d^z + S_0^z + S_1^z$ are the total number operator and total magnetisation operator respectively for the impurity, bath zeroth and first sites taken together. It is worth observing that

- the presence of the unscreened states $|N_{\text{tot}} = 3, S_{\text{tot}}^z = \pm \frac{1}{2}\rangle$ in the ground-state subspace is a result of the inexact screening at the critical point, and
- the presence of a degenerate ground-state manifold indicates that these excitations of the bath will likely be of the non-Fermi liquid (NFL) kind [203, 261, 262].

The precise form of the effective Hamiltonian for this non-Fermi liquid, as well as the behaviour of various correlation functions, is obtained by considering the ground-state manifold in conjunction with the excited states at energy $-t$.

Since the total Hamiltonian conserves the total spin S_{tot}^z , the effective Hamiltonian separates into two sectors, $S_{\text{tot}}^z = 0$ and $|S_{\text{tot}}^z| = \frac{1}{2}$. Detailed calculations on obtaining this effective Hamiltonian from the RG fixed point theory are shown in Sec. 7 of the Supplementary Materials [237]. In order to highlight certain distinct features, we present simplified effective Hamiltonians only for the $S_{\text{tot}}^z = 0$ and $S_{\text{tot}}^z = \frac{1}{2}$ sectors. We first take a look at the $S_{\text{tot}}^z = 0$ sector:

$$H_{\text{eff}}^{S_{\text{tot}}^z=0} = t \vec{S}_d \cdot (\vec{\mathcal{S}}_{1,-} + \vec{\mathcal{S}}_{3,-}) . \quad (4.34)$$

The effective spin-1/2 ladder operators $\vec{\mathcal{S}}_{1,\pm}$ act on the positive and negative parity sectors (labelled by \pm) of the $\hat{n}_0 + \hat{n}_1 = 1$ subspace spanned by the states

$$|\uparrow\rangle_{1,\pm} = |\uparrow\rangle_0 |0\rangle_1 \pm |0\rangle_0 |\uparrow\rangle_1 , \quad |\downarrow\rangle_{1,\pm} = |\downarrow\rangle_0 |0\rangle_1 \pm |0\rangle_0 |\downarrow\rangle_1 , \quad (4.35)$$

leading to a Pauli matrix representation of $\vec{\mathcal{S}}_{1,\pm}$ in that basis. The Pauli matrix operators $\vec{\mathcal{S}}_{3,\pm}$ similarly act on the $\hat{n}_0 + \hat{n}_1 = 3$ subspace spanned by the states $|\uparrow\rangle_{3,\pm} = |\uparrow\rangle_0 |2\rangle_1 \pm |2\rangle_0 |\uparrow\rangle_1$ and $|\downarrow\rangle_{3,\pm} = |\downarrow\rangle_0 |2\rangle_1 \pm |2\rangle_0 |\downarrow\rangle_1$, obtained by applying the transformation $|0\rangle \rightarrow 2$ on the $\hat{n}_0 + \hat{n}_1 = 1$ counterparts. We now point out two interesting features of this simplified effective Hamiltonian in eq. (4.34).

- The fact that the impurity is now interacting with emergent spins $\vec{\mathcal{S}}_1$ and $\vec{\mathcal{S}}_3$ that span over two lattice sites (0 and 1) instead of just the zeroth site indicates that the entanglement between the impurity and bath is now extended beyond the bath zeroth site, and that *the singlet is being stretched*.
- The presence of two spins that are trying to simultaneously screen the impurity spin introduces frustration in the dynamics of the impurity. This is reminiscent of the 2-channel Kondo effect, and the connection is made more precise in the concluding section of our work.

Both these features are precursors to the ultimate and complete destruction of screening in the local moment regime, and reflect the fact that the impurity-bath system *is now in an over-screened state*.

We now focus on the effective Hamiltonian of the $S_{\text{tot}}^z \neq 0$ subspace:

$$H_{\text{eff}}^{S_{\text{tot}}^z \neq 0} = -\frac{1}{2} t (S_d^- \mathcal{B}_\uparrow^+ + \text{h.c.}) . \quad (4.36)$$

The Pauli matrix operators \mathcal{B}_\uparrow^+ and \mathcal{B}_\uparrow^- flip between the doublet of states $|\uparrow\rangle_0 |\uparrow\rangle_1$ and $\frac{1}{\sqrt{2}} (|2\rangle_0 |0\rangle_1 + |0\rangle_0 |2\rangle_1)$:

$$\begin{aligned} \mathcal{B}_\uparrow^- |\uparrow\rangle_0 |\uparrow\rangle_1 &= \frac{1}{\sqrt{2}} (|2\rangle_0 |0\rangle_1 + |0\rangle_0 |2\rangle_1) , \\ \mathcal{B}_\uparrow^+ \frac{1}{\sqrt{2}} (|2\rangle_0 |0\rangle_1 + |0\rangle_0 |2\rangle_1) &= |\uparrow\rangle_0 |\uparrow\rangle_1 . \end{aligned} \quad (4.37)$$

The structure of the effective Hamiltonian in eq. (4.36) leads to another drastic difference from the behaviour of the local Fermi liquid: it allows for the electrons to be “Andreev scattered” into an orthogonal state by hopping from the first site into the zeroth site. This is easily seen by considering the scattering processes in eq. (4.37): a state $|\uparrow\rangle_0 |\uparrow\rangle_1$ (i.e., with site 1 in \uparrow configuration) has a finite probability of

being flipped into the $|\downarrow\rangle_0 |2\rangle_1$ state (i.e., with site 1 in the doublon configuration). An incident electron $c_{1\uparrow}^\dagger$ can therefore emerge as a doublon $c_{1\uparrow}^\dagger c_{1\downarrow}^\dagger$ or a hole $c_{1\uparrow}$ upon scattering from the zeroth site. This is a direct consequence of the entanglement between the singlet and the first site at the critical point that was absent in the metallic regime of the e-SIAM. We note that similar orthogonal scattering processes also occur in a two-channel Kondo problem between effective pseudo-particles and pseudo-holes [263].

At this point, it is worth noting that the polarised ground-state $|S_{\text{tot}}^z = \frac{1}{2}\rangle$ can be written as an equal superposition of the singlet state $|\text{SS}\rangle_{d0} \otimes |\uparrow\rangle_1$ and the local moment states $\frac{1}{\sqrt{2}}(|\uparrow, 0, 2\rangle - |\uparrow, 2, 0\rangle)$. This symmetry-broken ground state, along with its counterpart $|S_{\text{tot}}^z = -\frac{1}{2}\rangle$, act as a bridge between the ground states of the metallic and insulating phases. They are thus important in displaying the breakdown of the Kondo cloud at the QCP, and the consequences arising from it. We will hence consider these states in the next subsection and demonstrate some exotic non-Fermi liquid properties of these states, e.g., inexact screening of the impurity, fractional impurity magnetisation and fractional impurity entanglement entropy.

Finally, by mapping the quantum impurity problem of the e-SIAM onto that of a classical Coulomb gas [203, 208], it can be shown that the local self-energies $\Sigma_{dd}(\omega)$ and $\Sigma_{00}(\omega)$ of the impurity and zeroth sites respectively and certain two-particle correlation functions have power-law behaviours in the frequency domain:

$$\text{Re} [\Sigma_{dd}] (\omega) \sim |\omega|^{\gamma_{dd}}, \quad \text{Re} [\Sigma_{00}] (\omega) \sim |\omega|^{\gamma_{00}}, \quad (4.38)$$

$$\langle S_d^+ \rangle \sim |\omega|^{(\alpha_1-1)/2}, \quad \langle c_{0\uparrow}^\dagger c_{0\downarrow}^\dagger \rangle \sim |\omega|^{(\alpha_3-1)/2}. \quad (4.39)$$

The precise forms of the exponents in terms of the conduction electron scattering phase shifts, as well as several other technical details of the calculation, are provided in Sec. 8 of the Supplementary Materials [237]. While the various exponents are found to be non-universal functions of the fixed point value of J and the coupling U_b for $r \rightarrow r_{c2}-$, we argue in subsection (4.7.4) that they assume universal values precisely at the QCP ($r = r_{c2}$). The algebraic behaviour of these local correlations is reminiscent of critical behaviour ascribed to the class of local quantum criticality [264, 265].

4.7.3 Impurity magnetisation and entanglement entropy

More indications of non-Fermi liquid behaviour at the QCP is obtained from a calculation of the impurity magnetisation and the impurity entanglement entropy ($S_{\text{EE}}(d)$) (shown in Sec. 9 of the Supplementary Materials [237]) for the symmetry-broken states $|S_{\text{tot}}^z = \sigma/2\rangle$. This leads to a fractional entanglement entropy (in units of $\log 2$) for each of the two states:

$$\begin{aligned} \rho_{\text{imp}} &= \begin{pmatrix} \frac{1}{2} + m_{\text{imp}}^z & 0 \\ 0 & \frac{1}{2} - m_{\text{imp}}^z \end{pmatrix} = \begin{pmatrix} \frac{3}{4} & 0 \\ 0 & \frac{1}{4} \end{pmatrix}, \\ S_{\text{EE}}(d) &= -\text{Tr} (\rho_{\text{imp}} \ln \rho_{\text{imp}}) \simeq 0.81 \log 2, \end{aligned} \quad (4.40)$$

where the impurity magnetisation m_{imp}^z takes the value $m_{\text{imp}}^z = 1/4$ at the QCP (i.e., half the value for a local moment). Further, $S_{\text{EE}}(d)$ can be written in terms of an effective impurity degeneracy g_{imp} , which we define using the impurity magnetisation: $g_{\text{imp}} \equiv 1 + 2|m_{\text{imp}}^z|$, such that it takes the expected values of 1 and 2 in the local Fermi liquid and local moment phases (with m_{imp}^z having values 0 and $\frac{1}{2}$ respectively). The effective degeneracy in the polarised subspace $S_{\text{tot}}^z = \pm 1/2$ at the QCP then turns out to be $3/2$, which is half-way between a unique state and a doublet. This corresponds to partial screening

of the impurity degrees of freedom at the QCP, in contrast to complete screening in the metallic phase ($g_{\text{imp}} = 1$) and the absence of screening in the insulating phase ($g_{\text{imp}} = 2$).

In Sec. 9 of the Supplementary Materials [237], we show that the incomplete magnetisation (and hence the fractional value of S_{EE}) arises from the mixing of the local Fermi liquid ground-state $|\phi\rangle = \otimes_{k <= k_F} |k \uparrow\rangle |k \downarrow\rangle$ and the gapless excitations above it, $|e\rangle_\sigma = e_\sigma^\dagger |\phi\rangle$, $e \equiv \sum_{k \in FS} c_{k\sigma}^\dagger$, leading to the decay of the local Fermi liquid quasiparticles [261]. This is captured by the modified ground-state $|-\rangle$ and lowest-lying excited states $|+\rangle$ at the QCP:

$$|\pm\rangle = \frac{1}{\sqrt{2}} (|SS\rangle \otimes |e\rangle_\sigma \pm |LM\rangle_\sigma \otimes |\phi\rangle) . \quad (4.41)$$

The spin-singlet state $|SS\rangle \sim \sum_\sigma \sigma |\sigma\rangle_d |\bar{\sigma}\rangle_0$ and the local moment state $|LM\rangle_\sigma = |\sigma\rangle_d |2\rangle_0$ represent the configurations of the impurity and the bath zeroth sites. Such a ground-state $|-\rangle$ should be contrasted with the local Fermi liquid ground-state $|SS\rangle \otimes |\phi\rangle$ that is stable in the metallic phase for $r_{c1} < r < r_{c2}$. This change in the ground-state manifests in the vanishing of the quasiparticle residue of the local Fermi liquid excitations: $Z = |\langle + | e_\sigma^\dagger | - \rangle|^2 = |\langle + | (|LM\rangle_\sigma \otimes |e\rangle_\sigma) | - \rangle|^2 = 0$, consistent with the orthogonality catastrophe [266] described below eq. (4.30). As the local Fermi liquid quasiparticles are rendered unstable, they are replaced by stable composite three-site excitations of the form, $S_d^- c_{0\bar{\sigma}} e_\sigma^\dagger$. This is further reflected in the fact that the corresponding residue for such three-site composite excitation is non-zero at the QCP: $|\langle + | S_d^- c_{0\bar{\sigma}} e_\sigma^\dagger | - \rangle|^2 > 0$.

4.7.4 Friedel scattering phase shift and fractional excess charge

The orthogonality catastrophe faced by the infrared excitations of the conduction bath at the QCP points towards the presence of an “unrenormalised” phase shift [267] of the scattering k -states. Indeed, using the Friedel sum rule [268–270], we obtain a $\pi/2$ phase shift for the extended states at the Fermi surface for the QCP, which is only half the unitary limit. This can be seen by recalling that the ground state in eq. (4.41) is an equal admixture of a decoupled local moment state and a singlet state. Through the singlet state, the impurity contributes an excess charge of unity to the Fermi surface of the conduction bath (because of the presence of gapless spin-flip fluctuations). The local moment state does not contribute any excess charge, because the impurity is decoupled from the bath. The net excess charge then comes out to be $n_{\text{exc}} = \frac{1}{2}(1+0) = \frac{1}{2}$. From the Friedel sum rule, the phase shift at the fixed point is $\delta^* = \pi n_{\text{exc}} = \pi/2$, as mentioned above. Expectedly, n_{exc} is zero in the local moment phase. Also, as the exponents of the algebraic form for the local quantities shown in eq. (4.38) are functions of the scattering phase shift, we find that these exponents take universal values precisely at the QCP.

The values of the excess charge at the QCP and in the local moment phase lead to important corollaries. Firstly, the jump in the excess charge by unity in going from $r < r_{c2}$ to $r > r_{c2}$ is in fact a reduction in the Luttinger volume V_L of the conduction bath [144, 271]. V_L counts the number of extended states present at and below the Fermi volume, and corresponds to a topological quantum number [1, 123, 124, 272]. Since the excess charge n_{exc} calculated above is simply the impurity contribution to V_L at the Fermi surface, the difference in the excess charge across the transition implies that the two phases acquire different values for the invariant V_L . Thus, n_{exc} tracks the change (ΔV_L) in the Luttinger volume, and the transition is topological in nature. Secondly, in a recent work, Sen et al. [273] have shown that the Mott MIT of the infinite-dimensional Hubbard model proceeds through the dissociation of domain walls in a fictitious Su-Schrieffer-Heeger chain connected to the physical lattice sites. If one couples their observation with the fact that the two dissociated domain walls at the ends of the

SSH chain are together known to host a single charge [274, 275], it becomes evident that the fractional excess charge we obtain at the QCP corresponds to the state that is localised in the SSH chain near the physical lattice site as obtained by Sen et al. The well-known bulk-boundary correspondence of the SSH model (see, e.g., [276]) suggests that the excess charge n_{exc} and the change ΔV_L in the Luttinger volume are the respective topological invariants of the boundary and bulk in the e-SIAM that are tied to one another. Further, the appearance of a half-quantised n_{exc} at the MIT of the e-SIAM corresponds, in the SSH model, to the dissociation of a domain wall-anti domain wall pair with each carrying a half charge [274, 275].

We show in Sec. 9 of the Supplementary Materials [237] that it is in fact possible to connect the scattering phase shift (δ^*), impurity magnetisation (m_{imp}^z), effective degeneracy (\tilde{g}) and excess charge (n_{exc}) in a single relation:

$$\delta^* = \pi n_{\text{exc}} = \left[1 + \left(\frac{2 - \tilde{g}}{\tilde{g} - 1} \right)^2 \right]^{-1} = \frac{4 m_{\text{imp}}^z {}^2}{1 - 4|m_{\text{imp}}^z| + 8 m_{\text{imp}}^z {}^2}. \quad (4.42)$$

As we now discuss, this provides a unified picture of the effect of frustration on the impurity spin. As we have seen earlier, the presence of U_b in the Hamiltonian of the e-SIAM introduces local moment states into the spectrum and leads to states with non-vanishing impurity magnetisation at the QCP. This non-zero magnetisation can be interpreted as a partial screening of the impurity spin, in turn resulting in an effective impurity degeneracy ($1 < \tilde{g} < 2$ between that of a unique screened state and an unscreened local moment. The partial screening also manifests in only half the excess charge being contributed to the conduction bath. This reduction in the excess charge acts as a change in the boundary conditions felt by the conduction electrons coupled to the impurity and manifests as a phase shift that is less than the unitarity limit of π .

4.8 Discussions and Outlook

In summary, we have shown that an attractive correlation on the bath zeroth site is enough to frustrate the Kondo effect and stabilise the local moment phase. The destruction of the Kondo cloud, and the associated local Fermi liquid, occurs through *pairing fluctuations in the bath and proximate to the impurity* (left panel of Fig. (4.8)). This is reminiscent of a subdominant superconducting tendency that was observed in the half-filled Hubbard model at $T = 0$ from a unitary RG treatment in Refs. [3, 121]. We also note the finding of non-local attractive effective interactions in a recent theoretical study of the 2D Hubbard model [277]. We find that the critical point displays non-Fermi liquid behaviour with a vanishing quasiparticle residue Z . The strong agreement of our results with several aspects of DMFT suggests that the local self-energy obtained self-consistently in that method can be represented quite faithfully through the e-SIAM. It will, thus, be important to test the predictions offered by our approach directly within the DMFT method. We note that the non-Fermi liquid at the critical point displays a *partial correlation of doublons and holons* that is distinct from not only the correlated Fermi liquid metal (unbound holons and doublons), but also the paramagnetic insulator (comprised of bound holons and doublons). The excitations that propagate through the two unscreened states in the ground-state subspace (Eq. (4.33)) involve the simultaneous creation of a doublon and a holon: in these channels, the doublons and holons cannot propagate in the absence of each other. Such an incomplete correlation is an intermediate step towards complete confinement in the local moment phase. It appears interesting to

experimentally test some of these ideas on a mesoscopic quantum dot [278,279] which is, apart from the usual electron tunnel coupling to an electronic reservoir, additionally coupled through the proximity effect to a superconducting lead.

We stress here that the e-SIAM analysed in this work represents an impurity model that (i) has a single correlated channel of conduction electrons, (ii) is consistent with the symmetries of a half-filled Hubbard model (SU(2)-spin, U(1)-charge and particle-hole), and (iii) shows a local metal-insulator transition. The model, therefore, provides a minimal route towards obtaining a Hamiltonian-based understanding of DMFT. Further, at the level of the renormalisation group flows that involve the frustration of Kondo screening, the effect of the attractive on-site interaction U_b introduced by us is equivalent to that of additional bath correlations that have been introduced in related impurity models. These include a single impurity Anderson model with multiple anisotropic conduction channels studied by Giamarchi et al. [280], and a periodic Anderson model enhanced with explicit s-d coupling (as well as a density-density interaction) between the conduction and impurity bands, studied by Si and Kotliar [203,215,281] as well as by Ruckenstein et al., [282]. In the former K -channel model of Ref. [280], the z -component (V_l , $l \in [1, K-1]$) of the Kondo interaction term in the $K-1$ additional conduction channels acts as a source of frustration for the spin-flip term γ_0 of the Kondo interaction in the original $l=0$ channel, leading to a breakdown of Kondo screening. The U_b coupling in the e-SIAM acts as a similar source of frustration: the equivalence lies at the level of the renormalisation group equations, such that both V_l and U_b oppose the RG relevance of γ_0 and J respectively. This can be made more precise by comparing the RG equations of our work (eqs.(4.70)) and that of Giamarchi et al. [280]: the mapping between the two frustration terms U_b and V_l is found to be of the form $U_b \sim \sum_{l=1}^{K-1} V_l^2 \rho$, where ρ is the conduction bath DOS. A similar relationship can be found between the RG equations obtained by us and those for the extended periodic Anderson model studied by Si and Kotliar [203]. In this sense, our analysis applies to a wide variety of models where the Kondo effect is stable in a certain regime of parameters but is destroyed in other parameter regimes by some form of quantum-mechanical frustration of the impurity spin degree of freedom.

Extensions of the present work involve analysing the mixed valence regime of the impurity site (i.e., away from half-filling) within the e-SIAM auxiliary model. This allows the possibility that the finite-temperature critical end-point of the DMFT first-order transition could turn into a quantum critical point from the merging of the $T = 0$ ESQPT and QPT observed in the present work. Recent DMFT calculations [283] show a shrinking of the coexistence region with hole doping but fall short of revealing a QCP. If such a QCP does exist, can it harbour pair fluctuations between the impurity and zeroth bath sites that become dominant upon doping, signalling thereby a putative superconducting instability of a related bulk model? We recall that a superconducting state of matter was indeed observed to be emergent from a QCP in the hole-doped Hubbard model at $T = 0$ via a unitary RG treatment in Refs. [4, 121]. The phenomenon of electronic differentiation in k -space can perhaps be captured by considering cluster variants of the e-SIAM, i.e., multiple impurities connected to one another through single-particle hopping and/or RKKY-like interactions [284, 285]. In general, the presence of multiple and varied classes of correlations in the auxiliary model - localisation from Mott physics, delocalisation from spin and charge fluctuations, and pairing from local attractive correlations - makes this a strong candidate for an auxiliary model that carries the potential for describing the emergence of a variety of novel phases of correlated quantum matter.

4.9 Appendix: Derivation of renormalisation group equations for the extended-SIAM

The Hamiltonian we are working with is the extended Anderson impurity model (described in Section III of the main manuscript):

$$\mathcal{H} = -\frac{1}{2}U(\hat{n}_{d\uparrow} - \hat{n}_{d\downarrow})^2 + \sum_{\vec{k},\sigma} \epsilon_{\vec{k}} \tau_{\vec{k},\sigma} + J \vec{S}_d \cdot \vec{S}_0 + V \sum_{\sigma} \left(c_{d\sigma}^\dagger c_{0\sigma} + \text{h.c.} \right) - \frac{1}{2}U_b(\hat{n}_{0\uparrow} - \hat{n}_{0\downarrow})^2 . \quad (4.43)$$

The renormalisation in the Hamiltonian $H_{(j)}$ at the j^{th} RG step, upon decoupling an electronic state $q\beta$, is given by the expression:

$$(\Delta H_{(j)})_{\vec{q},\beta} = H_{(j-1)} - H_{(j)} = c_{\vec{q},\beta}^\dagger T_{\vec{q},\beta} \frac{1}{\omega_e - H_D} T_{\vec{q},\beta}^\dagger c_{\vec{q},\beta} + T_{\vec{q},\beta}^\dagger c_{\vec{q},\beta} \frac{1}{\omega_h - H_D} c_{\vec{q},\beta}^\dagger T_{\vec{q},\beta} , \quad (4.44)$$

where $\omega_{e,h}$ are the quantum fluctuation scales for the electron and hole scattering channels, H_D is the part of the Hamiltonian that is diagonal in k -space, and $T_{\vec{q},\beta} + T_{\vec{q},\beta}^\dagger$ is the part of the Hamiltonian that does not commute with $\hat{n}_{\vec{q},\beta}$ (in short, it is the part that is off-diagonal with respect to a particular state \vec{q}, β). This off-diagonal part is made up of contributions from V, J and U_b : $T_{\vec{q}\uparrow} = \left[V c_{d\uparrow}^\dagger + J \sum_{\vec{k}} S_d^+ c_{\vec{k}\downarrow}^\dagger + U_b \sum_{\vec{k}_1, \vec{k}_2, \vec{k}_3} c_{\vec{k}_1\uparrow}^\dagger c_{\vec{k}_3\downarrow}^\dagger c_{\vec{k}_4\downarrow} \right] c_{\vec{q}\uparrow}$, while the diagonal part is given by $H_D = \epsilon_{\vec{q}} \tau_{q\uparrow} + \frac{1}{4} J S_d^z (\hat{n}_{q\uparrow} - \hat{n}_{q\downarrow}) - \frac{1}{2} U_b (\tau_{q\uparrow} - \tau_{q\downarrow})^2$. The contribution from U_b is obtained by taking the Hartree contributions corresponding to the states $|q\sigma\rangle$ from the full interacting term in the Hamiltonian. Note that we have ignored potential scattering terms in the off-diagonal part $T_{\vec{q}\beta}$. In order to allow both spin-flip and charge transfer scattering processes, we start from initial states with $\tau_{q\uparrow} = -\tau_{q\downarrow}$. As a result, the contribution to H_D from the kinetic energy is $\epsilon_q \tau_{q\uparrow} = (\pm D) \times (\pm \frac{1}{2}) = D/2$, while the contribution from U_b is $-\frac{1}{2} U_b (\pm \frac{1}{2} - (\mp \frac{1}{2}))^2 = -U_b/2$.

4.9.1 Renormalisation of U_b

U_b can renormalise only via itself. The relevant renormalisation term in the particle sector is

$$U_b^2 \sum_{q\beta} \sum_{\substack{k_1, k_2, k_3, \\ k'_1, k'_2, k'_3}} c_{q\beta}^\dagger c_{k_1\beta} c_{k'_3\bar{\beta}}^\dagger c_{k'_1\bar{\beta}} \frac{1}{\omega - H_D} c_{k'_2\bar{\beta}}^\dagger c_{k'_3\bar{\beta}} c_{k_2\beta} c_{q\beta} . \quad (4.45)$$

In order to renormalise U_b , we need to contract one more pair of momenta. There are two choices. The first is by setting $k_3 = k'_3 = q$. The two internal states, then, are $q\beta$ and $q\bar{\beta}$. As discussed above, the intermediate state energy is $-U_b/4$. We therefore have

$$\frac{U_b^2 n_j}{\omega - D/2 + \frac{U_b}{2}} \sum_{\beta} \sum_{k_1, k_2, k'_1, k'_2} c_{k_1\beta} c_{k'_1\bar{\beta}}^\dagger c_{k'_2\bar{\beta}}^\dagger c_{k_2\beta} = \frac{U_b^2 n_j}{\omega - D/2 + \frac{U_b}{2}} \sum_{\beta} \sum_{k_1, k_2, k'_1, k'_2} c_{k'_2\bar{\beta}}^\dagger c_{k'_1\bar{\beta}} c_{k_2\beta}^\dagger c_{k_1\beta} . \quad (4.46)$$

Another way to contract the momenta is by setting $k'_1 = k'_2 = q$, which gives a renormalisation of

$$\frac{U_b^2 n_j}{\omega - D/2 + \frac{U_b}{2}} \sum_{\beta} \sum_{k_1, k_2, k_3, k'_3} c_{k_1\beta} c_{k'_3\bar{\beta}}^\dagger c_{k_3\bar{\beta}} c_{k_2\beta}^\dagger = -\frac{U_b^2 n_j}{\omega - D/2} \sum_{\beta} \sum_{k_1, k_2, k_3, k'_3} c_{k'_3\bar{\beta}}^\dagger c_{k_3\bar{\beta}} c_{k_2\beta}^\dagger c_{k_1\beta} . \quad (4.47)$$

The two contributions cancel each other. The same cancellation happens in the hole sector as well.

4.9.2 Renormalisation of the impurity correlation U

The coupling U is renormalised by two kinds of vertices: V^2 and J^2 . We will consider these processes one at a time. For convenience, we define $\epsilon_d = -U/2$.

The renormalisation arising from the first kind of terms, in the particle sector, is

$$\begin{aligned} \sum_{q\beta} c_{q\beta}^\dagger c_{d\beta} \frac{V^2}{\omega - H_D} c_{d\beta}^\dagger c_{q\beta} &= \sum_{q\beta} V^2 \hat{n}_{q\beta} (1 - \hat{n}_{d\beta}) \left(\frac{1 - \hat{n}_{d\bar{\beta}}}{\omega_0 - E_0} + \frac{\hat{n}_{d\bar{\beta}}}{\omega_1 - E_1} \right) \\ &= V^2 n_j \sum_{\beta} (1 - \hat{n}_{d\beta}) \left(\frac{1 - \hat{n}_{d\bar{\beta}}}{\omega_0 - E_0} + \frac{\hat{n}_{d\bar{\beta}}}{\omega_1 - E_1} \right). \end{aligned} \quad (4.48)$$

q runs over the momentum states that are being decoupled at this RG step: $|q| = \Lambda_j$. $E_{1,0}$ are the diagonal parts of the Hamiltonian at $\hat{n}_{d\bar{\beta}} = 1, 0$ respectively: $E_1 = \frac{D}{2}$ and $E_0 = \frac{D}{2} + \epsilon_d - \frac{J}{4}$. In order to relate ω_0 and ω_1 with the common fluctuation scale ω for the conduction electrons, we will replace these quantum fluctuation scales with the current renormalised values of the single-particle self-energy for the initial state from which we started scattering. For $\hat{n}_{d\bar{\beta}} = 0$, there is no additional self-energy because the impurity does not have any spin: $\omega_0 = \omega$. For $\hat{n}_{d\bar{\beta}} = 1$, we have an additional self-energy of ϵ_d arising from the correlation on the impurity: $\omega_1 = \omega + \epsilon_d$. Substituting the values of $E_{0,1}$ and $\omega_{0,1}$, we get

$$V^2 n_j \sum_{\beta} (1 - \hat{n}_{d\beta}) \left(\frac{1 - \hat{n}_{d\bar{\beta}}}{\omega - \frac{D}{2} - \epsilon_d + \frac{J}{4}} + \frac{\hat{n}_{d\bar{\beta}}}{\omega - \frac{D}{2} + \epsilon_d} \right). \quad (4.49)$$

Performing a similar calculation for the hole sector gives the contribution:

$$V^2 n_j \sum_{\beta} \hat{n}_{d\beta} \left(\frac{1 - \hat{n}_{d\bar{\beta}}}{\omega - \frac{D}{2} + \epsilon_d} + \frac{\hat{n}_{d\bar{\beta}}}{\omega - \frac{D}{2} - \epsilon_d + \frac{J}{4}} \right). \quad (4.50)$$

We now come to the second class of terms: spin-spin. We first look at the particle sector:

$$\frac{J^2}{4} \sum_{q\beta} c_{d\bar{\beta}}^\dagger c_{d\beta} c_{q\beta}^\dagger c_{-q\bar{\beta}} \frac{1}{\omega - H_D} c_{d\beta}^\dagger c_{d\bar{\beta}} c_{q\bar{\beta}}^\dagger c_{q\beta} = \frac{J^2}{4} n_j \frac{1}{\omega - \frac{D}{2} + \frac{J}{4}} \sum_{\beta} \hat{n}_{d\bar{\beta}} (1 - \hat{n}_{d\beta}). \quad (4.51)$$

The diagonal part in the denominator was simple to deduce in this case because the nature of the scattering requires the spins S_d^z and $\frac{\beta}{2} (\hat{n}_{q\beta} - \hat{n}_{q\bar{\beta}})$ to be anti-parallel. This ensures that the intermediate state has an energy of $E = \frac{D}{2} + \epsilon_d - \frac{J}{4}$, and the quantum fluctuation scale is $\omega' = \omega + \epsilon_d$, such that $\omega' - E = \omega - \frac{D}{2} + \frac{J}{4}$. In the hole sector, we have

$$\frac{J^2}{4} n_j \frac{1}{\omega - \frac{D}{2} + \frac{J}{4}} \sum_{\beta} \hat{n}_{d\beta} (1 - \hat{n}_{d\bar{\beta}}). \quad (4.52)$$

From eqs. (4.49), (4.50), (4.51) and (4.52), we write

$$\begin{aligned} \Delta U &= \Delta \epsilon_2 + \Delta \epsilon_0 - 2 \Delta \epsilon_1 \\ &= -\frac{4V^2 n_j}{\omega + \frac{U_b}{2} - \frac{D}{2} - U/2} + \frac{4V^2 n_j}{\omega + \frac{U_b}{2} - \frac{D}{2} + U/2 + \frac{J}{4}} - \frac{J^2 n_j}{\omega + \frac{U_b}{2} - \frac{D}{2} + \frac{J}{4}}, \end{aligned} \quad (4.53)$$

where we have restored the contribution from U_b in the denominator.

4.9.3 Renormalisation of the hybridisation V

Renormalisation of V happens through two kinds of processes: VJ and VU_b . Within the first kind, the scattering can be either via S_d^z or through S_d^\pm . For the first kind, we have the following contribution in the particle sector:

$$\begin{aligned} & \sum_{q\beta} V c_{q\beta}^\dagger c_{d\beta} \frac{1}{\omega - H_D} \frac{1}{4} J \sum_k (\hat{n}_{d\beta} - \hat{n}_{d\bar{\beta}}) c_{k\beta}^\dagger c_{q\beta} \\ &= \frac{1}{4} V J n_j \frac{1}{2} \left(\frac{1}{\omega'_1 - E} + \frac{1}{\omega'_2 - E} \right) \sum_{k\beta} (1 - \hat{n}_{d\bar{\beta}}) c_{d\beta} c_{k\beta}^\dagger. \end{aligned} \quad (4.54)$$

The transformation from $\frac{1}{\omega - H_D}$ to $\frac{1}{2} \left(\frac{1}{\omega'_1 - E} + \frac{1}{\omega'_2 - E} \right)$ is made so that we can account for both the initial state and the final state energies through the two fluctuation scales ω'_1 and ω'_2 respectively; we calculate the denominators for both the initial and final states and then take the mean of the two (hence the factor of half in front). This was not required previously because, in the earlier scattering processes, the impurity returned to its initial state at the end, at least in terms of $\epsilon_d (\hat{n}_{d\uparrow} - \hat{n}_{d\downarrow})^2$, and so we had $\omega'_1 = \omega'_2 = \omega'$. Substituting the energies and the ω -scales, we get

$$- \left(\frac{\frac{n_j}{4} V J \frac{1}{2}}{\omega - \frac{D}{2} + \frac{J}{4}} + \frac{\frac{n_j}{4} V J \frac{1}{2}}{\omega - \frac{D}{2} - \epsilon_d + \frac{J}{4}} \right) \sum_{k\beta} (1 - \hat{n}_{d\bar{\beta}}) c_{k\beta}^\dagger c_{d\beta}. \quad (4.55)$$

One can generate another such process by exchanging the single-particle process and the spin-exchange process:

$$\sum_{q\beta} \frac{1}{4} J \sum_k (\hat{n}_{d\beta} - \hat{n}_{d\bar{\beta}}) c_{q\beta}^\dagger c_{k\beta} \frac{1}{\omega - H_D} V c_{d\beta}^\dagger c_{q\beta}. \quad (4.56)$$

This is simply the Hermitian conjugate of the previous contribution. Combining this with the previous then gives

$$-\frac{n_j}{8} V J \left(\frac{1}{\omega - \frac{D}{2} + \frac{J}{4}} + \frac{1}{\omega - \frac{D}{2} - \epsilon_d + \frac{J}{4}} \right) \sum_{k\beta} (1 - \hat{n}_{d\bar{\beta}}) \times (c_{d\beta}^\dagger c_{k\beta} + \text{h.c.}) . \quad (4.57)$$

If we similarly calculate the contributions from the spin-exchange processes involving S_d^\pm , we get

$$-\frac{1}{4} V J n_j \left(\frac{1}{\omega - \frac{D}{2} + \frac{J}{4}} + \frac{1}{\omega - \frac{D}{2} - \epsilon_d + \frac{J}{4}} \right) \sum_{k\beta} (1 - \hat{n}_{d\beta}) (c_{k\bar{\beta}}^\dagger c_{d\bar{\beta}} + \text{h.c.}) . \quad (4.58)$$

The contributions from the hole sector are obtained by making the transformation $\hat{n}_{d\bar{\beta}} \rightarrow 1 - \hat{n}_{d\bar{\beta}}$ on the particle sector contributions. The total renormalisation to V from VJ processes are

$$-\frac{3n_j}{8} V J \left(\frac{1}{\omega + U_b/4 - \frac{D}{2} + \frac{J}{4}} + \frac{1}{\omega + U_b/4 - \frac{D}{2} + U/2 + \frac{J}{4}} \right) \sum_{k\beta} (c_{d\beta}^\dagger c_{k\beta} + \text{h.c.}) . \quad (4.59)$$

The renormalisation in V from U_b arises through terms of VU_b and U_bV kind. The first term gives

$$-\sum_{k\beta} c_{d\beta}^\dagger c_{k\beta} \left[\frac{\hat{n}_{d\bar{\beta}}}{2} \left(\frac{n_j U_b V}{\omega - \frac{D}{2} - \frac{U}{2} + \frac{U_b}{4}} + \frac{n_j U_b V}{\omega - \frac{D}{2} + \frac{U_b}{4}} \right) + \frac{1 - \hat{n}_{d\bar{\beta}}}{2} \left(\frac{n_j U_b V}{\omega - \frac{D}{2} + \frac{U_b}{4} + \frac{U}{2} + \frac{J}{4}} + \frac{n_j U_b V}{\omega - \frac{D}{2} + \frac{U_b}{4} + \frac{J}{4}} \right) \right]. \quad (4.60)$$

The second term is of the form $\sum_{q\beta} \sum_k U_b V c_{q\beta}^\dagger c_{d\beta} \frac{1}{\omega - H_D} \hat{n}_{q\bar{\beta}} c_{k\beta}^\dagger c_{q\beta}$, and this is just the Hermitian conjugate of the previous term, so these two terms together lead to

$$-n_j U_b V \sum_{k\beta} \left(c_{d\beta}^\dagger c_{k\beta} + \text{h.c.} \right) \left[\frac{\hat{n}_{d\bar{\beta}}}{2} \left(\frac{1}{\omega - \frac{D}{2} - \frac{U}{2} + \frac{U_b}{4}} + \frac{1}{\omega - \frac{D}{2} + \frac{U_b}{4}} \right) + \frac{1 - \hat{n}_{d\bar{\beta}}}{2} \left(\frac{1}{\omega - \frac{D}{2} + \frac{U_b}{4} + \frac{U}{2} + \frac{J}{4}} + \frac{1}{\omega - \frac{D}{2} + \frac{U_b}{4} + \frac{J}{4}} \right) \right]. \quad (4.61)$$

In the hole sector, we have

$$-n_j U_b V \sum_{k\beta} c_{k\beta}^\dagger \left[\frac{\hat{n}_{d\bar{\beta}}}{2} \left(\frac{1}{\omega_1 - E_1} + \frac{1}{\omega'_1 - E_1} \right) + \frac{1 - \hat{n}_{d\bar{\beta}}}{2} \left(\frac{1}{\omega_0 - E_0} + \frac{1}{\omega'_0 - E_0} \right) \right] c_{d\beta}. \quad (4.62)$$

$E_1 = D/2 - U_b/4 - U/2 - J/4$, $E_0 = D/2 - U_b/4 - K/4$. The fluctuation scales are $\omega_1 = \omega = \omega'_0$, $\omega'_1 = \omega - U/2 = \omega_0$. Substituting these gives

$$-\sum_{k\beta} c_{d\beta}^\dagger c_{k\beta} \left[\frac{1 - \hat{n}_{d\bar{\beta}}}{2} \left(\frac{n_j U_b V}{\omega - \frac{D}{2} - \frac{U}{2} + \frac{U_b}{4}} + \frac{n_j U_b V}{\omega - \frac{D}{2} + \frac{U_b}{4}} \right) + \frac{\hat{n}_{d\bar{\beta}}}{2} \left(\frac{n_j U_b V}{\omega - \frac{D}{2} + \frac{U_b}{4} + \frac{U}{2} + \frac{J}{4}} + \frac{n_j U_b V}{\omega - \frac{D}{2} + \frac{U_b}{4} + \frac{J}{4}} \right) \right]. \quad (4.63)$$

The other term, obtained by exchanging V and U_b , gives the Hermitian conjugate, so the overall contribution from the hole sector is the same as the total contribution from the particle sector, but with $\hat{n}_{d\bar{\beta}} \rightarrow 1 - \hat{n}_{d\bar{\beta}}$. Combining both the sectors, we get

$$-\sum_{k\beta} \left(c_{d\beta}^\dagger c_{k\beta} + \text{h.c.} \right) \left[\left(\frac{n_j U_b V/2}{\omega - \frac{D}{2} - \frac{U}{2} + \frac{U_b}{4}} + \frac{n_j U_b V/2}{\omega - \frac{D}{2} + \frac{U_b}{4}} \right) + \left(\frac{n_j U_b V/2}{\omega - \frac{D}{2} + \frac{U_b}{4} + \frac{U}{2} + \frac{J}{4}} + \frac{n_j U_b V/2}{\omega - \frac{D}{2} + \frac{U_b}{4} + \frac{J}{4}} \right) \right]. \quad (4.64)$$

4.9.4 Renormalisation of the spin-exchange coupling J

The term $J \vec{S}_d \cdot \vec{S}_0$ can be split into three parts: $J^z S_d^z$, $\frac{1}{2} J^+ S_d^+ S_0^-$ and $\frac{1}{2} J^- S_d^- S_0^+$. We will only calculate the renormalisation in J^+ , which will be equal to that of J^- , J^z due to spin-rotation symmetry. The terms that renormalise J^+ are of the form $S_d^+ S_d^z$ and $S_d^z S_d^+$. In the particle sector, we have

$$\begin{aligned} -\sum_q \sum_{kk'} \frac{1}{4} J^2 S_d^+ c_{q\downarrow}^\dagger c_{k'\uparrow} \frac{1}{\omega - H_D} S_d^z c_{k\downarrow}^\dagger c_{q\downarrow} &= n_j \frac{1}{4} J^2 \left(-\frac{1}{2} S_d^+ \right) \sum_{kk'} c_{k\downarrow}^\dagger c_{k'\uparrow} \frac{1}{\omega + \frac{U_b}{2} - \frac{D}{2} + \frac{J}{4}}, \\ \sum_q \sum_{kk'} \frac{1}{4} J^2 S_d^z c_{q\uparrow}^\dagger c_{k'\uparrow} \frac{1}{\omega - H_D} S_d^+ c_{k\downarrow}^\dagger c_{q\uparrow} &= -n_j \frac{1}{4} J^2 \left(\frac{1}{2} S_d^+ \right) \sum_{kk'} c_{k\downarrow}^\dagger c_{k'\uparrow} \frac{1}{\omega + \frac{U_b}{2} - \frac{D}{2} + \frac{J}{4}}. \end{aligned} \quad (4.65)$$

The denominator is determined using $E = \frac{D}{2} + \epsilon_d - \frac{J}{4}$ and $\omega' = \omega + \epsilon_d$. In the hole sector, we similarly have

$$\begin{aligned} \sum_q \sum_{kk'} \frac{1}{4} J^2 S_d^+ c_{k\downarrow}^\dagger c_{q\uparrow} \frac{1}{\omega - H_D} S_d^z c_{q\uparrow}^\dagger c_{k'\uparrow} &= n_j \frac{1}{4} J^2 \left(-\frac{1}{2} S_d^+ \right) \sum_{kk'} c_{k\downarrow}^\dagger c_{k'\uparrow} \frac{1}{\omega + \frac{U_b}{2} - \frac{D}{2} + \frac{J}{4}} , \\ - \sum_q \sum_{kk'} \frac{1}{4} J^2 S_d^z c_{k\downarrow}^\dagger c_{q\uparrow} \frac{1}{\omega - H_D} S_d^+ c_{q\downarrow}^\dagger c_{k'\uparrow} &= -n_j \frac{1}{4} J^2 \left(\frac{1}{2} S_d^+ \right) \sum_{kk'} c_{k\downarrow}^\dagger c_{k'\uparrow} \frac{1}{\omega + \frac{U_b}{2} - \frac{D}{2} + \frac{J}{4}} . \end{aligned} \quad (4.66)$$

The renormalisation due to U_b also happens through multiple terms. One of the terms is

$$\frac{1}{2} J U_b \sum_q \sum_{k,k'} S_d^+ c_{q\downarrow}^\dagger c_{k\uparrow} \frac{1}{\omega - H_D} \hat{n}_{q\uparrow} c_{k'\downarrow}^\dagger c_{q\downarrow} = -\frac{1}{2} \frac{J U_b n_j}{\omega - \frac{D}{2} + \frac{U_b}{2} + \frac{J}{4}} \sum_{k,k'} S_d^+ c_{k'\downarrow}^\dagger c_{k\uparrow} . \quad (4.67)$$

The factor of half in front is the same half factor that appears in front of the $S_1^+ S_2^-$, $S_1^- S_2^+$ terms when we rewrite $\vec{S}_1 \cdot \vec{S}_2$ in terms of S^z , S^\pm . Another term is obtained by switching J and U_b :

$$\frac{1}{2} J U_b \sum_q \sum_{k,k'} \hat{n}_{q\downarrow} c_{q\uparrow}^\dagger c_{k\uparrow} \frac{1}{\omega - H_D} S_d^+ c_{k'\downarrow}^\dagger c_{q\uparrow} = -\frac{1}{2} \frac{J U_b n_j}{\omega - \frac{D}{2} + \frac{U_b}{2} + \frac{J}{4}} \sum_{k,k'} S_d^+ c_{k'\downarrow}^\dagger c_{k\uparrow} . \quad (4.68)$$

The corresponding terms in the hole sector are

$$-\frac{1}{2} \frac{J U_b n_j}{\omega - \frac{D}{2} + \frac{U_b}{2} + \frac{J}{4}} \sum_{k,k'} S_d^+ c_{k'\downarrow}^\dagger c_{k\uparrow} , -\frac{1}{2} \frac{J U_b n_j}{\omega - \frac{D}{2} + \frac{U_b}{2} + \frac{J}{4}} \sum_{k,k'} S_d^+ c_{k'\downarrow}^\dagger c_{k\uparrow} . \quad (4.69)$$

4.9.5 Final URG equations

In summary, the renormalisation in the couplings takes the form:

$$\begin{aligned} \Delta U &= 4V^2 n_j \left(\frac{1}{d_1} - \frac{1}{d_0} \right) - n_j \frac{J^2}{d_2} , & \Delta V &= -\frac{3n_j V}{8} \left[J \left(\frac{1}{d_2} + \frac{1}{d_1} \right) + \frac{4U_b}{3} \sum_{i=1}^4 \frac{1}{d_i} \right] , \\ \Delta J &= -\frac{n_j J (J+4U_b)}{d_2} , & \Delta U_b &= 0 , \end{aligned} \quad (4.70)$$

where the denominators d_i are given by

$$d_0 = \omega - \frac{D}{2} + \frac{U_b}{2} - \frac{U}{2} , \quad d_1 = \omega - \frac{D}{2} + \frac{U_b}{2} + \frac{U}{2} + \frac{J}{4} , \quad (4.71)$$

$$d_2 = \omega - \frac{D}{2} + \frac{U_b}{2} + \frac{J}{4} , \quad d_3 = \omega - \frac{D}{2} + \frac{U_b}{2} . \quad (4.72)$$

For the sake of completeness, we present the RG equation for a charge isospin Kondo coupling K between the impurity and the bath:

$$\Delta K = -\frac{n_j K (K+4U_b)}{\omega - \frac{D}{2} + \frac{U_b}{2} + \frac{K}{4}} . \quad (4.73)$$

Indeed, the RG equation for K is observed to be identical in form to that for the spin Kondo coupling J , obtained through the transformation $J \rightarrow K$. This indicates that charge fluctuations between the bath zeroth and first sites (that are incited by an attractive interaction U_b) lead to the RG irrelevance of $K(>0)$, and thereby a destabilisation of the charge Kondo effect similar to that presented in the main manuscript for J .

4.10 Appendix: Expressing correlation functions in terms of entanglement

We will first relate the impurity Greens function to the geometric entanglement. Given a ground state $|\Psi\rangle_{\text{gs}}$ and a spectrum of energies $\{E_n\}$, the retarded impurity Greens function (in time domain) is defined as $G_{d\sigma}(t) = -i\theta(t) \langle \{c_{d\sigma}(t), c_{d\sigma}^\dagger\} \rangle$. It can be given a spectral representation in terms of the eigenstates $\{|\Psi\rangle_n\}$ of the e-SIAM:

$$G_{d\sigma}(\omega) = \frac{1}{Z} \sum_n \left[\frac{|\langle \Psi_{\text{gs}} | c_{d\sigma} | \Psi_n \rangle|^2}{\omega + E_{\text{gs}} - E_n} + \frac{|\langle \Psi_n | c_{d\sigma} | \Psi_{\text{gs}} \rangle|^2}{\omega - E_{\text{gs}} + E_n} \right], \quad (4.74)$$

where $Z \equiv \sum_n e^{-\beta E_n}$ is the partition function. We will now insert a complete basis into the expression. The basis will be the set of eigenstates of the Hamiltonian $H = H_1 + H_2$, where H_1 is the two-site $J - U_b$ Hamiltonian formed by the impurity and zeroth sites, and H_2 is a tight-binding Hamiltonian formed by the remaining sites. Since the Hamiltonians are decoupled, the eigenstates $|\Psi\rangle_{m,n}$ will be direct product states formed by combining the eigenstates $|\phi\rangle_m, |\psi\rangle_n$ of the individual Hamiltonians H_1 and H_2 respectively: $|\Phi\rangle_{m,n} = |\phi\rangle_m \otimes |\psi\rangle_n$. Inserting this basis leads to the expression:

$$|\Psi\rangle_{\text{gs}} = \sum_{m,n} |\Phi\rangle_{m,n} (\langle \phi_m | \otimes \langle \psi_n |) |\Psi_{\text{gs}}\rangle. \quad (4.75)$$

The ground state of H_1 is the spin-singlet: $|\phi\rangle_0 = |ss\rangle$. We denote the ground state of the tight-binding Hamiltonian H_2 by $|\psi\rangle_0$. Because of the highly renormalised couplings V and J , the impurity site is almost maximally entangled with the zeroth site, such that the ground state $|\Psi\rangle_{\text{gs}}$ in the $r < 0.25$ regime can be thought of as a direct product of the two-site ground state, $c|ss\rangle + \sqrt{1-c^2}|ct\rangle$, in direct product with the tight-binding ground state:

$$|\Psi\rangle_{\text{gs}} \simeq \left(c|ss\rangle + \sqrt{1-c^2}|ct\rangle \right) \otimes |\psi\rangle_0 = |\Phi\rangle_{\text{ss}} + |\Phi\rangle_{\text{ct}}, \quad (4.76)$$

where $|\Phi\rangle_{\text{ss(ct)}} = |ss(\text{ct})\rangle \otimes |\psi\rangle_0$. This suggests that not all terms in the summation of eq. (4.75) contribute; out of all $\{|\psi\rangle_n\}$, only the ground state $n = 0$ contributes, while only $|ss\rangle$ and $|ct\rangle$ contribute from the set $\{|\phi\rangle_m\}$. The summation then simplifies to

$$|\Psi\rangle_{\text{gs}} = |\Phi\rangle_{\text{ss}} \langle ss | \Psi_{\text{gs}}^{(2)} \rangle + |\Phi\rangle_{\text{ct}} \langle ct | \Psi_{\text{gs}}^{(2)} \rangle, \quad (4.77)$$

where $|\Psi_{\text{gs}}^{(2)}\rangle$ is the two-site part of the ground state and can be obtained by starting with the full ground state $|\Psi\rangle_{\text{gs}}$ and tracing over the other lattice sites of the system.

We assume that the global phases of the wavefunctions are real, and since the internal weights of the wavefunctions are real as well, the overlaps $\langle ss | \Psi_{\text{gs}}^{(2)} \rangle, \langle ct | \Psi_{\text{gs}}^{(2)} \rangle$ are also real. We can use these overlaps to define a geometric measure of entanglement [16, 241, 242]:

$$\varepsilon(\psi_1, \psi_2) = 1 - |\langle \psi_1 | \psi_2 \rangle|^2. \quad (4.78)$$

If $|\psi_1\rangle$ is thought of as a separable state, then $|\psi_2\rangle$ should be less entangled if its overlap with $|\psi_1\rangle$ is large, which is indeed borne out by the definition. The overlaps then become $\langle ss | \Psi_{\text{gs}}^{(2)} \rangle = \sqrt{1 - \varepsilon(ss, \Psi_{\text{gs}}^{(2)})}$,

and similarly for the state $|ct\rangle$. For brevity, we will use the notation $\varepsilon_{ss} \equiv \varepsilon(ss, \Psi_{gs}^{(2)})$, $\varepsilon_{ct} \equiv \varepsilon(ct, \Psi_{gs}^{(2)})$. The retarded impurity Greens function for spin σ can now be written in terms of these measures:

$$G_{d\sigma}(\omega) = \frac{1}{Z} \sum_n \left[(1 - \varepsilon_{ss}) \left(\frac{|\langle \Phi_{ss} | c_{d\sigma} | \Psi_n \rangle|^2}{\omega + E_{gs} - E_n} + \frac{|\langle \Psi_n | c_{d\sigma} | \Phi_{ss} \rangle|^2}{\omega - E_{gs} + E_n} \right) + (1 - \varepsilon_{ct}) \frac{|\langle \Phi_{ct} | c_{d\sigma} | \Psi_n \rangle|^2}{\omega + E_{gs} - E_n} \right. \\ \left. + (1 - \varepsilon_{ct}) \frac{|\langle \Psi_n | c_{d\sigma} | \Phi_{ct} \rangle|^2}{\omega - E_{gs} + E_n} + \sqrt{(1 - \varepsilon_{ss})} \sqrt{(1 - \varepsilon_{ct})} \frac{\langle \Phi_{ss} | c_{d\sigma} | \Psi_n \rangle \langle \Psi_n | c_{d\sigma}^\dagger | \Phi_{ct} \rangle + h.c.}{\omega + E_{gs} - E_n} \right. \\ \left. + \sqrt{(1 - \varepsilon_{ss})} \sqrt{(1 - \varepsilon_{ct})} \frac{\langle \Phi_{ct} | c_{d\sigma} | \Psi_n \rangle \langle \Psi_n | c_{d\sigma}^\dagger | \Phi_{ss} \rangle + h.c.}{\omega - E_{gs} + E_n} \right]. \quad (4.79)$$

We now generalise this to any real-space two-particle correlation involving operators O_1, O_2 that are at most two-particle operators and act on the combined Hilbert space of the impurity site and the zeroth site. The so-called lesser Greens function corresponding to these operators is defined as

$$G_{O_1^\dagger, O_2}^<(t) \equiv i \langle O_1^\dagger O_2(t) \rangle, \quad G_{O_1^\dagger, O_2}^<(t \rightarrow \infty) = i \langle \Psi_{gs} | O_1^\dagger O_2 | \Psi_{gs} \rangle. \quad (4.80)$$

We focus on the static case ($t \rightarrow \infty$) here. Following eq. (4.77), we can rewrite the ground states in terms of the entanglement measures mentioned above.

$$|\Psi\rangle_{gs} = |\Phi\rangle_{ss} \sqrt{1 - \varepsilon_{ss}} + |\Phi\rangle_{ct} \sqrt{1 - \varepsilon_{ss}}, \quad (4.81)$$

where $|\Phi\rangle_{ss(ct)}$ are the zero spin and zero charge isospin eigenstates of the Hamiltonian $H = H_1 + H_2$ defined below eq. (4.74). Substituting this in the static lesser Greens function gives

$$\frac{1}{i} G_{O_1^\dagger, O_2}^<(t \rightarrow \infty) = (1 - \varepsilon_{ss}) \langle \Phi_{ss} | O_2 O_1^\dagger | \Phi_{ss} \rangle + (1 - \varepsilon_{ct}) \langle \Phi_{ct} | O_2 O_1^\dagger | \Phi_{ct} \rangle \\ + \sqrt{1 - \varepsilon_{ss}} \sqrt{1 - \varepsilon_{ct}} \left(\langle \Phi_{ss} | O_2 O_1^\dagger | \Phi_{ct} \rangle + \langle \Phi_{ct} | O_2 O_1^\dagger | \Phi_{ss} \rangle \right). \quad (4.82)$$

This can be extended to generalised retarded Greens functions $G_{O_1^\dagger, O_2}^R(t) \equiv -i\theta(t) \langle \{O_1^\dagger(t), O_2\} \rangle$, whose spectral representation is of the form

$$G_{O_1^\dagger, O_2}^R(\omega) = \frac{1}{Z} \sum_n \left[\frac{\langle \Psi_{gs} | O_2 | \Psi_n \rangle \langle \Psi_n | O_1^\dagger | \Psi_{gs} \rangle}{\omega + E_{gs} - E_n} + \frac{\langle \Psi_n | O_2 | \Psi_{gs} \rangle \langle \Psi_{gs} | O_1^\dagger | \Psi_n \rangle}{\omega - E_{gs} + E_n} \right]. \quad (4.83)$$

Following an approach very similar to the one that led to eq. (4.79), we can cast the generalised Greens function in terms of the geometric entanglement measures:

$$G_{O_1^\dagger, O_2}^R(\omega) = \frac{1}{Z} \sum_n \left[(1 - \varepsilon_{ss}) \left(\frac{(O_1)_{ss,n}^*(O_2)_{ss,n}}{\omega + E_{gs} - E_n} + \frac{(O_1)_{n,ss}^*(O_2)_{n,ss}}{\omega - E_{gs} + E_n} \right) + (1 - \varepsilon_{ct}) \frac{(O_1)_{ct,n}^*(O_2)_{ct,n}}{\omega + E_{gs} - E_n} \right. \\ \left. + (1 - \varepsilon_{ct}) \frac{(O_1)_{n,ct}^*(O_2)_{n,ct}}{\omega - E_{gs} + E_n} + \sqrt{(1 - \varepsilon_{ss})} \sqrt{(1 - \varepsilon_{ct})} \frac{(O_2)_{ss,n} (O_1)_{ct,n}^* + h.c.}{\omega + E_{gs} - E_n} \right. \\ \left. + \sqrt{(1 - \varepsilon_{ss})} \sqrt{(1 - \varepsilon_{ct})} \frac{(O_2)_{ct,n} (O_1)_{ss,n}^* + h.c.}{\omega - E_{gs} + E_n} \right], \quad (4.84)$$

where $(O_2)_{ss,n}$ is the matrix element $\langle \Phi_{ss} | O_2 | \Psi_n \rangle$, and similar definitions exist for $(O_1)_{ss,n}$ and its $|\Phi_{ct}\rangle$ counterparts.

Closely related to geometric entanglement is the quantum Fisher information (QFI) F_Q [243, 286], which quantifies how sensitive a state ρ is to unitary transformations generated by an observable \hat{O} . For a pure state $\rho = |\psi\rangle\langle\psi|$, $F_Q(\psi, \hat{O})$ is defined in terms of the variance of the operator \hat{O} (i.e., the connected correlation function):

$$F_Q(\psi, \hat{O}) = 4\Delta(\hat{O})^2 = 4 \left(\langle\psi|\hat{O}^2|\psi\rangle - \langle\psi|\hat{O}|\psi\rangle^2 \right), \quad (4.85)$$

and it provides an upper bound on the precision that can be achieved in measuring the parameter θ that is dual to the observable \hat{O} : $\mathcal{N}(\Delta\theta)^2 \geq F_Q^{-1}$, \mathcal{N} being the number of independent measurements [243, 286]. $F_Q(\psi, \hat{O})$ is thus a measure of the entanglement arising from quantum fluctuation content in $|\psi\rangle$ (considered with respect to an eigenstate of \hat{O}). This can be made more manifest by considering a traceless operator \hat{M} with eigenstates $\{|m\rangle\}$. Without loss of generality, we can rescale the operator such that $\sum m^2 = 1/2$. There are several examples of such operators in the context of the present work, such as the impurity magnetisation operator (S_d^z), the Kondo spin-flip operator ($S_d^+ S_0^- + \text{h.c.}$) and the Kondo isospin-flip operator ($C_d^+ C_0^- + \text{h.c.}$). If $\varepsilon_m(\psi) \equiv 1 - |\langle m|\psi\rangle|^2$ is the geometric entanglement between a given state $|\psi\rangle$ and the eigenstates of \hat{M} , the QFI corresponding to \hat{M} in the state ψ can be written as

$$F_Q(\psi, \hat{M}) = 4 \left[\frac{1}{2} - \sum_m m^2 \varepsilon_m - \left(\sum_m m \varepsilon_m \right)^2 \right]. \quad (4.86)$$

The total geometric entanglement $\sum_m \varepsilon_m$ is constrained to be $d_M - 1$, where d_M is the dimension of the operator \hat{M} . Because each eigenvalue m has a magnitude of at most $1/\sqrt{2}$ (all m^2 must add up to $1/2$), the maximum magnitude of the last two terms in eq. (4.86) (and hence the minimum value of the QFI) is attained for the case when some of the ε_m are zero. However, because the eigenstates are orthogonal, only one of them can have perfect overlap with the state $|\psi\rangle$ and only one ε_m can be zero at a time. The case of minimum QFI therefore corresponds to $\varepsilon_{m^*} = 0, \varepsilon_{m \neq m^*} = 1$, leading to $F_Q = 0$. The opposite situation arises when all the geometric entanglement measures are non-zero and equal, $\varepsilon_m = 1/d_M$, leading to a maximum QFI value of $F_Q = 2/d_M$. A uniformly spread geometric entanglement distribution, therefore, leads to a larger QFI, while a more focused distribution leads to a smaller QFI. This sums up the relation between the quantum Fisher information and geometric entanglement.

If the operator \hat{M} is such that its eigenstates are separable states from the perspective of a certain party, the vanishing QFI arises when $|\psi\rangle$ has zero geometric entanglement with respect to one of the separable states, and the QFI saturates when $|\psi\rangle$ has a finite geometric entanglement with all of the states. A large QFI can thus be associated with more entanglement. Moreover, if the eigenstates of \hat{M} are symmetry-broken states, a vanishing QFI indicates that $|\psi\rangle$ is very close to such a symmetry-broken state, while a large QFI indicates that $|\psi\rangle$ is a uniform superposition of such symmetry-broken states and therefore preserves the symmetry as a whole. A larger QFI points towards the presence of more quantum fluctuations and the lack of susceptibility towards symmetry-breaking.

In order to demonstrate these ideas in the present problem, we computed the QFI in the ground-state of the e-SIAM for a number of Hermitian operators, as a function of the parameter $r = -U_b/J_0$. These are shown in the left panel of Fig. (4.13) (left panel). In order to explain the behaviour depicted in the figure, we point out again that the ground-states for $r \ll r_{c2}, r \lesssim r_{c2}$ and $r > r_{c2}$ are $|\text{SS}\rangle + |\text{CT}\rangle$, $|\text{SS}\rangle$ and

$|LM\rangle$ respectively, where $|SS\rangle$, $|CT\rangle$ and $|LM\rangle$ are the spin-singlet state, charge triplet and local moment states respectively. We focus on the spin-flip QFI, corresponding to the operator $\hat{O} = S_d^+ S_0^- + \text{h.c.}$

- For $r < r_{c1}$, the ground-state involves both $|SS\rangle$ and $|CT\rangle$, meaning that neither of the two entanglement measures ε_{ss} or ε_{ct} will be zero. As mentioned in the preceding paragraph, this leads to the maximal QFI, as can be seen in the figure as well.
- At $r = r_{c1}$, the charge triplet content vanishes and the ground-state is purely a singlet beyond that point. As a result, in the range $r_{c1} < r < r_{c2}$, the geometric entanglement corresponding to the singlet state is zero, leading to a minimal and vanishing QFI. This is again shown in the figure.
- Finally, for $r > r_{c2}$, the local moment states become the ground-states, where the bath zeroth site displays all four configurations as a superposition, because of the hopping into the rest of the bath. This state is again not an eigenstate of the spin-flip operator, and the geometric entanglement will be uniformly distributed across the states, none being zero. This explains the large QFI in the local moment phase.

Similar explanations hold for the single-particle hopping FQI between the impurity and the zeroth site, and the charge isospin FQI between the zeroth site and the first site. In Fig. (4.13) (right panel), we show the QFI for the same three operators very close to the MIT (i.e., for $r \lesssim r_{c2}$). Two important quantities that track the local MIT and act as order parameters for the transition are the degree of compensation for the impurity ($\langle \vec{S}_d \cdot \vec{S}_0 \rangle$) and the impurity magnetisation ($\langle S_d^z \rangle$), and the first two QFI (red and blue curves) in Fig. 4.13 are therefore particularly important because they quantify the quantum fluctuations present in the system corresponding to these order parameters. Our analysis shows that the two phases on either side of the transition are characterised by distinct values of this pair of QFI: while the QFI corresponding to the degree of compensation zero in the Kondo screened phase, it becomes non-zero in the local moment phase, and the opposite is true for the QFI arising from the impurity magnetisation. The phase precisely at the transition is distinct from those on either side because it displays a non-zero value for both the QFI. While it is expected that a critical point would show enhanced fluctuations of multiple kinds (giving rise to universality), it is enlightening to find that this is also reflected in a measure of many-particle entanglement.

All three QFIs are observed to saturate to finite, non-zero values at the MIT, indicating that the non-Fermi liquid state therein possesses quantum fluctuations of all three varieties.

We will now relate the QFI to some other measures of correlation. The QFI corresponding to an observable can be directly related to the static lesser Greens functions associated with that observable:

$$F_Q(\psi, \hat{O}_2) = 4 \left(\langle \hat{O}_2 \hat{O}_1^\dagger \rangle \Big|_{\hat{O}_1^\dagger = \hat{O}_2} - \langle \hat{O}_2 \hat{O}_1^\dagger \rangle^2 \Big|_{\hat{O}_1 = 1} \right) = 4 \left[G_{O_2, O_2}^<(t \rightarrow \infty) - (G_{1, O_2}^<(t \rightarrow \infty))^2 \right] \quad (4.87)$$

In the context of the present work, eq. (4.82) allows relating the QFI to the geometric entanglement measured with respect to the spin-singlet and charge triplet states. By combining eqs. (4.82) and (4.87), we get

$$\begin{aligned} F_Q(\psi, \hat{O}_2) &= 4 \left[(1 - \varepsilon_{ss}) \langle \Phi_{ss} | \hat{O}_2^2 | \Phi_{ss} \rangle + (1 - \varepsilon_{ct}) \langle \Phi_{ct} | \hat{O}_2^2 | \Phi_{ct} \rangle \right. \\ &\quad + \sqrt{1 - \varepsilon_{ss}} \sqrt{1 - \varepsilon_{ct}} \left(\langle \Phi_{ss} | \hat{O}_2^2 | \Phi_{ct} \rangle + \langle \Phi_{ct} | \hat{O}_2^2 | \Phi_{ss} \rangle \right) - \left\{ (1 - \varepsilon_{ss}) \langle \Phi_{ss} | \hat{O}_2 | \Phi_{ss} \rangle \right. \\ &\quad \left. \left. + (1 - \varepsilon_{ct}) \langle \Phi_{ct} | \hat{O}_2 | \Phi_{ct} \rangle + \sqrt{1 - \varepsilon_{ss}} \sqrt{1 - \varepsilon_{ct}} \left(\langle \Phi_{ss} | \hat{O}_2 | \Phi_{ct} \rangle + \langle \Phi_{ct} | \hat{O}_2 | \Phi_{ss} \rangle \right) \right\}^2 \right]. \end{aligned} \quad (4.88)$$

Further, the retarded Greens function defined above in eq. (4.83) can very generally be related to the QFI. By using the simplified forms $\frac{i}{2}G_{O_2,O_2}^R(t \rightarrow \infty) = \langle(O_2)^2\rangle$ and $\frac{i}{2}G_{1,O_2}^R(t \rightarrow \infty) = \langle O_2 \rangle$, we get

$$F_Q(\psi, \hat{O}_2) = 2iG_{O_2,O_2}^R(t \rightarrow \infty) + (G_{1,O_2}^R(t \rightarrow \infty))^2. \quad (4.89)$$

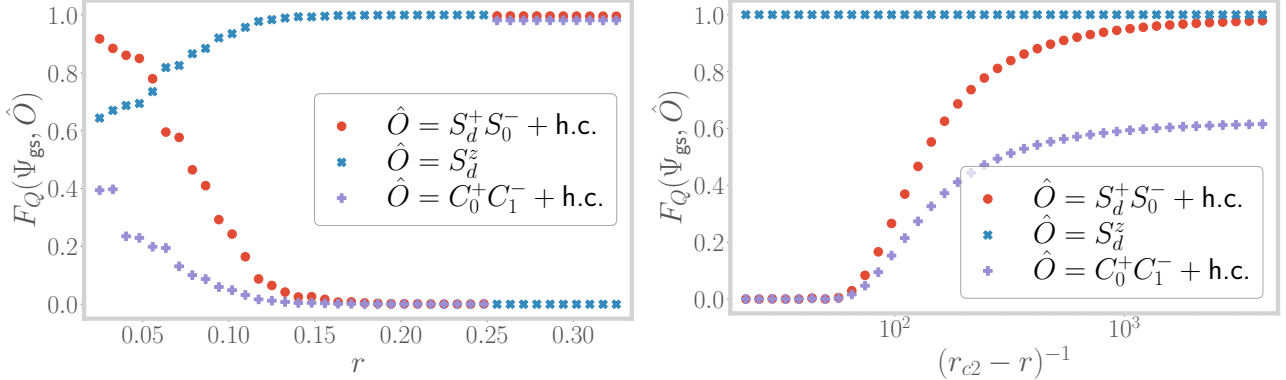


Figure 4.13: *Left:* Variation of the quantum Fisher information for three separate fluctuations, across the entire range of r . *Right:* The QFI corresponding to the same three operators, but very close to the QCP at r_{c2} .

For the sake of completeness, we generalise the above relations to finite temperatures by adopting the approach of Hauke et al. [243]. For a mixed state at inverse temperature β characterised by the density matrix $\rho = \sum_n f_n |n\rangle\langle n|$ where $(E_n, |n\rangle)$ are the eigenvalue-eigenstate pairs and $f_n = e^{-\beta E_n} / \sum_n e^{-\beta E_n}$ are the Boltzmann weights, the FQI can be assigned a spectral representation of the form [243]

$$F_Q(\rho, \hat{O}) = 2 \sum_{m,n} \frac{(f_m - f_n)^2}{f_m + f_n} |\langle m|\hat{O}|n\rangle|^2. \quad (4.90)$$

By using the identity $\frac{f_m - f_n}{f_m + f_n} = \int_{-\infty}^{\infty} d\omega \delta(\omega + E_m - E_n) \tanh(\beta\omega/2)$, the finite temperature FQI can be written in the form

$$F_Q(\rho, \hat{O}) = 2 \int_{-\infty}^{\infty} d\omega \tanh(\beta\omega/2) \sum_{m,n} (f_m - f_n) \delta(\omega + E_m - E_n) |\langle m|\hat{O}|n\rangle|^2. \quad (4.91)$$

In order to relate this with a correlation function, we now point out that the lesser Greens function $G^<$ defined in eq. (4.80), as well as the greater Greens function $G^>$ that we will now define, also admit spectral representations in terms of the eigenstates $|n\rangle$ of the full problem:

$$G_{O^\dagger, O}^<(t) \equiv i \langle \hat{O}^\dagger \hat{O}(t) \rangle \implies G_{O^\dagger, O}^<(\omega) = 2\pi i \sum_{m,n} f_n \delta(\omega + E_m - E_n) |\langle m|\hat{O}^\dagger|n\rangle|^2, \quad (4.92)$$

$$G_{O^\dagger, O}^>(t) \equiv -i \langle \hat{O}(t) \hat{O}^\dagger \rangle \implies G_{O^\dagger, O}^>(\omega) = -2\pi i \sum_{m,n} f_m \delta(\omega + E_m - E_n) |\langle m|\hat{O}|n\rangle|^2. \quad (4.93)$$

If \hat{O} is a Hermitian operator, eqs. (4.92) can be used to rewrite the QFI in terms of $G_{O^\dagger, O}^<(\omega)$. Indeed, by combining eqs. (4.92) and eq. (4.91) with the assumption $\hat{O} = \hat{O}^\dagger$, we get

$$F_Q(\rho, \hat{O}) = -\frac{1}{\pi i} \int_{-\infty}^{\infty} d\omega \tanh(\beta\omega/2) (G_{O, O}^>(\omega) + G_{O, O}^<(\omega)). \quad (4.94)$$

This constitutes the general relation between the finite temperature QFI for a general Hermitian many-particle operator \hat{O} and the corresponding many-particle correlations at zero and finite frequencies.

The Kubo linear response function associated with the operator $\hat{O}(t)$ due to a perturbation from the same operator is associated with a correlation function/susceptibility $\mathcal{C}_{\hat{O}}(t, t') = i\theta(t-t') \langle [\hat{O}(t), \hat{O}(t')] \rangle$. By going to the frequency domain, the imaginary part of such a function can be related to the sum of the lesser and greater Greens functions:

$$\begin{aligned} \mathcal{C}_{\hat{O}}(\omega) &= i \int_0^\infty d(t-t') e^{i\omega(t-t')} (\langle \hat{O}(t)\hat{O}(t') \rangle - \langle \hat{O}(t')\hat{O}(t) \rangle) \\ \implies \mathcal{C}_{\hat{O}}(\omega) - \mathcal{C}_{\hat{O}}(\omega)^* &= i \int_0^\infty d(t-t') (e^{i\omega(t-t')} - e^{-i\omega(t-t')}) (\langle \hat{O}(t)\hat{O}(t') \rangle - \langle \hat{O}(t')\hat{O}(t) \rangle) \\ &= i \int_{-\infty}^\infty d(t-t') e^{i\omega(t-t')} (\langle \hat{O}(t)\hat{O}(t') \rangle - \langle \hat{O}(t')\hat{O}(t) \rangle) \\ &= -(G_{O,O}^>(\omega) + G_{O,O}^<(\omega)) \end{aligned} \quad (4.95)$$

This allows us to connect the QFI with the imaginary part of the Kubo correlation function/susceptibility obtained in Ref. [243]:

$$F_Q(\rho, \hat{O}) = \frac{1}{\pi i} \int_{-\infty}^\infty d\omega \tanh(\beta\omega/2) (\mathcal{C}_{\hat{O}}(\omega) - \mathcal{C}_{\hat{O}}(\omega)^*) . \quad (4.96)$$

4.11 Appendix: One-shot decoupling of impurity from zeroth site

We will decouple the impurity states from the fixed point Hamiltonian using a single URG transformation. This will, of course, generate correlations on the zeroth site. The resulting Hamiltonian will be an AIM with the hopping between the zeroth site and the rest of the chain acting as the effective hybridisation. Schematically, we will have

$$\begin{aligned} H^* = H_{\text{imp}} + V_{\text{imp-0}} + H_0 + H_{0-1} + H_{\text{rest}} &\xrightarrow{\text{decouple imp.}} E_{\text{imp}} + \tilde{H}_0 + H_{0-1} + H_{\text{rest}} \\ &= H_{\text{new imp}} + V_{\text{new imp - rest}} + H_{\text{rest}} . \end{aligned} \quad (4.97)$$

Since the impurity is not coupled with any site beyond the zeroth site, the parts of the Hamiltonian that involve "rest" will not change in the process. This also means that the decoupling can be performed by looking at the smaller Hamiltonian

$$\begin{aligned} H_{\text{imp+0}} = H_{\text{imp}} + H_0 + V_{\text{imp-0}} &= -\frac{U^*}{2} (\hat{n}_{d\uparrow} - \hat{n}_{d\downarrow})^2 - U_b (\hat{n}_{0\uparrow} - \hat{n}_{0\downarrow})^2 + J^* S_d^z S_0^z \\ &\quad + V^* \sum_\sigma \left(c_{d\sigma}^\dagger c_{0\sigma} + \text{h.c.} \right) + \frac{J^*}{2} \left(c_{d\uparrow}^\dagger c_{d\downarrow} c_{0\downarrow}^\dagger c_{0\uparrow} + \text{h.c.} \right) . \end{aligned} \quad (4.98)$$

4.11.1 Renormalisation from V^*

From the off-diagonal term involving V^* , we generate the following term, in the particle sector for 0:

$$\sum_\sigma c_{0\sigma}^\dagger c_{d\sigma} \frac{V^{*2}}{\tilde{\omega} - H_d} c_{d\sigma}^\dagger c_{0\sigma} = \sum_\sigma c_{0\sigma}^\dagger c_{d\sigma} \frac{V^{*2}}{\tilde{\omega} + \frac{U^*}{2} (1 - \hat{n}_{d\bar{\sigma}})^2 + U_b \hat{n}_{0\bar{\sigma}} + \frac{J^*}{4} (1 - \hat{n}_{d\bar{\sigma}}) \hat{n}_{0\bar{\sigma}}} c_{d\sigma}^\dagger c_{0\sigma} . \quad (4.99)$$

where $\tilde{\omega}$ is the quantum fluctuation operator for the impurity site and $H_d = -\frac{U^*}{2} (\hat{n}_{d\uparrow} - \hat{n}_{d\downarrow})^2 - U_b (\hat{n}_{0\uparrow} - \hat{n}_{0\downarrow})^2 + J^* S_d^z S_0^z$, is the diagonal part of the Hamiltonian for the imp+0 system. In order

to resolve the operators in the denominator, we expand the unity in the numerator using the identity $1 = \hat{n}_{d\bar{\sigma}}\hat{n}_{0\bar{\sigma}} + \hat{n}_{d\bar{\sigma}}\hat{h}_{0\bar{\sigma}} + \hat{h}_{d\bar{\sigma}}\hat{n}_{0\bar{\sigma}} + \hat{h}_{d\bar{\sigma}}\hat{h}_{0\bar{\sigma}}$, where $\hat{h} = 1 - \hat{n}$ is hole operator. On Substituting this, we get

$$\begin{aligned} \sum_{\sigma} c_{0\sigma}^{\dagger} c_{d\sigma} \frac{V^{*2}}{\tilde{\omega} - H_d} c_{d\sigma}^{\dagger} c_{0\sigma} &= V^{*2} \sum_{\sigma} c_{0\sigma}^{\dagger} c_{d\sigma} \frac{\hat{h}_{d\bar{\sigma}}\hat{h}_{0\bar{\sigma}} + \hat{h}_{d\bar{\sigma}}\hat{n}_{0\bar{\sigma}} + \hat{n}_{d\bar{\sigma}}\hat{h}_{0\bar{\sigma}} + \hat{n}_{d\bar{\sigma}}\hat{n}_{0\bar{\sigma}}}{\tilde{\omega} + \frac{U^*}{2}\hat{h}_{d\bar{\sigma}} + U_b\hat{n}_{0\bar{\sigma}} + \frac{J^*}{4}\hat{h}_{d\bar{\sigma}}\hat{n}_{0\bar{\sigma}}} c_{d\sigma}^{\dagger} c_{0\sigma} \\ &= V^{*2} \sum_{\sigma} \hat{h}_{d\sigma} \hat{n}_{0\sigma} \left[\frac{\hat{h}_{d\bar{\sigma}}\hat{h}_{0\bar{\sigma}}}{\tilde{\omega}_{00} + \frac{U^*}{2}} + \frac{\hat{h}_{d\bar{\sigma}}\hat{n}_{0\bar{\sigma}}}{\tilde{\omega}_{01} + \frac{U^*}{2} + U_b + \frac{J^*}{4}} + \frac{\hat{n}_{d\bar{\sigma}}\hat{h}_{0\bar{\sigma}}}{\tilde{\omega}_{10}} + \frac{\hat{n}_{d\bar{\sigma}}\hat{n}_{0\bar{\sigma}}}{\tilde{\omega}_{11} + U_b} \right]. \end{aligned} \quad (4.100)$$

$\tilde{\omega}_{(0,1),(0,1)}$ represents the quantum fluctuation scale corresponding to the configuration in the numerator.

In order to "freeze" the impurity dynamics, we will substitute $\hat{n}_{d\sigma} = \hat{n}_{d\bar{\sigma}} = \frac{1}{2}$, because of the Z_2 symmetry and the particle-hole symmetry of the impurity levels. This gives

$$\frac{1}{4} V^{*2} \sum_{\sigma} \hat{n}_{0\sigma} \left[\frac{\hat{h}_{0\bar{\sigma}}}{\tilde{\omega}_{00} + \frac{U^*}{2}} + \frac{\hat{n}_{0\bar{\sigma}}}{\tilde{\omega}_{01} + \frac{U^*}{2} + U_b + \frac{J^*}{4}} + \frac{\hat{h}_{0\bar{\sigma}}}{\tilde{\omega}_{10}} + \frac{\hat{n}_{0\bar{\sigma}}}{\tilde{\omega}_{11} + U_b} \right]. \quad (4.101)$$

The state that most closely represents the metallic ground state is $\tilde{\omega}_{10}$, we take that as the reference quantum fluctuation scale $\bar{\omega}$. It is of the order of $\bar{\omega} \sim -\frac{J^*}{4} - \frac{U^*}{2} - U_b$. We will now relate the other scales to $\bar{\omega}$ by expressing them in terms of the energy of the initial state:

$$\tilde{\omega}_{00} \sim -U_b = \bar{\omega} + \frac{J^*}{4} + \frac{U^*}{2}, \quad \tilde{\omega}_{01} \sim 0 = \bar{\omega} + \frac{J^*}{4} + \frac{U^*}{2} + U_b, \quad \tilde{\omega}_{11} \sim -\frac{U^*}{2} = \bar{\omega} + \frac{J^*}{4} + U_b. \quad (4.102)$$

Substituting these gives

$$\frac{1}{4} V^{*2} \sum_{\sigma} \hat{n}_{0\sigma} \left[\hat{h}_{0\bar{\sigma}} \alpha_1 + \hat{n}_{0\bar{\sigma}} \alpha_2 \right], \quad (4.103)$$

where $\alpha_1 = (\bar{\omega} + U^* + \frac{J^*}{4})^{-1} + (\bar{\omega})^{-1}$ and $\alpha_2 = (\bar{\omega} + U^* + 2U_b + \frac{J^*}{2})^{-1} + (\bar{\omega} + 2U_b + \frac{J^*}{4})^{-1}$.

Because of the particle-hole symmetry on the impurity as well as in the bath, the renormalisation from the hole sector is obtained simply by transforming $\hat{n} \leftrightarrow \hat{h}$:

$$\frac{1}{4} V^{*2} \sum_{\sigma} \hat{h}_{0\sigma} \left[\hat{n}_{0\bar{\sigma}} \alpha_1 + \hat{h}_{0\bar{\sigma}} \alpha_2 \right]. \quad (4.104)$$

The total renormalisation arising from V is therefore

$$\frac{1}{4} V^{*2} \sum_{\sigma} \left[\alpha_1 \left(\hat{n}_{0\sigma} \hat{h}_{0\bar{\sigma}} + \hat{h}_{0\sigma} \hat{n}_{0\bar{\sigma}} \right) + \alpha_2 \left(\hat{n}_{0\sigma} \hat{n}_{0\bar{\sigma}} + \hat{h}_{0\sigma} \hat{h}_{0\bar{\sigma}} \right) \right] = \frac{1}{2} V^{*2} (\alpha_1 - \alpha_2) (\hat{n}_{0\uparrow} - \hat{n}_{0\downarrow})^2 + \text{constant}. \quad (4.105)$$

4.11.2 Renormalisation from J^*

The renormalisation arising from decoupling the Kondo coupling has two terms. The first term arises when the spin of the zeroth site is initially up:

$$\begin{aligned} \frac{J^{*2}}{4} c_{d\downarrow}^{\dagger} c_{d\uparrow} c_{0\uparrow}^{\dagger} c_{0\downarrow} \frac{1}{\tilde{\omega} - H_d} c_{0\downarrow}^{\dagger} c_{0\uparrow} c_{d\uparrow}^{\dagger} c_{d\downarrow} &= c_{d\downarrow}^{\dagger} c_{d\uparrow} c_{0\uparrow}^{\dagger} c_{0\downarrow} \frac{J^{*2}/4}{\tilde{\omega} + \frac{U^*}{2} + U_b + \frac{J^*}{4}} c_{0\downarrow}^{\dagger} c_{0\uparrow} c_{d\uparrow}^{\dagger} c_{d\downarrow} \\ &= \frac{J^{*2}}{4} \frac{\hat{n}_{d\downarrow} \hat{h}_{d\uparrow} \hat{n}_{0\uparrow} \hat{h}_{0\downarrow}}{\tilde{\omega} + \frac{U^*}{2} + U_b + \frac{J^*}{4}}. \end{aligned} \quad (4.106)$$

The quantum fluctuation scale $\tilde{\omega}$ for this process can be similarly related to $\bar{\omega}$: $\tilde{\omega} \sim -\frac{U^*}{2} - U_b - \frac{J^*}{4} = \bar{\omega}$. This gives

$$\frac{J^{*2}}{4} \frac{\hat{n}_{d\downarrow} \hat{h}_{d\uparrow} \hat{n}_{0\uparrow} \hat{h}_{0\downarrow}}{\bar{\omega} + \frac{U^*}{2} + U_b + \frac{3J^*}{4}} = \frac{J^{*2}}{16} \frac{\hat{n}_{0\uparrow} \hat{h}_{0\downarrow}}{\bar{\omega} + \frac{U^*}{2} + U_b + \frac{J^*}{4}}, \quad (4.107)$$

as the renormalisation for this configuration. At the final step, we substituted $\hat{n}_{d\sigma} = \hat{h}_{d\sigma} = \frac{1}{2}$. For the other configuration where the spin of the zeroth site is down, we get

$$\frac{J^{*2}}{16} \frac{\hat{n}_{0\downarrow} \hat{h}_{0\uparrow}}{\bar{\omega} + \frac{U^*}{2} + U_b + \frac{J^*}{4}}. \quad (4.108)$$

Adding both sectors, we get

$$\frac{J^{*2}}{16} \frac{1}{\bar{\omega} + \frac{U^*}{2} + U_b + \frac{J^*}{4}} (\hat{n}_{0\uparrow} - \hat{n}_{0\downarrow})^2. \quad (4.109)$$

4.11.3 Total renormalisation

Adding the contributions from both V^* and J^* , the net renormalisation is the generation of a local correlation term $-U' (\hat{n}_{0\uparrow} - \hat{n}_{0\downarrow})^2$ on the zeroth site, where U' is given by

$$U' = \frac{-J^{*2}/16}{\bar{\omega} + \frac{U^*}{2} + U_b + \frac{J^*}{4}} - \frac{1}{2} V^{*2} \left(\frac{1}{\bar{\omega} + U^* + \frac{J^*}{4}} + \frac{1}{\bar{\omega}} - \frac{1}{\bar{\omega} + U^* + 2U_b + \frac{J^*}{2}} - \frac{1}{\bar{\omega} + 2U_b + \frac{J^*}{4}} \right) \quad (4.110)$$

The effective Hamiltonian for the zeroth site is therefore

$$H_{0+\text{rest}} = \underbrace{-(U' + U_b)(\hat{n}_{0\uparrow} - \hat{n}_{0\downarrow})^2}_{\text{new correlated impurity}} - t \underbrace{\sum_{j \in \text{n.n. of } 0, \sigma} (c_{0\sigma}^\dagger c_{j\sigma} + \text{h.c.})}_{\text{hopping between new impurity \& new bath}} - t \underbrace{\sum_{\langle i,j \rangle} (c_{i\sigma}^\dagger c_{j\sigma} + \text{h.c.})}_{\text{K.E. of new bath}}. \quad (4.111)$$

4.12 Appendix: Effective Hamiltonian for the excitations within the Hubbard sidebands

Beyond r_{c1} , the Hubbard sidebands can be seen to separate from the central Kondo resonance in the impurity spectral function. These sidebands are broad, indicating that the impurity site is hybridising with the bath from within the sidebands, at high energies $\omega \sim U/2$. These processes lead to the presence of gapless excitations within the rest of the bath, outside the Mott gap. To find the effective Hamiltonian for the rest of the bath (sites 1 and onwards), we will take the eigenstates of the two-site Hamiltonian H that reside within the sideband as our ground-states, and treat the hopping from the zeroth site to the rest of the bath as a perturbation. The two-site Hamiltonian is

$$H_{\text{two site}} = V \sum_{\sigma} (c_{d\sigma}^\dagger c_{0\sigma} + \text{h.c.}) + J \vec{S}_d \cdot \vec{S}_0 - \frac{U}{2} (\hat{n}_{d\uparrow} - \hat{n}_{d\downarrow})^2 + \frac{U}{2}. \quad (4.112)$$

In order to align the doubly-occupied impurity level at the more conventional value of $U/2$, we have shifted the Hamiltonian by the same constant value. The effect of U_b has been ignored because it is small compared to U at the frequencies pertinent to the physics of the sidebands. The two-site states that reside within the Hubbard sidebands are

$$\begin{aligned} |\Psi_{cc}\rangle &\equiv |c\rangle_d |c\rangle_0; \quad c \in \{0, 2\}; \quad |\Psi_{cs}\rangle \equiv \frac{1}{\sqrt{2}} (|2\rangle_d |0\rangle_0 - |0\rangle_d |2\rangle_0); \\ |\Psi_{\sigma,c}\rangle &= \alpha |\sigma\rangle_d |c\rangle_0 + \sqrt{1-\alpha^2} |c\rangle_d |\sigma\rangle_0; \quad \sigma \in \{\uparrow, \downarrow\}; \\ |\Psi_{ct}\rangle &= \beta \frac{1}{\sqrt{2}} (|\uparrow\rangle_d |\downarrow\rangle_0 - |\downarrow\rangle_d |\uparrow\rangle_0) + \sqrt{1-\beta^2} \frac{1}{\sqrt{2}} (|2\rangle_d |0\rangle_0 + |0\rangle_d |2\rangle_0), \end{aligned} \quad (4.113)$$

where the coefficients of the eigenstates are given by

$$\alpha \simeq \frac{V}{\sqrt{V^2 + (E_{X1} + \frac{U}{2})^2}}, \quad \beta = \frac{2V}{\sqrt{4V^2 + (E_{CS} + \frac{U}{2} + \frac{3J}{4})^2}}. \quad (4.114)$$

The energies of the states are

$$\begin{aligned} E_{gs} \equiv E_{00} = E_{22} = E_{CS} &= \frac{U}{2}, \quad E_{X1} \equiv E_{\sigma,c} = \frac{U}{4} + \sqrt{V^2 + \frac{U^2}{16}}, \\ E_{X2} \equiv E_{CS} &= \frac{U}{4} - \frac{3J}{8} + \sqrt{4V^2 + \left(\frac{U}{4} + \frac{3J}{8}\right)^2}. \end{aligned} \quad (4.115)$$

The ground state (comprising the states shown in eq. (4.113)) is triply degenerate. In order to study the dynamics of the bath, we now introduce the perturbation $H_I = -t \sum_{\sigma} (c_{0\sigma}^\dagger c_{1\sigma} + \text{h.c.})$. We also take an expanded set of eigenstates $\{|\Psi_n\rangle \otimes |a\rangle\}$, where $\{|\Psi_n\rangle\}$ is the set of eigenstates of $H_{\text{two site}}$, and $|a\rangle \in \{|0\rangle, |\uparrow\rangle, |\downarrow\rangle, |2\rangle\}$ represents the configuration of the first site. The eigenstates of $H_{\text{two site}}$ are also eigenstates the total number operator $\hat{n}_d + \hat{n}_0 + \hat{n}_1$, and since H_I does not conserve the total number, all odd order shifts are zero: $\langle \Psi_n | H_I^b | \Psi_n \rangle, b = 1, 3, \dots$, is zero for all the eigenstates.

For the second order shift, we need to calculate the overlaps $\langle \Psi_m | H_I | \Psi_n \rangle, m \neq n$ for n in the ground state. Since all three ground-states involve the impurity and zeroth sites in charge configuration (0 or 2), $H_I |\Psi\rangle_n$ will result in states of the form $|0(2)\rangle_d |\sigma\rangle_0 |a\rangle_1$. This resulting state has non-zero overlap only with the part $\sqrt{1-\alpha^2} |c\rangle_d |\sigma\rangle_0 |a\rangle$ of the expanded state $|\Psi_{\sigma,c}\rangle |a\rangle$. The square of each such overlap is, therefore, $t^2 (1 - \alpha^2)$.

- Excitations from the ground-states $|\Psi_{00}\rangle |0\rangle$ and $|\Psi_{22}\rangle |2\rangle$ have zero overlap with any other state, such that the second order shifts in these states is zero.
- Excitations from the ground-states $|\Psi_{00}\rangle |\sigma\rangle$ and $|\Psi_{22}\rangle |\sigma\rangle$ have non zero overlap with one excited state each, such that the second order shift in these states are $\gamma^2 \equiv t^2 (1 - \alpha^2) / (E_{X1} - E_{gs})$.
- Excitations from the remaining ground states have non-zero overlaps with two excited states each, such that the second order shift in these states are $2\gamma^2$.

Upon dropping the zeroth order part (because it has no dynamics for the rest of the bath), the effective Hamiltonian at second order in t takes the form

$$\begin{aligned} H_{\text{eff}}^{(2)} &= \gamma^2 [(|\Psi_{00}\rangle \langle \Psi_{00}| + |\Psi_{22}\rangle \langle \Psi_{22}| + 2 |\Psi_{CS}\rangle \langle \Psi_{CS}|) (\sum_{\sigma} |\sigma\rangle_1 \langle \sigma|_1) \\ &\quad + 2 (|\Psi_{22}\rangle \langle \Psi_{22}| + |\Psi_{CS}\rangle \langle \Psi_{CS}|) |0\rangle_1 \langle 0|_1 + 2 (|\Psi_{00}\rangle \langle \Psi_{00}| + |\Psi_{CS}\rangle \langle \Psi_{CS}|) |2\rangle_1 \langle 2|_1] \end{aligned} \quad (4.116)$$

By using the completeness relation $1 = \sum_{\sigma} |\sigma\rangle_1 \langle \sigma|_1 + |0\rangle_1 \langle 0|_1 + |2\rangle_1 \langle 2|_1$ of the Hilbert space of the first site, this evaluates to

$$H_{\text{eff}}^{(2)} = \text{constant} + \gamma^2 (|\Psi_{22}\rangle \langle \Psi_{22}| - |\Psi_{00}\rangle \langle \Psi_{00}|) (|2\rangle_1 \langle 2|_1 - |0\rangle_1 \langle 0|_1) , \quad (4.117)$$

where the "constant" term refers to operators that do not depend on the dynamics of the rest of the bath. By defining the charge isospin operator $C^z |2(0)\rangle = +(-)^{\frac{1}{2}} |2(0)\rangle$, the effective Hamiltonian can be written as (dropping the non-dynamical part)

$$H_{\text{eff}}^{(2)} = 4\gamma^2 C_{\text{tot}}^z C_1^z , \quad (4.118)$$

where C_i^z is the charge isospin for site i and $C_{\text{tot}}^z \equiv C_d^z + C_0^z$ is the z-component of the total charge isospin for the impurity and the zeroth sites.

The fourth order shift in the energy of the eigenstate $|\Psi_n\rangle$ will be given by

$$E_n^{(4)} = \sum_{j,k,l} \frac{(H_I)_{nl} (H_I)_{lk} (H_I)_{kj} (H_I)_{jn}}{(E_l - E_n)(E_k - E_n)(E_j - E_n)} - E_n^{(2)} \left[\frac{(H_I)_{kn}}{E_k - E_n} \right]^2 , \quad (4.119)$$

where the matrix elements $(H_I)_{in}$ are defined as $\langle i|H_I|n\rangle$. This fourth-order shift vanishes for almost all the ground-states. For the remaining states, it becomes important to treat their degeneracy. The "appropriate" combinations of states that provide non-zero fourth order contribution are

$$|+\rangle = \sqrt{\frac{2}{3}} |\Psi_{22}\rangle |0\rangle_1 + \sqrt{\frac{1}{3}} |\Psi_{\text{CS}}\rangle |2\rangle_1 , \quad |-\rangle = -\sqrt{\frac{2}{3}} |\Psi_{00}\rangle |2\rangle_1 + \sqrt{\frac{1}{3}} |\Psi_{\text{CS}}\rangle |0\rangle_1 . \quad (4.120)$$

Corresponding to these ground states, the fourth-order shift in the eigenvalue is

$$E^{(4)} = \frac{3\gamma^4 \alpha^2 \beta^2}{(1-\alpha^2)(E_{\text{X2}} - E_{\text{gs}})} , \quad (4.121)$$

such that the fourth-order contribution to the effective Hamiltonian is

$$\begin{aligned} H_{\text{eff}}^{(4)} &= E^{(4)} (|+\rangle \langle +| + |-\rangle \langle -|) \\ &= \frac{\gamma^4 \alpha^2 \beta^2}{(1-\alpha^2)(E_{\text{X2}} - E_{\text{gs}})} [-C_{\text{tot}}^z C_{\text{tot}}^2 C_1^z + \sqrt{2} \mathcal{P}_{\text{tot}}^4 (C_0^+ - C_d^+) C_1^- + \text{h.c.}] . \end{aligned} \quad (4.122)$$

The operator $\mathcal{P}_{\text{tot}}^4$ acts on states belonging to the combined $d+0$ Hilbert space and projects on to the $\hat{n}_d + \hat{n}_0 = 4$ subspace.

4.13 Appendix: Behaviour of the Kondo scale T_K close to the transition

Towards obtaining the emergent Kondo temperature scale T_K close to the transition, we follow the approach used by Moeller et al. 1995 [244] and Held et al. 2013 [245]. Near the transition, they obtained a Kondo model from the full AIM by applying a Schrieffer-Wolff transition that removes the charge fluctuations of the impurity site and retains the physics of only the s-d coupling J . This amounts to removing the side peaks from the impurity spectral function and focusing on the low-energy central

peak. Held et al. then integrated the RG equation for this Kondo model by using a Lorentzian DOS in the bath. This is motivated by the fact that the central peak of the impurity spectral function is a Lorentzian, and the bath becomes equivalent to the impurity site under self-consistency. We implement the same approach but on our extended impurity model, such that the transformation then leads to a $J - U_b$ model. The relevant RG equations are mentioned in Section IV of the main manuscript:

$$\Delta J = -\frac{n_j J (J + 4U_b)}{\omega - D/2 + U_b/2 + J/4}, \quad \Delta U_b = 0, \quad (4.123)$$

where $n_j = \rho(D)|\Delta D|$ is proportional to the bath density of states. In Section VII of the main manuscript, we show that the spectral function of the zeroth site is tracked by that on the impurity site through the coherent spin-flip fluctuations, and this shows that the appropriate density of states for the bath in this regime is of the Lorentzian kind (same as the shape of the central peak of the impurity spectral function). We therefore set

$$\rho(D) = \frac{\rho_0 \Gamma^2}{D^2 + \Gamma^2}, \quad (4.124)$$

where Γ represents the half-width of the Lorentzian. A similar line of arguments was presented by Held et al. [245]. Close to the transition, the RG flow of the Kondo coupling J is stunted by the competing pairing term, and the RG equation can be simplified into the Poor man's scaling 1-loop form:

$$\frac{dJ}{dD} \simeq -2\rho_0 \Gamma^2 \frac{J (J + 4U_b)}{(\Gamma^2 + D^2) D}. \quad (4.125)$$

We now integrate this RG equation over the range $D \in [D_0, D^*]$, where D_0 is the bare bandwidth, and D^* is the fixed-point bandwidth. D^* represents the energy scale for the conduction electrons in the IR.

$$\begin{aligned} \int_{J_0}^{J^*} \frac{dJ}{J (J + 4U_b)} &= - \int_{D_0}^{D^*} \frac{2\rho_0 \Gamma^2 dD}{(\Gamma^2 + D^2) D} \\ \implies \frac{1}{4U_b \rho_0} \left(\ln \frac{J^*}{J_0} - \ln \frac{J^* + 4U_b}{J_0 + 4U_b} \right) &= \ln \frac{D^* + \Gamma^2}{D_0 + \Gamma^2} - \ln \frac{D^*}{D_0}. \end{aligned} \quad (4.126)$$

We will now take the limit of $J_0 + 4U_b \rightarrow 0^-$ and equate the singular terms on both sides of the equation:

$$\ln \frac{D^*}{D_0} = -\frac{1}{4U_b \rho_0} \ln \frac{J_0 + 4U_b}{J_0} = -\frac{1}{4U_b \rho_0} \ln (r_{c2} - r) + \text{non-singular part}. \quad (4.127)$$

We have replaced the couplings J and U_b with the dimensionless parameters $r = -U_b/J_0$ and $r_{c2} = 1/4$. Dropping the non-singular part and solving for D^* then gives the IR energy scale:

$$D^* = D_0 \exp \left[-\frac{\ln (r_{c2} - r)}{4U_b \rho_0} \right]. \quad (4.128)$$

The dynamically generated Kondo temperature scale is then obtained as

$$T_K = \frac{D^*}{k_B} = \frac{D_0}{k_B} \exp \left[-\frac{\ln (r_{c2} - r)}{4U_b \rho_0} \right]. \quad (4.129)$$

Note that the prefactor of the logarithm is positive because U_b is negative: $-4U_b \rho_0 = |4U_b \rho_0|$. As we approach the transition, the parameter r takes the limit $r \rightarrow r_{c2}^-$, and the Kondo temperature scale vanishes:

$$\lim_{r \rightarrow r_{c2}^-} T_K = \frac{D_0}{k_B} \lim_{r \rightarrow r_{c2}^-} (r_{c2} - r)^{4|U_b \rho_0|} \rightarrow 0. \quad (4.130)$$

4.14 Appendix: Effective Hamiltonian for the low-lying excitations at the critical point

In order to obtain an effective Hamiltonian for the low-lying excitations in the bath, we will introduce a hopping term V between the zeroth site and the first site into the two-site Hamiltonian H_0 , and treat that term perturbatively.

$$H = \underbrace{J\vec{S}_d \cdot \vec{S}_0 - U_b (\hat{n}_{0\uparrow} - \hat{n}_{0\downarrow})^2}_{H_0} - t \underbrace{\sum_{\sigma} (c_{0\sigma}^\dagger c_{1\sigma} + \text{h.c.})}_{V}. \quad (4.131)$$

As mentioned before, H_0 is our zeroth Hamiltonian, while V is the perturbation. At the critical point, the zeroth Hamiltonian has a 20-fold degenerate ground-state manifold, and we will show later that it is this degeneracy that leads to NFL excitations. The ground-states are

$$\{|S = S^z = 0\rangle, |\uparrow, 0\rangle, |\uparrow, 2\rangle, |\downarrow, 0\rangle, |\downarrow, 2\rangle\} \otimes \{|0\rangle, |\uparrow\rangle, |\downarrow\rangle, |\uparrow\downarrow\rangle\}. \quad (4.132)$$

The ket to the left of \otimes describes the configuration of the impurity and zeroth sites; $S = S^z = 0$ represents the singlet, while the remaining four states $|\sigma, 0\rangle, |\sigma, 2\rangle$ are local moment states. The ket to the right of \otimes represents the configuration of the first site. Eight of these states have zero matrix elements within the ground-state subspace, even in the presence of the perturbation, so we drop these states. Since the full Hamiltonian conserves the total number of particles $N_{\text{tot}} = \sum_{\sigma} (\hat{n}_{d\sigma} + \hat{n}_{0\sigma} + \hat{n}_{1\sigma})$ and the total spin $S_{\text{tot}}^z = S_d^z + S_0^z + S_1^z$, the remaining 12 states can be split into decoupled blocks based on the values of these two operators:

$$\begin{aligned} N_{\text{tot}} = c + 2, S_{\text{tot}}^z = 0 &: |S = S^z = 0\rangle |c\rangle, |\uparrow, c, \downarrow\rangle, |\downarrow, c, \uparrow\rangle; c = 0, 2, \\ N_{\text{tot}} = 3, S_{\text{tot}}^z = \pm \frac{1}{2} &: |S = S^z = 0\rangle |\sigma\rangle, |\sigma, 0, 2\rangle, |\sigma, 2, 0\rangle; \sigma = \uparrow, \downarrow. \end{aligned} \quad (4.133)$$

The perturbation V will lift the degeneracy in each block; to calculate the modified spectrum, we diagonalise each block in the presence of V . We will first write down the action of the perturbation on the singlet ground-states: this will make it easier to identify the true eigenstates.

$$\begin{aligned} N_{\text{tot}} = c + 2, S_{\text{tot}}^z = 0 &: V |SS_c\rangle = \frac{t}{\sqrt{2}} (|\downarrow, c, \uparrow\rangle - |\uparrow, c, \downarrow\rangle), c = 0, 2, \\ N_{\text{tot}} = 3, S_{\text{tot}}^z = \frac{\sigma}{2} &: V |SS_{\sigma}\rangle = \frac{t}{\sqrt{2}} |\sigma\rangle \otimes (|0, 2\rangle + |2, 0\rangle), \sigma = \uparrow (1), \downarrow (-1), \end{aligned} \quad (4.134)$$

where we have introduced the notation $|SS_{\alpha}\rangle = |S = S^z = 0\rangle \otimes |\alpha\rangle, \alpha = 0, \uparrow, \downarrow, 2$. This shows that the action of the perturbation on the singlet state is to create linear combinations of the local moment states in the respective blocks. We therefore define the two possible linear combinations $|\text{LM}_{\pm}^{N_{\text{tot}}, S_{\text{tot}}^z}\rangle$ within each block:

$$\begin{aligned} N_{\text{tot}} = c + 2, S_{\text{tot}}^z = 0 &: |\text{LM}_{\pm}^{c+2, 0}\rangle = \frac{1}{\sqrt{2}} (|\uparrow, c, \downarrow\rangle \pm |\downarrow, c, \uparrow\rangle), c = 0, 2, \\ N_{\text{tot}} = 3, S_{\text{tot}}^z = \frac{\sigma}{2} &: |\text{LM}_{\sigma}^{3, \frac{1}{2}}\rangle = \frac{1}{\sqrt{2}} (|\sigma, 0, 2\rangle \pm |\sigma, 2, 0\rangle), \sigma = \uparrow (1), \downarrow (-1). \end{aligned} \quad (4.135)$$

In terms of these linear combinations, we then get

$$\begin{aligned} V |SS_0\rangle &= t |\text{LM}_{-}^{2, 0}\rangle, V |\text{LM}_{-}^{2, 0}\rangle = t |SS_0\rangle, V |\text{LM}_{+}^{2, 0}\rangle = 0; V |SS_{\uparrow}\rangle = t |\text{LM}_{+}^{3, \uparrow}\rangle, \\ V |\text{LM}_{+}^{3, \uparrow}\rangle &= t |SS_{\uparrow}\rangle, V |\text{LM}_{-}^{3, \uparrow}\rangle = 0, V |SS_{\downarrow}\rangle = t |\text{LM}_{+}^{3, \downarrow}\rangle, V |\text{LM}_{+}^{3, \downarrow}\rangle = t |SS_{\downarrow}\rangle, \\ V |\text{LM}_{-}^{3, \downarrow}\rangle &= 0; V |SS_2\rangle = t |\text{LM}_{-}^{4, 0}\rangle, V |\text{LM}_{-}^{4, 0}\rangle = t |SS_2\rangle, V |\text{LM}_{+}^{4, 0}\rangle = 0. \end{aligned} \quad (4.136)$$

The zero matrix elements at the far right of each line should be understood as the fact that V takes those states out of the ground-state subspace. For e.g., the state $V |LM_-^{2,0}\rangle$ is not really zero, but the overlap of $V |LM_-^{2,0}\rangle$ with any other state in the ground-state subspace spanned by the 20 degenerate states is zero. We now see that each of the 3×3 blocks decouples into a 2×2 block $\begin{pmatrix} 0 & t \\ t & 0 \end{pmatrix}$ and a 1×1 block (0) when written in terms of the linear combinations $|LM_\pm\rangle$. The state in the final block is therefore already an eigenstate, but with zero energy, so that will drop out from the effective Hamiltonian. The remaining 2×2 block has eigenstates $|\pm^{N_{\text{tot}}, S_{\text{tot}}^z}\rangle$ that are linear combinations of the singlet states and the surviving local moment combination, with eigenvalues $\pm t$:

$$\begin{aligned} N_{\text{tot}} = 2, S_{\text{tot}}^z = 0 : |\pm^{2,0}\rangle &= \frac{1}{\sqrt{2}} (|SS_0\rangle \pm |LM_-^{2,0}\rangle) , \\ N_{\text{tot}} = 3, S_{\text{tot}}^z = \frac{1}{2} : |\pm^{3,\frac{1}{2}}\rangle &= \frac{1}{\sqrt{2}} (|SS_\uparrow\rangle \pm |LM_+^{3,\frac{1}{2}}\rangle) , \\ N_{\text{tot}} = 3, S_{\text{tot}}^z = -\frac{1}{2} : |\pm^{3,-\frac{1}{2}}\rangle &= \frac{1}{\sqrt{2}} (|SS_\downarrow\rangle \pm |LM_+^{3,-\frac{1}{2}}\rangle) , \\ N_{\text{tot}} = 4, S_{\text{tot}}^z = 0 : |\pm^{4,0}\rangle &= \frac{1}{\sqrt{2}} (|SS_2\rangle \pm |LM_-^{4,0}\rangle) . \end{aligned} \quad (4.137)$$

At this point, it is worth noting that the polarised ground-states $|S_{\text{tot}}^z = \sigma \frac{1}{2}\rangle, \sigma = \pm 1$ can be written as an equal superposition of the singlet states $|SS\rangle_{d0} \otimes |\sigma\rangle_1$ and the local moment states $\frac{1}{\sqrt{2}} (|\sigma, 0, 2\rangle - |\sigma, 2, 0\rangle)$. The polarised symmetry-broken states therefore act as a bridge between the ground states of the two phases and are important in displaying the breakdown of the Kondo cloud at the QCP and the consequences arising from it (like inexact screening of the impurity and fractional magnetisation and entanglement entropy, which will be discussed in the next section).

By combining the two eigenstates $|\pm\rangle$ for each block, one can then reconstruct the effective Hamiltonian $\mathcal{H}_{\text{eff}}^{N_{\text{tot}}, S_{\text{tot}}^z}$ that describes the dynamics of the first site from within the ground-state subspace of the zeroth Hamiltonian. Formally, this is written as

$$\begin{aligned} \mathcal{H}_{\text{eff}}^{N_{\text{tot}}, S_{\text{tot}}^z} &= t |+\rangle^{N_{\text{tot}}, S_{\text{tot}}^z} \langle +| - t |-\rangle^{N_{\text{tot}}, S_{\text{tot}}^z} \langle -| , \\ &= \begin{cases} t \left[|SS_\alpha\rangle \langle LM_-^{N_{\text{tot}}, S_{\text{tot}}^z}| + |LM_-^{N_{\text{tot}}, S_{\text{tot}}^z}\rangle \langle SS_\alpha| \right], & \alpha = 0, 2 , \\ t \left[|SS_\alpha\rangle \langle LM_+^{N_{\text{tot}}, S_{\text{tot}}^z}| + |LM_+^{N_{\text{tot}}, S_{\text{tot}}^z}\rangle \langle SS_\alpha| \right], & \alpha = \uparrow, \downarrow . \end{cases} \end{aligned} \quad (4.138)$$

We first write down the effective Hamiltonian for $\alpha = 0$ which corresponds to $N_{\text{tot}} = 2, S_{\text{tot}}^z = 0$:

$$\mathcal{H}_{\text{eff}}^{2,0} = t [|SS_0\rangle \langle LM_-^{2,0}| + |LM_-^{2,0}\rangle \langle SS_0|] . \quad (4.139)$$

In order to convert this into a second-quantised form, we will use the following identities:

$$|SS_0\rangle = \frac{1}{\sqrt{2}} \left(P_d^\uparrow c_{0\downarrow}^\dagger - P_d^\downarrow c_{0\uparrow}^\dagger \right) P_0^{(0)} P_1^{(0)} |0\rangle ; \quad |LM_-^{2,0}\rangle = \frac{1}{\sqrt{2}} \left(P_d^\uparrow c_{1\downarrow}^\dagger - P_d^\downarrow c_{1\uparrow}^\dagger \right) P_0^{(0)} P_1^{(0)} |0\rangle \quad (4.140)$$

where $P_i^{(m)} (m = 0, 1, 2)$ projects onto the $\hat{n}_i = m$ subspace on the i^{th} site, and P_d^σ projects the impurity spin into $|\sigma\rangle ; \sigma = \uparrow, \downarrow$ configuration. We then have

$$\begin{aligned} |SS_0\rangle \langle LM_-^{2,0}| &= \frac{1}{2} \left(P_d^\uparrow c_{0\downarrow}^\dagger - P_d^\downarrow c_{0\uparrow}^\dagger \right) P_0^{(0)} P_1^{(0)} \left(P_d^\uparrow c_{1\downarrow}^\dagger - P_d^\downarrow c_{1\uparrow}^\dagger \right) \\ &= P_1^{(0)} \frac{1}{2} \left(P_d^\uparrow c_{0\downarrow}^\dagger c_{1\downarrow} + P_d^\downarrow c_{0\uparrow}^\dagger c_{1\uparrow} - S_d^+ c_{0\downarrow}^\dagger c_{1\uparrow} - S_d^- c_{0\uparrow}^\dagger c_{1\downarrow} \right) P_0^{(0)} , \end{aligned} \quad (4.141)$$

where we have used $P^2 = P$ if P is a projector, and that $P_d^\uparrow P_d^\downarrow = S_d^+$. Substituting these into the effective Hamiltonian and recognising that $P_d^\uparrow = \frac{1}{2} + S_d^z$, $P_d^\downarrow = \frac{1}{2} - S_d^z$ gives

$$\mathcal{H}_{\text{eff}}^{2,0} = \frac{t}{2} \left[\left(\frac{1}{2} + S_d^z \right) c_{0\downarrow}^\dagger P_0^{(0)} P_1^{(0)} c_{1\downarrow} - S_d^+ c_{0\downarrow}^\dagger P_0^{(0)} P_1^{(0)} c_{1\uparrow} - S_d^- c_{0\uparrow}^\dagger P_0^{(0)} P_1^{(0)} c_{1\downarrow} \right. \right. \\ \left. \left. + \left(\frac{1}{2} - S_d^z \right) c_{0\uparrow}^\dagger P_0^{(0)} P_1^{(0)} c_{1\uparrow} \right] + \text{h.c.} \right] \quad (4.142)$$

In order to make this more illuminating, we define the holon excitation operators $h_{i\sigma}^\dagger = c_{i\sigma}^\dagger P_i^{(0)}$. In terms of these operators, the effective Hamiltonian becomes

$$\begin{aligned} \mathcal{H}_{\text{eff}}^{2,0} &= \frac{t}{2} \left[\left(\frac{1}{2} + S_d^z \right) \left(h_{0\downarrow}^\dagger h_{1\downarrow} + h_{1\downarrow}^\dagger h_{0\downarrow} \right) - S_d^+ \left(h_{0\downarrow}^\dagger h_{1\uparrow} + h_{1\downarrow}^\dagger h_{0\uparrow} \right) - S_d^- \left(h_{0\uparrow}^\dagger h_{1\downarrow} + h_{1\uparrow}^\dagger h_{0\downarrow} \right) + \right. \\ &\quad \left. \left(\frac{1}{2} - S_d^z \right) \left(h_{0\uparrow}^\dagger h_{1\uparrow} + h_{1\uparrow}^\dagger h_{0\uparrow} \right) \right] \\ &= -t \left[S_d^z \frac{1}{2} \left(h_{0\uparrow}^\dagger h_{1\uparrow} + h_{1\uparrow}^\dagger h_{0\uparrow} - h_{0\downarrow}^\dagger h_{1\downarrow} - h_{1\downarrow}^\dagger h_{0\downarrow} \right) + \frac{1}{2} S_d^+ \left(h_{0\downarrow}^\dagger h_{1\uparrow} + h_{1\downarrow}^\dagger h_{0\uparrow} \right) \right. \\ &\quad \left. + \frac{1}{2} S_d^- \left(h_{0\uparrow}^\dagger h_{1\downarrow} + h_{1\uparrow}^\dagger h_{0\downarrow} \right) \right] + \frac{t}{4} \left(h_{0\uparrow}^\dagger h_{1\uparrow} + h_{1\uparrow}^\dagger h_{0\uparrow} + h_{0\downarrow}^\dagger h_{1\downarrow} + h_{1\downarrow}^\dagger h_{0\downarrow} \right). \end{aligned} \quad (4.143)$$

The first part of the Hamiltonian (with a $-t$ factor in front) is reminiscent of a two-spin Heisenberg Hamiltonian. To investigate this, we write down the potential second spin:

$$\mathcal{S}_1^z \equiv \frac{1}{2} \left(h_{0\uparrow}^\dagger h_{1\uparrow} + h_{1\uparrow}^\dagger h_{0\uparrow} - h_{0\downarrow}^\dagger h_{1\downarrow} - h_{1\downarrow}^\dagger h_{0\downarrow} \right). \quad (4.144)$$

Note that each term that comprises the full operator \mathcal{S}_1^z has a combined projector $P_{01}^{(0)} = P_0^{(0)} P_1^{(0)} = P_1^{(0)} P_0^{(0)}$ in the middle with a single annihilation operator to the right. This means that \mathcal{S}_1^z projects onto the smaller set of only those states that satisfy $\hat{n}_0 + \hat{n}_1 = 1$. That is also the meaning of the subscript 1 in \mathcal{S}_1^z . There are four such states: $|\uparrow, 0\rangle, |\downarrow, 0\rangle, |0, \uparrow\rangle, |0, \downarrow\rangle$. In fact, it is easy to see that the eigenstates of \mathcal{S}_1^z are

$$|\uparrow\rangle_{1,\pm} = \frac{1}{\sqrt{2}} (|\uparrow, 0\rangle \pm |0, \uparrow\rangle), \quad \mathcal{S}_1^z |\uparrow\rangle_{1,\pm} = \pm \frac{1}{2} |\uparrow\rangle_{1,\pm}, \quad (4.145)$$

$$|\downarrow\rangle_{1,\pm} = \frac{1}{\sqrt{2}} (|\downarrow, 0\rangle \pm |0, \downarrow\rangle), \quad \mathcal{S}_1^z |\downarrow\rangle_{1,\pm} = \mp \frac{1}{2} |\downarrow\rangle_{1,\pm}. \quad (4.146)$$

The label \pm on top of the eigenstates indicates that these are also eigenstates of the parity operator \mathcal{P}_{01} that switches the site labels 0 and 1:

$$\mathcal{P}_{01} |\alpha, \alpha'\rangle = |\alpha', \alpha\rangle; \quad \alpha, \alpha' \in \{0, \uparrow, \downarrow, 2\}. \quad (4.147)$$

In fact, the eigenstates $|\uparrow\rangle_{1,+1}$ and $|\downarrow\rangle_{1,-1}$ both have $\mathcal{S}_1^z = \frac{1}{2}$, but are orthogonal because they have different parities. Analogous to the \mathcal{S}_1^z operator, we can also read off the potential \mathcal{S}_1^\pm ladder operators from the effective Hamiltonian:

$$\mathcal{S}_1^+ = h_{0\uparrow}^\dagger h_{1\downarrow} + h_{1\uparrow}^\dagger h_{0\downarrow}, \quad \mathcal{S}_1^- = (\mathcal{S}_1^+)^{\dagger}. \quad (4.148)$$

Applying these ladder operators on the eigenstates of \mathcal{S}_1^z gives

$$\mathcal{S}_1^+ |\downarrow\rangle_{1,\pm} = \pm |\uparrow\rangle_{1,\pm}; \quad \mathcal{S}_1^- |\uparrow\rangle_{1,\pm} = \pm |\downarrow\rangle_{1,\pm}; \quad \mathcal{S}_1^+ |\uparrow\rangle_{1,\pm} = \mathcal{S}_1^- |\downarrow\rangle_{1,\pm} = 0. \quad (4.149)$$

This makes it clear that the pair of states $|\uparrow\rangle_1^+$ and $|\downarrow\rangle_1^+$ form a spin-half doublet, as does the other pair $|\uparrow\rangle_1^-$ and $|\downarrow\rangle_1^-$. We can define new spin operators that act only on a single parity subspace:

$$\mathcal{S}_{1,\pm}^a = \pm \mathcal{S}^a \frac{1}{2} (1 \pm \mathcal{P}_{01}); \quad a = x, y, z. \quad (4.150)$$

The operator $\frac{1}{2} (1 \pm \mathcal{P}_{01})$ projects on to the subspace with ± 1 parity. In the notation $\mathcal{S}_{1,\pm}^a$, the label \pm indicates the parity sector to which the operator applies, while 1 indicates that we are operating in the subspace with $\hat{n}_0 + \hat{n}_1 = 1$. Two operators corresponding to different parity subspaces will commute because they act on disjoint Hilbert spaces: $[\mathcal{S}_{+1}^a, \mathcal{S}_{-1}^b] = 0$. In terms of these projected spin operators, we recover the usual spin-half SU(2) algebra:

$$\begin{aligned} \mathcal{S}_{1,\pm}^z |\uparrow\rangle_{1,\pm} &= \frac{1}{2} |\uparrow\rangle_{1,\pm}; & \mathcal{S}_{1,\pm}^z |\downarrow\rangle_{1,\pm} &= -\frac{1}{2} |\downarrow\rangle_{1,\pm}; \\ \mathcal{S}_{1,\pm}^+ |\downarrow\rangle_{1,\pm} &= |\uparrow\rangle_{1,\pm}; & \mathcal{S}_{1,\pm}^- |\uparrow\rangle_{1,\pm} &= |\downarrow\rangle_{1,\pm}. \end{aligned} \quad (4.151)$$

The part of the effective Hamiltonian that involves the impurity can now be written in terms of these new spin operators:

$$t \left(\vec{\mathcal{S}}_d \cdot \vec{\mathcal{S}}_{-,1} - \vec{\mathcal{S}}_d \cdot \vec{\mathcal{S}}_{+,1} \right); \quad \vec{\mathcal{S}}_\pm = (\mathcal{S}_\pm^x \ \mathcal{S}_\pm^y \ \mathcal{S}_\pm^z). \quad (4.152)$$

The last term in eq. (4.143) (with a prefactor of $\frac{t}{4}$) can now be identified as the parity operator \mathcal{P}_{01} acting within the subspace $\hat{n}_0 + \hat{n}_1 = 1$, because it has eigenstates $|\uparrow, 0\rangle \pm |0, \uparrow\rangle$ and $|\downarrow, 0\rangle \pm |0, \downarrow\rangle$ with eigenvalues ± 1 . The full effective Hamiltonian in the $N_{\text{tot}} = 2$ subspace then takes the compact form

$$\mathcal{H}_{\text{eff}}^{2,0} = t \left(\vec{\mathcal{S}}_d \cdot \vec{\mathcal{S}}_{1,-1} - \vec{\mathcal{S}}_d \cdot \vec{\mathcal{S}}_{1,+} \right) + \frac{t}{4} \mathcal{P}_{01} P_{01}^{(1)}, \quad (4.153)$$

where $P_{01}^{(1)} = P_0^{(1)} P_1^{(0)} + P_0^{(0)} P_1^{(1)}$ projects on to the $\hat{n}_0 + \hat{n}_1 = 1$ subspace. In light of these new spin operators, the original eigenstates $|\pm^{2,0}\rangle$ can be written in terms of these emergent spins $|\uparrow\rangle_{1,\pm}$ and $|\downarrow\rangle_{1,\pm}$:

$$\begin{aligned} |\pm^{2,0}\rangle &= \frac{1}{2} (|\uparrow, \downarrow, 0\rangle - |\downarrow, \uparrow, 0\rangle \pm |\uparrow, 0, \downarrow\rangle \mp |\downarrow, 0, \uparrow\rangle) = \frac{1}{2} [|\uparrow\rangle (|\downarrow, 0\rangle \pm |0, \downarrow\rangle) - |\downarrow\rangle (|\uparrow, 0\rangle \pm |0, \uparrow\rangle)] \\ &= \frac{1}{\sqrt{2}} (|\uparrow\rangle |\downarrow\rangle_{1,\pm} - |\downarrow\rangle |\uparrow\rangle_{1,\pm}). \end{aligned} \quad (4.154)$$

Both the ground and excited states are therefore spin-singlet states, but they belong to the negative and positive parity sectors respectively.

We now proceed to the $N_{\text{tot}} = 4$ sector, which is equivalent to $\alpha = 2$ and $\hat{n}_0 + \hat{n}_1 = 3$. From eq. (4.138), we note that the effective Hamiltonian of the $\alpha = 2$ sector is obtained from that of the $\alpha = 0$ sector by replacing the holons with doublons, $|0\rangle \rightarrow |2\rangle$. This allows us to use the results of the $N_{\text{tot}} = 2$ sector simply by making the above-mentioned holon-doublon transformation. Accordingly, the composite up and down spins of the 0 + 1-site system become

$$|\uparrow\rangle_{3,\pm} = \frac{1}{\sqrt{2}} (|\uparrow, 2\rangle \pm |2, \uparrow\rangle), \quad |\downarrow\rangle_{3,\pm} = \frac{1}{\sqrt{2}} (|\downarrow, 2\rangle \pm |2, \downarrow\rangle), \quad (4.155)$$

which then allow us to define spin operators for the positive and negative parity sectors:

$$\mathcal{S}_{\pm}^z = \frac{1}{2} \left(|\uparrow\uparrow\rangle_{3,\pm} - |\downarrow\downarrow\rangle_{3,\pm} \right), \quad \mathcal{S}_{\pm}^{+} = |\uparrow\uparrow\rangle_{3,\pm} \langle \downarrow\downarrow|_{3,\pm}, \quad (4.156)$$

analogous to those of the $N_{\text{tot}} = 2$ sector in eqs. (4.145) and (4.148). These definitions then allow us to rewrite the effective Hamiltonian in terms of the eigenstates of \mathcal{S}_{\pm}^z , and hence in terms of the spin operators $\vec{\mathcal{S}}_{3,\pm}$. The eigenstates $|\pm^{4,0}\rangle$ and the effective Hamiltonian $H_{\text{eff}}^{4,0}$ for this sector can be written as

$$|\pm^{4,0}\rangle = \frac{1}{\sqrt{2}} \left(|\uparrow\uparrow\rangle_d |\downarrow\downarrow\rangle_{3,\pm} - |\downarrow\downarrow\rangle_d |\uparrow\uparrow\rangle_{3,\pm} \right). \quad (4.157)$$

The effective Hamiltonian can then be written in terms of these emergent spins

$$H_{\text{eff}}^{4,0} = \frac{t}{2} \left[\left(|\uparrow\uparrow\rangle_d |\downarrow\downarrow\rangle_{3,+} - |\downarrow\downarrow\rangle_d |\uparrow\uparrow\rangle_{3,+} \right) \left(\langle \uparrow|_d \langle \downarrow|_{3,+} - \langle \downarrow|_d \langle \uparrow|_{3,+} \right) \right. \\ \left. - \left(|\uparrow\uparrow\rangle_d |\downarrow\downarrow\rangle_{3,-} - |\downarrow\downarrow\rangle_d |\uparrow\uparrow\rangle_{3,-} \right) \left(\langle \uparrow|_d \langle \downarrow|_{3,-} - \langle \downarrow|_d \langle \uparrow|_{3,-} \right) \right]. \quad (4.158)$$

By replacing the emergent spins with the spin operators $\vec{\mathcal{S}}_{3,\pm}$, we get the final form of the Hamiltonian

$$H_{\text{eff}}^{4,0} = t \left(\vec{S}_d \cdot \vec{\mathcal{S}}_{3,-} - \vec{S}_d \cdot \vec{\mathcal{S}}_{3,+} \right) + \frac{t}{4} \mathcal{P}_{01} P_{01}^{(3)}, \quad (4.159)$$

where \mathcal{P}_{01} is the parity transformation operator defined in eq. (4.147) and $P_{01}^{(3)}$ projects on to the $\hat{n}_0 + \hat{n}_1 = 3$ subspace. This completes the effective Hamiltonian for the $S_{\text{tot}}^z = 0$ sector.

We now come to the $S_{\text{tot}}^z = +1/2$ sector. From eq. (4.138), the effective Hamiltonian for this sector is

$$H_{\text{eff}}^{3,\frac{1}{2}} = t \left[|\text{SS}\uparrow\rangle \langle \text{LM}^{3,\frac{1}{2}}| + |\text{LM}^{3,\frac{1}{2}}\rangle \langle \text{SS}\uparrow| \right], \quad (4.160)$$

where

$$|\text{SS}\uparrow\rangle = \frac{1}{\sqrt{2}} \left(P_d^{\uparrow} c_{0\downarrow}^{\dagger} - P_d^{\downarrow} c_{0\uparrow}^{\dagger} \right) c_{1\uparrow}^{\dagger} |0\rangle; \quad |\text{LM}^{3,\frac{1}{2}}\rangle = \frac{1}{\sqrt{2}} P_d^{\uparrow} \left(c_{0\uparrow}^{\dagger} c_{0\downarrow}^{\dagger} + c_{1\uparrow}^{\dagger} c_{1\downarrow}^{\dagger} \right) |0\rangle, \quad (4.161)$$

such that

$$|\text{SS}\uparrow\rangle \langle \text{LAM}^{3,\frac{1}{2}}| = \frac{1}{2} \left(P_d^{\uparrow} c_{0\downarrow}^{\dagger} - P_d^{\downarrow} c_{0\uparrow}^{\dagger} \right) c_{1\uparrow}^{\dagger} (c_{0\downarrow} c_{0\uparrow} + c_{1\downarrow} c_{1\uparrow}) P_d^{\uparrow} \quad (4.162)$$

$$= -\frac{1}{2} \left[P_d^{\uparrow} \left(c_{1\uparrow}^{\dagger} c_{0\uparrow} \hat{n}_{0\downarrow} + c_{0\downarrow}^{\dagger} c_{1\downarrow} \hat{n}_{1\uparrow} \right) + S_d^{-} \left(c_{1\uparrow}^{\dagger} c_{0\downarrow} \hat{n}_{0\uparrow} - c_{0\uparrow}^{\dagger} c_{1\downarrow} \hat{n}_{1\uparrow} \right) \right]. \quad (4.163)$$

The full effective Hamiltonian then becomes

$$H_{\text{eff}}^{3,\frac{1}{2}} = -\frac{t}{2} \left[P_d^{\uparrow} \left\{ \left(c_{1\uparrow}^{\dagger} c_{0\uparrow} + c_{0\downarrow}^{\dagger} c_{1\downarrow} \right) \left(P_0^{(2)} P_1^{(0)} + P_0^{(0)} P_1^{(2)} \right) + \left(c_{0\uparrow}^{\dagger} c_{1\uparrow} + c_{1\downarrow}^{\dagger} c_{0\downarrow} \right) P_0^{(1)} P_1^{(1)} \right\} \right. \\ \left. + S_d^{-} \left(c_{1\uparrow}^{\dagger} c_{0\downarrow} - c_{0\uparrow}^{\dagger} c_{1\downarrow} \right) \left(P_0^{(2)} P_1^{(0)} + P_0^{(0)} P_1^{(2)} \right) + S_d^{+} \left(c_{0\downarrow}^{\dagger} c_{1\uparrow} - c_{1\downarrow}^{\dagger} c_{0\uparrow} \right) P_0^{(1)} P_1^{(1)} \right] \\ = t \left[P_d^{\uparrow} \sqrt{2} \mathcal{A}_{\frac{1}{2}}^z - \frac{1}{2} S_d^{+} \mathcal{B}_{\frac{1}{2}}^{-} - \frac{1}{2} S_d^{-} \mathcal{B}_{\frac{1}{2}}^{+} \right], \quad (4.164)$$

where we have defined

$$\mathcal{A}_{\frac{1}{2}}^z = -\frac{1}{2\sqrt{2}} \left[\left(c_{1\uparrow}^\dagger c_{0\uparrow} + c_{0\downarrow}^\dagger c_{1\downarrow} \right) \left(P_0^{(2)} P_1^{(0)} + P_0^{(0)} P_1^{(2)} \right) + \left(c_{0\uparrow}^\dagger c_{1\uparrow} + c_{1\downarrow}^\dagger c_{0\downarrow} \right) P_0^{(1)} P_1^{(1)} \right], \quad (4.165)$$

and

$$\mathcal{B}_{\frac{1}{2}}^+ = \left(c_{1\uparrow}^\dagger c_{0\downarrow} - c_{0\uparrow}^\dagger c_{1\downarrow} \right) \left(P_0^{(2)} P_1^{(0)} + P_0^{(0)} P_1^{(2)} \right); \quad \mathcal{B}_{\frac{1}{2}}^- = \left(c_{0\downarrow}^\dagger c_{1\uparrow} - c_{1\downarrow}^\dagger c_{0\uparrow} \right) P_0^{(1)} P_1^{(1)}. \quad (4.166)$$

The effective Hamiltonian for the $S_{\text{tot}}^z = -1/2$ sector is obtained by applying the transformations $P_d^\sigma \rightarrow P_d^{\bar{\sigma}}$, $c_{i\sigma} \rightarrow c_{i\bar{\sigma}}$ on the Hamiltonian. This is motivated by the fact that applying the same transformations on the $S_{\text{tot}}^z = 1/2$ eigenstates give the $S_{\text{tot}}^z = -1/2$ eigenstates.

$$H_{\text{eff}}^{3,-\frac{1}{2}} = t \left[P_d^\uparrow \sqrt{2} \mathcal{A}_{-\frac{1}{2}}^z - \frac{1}{2} S_d^+ \mathcal{B}_{-\frac{1}{2}}^- - \frac{1}{2} S_d^- \mathcal{B}_{-\frac{1}{2}}^+ \right]. \quad (4.167)$$

The operators $\mathcal{A}_{-\frac{1}{2}}^z$ and $\mathcal{B}_{-\frac{1}{2}}^\pm$ are obtained by applying the above mentioned transformation on their $S_{\text{tot}}^z = +1/2$ counterparts.

4.15 Appendix: Non-Fermi liquid exponents in self-energy and two-particle correlations

The one-particle self-energies relating to the impurity and zeroth sites, as well as some relevant two-particle correlation functions, can be shown to follow power-law behaviour close to the Brinkman-Rice transition at r_{c2} , by mapping the impurity model to a classical Coulomb gas, similar to the work of Anderson, Yuval and Hamman for the Kondo model [208] and that of Si and Kotliar for a periodic Anderson model [203]. Indeed, the latter work uses an auxiliary that is similar to our extended Anderson impurity model. In the following, we adapt their results to our model. These non-universal power-laws are signatures of the non-Fermi liquid excitations that emerge at r_{c2} .

Near r_{c2} , extended SIAM can be reduced to a $J - U_b$ model (shown in subsection V.A of the main manuscript). The conduction electrons scattering off the impurity suffer phase shifts because of the presence of the potentials J and U_b . These phase shifts are given by $\delta_{\text{sp}} = \arctan(\pi\rho_0 J/2)$ and $\delta_{\text{ch}} = \arctan(\pi\rho_0 U_b/2)$ [203, 287], where ρ_0 is the electronic density of states in the conduction bath. The low-energy behaviour of the local impurity and bath self-energies can be expressed in terms of these phase shifts [203]:

$$\begin{aligned} \Sigma_{dd}(\omega) &\sim \omega^{\gamma_{dd}}, \quad \Sigma_{d0}(\omega) \sim \omega^{\gamma_{d0}}, \quad \Sigma_{00}(\omega) \sim \omega^{\gamma_{00}}, \\ \gamma_{dd} &= \frac{5}{4} - \left(\frac{\delta_{\text{tot}}^*}{\pi} \right)^2 - \left(\frac{\delta_{\text{ch}}^*}{\pi} \right)^2, \quad \gamma_{d0} = 2 \left[\left(\frac{\delta_{\text{ch}}^*}{\pi} \right)^2 + \left(\frac{\delta_{\text{tot}}^*}{\pi} \right)^2 - \frac{1}{4} \right], \\ \gamma_{00} &= \left(\frac{\delta_{\text{tot}}^*}{\pi} - \frac{1}{2} \right)^2 + \left(\frac{\delta_{\text{ch}}^*}{\pi} \right)^2 - 2, \end{aligned} \quad (4.168)$$

where we have defined a total phase shift parameter $\frac{\delta_{\text{tot}}}{\pi} \equiv \frac{\delta_{\text{sp}} + \delta_{\text{ch}}}{\pi} - \frac{1}{2}$. This can be extended to certain correlation functions as well. The impurity spin-flip correlation, the impurity-bath excitonic correlation

and the zeroth-site pairing correlation [203]:

$$\begin{aligned} \langle S_d^+(\tau)S_d^-(0) \rangle &\sim \tau^{-\alpha_1} & \implies \langle S_d^+ \rangle(\omega) &\sim \omega^{(\alpha_1-1)/2}, \\ \left\langle (c_{d\uparrow}^\dagger c_{0\uparrow})(\tau)(c_{0\uparrow}^\dagger c_{d\uparrow})(0) \right\rangle &\sim \tau^{-\alpha_2} & \implies \left\langle c_{d\uparrow}^\dagger c_{0\uparrow} c_{0\uparrow}^\dagger c_{d\uparrow} \right\rangle(\omega) &\sim \omega^{(\alpha_2-1)/2}, \\ \left\langle (c_{0\uparrow}^\dagger c_{0\downarrow}^\dagger)(\tau)(c_{0\downarrow} c_{0\uparrow})(0) \right\rangle &\sim \tau^{-\alpha_3} & \implies \left\langle c_{0\uparrow}^\dagger c_{0\downarrow}^\dagger \right\rangle(\omega) &\sim \omega^{(\alpha_3-1)/2}, \end{aligned} \quad (4.169)$$

where the exponents are given by

$$\alpha_1 = 2 \left(1 - \frac{\delta_{\text{sp}}^*}{\pi} \right)^2, \alpha_2 = \left(\frac{\delta_{\text{tot}}^*}{\pi} - \frac{1}{2} \right)^2 + \left(\frac{\delta_{\text{ch}}^*}{\pi} \right)^2, \alpha_3 = \left(\frac{\delta_{\text{tot}}^*}{\pi} + \frac{1}{2} \right)^2 + \left(1 + \frac{\delta_{\text{ch}}^*}{\pi} \right)^2. \quad (4.170)$$

4.16 Appendix: Entanglement entropy, magnetisation and phase shift, at the QCP

As mentioned in the previous section, the polarised ground-states $|-\rangle^{3,\pm\frac{1}{2}}$ of eq. (4.137) are special because they involve the strong-coupling ground-state as well as the local moment ground-state. The overall ground states, therefore, contain both entangled and non-entangled impurity contributions, leading to a departure from maximal entanglement. We will now calculate the impurity entanglement entropy $S_{\text{EE}}(d)$ in this polarised ground-state(s) that emerges exactly at the QCP, and show that $S_{\text{EE}}(d)$ has a fractional value (in units of $\log 2$). This turns out to be linked to the fact that the impurity is screened partially in these states, leading to an impurity magnetisation that is non-vanishing but only half of that in the local moment phase.

The fractional entropy arises because of the singular scattering of the gapless excitations at the Fermi surface leading to the destruction of the local Fermi liquid. In order to access these processes, we will work with a *semi-continuous* conduction bath beyond the zeroth site (total number of lattice sites $N \rightarrow \infty$): $H_{\text{bath}} = \sum_{k,\sigma} \epsilon(k) \psi_\sigma^\dagger(k) \psi_\sigma^\dagger(k)$. This conduction bath that is composed of the k -states formed from the Hilbert space of the lattice sites beyond the zeroth site will be referred to as the reduced conduction bath. This is in addition to the Hamiltonian for the impurity and zeroth sites: $H_{d0} = J \vec{S}_d \cdot \vec{S}_0 - \frac{U_b}{2} \left(c_{0\uparrow}^\dagger c_{0\uparrow} - c_{0\downarrow}^\dagger c_{0\downarrow} \right)^2$, where \vec{S}_d is the spin operator for the impurity site, and $c_{0\sigma}^\dagger$ creates an electron of spin σ at the zeroth site. The full Hamiltonian also involves a single-particle hopping term that couples these two Hamiltonians: $H = H_{d0} + H_{\text{bath}} + H_{\text{int}}$, where

$$H_{\text{int}} = -t \sum_{\sigma} \left(c_{0\sigma}^\dagger c_{1\sigma} + \text{h.c.} \right) = -\frac{t}{N} \sum_{k,\sigma} \left[c_{0\sigma}^\dagger \psi_\sigma(k) + \text{h.c.} \right]. \quad (4.171)$$

$c_{1\sigma}^\dagger = \frac{1}{N} \sum_k \psi_\sigma^\dagger(k)$ is the creation operator for the first site of the conduction bath of N sites (but effectively the zeroth site for the reduced conduction bath defined by H_{bath}). We will treat H_{int} perturbatively in t/J , in order to obtain the set of renormalised g -fold degenerate ground-states $\{ |\psi_{\text{gs}}^{(n)} \rangle ; n = 1, \dots, g \}$.

As mentioned before, the intention here is to calculate magnetisation and entanglement entropy in the non-Fermi liquid ground states. In the case of a degenerate subspace with $S_{\text{tot}}^z = \pm 1/2$ where $S_{\text{tot}}^z = S_d^z + S_0^z + S_1^z$ is the total spin operator, the magnetisation m_d^z must be calculated in any *one* of the degenerate states for our problem. This is accomplished by solving the problem in the presence of

an infinitesimal magnetic field term $-hS_{\text{tot}}^z$ that lifts the degeneracy and chooses one of the symmetry-broken ground-states. This is similar to the "two self-energy description" introduced by David Logan for computing quantities in the local moment phase/Mott insulating phase in terms of different self-energies obtained by inserting positive and negative magnetic fields [196, 288, 289]. Due to the symmetry of the Hamiltonian under $S_{\text{tot}}^z \rightarrow -S_{\text{tot}}^z$, both the limits $h = 0^+$ and $h = 0^-$ give the same results for the density matrix and the entanglement entropy. We will work with $h = 0^+$. Since the total Hamiltonian H and the perturbation H_{int} preserve the total spin $S_{\text{tot}}^z = S_d^z + S_0^z + \int dk S_k^z$, it is sufficient to solve only for the sector with the most positive value of S_{tot}^z , since those are the states that will be selected by the positive magnetic field $h = 0^+$.

In the absence of H_{int} , the set of ground-states with a positive S_{tot}^z will contain, to begin with, the local moment states $|\uparrow\rangle_d |0\rangle_0 |\phi\rangle$ and $|\uparrow\rangle_d |2\rangle_0 |\phi\rangle$, where $|\phi\rangle$ represents the filled Fermi sea of the reduced conduction bath, acting as its spinless ground-state. These states have $S_{\text{tot}}^z = 1/2$. We can label these states as $|n_{\text{tot}}, \mu_d^z\rangle$, using the total number of particles $n_{\text{tot}} = n_d + n_0 + n_{\text{bath}}$ (which is also conserved, and where we set $n_{\text{bath}} = 1$ for the set $|\phi\rangle$), and the average magnetisation μ_d^z of the impurity state: $|2, \frac{1}{2}\rangle \equiv |\uparrow\rangle_d |0\rangle_0 |\phi\rangle$, $|4, \frac{1}{2}\rangle \equiv |\uparrow\rangle_d |2\rangle_0 |\phi\rangle$. Since the singlet state $|SS\rangle_{d0}$ (on the d and zeroth sites) is degenerate with the local moment states $|\uparrow\rangle_d |0(2)\rangle_0$, one can construct other states with $S_{\text{tot}}^z = 1/2$ by creating magnetic excitations at the Fermi surface. The fact that we are working with a thermodynamically large bath ($N \rightarrow \infty$) means that there will be gapless excitations vanishingly close to the Fermi surface. Such states are of the form $|SS\rangle_{d0} |e_\uparrow\rangle$ (labeled as $|4, 0\rangle$ in the $|n_{\text{tot}}, \mu_d^z\rangle$ notation) and $|SS\rangle_{d0} |h_\downarrow\rangle$ (labeled as $|2, 0\rangle$), where $|e_\sigma\rangle$ and $|h_\downarrow\rangle$ are electron and hole states respectively:

$$|e_\sigma\rangle = \sum_k^{\text{FS}} \psi_\sigma^\dagger(k) |\phi\rangle, \quad |h_\sigma\rangle = \sum_k^{\text{FS}} \psi_\sigma(k) |\phi\rangle. \quad (4.172)$$

The sum is over k -states on the Fermi surface. The singlet state was set to have zero spin on the impurity site in the state notation, because $\langle S_d^z \rangle$ vanishes in the singlet state. The full set of relevant degenerate ground-states, classified by the total number of particles, is

$$n_{\text{tot}} = 4 : |4, 0\rangle, |4, \frac{1}{2}\rangle; \quad n_{\text{tot}} = 2 : |2, 0\rangle, |2, \frac{1}{2}\rangle. \quad (4.173)$$

Within each 2×2 block, the interaction matrix H_{int} takes the form (in the basis of the states in eq. (4.173))

$$(H_{\text{int}})_{\text{gs}}^{n_{\text{tot}}=2} = \frac{t}{N} \times \begin{pmatrix} 0 & 1/\sqrt{2} \\ 1/\sqrt{2} & 0 \end{pmatrix} = - (H_{\text{int}})_{\text{gs}}^{n_{\text{tot}}=4}, \quad (4.174)$$

and the $S_{\text{tot}}^z = +\frac{1}{2}$ ground-states are then easily obtained to be of the form $|\psi_{\text{gs}}\rangle^{(n_{\text{tot}})} = \frac{1}{\sqrt{2}} (|n_{\text{tot}}, 0\rangle - |n_{\text{tot}}, \frac{1}{2}\rangle)$, $n_{\text{tot}} = 2 \& 4$, independent of N . Both ground-states involve an equal superposition of a $\mu_d^z = 1/2$ state and a $\mu_d^z = 0$ state, such that the net impurity magnetisation in either of the renormalised polarised states is

$$m_d^z = \frac{1}{2} \left(0 + \frac{1}{2} \right) = \frac{1}{4}. \quad (4.175)$$

The reduced density matrix $\rho_{\text{imp}} = \text{Tr}' \left(|\psi_{\text{gs}}\rangle^{(n_{\text{tot}})} \langle \psi_{\text{gs}}|^{(n_{\text{tot}})} \right)$ (where Tr' indicates partial trace over all states apart from those of the impurity) for the impurity spin in the polarised states can now be immediately obtained. It is independent of n_{tot} , and actually turns out to be halfway between the maximally

mixed density matrix $\rho_{\text{MM}} = \frac{1}{2}I$ and the non-entangled density matrix $\rho_{\text{NE}} = \begin{pmatrix} 1 & 0 \\ 0 & 0 \end{pmatrix}$:

$$\rho_{\text{imp}} = \begin{pmatrix} 3/4 & 0 \\ 0 & 1/4 \end{pmatrix} = \frac{1}{2} (\rho_{\text{MM}} + \rho_{\text{NE}}), \quad S_{\text{EE}}(d) = -\text{Tr}(\rho_{\text{imp}} \ln \rho_{\text{imp}}) \simeq 0.81 \log 2. \quad (4.176)$$

This fractional value of the entropy in units of $\log 2$ is another signature of the non-Fermi liquid. We can express this in terms of an effective degeneracy \tilde{g} of the impurity degree of freedom. We define this effective degeneracy as $\tilde{g} = 1 + 2|m_d^z|$, in order to recover the unique ground-state in the local Fermi liquid phase (that has $m_d^z = 0, \tilde{g} = 1$) and the magnetic doublet in the local moment phase (that has $m_d^z = 1/2, \tilde{g} = 2$). The proposed form also results in a non-integer impurity degeneracy for the NFL at the QCP, $\tilde{g}^* = 3/2$. Using the effective degeneracy \tilde{g} , one can also write down a general ground-state

$$|\psi_{\text{gs}}(g)\rangle = \frac{1}{\sqrt{(2-\tilde{g})^2 + (\tilde{g}-1)^2}} [(2-\tilde{g}) |n_{\text{tot}}, 0\rangle - (\tilde{g}-1) |n_{\text{tot}}, 1/2\rangle], \quad (4.177)$$

that interpolates between the strong-coupling ground-state for $r < r_{c2}$ (therefore $\tilde{g} = 1$) and the weak coupling ground-state $r > r_{c2}$ (therefore $\tilde{g} = 2$), also describing the QCP in between ($\tilde{g} = 3/2$). The entanglement entropy, when written in terms of \tilde{g} , takes the form

$$\rho_{\text{imp}} = \frac{1}{2} \begin{pmatrix} 2-\tilde{g} & 0 \\ 0 & \tilde{g} \end{pmatrix} = \frac{1}{2} + \begin{pmatrix} m_d^z & 0 \\ 0 & -m_d^z \end{pmatrix}, \quad (4.178)$$

$$S_{\text{EE}}(d) = - \left(1 - \frac{\tilde{g}}{2}\right) \ln \left(1 - \frac{\tilde{g}}{2}\right) - \frac{\tilde{g}}{2} \ln \frac{\tilde{g}}{2}. \quad (4.179)$$

The relation between the reduced density matrix ρ_{imp} and the impurity magnetisation m_d^z is consistent with that obtained by Kopp et al., [290].

The general form $|\psi_{\text{gs}}(g)\rangle$ of polarised interpolating ground-state also allows us to calculate the excess charge (n_{exc}) added, by the impurity, to the conduction bath Fermi surface (through gapless excitations). This then allows the scattering phase shift of the conduction electrons (obtained via the Friedel sum rule, [268–270]) to be linked with the impurity magnetisation m_d^z . From the definitions of the states $|n_{\text{tot}}, 0\rangle$ and $|n_{\text{tot}}, 1/2\rangle$, we note that the former state involves an impurity-bath singlet while the latter involves a decoupled local moment. The singlet state contributes an excess charge of unity to the conduction bath: $n_{\text{exc}}^{\text{SS}} = 1$, because of the impurity-bath entanglement within it. The local state moment does not contribute any excess charge, because the impurity spin is no longer hybridising with the bath in that state: $n_{\text{exc}}^{\text{LM}} = 0$. Putting these together, the net excess charge contributed by the state in eq. (4.177) is

$$n_{\text{exc}} = \frac{1}{(2-\tilde{g})^2 + (\tilde{g}-1)^2} [(2-\tilde{g})^2 n_{\text{exc}}^{\text{SS}} + (\tilde{g}-1)^2 n_{\text{exc}}^{\text{LM}}] = \left[1 + \left(\frac{2-\tilde{g}}{\tilde{g}-1} \right)^2 \right]^{-1}. \quad (4.180)$$

At the QCP, the excess charge acquires a fractional value of $1/2$, indicating once more that only half of the impurity remains coupled with the bath at the transition. The Friedel sum rule can be used to

equate this excess charge with the phase shift δ^* suffered by conduction electrons as they scatter off the impurity, at the fixed point:

$$\delta^* = \pi n_{\text{exc}} = \left[1 + \left(\frac{2 - \tilde{g}}{\tilde{g} - 1} \right)^2 \right]^{-1} = \frac{4m_d^{z^2}}{1 - 4|m_d^z| + 8m_d^{z^2}}. \quad (4.181)$$

Equation (4.181) unifies the effect of several important quantities that lead to the frustration of the impurity and the destruction of the Kondo effect. The presence of U_b introduces local moment states into the spectrum and leads to states with non-vanishing impurity magnetisation m_d^z at the QCP; this non-zero m_d^z can be interpreted as an effective impurity degeneracy \tilde{g} that is only partially screened, resulting in only half the excess charge n_{exc} being contributed to the conduction bath. This reduction in the excess charge acts as a shift in the boundary conditions felt by the conduction electrons and manifests as a phase shift that is less than the unitarity limit of π .

4.17 Appendix: Additional correlations near the ESQPT and the QCP

We have included some additional correlations for the extended SIAM here to highlight the features that are mentioned in the main manuscript. Left panel of Fig. (4.14) shows the impurity and zeroth site double occupancy. Both vanish at r_{c1} , indicating the emergence of the Kondo model. Very close to r_{c2} , the zeroth site doublon occupancy picks up (see inset), showing the destruction of the Kondo cloud. Right panel of Fig. (4.14) shows various measures of entanglement close to r_{c2} . The impurity-bath mutual information (blue) decreases as the transition is approached, showing the breakdown of impurity screening. The impurity and first site MI (violet), the zeroth site and first site MI (red) and the impurity, zeroth site and first site tripartite information (grey) increase, showing the emergence of long-ranged correlations near the transition. Fig. (4.15) shows the emergence of long-ranged intra-bath mutual information near r_{c1} and r_{c2} , signalling critical behaviour near the ESQPT and QCP respectively. Intra-bath CDW correlations and impurity-bath Ising correlations in Fig. (4.16) also show the previously-mentioned emergence of long-ranged correlations.

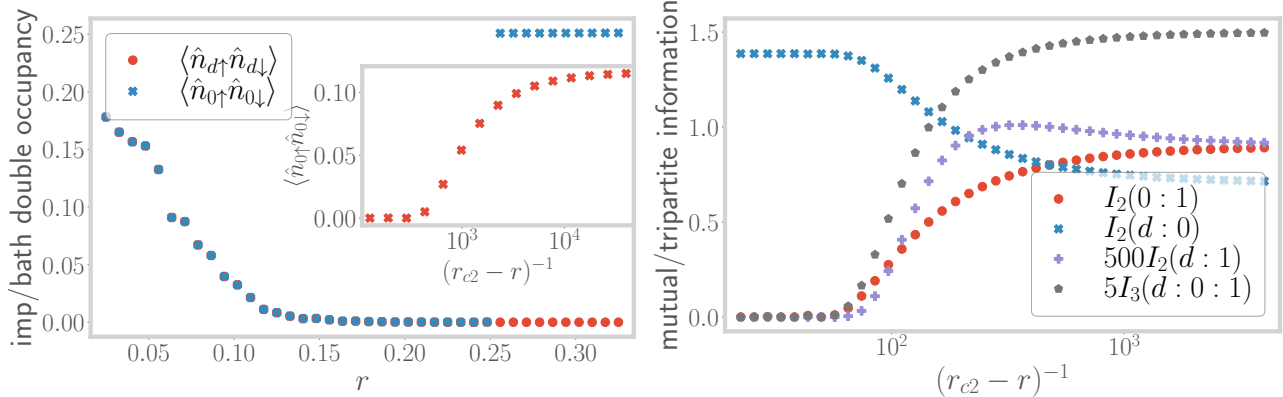


Figure 4.14: Left: Evolution of the double occupancy of impurity (red) and zeroth sites (blue) ground-state double occupancy, with r . Right: Evolution of various quantum information-theoretic measures, very close to the transition.

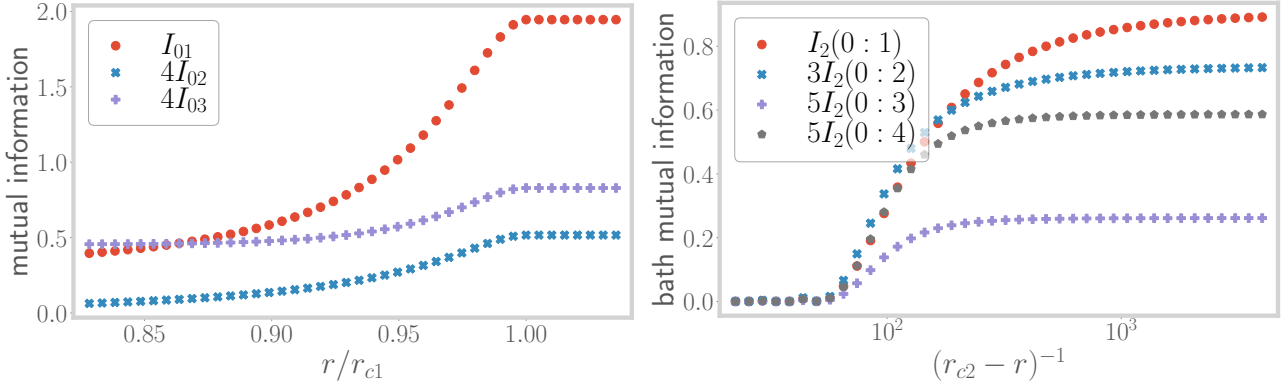


Figure 4.15: Variation of intra-bath mutual information between zeroth site and sites 1, 2 and 3, near r_{c1} (left) and r_{c2} (right).

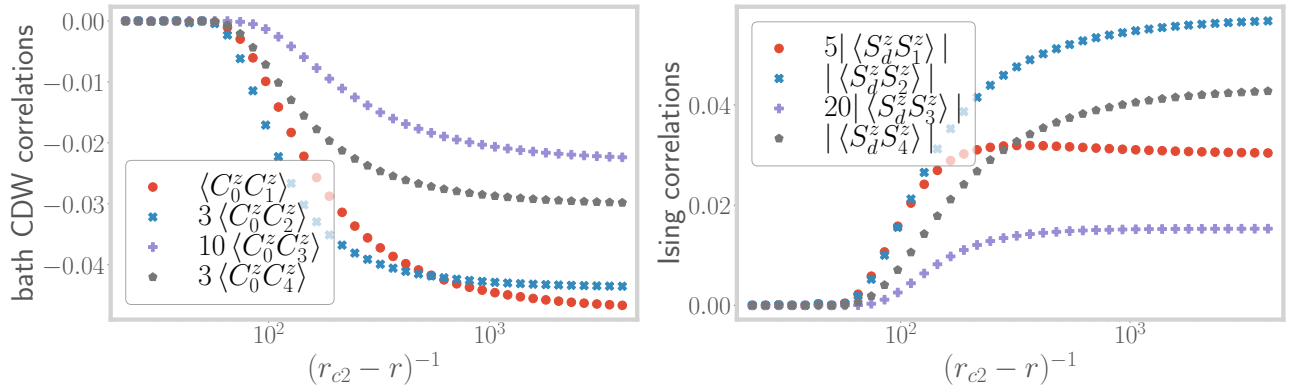


Figure 4.16: Left: Variation of charge isospin Ising correlations between the zeroth site and bath sites further down the chain. Right: Ising correlations between the impurity site and bath sites beyond the zeroth site. Both sets of correlations show an overall increase as $r \rightarrow r_{c2}$.

Chapter 5

Tiling Hubbard

5.1 The philosophy of auxiliary model methods

The present method is a realisation of the general method of using simpler systems called auxiliary models to study bulk systems [291]. In general, a full Hamiltonian can be separated into the Hamiltonians for a particular subsystem S , the rest of the system R , and the interactions between S and R .

$$\begin{aligned} \mathcal{H} &= \mathcal{H}_S |S\rangle\langle S| + \mathcal{H}_R |R\rangle\langle R| + \mathcal{H}_{SR} |S\rangle\langle R| \\ &\quad + \mathcal{H}_{RS} |S\rangle\langle R| = \begin{bmatrix} \mathcal{H}_R & \mathcal{H}_{RS} \\ \mathcal{H}_{RS}^* & \mathcal{H}_S \end{bmatrix} \end{aligned} \quad (5.1)$$

where $|S\rangle$ and $|R\rangle$ actually represents sums over all basis kets of S and R respectively. As an example, we can split the Hubbard model Hamiltonian between a particular site $i = p$ and the rest of the lattice into three parts $H_{\text{hubb}} = H_S + H_R + H_{SR} + H_{RS}$ (fig. 5.1), where

$$\begin{aligned} H_S &= U^H \hat{n}_{p\uparrow} \hat{n}_{p\downarrow} - \mu^H \sum_{\sigma} \hat{n}_{p\sigma} \\ H_R &= U^H \sum_{i \neq p} \hat{n}_{i\uparrow} \hat{n}_{i\downarrow} - \mu^H \sum_{i \neq p, \sigma} \hat{n}_{i\sigma} \\ &\quad - t^H \sum_{\substack{\sigma, (i,j) \\ i \neq p \neq j}} \left(c_{i\sigma}^\dagger c_{j\sigma} + \text{h.c.} \right) \\ H_{SR} + H_{RS} &= -t^H \sum_{\substack{\sigma, \\ i \in \text{N.N. of } p}} \left(c_{i\sigma}^\dagger c_{p\sigma} + \text{h.c.} \right). \end{aligned} \quad (5.2)$$

The Greens function of the full Hamiltonian can also be split in a similar fashion:

$$G(\omega) = \begin{bmatrix} G_S & G_{SR} \\ G_{RS} & G_R \end{bmatrix} \quad (5.3)$$

Each Greens function can be written in terms of the non-interacting counterpart and the self-energy through the Dyson equation: $\Sigma_i = 1/G_{i,0} - 1/G_i$.

The subsystem S is usually taken to be the "cluster", and consequently, R represents the "bath". The smaller system is typically chosen such that its eigenstates are known exactly. Progress is then made

by choosing a simpler version of H_R and a simpler form also for its coupling H_{RS} with the smaller system. This combination of the cluster and the simpler bath is then called the *auxiliary system*. A typical auxiliary system for the Hubbard model could, potentially, be the single-impurity Anderson model (SIAM), where the impurity represents an arbitrary site p of the lattice, the bath represents the rest of the lattice sites and the hybridisation term between the impurity and the bath represents the coupling term H_{RS} :

$$\mathcal{H}_{\text{SIAM}} = \underbrace{\epsilon_d \hat{n}_d + U \hat{n}_{d\uparrow} \hat{n}_{d\downarrow}}_{H_S} + \underbrace{-t \sum_{\langle i,j \rangle, \sigma} (c_{i\sigma}^\dagger c_{j\sigma} + \text{h.c.})}_{H_R} + \underbrace{V \sum_{\sigma} (c_{d\sigma}^\dagger c_{0\sigma} + \text{h.c.})}_{H_{SR}}. \quad (5.4)$$

Such a construction is shown in fig. 5.1. *It should be noted that any reasonable choice of the cluster and*

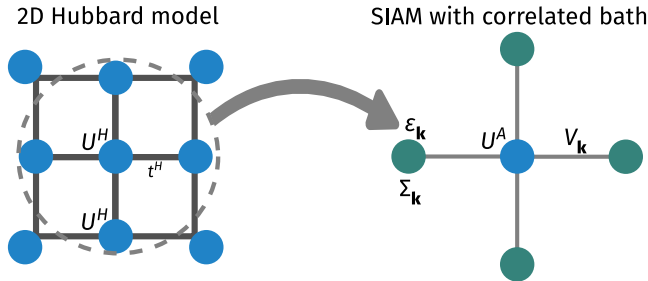


Figure 5.1: *Left:* Full Hubbard model lattice with onsite repulsion U^H on all sites and hopping between nearest neighbour sites with strength t^H . *Right:* Extraction of the auxiliary (cluster+bath) system from the full lattice. The central site on left becomes the impurity site (red) on the right (with an onsite repulsion ϵ_d), while the rest of the $N - 1$ sites on the left form a conduction bath (green circles) (with dispersion ϵ_k and correlation modelled by the self-energy $\Sigma_k(\omega)$) that hybridizes with the impurity through the coupling V .

bath would break the translational symmetry of the full model. To allow computing quantities, one would need to make the bath (which is a much larger system) simpler than the cluster (which is a single site). This distinction breaks the translational symmetry of the Hubbard model. For eg., if one chooses eq. 5.4 as the auxiliary system, then the fact that the impurity has an onsite correlation while the bath does not means we have broken the symmetry between the cluster and the bath.

5.2 A “bottoms-up” approach to using auxiliary models

The present work is aimed towards developing a new auxiliary model method to study correlated electronic systems. We first outline the main steps of the method, to make it more convenient for the reader to following the next sections:

- The first step is to identify the correct impurity model which can faithfully capture the physics of lattice model we are trying to solve (see Subsection 5.2.2). This model must be solved using an impurity solver. In the present work, we use the recently-developed unitary renormalisation group method [1–4, 141, 235].

- The leap to the bulk model is then made by applying lattice translation operators on the impurity model. This process, referred to as tiling here, allows us to reconstruct the lattice model Hamiltonian from that of the auxiliary model (see Subsection 5.2.1).
- Once the Hamiltonians are linked, it is possible to relate the eigenstates and correlations functions between the auxiliary model and lattice model, using a manybody version of Bloch’s theorem (see Section 5.3).

5.2.1 Formal description of the “tiling” procedure

We will now define the *tiling* procedure by which we can recreate the complete lattice model by using instances of an auxiliary model Hamiltonian. The first step is of course to identify an impurity model that can act as a good auxiliary model for our lattice model. The local behaviour of this impurity model should reflect the essential local physics of the lattice model. Typically, we will consider impurity model geometries where the real-space bath site connected directly to the impurity also harbours some kind of local interaction. We will henceforth refer to this site as the zeroth site. In the case where multiple sites are connected directly to the impurity, we will choose one of these sites for reference and call that the *bath zeroth site* throughout.

In order to identify a *unit cell* for our tiling procedure, we place the impurity site at a reference site \mathbf{r}_d of our lattice, and the bath zeroth site at a nearest-neighbour site \mathbf{z} , and label the corresponding auxiliary model Hamiltonian as $\mathcal{H}_{\text{aux}}(\mathbf{r}_d, \mathbf{z})$. The unit cell at the position \mathbf{r}_d is then obtained by placing the zeroth site on all nearest-neighbours of \mathbf{r}_d and averaging over these configurations:

$$\mathcal{H}_{\text{aux}}(\mathbf{r}_d) = \frac{1}{Z} \sum_{\mathbf{z} \in \text{NN}(\mathbf{r}_d)} \mathcal{H}_{\text{aux}}(\mathbf{r}_d, \mathbf{z}) , \quad (5.5)$$

where \mathbf{z} is summed over all nearest-neighbours of \mathbf{r}_d and Z is the number of such nearest-neighbours.

In order to create the bulk model, we now need to translate this auxiliary model over the entire lattice. For this, we define *many-particle global* translation operators $T(\mathbf{a})$ that translate all positions by a vector \mathbf{a} . In terms of manybody states and operators, their action is defined as

$$\begin{aligned} T^\dagger(\mathbf{a}) |\mathbf{r}_1, \mathbf{r}_2, \dots\rangle &= |\mathbf{r}_1 + \mathbf{a}\rangle \otimes |\mathbf{r}_2 + \mathbf{a}\rangle \dots \otimes |\mathbf{r}_n + \mathbf{a}\rangle \\ T^\dagger(\mathbf{a}) \mathcal{O}(\mathbf{r}_1, \mathbf{r}_2, \dots) T(\mathbf{a}) &= \mathcal{O}(\mathbf{r}_1 + \mathbf{a}, \mathbf{r}_2 + \mathbf{a}, \dots) , \end{aligned} \quad (5.6)$$

where $|\mathbf{r}_1, \mathbf{r}_2, \dots\rangle$ is a state in the manyparticle Fock-space basis with the particles localised at the specified positions. For example, for a local fermionic creation operator $c^\dagger(\mathbf{r})$, we have

$$T^\dagger(\mathbf{a}) c^\dagger(\mathbf{r}) T(\mathbf{a}) = c^\dagger(\mathbf{r} + \mathbf{a}) . \quad (5.7)$$

It acts similarly on the auxiliary model Hamiltonian:

$$T^\dagger(\mathbf{a}) \mathcal{H}_{\text{aux}}(\mathbf{r}_d) T(\mathbf{a}) = \mathcal{H}_{\text{aux}}(\mathbf{r}_d + \mathbf{a}) , \quad (5.8)$$

translating all sites by the vector \mathbf{a} . By introducing the Fourier transform to momentum space,

$$|\mathbf{r}_1, \mathbf{r}_2, \dots\rangle = \otimes_{j=1}^N \int d\mathbf{k}_j e^{-i\mathbf{r}_j \cdot \mathbf{k}_j} |\mathbf{k}_j\rangle , \quad (5.9)$$

it is easy to see that the total momentum states are eigenstates of the global translation operators:

$$\begin{aligned}
T^\dagger(\mathbf{a}) |\mathbf{k}_1, \mathbf{k}_2, \dots\rangle &= \otimes_{j=1}^N \int d\mathbf{r}_j e^{i\mathbf{r}_j \cdot \mathbf{k}_j} T^\dagger(\mathbf{a}) |\mathbf{r}_j\rangle , \\
&= \otimes_{j=1}^N \int d\mathbf{r}_j e^{i\mathbf{r}_j \cdot \mathbf{k}_j} |\mathbf{r}_j + \mathbf{a}\rangle \\
&= e^{-i\mathbf{a}_j \cdot \mathbf{k}_{\text{tot}}} |\mathbf{k}_1, \mathbf{k}_2, \dots\rangle ,
\end{aligned} \tag{5.10}$$

where $\mathbf{k}_{\text{tot}} = \sum_j \mathbf{k}_j$ is the total momentum.

The auxiliary model, being an impurity model, lacks translation symmetry. The lattice model does remain invariant under global translation operations. In order to reconstruct the full lattice model and restore its translation invariance, we translate the unit cell across all sites of the lattice:

$$\begin{aligned}
\mathcal{H}_{\text{tiled}} &= \sum_{\mathbf{r}} \mathcal{H}_{\text{aux}}(\mathbf{r}) \\
&= \sum_{\mathbf{r}} T^\dagger(\mathbf{r} - \mathbf{r}_d) \mathcal{H}_{\text{aux}}(\mathbf{r}_d) T(\mathbf{r} - \mathbf{r}_d) \\
&= \frac{1}{Z} \sum_{\mathbf{r}} \sum_{\mathbf{z} \in \text{NN}(\mathbf{r}_d)} T^\dagger(\mathbf{r} - \mathbf{r}_d) \mathcal{H}_{\text{aux}}(\mathbf{r}_d, \mathbf{z}) T(\mathbf{r} - \mathbf{r}_d)
\end{aligned} \tag{5.11}$$

where \mathbf{r} sums over all lattice sites.

5.2.2 Extending the Anderson impurity model: Identifying the correct auxiliary model

The standard Anderson model consists of a correlated impurity site coupled with a non-interacting conduction bath. The double occupancy cost on the impurity is U , while the single-particle hopping strength between the impurity and the conduction bath is V . If the impurity site hybridises with a *non-interacting* bath defined by a uniform density of states, the impurity spectral function is found to have a well-defined Kondo resonance at low temperatures. Such a model does not exhibit a phase transition; the low-energy phase is one of strong-coupling for all parameter regimes. Increasing the impurity correlation U only serves to reduce the width of the central peak at the cost of the appearance of side bands at energy scales of the order of U , but the resonance never dies. The situation is however different if the impurity is embedded in a correlated conduction bath with a non-trivial density of states. For the case of a conduction band with the DOS shown in the right of the figure below, the impurity hybridises into a reduced bandwidth because of the correlation on the lattice [245].

This difference in the type of conduction baths is utilised in dynamical mean-field theory to describe various phases of the bulk system. This is done through the DMFT algorithm: one starts with a non-interacting bath, but depending on the value of U , the conduction bath then gets modified and we ultimately end up with something that is different from what we started with. For small U , the bath does not change much and we retain the central resonance of the impurity spectral function. This then describes a metal in the bulk. For larger values of U , however, the bath changes significantly such that its density of states becomes non-constant. Above a critical U_c , the impurity spectral function gets gapped out, and that then describes the insulating phase in the bulk. *This leaves open the following question: What is the minimal correlation one can insert into the non-interacting bath (of a single-impurity Anderson model) that can capture both the metallic and insulating phases of the bulk model?*

We have recently studied an extended Anderson impurity model (e-SIAM) where we introduced an explicit Kondo coupling J and a local correlation W on the bath zeroth site, which is the site connected to the impurity (see [277] for some recent findings of non-local effective attractive interactions within the Hubbard model). The Hamiltonian of the e-SIAM for a half-filled impurity site is of the form

$$\mathcal{H}_{\text{E-S}} = \mathcal{H}_{\text{cbath}} + \mathcal{H}_{\text{imp}} + \mathcal{H}_{\text{imp-cbath}}, \quad (5.12)$$

where

- $\mathcal{H}_{\text{cbath}} = -\frac{1}{Z}t \sum_{i=0,1,\dots;\sigma} (c_{i,\sigma}^\dagger c_{i+1,\sigma} + \text{h.c.}) - \frac{1}{2}W (\hat{n}_{0\uparrow} - \hat{n}_{0\downarrow})^2$ is the Hamiltonian of the conduction bath consisting of a kinetic energy term and some local interaction terms on the zeroth site,
- $\mathcal{H}_{\text{imp}} = -\frac{U}{2} (\hat{n}_{d\uparrow} - \hat{n}_{d\downarrow})^2$ is the Hamiltonian for the localised impurity site, and
- $\mathcal{H}_{\text{imp-bath}} = JS_d \cdot \mathbf{S}_0 - V \sum_\sigma (c_{0\sigma}^\dagger c_{d\sigma} + \text{h.c.})$ describes the interaction between the impurity orbitals and the conduction bath.

Here, $c_{d\sigma}$ is the impurity electron operator, $c_{i\sigma}$ is the conduction bath electron operator, $c_{0,\sigma}$ is the bath zeroth site operator, \mathbf{S}_d is the impurity spin operator and $\mathbf{S}_0 = \sum_{\alpha,\beta} \sigma c_{0,\alpha}^\dagger c_{0,\beta}$ is the operator for the local spin in the conduction bath. We have found that the e-SIAM has a stable local moment phase for $W < -J/4$ with an antiferromagnetic Kondo coupling ($J > 0$). We have also shown that this model captures much of the phenomenology of the infinite dimensional Hubbard model (as discovered via DMFT), such as a second-order phase transition at $T = 0$ and the presence of an optical gap in the local spectral function beyond a certain value of interaction strength. Note that the impurity site and the conduction bath are both at half-filling.

5.2.3 Tiling towards a Hubbard-Heisenberg model with an embedded extended SIAM

In this subsection, we provide an explicit example of constructing a lattice model. We will consider a slightly more generalised version of the extended SIAM described in the previous section, where the impurity site coupled to the conduction bath purely through the s-wave channel. We will show that that model leads to a form of a Hubbard-Heisenberg model upon restoring translation invariance via repeated translation operations. The generalisation involve allowing an arbitrary filling on the impurity site and in the conduction bath, through two additional parameter: (i) a particle-hole asymmetry parameter η for the impurity site, (ii) a chemical potential for the conduction bath, and (iii) embedding the impurity into the lattice of the 2D conduction bath. This modified impurity model is shown in Fig. 6.1. The first term modifies the impurity Hamiltonian \mathcal{H}_{imp} into

$$\mathcal{H}_{\text{imp}} = -\frac{U}{2} (\hat{n}_{\mathbf{r}_d\uparrow} - \hat{n}_{\mathbf{r}_d\downarrow})^2 - \eta \sum_\sigma \hat{n}_{\mathbf{r}_d\sigma}. \quad (5.13)$$

where we have placed the impurity site at the position \mathbf{r}_d . The second term modifies the conduction bath Hamiltonian $\mathcal{H}_{\text{cbath}}$:

$$\mathcal{H}_{\text{cbath}} = -\frac{1}{\sqrt{Z}}t \sum_{\langle \mathbf{r}_i, \mathbf{r}_j \rangle \neq \mathbf{r}_d; \sigma} (c_{\mathbf{r}_i,\sigma}^\dagger c_{\mathbf{r}_j,\sigma} + \text{h.c.}) - \frac{1}{2Z}W \sum_{\mathbf{z} \in \text{NN}(\mathbf{r}_d)} (\hat{n}_{\mathbf{z},\uparrow} - \hat{n}_{\mathbf{z},\downarrow})^2 - \mu \sum_{\mathbf{r}_i \neq \mathbf{r}_d} \hat{n}_{\mathbf{r}_i,\sigma}, \quad (5.14)$$

where $\langle \mathbf{r}_i, \mathbf{r}_j \rangle \neq \mathbf{r}_d$ indicates that the sum is over all nearest-neighbour pairs of sites avoiding the impurity site \mathbf{r}_d .

In this notation, the interaction Hamiltonian can be written as

$$\mathcal{H}_{\text{imp-cbath}} = \frac{J}{Z} \sum_{\sigma, \sigma'} \sum_{\mathbf{z} \in \text{NN}(\mathbf{r}_d)} \mathbf{S}_{\mathbf{r}_d} \cdot \boldsymbol{\tau}_{\sigma, \sigma'} c_{\mathbf{z}, \sigma}^\dagger c_{\mathbf{z}, \sigma'} - \frac{V}{\sqrt{Z}} \sum_{\sigma} \sum_{\mathbf{z} \in \text{NN}(\mathbf{r}_d)} (c_{\mathbf{r}_d, \sigma}^\dagger c_{\mathbf{z}, \sigma} + h.c.) \quad (5.15)$$

where $\boldsymbol{\tau} = (\tau_x, \tau_y, \tau_z)$ is the vector of Pauli matrices. σ and σ' can be ± 1 and represent up and down configurations.

We now follow the prescription laid out in eq. 5.11. The tiled Hamiltonian can be written as

$$\mathcal{H}_{\text{tiled}} = \sum_{\mathbf{r}} T^\dagger(\mathbf{r} - \mathbf{r}_d) [\mathcal{H}_{\text{cbath}} + \mathcal{H}_{\text{imp}} + \mathcal{H}_{\text{imp-cbath}}] T(\mathbf{r} - \mathbf{r}_d). \quad (5.16)$$

Note that in comparison to eq. 5.11, we have dropped the sum over the zeroth sites, because our impurity model Hamiltonian (defined using eqs. 5.13 through 5.15) already contains a sum over these zeroth sites.

We consider the effect of the translation operations on each part of the Hamiltonian. We first have

$$\begin{aligned} & \sum_{\mathbf{r}} T^\dagger(\mathbf{r} - \mathbf{r}_d) \mathcal{H}_{\text{cbath}}(\mathbf{r}_d, \mathbf{z}) T(\mathbf{r} - \mathbf{r}_d) \\ &= \sum_{\mathbf{r}} T^\dagger(\mathbf{r} - \mathbf{r}_d) \left[-\frac{1}{\sqrt{Z}} t \sum_{\langle \mathbf{r}_i, \mathbf{r}_j \rangle \neq \mathbf{r}_d; \sigma} (c_{\mathbf{r}_i, \sigma}^\dagger c_{\mathbf{r}_j, \sigma} + \text{h.c.}) - \frac{W}{2Z} \sum_{\mathbf{z} \in \text{NN}(\mathbf{r}_d)} (\hat{n}_{\mathbf{z}, \uparrow} - \hat{n}_{\mathbf{z}, \downarrow})^2 - \mu \sum_{\mathbf{r}_i \neq \mathbf{r}_d} \hat{n}_{\mathbf{r}_i, \sigma} \right] T(\mathbf{r} - \mathbf{r}_d) \\ &= -\frac{1}{\sqrt{Z}} t \sum_{\langle \mathbf{r}_i, \mathbf{r}_j \rangle; \sigma} \sum_{\mathbf{r} \neq \mathbf{r}_i, \mathbf{r}_j} (c_{\mathbf{r}_i, \sigma}^\dagger c_{\mathbf{r}_j, \sigma} + \text{h.c.}) - \frac{W}{2Z} \sum_{\mathbf{r}} \sum_{\mathbf{z} \in \text{NN}(\mathbf{r})} (\hat{n}_{\mathbf{z}, \uparrow} - \hat{n}_{\mathbf{z}, \downarrow})^2 - \mu \sum_{\mathbf{r}_i} \sum_{\mathbf{r} \neq \mathbf{r}_i} \hat{n}_{\mathbf{r}_i, \sigma} \\ &= -\frac{1}{\sqrt{Z}} (N-2) t \sum_{\langle \mathbf{r}_i, \mathbf{r}_j \rangle; \sigma} (c_{\mathbf{r}_i, \sigma}^\dagger c_{\mathbf{r}_j, \sigma} + \text{h.c.}) - \frac{1}{2} W \sum_{\mathbf{r}} (\hat{n}_{\mathbf{r}, \uparrow} - \hat{n}_{\mathbf{r}, \downarrow})^2 - \mu(N-1) \sum_{\mathbf{r}} \hat{n}_{\mathbf{r}, \sigma} \end{aligned} \quad (5.17)$$

In the first step, the factor of Z is cancelled out by the trivial sum over \mathbf{r}_0 in the first and third terms. At the last step, the three terms simplified for the following reasons. The inequality $\langle \mathbf{r}_i, \mathbf{r}_j \rangle \neq \mathbf{r}$ in the first term ensures that each nearest-neighbour pair appears in $N-2$ instances of the auxiliary model, N being the total number of lattice sites; the two instances that do not contribute are the ones in which the impurity site itself is at \mathbf{r}_i or \mathbf{r}_j . For the second term, the double sum $\sum_{\mathbf{r}} \sum_{\mathbf{z} \in \text{NN}(\mathbf{r})}$ evaluates to $Z \sum_{\mathbf{r}}$, because each point on the lattice appears W times in the summation. This factor of W cancels the one in the denominator. In the third term, the inner summation simply evaluates to $N-1$, and we finally replace the dummy index \mathbf{r}_i with \mathbf{r} .

The next part is

$$\sum_{\mathbf{r}} T^\dagger(\mathbf{r} - \mathbf{r}_d) \mathcal{H}_{\text{imp}} T(\mathbf{r} - \mathbf{r}_d) = -\frac{U}{2} \sum_{\mathbf{r}} (\hat{n}_{\mathbf{r}\uparrow} - \hat{n}_{\mathbf{r}\downarrow})^2 - \eta \sum_{\mathbf{r}, \sigma} \hat{n}_{\mathbf{r}\sigma}. \quad (5.18)$$

This is obtained simply by replacing the impurity position \mathbf{r}_d with the translated position \mathbf{r} , generating a translation-invariant Hubbard term (the first term) and a finite chemical potential (second term).

We now consider the final term:

$$\begin{aligned}
& \sum_{\mathbf{r}} T^\dagger(\mathbf{r} - \mathbf{r}_d) \mathcal{H}_{\text{imp-cbath}} T(\mathbf{r} - \mathbf{r}_d) \\
&= \sum_{\mathbf{r}} T^\dagger(\mathbf{r} - \mathbf{r}_d) \left[\frac{1}{Z} \sum_{\mathbf{z} \in \text{NN}(\mathbf{r}_d)} \sum_{\sigma, \sigma'} J \mathbf{S}_{\mathbf{r}_d} \cdot \boldsymbol{\tau}_{\sigma, \sigma'} c_{\mathbf{z}, \sigma}^\dagger c_{\mathbf{z}, \sigma'} - \frac{1}{\sqrt{Z}} \sum_{\mathbf{z} \in \text{NN}(\mathbf{r}_d)} \sum_{\sigma} V (c_{\mathbf{r}_d, \sigma}^\dagger c_{\mathbf{z}, \sigma} + h.c.) \right] T(\mathbf{r} - \mathbf{r}_d) \\
&= \sum_{\mathbf{r}} \sum_{\mathbf{z} \in \text{NN}(\mathbf{r})} \left[\frac{1}{Z} \sum_{\sigma, \sigma'} J \mathbf{S}_{\mathbf{r}} \cdot \boldsymbol{\tau}_{\sigma, \sigma'} c_{\mathbf{z}, \sigma}^\dagger c_{\mathbf{z}, \sigma'} - \frac{1}{\sqrt{Z}} \sum_{\sigma} V (c_{\mathbf{r}_d, \sigma}^\dagger c_{\mathbf{z}, \sigma} + h.c.) \right] \\
&= \sum_{\langle \mathbf{r}_i, \mathbf{r}_j \rangle} \left[\frac{2}{Z} J \mathbf{S}_{\mathbf{r}_i} \cdot \mathbf{S}_{\mathbf{r}_j} - \frac{2}{\sqrt{Z}} V \sum_{\sigma} (c_{\mathbf{r}_i, \sigma}^\dagger c_{\mathbf{r}_j, \sigma} + h.c.) \right]
\end{aligned} \tag{5.19}$$

At the last step, each nearest-neighbour pair of sites $\mathbf{r}_i, \mathbf{r}_j$ appear 2 times in the summation, because any site is a member of two distinct nearest-neighbour pairs. We have also defined $\mathbf{S}_{\mathbf{r}_j} = \sum_{\sigma, \sigma'} \boldsymbol{\tau}_{\sigma, \sigma'} c_{\mathbf{z}, \sigma}^\dagger c_{\mathbf{z}, \sigma'}$ as the local spin operator.

The total tiled Hamiltonian is therefore

$$\begin{aligned}
\mathcal{H}_{\text{tiled}} &= -\frac{N-2}{\sqrt{Z}} t \sum_{\langle \mathbf{r}_i, \mathbf{r}_j \rangle, \sigma} (c_{\mathbf{r}_i, \sigma}^\dagger c_{\mathbf{r}_j, \sigma} + h.c.) - \mu(N-1) \sum_{\mathbf{r}} \hat{n}_{\mathbf{r}, \sigma} - \frac{1}{2} W \sum_{\mathbf{r}} (\hat{n}_{\mathbf{r}, \uparrow} - \hat{n}_{\mathbf{r}, \downarrow})^2 - \frac{U}{2} \sum_{\mathbf{r}} (\hat{n}_{\mathbf{r}\uparrow} - \hat{n}_{\mathbf{r}\downarrow})^2 - \dots \\
&\quad + \sum_{\langle \mathbf{r}_i, \mathbf{r}_j \rangle} \left[\frac{2}{Z} J \mathbf{S}_{\mathbf{r}_i} \cdot \mathbf{S}_{\mathbf{r}_j} - \frac{2}{\sqrt{Z}} V \sum_{\sigma} (c_{\mathbf{r}_i, \sigma}^\dagger c_{\mathbf{r}_j, \sigma} + h.c.) \right]
\end{aligned} \tag{5.20}$$

While constructing the tiled Hamiltonian, we have added extra copies of the non-interacting Hamiltonian $\mathcal{H}_{\text{cbath-nint}} = -\frac{1}{\sqrt{Z}} t \sum_{\langle \mathbf{r}_i, \mathbf{r}_j \rangle; \sigma} (c_{\mathbf{r}_i, \sigma}^\dagger c_{\mathbf{r}_j, \sigma} + h.c.) - \mu \sum_{\mathbf{r}} \hat{n}_{\mathbf{r}, \sigma}$ for the conduction bath (this results in the factors of $N-2$ and $N-1$ in front of the first and third terms). Upon removing these repeated terms, the tiled Hamiltonian becomes

$$\begin{aligned}
\mathcal{H}_{\text{tiled}} &= \sum_{\mathbf{r}} \mathcal{H}_{\text{aux}}(\mathbf{r}) - (N-3) \mathcal{H}_{\text{cbath-nint}} \\
&= -\frac{1}{\sqrt{Z}} (t+2V) \sum_{\langle \mathbf{r}_i, \mathbf{r}_j \rangle; \sigma} (c_{\mathbf{r}_i, \sigma}^\dagger c_{\mathbf{r}_j, \sigma} + h.c.) - \frac{1}{2} (U+W) \sum_{\mathbf{r}} (\hat{n}_{\mathbf{r}, \uparrow} - \hat{n}_{\mathbf{r}, \downarrow})^2 - (\eta+2\mu) \sum_{\mathbf{r}} \hat{n}_{\mathbf{r}, \sigma} + \frac{2}{Z} J \sum_{\langle \mathbf{r}_i, \mathbf{r}_j \rangle} \mathbf{S}_{\mathbf{r}_i} \cdot \mathbf{S}_{\mathbf{r}_j}
\end{aligned} \tag{5.21}$$

The result of the tiling operations is a Hubbard-Heisenberg model, of the form

$$\mathcal{H}_{\text{HH}} = -\frac{1}{\sqrt{Z}} \tilde{t} \sum_{\langle \mathbf{r}_i, \mathbf{r}_j \rangle; \sigma} (c_{\mathbf{r}_i, \sigma}^\dagger c_{\mathbf{r}_j, \sigma} + h.c.) - \tilde{\mu} \sum_{\mathbf{r}} \hat{n}_{\mathbf{r}, \sigma} + \frac{1}{Z} \tilde{J} \sum_{\langle \mathbf{r}_i, \mathbf{r}_j \rangle} \mathbf{S}_{\mathbf{r}_i} \cdot \mathbf{S}_{\mathbf{r}_j} - \frac{1}{2} \tilde{U} \sum_{\mathbf{r}} (\hat{n}_{\mathbf{r}, \uparrow} - \hat{n}_{\mathbf{r}, \downarrow})^2, \tag{5.22}$$

where the tilde symbol indicates that the parameters are for the lattice model (and not the auxiliary model). By comparing the tiled model and the general lattice model, the lattice model parameters and the auxiliary model parameters can be mapped to each other:

$$\tilde{t} = t + 2V, \quad \tilde{U} = U + W, \quad \tilde{\mu} = 2\mu + \eta, \quad \tilde{J} = 2J. \tag{5.23}$$

In summary, the appropriate method for reconstructing the lattice model Hamiltonian is therefore

$$\mathcal{H}_{\text{tiled}} = \sum_{\mathbf{r}} \mathcal{H}_{\text{aux}}(\mathbf{r}) - N \mathcal{H}_{\text{cbath-nint}}, \quad (5.24)$$

where we replaced $N - 3$ with N assuming a large number of sites. Using this, the extended-SIAM gets “expanded” into a Hubbard-Heisenberg model.

5.2.4 Translation symmetry and a conserved total momentum

From the form in eq. 5.24, the tiled Hamiltonian is symmetric under global many-body translations of the kind defined in eq. 5.6, by arbitrary lattice spacings:

$$\begin{aligned} T(\mathbf{a})^\dagger \sum_{\mathbf{r}} \mathcal{H}_{\text{aux}}(\mathbf{r}) T(\mathbf{a}) &= \sum_{\mathbf{r}} \mathcal{H}_{\text{aux}}(\mathbf{r} + \mathbf{a}) = \sum_{\mathbf{r}'} \mathcal{H}_{\text{aux}}(\mathbf{r}') \\ T(\mathbf{a})^\dagger \sum_{\mathbf{r}} \mathcal{H}_{\text{cbath-nint}} T(\mathbf{a}) &= \mathcal{H}_{\text{cbath-nint}} \\ \implies T(\mathbf{a})^\dagger \mathcal{H}_{\text{tiled}} T(\mathbf{a}) &= \mathcal{H}_{\text{tiled}}. \end{aligned} \quad (5.25)$$

In the first equation, we used the fact that the translation operator simply translates the auxiliary model at the position \mathbf{r} into another one at the position $\mathbf{r} + \mathbf{a}$. Since both are part of the summation, the summation remains unchanged. The second equation uses the fact that the Hamiltonian $\mathcal{H}_{\text{cbath-nint}}$ is that of a tight-binding model and is therefore translation-invariant. The fact that the Hamiltonian $\mathcal{H}_{\text{tiled}}$ commutes with the many-body translation operator implies that the total crystal momentum \vec{k} is a conserved quantity.

5.2.5 Form of the eigenstates: Bloch’s theorem

In the tight-binding approach to lattice problems, the full Hamiltonian is described by adding the localised Hamiltonians at each site, and the full eigenstate $|\Psi\rangle$ is then obtained by constructing linear combinations of the eigenstates $|\psi_i\rangle$ of the local Hamiltonians such that $|\Psi\rangle$ satisfies Bloch’s theorem: $|\Psi_{\mathbf{k}}\rangle = \sum_i e^{i\mathbf{k}\cdot\mathbf{r}_i} |\psi_i\rangle$, where \mathbf{r}_i sums over the positions of the local Hamiltonians. Bloch’s theorem ensures that eigenstates satisfy the following relation under a translation operation by an arbitrary number of lattice spacings $n\mathbf{a}$:

$$T^\dagger(n\mathbf{a}) |\Psi_{\mathbf{k}}\rangle = \sum_i e^{i\mathbf{k}\cdot\mathbf{r}_i} |\psi_{i+n}\rangle = e^{-in\mathbf{k}\cdot\mathbf{a}} |\Psi_{\mathbf{k}}\rangle \quad (5.26)$$

The definition and some properties of these global translation operations were provided in Appendix 5.4. It was shown there that they share eigenstates with the total momentum operator. In a lattice model, this continuous symmetry gets lowered to its discrete form: the total *crystal* momentum is conserved by any scattering process. As a result, the eigenstates can be labelled using the combined index $s = (\mathbf{k}, n)$ where \mathbf{k} is the total crystal momentum and n is a band index n .

The eigenstates $|\Psi_s\rangle$ ($s = (\mathbf{k}, n)$) of the lattice Hamiltonians obtained using eq. 5.24 also enjoy a *many-body* Bloch’s theorem [292], because the tiling procedure restores the translation symmetry of the Hamiltonian (as shown in eq. 5.25). This means that the *local* eigenstates $|\psi_n(\mathbf{r}_d)\rangle$ (with the impurity

located at an arbitrary position \mathbf{r}_d) of the unit cell auxiliary model Hamiltonian $\mathcal{H}_{\text{aux}}(\mathbf{r}_d)$ defined in eq. 5.5 can be used to construct eigenstates of the lattice Hamiltonian. The index $n (= 0, 1, \dots)$ in the subscript indicates that it is the n^{th} eigenstate of the auxiliary model.

The state $|\psi_n(\mathbf{r}_d)\rangle$ does not specify the position of the zeroth site, because the unit cell Hamiltonian $\mathcal{H}_{\text{aux}}(\mathbf{r}_d)$ itself has been averaged over \mathcal{Z} zeroth sites. Accordingly, we can express the averaged eigenstate $|\psi_n(\mathbf{r}_d)\rangle$ as

$$|\psi_n(\mathbf{r}_d)\rangle = \frac{1}{\sqrt{\mathcal{Z}}} \sum_{\mathbf{z} \in \text{NN}(\mathbf{r}_d)} |\psi_n(\mathbf{r}_d, \mathbf{z})\rangle , \quad (5.27)$$

where $|\psi_n(\mathbf{r}_d, \mathbf{z})\rangle$ is an auxiliary model eigenstate with the impurity and zeroth sites placed at \mathbf{r}_d and \mathbf{z} . With this in mind, the following unnormalised combination of the auxiliary model eigenstates satisfies a many-particle equivalent of Bloch's theorem [292]:

$$|\Psi_s\rangle \equiv |\Psi_{\mathbf{k},n}\rangle = \frac{1}{\sqrt{N}} \sum_{\mathbf{r}_d} e^{i\mathbf{k} \cdot \mathbf{r}_d} |\psi_n(\mathbf{r}_d)\rangle = \frac{1}{\sqrt{\mathcal{Z}N}} \sum_{\mathbf{r}_d} \sum_{\mathbf{z} \in \text{NN}(\mathbf{r}_d)} e^{i\mathbf{k} \cdot \mathbf{r}_d} |\psi_n(\mathbf{r}_d, \mathbf{z})\rangle , \quad (5.28)$$

where N is the total number of lattice sites and \mathbf{r}_d is summed over all lattice spacings. The set of $n = 0$ states form the lowest band in the spectrum of the lattice, while higher values of n produce the more energetic bands. The ground state $s = s_0$ is obtained by setting \mathbf{k} and n to 0:

$$|\Psi_{\text{gs}}\rangle \equiv |\Psi_{s_0}\rangle = \frac{1}{\sqrt{N}} \sum_{\mathbf{r}_d} e^{i\mathbf{k} \cdot \mathbf{r}_d} |\psi_{\text{gs}}(\mathbf{r}_d)\rangle = \frac{1}{\sqrt{\mathcal{Z}N}} \sum_{\mathbf{r}_d} \sum_{\mathbf{z} \in \text{NN}(\mathbf{r}_d)} e^{i\mathbf{k} \cdot \mathbf{r}_d} |\psi_{\text{gs}}(\mathbf{r}_d, \mathbf{z})\rangle \quad (5.29)$$

5.3 Mapping Static and Dynamic Correlations from the Auxiliary Model to the Lattice Model

5.3.1 One-Particle Greens Functions: Momentum-space

In the previous part, we proposed a form for the ground state $|\Psi_{\text{gs}}\rangle$ of the bulk Hamiltonian in terms of the ground-states $|\psi_{\text{gs}}\rangle$ of the auxiliary models. In this section, we will relate one-particle Greens functions of the bulk lattice to those of the auxiliary model. We will assume that the auxiliary model Hilbert space has the same dimensions as that of the bulk lattice model. We define the retarded time-domain lattice k -space Greens function at zero temperature as

$$\tilde{G}(\mathbf{K}\sigma; t) = -i\theta(t) \langle \Psi_{\text{gs}} | \left\{ c_{\mathbf{K}\sigma}(t), c_{\mathbf{K}\sigma}^\dagger \right\} | \Psi_{\text{gs}} \rangle . \quad (5.30)$$

where the bulk Hamiltonian H_{tiled} leads to the dynamics of the annihilation operators at time t :

$$c_{\mathbf{K}\sigma}(t) = e^{itH_{\text{tiled}}} c_{\mathbf{K}\sigma} e^{-itH_{\text{tiled}}} . \quad (5.31)$$

We now proceed to simplify one of the terms of the anticommutator (for simplicity of notation):

$$\langle \Psi_{\text{gs}} | c_{\mathbf{K}\sigma}(t) c_{\mathbf{K}\sigma}^\dagger | \Psi_{\text{gs}} \rangle = \frac{1}{N^2} \sum_{\vec{r}, \vec{\Delta}} e^{-i\mathbf{K}_0 \cdot \vec{\Delta}} \langle \psi_0(\vec{r} + \vec{\Delta}) | c_{\mathbf{K}\sigma}(t) c_{\mathbf{K}\sigma}^\dagger | \psi_0(\vec{r}) \rangle . \quad (5.32)$$

To make further progress, we insert the identity resolution $1 = \sum_s |\Psi_s\rangle \langle \Psi_s|$ in between the two operators, where $s = (\mathbf{k}, n)$ sums over all eigenstates (with energies \tilde{E}_s). The lattice eigenstates themselves can again be written in terms of those of the auxiliary model, using eq. 5.28:

$$|\Psi_s\rangle \langle \Psi_s| = \sum_{\vec{r}', \vec{\Delta}'} e^{i\vec{k}\cdot\vec{\Delta}'} |\psi_n(\vec{r}' + \vec{\Delta}')\rangle \langle \psi_n(\vec{r}')| . \quad (5.33)$$

With this, eq. 5.32 becomes

$$\langle \Psi_{\text{gs}} | c_{\mathbf{K}\sigma}(t) c_{\mathbf{K}\sigma}^\dagger | \Psi_{\text{gs}} \rangle = \frac{1}{N^2} \sum_s \sum_{\vec{r}, \vec{\Delta}} \sum_{\vec{r}', \vec{\Delta}'} e^{-i\vec{k}_0 \cdot \vec{\Delta}} e^{i\vec{k} \cdot \vec{\Delta}'} \langle \psi_0(\vec{r} + \vec{\Delta}) | c_{\mathbf{K}\sigma}(t) | \psi_n(\vec{r}' + \vec{\Delta}') \rangle \langle \psi_n(\vec{r}') | c_{\mathbf{K}\sigma}^\dagger | \psi_0(\vec{r}) \rangle . \quad (5.34)$$

In order to bring this expression closer to the form of an auxiliary model Greens function, we would like to transform the initial and final states $|\psi(\vec{r})\rangle$ and $|\psi(\vec{r} + \vec{\Delta})\rangle$ to apply to the same auxiliary model. This is done by using the relation: $|\psi(\vec{r} + \vec{\Delta})\rangle = T^\dagger(\vec{\Delta}) |\psi(\vec{r})\rangle$, where $T^\dagger(\vec{\Delta})$ translates all lattice sites by the vector $\vec{\Delta}$.

$$\langle \psi_0(\vec{r} + \vec{\Delta}) | c_{\mathbf{K}\sigma}(t) | \psi_n(\vec{r}' + \vec{\Delta}') \rangle = \langle \psi_0(\vec{r}) | T(\vec{\Delta}) c_{\mathbf{K}\sigma}(t) | \psi_n(\vec{r}' + \vec{\Delta}') \rangle = \langle \psi_0(\vec{r}) | T(\vec{\Delta}) c_{\mathbf{K}\sigma}(t) T^\dagger(\vec{\Delta}) | \psi_n(\vec{r}' + \vec{\Delta}' - \vec{\Delta}) \rangle \quad (5.35)$$

The effect of the translation operators on the k -space annihilation operator can be easily ascertained by transforming it to real-space, using the Fourier transform definition

$$c(\mathbf{K}) = \frac{1}{\sqrt{N}} \sum_{\mathbf{r}} e^{-i\mathbf{K}\cdot\mathbf{r}} c(\mathbf{r}) . \quad (5.36)$$

Upon applying this, we get

$$T(\vec{a}) c(\mathbf{K}) T^\dagger(\vec{a}) = \frac{1}{N} \sum_{\mathbf{r}} e^{-i\mathbf{K}\cdot\mathbf{r}} T(\vec{a}) c(\mathbf{r}) T^\dagger(\vec{a}) = \frac{1}{N} \sum_{\mathbf{r}} e^{-i\mathbf{K}\cdot\mathbf{r}} c(\mathbf{r} - \vec{a}) = e^{-i\mathbf{K}\cdot\vec{a}} c(\mathbf{K}) . \quad (5.37)$$

Using this identity on the above expression gives

$$\langle \psi_0(\vec{r} + \vec{\Delta}) | c_{\mathbf{K}\sigma}(t) | \psi_n(\vec{r}' + \vec{\Delta}') \rangle = e^{-i\mathbf{K}\cdot\vec{\Delta}} \langle \psi_0(\vec{r}) | c_{\mathbf{K}\sigma}(t) | \psi_n(\vec{r}' + \vec{\Delta}' - \vec{\Delta}) \rangle \quad (5.38)$$

Finally replacing this all the way back into eq. 5.34 gives

$$\langle \Psi_{\text{gs}} | c_{\mathbf{K}\sigma}(t) c_{\mathbf{K}\sigma}^\dagger | \Psi_{\text{gs}} \rangle = \frac{1}{N^2} \sum_s \sum_{\vec{r}, \vec{\Delta}} \sum_{\vec{r}', \vec{\Delta}'} e^{-i(\vec{k}_0 + \mathbf{K}) \cdot \vec{\Delta}} e^{i\vec{k} \cdot \vec{\Delta}'} \langle \psi_0(\vec{r}) | c_{\mathbf{K}\sigma}(t) | \psi_n(\vec{r}' + \vec{\Delta}' - \vec{\Delta}) \rangle \langle \psi_n(\vec{r}') | c_{\mathbf{K}\sigma}^\dagger | \psi_0(\vec{r}) \rangle . \quad (5.39)$$

To further unify the operators, we make the substitution $\vec{\Delta}' \rightarrow \vec{\Delta}' + \vec{\Delta}$, leading to the expression

$$\langle \Psi_{\text{gs}} | c_{\mathbf{K}\sigma}(t) c_{\mathbf{K}\sigma}^\dagger | \Psi_{\text{gs}} \rangle = \frac{1}{N^2} \sum_s \sum_{\vec{r}, \vec{\Delta}} \sum_{\vec{r}', \vec{\Delta}'} e^{-i(\vec{k}_0 + \mathbf{K} - \vec{k}) \cdot \vec{\Delta}} e^{i\vec{k} \cdot \vec{\Delta}'} \langle \psi_0(\vec{r}) | c_{\mathbf{K}\sigma}(t) | \psi_n(\vec{r}' + \vec{\Delta}') \rangle \langle \psi_n(\vec{r}') | c_{\mathbf{K}\sigma}^\dagger | \psi_0(\vec{r}) \rangle . \quad (5.40)$$

The sum over $\vec{\Delta}$ can now be carried out, resulting in

$$\langle \Psi_{\text{gs}} | c_{\mathbf{K}\sigma}(t) c_{\mathbf{K}\sigma}^\dagger | \Psi_{\text{gs}} \rangle = \frac{1}{N} \sum_n \sum_{\vec{r}, \vec{r}', \vec{\Delta}'} e^{i(\vec{k}_0 + \mathbf{K}) \cdot \vec{\Delta}'} \langle \psi_0(\vec{r}) | c_{\mathbf{K}\sigma}(t) | \psi_n(\vec{r}' + \vec{\Delta}') \rangle \langle \psi_n(\vec{r}') | c_{\mathbf{K}\sigma}^\dagger | \psi_0(\vec{r}) \rangle , \quad (5.41)$$

where the sum over $s = (\vec{k}, n)$ has been reduced to a sum over the auxiliary model eigenstate index n because of the Kronecker delta $\delta(\vec{k}_0 + \mathbf{K} - \vec{k})$. This can be further simplified by splitting the sum over $\vec{\Delta}'$ into positive and negative parts and then making the transformation $\vec{r}' \rightarrow \vec{r}' + \vec{\Delta}'$:

$$\begin{aligned} \sum_{\vec{r}', \vec{\Delta}'} e^{i(\vec{k}_0 + \mathbf{K}) \cdot \vec{\Delta}'} |\psi_n(\vec{r}' + \vec{\Delta}')\rangle \langle \psi_n(\vec{r}')| &= \frac{1}{2} \sum_{\vec{r}', \vec{\Delta}'} \left[e^{i(\vec{k}_0 + \mathbf{K}) \cdot \vec{\Delta}'} |\psi_n(\vec{r}' + \vec{\Delta}')\rangle \langle \psi_n(\vec{r}')| + e^{-i(\vec{k}_0 + \mathbf{K}) \cdot \vec{\Delta}'} |\psi_n(\vec{r}' - \vec{\Delta}')\rangle \langle \psi_n(\vec{r}')| \right] \\ &= \frac{1}{2} \sum_{\vec{r}', \vec{\Delta}'} \left[e^{i(\vec{k}_0 + \mathbf{K}) \cdot \vec{\Delta}'} |\psi_n(\vec{r}' + \vec{\Delta}')\rangle \langle \psi_n(\vec{r}')| + e^{-i(\vec{k}_0 + \mathbf{K}) \cdot \vec{\Delta}'} |\psi_n(\vec{r}')\rangle \langle \psi_n(\vec{r}' + \vec{\Delta}')| \right] \end{aligned} \quad (5.42)$$

For each pair of \vec{r}' and $\vec{\Delta}'$, the term within the box brackets has the form of a two-level Hamiltonian between the states $|\psi_n(\vec{r}')\rangle$ and $|\psi_n(\vec{r}' + \vec{\Delta}')\rangle$, with a tunnelling amplitude $e^{i(\vec{k}_0 + \mathbf{K}) \cdot \vec{\Delta}'}$. The term can therefore be written in the eigenbasis of this Hamiltonian:

$$\sum_{\vec{r}', \vec{\Delta}'} e^{i(\vec{k}_0 + \mathbf{K}) \cdot \vec{\Delta}'} |\psi_n(\vec{r}' + \vec{\Delta}')\rangle \langle \psi_n(\vec{r}')| = \frac{1}{2} \sum_{\vec{r}', \vec{\Delta}'} \left[|\chi_n^+(\vec{r}', \vec{\Delta}')\rangle \langle \chi_n^+(\vec{r}', \vec{\Delta}')| - |\chi_n^-(\vec{r}', \vec{\Delta}')\rangle \langle \chi_n^-(\vec{r}', \vec{\Delta}')| \right], \quad (5.43)$$

where $|\chi_n^\pm(\vec{r}', \vec{\Delta}')\rangle = \frac{1}{\sqrt{2}} \left[|\psi_n(\vec{r}')\rangle \pm e^{i(\vec{k}_0 + \mathbf{K}) \cdot \vec{\Delta}'} |\psi_n(\vec{r}' + \vec{\Delta}')\rangle \right]$ are the eigenvectors of the tunnelling Hamiltonian with eigenvalues ± 1 respectively. With this basis transformation, we can rewrite eq. 5.41 as

$$\langle \Psi_{\text{gs}} | c_{\mathbf{K}\sigma}(t) c_{\mathbf{K}\sigma}^\dagger | \Psi_{\text{gs}} \rangle = \frac{1}{2N} \sum_n \sum_{\vec{r}, \vec{r}', \vec{\Delta}'} \langle \psi_0(\vec{r}) | c_{\mathbf{K}\sigma}(t) \left[|\chi_n^+(\vec{r}', \vec{\Delta}')\rangle \langle \chi_n^+(\vec{r}', \vec{\Delta}')| - |\chi_n^-(\vec{r}', \vec{\Delta}')\rangle \langle \chi_n^-(\vec{r}', \vec{\Delta}')| \right] c_{\mathbf{K}\sigma}^\dagger | \psi_0(\vec{r}') \rangle. \quad (5.44)$$

In order to make the expression more transparent, we consider the various components separately:

$\vec{r}' = \vec{r}$, $\vec{\Delta}' = 0$:

$$\langle \Psi_{\text{gs}} | c_{\mathbf{K}\sigma}(t) c_{\mathbf{K}\sigma}^\dagger | \Psi_{\text{gs}} \rangle \rightarrow \frac{1}{N} \sum_n \sum_{\vec{r}} \langle \psi_0(\vec{r}) | c_{\mathbf{K}\sigma}(t) | \psi_n(\vec{r}) \rangle \langle \psi_n(\vec{r}) | c_{\mathbf{K}\sigma}^\dagger | \psi_0(\vec{r}) \rangle. \quad (5.45)$$

These terms represent those contributions to the total Greens function that arise from excitations that start and end at a specific auxiliary model (at \vec{r}), and also evolve dynamically within the same auxiliary model. These terms are therefore exactly equal to the auxiliary model Greens function at position \vec{r} , and are the most dominant contribution due to the localised nature of the impurity model.

$\vec{r}' \neq \vec{r}$, $\vec{\Delta}' = 0$:

$$\langle \Psi_{\text{gs}} | c_{\mathbf{K}\sigma}(t) c_{\mathbf{K}\sigma}^\dagger | \Psi_{\text{gs}} \rangle \rightarrow \frac{1}{N} \sum_n \sum_{\vec{r}, \vec{r}' \neq \vec{r}} \langle \psi_0(\vec{r}) | c_{\mathbf{K}\sigma}(t) | \psi_n(\vec{r}') \rangle \langle \psi_n(\vec{r}') | c_{\mathbf{K}\sigma}^\dagger | \psi_0(\vec{r}) \rangle. \quad (5.46)$$

These are more non-local contributions; they involve excitations whose time evolution is governed by a different auxiliary model than the terminal one. These contributions are highly suppressed in the Kondo screened phase because of the strong entanglement of the singlet ground state.

$\vec{r}' \neq \vec{r}$, $\vec{\Delta}' \neq 0$:

$$\langle \Psi_{\text{gs}} | c_{\mathbf{K}\sigma}(t) c_{\mathbf{K}\sigma}^\dagger | \Psi_{\text{gs}} \rangle \rightarrow \frac{1}{2N} \sum_n \sum_{\vec{r}, \vec{r}' \neq \vec{r}, \vec{\Delta}' \neq 0} \langle \psi_0(\vec{r}) | c_{\mathbf{K}\sigma}(t) \left[|\chi_n^+(\vec{r}', \vec{\Delta}')\rangle \langle \chi_n^+(\vec{r}', \vec{\Delta}')| - |\chi_n^-(\vec{r}', \vec{\Delta}')\rangle \langle \chi_n^-(\vec{r}', \vec{\Delta}')| \right] c_{\mathbf{K}\sigma}^\dagger | \Psi_{\text{gs}} \rangle . \quad (5.47)$$

These are the most non-local contributions; they involve excitations whose time evolution is governed by three different auxiliary models. Accordingly, these contributions are further suppressed.

We now consider each type of contribution in more detail.

5.3.2 $\vec{r}' = \vec{r}$, $\vec{\Delta}' = 0$

Restricting ourselves to just the single auxiliary model contributions gives

$$\langle \Psi_{\text{gs}} | c_{\mathbf{K}\sigma}(t) c_{\mathbf{K}\sigma}^\dagger | \Psi_{\text{gs}} \rangle = \frac{1}{N} \sum_n \sum_{\vec{r}} \langle \psi_0(\vec{r}) | c_{\mathbf{K}\sigma}(t) | \psi_n(\vec{r}) \rangle \langle \psi_n(\vec{r}) | c_{\mathbf{K}\sigma}^\dagger | \psi_0(\vec{r}) \rangle . \quad (5.48)$$

We first consider more carefully the transition operator $\mathcal{T}_{\mathbf{K}\sigma} = c_{\mathbf{K}\sigma}$ for the 1-particle excitation giving rise to the above Greens function. Within our auxiliary model approach, gapless excitations within the lattice model are represented by gapless excitations of the impurity site, specifically those that screen the impurity site and form the local Fermi liquid. As a result, the uncoordinated \mathcal{T} -matrix for the lattice model must be replaced by a combined \mathcal{T} -matrix within the impurity model that captures those gapless excitations that occur in connection with the impurity, and projects out the uncorrelated excitations that take place even when the impurity site is decoupled from the bath.

In order to construct this auxiliary model \mathcal{T} -matrix, we note that the impurity site can have both spin and charge excitations. Considering both excitations, the modified \mathcal{T} -matrix that constructs k -space excitations in correlation with the impurity site are

$$\mathcal{T}_{\mathbf{K}\sigma} = c_{\mathbf{K}\sigma} \left(\sum_{\sigma'} c_{d\sigma}^\dagger + \text{h.c.} \right) + c_{\mathbf{K}\sigma} (S_d^+ + \text{h.c.}) , \quad (5.49)$$

leading to the updated expression for the complete Greens function:

$$\tilde{G}(\mathbf{K}\sigma; t) = -i\theta(t) \frac{1}{N} \sum_n \sum_{\vec{r}} \langle \psi_0(\vec{r}) | \left[\mathcal{T}_{\mathbf{K}\sigma}(t) | \psi_n(\vec{r}) \rangle \langle \psi_n(\vec{r}) | \mathcal{T}_{\mathbf{K}\sigma}^\dagger + \mathcal{T}_{\mathbf{K}\sigma}^\dagger | \psi_n(\vec{r}) \rangle \langle \psi_n(\vec{r}) | \mathcal{T}_{\mathbf{K}\sigma}(t) \right] | \psi_0(\vec{r}) \rangle . \quad (5.50)$$

In order to convert this into a more useful form, we use eq. 5.31:

$$\langle \psi_0(\vec{r}) | \mathcal{T}_{\mathbf{K}\sigma}(t) | \psi_n(\vec{r}) \rangle = \langle \psi_0(\vec{r}) | e^{itH_{\text{tiled}}} \mathcal{T}_{\mathbf{K}\sigma} e^{-itH_{\text{tiled}}} | \psi_n(\vec{r}) \rangle . \quad (5.51)$$

Guided by the relation in eq. 5.24 $H_{\text{tiled}} = \sum_{\mathbf{r}} \mathcal{H}_{\text{aux}}(\mathbf{r}) - N\mathcal{H}_{\text{cbath-nint}}$ between the tiled Hamiltonian and the auxiliary model, we assume that the operator $e^{-itH_{\text{tiled}}}$ acting on the state $|\psi_n(\vec{r})\rangle$ involves the excitation energy E_n of only a single auxiliary model. Specifically, E_n is the energy of the eigenstate $|\psi_n(\vec{r})\rangle$. This is supported by the fact that this class of contributions to the Greens function is completed within a single auxiliary model. Accordingly, we replace H_{tiled} with $E_n - \varepsilon_{\mathbf{k}}$, where $\varepsilon_{\mathbf{k}}$ are the eigenenergies of the non-interacting conduction bath $\mathcal{H}_{\text{cbath-nint}}$ and \mathbf{k} is the crystal momentum associated with the state $|\psi_n(\vec{r})\rangle$. This momentum was found to be constrained to $\mathbf{k}_0 + \mathbf{K}$ below eq. 5.41. In the same way,

the action of H_{tiled} on the terminal state $|\psi_0(\vec{r})\rangle$ gives $E_0 - \varepsilon_{\mathbf{k}_0}$, where E_0 is the ground state energy of the auxiliary model at \mathbf{r} . Applying this to our expression gives

$$\tilde{G}(\mathbf{K}\sigma; t) = -i\theta(t) \frac{1}{N} \sum_n \sum_{\vec{r}} \langle \psi_0(\vec{r}) | \left[e^{-it\omega_p} \mathcal{T}_{\mathbf{K}\sigma}(t) |\psi_n(\vec{r})\rangle \langle \psi_n(\vec{r})| \mathcal{T}_{\mathbf{K}\sigma}^\dagger + e^{-it\omega_h} \mathcal{T}_{\mathbf{K}\sigma}^\dagger |\psi_n(\vec{r})\rangle \langle \psi_n(\vec{r})| \mathcal{T}_{\mathbf{K}\sigma}(t) \right] |\psi_0(\vec{r})\rangle . \quad (5.52)$$

where $\omega_p = (E_n - \varepsilon_{\mathbf{k}_0 + \mathbf{K}}) - (E_0 - \varepsilon_{\mathbf{k}_0})$ is the particle-excitation cost and $\omega_h = -\omega_p$ is the hole-excitation cost. We now introduce the Fourier transform $g(\omega) = \int dt e^{i\omega T} f(t)$ to obtain the frequency-domain Greens function in its spectral representation:

$$\tilde{G}(\mathbf{K}\sigma; \omega) = \frac{1}{N} \sum_{\vec{r}} \sum_n \langle \psi_0(\vec{r}) | \left[\frac{1}{\omega - \omega_p} \mathcal{T}_{\mathbf{K}\sigma} |\psi_n(\vec{r})\rangle \langle \psi_n(\vec{r})| \mathcal{T}_{\mathbf{K}\sigma}^\dagger + \frac{1}{\omega - \omega_h} \mathcal{T}_{\mathbf{K}\sigma}^\dagger |\psi_n(\vec{r})\rangle \langle \psi_n(\vec{r})| \mathcal{T}_{\mathbf{K}\sigma} \right] |\psi_0(\vec{r})\rangle . \quad (5.53)$$

For each value of \vec{r} , the term within that summation is simply the Greens function (for the excitation $\mathcal{T}_{\mathbf{K}\sigma}$) of the auxiliary model with the impurity site at \vec{r} . Since all these impurity models are physically equivalent (because of translation invariance), we can replace the average over \mathbf{r} with the value obtained from any one auxiliary model.

$$\begin{aligned} \tilde{G}(\mathbf{K}\sigma; \omega) &= \sum_n \langle \psi_0 | \left[\frac{1}{\omega - \omega_p} \mathcal{T}_{\mathbf{K}\sigma} |\psi_n\rangle \langle \psi_n| \mathcal{T}_{\mathbf{K}\sigma}^\dagger + \frac{1}{\omega - \omega_h} \mathcal{T}_{\mathbf{K}\sigma}^\dagger |\psi_n\rangle \langle \psi_n| \mathcal{T}_{\mathbf{K}\sigma} \right] |\psi_0\rangle \\ &= G^>(\mathcal{T}_{\mathbf{K}\sigma}^\dagger, \omega - \varepsilon_{\mathbf{k}_0 + \mathbf{K}}) + G^<(\mathcal{T}_{\mathbf{K}\sigma}^\dagger, \omega + \varepsilon_{\mathbf{k}_0 + \mathbf{K}}) , \end{aligned} \quad (5.54)$$

where $G^>(\mathcal{O}^\dagger, t) = -i \langle \mathcal{O}(t) \mathcal{O}^\dagger \rangle$ and $G^<(\mathcal{O}^\dagger, t) = -i \langle \mathcal{O}^\dagger \mathcal{O}(t) \rangle$ are the greater and lesser Greens function for the auxiliary model.

5.3.3 $\vec{r}' \neq \vec{r}$, $\vec{\Delta}' = 0$

Allowing for more non-local contributions, and updating the \mathcal{T} -matrix similar to the previous section gives the following Greens function:

$$\tilde{G}(\mathbf{K}\sigma; t) = -i\theta(t) \frac{1}{N} \sum_n \sum_{\vec{r}, \vec{r}'} \langle \psi_0(\vec{r}) | \left[\mathcal{T}_{\mathbf{K}\sigma}(t) |\psi_n(\vec{r}')\rangle \langle \psi_n(\vec{r}')| \mathcal{T}_{\mathbf{K}\sigma}^\dagger + \mathcal{T}_{\mathbf{K}\sigma}^\dagger |\psi_n(\vec{r}')\rangle \langle \psi_n(\vec{r}')| \mathcal{T}_{\mathbf{K}\sigma}(t) \right] |\psi_0(\vec{r})\rangle . \quad (5.55)$$

In order to allow computations within a single auxiliary model, we replace the translated state $|\psi_n(\vec{r}')\rangle$ with $T^\dagger(\vec{r} \rightarrow \vec{r}') |\psi_n(\vec{r})\rangle$, where $T^\dagger(\vec{r} - \vec{r}')$ translates all sites by the vector $\vec{r}' - \vec{r}$. This leads to a modified correlation function but within a single auxiliary model:

$$\begin{aligned} \tilde{G}(\mathbf{K}\sigma; t) &= -i\theta(t) \frac{1}{N} \sum_{n, \vec{r}, \vec{r}'} \langle \psi_0(\vec{r}) | \left[\mathcal{T}_{\mathbf{K}\sigma}(t) T^\dagger(\vec{r} - \vec{r}') |\psi_n(\vec{r})\rangle \langle \psi_n(\vec{r})| T(\vec{r} - \vec{r}') \mathcal{T}_{\mathbf{K}\sigma}^\dagger + \right. \\ &\quad \left. \mathcal{T}_{\mathbf{K}\sigma}^\dagger T^\dagger(\vec{r} - \vec{r}') |\psi_n(\vec{r})\rangle \langle \psi_n(\vec{r})| T(\vec{r} - \vec{r}') \mathcal{T}_{\mathbf{K}\sigma}(t) \right] |\psi_0(\vec{r})\rangle . \end{aligned} \quad (5.56)$$

In fact, by the same arguments as in the previous section, we can obtain a frequency-resolved Greens function:

$$\begin{aligned} \tilde{G}(\mathbf{K}\sigma; \omega) &= \sum_n \langle \psi_0 | \left[\frac{1}{\omega - \omega_p} \mathcal{T}_{\mathbf{K}\sigma}(t) T^\dagger(\vec{r} - \vec{r}') |\psi_n\rangle \langle \psi_n| T(\vec{r} - \vec{r}') \mathcal{T}_{\mathbf{K}\sigma}^\dagger + \right. \\ &\quad \left. \frac{1}{\omega - \omega_h} \mathcal{T}_{\mathbf{K}\sigma}^\dagger T^\dagger(\vec{r} - \vec{r}') |\psi_n\rangle \langle \psi_n| T(\vec{r} - \vec{r}') \mathcal{T}_{\mathbf{K}\sigma}(t) \right] |\psi_0\rangle . \end{aligned} \quad (5.57)$$

To obtain the above, we used the fact that H_{tiled} commutes with the translation operator.

5.3.4 Equal-Time Ground State Correlators: Real-space

We first consider a real-space operator $\mathcal{O}(\mathbf{r} + \Delta)\mathcal{O}^\dagger(\mathbf{r})$ that quantifies the presence of correlations over a distance Δ . The correlation function itself is given by the expectation value of this operator in the ground state:

$$C_{\mathcal{O}}(\Delta) = \langle \Psi_{\text{gs}} | \mathcal{O}(\mathbf{r} + \Delta)\mathcal{O}^\dagger(\mathbf{r}) | \Psi_{\text{gs}} \rangle . \quad (5.58)$$

To obtain a tractable expression for this, we first replace the full ground state with its expression in terms of the auxiliary model ground states (eq. 5.29):

$$C_{\mathcal{O}}(\Delta) = \frac{1}{N} \sum_{\mathbf{r}_1, \mathbf{r}'} \langle \psi_{\text{gs}}(\mathbf{r}_1 + \mathbf{r}' + \mathbf{r}_c + \mathbf{r}) | \mathcal{O}(\mathbf{r} + \Delta)\mathcal{O}^\dagger(\mathbf{r}) | \psi_{\text{gs}}(\mathbf{r}_1 + \mathbf{r}_c + \mathbf{r}) \rangle e^{-i\mathbf{k}_0 \cdot (\mathbf{r}_1 - \mathbf{r}_2)} , \quad (5.59)$$

where \mathbf{r}_1 and $\mathbf{r}_1 + \mathbf{r}'$ are the positions of the incoming and outgoing auxiliary model states, relative to $\mathbf{r}_c + \mathbf{r}$, and \mathbf{k}_0 is the crystal momentum of the ground state (which we will immediately set to zero). In order to convert the incoming and outgoing states into the same auxiliary mode at a reference location \mathbf{r}_c (which would then allow computations purely within a single auxiliary model), we use the relation: $|\psi_{\text{gs}}(\mathbf{x})\rangle = T^\dagger(\mathbf{x} - \mathbf{r}_c)\psi_{\text{gs}}|\psi(\mathbf{r}_c)\rangle$. Substituting this appropriately for both the auxiliary model states gives:

$$\begin{aligned} C_{\mathcal{O}}(\Delta) &= \frac{1}{N} \sum_{\mathbf{r}_1, \mathbf{r}'} \langle \psi_{\text{gs}}(\mathbf{r}_c) | T(\mathbf{r}_1 + \mathbf{r}' + \mathbf{r}) \mathcal{O}(\mathbf{r} + \Delta)\mathcal{O}^\dagger(\mathbf{r}) T^\dagger(\mathbf{r}_1 + \mathbf{r}) | \psi_{\text{gs}}(\mathbf{r}_c) \rangle \\ &= \frac{1}{N} \sum_{\mathbf{r}_1, \mathbf{r}'} \langle \psi_{\text{gs}}(\mathbf{r}_c) | T(\mathbf{r}') \mathcal{O}(\Delta - \mathbf{r}_1)\mathcal{O}^\dagger(-\mathbf{r}_1) | \psi_{\text{gs}}(\mathbf{r}_c) \rangle \\ &= \frac{1}{N} \sum_{\mathbf{r}_1, \mathbf{r}'} \langle \psi_{\text{gs}}(\mathbf{r}_c + \mathbf{r}') | \mathcal{O}(\Delta - \mathbf{r}_1)\mathcal{O}^\dagger(-\mathbf{r}_1) | \psi_{\text{gs}}(\mathbf{r}_c) \rangle . \end{aligned} \quad (5.60)$$

As a final cosmetic change, we transform $\mathbf{r}_1 \rightarrow -\mathbf{r}$:

$$C_{\mathcal{O}}(\Delta) = \frac{1}{N} \sum_{\mathbf{r}, \mathbf{r}'} \langle \psi_{\text{gs}}(\mathbf{r}_c + \mathbf{r}') | \mathcal{O}(\Delta + \mathbf{r})\mathcal{O}^\dagger(\mathbf{r}) | \psi_{\text{gs}}(\mathbf{r}_c) \rangle . \quad (5.61)$$

Like in the Greens function calculation, we now consider the various kinds of contributions separately.

Intra-auxiliary model contributions: $\mathbf{r}' = 0$

These terms describe excitations that start and propagate within the same auxiliary model, upto a distance Δ :

$$C_{\mathcal{O}}(\Delta) \rightarrow \frac{1}{N} \sum_{\mathbf{r}} \langle \psi_{\text{gs}}(\mathbf{r}_c) | \mathcal{O}(\Delta + \mathbf{r})\mathcal{O}^\dagger(\mathbf{r}) | \psi_{\text{gs}}(\mathbf{r}_c) \rangle . \quad (5.62)$$

With an eye towards introducing the impurity operators into the correlations, we insert a complete basis defined by the eigenstates $\{|\psi_n(\mathbf{r}_c)\rangle\}$ of the auxiliary model into the expression:

$$C_{\mathcal{O}}(\Delta) \rightarrow \frac{1}{N} \sum_{\mathbf{r}} \sum_n \langle \psi_{\text{gs}}(\mathbf{r}_c) | \mathcal{O}(\Delta + \mathbf{r}) | \psi_n(\mathbf{r}_c) \rangle \langle \psi_n(\mathbf{r}_c) | \mathcal{O}^\dagger(\mathbf{r}) | \psi_{\text{gs}}(\mathbf{r}_c) \rangle . \quad (5.63)$$

For the excitations that exist purely in the conduction bath ($\mathbf{r} \neq \mathbf{r}_c$), the excitation operators must be suitably modified (see the arguments around eq. 5.49) in order to incorporate Kondo screening. The modified excitation operators are generally defined as

$$\tilde{\mathcal{O}}(\mathbf{r}) = \mathcal{O}(\mathbf{r})\mathcal{O}^\dagger(d)\mathcal{P}_{\text{gs}} , \quad (5.64)$$

where $\mathcal{O}^\dagger(d)$ is the hermitian conjugate of the correlation operator \mathcal{O} , but applied on the impurity sites. This therefore constitutes a time-reversed scattering process on the impurity site relative to the process in the bath. The operator \mathcal{P}_{gs} projects onto the ground state of the auxiliary model, since we are interested in ground state correlations. The operator multiplying the old correlation operator represents all possible excitations of the impurity site, and ensure that the bath and impurity excitation processes take place coherently. The projector ensures that only tripartite correlations between the impurity site and the two momentum states are captured by the correlation, which is what's desired within the tiling method.

With this modified operator, this class of correlation functions can be written as

$$C_{\mathcal{O}}(\Delta) \rightarrow \frac{1}{N} \sum_{\mathbf{r}} \langle \psi_{\text{gs}}(\mathbf{r}_c) | \tilde{\mathcal{O}}(\Delta + \mathbf{r}) | \psi_{\text{gs}}(\mathbf{r}_c) \rangle \langle \psi_{\text{gs}}(\mathbf{r}_c) | \tilde{\mathcal{O}}^\dagger(\mathbf{r}) | \psi_{\text{gs}}(\mathbf{r}_c) \rangle . \quad (5.65)$$

This can be interpreted as the fact that within our auxiliary model formalism, the correlation between the sites \mathbf{r} and $\Delta + \mathbf{r}$ can only occur through a transition process that connect one of the sites with the impurity site and then a return process that connects the impurity site with the other site.

Inter-auxiliary model contributions: $\mathbf{r}' \neq 0$

These are the most non-local contributions, and involve excitations that connect different auxiliary models:

$$C_{\mathcal{O}}(\Delta) \rightarrow \frac{1}{N} \sum_{\mathbf{r}' \neq 0} \langle \psi_{\text{gs}}(\mathbf{r}_c + \mathbf{r}') | \tilde{\mathcal{O}}(\Delta + \mathbf{r}) | \psi_{\text{gs}}(\mathbf{r}_c) \rangle \langle \psi_{\text{gs}}(\mathbf{r}_c) | \tilde{\mathcal{O}}^\dagger(\mathbf{r}) | \psi_{\text{gs}}(\mathbf{r}_c) \rangle . \quad (5.66)$$

5.3.5 Equal-Time Ground State Correlators: Momentum-space

We now consider momentum space correlations, through a general operator $\mathcal{O}(\mathbf{k}_2)\mathcal{O}^\dagger(\mathbf{k}_1)$:

$$C_{\mathcal{O}}(\mathbf{k}_1, \mathbf{k}_2) = \langle \Psi_{\text{gs}} | \mathcal{O}(\mathbf{k}_2) \mathcal{O}^\dagger(\mathbf{k}_1) | \Psi_{\text{gs}} \rangle . \quad (5.67)$$

Note that \mathcal{O} itself is a two-particle operator. To obtain a tractable expression for this, we first replace the full ground state with its expression in terms of the auxiliary model ground states (eq. 5.29):

$$C_{\mathcal{O}}(\mathbf{k}_1, \mathbf{k}_2) = \frac{1}{N} \sum_{\mathbf{r}_1, \mathbf{r}_2} \langle \psi_{\text{gs}}(\mathbf{r}_2) | \mathcal{O}(\mathbf{k}_2) \mathcal{O}^\dagger(\mathbf{k}_1) | \psi_{\text{gs}}(\mathbf{r}_1) \rangle , \quad (5.68)$$

where \mathbf{r}_1 and \mathbf{r}_2 are the positions of the incoming and outgoing auxiliary model states. In order to convert the incoming and outgoing states into the same auxiliary mode at a reference location \mathbf{r}_c (which would then allow computations purely within a single auxiliary model), we use the relation: $|\psi_{\text{gs}}(\mathbf{x})\rangle = T^\dagger(\mathbf{x} - \mathbf{r}_c) \psi_{\text{gs}} |\psi(\mathbf{r}_c)\rangle$. Substituting this appropriately for both the auxiliary model states gives:

$$C_{\mathcal{O}}(\mathbf{k}_1, \mathbf{k}_2) = \frac{1}{N} \sum_{\mathbf{r}_1, \mathbf{r}_2} \langle \psi_{\text{gs}}(\mathbf{r}_c) | T(\mathbf{r}_2 - \mathbf{r}_c) \mathcal{O}(\mathbf{k}_2) \mathcal{O}^\dagger(\mathbf{k}_1) T^\dagger(\mathbf{r}_1 - \mathbf{r}_c) | \psi_{\text{gs}}(\mathbf{r}_c) \rangle . \quad (5.69)$$

In order to simplify the translation operators, we can use eq. 5.37. For that, we would need to know whether the operator \mathcal{O} involves a net transfer of momentum. If $\mathcal{O}(\mathbf{k})$ commutes with the total number operator $n_{\mathbf{k}} = \sum_{\sigma} n_{\mathbf{k},\sigma}$, there is no momentum transfer. Examples of such operators are spin operators, $S_{\alpha\beta}(\mathbf{k}) \equiv c_{\mathbf{k}\alpha}^{\dagger} c_{\mathbf{k}\beta}$, and density operators $n_{\mathbf{k}\alpha}$. If $\mathcal{O}(\mathbf{k})$ does not commute with $n_{\mathbf{k}}$, there is a net transfer of momentum, and one such operator would be the charge isospin operator $C^{+}(\mathbf{k}) = c_{\mathbf{k}\uparrow}^{\dagger} c_{\mathbf{k}\downarrow}^{\dagger}$. For the first kind of operators, we have $T(\mathbf{a})\mathcal{O}(\mathbf{k})T^{\dagger}(\mathbf{a}) = \mathcal{O}(\mathbf{k})$, while for the latter, we get $T(\mathbf{a})\mathcal{O}(\mathbf{k})T^{\dagger}(\mathbf{a}) = e^{-\mathbf{a}\cdot 2\mathbf{k}}\mathcal{O}(\mathbf{k})$, where $2\mathbf{k}$ represents the momentum being transferred by the operator. We consider the two cases separately.

Momentum-conserving operators: $[\mathcal{O}(\mathbf{k}), n_{\mathbf{k}}] = 0$

For these operators, the expression for the correlation gives

$$\begin{aligned} C_{\mathcal{O}}(\mathbf{k}_1, \mathbf{k}_2) &= \frac{1}{N} \sum_{\mathbf{r}_1, \mathbf{r}_2} \langle \psi_{\text{gs}}(\mathbf{r}_c) | T(\mathbf{r}_2 - \mathbf{r}_1) \mathcal{O}(\mathbf{k}_2) \mathcal{O}^{\dagger}(\mathbf{k}_1) | \psi_{\text{gs}}(\mathbf{r}_c) \rangle \\ &= \sum_{\Delta} \langle \psi_{\text{gs}}(\mathbf{r}_c + \Delta) | \mathcal{O}(\mathbf{k}_2) \mathcal{O}^{\dagger}(\mathbf{k}_1) | \psi_{\text{gs}}(\mathbf{r}_c) \rangle . \end{aligned} \quad (5.70)$$

To obtain the last form, we defined $\Delta = \mathbf{r}_2 - \mathbf{r}_1$ as the distance between the incoming and outgoing auxiliary model states, and performed the sum over the free variable \mathbf{r}_1 to cancel out the factor of $1/N$. Just like before, this expression can be decomposed into a term that involves a single auxiliary model and other terms that involve two distinct auxiliary models. By making the identification of the right transition operator $\tilde{\mathcal{O}}(\mathbf{k}) = \mathcal{O}(\mathbf{k})\mathcal{O}^{\dagger}(d)\mathcal{P}_{\text{gs}}$, we get

$$C_{\mathcal{O}}(\mathbf{k}_1, \mathbf{k}_2) = \sum_{\Delta} \langle \psi_{\text{gs}}(\mathbf{r}_c + \Delta) | \tilde{\mathcal{O}}(\mathbf{k}_2) | \psi_{\text{gs}}(\mathbf{r}_c) \rangle \langle \psi_{\text{gs}}(\mathbf{r}_c) | \tilde{\mathcal{O}}^{\dagger}(\mathbf{k}_1) | \psi_{\text{gs}}(\mathbf{r}_c) \rangle . \quad (5.71)$$

Non-momentum-conserving operators: $[\mathcal{O}(\mathbf{k}), n_{\mathbf{k}}] \neq 0$

This class of operators incur an additional phase factor of $e^{-\mathbf{a}\cdot 2\mathbf{k}}$ when the translation operators are translated across them:

$$\begin{aligned} C_{\mathcal{O}}(\mathbf{k}_1, \mathbf{k}_2) &= \frac{1}{N} \sum_{\mathbf{r}_1, \mathbf{r}_2} \langle \psi_{\text{gs}}(\mathbf{r}_c) | T(\mathbf{r}_2 - \mathbf{r}_1) \mathcal{O}(\mathbf{k}_2) \mathcal{O}^{\dagger}(\mathbf{k}_1) | \psi_{\text{gs}}(\mathbf{r}_c) \rangle e^{2i(\mathbf{r}_1 - \mathbf{r}_c) \cdot (\mathbf{k}_1 - \mathbf{k}_2)} \\ &= \delta_{\mathbf{k}_1, \mathbf{k}_2} \sum_{\Delta} \langle \psi_{\text{gs}}(\mathbf{r}_c + \Delta) | \mathcal{O}(\mathbf{k}_2) \mathcal{O}^{\dagger}(\mathbf{k}_1) | \psi_{\text{gs}}(\mathbf{r}_c) \rangle . \end{aligned} \quad (5.72)$$

For this expression, we again defined Δ similar to before, and carried out the sum of \mathbf{r}_1 involving the exponential to obtain a factor of $N\delta_{\mathbf{k}_1, \mathbf{k}_2}$. The Kronecker delta factor is a manifestation of translational invariance and the associated total momentum conservation.

As it stands, operators like $\mathcal{O}(\mathbf{k}_1)$ act purely on the conduction bath degrees of freedom. In order to incorporate impurity-bath correlation effects, we modify these operators using the appropriate T -matrices, by employing eq. 5.64. The final computations are carried out using these modified operators.

5.3.6 Entanglement Measures

We will now describe the prescription of calculating entanglement measures of the lattice model from within our auxiliary model treatment. In this section, we are interested mainly in two such measures, the entanglement entropy and the mutual information. Given a pure state $|\Psi\rangle$ describing the complete system, the entanglement entropy $S_{\text{EE}}(\nu)$ of a subsystem ν quantifies the entanglement of ν with the rest of the subsystem, and is defined as

$$S_{\text{EE}}(\nu) = -\text{Tr} [\rho(\nu) \log \rho(\nu)], \quad \rho(\nu) = \text{Tr}_\nu [|\Psi\rangle \langle \Psi|] \quad (5.73)$$

where $\text{Tr}[\cdot]$ is the trace operator, and $\rho(\nu)$ is the reduced density matrix (RDM) for the subsystem ν obtained by taking the partial trace Tr_ν (over the states of ν) of the full density matrix $\rho = |\Psi\rangle \langle \Psi|$. If the subsystem ν describes local regions in real space (or states in k -space), we might be interested in the entanglement between two such subsystems ν_1 and ν_2 . The correct measure to quantify such entanglement is the mutual information:

$$I_2(\nu_1, \nu_2) = S_{\text{EE}}(\nu_1) + S_{\text{EE}}(\nu_2) - S_{\text{EE}}(\nu_1 \cup \nu_2), \quad (5.74)$$

where $\nu_1 \cup \nu_2$ is a larger subsystem formed by combining ν_1 and ν_2 .

Real-space entanglement

Real-space entanglement measures can be used to probe delocalisation-localisation transitions. The simplest such measure is the entanglement of a local mode. Since the local entanglement entropy will be uniform at each lattice site for a system with translation invariance, it suffices to calculate the real-space averaged entanglement entropy $S_{\text{EE}}^{\text{loc}} = \frac{1}{N} \sum_{\mathbf{r}} S_{\text{EE}}(\mathbf{r})$. By visualising the lattice model as a superposition of auxiliary models placed at various sites (eq. 5.24), the real space average of the lattice model can be thought of as an average over sites of a particular impurity model, and then a second average over all the impurity models. But since all all impurity models are equivalent to each other, the second average is redundant. Secondly, all correlations must derive from the impurity site, which can be formally encoded by subtracting, from this average, the corresponding contribution obtained in the absence of the impurity site. In total, the lattice-auxiliary model relation for the local entanglement entropy can be written as

$$S_{\text{EE}}^{\text{loc}} = \frac{1}{N} \sum_{\mathbf{r}} \left[S_{\text{EE}}(\mathbf{r}_d + \mathbf{r}) - S_{\text{EE}}^{(0)}(\mathbf{r}_d + \mathbf{r}) \right], \quad (5.75)$$

where \mathbf{r}_d is the impurity site position, \mathbf{r} is the distance of a conduction bath site from the impurity site (can be zero), and $S_{\text{EE}}(\mathbf{r}_d + \mathbf{r})$ is the entanglement entropy, calculated within the impurity model, at the location $\mathbf{r}_d + \mathbf{r}$. $S_{\text{EE}}^{(0)}(\mathbf{r}_d + \mathbf{r})$ is the same entanglement entropy, but calculated for an impurity model with vanishing impurity-bath hybridisation and bath interaction.

Momentum-space entanglement

Entanglement measures in k -space can provide valuable information regarding the Fermi surface structure and the nature of gapless excitations proximate to it. The most elementary measure is the entanglement entropy $S_{\text{EE}}(\mathbf{q})$ of a single excitation carrying momentum \mathbf{q} . Unlike $S_{\text{EE}}^{\text{loc}}$, this does not involve an average, and involves a single computation:

$$\tilde{S}_{\text{EE}}(\mathbf{q}) = S_{\text{EE}}(\mathbf{q}) - S_{\text{EE}}^{(0)}(\mathbf{q}). \quad (5.76)$$

It is possible to improve this by considering inter-auxiliary model contributions in the reduced density matrix $\rho(\mathbf{q})$. On the lattice model, $\rho(\mathbf{q})$ is defined as

$$\rho(\mathbf{q}) = \text{Tr}_{\mathbf{q}} [|\Psi_{\text{gs}}\rangle \langle \Psi_{\text{gs}}|] , \quad (5.77)$$

where $\text{Tr}_{\mathbf{q}} [\cdot]$ is the partial trace over the Hilbert space of \mathbf{q} , and $|\Psi_{\text{gs}}\rangle$ is the tiled ground state. Using eq. 5.29, we can write the ground state in terms of those of the auxiliary model. These leads to two classes of terms, one purely within a single auxiliary model ground state $|\psi_{\text{gs}}\rangle$, and the other involving transitions across auxiliary models:

$$\rho(\mathbf{q}) \sim \text{Tr}_{\mathbf{q}} [|\psi_{\text{gs}}(\mathbf{r}_d)\rangle \langle \psi_{\text{gs}}(\mathbf{r}_d)|] + \frac{1}{N} \text{Tr}_{\mathbf{q}} \sum_{\mathbf{r}} [|\psi_{\text{gs}}(\mathbf{r}_d)\rangle \langle \psi_{\text{gs}}(\mathbf{r}_d + \mathbf{r})|] , \quad (5.78)$$

where $|\psi_{\text{gs}}(\mathbf{r}_d)\rangle$ is a reference auxiliary model ground state, and $|\psi_{\text{gs}}(\mathbf{r}_d + \mathbf{r})\rangle$ sums over other auxiliary models at increasing distances from this reference model. The \sim indicates that the RDM needs to be normalised. The first term leads to the expression in eq. 5.77, while the second term can be used to improve this estimate. Away from any quantum critical points, the localised nature of the impurity-bath hybridisation ensures that impurity correlations decay exponentially away from the transition. This ensures that the second term is very small away from a critical point. We therefore restrict ourselves to just the first term in the present work.

5.4 Properties of the Bloch states

5.4.1 Translation invariance

It is easy to verify that $\Psi_{\vec{k}}(\{\mathbf{r}_k\})$ transforms like Bloch functions under translation by a displacement \mathbf{r} :

$$\Psi_{\vec{k}}(\{\mathbf{r}_k + \mathbf{r}\}) = \frac{1}{\lambda_{|\vec{k}|} \mathcal{Z} N} \sum_{\mathbf{r}_i, \mathbf{a}} e^{i\vec{k} \cdot \vec{R}_i} \psi_{\text{aux}}(\mathbf{r}_i - \mathbf{r}, \mathbf{a}) = \frac{1}{\lambda_{|\vec{k}|} \mathcal{Z} N} \sum_{\mathbf{r}_j, \mathbf{a}} e^{i\vec{k} \cdot (\vec{R}_j + \mathbf{r})} \psi_{\text{aux}}(\mathbf{r}_j, \mathbf{a}) = e^{i\vec{k} \cdot \vec{R}} \Psi_{\vec{k}}(\{\mathbf{r}_k\}) \quad (5.79)$$

In the last equation, we transformed $\mathbf{r}_i \rightarrow \mathbf{r}_j = \mathbf{r}_i - \mathbf{r}$. Note that the argument \mathbf{a} does not change under a translation of the system, because that vector always represents the difference between the impurity lattice position and its nearest neighbours, irrespective of the absolute position of the impurity.

The wavefunction can be even brought into the familiar Bloch function form:

$$\begin{aligned} \Psi_{\vec{k}}^n(\{\mathbf{r}_k\}) &= \sum_{\mathbf{r}_i, \mathbf{a}} \frac{e^{i\vec{k} \cdot \vec{R}_i}}{\lambda_{|\vec{k}|} \mathcal{Z} N} \psi_{\text{aux}}(\{\mathbf{r}_d - \mathbf{r}_i, \mathbf{r}_0 - \mathbf{r}_i - \mathbf{a}\}) = \frac{e^{i\vec{k} \cdot \frac{1}{N} \sum_k \vec{r}_k}}{\lambda_{|\vec{k}|} \mathcal{Z} N} \sum_{\mathbf{r}_i, \mathbf{a}} e^{-i\vec{k} \cdot \left(\frac{1}{N} \sum_k \mathbf{r}_k - \vec{R}_i\right)} \psi_{\text{aux}}(\{\mathbf{r}_d - \mathbf{r}_i, \mathbf{r}_0 - \mathbf{r}_i - \mathbf{a}\}) \\ &= e^{i\vec{k} \cdot \vec{r}_{\text{COM}}} \eta_{\vec{k}}(\{\mathbf{r}_k\}) \end{aligned} \quad (5.80)$$

where $\mathbf{r}_{\text{COM}} = \frac{1}{N} \sum_k \mathbf{r}_k$ is the center-of-mass coordinate and $\eta_{\vec{k}}(\{\mathbf{r}_k\}) = \frac{1}{\lambda_{|\vec{k}|} \mathcal{Z} N} \sum_{\mathbf{r}_i} e^{-i\vec{k} \cdot \left(\frac{1}{N} \sum_k \mathbf{r}_k - \vec{R}_i\right)} \psi_{\text{aux}}^n(\{\mathbf{r}_k - \mathbf{r}_i\})$ is the translation symmetric function. This form of the eigenstate allows the interpretation that tuning the Bloch momentum \vec{k} corresponds to a translation of the center of mass of the system (or in this case, of the auxiliary models that comprise the system).

5.4.2 Orthonormality

It is straightforward to show that these states form an orthonormal basis. We start by writing down the inner product of two distinct such states:

$$\begin{aligned} \langle \Psi_{\vec{k}'} | \Psi_{\vec{k}} \rangle &= \frac{1}{\lambda_{|\vec{k}'\rangle}^* \lambda_{|\vec{k}\rangle} \mathcal{Z}^2 N^2} \sum_{\mathbf{r}_i, \mathbf{r}_j, \mathbf{a}, \mathbf{a}'} e^{i(\vec{k} \cdot \vec{R}_i - \vec{k}' \cdot \vec{R}_j)} \langle \psi_{\text{aux}}(\mathbf{r}_j, \mathbf{a}') | \psi_{\text{aux}}(\mathbf{r}_i, \mathbf{a}) \rangle \\ &= \frac{1}{\lambda_{|\vec{k}'\rangle}^* \lambda_{|\vec{k}\rangle} \mathcal{Z}^2 N^2} \sum_{\mathbf{r}_i, \mathbf{r}_j, \mathbf{a}, \mathbf{a}'} e^{i(\vec{k} \cdot \vec{R}_i - \vec{k}' \cdot \vec{R}_j)} \langle \psi_{\text{aux}}(\mathbf{r}_0, \mathbf{a}') T^\dagger(\mathbf{r}_0 - \mathbf{r}_j) T(\mathbf{r}_0 - \mathbf{r}_i) | \psi_{\text{aux}}(\mathbf{r}_0, \mathbf{a}) \rangle \end{aligned} \quad (5.81)$$

At this point, we insert a complete basis of momentum eigenkets $1 = \sum_{\vec{q}} |\vec{q}\rangle \langle \vec{q}|$ to resolve the translation operators:

$$\begin{aligned} \langle \Psi_{\vec{k}'} | \Psi_{\vec{k}} \rangle &= \frac{1}{\lambda_{|\vec{k}'\rangle}^* \lambda_{|\vec{k}\rangle} \mathcal{Z}^2 N^2} \sum_{\mathbf{r}_i, \mathbf{r}_j, \mathbf{a}, \mathbf{a}', \vec{q}} e^{i(\vec{k} \cdot \vec{R}_i - \vec{k}' \cdot \vec{R}_j)} \langle \psi_{\text{aux}}(\mathbf{r}_0, \mathbf{a}') T(\mathbf{r}_j - \mathbf{r}_i) | \vec{q} \rangle \langle \vec{q} | \psi_{\text{aux}}(\mathbf{r}_0, \mathbf{a}) \rangle \\ &= \frac{1}{\lambda_{|\vec{k}'\rangle}^* \lambda_{|\vec{k}\rangle} \mathcal{Z}^2 N^2} \sum_{\mathbf{r}_i, \mathbf{r}_j, \mathbf{a}, \mathbf{a}', \vec{q}} e^{i(\vec{k} \cdot \vec{R}_i - \vec{k}' \cdot \vec{R}_j)} \langle \psi_{\text{aux}}(\mathbf{r}_0, \mathbf{a}') e^{i\vec{q} \cdot (\mathbf{r}_j - \mathbf{r}_i)} | \vec{q} \rangle \langle \vec{q} | \psi_{\text{aux}}(\mathbf{r}_0, \mathbf{a}) \rangle \\ &= \frac{1}{|\lambda_{|\vec{k}\rangle}|^2 \mathcal{Z}^2} \delta_{\vec{k}, \vec{k}'} \sum_{\mathbf{a}, \mathbf{a}'} \langle \psi_{\text{aux}}(\mathbf{r}_0, \mathbf{a}') | \vec{k} \rangle \langle \vec{k} | \psi_{\text{aux}}(\mathbf{r}_0, \mathbf{a}) \rangle \end{aligned} \quad (5.82)$$

At the last step, we used the summation form of the Kronecker delta function: $\sum_{\mathbf{r}_i} e^{i\mathbf{r}_i \cdot (\vec{k} - \vec{q})} \sum_{\mathbf{r}_j} e^{i\mathbf{r}_j \cdot (\vec{q} - \vec{k}')} = N \delta_{\vec{k}, \vec{q}} N \delta_{\vec{k}', \vec{q}}$. The final remaining step is to identify that the inner products inside the summation are actually independent of the direction \mathbf{a}, \mathbf{a}' of the connecting vector, and both are equal to the normalisation factor $\lambda_{|\vec{k}\rangle}$:

$$\langle \Psi_{\vec{k}'} | \Psi_{\vec{k}} \rangle = \frac{1}{|\lambda_{|\vec{k}\rangle}|^2 \mathcal{Z}^2} \delta_{\vec{k}, \vec{k}'} \sum_{\mathbf{a}, \mathbf{a}'} |\lambda_{|\vec{k}\rangle}|^2 = \frac{1}{|\lambda_{|\vec{k}\rangle}|^2 \mathcal{Z}^2} \delta_{\vec{k}, \vec{k}'} w^2 |\lambda_{|\vec{k}\rangle}|^2 = \delta_{\vec{k}, \vec{k}'} \quad (5.83)$$

This concludes the proof of orthonormality.

5.4.3 Eigenstates

To demonstrate that these are indeed eigenstates of the bulk Hamiltonian, we will calculate the matrix elements of the full Hamiltonian between these states:

$$\begin{aligned} \langle \Psi_{\vec{k}'} | H_{\text{H-H}} | \Psi_{\vec{k}} \rangle &= \frac{1}{\lambda_{|\vec{k}'\rangle}^* \lambda_{|\vec{k}\rangle} \mathcal{Z}^2 N^2} \sum_{\mathbf{r}_i, \mathbf{r}_j, \mathbf{r}_k, \mathbf{a}, \mathbf{a}'} e^{i(\vec{k} \cdot \vec{R}_i - \vec{k}' \cdot \vec{R}_j)} \langle \psi_{\text{aux}}(\mathbf{r}_j, \mathbf{a}') | H_{\text{aux}}(\mathbf{r}_k) | \psi_{\text{aux}}(\mathbf{r}_i, \mathbf{a}) \rangle \\ &= \frac{1}{\lambda_{|\vec{k}'\rangle}^* \lambda_{|\vec{k}\rangle} \mathcal{Z}^2 N^2} \sum_{\mathbf{r}_i, \mathbf{r}_j, \mathbf{r}_k, \mathbf{a}, \mathbf{a}'} e^{i(\vec{k} \cdot \vec{R}_i - \vec{k}' \cdot \vec{R}_j)} \langle \psi_{\text{aux}}(\mathbf{r}_0, \mathbf{a}') | T_{\mathbf{r}_0 - \mathbf{r}_j}^\dagger T_{\mathbf{r}_0 - \mathbf{r}_k} H_{\text{aux}}(\mathbf{r}_0) T_{\mathbf{r}_0 - \mathbf{r}_k}^\dagger T_{\mathbf{r}_0 - \mathbf{r}_i} | \psi_{\text{aux}}(\mathbf{r}_0, \mathbf{a}) \rangle \\ &= \frac{1}{\lambda_{|\vec{k}'\rangle}^* \lambda_{|\vec{k}\rangle} \mathcal{Z}^2 N^2} \sum_{\mathbf{r}_i, \mathbf{r}_j, \mathbf{r}_k, \mathbf{a}, \mathbf{a}'} e^{i(\vec{k} \cdot \vec{R}_i - \vec{k}' \cdot \vec{R}_j)} \langle \psi_{\text{aux}}(\mathbf{r}_0, \mathbf{a}') | T_{\mathbf{r}_k - \mathbf{r}_j}^\dagger H_{\text{aux}}(\mathbf{r}_0) T_{\mathbf{r}_k - \mathbf{r}_i} | \psi_{\text{aux}}(\mathbf{r}_0, \mathbf{a}) \rangle \end{aligned} \quad (5.84)$$

To resolve the translation operators, we will now insert the momentum eigenstates $|\vec{k}\rangle$ of the full model: $1 = \sum_{\vec{q}} |\vec{q}\rangle \langle \vec{q}|$ in between the operators.

$$\begin{aligned}
\langle \Psi_{\vec{k}'} | H_{\text{H-H}} | \Psi_{\vec{k}} \rangle &= \sum_{\substack{\mathbf{r}_i, \mathbf{r}_j, \mathbf{r}_k, \\ \mathbf{a}, \mathbf{a}', \vec{q}, \vec{q}'}} \frac{e^{i(\vec{k} \cdot \vec{R}_i - \vec{k}' \cdot \vec{R}_j)}}{\lambda_{|\vec{k}'}^* \lambda_{|\vec{k}|} \mathcal{Z}^2 N^2} \langle \psi_{\text{aux}}(\mathbf{r}_0, \mathbf{a}') | \vec{q}' \rangle \langle \vec{q}' | T_{\mathbf{r}_k - \mathbf{r}_j}^\dagger H_{\text{aux}}(\mathbf{r}_0) T_{\mathbf{r}_k - \mathbf{r}_i} | \vec{q} \rangle \langle \vec{q} | \psi_{\text{aux}}(\mathbf{r}_0, \mathbf{a}) \rangle \\
&= \sum_{\substack{\mathbf{r}_i, \mathbf{r}_j, \mathbf{r}_k, \\ \mathbf{a}, \mathbf{a}', \vec{q}, \vec{q}'}} \frac{e^{i(\vec{k} \cdot \vec{R}_i - \vec{k}' \cdot \vec{R}_j)}}{\lambda_{|\vec{k}'}^* \lambda_{|\vec{k}|} \mathcal{Z}^2 N^2} \langle \psi_{\text{aux}}(\mathbf{r}_0, \mathbf{a}') | \vec{q}' \rangle e^{-i\vec{q}' \cdot (\mathbf{r}_k - \mathbf{r}_j)} e^{i\vec{q}' \cdot (\mathbf{r}_k - \mathbf{r}_i)} \langle \vec{q}' | H_{\text{aux}}(\mathbf{r}_0) | \vec{q} \rangle \langle \vec{q} | \psi_{\text{aux}}(\mathbf{r}_0, \mathbf{a}) \rangle \\
&= \frac{N}{\lambda_{|\vec{k}'}^* \lambda_{|\vec{k}|} \mathcal{Z}^2} \sum_{\mathbf{a}, \mathbf{a}', \vec{q}, \vec{q}'} \delta_{\vec{k}, \vec{q}} \delta_{\vec{q}, \vec{q}'} \delta_{\vec{q}', \vec{k}} \langle \psi_{\text{aux}}(\mathbf{r}_0, \mathbf{a}') | \vec{q}' \rangle \langle \vec{q}' | H_{\text{aux}}(\mathbf{r}_0) | \vec{q} \rangle \langle \vec{q} | \psi_{\text{aux}}(\mathbf{r}_0, \mathbf{a}) \rangle \\
&= \frac{N}{|\lambda_{|\vec{k}|}|^2 \mathcal{Z}^2} \delta_{kk'} \sum_{\mathbf{a}, \mathbf{a}'} \langle \psi_{\text{aux}}(\mathbf{r}_0, \mathbf{a}') | \vec{k} \rangle \langle \vec{k} | H_{\text{aux}}(\mathbf{r}_0) | \vec{k} \rangle \langle \vec{k} | \psi_{\text{aux}}(\mathbf{r}_0, \mathbf{a}) \rangle \\
&= \frac{N}{|\lambda_{|\vec{k}|}|^2 \mathcal{Z}^2} \delta_{kk'} \underbrace{\langle \vec{k} | H_{\text{aux}}(\mathbf{r}_0) | \vec{k} \rangle}_{w^2 |\lambda_{|\vec{k}|}|^2} \sum_{\mathbf{a}, \mathbf{a}'} \langle \psi_{\text{aux}}(\mathbf{r}_0, \mathbf{a}') | \vec{k} \rangle \langle \vec{k} | \psi_{\text{aux}}(\mathbf{r}_0, \mathbf{a}) \rangle \\
&= N \delta_{kk'} \langle \vec{k} | H_{\text{aux}}(\mathbf{r}_0) | \vec{k} \rangle
\end{aligned} \tag{5.85}$$

The momentum eigenket $|\vec{k}\rangle$ can be expressed as a sum over position eigenkets at varying distances from \mathbf{r}_0 . This form allows a systematic method of improving the energy eigenvalue estimate, because the interacting in the impurity model is extremely localised, so the overlap between two auxiliary models decreases rapidly with distance. The majority of the contribution will come from the state at \mathbf{r}_0 , and improvements are then made by considering auxiliary models at further distances.

Chapter 6

Embedded eSIAM

6.1 Extending the Anderson Model To a Lattice-Embedded Impurity Model

Crucial to our method is the choice of an impurity auxiliary model that is able to capture important aspects of the lattice model in a local sense. Some of us have shown in a previous work [293] that almost all aspects of the Mott metal-insulator transition on the infinite dimensional Hubbard model on the Bethe lattice (as seen, for example, from dynamical mean-field theory [186]) can be captured from a simple extension of the Anderson impurity model (eSIAM). The extension involves including a local attractive interacting W on the conduction bath site coupled to the impurity site; by tuning the ratio of $|W|$ and the Kondo coupling J , we obtained an impurity phase transition from a screened phase to an unscreened local moment phase. Since the impurity site of the auxiliary model is a representative of each correlated site on the lattice, the mapping to the lattice model then involves identifying the locally gapless impurity phase with the bulk gapless of the lattice model. In other words, the ability of the impurity site to participate in low-energy excitations corresponds to the ability of an electron, within the lattice model, to delocalise from one site into the rest of the lattice. In the same vein, a local moment phase of the impurity model maps to a gapped Mott insulating phase on the lattice model, where there's a charge gap to electron hopping processes.

In the present work, the goal is to tackle interacting fermions on a 2D square lattice, which makes it important for us to incorporate the effects of the lattice within the impurity model. More specifically, while the impurity-bath interactions on the infinite dimensional Bethe lattice are s -wave symmetric, that is not a realistic form for a 2D lattice. To make a realistic impurity model, we embed the impurity site into the lattice of a 2D conduction bath, and lower the s -wave symmetry of the interactions down to the C_4 symmetry of the 2D square lattice. A general structure of such a model is shown in fig. 6.1; one of the sites of the 2D square lattice is identified as the impurity (red), while the four nearest-neighbours (navy blue) interact directly with this impurity site through a C_4 -symmetric interaction.

6.1.1 Hamiltonian

We consider an impurity site \vec{S}_d interacting with a two-dimensional tight-binding conduction bath through a highly localised interaction, described by the Hamiltonian

$$\mathcal{H} = H_{\text{cbath}} + H_{\text{imp}} + H_{\text{imp-cbath}} + H_{\text{cbath-int}}, \quad (6.1)$$

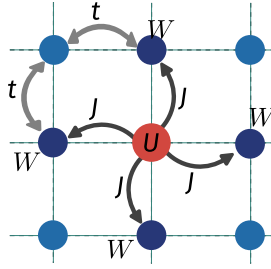


Figure 6.1: General structure of an embedded extended SIAM, where the impurity site is a part of the 2D square lattice. The four nearest-neighbour sites (dark blue) interact with the impurity site through one or more processes, and can host local interactions. The other lattice sites (light blue) are completely non-interacting.

where H_{cbath} is the kinetic energy arising out of nearest-neighbour hopping processes and H_{imp} is the particle-hole symmetric impurity-local term,

$$H_{\text{cbath}} = -2t \sum_{\mathbf{k}} [\cos(ak_x) + \cos(ak_y)] c_{\mathbf{k},\sigma}^\dagger c_{\mathbf{k},\sigma}, \quad H_{\text{imp}} = -\frac{U}{2} (n_{d\uparrow} - n_{d\downarrow})^2. \quad (6.2)$$

For the impurity-bath interaction $H_{\text{imp-cbath}}$ and the local interaction $H_{\text{cbath-int}}$ in the bath, we take the simplest choices consistent with the 2D square lattice geometry:

$$\begin{aligned} H_{\text{imp-cbath}} &= \frac{1}{2} J \sum_{\sigma_1, \sigma_2} \sum_Z \mathbf{S}_d \cdot c_{Z\sigma_1}^\dagger \boldsymbol{\tau}_{\sigma_1, \sigma_2} c_{Z\sigma_2} - V \sum_{\sigma, Z} (c_{d\sigma}^\dagger c_{Z\sigma} + \text{h.c.}), \\ H_{\text{cbath-int}} &= -\frac{W}{2} \sum_Z (n_{Z\uparrow} - n_{Z\downarrow})^2, \end{aligned} \quad (6.3)$$

where Z sums over all nearest-neighbour sites of the impurity site (navy blue circles in Fig. 6.1, henceforth referred to as bath zeroth sites). The impurity interacts with the bath zeroth sites in $H_{\text{imp-cbath}}$ through four single-particle hybridisation terms of strength V and spin-exchange terms of strength J . The other term $H_{\text{cbath-int}}$ represents local Hubbard interactions on the four zeroth sites, again of uniform strength.

The 2D structure of the impurity model and its distinction from the infinite-dimensional counterpart becomes apparent once we transform the Hamiltonian to momentum space. The conduction bath operators transform as

$$c_{\mathbf{r}}^\dagger = \sum_{\mathbf{k}} e^{-i\mathbf{k}\cdot\mathbf{r}} c_{\mathbf{k}}^\dagger, \quad (6.4)$$

where the momentum states \mathbf{k} are the plane wave solutions of the tight-binding model obtained in the non-interacting limit: $U = J = 0, V = t$. Transforming all bath operators leads to the following form:

$$\begin{aligned} H_{\text{imp-cbath}} &= \frac{1}{2} \sum_{\sigma_1, \sigma_2, \mathbf{k}, \mathbf{k}'} J_{\mathbf{k}, \mathbf{k}'} \mathbf{S}_d \cdot c_{\mathbf{k}\sigma_1}^\dagger \boldsymbol{\tau}_{\sigma_1, \sigma_2} c_{\mathbf{k}'\sigma_2}, \\ H_{\text{cbath-int}} &= -\frac{1}{2} \sum_{\mathbf{k}, \mathbf{k}', \mathbf{q}, \mathbf{q}'} W_{\mathbf{k}, \mathbf{k}', \mathbf{q}, \mathbf{q}'} c_{\mathbf{k}}^\dagger c_{\mathbf{k}'} c_{\mathbf{q}}^\dagger c_{\mathbf{q}'}, \end{aligned} \quad (6.5)$$

where the momentum-dependent couplings are defined as

$$\begin{aligned} J_{\mathbf{k}, \mathbf{k}'} &= \frac{J}{2} [\cos(\mathbf{k}_x - \mathbf{k}'_x) + \cos(\mathbf{k}_y - \mathbf{k}'_y)] , \\ W_{\mathbf{k}, \mathbf{k}', \mathbf{q}, \mathbf{q}'} &= W [\cos(\mathbf{k}_x - \mathbf{k}'_x + \mathbf{q}_x - \mathbf{q}'_x) + \cos(\mathbf{k}_y - \mathbf{k}'_y + \mathbf{q}_y - \mathbf{q}'_y)] . \end{aligned} \quad (6.6)$$

where the subscripts x and y represent components of the momenta vector. This form shows that the Kondo coupling is no longer independent of the exchange momentum, and encodes information of the lattice geometry in it.

6.1.2 The unitary renormalisation group method

In order to obtain the various low-energy phases of our impurity model, we perform a scaling analysis of the associated Hamiltonian using the recently developed unitary renormalisation group (URG) method [1, 2]. The method has been applied successfully on a wide variety of problems of correlated fermions [1–4, 141, 219, 234–236]. The method proceeds by resolving quantum fluctuations in high-energy degrees of freedom, leading to a low-energy Hamiltonian with renormalised couplings and new emergent degrees of freedom. Typically, for a system with Fermi energy ϵ_F and bandwidth E_N , the sequence of isoenergetic shells $\{E_{(j)}\}$, $E_j \in [E_0, E_N]$ define the states whose quantum fluctuations we sequentially resolve. The momentum states lying on shells E_N that are far away from the Fermi surface comprise the UV states, while those on shells near the Fermi surface comprise the IR states. This scheme is shown in Fig. (6.2).

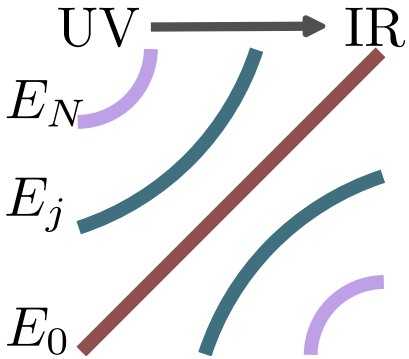


Figure 6.2: High energy - low energy scheme defined and used in the URG method. The states away from the Fermi surface (E_N in the figure) form the UV subspace and are decoupled first, leading to a Hamiltonian which is more block-diagonal and comprised of only the IR states near the Fermi surface (E_0 in the figure).

As a result of the URG transformations, the Hamiltonian $H_{(j)}$ at a given RG step j involves scattering processes between the k -states that have energies lower than $D_{(j+1)}$. The unitary transformation $U_{(j)}$ is then defined so as to remove the number fluctuations of the currently most energetic set of states $D_{(j)}$ [1, 2]:

$$H_{(j-1)} = U_{(j)} H_{(j)} U_{(j)}^\dagger , \text{ such that } [H_{(j-1)}, \hat{n}_j] = 0 . \quad (6.7)$$

The eigenvalue of \hat{n}_j has, thus, been rendered an integral of motion (IOM) under the RG transformation.

The unitary transformations can be expressed in terms of a generator $\eta_{(j)}$ that has fermionic algebra [1, 2]:

$$U_{(j)} = \frac{1}{\sqrt{2}} \left(1 + \eta_{(j)} - \eta_{(j)}^\dagger \right) , \quad \left\{ \eta_{(j)}, \eta_{(j)}^\dagger \right\} = 1 , \quad (6.8)$$

where $\{\cdot\}$ is the anticommutator. The unitary operator $U_{(j)}$ that appears in Eq. (6.8) can be cast into the well-known general form $U = e^S$, $S = \frac{\pi}{4} \left(\eta_{(j)}^\dagger - \eta_{(j)} \right)$ that a unitary operator can take, defined by an anti-Hermitian operator S . The generator $\eta_{(j)}$ is given by the expression [1, 2]

$$\eta_{(j)}^\dagger = \frac{1}{\hat{\omega}_{(j)} - \text{Tr} (H_{(j)} \hat{n}_j)} c_j^\dagger \text{Tr} (H_{(j)} c_j) . \quad (6.9)$$

The operators $\eta_{(j)}, \eta_{(j)}^\dagger$ behave as the many-particle analogues of the single-particle field operators c_j, c_j^\dagger - they change the occupation number of the single-particle Fock space $|n_j\rangle$. The important operator $\hat{\omega}_{(j)}$ originates from the quantum fluctuations that exist in the problem because of the non-commutation of the kinetic energy terms and the interaction terms in the Hamiltonian:

$$\hat{\omega}_{(j)} = H_{(j-1)} - H_{(j)}^i . \quad (6.10)$$

$H_{(j)}^i$ is the part of $H_{(j)}$ that commutes with \hat{n}_j but does *not* commute with at least one \hat{n}_l for $l < j$. The RG flow continues up to energy D^* , where a fixed point is reached from the vanishing of the RG function. Detailed comparisons of the URG with other methods (e.g., the functional RG, spectrum bifurcation RG etc.) can be found in Refs. [1, 3].

6.1.3 Unitary RG analysis of the embedded eSIAM

We studied the low-energy physics of this model through a unitary renormalisation group calculation that decouples the high-energy modes of the conduction bath and incorporates their effects in the form of renormalised Hamiltonian couplings. We find that the bath interaction W remains marginal (does not undergo any renormalisation), while the renormalisation in the momentum-resolved Kondo coupling $J^{(j)}$ at the j^{th} step is of the form

$$\Delta J_{\mathbf{k}_1, \mathbf{k}_2}^{(j)} = - \sum_{\mathbf{q} \in \text{PS}} \frac{J_{\mathbf{k}_2, \mathbf{q}}^{(j)} J_{\mathbf{q}, \mathbf{k}_1}^{(j)} + 4 J_{\mathbf{q}, \bar{\mathbf{q}}}^{(j)} W_{\bar{\mathbf{q}}, \mathbf{k}_2, \mathbf{k}_1, \mathbf{q}}}{\omega - \frac{1}{2} |\varepsilon_j| + J_{\mathbf{q}}^{(j)}/4 + W_{\mathbf{q}}/2} , \quad (6.11)$$

where ε_j is the energy of the shell being decoupled at the j^{th} step, and the sum is over all momentum states \mathbf{q} in the particle sector (PS) of the shell ε_j (that is, all states that are occupied at $T = 0$ and in the absence of any quantum fluctuations). The Kondo coupling and the RG equation as well have certain symmetries under transformations in the Brillouin zone. If any one of the momenta \mathbf{k}_1 or \mathbf{k}_2 are translated by π ($k_{1x} \rightarrow k_{1x} + \pi, k_{1y} \rightarrow k_{1y} + \pi$), the coupling as well as the RG equation changes sign. Translating both the momenta leads to the reversal of the sign change.

$$\Delta J_{\mathbf{k}_1 + \boldsymbol{\pi}, \mathbf{k}_2}^{(j)} = \Delta J_{\mathbf{k}_1, \mathbf{k}_2 + \boldsymbol{\pi}}^{(j)} = -\Delta J_{\mathbf{k}_1 + \boldsymbol{\pi}, \mathbf{k}_2 + \boldsymbol{\pi}}^{(j)} = -\Delta J_{\mathbf{k}_1, \mathbf{k}_2}^{(j)} . \quad (6.12)$$

These transformations involve translating one or both momenta through the center of the Brillouin zone.

With our chosen momentum-space dependence of the Kondo coupling and bath interaction, the form of the Kondo coupling morphs during the RG flow, allowing the emergence of new degrees of freedom that screen the impurity at low-energies. At the first step, the RG equation can be written down explicitly as

$$\Delta J_{\mathbf{k}, \mathbf{k}'}^{(0)} = - \sum_{\mathbf{q} \in \text{PS}} \frac{J^2 \frac{1}{2} \sum_a \cos(\mathbf{k}'_a - \mathbf{q}_a) \frac{1}{2} \sum_a \cos(\mathbf{q}_a - \mathbf{k}_a) - 2JW \sum_a \cos(\mathbf{k}'_a - \mathbf{k}_a)}{\omega - \frac{1}{2}|\varepsilon_j| + \frac{J}{4}f_D(\mathbf{q})^2 + \frac{W}{4}}, \quad (6.13)$$

where a sums over the x and y components of the momenta. We see that unlike the bare Kondo coupling $J_{\mathbf{k}, \mathbf{k}'}$ that depends only on the momentum difference $\mathbf{k} - \mathbf{k}'$, the renormalisation $\Delta J^{(0)}$ depends on products of the momenta. This shows the form of the Kondo coupling continuously changes under renormalisation.

6.2 Low-energy description of the embedded eSIAM

6.2.1 Zero temperature phase diagram and impurity site dynamics

The ground state phase diagram of the impurity model is shown in the left panel of Fig. 6.3. We find that upon tuning the ratio W/J of the bath interaction strength W and the Kondo coupling J , the impurity site undergoes a transition from a screened paramagnetic phase (dark green) to an unscreened local moment phase (yellow), through an intermediate pseudogapped regime (pink). The nature of pseudogapped phase will be clarified in the upcoming sections. The phase transition is seen through the evolution of the local spectral function (middle panel of Fig. 6.3); increasing the ratio W/J leads to the sharpening of the central Kondo resonance, indicating that the local Fermi liquid excitations are becoming poorer. At the transition, the extremely sharp peak disappears and we are left with a hard gap at zero frequency. A complimentary picture is painted by the imaginary part Σ'' of the impurity self-energy. The poles in Σ'' are the edges of the central Kondo resonance, and its sharpening leads to the coalescing of the poles.

6.2.2 Presence of a local pseuodogapping transition with electronic differentiation in momentum space

We now discuss the intervening pseudogapped regime (pink region) of the phase diagram. We find that the process of Kondo breakdown in our model occurs anisotropically in our model - the transition starts through the removal, from the Kondo cloud, of the antinodal points of the conduction bath Fermi surface. This is followed by the sequential removal of points away from the antinodes, with the nodal points being removed at the very end. This electronic differentiation is a novel feature of this model that arises because of the more realistic embedding of the impurity site into the conduction bath lattice.

We quantify the removal of these points by the vanishing (up to a tolerance) of the average renormalised scattering probability

$$\Gamma^*(\mathbf{k}) = \sum_{\mathbf{q} < \Lambda^*} (J_{\mathbf{k}, \mathbf{q}}^*)^2, \quad (6.14)$$

where the other momentum \mathbf{q} is summed over all the momentum states that reside within the fixed point window. The quantity $\Gamma(\mathbf{k})$ therefore quantifies the degree to which the state \mathbf{k} is participating in

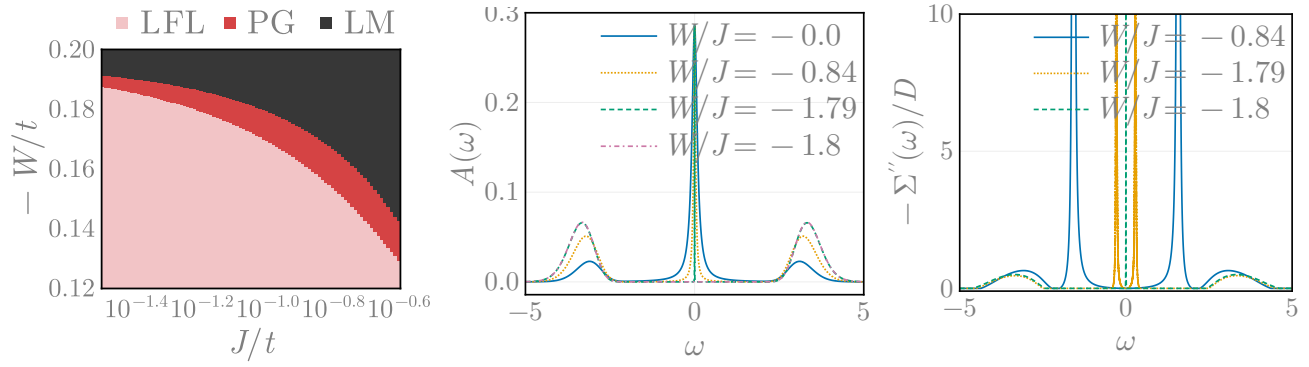


Figure 6.3: **Left:** Zero temperature phase diagram of the embedded impurity model, obtained by tracking impurity-bath spin correlations. The pink phase is characterised by perfect Kondo screening and local Fermi liquid excitations (L-FL), leading to non-zero spin-correlations all over the Fermi surface of the conduction electrons. The red phase is a local pseudogap (L-PG) phase, where a part of the Fermi surface (starting from the antinodal regions) no longer participates in Kondo screening. This leads to "Fermi arc"-like behaviour in the spin-correlations and the k -space density of states. The black phase is a local moment (LM) phase, where the impurity is completely decoupled from the conduction electrons. **Middle:** Local spectral function of the impurity site. The blue curve is the normal Kondo resonance in the absence of any bath interaction. The yellow and green curves show the sharpening the spectral function through the locally pseudogapped phase, as momentum states are expelled from the Kondo cloud. The final pink curve shows the charge gap in the local moment phase. **Right:** Imaginary part of impurity self-energy. Poles represent the beginning of the optical gap between the central Kondo resonance and the Hubbard sidebands. Increasing the bath interaction leads to the coalescing of the poles (due to the sharpening of the Kondo resonance), ultimately leading to a zero frequency pole in the local moment phase.

screening the impurity at low energies. The k -space forms of this quantity at various values of W/J is shown in fig. 6.4, and the difference in the behaviour of the nodal and antinodal points is apparent.

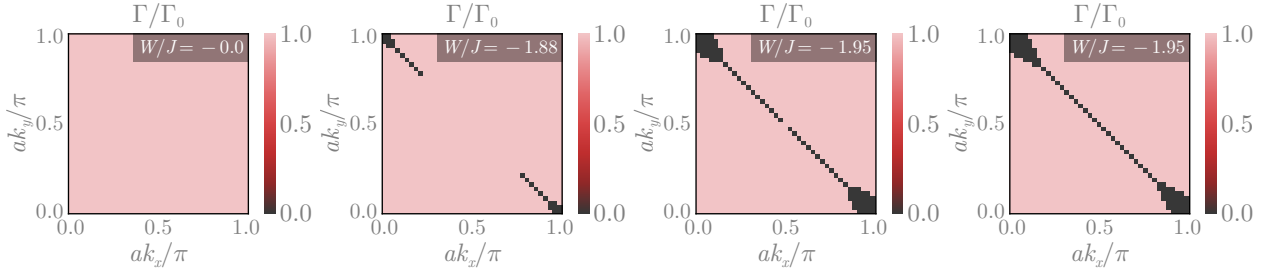


Figure 6.4: Variation of the total scattering probability $\Gamma(\mathbf{k})$ (defined in the main text) as W/J is increased from left to right. Each plot shows whether $\Gamma(\mathbf{k})$ is RG-relevant (pink) or irrelevant (black). RG-relevant values of $\Gamma(\mathbf{k})$ indicate that the k -point participates in Kondo screening at low-energies, while an irrelevant value indicates that the k -point is decoupled from the impurity site. As W/J is made more negative, the antinodal points are the first state to be removed from the Kondo cloud, while the node is the last to be removed.

6.2.3 Spin-correlations across the pseudogap

In figure 6.5, we show the evolution of the spin-spin correlation $\chi_s(d, \vec{k}) = \langle \mathbf{S}_d \cdot \mathbf{S}_{\vec{k}} \rangle$ in k -space, as the system is tuned through the pseudogap. At vanishing value of the interaction W , the spin correlations are concentrated around the antinode, because of the p -wave nature of the Kondo interaction. At the entry into the pseudogap, the correlations become more pronounced near the nodes and become suppressed near the antinodes, signalling that the latter parts will gap out first. The last three figures ($W/J = -1.74, -1.83, -1.84$) show how k -points starting from the antinode progressively exit the Kondo cloud, the node being the last to decouple from the impurity.

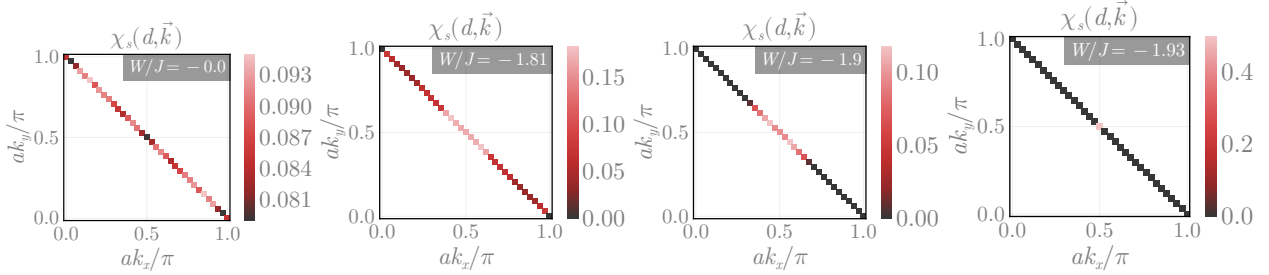


Figure 6.5: k -space distribution of spin-spin correlation $\chi_s(d, \vec{k})$ (defined in the main text). The last three figures show how k -points starting from the antinode progressively exit the Kondo cloud, the node being the last k -point to decouple from the impurity.

6.2.4 Charge correlations

In order to study the mechanism behind the destabilisation of the Kondo cloud through the pseudogap, we calculate the k -space double occupancy $\langle n_{\vec{k}\uparrow} n_{\vec{k}\downarrow} \rangle$ and k -space charge-transfer correlation

$\chi_c(\vec{k}, \vec{q}) = \left\langle c_{\vec{k}\uparrow}^\dagger c_{\vec{k}\downarrow}^\dagger c_{\vec{q}\downarrow} c_{\vec{q}\uparrow} \right\rangle$ (Fig. 6.6). We find that the entry into the pseudogap is marked by an increase of doubly-occupied states near the antinode in comparison to $W = 0$. These pairs likely lead to the concomitant vanishing of spin-correlations near the antinode at the same value of W , as seen in Fig. 6.5. More insight on the nature of these correlations are obtained from the fluctuations $\chi_c(\vec{k}, \vec{q})$ starting from the node ($\vec{q} = k_N$) and antinode ($\vec{q} = k_{AN}$). Interestingly, we find strong pair-transfer interactions between the node and antinode. Within the pseudogap, this leads to charge-isospin flip correlations between the decoupled antinodal region and the still-coupled nodal region.

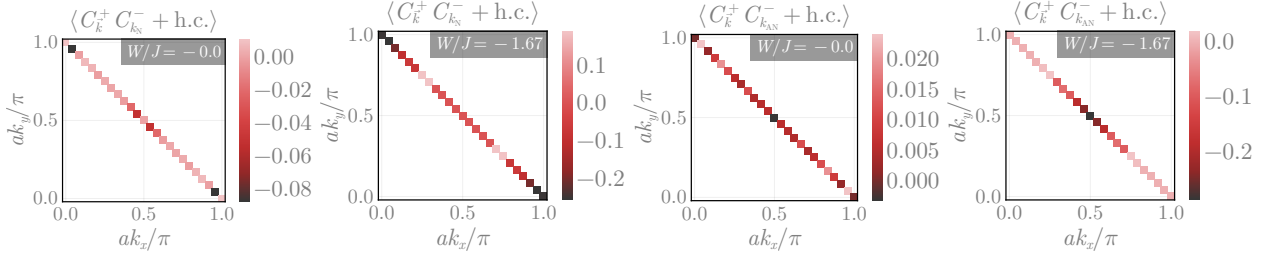


Figure 6.6: *Top panels:* Distribution of double occupancy at $W = 0$ and $W = -1.74$ (entry into the pseudogap). While the double occupancy is concentrated near the nodes at $W = 0$, it rises near the antinodes at the start of the pseudogap, signalling its destabilisation. *Bottom panels:* Charge-transfer correlation χ_c (defined in main text) starting from antinode (left) and node (right), at the beginning of the pseudogap phase. Strong node-antinode correlations are clearly visible.

6.3 Nature of Gapless Excitations in the Impurity Pseudogap

6.3.1 Emergence of a two-channel Kondo Model

As the bath interaction W is tuned through the L-PG phase, the four nodal points in the Brillouin zone are the last to decouple from the impurity. This allows us to write down a simpler Kondo model near the transition, focusing on scattering processes involving the nodal region. Specifically, for the Kondo term $J_{\mathbf{k}_1, \mathbf{k}_2}$, we find that only the following classes of scattering processes survive close to the critical point:

- Both momenta in a neighbourhood around \mathbf{k}_N , where \mathbf{k}_N can be any of the four nodal points,
- One momentum from the neighbourhood around \mathbf{k}_N , while the other from the neighbourhood around $\mathbf{k}_N + (\pi, \pi)$.

The second class is tied to the first through a symmetry of the Hamiltonian (eq. 6.12). The crucial feature of these processes is that each node only interacts with the other node directly opposite to it across the origin. That is, $(\pi/2, \pi/2)$ and $(-\pi/2, -\pi/2)$ only interact between themselves, while $(\pi/2, -\pi/2)$ and $(-\pi/2, \pi/2)$ form their own pair of connected regions.

Let S^\pm be the set of momentum states in a small window around nodes along $k_x = \pm k_y$. As discussed immediately above, the Kondo spin-exchange term close to the transition does not lead to scattering of any k -state from S^+ to S^- . This is verified by calculating the ratio $\max \left\{ J_{k_1^+, k_2^-} \right\} / \max \left\{ J_{k_1^+, k_2^+} \right\}$,

where the maximum in the numerator is calculated from all the low-energy (fixed point) Kondo scattering processes that connect the two sets S^\pm , while the denominator maximum is from within the set S^+ . This ratio vanishes (left panel of Fig. 6.7) within the local pseudogap regime, indicating that no direct Kondo scattering process persists between the two sectors S^\pm at low energies, deep within the pseudogap regime. We call the value of W at which this ratio vanishes W^* .

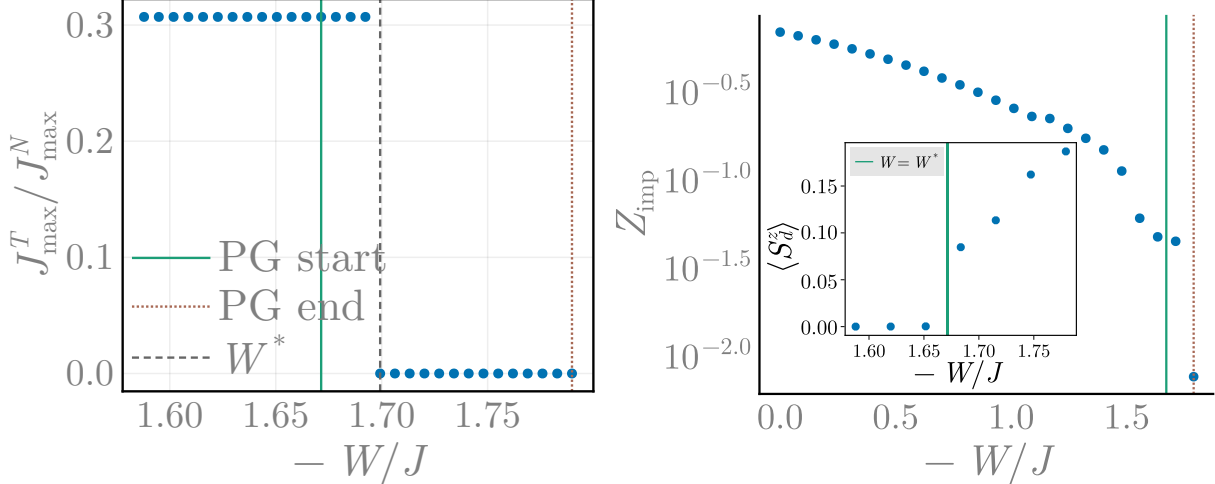


Figure 6.7: Left: Ratio between the maximum values of the fixed point values of the Kondo couplings for scattering processes between and within the regions S^+ and S^- . The vanishing of the fixed point ratio indicates that the pseudogap regime features a singular low-energy effective theory, where the Fermi surface neighbourhood splits into two disconnected regions with no explicit term in the Hamiltonian connecting them directly. Right: The quasiparticle residue Z_{imp} of the local gapless excitations in various regions. The vanishingly small values of Z_{imp} lend more support to the two-channel (and hence the non-Fermi liquid) nature of the low-energy physics in the pseudogap regime.

The decoupling of the k -space regions S^\pm is captured by the following simplified low-energy Hamiltonian:

$$H_{\text{eff}} = H(S^+) + H(S^-); H(S) = \sum_{\mathbf{q} \in S, \sigma} \varepsilon_{\mathbf{q}} c_{\mathbf{q}\sigma}^\dagger c_{\mathbf{q}\sigma} + \sum_{\mathbf{q}_1 \in S, \mathbf{q}_2 \in S} \sum_{\alpha, \beta} J^*(\mathbf{q}_1, \mathbf{q}_2) \mathbf{S}_d \cdot \sigma_{\alpha\beta} c_{\mathbf{q}_1\alpha}^\dagger c_{\mathbf{q}_2\beta}, \quad (6.15)$$

where $H(S^\pm)$ represents the dynamics of momentum states residing in regions S^\pm . The only source of information transfer between the two regions is the fact that they interact with the same impurity local moment. Eq. 6.15 tells us that the low-energy dynamics of the embedded eSIAM close to the Kondo-breakdown transition is governed by an emergent **two-channel Kondo model**, with the conduction bath states in the sets S^\pm making up the two channels.

6.3.2 Non-Fermi liquid behaviour in the pseudogap

It is well-known that the two-channel Kondo model hosts non-Fermi liquid excitations at low-energies [294, 295]; that this also happens in the present model is corroborated by our calculations of the quasiparticle residue Z_{imp} for the local gapless excitations. For a single-particle Greens function of an interacting model, the quasiparticle residue Z is defined as the spectral weight of low-energy resonance within the

spectral function:

$$G_k = \frac{Z}{\omega - \varepsilon_k - i\Sigma''} + G_{\text{incoh}}, \quad 1/Z = 1 - \frac{d\Sigma'}{d\omega}, \quad (6.16)$$

where Σ' and Σ'' are the real and imaginary parts of the self-energy, and G_{incoh} is contribution to the Greens function arising from incoherent short-lived excitations as well as high-energy features that are decoupled from the low-energy excitations [296]. Small values of Z indicate that the excitations cannot be described in terms of a Fermi liquid theory. Indeed, as shown in the right panel of Fig. 6.7, the quasiparticle residue Z_{imp} of the impurity excitations becomes vanishingly small in the pseudogap region, signalling that the excitations are of a non-Fermi liquid nature. Given that the pseudogap phase is close to a critical point in the impurity model phase diagram (separating the local Fermi liquid and local moment phases), it is not surprising that a quantum critical model emerges at that point.

Coleman and Ioffe have shown that by mapping the two-channel Kondo problem to a “compactified” form where the impurity spin hybridises with the spin and isospin degrees of freedom of a single conduction channel, the impurity self-energy $\Sigma = \Sigma' + i\Sigma''$ can be shown to display marginal Fermi liquid behaviour [?, 297]:

$$\Sigma' \propto \omega \ln \omega, \quad \Sigma'' \propto \omega. \quad (6.17)$$

Some of us have shown in a previous work [236] that this can also be obtained from a renormalisation group calculation of the low-energy excitations of the two-channel overscreened fixed point. For the sake of completeness, we have reproduced the calculation in Appendix .0.5.

6.3.3 Emergence of long-ranged interactions near the NFL-Mott insulator transition

We will now obtain a low-energy Hamiltonian for the excitations very close to the transition, where the Kondo coupling is about to turn irrelevant. In order to do this, we carry out a perturbation-theoretic treatment of the fixed point Hamiltonian in this region of the phase diagram, by considering the effects of a small fixed point Kondo scattering probability J^* in the backdrop of a larger bath interaction parameter W . We note that this is in contrast to the state of affairs that gave rise to the marginal Fermi liquid excitations in Subsection 6.3.2, where the Kondo coupling fixed the ground state and the conduction bath hopping processes led to the low-energy excitations; it is this contrast that leads to the emergence of a new effective Hamiltonian close to the transition.

The complete Hamiltonian (details described in Appendix .0.6) is

$$\Delta \tilde{H} = \sum_{\mathbf{q}, \sigma} \text{sign}(\varepsilon_{\mathbf{N}_1 + \mathbf{q}}) \frac{\varepsilon_{\mathbf{N}_1 + \mathbf{q}}^2}{-W} r_{\mathbf{q}, \sigma} + \sum_{\mathbf{q}_1, \mathbf{q}_2, \sigma} \frac{J^{*2}}{-4W} \left[r_{\mathbf{q}_1 \sigma} (1 - r_{\mathbf{q}_2 \bar{\sigma}}) - (1 - \delta_{\mathbf{q}_1, \mathbf{q}_2}) \phi_{\mathbf{q}_1, \bar{\sigma}}^\dagger \phi_{\mathbf{q}_1, \sigma}^\dagger \phi_{\mathbf{q}_2, \sigma} \phi_{\mathbf{q}_2, \bar{\sigma}} \right], \quad (6.18)$$

where the fermionic operator $\phi_{\mathbf{q}, \sigma}$ defines emergent relative modes,

$$\phi_{\mathbf{q}, \sigma} = \frac{1}{\sqrt{2}} (c_{\mathbf{N}_1 + \mathbf{q}, \sigma} - c_{\mathbf{N}_1 + \mathbf{Q}_1 - \mathbf{q}, \sigma}), \quad (6.19)$$

that are shifted by an excitation momentum \mathbf{q} away from the nodal point $\mathbf{N}_1 = (\pi/2, \pi/2)$ and its nested partner $\mathbf{N}_1 + \mathbf{Q}_1 = (-\pi/2, -\pi/2)$. The number operator $r_{\mathbf{q}\sigma}$ is defined as $r_{\mathbf{q}\sigma} = \phi_{\mathbf{q}, \sigma}^\dagger \phi_{\mathbf{q}, \sigma}$. $\varepsilon_{\mathbf{N}_1 + \mathbf{q}}$ represents the non-interacting kinetic energy of the conduction bath.

In order to extract the singular, critical part of the Hamiltonian, we focus on the $\mathbf{q}_1 = \mathbf{q}_2$ forward scattering processes:

$$\Delta\tilde{H}_{\mathbf{q}_1=\mathbf{q}_2} = \sum_{\mathbf{q},\sigma} \epsilon_{\mathbf{q}} r_{\mathbf{q},\sigma} + u \sum_{\mathbf{q},\sigma} r_{\mathbf{q}\sigma} r_{\mathbf{q}\bar{\sigma}} \quad (6.20)$$

where $\epsilon_{\mathbf{q}}$ and u are emergent energy scales:

$$\epsilon_{\mathbf{q}} = \text{sign}(\varepsilon_{\mathbf{N}_1+\mathbf{q}}) \frac{\varepsilon_{\mathbf{N}_1+\mathbf{q}}^2}{-W} + \frac{J^{*2}}{-4W}, \quad u = \frac{J^{*2}}{4W}. \quad (6.21)$$

Eq. 6.20 describes a Hatsugai-Kohmoto model [?, ?], an exactly solvable model of correlated electrons; by tuning the ratio of the interaction strength u and the bandwidth w , the model describes a transition between a non-Fermi liquid and a Mott insulator. The non-Fermi liquid nature of the gapless excitations in the metallic phase of the model manifests in the form of a divergent one-particle self-energy at the non-interacting Fermi surface [?]:

$$\Sigma_{\mathbf{q}}(\omega) = -\frac{u^2/4}{\omega - \epsilon_{\mathbf{q}}}, \quad \Sigma_{\epsilon_{\mathbf{q}}=0}(\omega \rightarrow 0) \rightarrow \infty, \quad (6.22)$$

while the spectral function $A(k, \omega = 0)$ shows a sharp peak at each of the four nodal Fermi surface points. This will be observed to lead to a nodal non-Fermi liquid metal shown below in Fig.6.8 (fourth panel). Beyond the transition and inside the Mott insulating phase, this zero frequency pole continues to exist and marks the hard gap in the spectral function for charge excitations. We note that the $\mathbf{q}_1 \neq \mathbf{q}_2$ scattering processes correspond to the forward and tangential scattering of the coherent superposition of $\mathbf{N}_1 = (\pi/2, \pi/2)$ and its nested partner $\mathbf{N}_1 + \mathbf{Q}_1 = (-\pi/2, -\pi/2)$ along the respective Fermi arcs. Such scattering processes add non-singular contributions to the self-energy, and do not open gaps at the Fermi surface. WE EXPECT SUCH A NODAL NON-FERMI LIQUID METAL TO EXHIBIT VOLUME LAW SCALING OF THE BIPARTITION ENTANGLEMENT ENTROPY.

6.4 Journey Through the Pseudogap on The Lattice model: Spectral Function, Spin Correlations and Entanglement

Having studied the phase diagram of the lattice-embedded impurity model, we now proceed to translate our results into the translation-invariant lattice model. For this, we use the results that we obtained in Sec. 5.3. In particular, we focus in this section on the implications of the impurity model pseudogap phase on the lattice model. We find that the anisotropic decoupling, from the impurity dynamics, of the conduction bath low-energy states leads to the formation of a partially gapped Fermi surface in the correlated model. The partial gapping is signalled by the replacement of Greens function poles with zeroes in the antinodal region.

6.4.1 k -space spectral function and self-energy

The primary indicator of the pseudogapping nature of the transition is of course the k -space density of states or the spectral function $\tilde{A}_{\mathbf{k}}(\omega)$. We calculate $\tilde{A}_{\mathbf{k}}(\omega)$ from the impurity-bath spectral function

computations carried out for the impurity model, using the following expression that was obtained previously (eq. 5.54):

$$\tilde{G}(\mathbf{K}\sigma; \omega) = G^>(\mathcal{T}_{\mathbf{K}\sigma}^\dagger, \omega - \varepsilon_{\mathbf{K}}) + G^<(\mathcal{T}_{\mathbf{K}\sigma}^\dagger, \omega + \varepsilon_{\mathbf{K}}) , \quad (6.23)$$

where $\mathcal{T}_{\mathbf{K}\sigma} = c_{\mathbf{K}\sigma} \left(\sum_{\sigma'} c_{d\sigma'}^\dagger + \text{h.c.} \right) + c_{\mathbf{K}\sigma} (S_d^+ + \text{h.c.})$ was defined in eq. 5.49, and $G^>(\mathcal{O}^\dagger, t) = -i \langle \mathcal{O}(t) \mathcal{O}^\dagger \rangle$ and $G^<(\mathcal{O}^\dagger, t) = -i \langle \mathcal{O}^\dagger \mathcal{O}(t) \rangle$ are the greater and lesser Greens function for the auxiliary model, and $\varepsilon_{\mathbf{K}}$ is the excitation energy associated with the momentum state \mathbf{K} , as determined by the dispersion on the lattice. In order to determine the low-energy behaviour in k -space, the zero frequency value $\tilde{A}_k(\omega \simeq 0)$ of the spectral function on the Fermi surface points is shown in Fig. 6.8 for various values of W/J .

We find that the Fermi surface remains completely gapless (seen through large non-zero values at zero frequency) for small values of W (first plot). However, if W is made sufficiently large, a partial gap opens up on the Fermi surface, starting from the antinode. Increasing the value of W/J leads to enlargement of the gapped region; exactly at the transition, we end up with a singular Fermi surface composed of just the nodal points.

In order to better understand the nature of the metal in the partially gapped region, we have also calculated the k -space self-energy $\tilde{\Sigma}(\mathbf{k}(\omega))$, using Dyson's equation:

$$\tilde{\Sigma}(\mathbf{k}(\omega)) = 1/\tilde{G}_k^{(0)}(\omega) - 1/\tilde{G}_k(\omega) , \quad (6.24)$$

where \tilde{G}_k is the interacting k -space Greens function (whose spectral function is shown in Fig. 6.8) while $\tilde{G}_k^{(0)}$ is the non-interacting $W = 0$ Greens function. We show the zero frequency value of the self-energy in Fig. 6.9, and the partial gapping of the Fermi surface is seen to arise from the appearance of poles in the self-energy at the antinodal region. As the partial gap expands, more and more k -space points exhibit poles in their self-energy. This, along with the behaviour of the spectral function, indicates that in the pseudogap region, the disconnected Fermi surface coexists with a Luttinger surface. WE EXPECT THAT THE JOURNEY THROUGH THE PSEUDOGAP DOES NOT VIOLATE LUTTINGER'S THEOREM; THIS CAN BE SEEN BY COUNTING BOTH THE POLES AND THE ZEROS OF THE SINGLE PARTICLE GREENS FUNCTION. CHECK.

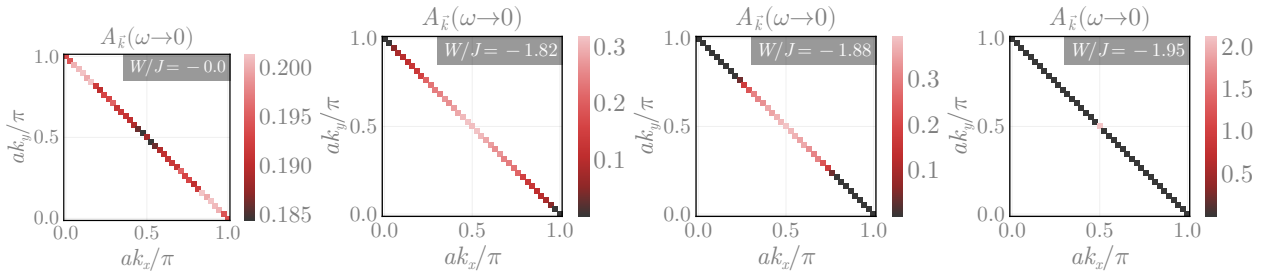


Figure 6.8: One-particle k -space spectral function. In the absence of bath interactions, all points on Fermi surface are gapless (first panel). Proceeding through the pseudogap results in the gapping out of Fermi surface points starting from the antinode (second panel) and approaching the node (third panel), until finally only the node remains at the critical point (fourth panel).

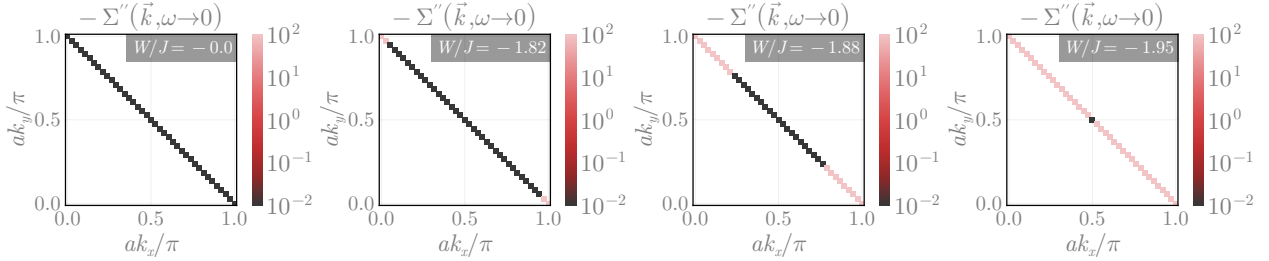


Figure 6.9: k -space self-energy. For $W = 0$, the self-energy is vanishingly small, leading to a Fermi liquid phase described by well-defined quasiparticles. Inside the pseudogap, the self-energy diverges near the antinodes, leading to their gapping. The coexistence of gapped and gapless points on the Fermi surface in the pseudogapped region leads to non-Fermi liquid behaviour of the gapless excitations, as captured by the emergent two-channel behaviour within the impurity model. The metal at the transition is supported only the four nodal points.

6.4.2 Momentum-space spin-correlations

To gain more insight on the nature of the fluctuations in various phases, we study the spin-spin correlation, $\tilde{\chi}_s(\mathbf{k}_1, \mathbf{k}_2) = \frac{1}{2} \langle \mathbf{S}_{\mathbf{k}_1} \cdot \mathbf{S}_{\mathbf{k}_2} \rangle$, where $\mathbf{S}(\mathbf{k}) = \sum_{\alpha\beta} c_{\mathbf{k}\alpha}^\dagger \boldsymbol{\sigma}_{\alpha\beta} c_{\mathbf{k}\beta}$. These correlations are again obtained from computations within the auxiliary model, using the relation obtained in eq. 5.71. While the full expression contains contributions from various combinations of auxiliary models, in the present work we focus on the intra-auxiliary model contribution which is the largest term:

$$C_{\mathcal{O}}(\mathbf{k}_1, \mathbf{k}_2) = \langle \psi_{\text{gs}}(\mathbf{r}_c) | \tilde{\mathcal{O}}(\mathbf{k}_2) | \psi_{\text{gs}}(\mathbf{r}_c) \rangle \langle \psi_{\text{gs}}(\mathbf{r}_c) | \tilde{\mathcal{O}}^\dagger(\mathbf{k}_1) | \psi_{\text{gs}}(\mathbf{r}_c) \rangle . \quad (6.25)$$

The results for Fermi surface points are shown in Fig. 6.10. We find that at small values of the bath interaction (first plot from left), the spin correlations are spread out uniformly on the Fermi surface, and are quite small in magnitude. This is likely because of the weakly correlated nature of the Fermi liquid. As we enter the pseudogap (second plot from left and beyond), the spin correlations of the antinodal region vanish. Along with the divergence of self-energy observed along the same points, this indicates that the antinodal region no longer participates in scattering processes that can renormalise the metal. The nodal region, however, sees an enhancement of spin correlations, particularly in its neighbourhood. This is a sign that the metallic excitations are becoming highly correlated through the pseudogap.

6.4.3 Entanglement entropy and Mutual information

We have also used our method to study the k -space entanglement entropy and mutual information within the lattice model, in order to probe the transition and the pseudogap. Given a pure state $|\Psi\rangle$ describing the complete system, the entanglement entropy $S_{\text{EE}}(\nu)$ of a subsystem ν quantifies the entanglement of ν with the rest of the subsystem, and is defined as

$$S_{\text{EE}}(\nu) = -\text{Tr} [\rho(\nu) \log \rho(\nu)], \quad \rho(\nu) = \text{Tr}_\nu [|\Psi\rangle \langle \Psi|] \quad (6.26)$$

where $\text{Tr} [\cdot]$ is the trace operator, and $\rho(\nu)$ is the reduced density matrix (RDM) for the subsystem ν obtained by taking the partial trace Tr_ν (over the states of ν) of the full density matrix $\rho = |\Psi\rangle \langle \Psi|$. If the subsystem ν describes local regions in real space (or states in k -space), we might be interested

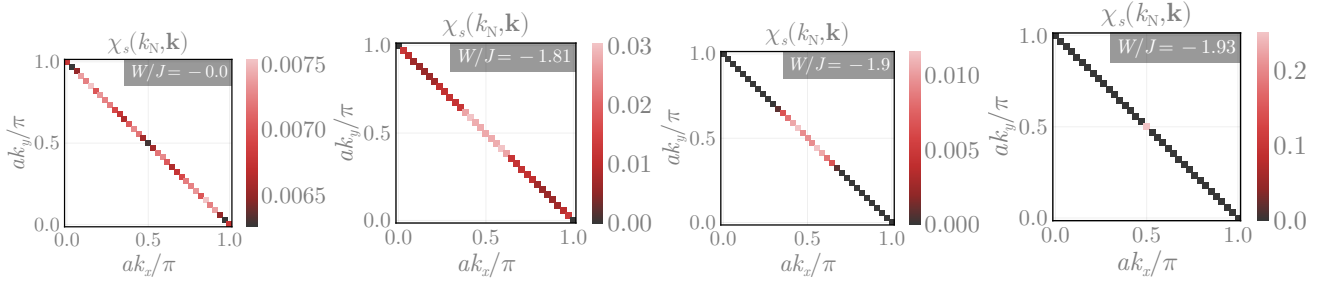


Figure 6.10: Spin-spin correlations χ_s (defined in main text) between the nodal point $k_N = (-\pi/2, -\pi/2)$ and an arbitrary k -point on the Fermi surface. In the absence of bath interaction (first panel), the correlations are somewhat uniformly distributed along the Fermi surface, and quite small. This describes the Fermi liquid phase of the lattice model. As we enter the pseudogap (second panel and beyond), the spin-correlations near the antinode vanish, indicating that they have been removed from the metallic excitations, while the correlations near the nodal point become enhanced because of the increasingly correlated nature of the metal.

in the entanglement between two such subsystems ν_1 and ν_2 . The correct measure to quantify such entanglement is the mutual information:

$$I_2(\nu_1, \nu_2) = S_{\text{EE}}(\nu_1) + S_{\text{EE}}(\nu_2) - S_{\text{EE}}(\nu_1 \cup \nu_2), \quad (6.27)$$

where $\nu_1 \cup \nu_2$ is a larger subsystem formed by combining ν_1 and ν_2 .

We have already shown how to obtain the RDM for a k -state from our approach, in eq. 5.78:

$$\tilde{\rho}(\mathbf{k}) \sim \text{Tr}_{\mathbf{k}} [|\psi_{\text{gs}}(\mathbf{r}_d)\rangle \langle \psi_{\text{gs}}(\mathbf{r}_d)|] + \frac{1}{N} \text{Tr}_{\mathbf{k}} \sum_{\mathbf{r}} [|\psi_{\text{gs}}(\mathbf{r}_d)\rangle \langle \psi_{\text{gs}}(\mathbf{r}_d + \mathbf{r})|], \quad (6.28)$$

where $|\psi_{\text{gs}}(\mathbf{r}_d)\rangle$ is a reference auxiliary model ground state, and $|\psi_{\text{gs}}(\mathbf{r}_d + \mathbf{r})\rangle$ sums over other auxiliary models at increasing distances from this reference model. The \sim indicates that the RDM needs to be normalised. In the present work, we have restricted our results to the intra-auxiliary model contribution (first term). We show, in Fig. 6.11, the results of entanglement calculations on the Fermi surface. The entanglement entropy distribution (top panel) in k -space shows how the partial gapping leads to the elimination of the antinodal k -modes from the ground state and excitations and the consequent vanishing of their entanglement. We also plot, in the lower panel, the mutual information between (i) an arbitrary k -state and the nodal point, and (ii) an arbitrary k -state and the edge of the disconnected Fermi surface in the pseudogap. While the nodal point is seen to remain somewhat strongly entangled with the other Fermi surface points, the edge of the “Fermi arc” has minimal entanglement until the system comes close to the critical point.

6.5 Nature of Low-Energy Excitations in Various Regimes

6.5.1 Fermi liquid excitations, $|W| < |W|^*$

As discussed in Sec. 6.3.1, the effective description of the impurity model for $|W| > |W|^*$ becomes that of a two-channel Kondo (2CK) model. Prior to that ($|W| < |W|^*$), the entire Fermi surface continues to

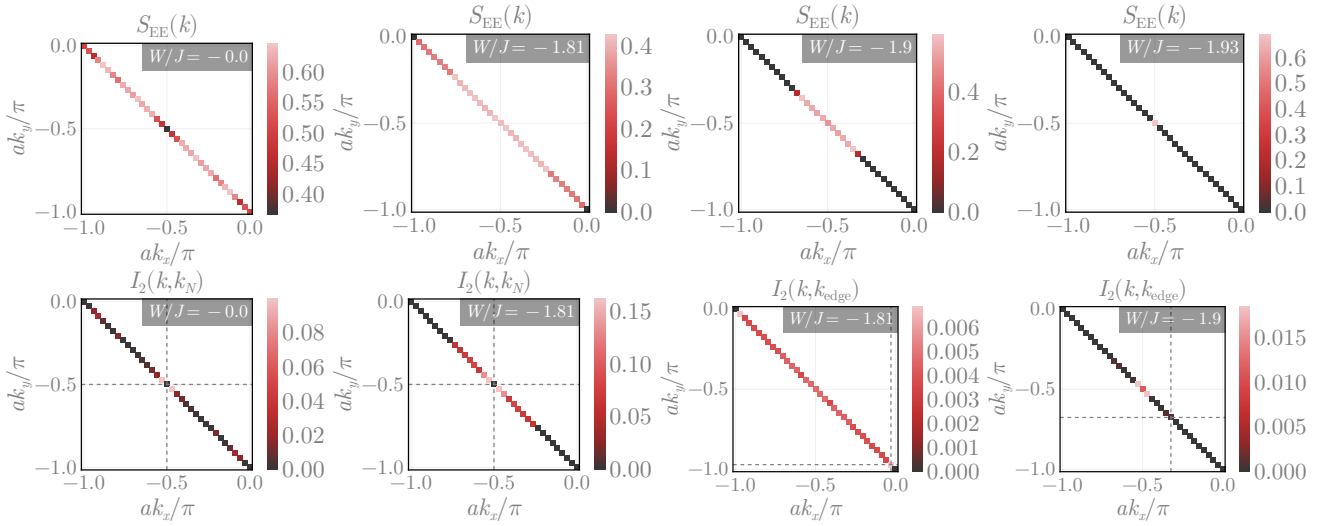


Figure 6.11: Top panel: Entanglement entropy $S_{\text{EE}}(\mathbf{k})$ on the Fermi surface. Similar to the correlations, the entanglement in the $W = 0$ model remains uniformly spread out over the Fermi surface. As the Fermi surface progressively shrinks, the entanglement gets concentrated to the nodal points. Bottom panel: Mutual information I_2 between (i) an arbitrary k -state and the nodal point (first and second plots), and (ii) an arbitrary k -state and the edge of the disconnected Fermi surface in the pseudogap (third and fourth plots). The ends of the partial Fermi surface appear to be weakly entangled to the rest of the Fermi surface, while the nodal points remain strongly entangled all the way through to the transition.

screen the impurity, and this leads to local Fermi liquid description of the impurity excitations. Using our translation operator prescription for mapping an impurity model to a lattice model (eq. 5.11), these local Fermi liquid excitations arising from each auxiliary model coherently combine to create extended Fermi liquid excitations in the lattice model. This is therefore the nature of the metal for $|W| < |W|^*$, and further support for this is found from the non-zero values of the quasiparticle residue in this regime (right panel of Fig. 6.7).

6.5.2 Marginal Fermi liquid, $|W| > |W|^*$

We have demonstrated in Subsection 6.3.2 that the low-lying excitations of the pseudogap phase are described by a marginal Fermi liquid. This is linked to the fact that the excitations within the impurity model become many-particle in nature - they involve fluctuations on multiple sites. This should be contrasted with the local Fermi liquid excitations that involve only the conduction bath site next to the zeroth site. Upon tiling, we can immediately see that the resulting metal is not a Fermi liquid; the extended excitations will involve excitations of multiple k -states, and just not a simple superposition of 1-particle excitations (that gave rise to the Fermi liquid). The build up of additional correlations within the marginal Fermi liquid (in comparison to the Fermi liquid) can also be ascertained from the fact that the local physics is determined by an impurity model which is highly local in k -space (due to the decoupling of the Fermi arms, see Sec. 6.3.1). Such a local-in- k -space impurity model is highly non-local in real-space, consisting of long-ranged interactions between the impurity and the conduction bath. This is another signature of the non-Fermi liquid nature of the excitations obtained upon tiling.

6.5.3 At the critical point, $|W| \lesssim |W|^*$

Crucially, we find that during the passage through the pseudogap phase, the nature of the non-Fermi liquid metal itself morphs; the marginal Fermi liquid description is found to break down at the transition, and is replaced by the non-Fermi liquid excitations of a Hatsugai-Kohmoto model. The singular nature of the excitations in this regime can be ascertained from the self-energy displaying divergent behaviour (see Subsection 6.3.3). This can be attributed to the extremely non-local form of the impurity model (arising from the fact that it couples to only the nodal points in k -space). This divergent self-energy is consistent with our numerical calculations of the impurity self-energy which showed that the self-energy poles approach the $\omega = 0$ point as the system is tuned towards the transition.

In order to probe how the metal becomes increasingly correlated as it is tuned through the pseudogap, we compare the quasiparticle residue Z_{imp} and the scattering rate Γ of the quasiparticles, at the beginning and end of the pseudogap. For the regime $|W| \gtrsim |W|^*$, the low-energy excitations obey the marginal Fermi liquid theory: $\Sigma' \sim \omega \ln \omega$, $\Sigma'' \sim -\omega$. This gives rise to a linear scattering rate $\Gamma \sim \omega$ (arising from the imaginary part of the self-energy), and a logarithmically vanishing quasiparticle residue [261]

$$Z_{\text{imp}}(\omega) = (1 - \frac{d\Sigma'}{d\omega})^{-1} \sim (c - \ln \omega)^{-1} \quad (6.29)$$

where c is a constant. Close to the transition ($|W| \lesssim |W_c|$), the low-energy theory is described by a Hatsugai-Kohmoto model, with a diverging self-energy:

$$\Sigma(\mathbf{k}) = U^2 / (\omega - \epsilon_{\mathbf{k}}) = U^2 \left[\mathcal{P}\left(\frac{1}{\omega - \epsilon_{\mathbf{k}}}\right) - i\pi\delta(\omega - \epsilon_{\mathbf{k}}) \right], \quad (6.30)$$

where $\mathcal{P}(\cdot)$ represents the principal value, and we used the Sokhotski–Plemelj theorem to write down the final expression. For small but non-zero values of $\omega - \epsilon_{\mathbf{k}}$, we get $Z_{\text{imp}} \sim \omega^2/U^2$. The metal near the transition therefore displays a much more rapid vanishing of the quasiparticle residue compared to the logarithmic vanishing for the marginal Fermi liquid. The scattering rate precisely at the surface $\omega = \epsilon_{\mathbf{k}}$, in fact, diverges: $\Gamma \sim U^2\delta(\omega - \epsilon_{\mathbf{k}})$, in contrast to the linearly vanishing scattering rate of the MFL.

6.5.4 Heisenberg model as a low-energy description of the Mott insulator

In the insulating phase, the ground state of each auxiliary model hosts a decoupled local moment. Upon applying the tiling procedure, the lattice model ground state becomes that of the Hubbard model in the atomic limit. In order to lift the extensive degeneracy of the state, we will now take into consideration inter-auxiliary model virtual scattering processes that were subdominant in the metallic phase and were hence ignored. These one-particle scattering processes lead to the emergence of a nearest-neighbour superexchange interaction. The calculation is a straightforward application of second order perturbation theory (Schrieffer-Wolff transformation). In order to allow virtual fluctuations that can lift the large ground state degeneracy and lower the energy, we consider (perturbatively) the effects of an irrelevant single-particle hybridisation that connects the nearest-neighbour sites. This perturbation Hamiltonian is therefore of the form

$$H_t = \sum_{\omega} V(\omega) \mathcal{P}(\omega) \sum_{\sigma} \left(c_{1\sigma}^\dagger c_{2\sigma} + \text{h.c.} \right), \quad (6.31)$$

where $V(\omega)$ only acts on states at the energy scale ω ; the renormalisation of V is encoded in the fact that $V(\omega)$ is largest for the excited states and vanishes at low-energies: $V(\omega \rightarrow 0) = 0$.

We show the details in Appendix .0.7. The final result is the emergence of the following effective Hamiltonian for the low-energy dynamics between any two nearest-neighbour sites i and j :

$$H_{\text{eff}} = 2 \frac{V_H^2}{U/2} (2S_i^z S_j^z + S_i^+ S_j^- + S_i^- S_j^+) = J_{\text{eff}} \mathbf{S}_i \cdot \mathbf{S}_j , \quad (6.32)$$

where the effective antiferromagnetic Heisenberg coupling is $J_{\text{eff}} = \frac{8V_H^2}{U}$ and $V_H \equiv V(\omega \rightarrow U/2)$ is the impurity-bath hybridisation at energy scales of the order of the Mott gap, in the sense of an RG flow.

Appendices

.0.5 Marginal Fermi liquid excitations in a two-channel Kondo model

By considering minimal hopping into the conduction bath and treating the effects of this hopping perturbatively against the overscreened screened ground state (determined by an intermediate coupling J^*), the low-energy excitations above the ground state of the two-channel Kondo (2CK) model are described by the following Hamiltonian [236]:

$$H_{\text{eff}} = \frac{8t^2}{J} \left[(S_{0,1}^z)^2 S_{0,2}^+ + (S_{0,2}^z)^2 S_{0,1}^+ \right] (S_{1,1}^- + S_{1,2}^-) + \text{h.c.}; \quad (33)$$

where $S_{i,l} = \frac{1}{2} \sum_{\sigma_1, \sigma_2} c_{i,\sigma_1,l}^\dagger \boldsymbol{\sigma}_{\sigma_1, \sigma_2} c_{i,\sigma_2,l}$ are spin operators for the i^{th} site on the l^{th} conduction channel (l can be 1 or 2 for a two-channel model). The labels σ_1 and σ_2 are spin indices that can be ± 1 . The site index 0 represents the bath sites connected immediately to the impurity site. The operator $c_{i,\sigma,l}^\dagger$ creates an electron with spin σ on the i^{th} site of the l^{th} conduction channel.

We will Fourier transform this effective Hamiltonian into k -space:

$$\frac{2t^2}{J} \sum_{\{k_i, k'_i\}} \sum_{\sigma, l} \left(e^{i(k_1 - k'_1)a} c_{k\sigma,l}^\dagger c_{k'\sigma,l} c_{k'_2 \uparrow, \bar{l}}^\dagger c_{k'_2 \downarrow, \bar{l}} c_{k'_1 \uparrow, \bar{l}}^\dagger c_{k'_1 \downarrow, \bar{l}} + \text{h.c.} \right). \quad (34)$$

Such a three particle interaction term was also obtained for the NFL phase of the 2D Hubbard model from a URG treatment (see Appendix B of Ref. [3]). The channel indices in Eq. 34 can be mapped to the normal directions in [3]. The 2 particle-1 hole interaction in Eq. 34 has a diagonal component which can be obtained by setting $k = k'$, $k_1 = k'_2$ and $k_2 = k'_1$:

$$\begin{aligned} H_{\text{MFL}} &= \sum_{k_1, k_2, \sigma, l} \frac{2t^2 e^{i(k_1 - k_2)a}}{J} \hat{n}_{k\sigma,l} \hat{n}_{k_2 \uparrow, \bar{l}} (1 - \hat{n}_{k_1 \downarrow, \bar{l}}) + \text{h.c.} \\ &= \sum_{k_1, k_2, \sigma, l} \frac{4t^2}{J} \cos a (k_1 - k_2) \hat{n}_{k\sigma,l} \hat{n}_{k_2 \uparrow, \bar{l}} (1 - \hat{n}_{k_1 \downarrow, \bar{l}}). \end{aligned} \quad (35)$$

The most dominant contribution comes from $k_1 = k_2 = k'$, revealing the non-Fermi liquid metal [?, 298]:

$$H_{\text{MFL}}^* = \frac{4t^2}{J} \sum_{\sigma, k, k', l} \hat{n}_{k\sigma,l} \hat{n}_{k' \uparrow, \bar{l}} (1 - \hat{n}_{k' \downarrow, \bar{l}}). \quad (36)$$

A non-local version of this effective Hamiltonian was found to describe the normal phase of the Mott insulator of the 2D Hubbard model, as seen from a URG analysis [3, 4]. Following [3], one can track the RG evolution of the dual coupling $R_j = \frac{4t^2}{J_j}$ at the j^{th} RG step, in the form of the URG equation

$$\Delta R_j = - \frac{R_j^2}{\omega - \epsilon_j/2 - R_j/8}. \quad (37)$$

In the RG equation, ϵ_j represents the energy of the j^{th} isoenergetic shell. It is seen from the RG equation that R is relevant in the range of $\omega < \frac{1}{2}\epsilon_j$ that has been used throughout, leading to a fixed-point at $R^*/8 = \omega - \frac{1}{2}\epsilon^*$). The relevance of R is expected because the strong coupling J is irrelevant and $R \sim 1/J$.

The renormalisation in R leads to a renormalisation in the real part of the single-particle self-energy [3]. The k -space-averaged self-energy renormalisation is

$$\Delta\Sigma'(\omega) = \rho R^{*2} \int_0^{\epsilon^*} \frac{d\epsilon_j}{\omega - \epsilon_j/2 + R_j/8}. \quad (38)$$

The density of states can be approximated to be N^*/R^* , where N^* is the total number of states over the interval R^* . As suggested by the fixed point value of R_j , we can approximate its behaviour near the fixed point by a linear dependence on the dispersion ϵ_j . The two limits of the integration are the starting and ending points of the RG. We start the RG very close to the Fermi surface and move towards the fixed point ϵ^* . Near the starting point, we substitute $\epsilon = 0$ and $R = \omega$, following the fixed point condition. From the fixed point condition, we also substitute $R^*/8 = \omega - \frac{1}{2}\epsilon^*$. On defining $\bar{\omega} = N^*(\omega - \frac{1}{2}\epsilon^*)$, we can write

$$\Delta\Sigma'(\omega) \sim \bar{\omega} \ln \frac{N^*\omega}{\bar{\omega}}. \quad (39)$$

The imaginary part of the self-energy can be obtained using the Kramers-Kronig relations:

$$\Delta\Sigma''(\omega) = \frac{1}{\pi} \mathcal{P} \int_{-\infty}^{\infty} d\omega' \frac{\Sigma'(\omega')}{\omega - \omega'} \sim -\bar{\omega}. \quad (40)$$

The self-energy also provides the quasiparticle residue for each channel [3]:

$$Z(\bar{\omega}) = \left(2 - \ln \frac{2\bar{\omega}}{N^*\omega} \right)^{-1}. \quad (41)$$

As $\omega \rightarrow 0$, the Z vanishes, implying that the ground state is *not adiabatically connected* to the Fermi gas in the presence of the NFL terms. This is the orthogonality catastrophe [261, 299–301] in the two-channel Kondo problem, and it is brought about by the presence of the channel-non diagonal terms in Eq. 36.

.0.6 Emergence of Hatsugai-Kohmoto model near the NFL-Mott insulator transition

As the bath interaction W is tuned through the L-PG phase, the nodal region is the last to decouple from the impurity. This allows us to write down a simpler Kondo model near the transition, where only the nodal region is hybridising with the impurity spin through Kondo interactions. This is done by retaining only those scattering processes $\mathbf{k}_1 \rightarrow \mathbf{k}_2$ that originate from and end at k -points within a small neighborhood of width $|\mathbf{q}|$ around the four nodal points: $\mathbf{k}_1, \mathbf{k}_2 \in \mathbf{N} + \mathbf{q}$, $|\mathbf{q}| \ll \pi$, where \mathbf{N} can be any one of the four nodal points $\mathbf{N}_1 = (\pi/2, \pi/2)$, $\mathbf{N}_2 = (-\pi/2, \pi/2)$ and $\mathbf{N}_1 + \mathbf{Q}_1$ and $\mathbf{N}_2 + \mathbf{Q}_2$, where $\mathbf{Q}_1 = (-\pi, -\pi)$ and $\mathbf{Q}_2 = (\pi, -\pi)$ are the two nesting vectors. We have already seen, in Subsection 6.3.1, that the pseudogap regime displays a decoupling of the Brillouin zone into sets of points that have no explicit connecting term in the Hamiltonian. Near the transition, the neighbourhoods of \mathbf{N}_1 and $\mathbf{N}_1 + \mathbf{Q}_1$ form one such connected set, while the other two nodes \mathbf{N}_2 and $\mathbf{N}_2 + \mathbf{Q}_2$ form another connected set, but these two sets are disconnected from each other, in the sense of a two-channel model. We also assume that the window of \mathbf{q} is small enough so that the fixed point Kondo coupling values $J^*(\mathbf{q}_1, \mathbf{q}_2)$ for the scattering processes involving \mathbf{q}_1 and \mathbf{q}_2 can be replaced by an average value J^* .

With these considerations, the simplified low-energy model near the transition describing the Kondo scattering processes can be written as

$$\tilde{H}_{\text{imp-cbath}} = J^* \frac{1}{2} \sum_{l=1,2} \sum_{\mathbf{q}_1, \mathbf{q}_2} \sum_{\alpha, \beta} \mathbf{S}_d \cdot \boldsymbol{\sigma}_{\alpha\beta} \left(c_{\mathbf{N}_l + \mathbf{q}_1, \alpha}^\dagger c_{\mathbf{N}_l + \mathbf{q}_2, \beta} + c_{\mathbf{N}_l + \mathbf{Q}_l + \mathbf{q}_1, \alpha}^\dagger c_{\mathbf{N}_l + \mathbf{Q}_l + \mathbf{q}_2, \beta} - c_{\mathbf{N}_l + \mathbf{Q}_l + \mathbf{q}_1, \alpha}^\dagger c_{\mathbf{N}_l + \mathbf{q}_2, \beta} - c_{\mathbf{N}_l + \mathbf{q}_1, \alpha}^\dagger c_{\mathbf{N}_l + \mathbf{Q}_l + \mathbf{q}_2, \beta} \right) . \quad (42)$$

For scattering processes that involve two opposite nodal points (that is, connected by one of the nesting vectors \mathbf{Q}_l , the Kondo coupling is $-J^*$, which explains the negative signs in the third and fourth terms. An explanation of the various dummy indices is in order. The label l can take values 1 or 2, allowing us to consider both the decoupled sets (associated with \mathbf{N}_1 and \mathbf{N}_2). It also labels the nesting vectors \mathbf{Q}_l associated with the two sets. α and β indicate spin indices, and \mathbf{q}_1 and \mathbf{q}_2 represent incoming and outgoing momenta in the scattering processes.

Because of the decoupling of the channel $l = 1$ and $l = 2$, we consider only the $l = 1$ channel for the rest of the calculations in this section, and we comment at the end on what the presence of two channels means for the results. In order to simplify the Hamiltonian, we define new fermionic operators

$$\psi_{\mathbf{q}, \sigma} = \frac{1}{\sqrt{2}} (c_{\mathbf{N}_1 + \mathbf{q}, \sigma} + c_{\mathbf{N}_1 + \mathbf{Q}_1 - \mathbf{q}, \sigma}) , \phi_{\mathbf{q}, \sigma} = \frac{1}{\sqrt{2}} (c_{\mathbf{N}_1 + \mathbf{q}, \sigma} - c_{\mathbf{N}_1 + \mathbf{Q}_1 - \mathbf{q}, \sigma}) , \quad (43)$$

The operator satisfy fermionic anticommutation relations:

$$\begin{aligned} \left\{ \psi_{\mathbf{q}, \sigma}, \psi_{\mathbf{q}', \sigma'}^\dagger \right\} &= \left[\delta_{\mathbf{q}, \mathbf{q}'} + \frac{1}{2} (\delta_{\mathbf{Q}_1 - \mathbf{q}, \mathbf{q}'} + \delta_{\mathbf{q}, \mathbf{Q}_1 - \mathbf{q}'}) \right] \delta_{\sigma, \sigma'} \\ &= \delta_{\mathbf{q}, \mathbf{q}'} \delta_{\sigma, \sigma'} , \\ \left\{ \phi_{\mathbf{q}, \sigma}, \phi_{\mathbf{q}', \sigma'}^\dagger \right\} &= \left[\delta_{\mathbf{q}, \mathbf{q}'} - \frac{1}{2} (\delta_{\mathbf{Q}_1 - \mathbf{q}, \mathbf{q}'} + \delta_{\mathbf{q}, \mathbf{Q}_1 - \mathbf{q}'}) \right] \delta_{\sigma, \sigma'} \\ &= \delta_{\mathbf{q}, \mathbf{q}'} \delta_{\sigma, \sigma'} , \\ \left\{ \psi_{\mathbf{q}, \sigma}, \phi_{\mathbf{q}', \sigma'}^\dagger \right\} &= \left\{ \phi_{\mathbf{q}, \sigma}, \psi_{\mathbf{q}', \sigma'}^\dagger \right\} = 0 , \end{aligned} \quad (44)$$

where both \mathbf{q} and \mathbf{q}' are chosen from a small window around the nodes, so their difference is also small and it is therefore guaranteed that $|\mathbf{q} + \mathbf{q}'| \neq |\mathbf{Q}_1|$, rendering both $\delta_{\mathbf{q}, \mathbf{Q}_1 - \mathbf{q}'}$ and $\delta_{\mathbf{Q}_1 - \mathbf{q}, \mathbf{q}'}$ zero. For convenience, we define new number operators for the sum and relative degrees of freedom:

$$s_{\mathbf{q}, \sigma} = \psi_{\mathbf{q}, \sigma}^\dagger \psi_{\mathbf{q}, \sigma}, r_{\mathbf{q}, \sigma} = \phi_{\mathbf{q}, \sigma}^\dagger \phi_{\mathbf{q}, \sigma} . \quad (45)$$

We then have the following useful relation between the corresponding number operators $n = c^\dagger c$:

$$n_{\mathbf{N}_1 + \mathbf{q}, \sigma} + n_{\mathbf{N}_1 + \mathbf{Q}_1 - \mathbf{q}, \sigma} = s_{\mathbf{q}, \sigma} + r_{\mathbf{q}, \sigma} . \quad (46)$$

We find that the sum degrees of freedom $s_{\mathbf{q}, \sigma}$ do not enter the Kondo scattering Hamiltonian $\tilde{H}_{\text{imp-cbath}}$ (for the single channel $l = 1$), and it is expressed purely in terms of the relative degrees of freedom:

$$\tilde{H}_{\text{imp-cbath}} = J^* \sum_{\mathbf{q}_1, \mathbf{q}_2, \alpha, \beta} \mathbf{S}_d \cdot \boldsymbol{\sigma}_{\alpha\beta} \phi_{\mathbf{q}_1 \alpha}^\dagger \phi_{\mathbf{q}_2 \beta} . \quad (47)$$

We now proceed to rewrite the other parts of the Hamiltonian in terms of these new degrees of freedom. The kinetic energy can be written as

$$\begin{aligned}\tilde{H}_{\text{cbath}} &= \sum_{\mathbf{q},\sigma} \varepsilon_{\mathbf{N}_1+\mathbf{q}} (n_{\mathbf{N}_1+\mathbf{q},\sigma} + n_{\mathbf{N}_1+\mathbf{Q}_1-\mathbf{q},\sigma}) \\ &= \sum_{\mathbf{q},\sigma} \varepsilon_{\mathbf{N}_1+\mathbf{q}} (\psi_{\mathbf{q},\sigma}^\dagger \phi_{\mathbf{q},\sigma} + \phi_{\mathbf{q},\sigma}^\dagger \psi_{\mathbf{q},\sigma}) ,\end{aligned}\quad (48)$$

We also consider a simplified form of the bath interaction (for the channel $l = 1$), taking into account the density-density correlations in k -space:

$$\begin{aligned}\tilde{H}_{\text{cbath-int}} &= -W \sum_{\mathbf{q},\sigma} (n_{\mathbf{N}_1+\mathbf{q},\sigma} + n_{\mathbf{N}_1+\mathbf{Q}_1-\mathbf{q},\sigma}) + W \sum_{\mathbf{q}_1,\mathbf{q}_2} (n_{\mathbf{N}_1+\mathbf{q}_1,\uparrow} + n_{\mathbf{N}_1+\mathbf{Q}_1-\mathbf{q}_1,\uparrow}) (n_{\mathbf{N}_1+\mathbf{q}_2,\downarrow} + n_{\mathbf{N}_1+\mathbf{Q}_1-\mathbf{q}_2,\downarrow}) , \\ &= -W \sum_{\mathbf{q},\sigma} (s_{\mathbf{q},\sigma} + r_{\mathbf{q},\sigma}) + W \sum_{\mathbf{q}_1,\mathbf{q}_2} (s_{\mathbf{q}_1,\uparrow} + r_{\mathbf{q}_1,\uparrow}) (s_{\mathbf{q}_2,\downarrow} + r_{\mathbf{q}_2,\downarrow}) .\end{aligned}\quad (49)$$

We used eq. 46 in order to obtain the final form.

Since both $\tilde{H}_{\text{imp-cbath}}$ and $\tilde{H}_{\text{cbath-int}}$ commute with $s_{\mathbf{q},\sigma}$, we replace the local objects $\sum_{\mathbf{q}} s_{\mathbf{q},\sigma}$ in $\tilde{H}_{\text{cbath-int}}$ with $\frac{1}{2}$ since the bath is always at half-filling. This results in a simplified Hamiltonian for just the $\phi_{\mathbf{q},\sigma}$ degrees of freedom:

$$\tilde{H} = -\frac{1}{2}W \sum_{\mathbf{q},\sigma} r_{\mathbf{q},\sigma} + W \sum_{\mathbf{q}_1,\mathbf{q}_2} r_{\mathbf{q}_1,\uparrow} r_{\mathbf{q}_2,\downarrow} + \sum_{\mathbf{q}_1,\mathbf{q}_2,\alpha,\beta} J^* \mathbf{S}_d \cdot \boldsymbol{\sigma}_{\alpha\beta} \phi_{\mathbf{q}_1\alpha}^\dagger \phi_{\mathbf{q}_2\beta} \quad (50)$$

For bath interaction strength close to the critical value ($W \lesssim W_c$), the fixed point coupling value J^* is much smaller than W . In order to obtain the gapless excitations of the system arising from the presence of the impurity site, we integrate out the impurity dynamics via a Schrieffer-Wolff transformation. The perturbation term \mathcal{V} then consists of Hamiltonian terms that modify the impurity configuration,

$$\mathcal{V} = \sum_{\mathbf{q}_1,\mathbf{q}_2} J^* S_d^+ \phi_{\mathbf{q}_1\downarrow}^\dagger \phi_{\mathbf{q}_2\uparrow} + \text{h.c.} , \quad (51)$$

while the “non-interacting” Hamiltonian is

$$H_D = -\frac{1}{2}W \sum_{\mathbf{q},\sigma} r_{\mathbf{q},\sigma} + W \sum_{\mathbf{q}_1,\mathbf{q}_2} r_{\mathbf{q}_1,\uparrow} r_{\mathbf{q}_2,\downarrow} . \quad (52)$$

The renormalisation in the dynamics of $b_{\vec{k},\sigma}^\dagger$ are given by

$$\Delta \tilde{H} = \mathcal{P}_L \mathcal{V} \mathcal{P}_H \frac{1}{E_L - H_D} \mathcal{V} \mathcal{P}_L , \quad (53)$$

where E_L is the energy of the ground state of H_D , $-(E_L - H_D)$ is the excitation energy of the state generated upon applying the perturbation \mathcal{V} , and $\mathcal{P}_{L(H)}$ projects onto the low(high)-energy subspace. For the present Hamiltonian, the low-energy state (associated with E_L) is the one that minimises the

bath interaction term $\tilde{H}_{\text{bath-int}}$; since the coupling W is negative, the minimal configuration is one in which the local operators $\sum_{\mathbf{q}} r_{\mathbf{q},\sigma}$ (for $\sigma = \pm 1$) are unity. This leads to the following low-energy state:

$$|L\rangle = \frac{1}{N} \sum_{\mathbf{q}_1 \mathbf{q}_2} \phi_{\mathbf{q}_1, \uparrow}^\dagger \phi_{\mathbf{q}_2, \downarrow}^\dagger |0\rangle \quad (54)$$

where $|0\rangle$ is the $r_{\mathbf{q}\uparrow} = r_{\mathbf{q}\downarrow} = 0$ state. The state $|L\rangle$ is at zero energy. High-energy states are obtained by applying, on the state $|L\rangle$, the excitation operator $\phi_{\mathbf{q}_1, \sigma}^\dagger \phi_{\mathbf{q}_2, \bar{\sigma}}$ or its hermitian conjugate. The operator converts a double and a hole to spin states, incurring a total excitation cost of $-W = |W|$.

We now calculate the various terms in $\Delta\tilde{H}$:

$$\begin{aligned} \mathcal{P}_L \mathcal{V} \mathcal{P}_H \frac{1}{E_L - H_D} \mathcal{V} \mathcal{P}_L &= \left(\frac{1}{2} + S_d^z \right) \sum_{\mathbf{q}_1, \mathbf{q}_2} \frac{J^{*2}}{-4W} \phi_{\mathbf{q}_1, \downarrow}^\dagger \phi_{\mathbf{q}_2, \uparrow} \left(\phi_{\mathbf{q}_2, \uparrow}^\dagger \phi_{\mathbf{q}_1, \downarrow} + (1 - \delta_{\mathbf{q}_1, \mathbf{q}_2}) \phi_{\mathbf{q}_1, \uparrow}^\dagger \phi_{\mathbf{q}_2, \downarrow} \right) \\ &= - \sum_{\mathbf{q}_1, \mathbf{q}_2} \frac{J^{*2}}{4W} \left[r_{\mathbf{q}_1 \downarrow} (1 - r_{\mathbf{q}_2 \uparrow}) - (1 - \delta_{\mathbf{q}_1, \mathbf{q}_2}) \phi_{\mathbf{q}_1, \uparrow}^\dagger \phi_{\mathbf{q}_1, \downarrow}^\dagger \phi_{\mathbf{q}_2, \downarrow} \phi_{\mathbf{q}_2, \uparrow} \right] \\ \mathcal{P}_L \mathcal{V} \mathcal{P}_H \frac{1}{E_L - H_D} \mathcal{V} \mathcal{P}_L &= \sum_{\mathbf{q}_1, \mathbf{q}_2} \frac{J^{*2}}{-4W} \left[r_{\mathbf{q}_1 \uparrow} (1 - r_{\mathbf{q}_2 \downarrow}) - (1 - \delta_{\mathbf{q}_1, \mathbf{q}_2}) \phi_{\mathbf{q}_1, \downarrow}^\dagger \phi_{\mathbf{q}_1, \uparrow}^\dagger \phi_{\mathbf{q}_2, \uparrow} \phi_{\mathbf{q}_2, \downarrow} \right] \end{aligned} \quad (55)$$

In both terms, we set $S_d^z = 0$ owing to local SU(2) symmetry on the impurity site. In the same way, we treat the effects of the dispersion term (eq. 48) to second order:

$$\begin{aligned} \mathcal{P}_L \mathcal{V} \mathcal{P}_H \frac{1}{E_L - H_D} \mathcal{V} \mathcal{P}_L &= \sum_{\mathbf{q}, \sigma} \frac{\varepsilon_{\mathbf{N}_1 + \mathbf{q}}^2}{-W} [\psi_{\mathbf{q}, \sigma}^\dagger \phi_{\mathbf{q}, \sigma} \phi_{\mathbf{q}, \sigma}^\dagger \psi_{\mathbf{q}, \sigma} + \phi_{\mathbf{q}, \sigma}^\dagger \psi_{\mathbf{q}, \sigma} \psi_{\mathbf{q}, \sigma}^\dagger \phi_{\mathbf{q}, \sigma}] \\ &= \sum_{\mathbf{q}, \sigma} \frac{\varepsilon_{\mathbf{N}_1 + \mathbf{q}}^2}{-W} [s_{\mathbf{q}, \sigma} (1 - r_{\mathbf{q}, \sigma}) + r_{\mathbf{q}, \sigma} (1 - s_{\mathbf{q}, \sigma})] . \end{aligned} \quad (56)$$

At the values of \mathbf{q} for which $\varepsilon_{\mathbf{N}_1 + \mathbf{q}} > 0$, we can set the number operator $s_{\mathbf{q}, \sigma} = 0$ (these positive energy modes are unoccupied in the ground state), while for $\varepsilon_{\mathbf{N}_1 + \mathbf{q}} < 0$, we have $s_{\mathbf{q}, \sigma} = 1$:

$$\mathcal{P}_L \mathcal{V} \mathcal{P}_H \frac{1}{E_L - H_D} \mathcal{V} \mathcal{P}_L = \sum_{\mathbf{q} (\varepsilon_{\mathbf{N}_1 + \mathbf{q}} > 0), \sigma} \frac{\varepsilon_{\mathbf{N}_1 + \mathbf{q}}^2}{-W} r_{\mathbf{q}, \sigma} + \sum_{\mathbf{q} (\varepsilon_{\mathbf{N}_1 + \mathbf{q}} < 0), \sigma} \frac{\varepsilon_{\mathbf{N}_1 + \mathbf{q}}^2}{-W} (1 - r_{\mathbf{q}, \sigma}) . \quad (57)$$

The complete Hamiltonian (combining eqs. 57 and 55) is

$$\Delta\tilde{H} = \sum_{\mathbf{q}, \sigma} \text{sign}(\varepsilon_{\mathbf{N}_1 + \mathbf{q}}) \frac{\varepsilon_{\mathbf{N}_1 + \mathbf{q}}^2}{-W} r_{\mathbf{q}, \sigma} + \sum_{\mathbf{q}_1, \mathbf{q}_2, \sigma} \frac{J^{*2}}{-4W} \left[r_{\mathbf{q}_1 \sigma} (1 - r_{\mathbf{q}_2 \bar{\sigma}}) - (1 - \delta_{\mathbf{q}_1, \mathbf{q}_2}) \phi_{\mathbf{q}_1, \bar{\sigma}}^\dagger \phi_{\mathbf{q}_1, \sigma}^\dagger \phi_{\mathbf{q}_2, \sigma} \phi_{\mathbf{q}_2, \bar{\sigma}} \right] . \quad (58)$$

.0.7 Heisenberg Model as a low-energy description of the tiled Mott insulator

For simplicity, we consider two impurity sites labelled 1 and 2 associated with two nearest-neighbour auxiliary models. The ground state subspace is four-fold degenerate:

$$|\Psi_L\rangle = \{|\sigma_1, \sigma_2\rangle\} , \quad \sigma_i = \pm 1 , \quad (59)$$

where σ_i is the spin state of site i . This ground state is derived from the following "zeroth order" Hamiltonian that emerges in the local moment phase of the auxiliary models when all scattering processes between the impurity and conduction bath are RG-irrelevant:

$$H_0 = -\frac{U}{2} \sum_{i=1,2} (n_{i\uparrow} - n_{i\downarrow})^2 ; \quad (60)$$

the local correlation on the impurity site becomes the largest scale in the problem in this phase and pushes the $|n_i = 2\rangle$ and $|n_i = 0\rangle$ states to high energies. This then defines the high-energy subspace for our calculation:

$$|\Psi_H\rangle = |C_1, C_2\rangle , \quad (61)$$

where C_i can take values 0 or 2, indicating that the state i is either empty or full, respectively. Both the double and hole states exist at a charge gap of the order of $U/2$ above the low-energy singly-occupied subspace defined by the states $|\Psi_L\rangle$.

In order to allow virtual fluctuations that can lift the large ground state degeneracy and lower the energy, we consider (perturbatively) the effects of an irrelevant single-particle hybridisation that connects the nearest-neighbour sites. This perturbation Hamiltonian is therefore of the form

$$H_t = \sum_{\omega} V(\omega) \mathcal{P}(\omega) \sum_{\sigma} (c_{1\sigma}^\dagger c_{2\sigma} + \text{h.c.}) , \quad (62)$$

where $V(\omega)$ only acts on states at the energy scale ω ; the renormalisation of V is encoded in the fact that $V(\omega)$ is largest for the excited states and vanishes at low-energies: $V(\omega \rightarrow 0) = 0$.

In order to obtain a low-energy effective Hamiltonian for the impurity sites arising from this hybridisation, we integrate out H_t via a Schrieffer-Wolff transformation. This leads to the following second-order Hamiltonian:

$$H_{\text{eff}} = \mathcal{P}_L H_t G \mathcal{H}_t \mathcal{P}_L . \quad (63)$$

The operator \mathcal{P}_L projects onto the low-energy subspace $|\Psi_L\rangle$ - this ensures that we remain in the low-energy subspace at the beginning and at the end of the total process. The Greens function $G = (E_L - H_0)^{-1}$ incorporates the excitation energy to go from the low-energy subspace $|\Psi\rangle_L$ (of energy E_L) to the excited subspace $|\Psi\rangle_H$ of energy $E_L + U/2$. Substituting the form of the perturbation Hamiltonian and the excitation energy into the above expression gives

$$H_{\text{eff}} = \frac{V_H^2}{-U/2} \sum_{\sigma, \sigma'} \left[c_{1\sigma}^\dagger c_{2\sigma} c_{2\sigma'}^\dagger c_{1\sigma'} + c_{2\sigma}^\dagger c_{1\sigma} c_{1\sigma'}^\dagger c_{2\sigma'} \right] . \quad (64)$$

where $V_H \equiv V(\omega \rightarrow U/2)$ is the impurity-bath hybridisation at energy scales of the order of the Mott gap, in the sense of an RG flow. Terms with consecutive creation or annihilation operators on the same site are prohibited because each site is singly-occupied in the ground state. It is now easy to cast this Hamiltonian into a more recognizable form. For $\sigma' = \sigma$, we get

$$\sum_{\sigma} \delta_{\sigma, \sigma'} c_{1\sigma}^\dagger c_{2\sigma} c_{2\sigma'}^\dagger c_{1\sigma'} = \sum_{\sigma} (n_{1\sigma} - n_{1\sigma} n_{2\sigma}) , \quad (65)$$

while $\sigma = -\sigma' = \pm 1$ gives

$$\sum_{\sigma} \delta_{\sigma, -\sigma'} c_{1\sigma}^\dagger c_{2\sigma} c_{2\sigma'}^\dagger c_{1\sigma'} = - (S_1^+ S_2^- + \text{h.c.}) . \quad (66)$$

For the latter expression, we introduced the local spin-flip operators S_i^\pm . The expression above it can also be cast into spin variables, using the equations

$$\begin{aligned} \frac{1}{2} \sum_{\sigma} n_{i\sigma} &= \frac{1}{2}, \\ \frac{1}{2} \sum_{\sigma} \sigma n_{i\sigma} &= S_i^z, \end{aligned} \tag{67}$$

where the first equation is simply the condition of half-filling at each site, and the second equation is the definition of the local spin operator in z -direction. Adding and subtracting the equations gives $n_{i\sigma} = \frac{1}{2} + \sigma S_i^z$.

Substituting everything back into eq. 64 and dropping constant terms gives

$$H_{\text{eff}} = 2 \frac{V_H^2}{U/2} (2S_1^z S_2^z + S_1^+ S_2^- + S_1^- S_2^+) = J_{\text{eff}} \mathbf{S}_1 \cdot \mathbf{S}_2, \tag{68}$$

where the effective antiferromagnetic Heisenberg coupling is $J_{\text{eff}} = \frac{8V_H^2}{U}$.

.1 Effective action for the Hubbard-Heisenberg model and the eSIAM

In order to better understand the similarities and differences between the tiling approach outlined here and the approach adopted in dynamical mean-field approximations, we compute the effective action for the local impurity as well as the impurity-zeroth site system, in both the auxiliary and bulk models. This will be done in the limit of infinite coordination number, in order to create a tractable effective theory.

.1.1 Local theory for the Hubbard-Heisenberg model

We will first work with the Hubbard-Heisenberg model. Let us recall that within the eSIAM, most of the dynamics is governed by the physics of the impurity site and the bath site coupled to the impurity. Accordingly, we will first obtain an effective action within the Hubbard-Heisenberg model for the small system consisting of a local site and all its nearest-neighbours.

We choose a certain local site that we call 0, whose nearest-neighbours will be denoted as $\{\bar{0}\}$. The action for the full Hubbard-Heisenberg model can be formally separated into three parts:

$$S_{\text{H-H}} = S_{0,\bar{0}} + S^{(0,\bar{0})} + S_{\text{int}}, \tag{69}$$

where $S_{0,\bar{0}}$ represents the part of the action that involves only the sites 0 and $\{\bar{0}\}$, $S^{(0,\bar{0})}$ represents the part that has all the sites apart from 0 and $\{\bar{0}\}$, while S_{int} contains all terms that connect these two parts. These three parts have the forms

$$\begin{aligned} S_{0,\bar{0}} &= \sum_{i=0,\bar{0}} \sum_{\sigma} \int_0^{\beta} d\tau c_{i\sigma}^\dagger(\tau) \partial_\tau c_{i\sigma}(\tau) - t \sum_{\bar{0},\sigma} \int_0^{\beta} d\tau \left[c_{0\sigma}^\dagger(\tau) c_{\bar{0}\sigma}(\tau) + \text{h.c.} \right] \\ &\quad - \frac{U}{2} \sum_{i=0,\bar{0}} \int_0^{\beta} d\tau (n_{i\uparrow}(\tau) - n_{i\downarrow}(\tau))^2 + J \sum_{\bar{0}} \int_0^{\beta} d\tau \vec{S}_0(\tau) \cdot \vec{S}_{\bar{0}}(\tau), \end{aligned} \tag{70}$$

$$S^{(0,\bar{0})} = \sum_{j \neq (0,\bar{0})} \sum_{\sigma} \int_0^{\beta} d\tau c_{j\sigma}^{\dagger}(\tau) \partial_{\tau} c_{j\sigma}(\tau) - t \sum_{\langle j,l \rangle \neq (0,\bar{0}), \sigma} \int_0^{\beta} d\tau \left[c_{j\sigma}^{\dagger}(\tau) c_{l\sigma}(\tau) + \text{h.c.} \right] \\ - \frac{U}{2} \sum_{j \neq (0,\bar{0})} \int_0^{\beta} d\tau (n_{j\uparrow}(\tau) - n_{j\downarrow}(\tau))^2 + J \sum_{\langle j,l \rangle \neq (0,\bar{0})} \int_0^{\beta} d\tau \vec{S}_l(\tau) \cdot \vec{S}_j(\tau), \quad (71)$$

$$S_{\text{int}} = -t \sum_{i \in \bar{0}} \sum_{j \in \text{NN of } i} \sum_{\sigma} \int_0^{\beta} d\tau \left(c_{i\sigma}^{\dagger}(\tau) c_{j\sigma}(\tau) + \text{h.c.} \right) + J \sum_{i \in \bar{0}} \sum_{j \in \text{NN of } i} \int_0^{\beta} d\tau \vec{S}_i(\tau) \cdot \vec{S}_j(\tau) = S_{\text{int}}^{\text{hop}} + S_{\text{int}}^{\text{spin}} \quad (72)$$

In order to obtain an effective theory $S_{\text{eff}}^{0,\bar{0}}$ purely for the local system $(0,\bar{0})$, we need to trace over all the other degrees of freedom. This partial trace will be carried out over the states of the so-called ‘‘cavity’’ system $S^{(0,\bar{0})}$. The effective action can be constructed by tracing over scattering processes of all orders that leave the final action diagonal in the system $(0,\bar{0})$. The formal expression can be written as

$$S_{\text{eff}}^{0,\bar{0}} = S_{0,\bar{0}} + \sum_{n=1}^{\infty} \langle \left(S_{\text{int}}^{\text{hop}} \right)^{2n} \rangle_{(0,\bar{0})} + \sum_{n=1}^{\infty} \langle \left(S_{\text{int}}^{\text{spin}} \right)^{2n} \rangle_{(0,\bar{0})} \quad (73)$$

where, as mentioned before, the average is carried out in the cavity system $S^{(0,\bar{0})}$. Each hopping term in the expansion is of the form

$$\begin{aligned} \left(S_{\text{int}}^{\text{hop}} \right)^{2n} &= t^{2n} \sum_{\sigma} \sum_{(i_1, i'_1), \dots, (i_n, i'_n)} \sum_{(j_1, j'_1), \dots, (j_n, j'_n)} \int_0^{\beta} d\tau_1 \dots d\tau_n d\tau'_1 \dots d\tau'_{j_n} \\ &\quad c_{i_1\sigma}^{\dagger}(\tau_{i_1}) c_{i_2\sigma}^{\dagger}(\tau_2) \dots c_{i_n\sigma}^{\dagger}(\tau_n) c_{i'_1\sigma}^{\dagger}(\tau'_1) c_{i'_2\sigma}^{\dagger}(\tau'_2) \dots c_{i'_n\sigma}^{\dagger}(\tau'_n) \left\langle c_{j_1\sigma}(\tau_1) c_{j_2\sigma}(\tau_2) \dots c_{j_n\sigma} c_{j'_1\sigma}^{\dagger}(\tau'_1) \dots c_{j'_n\sigma}^{\dagger}(\tau'_n) \right\rangle_{(0,\bar{0})} \\ &= t^{2n} \sum_{\sigma} \sum_{(i_1, i'_1), \dots, (i_n, i'_n)} \sum_{(j_1, j'_1), \dots, (j_n, j'_n)} \int_0^{\beta} d\tau_1 \dots d\tau'_{j_n} c_{i_1\sigma}^{\dagger}(\tau_{i_1}) \dots c_{i_n\sigma}^{\dagger}(\tau_n) c_{i'_1\sigma}^{\dagger}(\tau'_1) \dots c_{i'_n\sigma}^{\dagger}(\tau'_n) \\ &\quad G_n^{(0,\bar{0})}(\tau_1 \dots \tau_n; \tau'_1 \dots \tau'_n), \end{aligned} \quad (74)$$

where the indices i_1 through i_n and their primed counterparts run through $\bar{0}$, while j_l ($\in \{j_1, \dots, j'_n\}$) runs through the nearest-neighbours of the corresponding i_l index. The n -particle Greens function $G_n^{(0,\bar{0})}(\tau_1 \dots \tau_n; \tau'_1 \dots \tau'_n)$ for the cavity system is defined in the usual fashion

$$G_n^{(0,\bar{0})}(\tau_1 \dots \tau_n; \tau'_1 \dots \tau'_n) = \left\langle c_{j_1\sigma}(\tau_1) c_{j_2\sigma}(\tau_2) \dots c_{j_n\sigma} c_{j'_1\sigma}^{\dagger}(\tau'_1) \dots c_{j'_n\sigma}^{\dagger}(\tau'_n) \right\rangle_{(0,\bar{0})} \quad (75)$$

In the limit of infinite coordination number, only the $n = 1$ term survives:

$$\begin{aligned} \lim_{z \rightarrow \infty} \sum_{n=1}^{\infty} \langle \left(S_{\text{int}}^{\text{hop}} \right)^{2n} \rangle_{(0,\bar{0})} &= t^2 \sum_{\sigma} \sum_{i, i'} \int_0^{\beta} d\tau d\tau' c_{i\sigma}^{\dagger}(\tau) c_{i'\sigma}(\tau') \sum_{j, j'} G_1^{(0,\bar{0})}(j\tau; j'\tau') \\ &= \sum_{\sigma} \sum_{i, i'} \int_0^{\beta} d\tau d\tau' \Delta_{ii', \sigma}(\tau - \tau') c_{i\sigma}^{\dagger}(\tau) c_{i'\sigma}(\tau'), \end{aligned} \quad (76)$$

where we have defined the bath hybridisation function $\Delta_{ii', \sigma}(\tau - \tau')$ as

$$\Delta_{ii', \sigma}(\tau - \tau') = t^2 \sum_{j \in \text{NN of } i} \sum_{j' \in \text{NN of } i'} G_1^{(0,\bar{0})}(j\sigma\tau; j'\sigma\tau'). \quad (77)$$

Under similar approximations, the spin term in the action reduces to

$$\lim_{\mathcal{Z} \rightarrow \infty} \sum_{n=1}^{\infty} \langle \left(S_{\text{int}}^{\text{spin}} \right)^{2n} \rangle_{(0, \bar{0})} = \sum_{i, i'} \int_0^{\beta} d\tau d\tau' \chi(\tau - \tau') \vec{S}_i(\tau) \cdot \vec{S}_{i'}(\tau') , \quad (78)$$

where the susceptibility $\chi_{ii'}(\tau - \tau')$ is defined as

$$\chi_{ii'}(\tau - \tau') = J^2 \sum_{j \in \text{NN of } i} \sum_{j' \in \text{NN of } i'} \vec{S}_j(\tau) \cdot \vec{S}_{j'}(\tau') . \quad (79)$$

The effective action for the $0, \bar{0}$ system, in the limit of large coordination number, simplifies to

$$\begin{aligned} S_{\text{eff}}^{0, \bar{0}} = & \sum_{i=0, \bar{0}} \sum_{\sigma} \int_0^{\beta} d\tau c_{i\sigma}^{\dagger}(\tau) \partial_{\tau} c_{i\sigma}(\tau) - t \sum_{0, \sigma} \int_0^{\beta} d\tau \left[c_{0\sigma}^{\dagger}(\tau) c_{0\sigma}(\tau) + \text{h.c.} \right] - \frac{U}{2} \sum_{i=0, \bar{0}} \int_0^{\beta} d\tau (n_{i\uparrow}(\tau) - n_{i\downarrow}(\tau))^2 \\ & + J \sum_{\bar{0}} \int_0^{\beta} d\tau \vec{S}_0(\tau) \cdot \vec{S}_{\bar{0}}(\tau) + \sum_{i, i'} \int_0^{\beta} d\tau d\tau' \left[\sum_{\sigma} \Delta_{ii', \sigma}(\tau - \tau') c_{i\sigma}^{\dagger}(\tau) c_{i'\sigma}(\tau') + \chi_{ii'}(\tau - \tau') \vec{S}_i(\tau) \cdot \vec{S}_{i'}(\tau') \right] \end{aligned} \quad (80)$$

One can also write down an effective action purely for the local site 0. The sites $\bar{0}$ will now be a part of the environment action $S^{(0)}$ instead of the system action, but since the system is thermodynamically large, the cavity action can be assumed to remain the same, such the expectation values are calculated in the same system. As a result, the hybridisation and susceptibility functions remain unchanged. S_{int} is now made of terms that connect 0 and $\bar{0}$, so the transformation from $S^{(0, \bar{0})}$ can be made by replacing the set $\{j\}$ with the set $\bar{0}$, and the set $\bar{0}$ itself will be replaced by the local site 0. We quote the final form of the local effective action:

$$\begin{aligned} S_{\text{eff}}^0 = & \sum_{\sigma} \int_0^{\beta} d\tau c_{0\sigma}^{\dagger}(\tau) \partial_{\tau} c_{0\sigma}(\tau) - \frac{U}{2} \int_0^{\beta} d\tau (n_{0\uparrow}(\tau) - n_{0\downarrow}(\tau))^2 \\ & + \int_0^{\beta} d\tau d\tau' \left[\sum_{\sigma} \Delta_{00, \sigma}(\tau - \tau') c_{0\sigma}^{\dagger}(\tau) c_{0\sigma}(\tau') + \chi_{00}(\tau - \tau') \vec{S}_i(\tau) \cdot \vec{S}_{i'}(\tau') \right] \end{aligned} \quad (81)$$

.1.2 Local theory for the extended SIAM

The Hamiltonian for the extended SIAM model is shown in eq. 5.12. We will denote the impurity with the label d and the bath sites with the label c . Among the bath sites, we will represent the site coupled to the impurity with z . The full action has the form

$$\begin{aligned} S_{\text{ES}} = & \sum_{d, c} \sum_{\sigma} \int_0^{\beta} d\tau c_{d\sigma}^{\dagger}(\tau) \partial_{\tau} c_{d\sigma}(\tau) - t \sum_{\langle i, j \rangle \in c, \sigma} \int_0^{\beta} d\tau \left[c_{i\sigma}^{\dagger}(\tau) c_{j\sigma}(\tau) + \text{h.c.} \right] - V \sum_{\sigma} \int_0^{\beta} d\tau \left[c_{d\sigma}^{\dagger}(\tau) c_{z\sigma}(\tau) + \text{h.c.} \right] \\ & + J \int_0^{\beta} d\tau \vec{S}_d(\tau) \cdot \vec{S}_z(\tau) - \frac{U}{2} \int_0^{\beta} d\tau (n_{d\uparrow}(\tau) - n_{d\downarrow}(\tau))^2 - \frac{W}{2} \int_0^{\beta} d\tau (n_{z\uparrow}(\tau) - n_{z\downarrow}(\tau))^2 , \end{aligned} \quad (82)$$

As in the Hubbard-Heisenberg model, we first obtain an effective action for the pair of sites (d, z) . As in the previous calculation, this will again generate a hybridisation function $\Delta_{zz, \sigma}$ for the bath site nearest

to the zeroth site. No susceptibility will be generated however, because there is no spin-exchange coupling within the bath. The net result is

$$\begin{aligned} S_{\text{eff}}^{d,z} = & \sum_{d,c} \sum_{\sigma} \int_0^{\beta} d\tau c_{i\sigma}^{\dagger}(\tau) \partial_{\tau} c_{i\sigma}(\tau) - V \sum_{\sigma} \int_0^{\beta} d\tau \left[c_{d\sigma}^{\dagger}(\tau) c_{z\sigma}(\tau) + \text{h.c.} \right] + J \int_0^{\beta} d\tau \vec{S}_d(\tau) \cdot \vec{S}_z(\tau) \\ & - \frac{U}{2} \int_0^{\beta} d\tau (n_{d\uparrow}(\tau) - n_{d\downarrow}(\tau))^2 - \frac{W}{2} \int_0^{\beta} d\tau (n_{z\uparrow}(\tau) - n_{z\downarrow}(\tau))^2 \\ & + \int_0^{\beta} d\tau d\tau' \sum_{\sigma} \Delta_{zz,\sigma}(\tau - \tau') c_{z\sigma}^{\dagger}(\tau) c_{z\sigma}(\tau') \end{aligned} \quad (83)$$

This hybridisation $\Delta_{zz,\sigma}$ is calculated in the cavity model of the eSIAM, obtained by removing the impurity and the zeroth site from the full model; it is a completely non-interacting system.

One can go one step further and also remove the zeroth site in order to obtain a theory for the impurity site. With this choice, the cavity model now also includes the zeroth site, and hence contains the correlation term associated with W . The one-particle connection V will lead to a modified hybridisation \mathcal{F} for this effective theory; the Kondo terms will generate a susceptibility. The resultant action is

$$\begin{aligned} S_{\text{eff}}^d = & \sum_{\sigma} \int_0^{\beta} d\tau c_{d\sigma}^{\dagger}(\tau) \partial_{\tau} c_{d\sigma}(\tau) - \frac{U}{2} \int_0^{\beta} d\tau (n_{d\uparrow}(\tau) - n_{d\downarrow}(\tau))^2 \\ & + \int_0^{\beta} d\tau d\tau' \left[\sum_{\sigma} \mathcal{F}_{\sigma}(\tau - \tau') c_{i\sigma}^{\dagger}(\tau) c_{i'\sigma}(\tau') + \chi_d(\tau - \tau') \vec{S}_i(\tau) \cdot \vec{S}_{i'}(\tau') \right] \end{aligned} \quad (84)$$

where \mathcal{F} is defined in terms of the local correlator of the zeroth site

$$\mathcal{F}_{\sigma}(\tau - \tau') = V^2 G_1^{(d)}(z\sigma\tau; z\sigma\tau') = V^2 \langle c_{z\sigma}(\tau) c_{z\sigma}^{\dagger}(\tau') \rangle_{(d)} \quad (85)$$

with the average computed in the interacting cavity model that has the impurity site removed. The interaction arises from the W -term. The susceptibility is also calculated in this interacting cavity model, and follows the same definition as in the bulk model:

$$\chi_d(\tau - \tau') = J^2 \vec{S}_z(\tau) \cdot \vec{S}_z(\tau') . \quad (86)$$

2 Zero temperature Greens function in frequency domain

2.1 Spectral representation of Greens function

The impurity retarded Green's function is defined as

$$G_{d\sigma}(t) = -i\theta(t) \langle \{ \mathcal{O}_{\sigma}(t), \mathcal{O}_{\sigma}^{\dagger} \} \rangle \quad (87)$$

where the average $\langle \rangle$ is over a canonical ensemble at temperature T , and \mathcal{O}_{σ} is the excitation whose spectral function we are interested in. What follows is a standard calculation where we write the Green's function in the spectral representation. The ensemble average for the operator \mathcal{O}_{σ} can be written in terms of the exact eigenstates of the Hamiltonian:

$$H |n\rangle = E_n |n\rangle , \quad \langle \mathcal{O}_{\sigma} \rangle \equiv \frac{1}{Z} \sum_n \langle n | \mathcal{O}_{\sigma} | n \rangle e^{-\beta E_n} \quad (88)$$

where $Z = \sum_n e^{-\beta E_n}$ is the partition function and $\{|n\rangle\}$ is the set of eigenfunctions of the Hamiltonian. We can therefore write

$$\begin{aligned}
& \langle \{\mathcal{O}_\sigma(t), \mathcal{O}_\sigma^\dagger\} \rangle \\
&= \frac{1}{Z} \sum_m e^{-\beta E_m} \langle m | \{\mathcal{O}_\sigma(t), \mathcal{O}_\sigma^\dagger\} | m \rangle \\
&= \frac{1}{Z} \sum_{m,n} e^{-\beta E_m} \langle m | (\mathcal{O}_\sigma(t) | n \rangle \langle n | \mathcal{O}_\sigma^\dagger + \mathcal{O}_\sigma^\dagger | n \rangle \langle n | \mathcal{O}_\sigma(t)) | m \rangle \\
&\quad \left[\sum_n | n \rangle \langle n | = 1 \right] \\
&= \frac{1}{Z} \sum_{m,n} e^{-\beta E_m} \langle m | (e^{iH^*t} \mathcal{O}_\sigma e^{-iH^*t} | n \rangle \langle n | \mathcal{O}_\sigma^\dagger + \mathcal{O}_\sigma^\dagger | n \rangle \langle n | e^{iH^*t} \mathcal{O}_\sigma e^{-iH^*t}) | m \rangle \\
&= \frac{1}{Z} \sum_{m,n} e^{-\beta E_m} (e^{i(E_m - E_n)t} \langle m | \mathcal{O}_\sigma | n \rangle \langle n | \mathcal{O}_\sigma^\dagger | m \rangle + e^{i(E_n - E_m)t} \langle m | \mathcal{O}_\sigma^\dagger | n \rangle \langle n | \mathcal{O}_\sigma | m \rangle) \\
&= \frac{1}{Z} \sum_{m,n} e^{i(E_m - E_n)t} |\langle m | \mathcal{O}_\sigma | n \rangle|^2 (e^{-\beta E_m} + e^{-\beta E_n})
\end{aligned} \tag{89}$$

The time-domain impurity Green's function can thus be written as (this is the so-called Lehmann-Kallen representation)

$$G_{d\sigma} = -i\theta(t) \frac{1}{Z} \sum_{m,n} e^{i(E_m - E_n)t} |\langle m | \mathcal{O}_\sigma | n \rangle|^2 (e^{-\beta E_m} + e^{-\beta E_n}) \tag{90}$$

We are interested in the frequency domain form.

$$\begin{aligned}
G_{dd}^\sigma(\omega) &= \int_{-\infty}^{\infty} dt e^{i(\omega)t} G_{dd}^\sigma(t) \\
&= \frac{1}{Z} \sum_{m,n} |\langle m | \mathcal{O}_\sigma | n \rangle|^2 (e^{-\beta E_m} + e^{-\beta E_n}) (-i) \int_{-\infty}^{\infty} dt \theta(t) e^{i(\omega + E_m - E_n)t}
\end{aligned} \tag{91}$$

To evaluate the time-integral, we will use the integral representation of the Heaviside function:

$$\theta(t) = -\frac{1}{2\pi i} \lim_{\eta \rightarrow 0^+} \int_{-\infty}^{\infty} \frac{1}{x + i\eta} e^{-ixt} dx \tag{92}$$

With this definition, the integral in $G_{d\sigma}(\omega)$ becomes

$$\begin{aligned}
(-i) \int_{-\infty}^{\infty} dt \theta(t) e^{i(\omega + i0^+ + E_m - E_n)t} &= (-i) \frac{-1}{2\pi i} \lim_{\eta \rightarrow 0^+} \int_{-\infty}^{\infty} dx \frac{1}{x + i\eta} \int_{-\infty}^{\infty} dt e^{i(\omega + i0^+ + E_m - E_n - x)t} \\
&= \frac{1}{2\pi} \lim_{\eta \rightarrow 0^+} \int_{-\infty}^{\infty} dx \frac{1}{x + i\eta} 2\pi \delta(\omega + i0^+ + E_m - E_n - x) \\
&= \frac{1}{\omega + E_m - E_n + i0^+}.
\end{aligned} \tag{93}$$

The frequency-domain Green's function is thus

$$G_{dd}^\sigma(\omega) = \frac{1}{Z} \sum_{m,n} |\langle m | \mathcal{O}_\sigma | n \rangle|^2 (e^{-\beta E_m} + e^{-\beta E_n}) \frac{1}{\omega + E_m - E_n + i0^+} \tag{94}$$

The infinitesimally positive imaginary part in the denominator shifts the poles onto the lower half of the complex plane, leaving it analytic in the upper half: this is necessary to make the retarded Greens function causal.

2.2 Real and imaginary parts - The Sokhotski-Plemelj theorem

In order to write down the real and imaginary parts of the Greens function, we first prove the *Sokhotski-Plemelj* formula:

$$\lim_{\eta \rightarrow 0^+} \frac{1}{x + i\eta} = P \left(\frac{1}{x} \right) - i\pi\delta(x). \quad (95)$$

where $P(f(x))$ is the Cauchy principal value, defined as

$$P \left[\int_{-\infty}^{\infty} \frac{dx}{x} \right] = \int_{-\infty}^{0^-} \frac{dx}{x} + \int_{0^+}^{\infty} \frac{dx}{x}. \quad (96)$$

To prove the above identity, we integrate the left-hand side using a test function $f(x)$:

$$\begin{aligned} \lim_{\eta \rightarrow 0^+} \int_{-\infty}^{\infty} dx \frac{f(x)}{x + i\eta} &= \lim_{\eta \rightarrow 0^+} \int_{-\infty}^{\infty} dx \frac{f(x)(x - i\eta)}{x^2 + \eta^2} \\ &= \lim_{\eta \rightarrow 0^+} \int_{-\infty}^{\infty} dx f(x) \left[\frac{x}{x^2 + \eta^2} - i\eta \frac{1}{x^2 + \eta^2} \right] \end{aligned} \quad (97)$$

The first integral can be split into three parts:

$$\lim_{\eta \rightarrow 0^+} \int_{-\infty}^{\infty} dx f(x) \frac{x}{x^2 + \eta^2} = \lim_{\eta \rightarrow 0^+} \lim_{\varepsilon \rightarrow 0^+} \left[\int_{-\infty}^{-\varepsilon} dx \frac{f(x)x}{x^2 + \eta^2} + \int_{\varepsilon}^{\infty} dx \frac{f(x)x}{x^2 + \eta^2} + \int_{-\varepsilon}^{\varepsilon} dx \frac{f(x)x}{x^2 + \eta^2} \right] \quad (98)$$

For the first two parts, it is safe to take the limit of η , because x is always non-vanishing there. For the third part, we can approximate $f(x)$ as $f(0)$ in the neighbourhood $x \in [-\varepsilon, \varepsilon]$, $\varepsilon \rightarrow 0$. This leaves an odd function $x/(x^2 + \eta^2)$ as the integrand, being integrated over a symmetric range. The third term therefore vanishes. In total, we get

$$\lim_{\eta \rightarrow 0^+} \int_{-\infty}^{\infty} dx f(x) \frac{x}{x^2 + \eta^2} = \int_{-\infty}^{-\varepsilon} dx \frac{f(x)}{x} + \int_{\varepsilon}^{\infty} dx \frac{f(x)}{x} = P \left(\int_{-\infty}^{\infty} dx \frac{f(x)}{x} \right). \quad (99)$$

To evaluate the second integral of eq. 97, we note that the only region in which the integrand is non-zero is when $|x| \simeq 0$; there, we again approximate $f(x)$ as $f(0)$. The remaining integral can then be evaluated easily:

$$-i \lim_{\eta \rightarrow 0^+} \eta \int_{-\infty}^{\infty} dx \frac{f(x)}{x^2 + \eta^2} = -i \lim_{\eta \rightarrow 0^+} \eta f(0) \int_{-\infty}^{\infty} \frac{dx}{x^2 + \eta^2} = -i\pi f(0), \quad (100)$$

where we used $\int \frac{dx}{x^2 + \eta^2} = \frac{1}{\eta} \arctan(x/\eta)$. Combining eqs. 97, 99 and 100, we get

$$\lim_{\eta \rightarrow 0^+} \int_{-\infty}^{\infty} dx \frac{f(x)}{x + i\eta} = P \left(\int_{-\infty}^{\infty} dx \frac{f(x)}{x} \right) - i\pi \int_{-\infty}^{\infty} dx f(x)\delta(x). \quad (101)$$

This proves eq. 95.

The Sokhotski-Plemelj formula allows us to split the spectral representation into a real and an imaginary part:

$$\begin{aligned} G'_{d\sigma} &= \frac{1}{Z} \sum_{m,n} \|\langle m | \mathcal{O}_\sigma | n \rangle\|^2 (e^{-\beta E_m} + e^{-\beta E_n}) P\left(\frac{1}{\omega + E_m - E_n}\right) \\ G''_{d\sigma} &= -\pi \frac{1}{Z} \sum_{m,n} \|\langle m | \mathcal{O}_\sigma | n \rangle\|^2 (e^{-\beta E_m} + e^{-\beta E_n}) \delta(\omega + E_m - E_n) . \end{aligned} \quad (102)$$

The spectral function, specifically, is defined as follows:

$$A_{d\sigma}(\omega) = -\frac{1}{\pi} G'_{d\sigma} = \frac{1}{Z} \sum_{m,n} \|\langle m | \mathcal{O}_\sigma | n \rangle\|^2 (e^{-\beta E_m} + e^{-\beta E_n}) \delta(\omega + E_m - E_n) \quad (103)$$

2.3 Zero temperature spectral function

We specialise to zero temperature by taking the limit of $\beta \rightarrow \infty$. In both the partition function as well as inside the summation, the only term that will survive is the exponential of the ground state energy E_{GS} .

$$Z \equiv \sum_m e^{-\beta E_m} \implies \lim_{\beta \rightarrow \infty} Z = d_{GS} e^{-\beta E_{GS}}, \quad E_{GS} \equiv \min \{E_n\}$$

where d_{GS} is the degeneracy of the ground state. The spectral function then simplifies to

$$\begin{aligned} A_{d\sigma} &= \frac{1}{d_{GS} e^{-\beta E_{GS}}} \sum_{m,n} \|\langle m | \mathcal{O}_\sigma | n \rangle\|^2 [e^{-\beta E_m} \delta_{E_m, E_{GS}} + e^{-\beta E_n} \delta_{E_n, E_{GS}}] \delta(\omega + E_m - E_n) \\ &= \frac{1}{d_{GS}} \sum_{n, n_{GS}} [\|\langle n_{GS} | \mathcal{O}_\sigma | n \rangle\|^2 \delta(\omega + E_{GS} - E_n) + \|\langle n | \mathcal{O}_\sigma | n_{GS} \rangle\|^2 \delta(\omega - E_{GS} + E_n)] \end{aligned} \quad (104)$$

The label n_{GS} sums over all states $|n_{GS}\rangle$ with energy E_{GS} . In practise, we evaluate this expression by replacing the formal Dirac delta functions with "nascent" ones, such as a Lorentzian function with a sufficiently sharp peak.

2.4 Reconstructing full Green function from spectral function: Kramers-Kronig relations

As mentioned earlier, the retarded Greens function $G_R(\omega + i0^+)$ has a complex pole in the lower half of the complex plane. In the following, the frequency ω is assumed to be complex. Consider the integral

$$I(\omega) = \oint_C d\omega' \frac{G_R(\omega')}{\omega' - \omega}, \quad \omega \in \mathbb{R} . \quad (105)$$

The contour C encloses the entirety of the upper half of the complex plane as well as almost all points of the real line but avoids the pole at $\omega' = \omega$ by forming a semicircle about that point that extends into the upper half of the plane. Since the integrand is completely analytic in the region enclosed by the contour (recall again that G_R is analytic in the upper half), the integral evaluates to zero (by Cauchy's theorem):

$$I(\omega) = 0 . \quad (106)$$

One can also evaluate the integral along each part of the contour. The semicircular part contributes zero: this is because while the length of the semicircular arc goes as $|\omega'|$, the integrand vanishes faster than $1/|\omega'|$ as $|\omega'| \rightarrow \infty$ (this assumes that the Green function vanishes in the limit of $\omega \rightarrow \infty$). The part of the contour along the real axis can now be evaluated. The two parts of the contour on either side of the pole contribute

$$\int_{-\infty}^{\omega-0^+} d\omega' \frac{G_R(\omega')}{\omega' - \omega} + \int_{\omega+0^+}^{\infty} d\omega' \frac{G_R(\omega')}{\omega' - \omega} = P \int_{-\infty}^{\infty} d\omega' \frac{G_R(\omega')}{\omega' - \omega} \quad (107)$$

To evaluate the part of the integral along the small semicircular around $\omega' = \omega$ (that extends into the upper half), we argue that this contribution should be equal to that obtained by taking the semicircle that goes instead into the lower half but circulates in the opposite direction. Each of these contributions should, in turn, be equal to that obtained from joining these two contours. But joining these contours leads to a closed integral about the pole at $\omega' = \omega$, which is equal to $2\pi G_R(\omega)$.

$$\int_{\text{upper}} d\omega' \frac{G_R(\omega')}{\omega' - \omega} = \int_{\text{lower}} d\omega' \frac{G_R(\omega')}{\omega' - \omega} = \frac{1}{2} \oint_{C(\omega)} d\omega' \frac{G_R(\omega')}{\omega' - \omega} = i\pi G_R(\omega) . \quad (108)$$

Combining the last two equations, we get

$$I(\omega) = P \int_{-\infty}^{\infty} d\omega' \frac{G_R(\omega')}{\omega' - \omega} + i\pi G_R(\omega) . \quad (109)$$

Comparing with eq. 106 and separating into real part G'_R and imaginary part G''_R gives

$$P \int_{-\infty}^{\infty} d\omega' \frac{[G'_R(\omega') + iG''_R(\omega')]}{\omega' - \omega} + \pi [-G''_R(\omega) + iG'_R(\omega)] = 0 . \quad (110)$$

Comparing the imaginary parts gives

$$G'_R(\omega) = \frac{1}{\pi} P \int_{-\infty}^{\infty} d\omega' \frac{G''_R(\omega')}{\omega' - \omega} = -\mathcal{H}[G''_R(\omega)] , \quad (111)$$

where $\mathcal{H}[g(\omega)] = \frac{1}{\pi} P \int_{-\infty}^{\infty} d\omega' \frac{g(\omega')}{\omega - \omega'}$ is the Hilbert transform of the function $g(\omega)$. The spectral function was defined above as $-1/\pi$ times the imaginary part of the Greens function. Exchanging G''_R for A gives

$$G'_R(\omega) = \pi \mathcal{H}[A(\omega)] . \quad (112)$$

This provides a method for calculating the real part of a Greens function if the spectral function is already known.

.3 Greens function in the insulating phase: the Hubbard bands and mottness

In the insulating state, the cluster becomes a local moment and the bulk system reduces to the atomic limit $H = -\frac{U}{2} \sum_i (\hat{n}_{i\uparrow} - \hat{n}_{i\downarrow})^2$. The Greens function in this limit is that of the atomic limit of the Hubbard model:

$$G_i(\omega) = \sum_{\sigma} G_{i,\sigma}(\omega) = \frac{1 + \langle \tau_i \rangle}{\omega - \frac{U}{2}} + \frac{1 - \langle \tau_i \rangle}{\omega + \frac{U}{2}} \quad (113)$$

where $\tau_i = \sum_\sigma \hat{n}_{i,\sigma} - 1$. At half-filling $\langle \tau_i \rangle = 0$, the low and high-energy poles have equal spectral weights. This is different from the situation in a band insulator, where the valence band has all the spectral weight in the ground state while the conduction band is empty. On doping holes into the system such that $\langle \tau_i \rangle = -x < 0$, spectral weight is transferred from the upper Hubbard band at $\omega = U/2$ to the lower one at $\omega = -U/2$:

$$G_i(\omega) = \sum_\sigma G_{i,\sigma}(\omega) = \frac{1-x}{\omega - \frac{U}{2}} + \frac{1+x}{\omega + \frac{U}{2}} \quad (114)$$

This transfer of spectral weight across energy scales of the order of U , as well as the lack of poles at zero energies, is referred to as mottness [302].

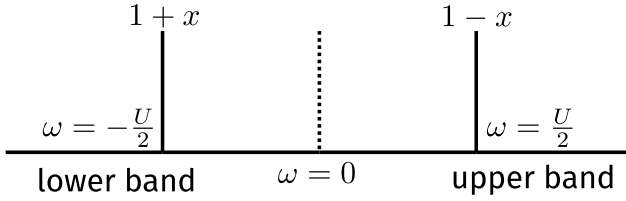


Figure 12: Structure of the Greens function in the atomic limit. The two poles at $\omega = \pm \frac{U}{2}$ form the two Hubbard bands. Doping the system leads to transfer of spectral weight between the bands.

.4 Nature of propagation: metal vs insulator

In the metallic state, the impurity in the auxiliary model hybridises with the bath through both 1-particle and 2-particle interactions. For any two auxiliary models differing by the locations i_1, i_2 of the impurity, the baths will always overlap. This means that an electron that starts out from the impurity site at i_1 can hop into the bath, and eventually reach i_2 by hopping out of the other bath and into the other impurity. Such processes connect all sites of the lattice and *allow spectral flow*.

In the insulating state, each auxiliary model separates into an impurity and a bath that decoupled from each other. This means that the impurity cannot hybridise into the bath, and hence cannot tunnel into any other impurity. This leads to the atomic limit of the system, where each site develops a local moment configuration because of the repulsive local correlation, but these local moments cannot communicate with each other, either through spin-exchange processes or by breaking into holons and doublons. Any attempt at spectral flow fails because the boundaries of the system become disconnected from each other.

A more accurate picture of the insulating and metallic phases can be obtained by working with a more complicated choice of the cluster. For instance, instead of a single impurity, one can take two correlated impurities interacting with each other through a single-particle hopping, and this cluster then interacts with the bath through the usual interactions. The ground state of such a cluster is actually a quantum liquid, consisting of the entangled spin and charge degrees of freedom. In the metallic state, various members of this liquid such as the holons, doublons and the spinons are free to propagate across the system through the baths. In the insulating state, it is this cluster that then gets decoupled from the other clusters. The composite degrees of freedom are then unable to propagate outside the cluster, and *the holons and the doublons are bound to each other* [191] within the confines of the cluster.

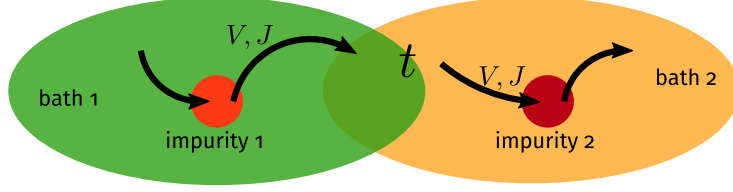


Figure 13: Propagation of electrons from one cluster to another through the bath, in the metallic state



Figure 14: The clusters get isolated from each other in the insulator, because they get decoupled from their baths.

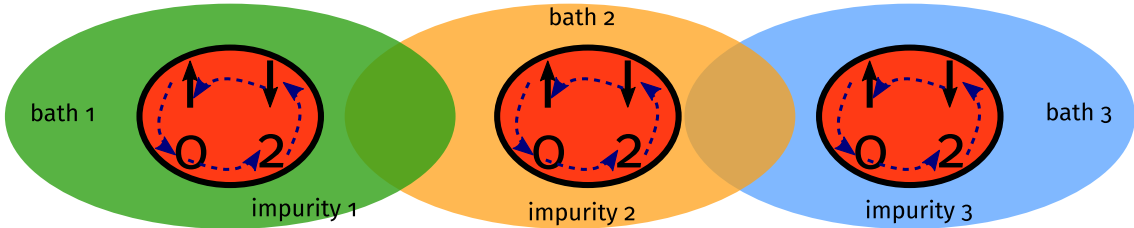


Figure 15: Each cluster is a quantum liquid composed of spin (\uparrow, \downarrow) and charge (0, 2) degrees of freedom. In the insulating state, these degrees of freedom get bound within the cluster and are unable to propagate outside.

.5 Presence of two self-energies under symmetry-breaking

The effective Hamiltonian that describes either the metallic or the insulating phase has SU(2) symmetry in both the spin and charge sectors. Since the repulsive correlation on the impurity picks out the spin sector, we focus on that for now. Applying a small magnetic field on the impurity breaks this spin-rotation symmetry and picks out either the up or the down state on the impurity, leading to two kinds of self-energies, one for each spin state [196, 289]. The Hamiltonian has the form $H(h)_i = -\frac{U}{2} (\hat{n}_{i\uparrow} - \hat{n}_{i\downarrow})^2 - h (\hat{n}_{i\uparrow} - \hat{n}_{i\downarrow})$. The unique ground-state is $|\hat{n}_{i,\sigma=\text{sgn}(h)} = 1, \hat{n}_{i,\sigma=-\text{sgn}(h)} = 0\rangle$, with an energy of $E_{\text{gs}} = -\frac{U}{2} - h$. The Greens function is easiest to obtain from the Lehmann-Kallen representation (eq. B.9):

$$G_{i,\sigma} = \sum_n \left[|\langle \text{GS} | c_{i\sigma} | n \rangle|^2 \frac{1}{\omega + E_{\text{GS}} - E_n} + |\langle n | c_{i\sigma} | \text{GS} \rangle|^2 \frac{1}{\omega - E_{\text{GS}} + E_n} \right] \quad (115)$$

We have $c_{i,\sigma} | \text{GS} \rangle = |\hat{n}_i = 0\rangle \delta_{\sigma, \text{sgn}(h)}$ and $c_{i,\sigma}^\dagger | \text{GS} \rangle = |\hat{n}_i = 2\rangle \delta_{\sigma, -\text{sgn}(h)}$, so that the only excited states that give non-zero inner product is $|n\rangle = |\hat{n}_i = 0\rangle$ for the second term and $|n\rangle = |\hat{n}_i = 2\rangle$ for the first term, with energies $E_n = 0$. Substituting these, we get

$$G_{i,\sigma}(h) = \frac{\delta_{\sigma, -\text{sgn}(h)}}{\omega - \frac{U}{2} - h} + \frac{\delta_{\sigma, \text{sgn}(h)}}{\omega + \frac{U}{2} + h} = \frac{1}{\omega + \left(\frac{U}{2} + h\right) \sigma \times \text{sgn}(h)} \quad (116)$$

Taking the limit of $h \rightarrow 0^\pm$ then gives

$$G_{i,\sigma}(h = 0^\pm) = \frac{1}{\omega \pm \frac{U}{2}\sigma} \quad (117)$$

The self-energies arising from the correlation U can also be obtained using Dyson's equation $\Sigma = G^{-1} - G_0^{-1}$, where $G_0^{-1} = \omega$ is the Greens function at $U = 0$. Using Dyson's equation, we get

$$\Sigma_{i,\sigma} = \pm \frac{U}{2}\sigma \quad (118)$$

.6 Derivation of RG equations for the embedded e-SIAM

.6.1 RG scheme

At any given step j of the RG procedure, we decouple the states $\{\mathbf{q}\}$ on the isoenergetic surface of energy ε_j . The diagonal Hamiltonian H_D for this step consists of all terms that do not change the occupancy of the states $\{\mathbf{q}\}$:

$$H_D^{(j)} = \varepsilon_j \sum_{q,\sigma} \tau_{q,\sigma} + \frac{1}{2} \sum_{\mathbf{q}} J_{\mathbf{q},\mathbf{q}} S_d^z (\hat{n}_{\mathbf{q},\uparrow} - \hat{n}_{\mathbf{q},\downarrow}) - \frac{1}{2} \sum_{\mathbf{q}} W_{\mathbf{q}} (\hat{n}_{\mathbf{q},\uparrow} - \hat{n}_{\mathbf{q},\downarrow})^2 , \quad (119)$$

where $\tau = \hat{n} - 1/2$ and $W_{\mathbf{q}}$ is a shorthand for $W_{\mathbf{q},\mathbf{q},\mathbf{q},\mathbf{q}}$. The three terms, respectively, are the kinetic energy of the momentum states on the isoenergetic shell that we are decoupling, the spin-correlation energy between the impurity spin and the spins formed by these momentum states and, finally, the local correlation energy associated with these states arising from the W term. The off-diagonal part of the Hamiltonian on the other hand leads to scattering in the states $\{\mathbf{q}\}$. We now list these terms, classified by the coupling they originate from.

Arising from the Kondo spin-exchange term

$$\begin{aligned} T_{KZ1}^\dagger + T_{KZ1} &= \frac{1}{2} \sum_{\mathbf{k},\mathbf{q},\sigma} \sigma J_{\mathbf{k},\mathbf{q}} S_d^z [c_{\mathbf{q}\sigma}^\dagger c_{\mathbf{k},\sigma} + \text{h.c.}] , \\ T_{KZ2}^\dagger + T_{KZ2} &= \frac{1}{2} \sum_{\mathbf{q},\sigma} \sigma J_{\mathbf{q},\bar{\mathbf{q}}} S_d^z [c_{\mathbf{q}\sigma}^\dagger c_{\bar{\mathbf{q}},\sigma} + \text{h.c.}] , \\ T_{KT1}^\dagger + T_{KT1} &= \frac{1}{2} \sum_{\mathbf{k},\mathbf{q}} J_{\mathbf{k},\mathbf{q}} \left[S_d^+ \left(c_{\mathbf{q}\downarrow}^\dagger c_{\mathbf{k}\uparrow} + c_{\mathbf{k}\downarrow}^\dagger c_{\mathbf{q}\uparrow} \right) + \text{h.c.} \right] , \\ T_{KT2}^\dagger + T_{KT2} &= \frac{1}{2} \sum_{\mathbf{q}} J_{\mathbf{q},\bar{\mathbf{q}}} \left[S_d^+ \left(c_{\mathbf{q}\downarrow}^\dagger c_{\bar{\mathbf{q}}\uparrow} + c_{\bar{\mathbf{q}}\downarrow}^\dagger c_{\mathbf{q}\uparrow} \right) + \text{h.c.} \right] , \end{aligned} \quad (120)$$

Arising from spin-preserving scattering within conduction bath

$$\begin{aligned}
T_{P1}^\dagger + T_{P1} &= - \sum_{\mathbf{q} \in \varepsilon_j} \sum_{\mathbf{k}_2, \mathbf{k}_3, \mathbf{k}_4 < \varepsilon_j} \sum_{\sigma} \left[W_{\mathbf{q}, \mathbf{k}_2, \mathbf{k}_3, \mathbf{k}_4} c_{\mathbf{q}, \sigma}^\dagger c_{\mathbf{k}_2, \sigma} c_{\mathbf{k}_3, \sigma}^\dagger c_{\mathbf{k}_4, \sigma} + \text{h.c.} \right] \\
T_{P2}^\dagger + T_{P3} &= - \sum_{\mathbf{q} \in \varepsilon_j} \sum_{\mathbf{k}_2 < \varepsilon_j} \sum_{\sigma} W_{\mathbf{q}, \mathbf{k}_2, \bar{\mathbf{q}}, \bar{\mathbf{q}}} c_{\mathbf{q}, \sigma}^\dagger c_{\mathbf{k}_2, \sigma} n_{\bar{\mathbf{q}}, \sigma} - \sum_{\mathbf{q} \in \varepsilon_j} \sum_{\mathbf{k}_1 < \varepsilon_j} \sum_{\sigma} W_{\mathbf{k}_1, \mathbf{q}, \mathbf{q}, \mathbf{q}} c_{\mathbf{k}_1, \sigma}^\dagger c_{\mathbf{q}, \sigma} n_{\mathbf{q}, \sigma} \\
T_{P4} &= - \sum_{\mathbf{q} \in \varepsilon_j} \sum_{\mathbf{k}_2, \mathbf{k}_3 < \varepsilon_j} \sum_{\sigma} W_{\mathbf{q}, \bar{\mathbf{q}}, \mathbf{k}_2, \mathbf{k}_3} c_{\mathbf{q}, \sigma}^\dagger c_{\bar{\mathbf{q}}, \sigma} c_{\mathbf{k}_2, \sigma}^\dagger c_{\mathbf{k}_3, \sigma} \\
T_{P5} &= - \sum_{\mathbf{q} \in \varepsilon_j} \sum_{\mathbf{k}_2, \mathbf{k}_3 < \varepsilon_j} \sum_{\sigma} W_{\mathbf{q}, \mathbf{k}_2, \mathbf{k}_3, \bar{\mathbf{q}}} c_{\mathbf{q}, \sigma}^\dagger c_{\mathbf{k}_2, \sigma} c_{\mathbf{k}_3, \sigma}^\dagger c_{\bar{\mathbf{q}}, \sigma} \\
&= + \sum_{\mathbf{q} \in \varepsilon_j} \sum_{\mathbf{k}_2, \mathbf{k}_3 < \varepsilon_j} \sum_{\sigma} W_{\mathbf{q}, \mathbf{k}_3, \mathbf{k}_2, \bar{\mathbf{q}}} c_{\mathbf{q}, \sigma}^\dagger c_{\bar{\mathbf{q}}, \sigma} c_{\mathbf{k}_2, \sigma}^\dagger c_{\mathbf{k}_3, \sigma} \\
&= -T_{P4}
\end{aligned} \tag{121}$$

Arising from spin-flip scattering within conduction bath

$$\begin{aligned}
T_{F1}^\dagger + T_{F1} &= \sum_{\mathbf{q} \in \varepsilon_j} \sum_{\mathbf{k}_2, \mathbf{k}_3, \mathbf{k}_4 < \varepsilon_j} \sum_{\sigma} \left[W_{\mathbf{q}, \mathbf{k}_2, \mathbf{k}_3, \mathbf{k}_4} c_{\mathbf{q}, \sigma}^\dagger c_{\mathbf{k}_2, \sigma} c_{\mathbf{k}_3, \bar{\sigma}}^\dagger c_{\mathbf{k}_4, \bar{\sigma}} + \text{h.c.} \right] \\
T_{F2} &= \sum_{\mathbf{q}, \mathbf{q}' \in \varepsilon_j} \sum_{\mathbf{k}_2, \mathbf{k}_3 < \varepsilon_j} \sum_{\sigma} W_{\mathbf{q}, \mathbf{q}', \mathbf{k}_2, \mathbf{k}_3} c_{\mathbf{q}, \sigma}^\dagger c_{\mathbf{q}', \sigma} c_{\mathbf{k}_2, \bar{\sigma}}^\dagger c_{\mathbf{k}_3, \bar{\sigma}} \\
T_{F3} &= \sum_{\mathbf{q}, \mathbf{q}' \in \varepsilon_j} \sum_{\mathbf{k}_2, \mathbf{k}_3 < \varepsilon_j} \sum_{\sigma} W_{\mathbf{q}, \mathbf{k}_2, \mathbf{k}_3, \mathbf{q}'} c_{\mathbf{q}, \sigma}^\dagger c_{\mathbf{k}_2, \sigma} c_{\mathbf{k}_3, \bar{\sigma}}^\dagger c_{\mathbf{q}', \bar{\sigma}} \\
T_{F4}^\dagger + T_{F4} &= \sum_{\mathbf{q}, \mathbf{q}' \in \varepsilon_j} \sum_{\mathbf{k}_1 < \varepsilon_j} \sum_{\sigma} \left[W_{\mathbf{q}, \mathbf{q}, \mathbf{q}', \mathbf{k}_1} n_{\mathbf{q}, \sigma} c_{\mathbf{q}', \bar{\sigma}}^\dagger c_{\mathbf{k}_1, \bar{\sigma}} + \text{h.c.} \right]
\end{aligned} \tag{122}$$

In all of the terms $T_{P[i]}$ and $T_{F[i]}$, the factor of $1/2$ in front has been cancelled out by a factor of 2 coming from the multiple possibilities of arranging the momentum labels. We will henceforth ignore T_{P4} and T_{P5} because they cancel each other out.

The renormalisation of the Hamiltonian is constructed from the general expression

$$\Delta H^{(j)} = H_X \frac{1}{\omega - H_D} H_X . \tag{123}$$

The states on the isoenergetic shell $\pm |\varepsilon_j|$ come in particle-hole pairs $(\mathbf{q}, \bar{\mathbf{q}})$ with energies of opposite signs (relative to the Fermi energy). If \mathbf{q} is defined as the hole state (unoccupied in the absence of quantum fluctuations), it will have positive energy, while the particle state $\bar{\mathbf{q}}$ will be of negative energy and hence below the Fermi surface. To be more specific, given a state \mathbf{q} with energy $\pm |\varepsilon_j|$, we define its particle-hole transformed counterpart as the state $\bar{\mathbf{q}} = \pi + \mathbf{q}$, having energy $\mp |\varepsilon_j|$ and residing in the opposite quadrant of the Brillouin zone. Given this definition, we have the important property that

$$\begin{aligned}
J_{\mathbf{k}, \bar{\mathbf{q}}} &= -J_{\mathbf{k}, \mathbf{q}}, \\
W_{\{\mathbf{k}\}, \bar{\mathbf{q}}} &= -W_{\{\mathbf{k}\}, \mathbf{q}} .
\end{aligned} \tag{124}$$

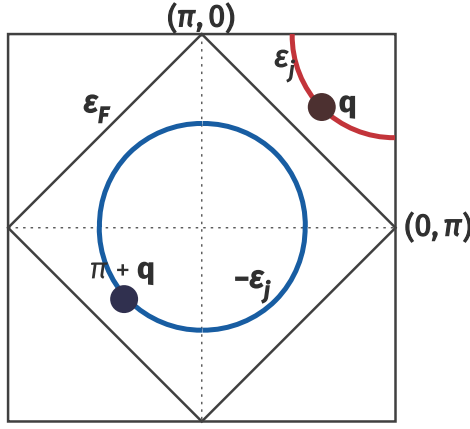


Figure 16: Particle and hole states.

.6.2 Renormalisation of the bath correlation term W

The bath correlation term W can undergo renormalisation only via scattering processes arising from itself. Irrespective of whether the state \mathbf{q} being decoupled is in a particle or hole configuration in the initial many-body state, the propagator $G = 1/(\omega - H_D)$ of the intermediate excited state is uniform, and equal to

$$G_W = 1/(\omega - |\varepsilon_j|/2 + W_q/2) , \quad (125)$$

where W_q is the same whether \mathbf{q} is above or below the Fermi surface. The $|\varepsilon_j|/2$ in H_D arises from the excited nature of the state after the initial scattering process.

Scattering arising purely from spin-preserving processes

In this subsection, we calculate the renormalisation to W arising from the terms T_{P1} , T_{P2} and T_{P3} . The first term is

$$\begin{aligned} T_{P1}^\dagger G_W T_{P3} &= \sum_\sigma \sum_{\mathbf{k}_1, \mathbf{k}_2, \mathbf{k}_3, \mathbf{k}_4} \sum_{\mathbf{q}} W_{\mathbf{q}, \mathbf{k}_2, \mathbf{k}_3, \mathbf{k}_4} c_{\mathbf{q}, \sigma}^\dagger c_{\mathbf{k}_2, \sigma} c_{\mathbf{k}_3, \sigma}^\dagger c_{\mathbf{k}_4, \sigma} G_W W_{\mathbf{k}_1, \mathbf{q}, \mathbf{q}, \mathbf{q}} c_{\mathbf{k}_1, \sigma}^\dagger c_{\mathbf{q}, \sigma} n_{\mathbf{q}, \sigma} \\ &= - \sum_\sigma \sum_{\mathbf{k}_1, \mathbf{k}_2, \mathbf{k}_3, \mathbf{k}_4} c_{\mathbf{k}_1, \sigma}^\dagger c_{\mathbf{k}_2, \sigma} c_{\mathbf{k}_3, \sigma}^\dagger c_{\mathbf{k}_4, \sigma} \sum_{\mathbf{q} \in \text{PS}} W_{\mathbf{q}, \mathbf{k}_2, \mathbf{k}_3, \mathbf{k}_4} G_W W_{\mathbf{k}_1, \mathbf{q}, \mathbf{q}, \mathbf{q}} . \end{aligned} \quad (126)$$

The operators acting on the states being decoupled contract to form a number operator $n_{\mathbf{q}, \sigma}$ which projects the sum over \mathbf{q} into the states that are initial occupied (particle sector, PS).

The second such contribution is obtained by flipping the sequence of scattering processes:

$$\begin{aligned} T_{P3} G_W T_{P1}^\dagger &= \sum_\sigma \sum_{\mathbf{k}_1, \mathbf{k}_2, \mathbf{k}_3, \mathbf{k}_4} \sum_{\mathbf{q}} W_{\mathbf{k}_1, \mathbf{q}, \mathbf{q}, \mathbf{q}} c_{\mathbf{k}_1, \sigma}^\dagger c_{\mathbf{q}, \sigma} n_{\mathbf{q}, \sigma} G_W W_{\mathbf{q}, \mathbf{k}_2, \mathbf{k}_3, \mathbf{k}_4} c_{\mathbf{q}, \sigma}^\dagger c_{\mathbf{k}_2, \sigma} c_{\mathbf{k}_3, \sigma}^\dagger c_{\mathbf{k}_4, \sigma} \\ &= \sum_\sigma \sum_{\mathbf{k}_1, \mathbf{k}_2, \mathbf{k}_3, \mathbf{k}_4} c_{\mathbf{k}_1, \sigma}^\dagger c_{\mathbf{k}_2, \sigma} c_{\mathbf{k}_3, \sigma}^\dagger c_{\mathbf{k}_4, \sigma} \sum_{\mathbf{q} \in \text{HS}} W_{\mathbf{q}, \mathbf{k}_2, \mathbf{k}_3, \mathbf{k}_4} G_W W_{\mathbf{k}_1, \mathbf{q}, \mathbf{q}, \mathbf{q}} . \end{aligned} \quad (127)$$

By virtue of eq. 124, the product of couplings $W_{\mathbf{q}, \mathbf{k}_2, \mathbf{k}_3, \mathbf{k}_4} G_W W_{\mathbf{k}_1, \mathbf{q}, \mathbf{q}, \mathbf{q}}$ is the same irrespective of whether \mathbf{q} belongs to the particle or hole sector. The two contributions therefore cancel each other. Moreover, the remaining contributions $T_{P3}^\dagger G_W T_{P1}$ and $T_{P1} G_W T_{P2}^\dagger$ are effectively hermitian conjugates of the two contributions considered above, and therefore also cancel each other.

Scattering arising from spin-flip processes

We now come to the processes that involve spin-flips. Considering T_{F1} and T_{F4} first, we get

$$\begin{aligned} T_{F1}^\dagger G_W T_{F4} &= \sum_\sigma \sum_{\mathbf{k}_1, \mathbf{k}_2, \mathbf{k}_3, \mathbf{k}_4} \sum_{\mathbf{q}} W_{\mathbf{q}, \mathbf{k}_2, \mathbf{k}_3, \mathbf{k}_4} c_{\mathbf{q}, \sigma}^\dagger c_{\mathbf{k}_2, \sigma} c_{\mathbf{k}_3, \bar{\sigma}}^\dagger c_{\mathbf{k}_4, \bar{\sigma}} G_W W_{\mathbf{k}_1, \mathbf{q}, \mathbf{q}, \mathbf{q}} c_{\mathbf{k}_1 \sigma}^\dagger c_{\mathbf{q} \sigma} n_{\mathbf{q} \bar{\sigma}} \\ &= - \sum_{1,2,3,4} \sum_\sigma c_{\mathbf{k}_1 \sigma}^\dagger c_{\mathbf{k}_2 \sigma} c_{\mathbf{k}_3 \bar{\sigma}}^\dagger c_{\mathbf{k}_4 \bar{\sigma}} \sum_{\mathbf{q} \in \text{PS}} W_{\mathbf{q}, \mathbf{k}_2, \mathbf{k}_4, \mathbf{k}_4} G_W W_{\mathbf{k}_1, \mathbf{q}, \mathbf{q}, \mathbf{q}}, \end{aligned} \quad (128)$$

$$\begin{aligned} T_{F4} G_W T_{F1}^\dagger &= \sum_\sigma \sum_{\mathbf{k}_1, \mathbf{k}_2, \mathbf{k}_3, \mathbf{k}_4} \sum_{\mathbf{q}} W_{\mathbf{k}_1, \mathbf{q}, \mathbf{q}, \mathbf{q}} c_{\mathbf{k}_1 \sigma}^\dagger c_{\mathbf{q} \sigma} n_{\mathbf{q} \bar{\sigma}} G_W W_{\mathbf{q}, \mathbf{k}_2, \mathbf{k}_3, \mathbf{k}_4} c_{\mathbf{q}, \sigma}^\dagger c_{\mathbf{k}_2, \sigma} c_{\mathbf{k}_3, \bar{\sigma}}^\dagger c_{\mathbf{k}_4, \bar{\sigma}} \\ &= \sum_{1,2,3,4} \sum_\sigma c_{\mathbf{k}_1 \sigma}^\dagger c_{\mathbf{k}_2 \sigma} c_{\mathbf{k}_3 \bar{\sigma}}^\dagger c_{\mathbf{k}_4 \bar{\sigma}} \sum_{\mathbf{q} \in \text{HS}} W_{\mathbf{q}, \mathbf{k}_2, \mathbf{k}_4, \mathbf{k}_4} G_W W_{\mathbf{k}_1, \mathbf{q}, \mathbf{q}, \mathbf{q}}. \end{aligned}$$

By the same arguments as in the previous subsection, these terms cancel each other out. Their hermitian conjugate contributions $T_{F1} G_W T_{F4}^\dagger$ and $T_{F4}^\dagger G_W T_{F1}$ also cancel out. The other two terms are T_{F2} and T_{F3} , and their contributions also cancel out for the same reason:

$$\begin{aligned} T_{F2} G_W T_{F2} &= \sum_\sigma \sum_{\mathbf{k}_1, \mathbf{k}_2, \mathbf{k}_3, \mathbf{k}_4} \sum_{\mathbf{q}} W_{\mathbf{q}, \bar{\mathbf{q}}, \mathbf{k}_3, \mathbf{k}_4} c_{\mathbf{q}, \sigma}^\dagger c_{\bar{\mathbf{q}}, \sigma} c_{\mathbf{k}_3, \bar{\sigma}}^\dagger c_{\mathbf{k}_4, \bar{\sigma}} G_W W_{\bar{\mathbf{q}}, \mathbf{q}, \mathbf{k}_1, \mathbf{k}_2} c_{\bar{\mathbf{q}}, \sigma}^\dagger c_{\mathbf{q}, \sigma} c_{\mathbf{k}_1, \bar{\sigma}}^\dagger c_{\mathbf{k}_2, \bar{\sigma}} \\ &= \sum_{1,2,3,4} \sum_\sigma c_{\mathbf{k}_1 \sigma}^\dagger c_{\mathbf{k}_2 \sigma} c_{\mathbf{k}_3 \bar{\sigma}}^\dagger c_{\mathbf{k}_4 \bar{\sigma}} \sum_{\mathbf{q} \in \text{PS}} W_{\mathbf{q}, \bar{\mathbf{q}}, \mathbf{k}_3, \mathbf{k}_4} G_W W_{\bar{\mathbf{q}}, \mathbf{q}, \mathbf{k}_1, \mathbf{k}_2}, \end{aligned} \quad (129)$$

$$\begin{aligned} T_{F3} G_W T_{F3} &= \sum_\sigma \sum_{\mathbf{k}_1, \mathbf{k}_2, \mathbf{k}_3, \mathbf{k}_4} \sum_{\mathbf{q}} W_{\mathbf{q}, \mathbf{k}_2, \mathbf{k}_3, \bar{\mathbf{q}}} c_{\mathbf{q}, \sigma}^\dagger c_{\mathbf{k}_2, \sigma} c_{\mathbf{k}_3, \bar{\sigma}}^\dagger c_{\bar{\mathbf{q}}, \bar{\sigma}} G_W W_{\bar{\mathbf{q}}, \mathbf{k}_4, \mathbf{k}_1, \mathbf{q}} c_{\bar{\mathbf{q}}, \bar{\sigma}}^\dagger c_{\mathbf{k}_4, \bar{\sigma}} c_{\mathbf{k}_1, \sigma}^\dagger c_{\mathbf{q}, \sigma} \\ &= - \sum_{1,2,3,4} \sum_\sigma c_{\mathbf{k}_1 \sigma}^\dagger c_{\mathbf{k}_2 \sigma} c_{\mathbf{k}_3 \bar{\sigma}}^\dagger c_{\mathbf{k}_4 \bar{\sigma}} \sum_{\mathbf{q} \in \text{PS}} W_{\mathbf{q}, \mathbf{k}_2, \mathbf{k}_3, \bar{\mathbf{q}}} G_W W_{\bar{\mathbf{q}}, \mathbf{k}_4, \mathbf{k}_1, \mathbf{q}}, \end{aligned}$$

Scattering involving both spin-flip and spin-preserving processes

These processes involve the combination of terms like T_{P1} with T_{F4} , and T_{P2} with T_{F1} . These again cancel each other out for the same reasons as outline above.

Net renormalisation for the bath correlation term

Since all the contributions cancel out in pairs, the bath correlation term W is *marginal*.

.6.3 Renormalisation of the Kondo scattering term \mathcal{J}

We focus on the renormalisation of the spin-flip part of the Kondo interaction. For these processes, the intermediate many-body state always involves the impurity spin being anti-correlated with the conduction electron spin, such that the propagator for that state is $G_J = 1 / (\omega - |\varepsilon_j|/2 + J_{\mathbf{q}}/4 + W_{\mathbf{q}}/2)$.

Impurity-mediated spin-flip scattering purely through Kondo-like processes

The following processes arising from the Kondo term renormalise the spin-flip interaction:

$$\begin{aligned}
T_{KT1}^\dagger G_J (T_{KZ1} + T_{KZ1}^\dagger) &= \frac{1}{4} \sum_{\mathbf{k}_1, \mathbf{k}_1, \mathbf{q}} J_{\mathbf{q}, \mathbf{k}_2} S_d^+ \left[-c_{\mathbf{q}\downarrow}^\dagger c_{\mathbf{k}_2\uparrow} G_J c_{\mathbf{k}_1\downarrow}^\dagger c_{\mathbf{q}\downarrow} + c_{\mathbf{k}_2\downarrow}^\dagger c_{\mathbf{q}\uparrow} G_J c_{\mathbf{q}\uparrow}^\dagger c_{\mathbf{k}_1\uparrow} \right] J_{\mathbf{k}_1, \mathbf{q}} S_d^z \\
&= -\frac{1}{8} \sum_{\mathbf{k}_1, \mathbf{k}_1, \mathbf{q}} J_{\mathbf{q}, \mathbf{k}_2} S_d^+ \left[c_{\mathbf{k}_1\downarrow}^\dagger c_{\mathbf{k}_2\uparrow} G_J n_{\mathbf{q}\downarrow} + c_{\mathbf{k}_2\downarrow}^\dagger c_{\mathbf{k}_1\uparrow} (1 - n_{\mathbf{q}\uparrow}) G_J \right] J_{\mathbf{k}_1, \mathbf{q}} \quad (130) \\
&= -\frac{1}{8} \sum_{\mathbf{k}_1, \mathbf{k}_1} S_d^+ c_{\mathbf{k}_1\downarrow}^\dagger c_{\mathbf{k}_2\uparrow} \sum_{\mathbf{q} \in \text{PS}} [J_{\mathbf{q}, \mathbf{k}_2} J_{\mathbf{k}_1, \mathbf{q}} + J_{\bar{\mathbf{q}}, \mathbf{k}_1} J_{\mathbf{k}_2, \bar{\mathbf{q}}}] G_J .
\end{aligned}$$

In getting the final expression, we used the sigma matrix relation $S_d^+ S_d^z = -\frac{1}{2} S_d^+$, and absorbed the projector $1 - n_{\mathbf{q}\uparrow}$ into the sum over the particle sector by replacing q with its particle-hole transformed counterpart \bar{q} . An identical contribution is obtained by switching the sequence of processes:

$$\begin{aligned}
(T_{KZ1} + T_{KZ1}^\dagger) G_J T_{KT1}^\dagger &= \frac{1}{4} \sum_{\mathbf{k}_1, \mathbf{k}_1, \mathbf{q}} J_{\mathbf{k}_1, \mathbf{q}} S_d^z \left[-c_{\mathbf{k}_1\downarrow}^\dagger c_{\mathbf{q}\downarrow} G_J c_{\mathbf{q}\downarrow}^\dagger c_{\mathbf{k}_2\uparrow} + c_{\mathbf{q}\uparrow}^\dagger c_{\mathbf{k}_1\uparrow} G_J c_{\mathbf{k}_2\downarrow}^\dagger c_{\mathbf{q}\uparrow} \right] J_{\mathbf{q}, \mathbf{k}_2} S_d^+ \\
&= -\frac{1}{8} \sum_{\mathbf{k}_1, \mathbf{k}_1} S_d^+ c_{\mathbf{k}_1\downarrow}^\dagger c_{\mathbf{k}_2\uparrow} \sum_{\mathbf{q} \in \text{PS}} [J_{\bar{\mathbf{q}}, \mathbf{k}_2} J_{\mathbf{k}_1, \bar{\mathbf{q}}} + J_{\mathbf{q}, \mathbf{k}_1} J_{\mathbf{k}_2, \mathbf{q}}] G_J . \quad (131)
\end{aligned}$$

Scattering processes involving interplay between the Kondo interaction and conduction bath interaction

Looking at T_{KT1}^\dagger first, we have

$$T_{KT1}^\dagger G_J (T_{F4} + T_{F4}^\dagger) = \frac{1}{2} \sum_{\mathbf{k}_1, \mathbf{k}_2, \mathbf{q}} J_{\mathbf{k}_2, \mathbf{q}} S_d^+ \left(c_{\mathbf{q}\downarrow}^\dagger c_{\mathbf{k}_2\uparrow} G_J W_{\mathbf{q}, \mathbf{q}, \mathbf{k}_1, \mathbf{q}} n_{\mathbf{q}\uparrow} c_{\mathbf{k}_1\downarrow}^\dagger c_{\mathbf{q}\downarrow} + c_{\mathbf{k}_2\downarrow}^\dagger c_{\mathbf{q}\uparrow} G_J W_{\bar{\mathbf{q}}, \bar{\mathbf{q}}, \mathbf{q}, \mathbf{k}_1} n_{\bar{\mathbf{q}}\downarrow} c_{\mathbf{q}\uparrow}^\dagger c_{\mathbf{k}_1\uparrow} \right) . \quad (132)$$

For either of the two choices of the functional form of W , it is easy to show that $W_{\mathbf{q}, \mathbf{q}, \mathbf{k}_1, \mathbf{q}} = W_{\bar{\mathbf{q}}, \bar{\mathbf{q}}, \mathbf{q}, \mathbf{k}_1}$.

$$T_{KT1}^\dagger G_J (T_{F4} + T_{F4}^\dagger) = \frac{1}{2} \sum_{\mathbf{k}_1, \mathbf{k}_2, \mathbf{q}} J_{\mathbf{k}_2, \mathbf{q}} W_{\mathbf{q}, \mathbf{q}, \mathbf{k}_1, \mathbf{q}} G_J S_d^+ \left[-c_{\mathbf{k}_1\downarrow}^\dagger c_{\mathbf{k}_2\uparrow} n_{\mathbf{q}\downarrow} n_{\mathbf{q}\uparrow} + c_{\mathbf{k}_2\downarrow}^\dagger c_{\mathbf{k}_1\uparrow} (1 - n_{\mathbf{q}\uparrow}) n_{\bar{\mathbf{q}}\downarrow} \right] . \quad (133)$$

Another contribution is obtained by switching the sequence of the scattering processes:

$$\begin{aligned}
(T_{F4} + T_{F4}^\dagger) G_J T_{KT1}^\dagger &= \frac{1}{2} \sum_{\mathbf{k}_1, \mathbf{k}_2, \mathbf{q}} \left(W_{\mathbf{q}, \mathbf{q}, \mathbf{k}_1, \mathbf{q}} n_{\bar{\mathbf{q}}\uparrow} c_{\mathbf{k}_1\downarrow}^\dagger c_{\mathbf{q}\downarrow} G_J c_{\mathbf{q}\downarrow}^\dagger c_{\mathbf{k}_2\uparrow} + W_{\bar{\mathbf{q}}, \bar{\mathbf{q}}, \mathbf{q}, \mathbf{k}_1} n_{\mathbf{q}\downarrow} c_{\mathbf{q}\uparrow}^\dagger c_{\mathbf{k}_1\uparrow} G_J c_{\mathbf{k}_2\downarrow}^\dagger c_{\mathbf{q}\uparrow} \right) J_{\mathbf{k}_2, \mathbf{q}} S_d^+ \\
&= \frac{1}{2} \sum_{\mathbf{k}_1, \mathbf{k}_2, \mathbf{q}} \left(c_{\mathbf{k}_1\downarrow}^\dagger c_{\mathbf{k}_2\uparrow} n_{\bar{\mathbf{q}}\uparrow} (1 - n_{\mathbf{q}\downarrow}) - c_{\mathbf{k}_2\downarrow}^\dagger c_{\mathbf{k}_1\uparrow} n_{\mathbf{q}\downarrow} n_{\mathbf{q}\uparrow} \right) W_{\mathbf{q}, \mathbf{q}, \mathbf{k}_1, \mathbf{q}} G_J J_{\mathbf{k}_2, \mathbf{q}} S_d^+
\end{aligned} \quad (134)$$

The two contributions (eqs. 133 and 134) arising from T_{KT1} cancel each other.

We now consider the other spin-exchange process T_{KT2}^\dagger . One such contribution is

$$\begin{aligned}
T_{KT2}^\dagger G_J T_{F3} &= \frac{1}{2} \sum_{\mathbf{k}_1, \mathbf{k}_2, \mathbf{q}} J_{\mathbf{q}, \bar{\mathbf{q}}} S_d^+ \left(c_{\mathbf{q}\downarrow}^\dagger c_{\bar{\mathbf{q}}\uparrow} G_J c_{\bar{\mathbf{q}}\uparrow}^\dagger c_{\mathbf{k}_2\uparrow} c_{\mathbf{k}_1\downarrow}^\dagger c_{\mathbf{q}\downarrow} + c_{\bar{\mathbf{q}}\downarrow}^\dagger c_{\mathbf{q}\uparrow} G_J c_{\mathbf{q}\uparrow}^\dagger c_{\mathbf{k}_2\uparrow} c_{\mathbf{k}_1\downarrow}^\dagger c_{\bar{\mathbf{q}}\downarrow} \right) W_{\bar{\mathbf{q}}, \mathbf{k}_2, \mathbf{k}_1, \mathbf{q}} \\
&= -\frac{1}{2} \sum_{\mathbf{k}_1, \mathbf{k}_2, \mathbf{q}} S_d^+ c_{\mathbf{k}_1\downarrow}^\dagger c_{\mathbf{k}_2\uparrow} [n_{\mathbf{q}\downarrow}(1 - n_{\bar{\mathbf{q}}\uparrow}) + n_{\bar{\mathbf{q}}\downarrow}(1 - n_{\mathbf{q}\uparrow})] J_{\mathbf{q}, \bar{\mathbf{q}}} G_J W_{\bar{\mathbf{q}}, \mathbf{k}_2, \mathbf{k}_1, \mathbf{q}} \\
&= -\frac{1}{2} \sum_{\mathbf{k}_1, \mathbf{k}_2} S_d^+ c_{\mathbf{k}_1\downarrow}^\dagger c_{\mathbf{k}_2\uparrow} \sum_{\mathbf{q} \in \text{PS}} (J_{\mathbf{q}, \bar{\mathbf{q}}} W_{\bar{\mathbf{q}}, \mathbf{k}_2, \mathbf{k}_1, \mathbf{q}} + J_{\bar{\mathbf{q}}, \mathbf{q}} W_{\mathbf{q}, \mathbf{k}_2, \mathbf{k}_1, \bar{\mathbf{q}}}) G_J .
\end{aligned} \tag{135}$$

An identical contribution is obtained from the reversed term:

$$\begin{aligned}
T_{F3} G_J T_{KT2}^\dagger &= \frac{1}{2} \sum_{\mathbf{k}_1, \mathbf{k}_2, \mathbf{q}} W_{\bar{\mathbf{q}}, \mathbf{k}_2, \mathbf{k}_1, \mathbf{q}} \left(c_{\bar{\mathbf{q}}\uparrow}^\dagger c_{\mathbf{k}_2\uparrow} c_{\mathbf{k}_1\downarrow}^\dagger c_{\mathbf{q}\downarrow} G_J c_{\mathbf{q}\downarrow}^\dagger c_{\bar{\mathbf{q}}\uparrow} + c_{\mathbf{q}\uparrow}^\dagger c_{\mathbf{k}_2\uparrow} c_{\mathbf{k}_1\downarrow}^\dagger c_{\bar{\mathbf{q}}\downarrow} G_J c_{\bar{\mathbf{q}}\downarrow}^\dagger c_{\mathbf{q}\uparrow} \right) J_{\mathbf{q}, \bar{\mathbf{q}}} S_d^+ \\
&= -\frac{1}{2} \sum_{\mathbf{k}_1, \mathbf{k}_2} S_d^+ c_{\mathbf{k}_1\downarrow}^\dagger c_{\mathbf{k}_2\uparrow} \sum_{\mathbf{q} \in \text{PS}} (J_{\mathbf{q}, \bar{\mathbf{q}}} W_{\bar{\mathbf{q}}, \mathbf{k}_2, \mathbf{k}_1, \mathbf{q}} + J_{\bar{\mathbf{q}}, \mathbf{q}} W_{\mathbf{q}, \mathbf{k}_2, \mathbf{k}_1, \bar{\mathbf{q}}}) G_J .
\end{aligned} \tag{136}$$

Net renormalisation to the Kondo interaction

Combining the results from eqs. 130, 131, 135 and 136, as well as using the properties $J_{\bar{\mathbf{q}}, \mathbf{k}_1} J_{\mathbf{k}_2, \bar{\mathbf{q}}} = J_{\mathbf{q}, \mathbf{k}_2} J_{\mathbf{k}_1, \mathbf{q}} = J_{\mathbf{k}_2, \mathbf{q}} J_{\mathbf{q}, \mathbf{k}_1}$ and $J_{\mathbf{q}, \bar{\mathbf{q}}} W_{\bar{\mathbf{q}}, \mathbf{k}_2, \mathbf{k}_1, \mathbf{q}} = J_{\bar{\mathbf{q}}, \mathbf{q}} W_{\mathbf{q}, \mathbf{k}_2, \mathbf{k}_1, \bar{\mathbf{q}}}$, the total renormalisation in the momentum-resolved Kondo coupling $J^{(j)}$ at the j^{th} step amounts to

$$\Delta J_{\mathbf{k}_1, \mathbf{k}_2}^{(j)} = - \sum_{\mathbf{q} \in \text{PS}} \frac{J_{\mathbf{k}_2, \mathbf{q}}^{(j)} J_{\mathbf{q}, \mathbf{k}_1}^{(j)} + 4 J_{\mathbf{q}, \bar{\mathbf{q}}}^{(j)} W_{\bar{\mathbf{q}}, \mathbf{k}_2, \mathbf{k}_1, \mathbf{q}}}{\omega - \frac{1}{2} |\varepsilon_j| + J_{\mathbf{q}}^{(j)}/4 + W_{\mathbf{q}}/2} \tag{137}$$

Appendix A

Heavy-fermions Project

A.1 Conclusions

Appendix B

Appendices

B.1 Zero temperature Greens function in frequency domain

The impurity retarded Green's function (assuming the Hamiltonian to be time-independent, which it is) is defined as

$$G_{dd}^\sigma(t) = -i\theta(t) \langle \{ \mathcal{O}_\sigma(t), \mathcal{O}_\sigma^\dagger \} \rangle \quad (\text{B.1})$$

where the average $\langle \cdot \rangle$ is over a canonical ensemble at temperature T , and $\mathcal{O}_\sigma = c_{d\sigma} + S_d^- c_{0\bar{\sigma}} + S_d^z c_{0\sigma}$ is the excitation whose spectral function we are interested in. The excitations defined in \mathcal{O} incorporates both single-particle excitations brought about by the hybridisation as well as two-particle spin excitations brought about by the spin-exchange term. What follows is a standard calculation where we write the Green's function in the Lehmann-Kallen representation. The ensemble average for an arbitrary operator \hat{M} can be written in terms of the exact eigenstates of the fixed point Hamiltonian:

$$H^* |n\rangle = E_n^* |n\rangle, \quad \langle \hat{M} \rangle \equiv \frac{1}{Z} \sum_n \langle n | \hat{M} | n \rangle e^{-\beta E_n^*} \quad (\text{B.2})$$

where $Z = \sum_n e^{-\beta E_n^*}$ is the fixed point partition function and $\{|n\rangle\}$ is the set of eigenfunctions of the fixed point Hamiltonian. We can therefore write

$$\begin{aligned} & \langle \{ \mathcal{O}_\sigma(t), \mathcal{O}_\sigma^\dagger \} \rangle \\ &= \frac{1}{Z} \sum_m e^{-\beta E_m} \langle m | \{ \mathcal{O}_\sigma(t), \mathcal{O}_\sigma^\dagger \} | m \rangle \\ &= \frac{1}{Z} \sum_{m,n} e^{-\beta E_m} \langle m | (\mathcal{O}_\sigma(t) |n\rangle \langle n| \mathcal{O}_\sigma^\dagger + \mathcal{O}_\sigma^\dagger |n\rangle \langle n| \mathcal{O}_\sigma(t)) |m\rangle \left[\sum_n |n\rangle \langle n| = 1 \right] \\ &= \frac{1}{Z} \sum_{m,n} e^{-\beta E_m} \langle m | (e^{iH^*t} \mathcal{O}_\sigma e^{-iH^*t} |n\rangle \langle n| \mathcal{O}_\sigma^\dagger + \mathcal{O}_\sigma^\dagger |n\rangle \langle n| e^{iH^*t} \mathcal{O}_\sigma e^{-iH^*t}) |m\rangle \\ &= \frac{1}{Z} \sum_{m,n} e^{-\beta E_m} (e^{i(E_m - E_n)t} \langle m | \mathcal{O}_\sigma |n\rangle \langle n| \mathcal{O}_\sigma^\dagger |m\rangle + e^{i(E_n - E_m)t} \langle m | \mathcal{O}_\sigma^\dagger |n\rangle \langle n| \mathcal{O}_\sigma |m\rangle) \\ &= \frac{1}{Z} \sum_{m,n} e^{i(E_m - E_n)t} |\langle m | \mathcal{O}_\sigma |n\rangle|^2 (e^{-\beta E_m} + e^{-\beta E_n}) \end{aligned} \quad (\text{B.3})$$

The time-domain impurity Green's function can thus be written as (this is the so-called Lehmann-Kallen representation)

$$G_{dd}^\sigma = -i\theta(t) \frac{1}{Z} \sum_{m,n} e^{i(E_m - E_n)t} \|\langle m | \mathcal{O}_\sigma | n \rangle\|^2 (e^{-\beta E_m} + e^{-\beta E_n}) \quad (\text{B.4})$$

We are interested in the frequency domain form.

$$\begin{aligned} G_{dd}^\sigma(\omega) &= \int_{-\infty}^{\infty} dt e^{i\omega t} G_{dd}^\sigma(t) \\ &= \frac{1}{Z} \sum_{m,n} \|\langle m | \mathcal{O}_\sigma | n \rangle\|^2 (e^{-\beta E_m} + e^{-\beta E_n}) (-i) \int_{-\infty}^{\infty} dt \theta(t) e^{i(\omega + E_m - E_n)t} \end{aligned} \quad (\text{B.5})$$

To evaluate the time-integral, we will use the integral representation of the Heaviside function:

$$\theta(t) = \frac{1}{2\pi i} \lim_{\eta \rightarrow 0^+} \int_{-\infty}^{\infty} \frac{1}{x - i\eta} e^{ixt} dx \quad (\text{B.6})$$

With this definition, the integral in $G_{dd}^\sigma(\omega)$ becomes

$$\begin{aligned} (-i) \int_{-\infty}^{\infty} dt \theta(t) e^{i(\omega + E_m - E_n)t} &= (-i) \frac{1}{2\pi i} \lim_{\eta \rightarrow 0^+} \int_{-\infty}^{\infty} dx \frac{1}{x - i\eta} \int_{-\infty}^{\infty} dt e^{i(\omega + E_m - E_n + x)t} \\ &= (-i) \frac{1}{2\pi i} \lim_{\eta \rightarrow 0^+} \int_{-\infty}^{\infty} dx \frac{1}{x - i\eta} 2\pi\delta(\omega + E_m - E_n + x) \\ &= (-i) \frac{1}{i} \lim_{\eta \rightarrow 0^+} \frac{-1}{\omega + E_m - E_n - i\eta} \\ &= \frac{1}{\omega + E_m - E_n} \end{aligned} \quad (\text{B.7})$$

The frequency-domain Green's function is thus

$$G_{dd}^\sigma(\omega) = \frac{1}{Z} \sum_{m,n} \|\langle m | \mathcal{O}_\sigma | n \rangle\|^2 (e^{-\beta E_m} + e^{-\beta E_n}) \frac{1}{\omega + E_m - E_n} \quad (\text{B.8})$$

The zero temperature Green's function is obtained by taking the limit of $\beta \rightarrow \infty$. In both the partition function as well as inside the summation, the only term that will survive is the exponential of the ground state energy E_0 .

$$Z \equiv \sum_m e^{-\beta E_m} \implies \lim_{\beta \rightarrow \infty} Z = d_0 e^{-\beta E_0}, \quad E_0 \equiv \min \{E_n\}$$

where d_0 is the degeneracy of the ground state. The Greens function then simplifies to

$$\begin{aligned} G_{dd}^\sigma(\omega, \beta \rightarrow \infty) &= \frac{1}{d_0 e^{-\beta E_0}} \sum_{m,n} \|\langle m | \mathcal{O}_\sigma | n \rangle\|^2 [e^{-\beta E_m} \delta_{E_m, E_0} + e^{-\beta E_n} \delta_{E_n, E_0}] \frac{1}{\omega + E_m - E_n} \\ &= \frac{1}{d_0} \sum_{n,0} \left[\|\langle 0 | \mathcal{O}_\sigma | n \rangle\|^2 \frac{1}{\omega + E_0 - E_n} + \|\langle n | \mathcal{O}_\sigma | 0 \rangle\|^2 \frac{1}{\omega - E_0 + E_n} \right] \end{aligned} \quad (\text{B.9})$$

The label 0 sums over all states $|0\rangle$ with energy E_0 . The spectral function is the imaginary part of this Green's function. To extract the imaginary part, we insert an infinitesimal imaginary part in the denominator:

$$G_{dd}^\sigma(\omega, \eta) = \frac{1}{d_0} \lim_{\eta \rightarrow 0^-} \sum_{n,0} \left[\|\langle 0 | \mathcal{O}_\sigma | n \rangle\|^2 \frac{1}{\omega + E_0 - E_n + i\eta} + \|\langle n | \mathcal{O}_\sigma | 0 \rangle\|^2 \frac{1}{\omega - E_0 + E_n + i\eta} \right] \quad (\text{B.10})$$

The spectral function at zero temperature can then be written as

$$\begin{aligned} \mathcal{A}(\omega) &= -\frac{1}{\pi} \operatorname{Im} [G_{dd}^\sigma(\omega)] \\ &= \frac{1}{d_0} \frac{1}{\pi} \operatorname{Im} \left[\lim_{\eta \rightarrow 0^-} \sum_{n,0} \left(\frac{-i\eta \|\langle 0 | \mathcal{O}_\sigma | n \rangle\|^2}{(\omega + E_0 - E_n)^2 + \eta^2} + \frac{-i\eta \|\langle n | \mathcal{O}_\sigma | 0 \rangle\|^2}{(\omega - E_0 + E_n)^2 + \eta^2} \right) \right] \\ &= \frac{1}{d_0} \frac{1}{\pi} \sum_{n,0} [\|\langle 0 | \mathcal{O}_\sigma | n \rangle\|^2 \pi \delta(\omega + E_0 - E_n) + \|\langle n | \mathcal{O}_\sigma | 0 \rangle\|^2 \pi \delta(\omega - E_0 + E_n)] \\ &= \frac{1}{d_0} \sum_{n,0} [\|\langle 0 | \mathcal{O}_\sigma | n \rangle\|^2 \delta(\omega + E_0 - E_n) + \|\langle n | \mathcal{O}_\sigma | 0 \rangle\|^2 \delta(\omega - E_0 + E_n)] \end{aligned} \quad (\text{B.11})$$

B.2 Spectrum of the Hubbard dimer

Here we document the spectrum of the Hubbard dimer Hamiltonian in eqs. ??.

eigenstate	symbol	eigenvalue
$ 0, 0\rangle$	$ 0\rangle$	$\frac{U^H}{2}$
$\frac{1}{\sqrt{2}} (\sigma, 0\rangle \pm 0, \sigma\rangle)$	$ 0\sigma_\pm\rangle$	$\mp t^H$
$ \sigma, \sigma\rangle$	$ \sigma\sigma\rangle$	$-\frac{U^H}{2}$
$\frac{1}{\sqrt{2}} (\uparrow, \downarrow\rangle + \downarrow, \uparrow\rangle)$	$ ST\rangle$	$-\frac{U^H}{2}$
$\frac{1}{\sqrt{2}} (2, 0\rangle - 0, 2\rangle)$	$ CS\rangle$	$\frac{U^H}{2}$
$a_1(U^H, t^H) \frac{1}{\sqrt{2}} (\uparrow, \downarrow\rangle - \downarrow, \uparrow\rangle) + a_2(U^H, t^H) \frac{1}{\sqrt{2}} (2, 0\rangle + 0, 2\rangle)$	$ -\rangle$	$-\frac{1}{2}\Delta(U^H, t^H)$
$-a_2(U^H, t^H) \frac{1}{\sqrt{2}} (\uparrow, \downarrow\rangle - \downarrow, \uparrow\rangle) + a_1(U^H, t^H) \frac{1}{\sqrt{2}} (2, 0\rangle + 0, 2\rangle)$	$ +\rangle$	$\frac{1}{2}\Delta(U^H, t^H)$
$\frac{1}{\sqrt{2}} (\sigma, 2\rangle \pm 2, \sigma\rangle)$	$ 2\sigma_\pm\rangle$	$\pm t^H$
$ 2, 2\rangle$	$ 4\rangle$	$\frac{U^H}{2}$

Table B.1: Spectrum of Hubbard dimer at half-filling

B.3 Greens function of Hubbard model in the atomic limit

The atomic limit is described by the Hamiltonian $H = -\frac{U}{2} \sum_i (\hat{n}_{i\uparrow} - \hat{n}_{i\downarrow})^2$. Since the Hamiltonian has decoupled into $\sum_i \equiv N$ single-site Hamiltonians, we can easily write down the retarded Greens function for a single site by identifying the ground state configuration of a site. The ground states are of course $|\Psi\rangle_i = |\uparrow\rangle, |\downarrow\rangle$, in the absence of any symmetry-breaking. The finite temperature retarded

Greens function in the time domain is given by

$$G_{i,\sigma}(T, t) = -i\theta(t) \frac{1}{Z} \sum_n e^{-\beta E_n} \langle n | \{c_{i\sigma}(t), c_{i\sigma}^\dagger\} | n \rangle \quad (\text{B.12})$$

where n labels the eigenstates of the H . At $T \rightarrow 0$, only the ground states will survive in the exponential and the partition function Z , such that the formula then reduces to

$$G_{i,\sigma}(T \rightarrow 0, t) = -i\theta(t) \langle GS | \{c_{i\sigma}(t), c_{i\sigma}^\dagger\} | GS \rangle \quad (\text{B.13})$$

Since the Hamiltonian is simple, we can compute the time-dependent operator $c_{i\sigma}(t) = e^{iHt} c_{i\sigma} e^{-iHt}$. Using the BCH lemma, we have

$$e^{iHt} c_{i\sigma} e^{-iHt} = \sum_{n=0}^{\infty} (it)^n \frac{1}{n!} [H, c_{i\sigma}]_n \quad (\text{B.14})$$

where $[H, c_{i\sigma}]_n = [H, [H, c_{i\sigma}]_{n-1}]$, $[H, c_{i\sigma}]_0 = c_{i\sigma}$. The first two non-trivial commutators are

$$[H, c_{i\sigma}]_1 = -U\tau_{i\bar{\sigma}} c_{i\sigma}, \quad \text{and} \quad [H, c_{i\sigma}]_2 = \frac{1}{4} U^2 c_{i\sigma}, \quad (\text{B.15})$$

such that

$$\begin{aligned} e^{iHt} c_{i\sigma} e^{-iHt} &= \left[c_{i\sigma} + \frac{i^2 t^2}{2!} \frac{U^2}{2^2} c_{i\sigma} + \frac{i^4 t^4}{4!} \frac{U^4}{2^4} c_{i\sigma} + \dots \right] + \left[-\frac{it}{1!} U \tau_{i\bar{\sigma}} c_{i\sigma} - \frac{i^3 t^3}{3!} \frac{U^3}{4} \tau_{i\bar{\sigma}} c_{i\sigma} + \dots \right] \\ &= c_{i\sigma} [\cos(Ut/2) - 2i\tau_{i\bar{\sigma}} \sin(Ut/2)] \end{aligned} \quad (\text{B.16})$$

Using this, we can write

$$\{c_{i\sigma}(t), c_{i\sigma}^\dagger\} = \{c_{i\sigma}, c_{i\sigma}^\dagger\} [\cos(Ut/2) - 2i\tau_{i\bar{\sigma}} \sin(Ut/2)] = [\cos(Ut/2) - 2i\tau_{i\bar{\sigma}} \sin(Ut/2)] \quad (\text{B.17})$$

and the Greens function becomes

$$G_{i,\sigma}(T \rightarrow 0, t) = -i\theta(t) \langle GS | [\cos(Ut/2) - 2i\tau_{i\bar{\sigma}} \sin(Ut/2)] | GS \rangle = -i\theta(t) \left[\cos \frac{Ut}{2} - 2i \sin \frac{Ut}{2} \langle \tau_{i\bar{\sigma}} \rangle \right] \quad (\text{B.18})$$

We now Fourier transform to frequency domain:

$$G_{i,\sigma}(\omega) = -i \int_0^\infty dt e^{i\omega t} \left[\cos \frac{Ut}{2} - 2i \sin \frac{Ut}{2} \langle \tau_{i\bar{\sigma}} \rangle \right] = \frac{1 + \langle \tau_{i\bar{\sigma}} \rangle}{\omega - \frac{U}{2}} + \frac{1 - \langle \tau_{i\bar{\sigma}} \rangle}{\omega + \frac{U}{2}} \quad (\text{B.19})$$

The spin-total Greens function for the site i is

$$G_i(\omega) = \sum_\sigma G_{i,\sigma}(\omega) = \frac{1 + \langle \tau_i \rangle}{\omega - \frac{U}{2}} + \frac{1 - \langle \tau_i \rangle}{\omega + \frac{U}{2}} \quad (\text{B.20})$$

At half-filling, we have $\tau_i = 1$.

B.4 Local Greens function for the Hubbard dimer

From the spectral representation, we have the following expression for the local Greens function for the Hubbard dimer at site 0:

$$G_{D,00}^\sigma(\omega) = \frac{1}{Z} \sum_{m,n} \left| \langle m | c_{i\sigma} | n \rangle \right|^2 (e^{-\beta E_m} + e^{-\beta E_n}) \frac{1}{\omega + E_m - E_n} \quad (\text{B.21})$$

m, n sum over the exact eigenstates. E_m, E_n are the corresponding energies. We are interested in the $T \rightarrow 0$ Greens function. In that limit, all exponentials except that for the ground state E_{gs} will die out. The exponential inside the summation will then cancel the exponential in the partition function.

$$\begin{aligned} G_{D,00}^\sigma(\omega, T \rightarrow 0) &= \sum_n \left[\left| \langle GS | c_{i\sigma} | n \rangle \right|^2 \frac{1}{\omega + E_{GS} - E_n} + \left| \langle n | c_{i\sigma} | GS \rangle \right|^2 \frac{1}{\omega + E_n - E_{GS}} \right] \\ &= \sum_n \left[\left| \langle n | c_{i\sigma}^\dagger | GS \rangle \right|^2 \frac{1}{\omega + E_{GS} - E_n} + \left| \langle n | c_{i\sigma} | GS \rangle \right|^2 \frac{1}{\omega + E_n - E_{GS}} \right] \end{aligned} \quad (\text{B.22})$$

The ground state $|GS\rangle$ is just the state $|-\rangle$ in the table B.1. We will choose to look at $\sigma = \uparrow$. Then,

$$\begin{aligned} c_{1\uparrow} |-\rangle &= \frac{a_1}{\sqrt{2}} |0, \downarrow\rangle + \frac{a_2}{\sqrt{2}} |\downarrow, 0\rangle \\ c_{1\uparrow}^\dagger |-\rangle &= -\frac{a_1}{\sqrt{2}} |2, \uparrow\rangle + \frac{a_2}{\sqrt{2}} |\uparrow, 2\rangle \end{aligned} \quad (\text{B.23})$$

The set of states $|n\rangle$ that give non-zero inner product $|GS\rangle$ are therefore

$$\begin{aligned} \{|n\rangle\} &= |0 \downarrow_\pm\rangle \\ \left| \langle n | c_{\uparrow\sigma} | GS \rangle \right|^2 &= \frac{1}{4} (a_2 \pm a_1)^2 = \frac{1}{4} (1 \pm 2a_1 a_2) \\ \{E_n\} &= \mp t \end{aligned} \quad (\text{B.24})$$

for the second inner product, and

$$\begin{aligned} \{|n\rangle\} &= |2 \uparrow_\pm\rangle \\ \left| \langle n | c_{\uparrow\sigma}^\dagger | GS \rangle \right|^2 &= \frac{1}{4} (a_2 \mp a_1)^2 = \frac{1}{4} (1 \mp 2a_1 a_2) \\ \{E_n\} &= \pm t \end{aligned} \quad (\text{B.25})$$

for the first. The Greens function is therefore

$$G_{D,00}^\uparrow(\omega, T \rightarrow 0) = \left(\frac{1}{2} + \frac{2t}{\Delta} \right) \frac{\omega}{\omega^2 - (t - \frac{\Delta}{2})^2} + \left(\frac{1}{2} - \frac{2t}{\Delta} \right) \frac{\omega}{\omega^2 - (t + \frac{\Delta}{2})^2} = G_{D,00}^\downarrow(\omega, T \rightarrow 0). \quad (\text{B.26})$$

In the atomic limit ($t = 0$), the Greens function simplifies to

$$G_{D,00}^\uparrow(\omega, T \rightarrow 0) \Big|_{\text{atomic}} = \frac{\omega}{\omega^2 - \frac{1}{4} U^2} \quad (\text{B.27})$$

In the atomic limit, the singly-occupied state has zero energy:

$$E_1(t=0) = \langle 1, 0 | (U\tau_{0\uparrow}\tau_{0\downarrow} + U\tau_{1\uparrow}\tau_{1\downarrow}) | 1, 0 \rangle = 0 \quad (\text{B.28})$$

We can write the atomic limit Greens function in terms of this energy and the self energy:

$$G_{D,00}^\uparrow(\omega, T \rightarrow 0) \Big|_{\text{atomic}} = \frac{1}{\omega - E_1(t=0) - \Sigma(t=0)} = \frac{1}{\omega - 0 - \frac{U^2}{4\omega}} \quad (\text{B.29})$$

The self energy in the atomic limit can be read off as

$$\Sigma(t=0) = \frac{U^2}{4\omega} \quad (\text{B.30})$$

The site local spectral function can also be calculated from the local Greens function:

$$\begin{aligned} A(0 \uparrow, \omega) &= -\frac{1}{\pi} \text{Im} G_{D,00}^\uparrow(\omega) \\ &= \left(\frac{1}{4} - \frac{t}{\Delta} \right) \left[\delta(\omega - \frac{1}{2}\Delta - t) + \delta(\omega + \frac{1}{2}\Delta + t) \right] \\ &\quad + \left(\frac{1}{4} + \frac{t}{\Delta} \right) \left[\delta(\omega - \frac{1}{2}\Delta + t) + \delta(\omega + \frac{1}{2}\Delta - t) \right] \\ &= A(0 \downarrow, \omega). \end{aligned} \quad (\text{B.31})$$

Finally, the inter-site Greens function for the Hubbard dimer is given by

$$G_{D,01}^\uparrow(\omega, T \rightarrow 0) = \left(\frac{1}{2} + \frac{2t}{\Delta} \right) \frac{t - \frac{\Delta}{2}}{\omega^2 - (t - \frac{\Delta}{2})^2} + \left(\frac{1}{2} - \frac{2t}{\Delta} \right) \frac{t + \frac{\Delta}{2}}{\omega^2 - (t + \frac{\Delta}{2})^2} = G_{D,01}^\downarrow(\omega, T \rightarrow 0). \quad (\text{B.32})$$

Using the diagonal and off-diagonal real space Greens functions, we can now compute the momentum-space Greens functions. The two momentum states are $ka = 0, \pi$. By Fourier transforming, these two Greens functions can be written as

$$\begin{aligned} G(k=0, \sigma) &= \sum_r e^{ikr} G(r, \sigma) = G(r=0, \sigma) + G(r=a, \sigma) = \frac{1/2 + 2t/\Delta}{\omega - t + \Delta/2} + \frac{1/2 - 2t/\Delta}{\omega - t - \Delta/2} \\ G(k=\pi, \sigma) &= \sum_r e^{ikr} G(r, \sigma) = G(r=0, \sigma) - G(r=a, \sigma) = \frac{1/2 + 2t/\Delta}{\omega + t - \Delta/2} + \frac{1/2 - 2t/\Delta}{\omega + t + \Delta/2} \end{aligned} \quad (\text{B.33})$$

B.5 Contributions of various excitations to the site local spectral function

The site local spectral function is

$$A(0 \uparrow, \omega) = \left(\frac{1}{4} - \frac{t}{\Delta} \right) \left[\delta(\omega - \frac{\Delta}{2} - t) + \delta(\omega + \frac{\Delta}{2} + t) \right] + \left(\frac{1}{4} + \frac{t}{\Delta} \right) \left[\delta(\omega - \frac{\Delta}{2} + t) + \delta(\omega + \frac{\Delta}{2} - t) \right]$$

If the eigenstates of the $N = 1, S^z = -\frac{1}{2}$ sector are $|1\pm\downarrow\rangle$ and those of $N = 3, S^z = \frac{1}{2}$ sector are $|3\pm\uparrow\rangle$, this spectral function originates from the expression:

$$A(0\uparrow, \omega) = \langle 1\downarrow_- | c_{0\uparrow} | GS \rangle \delta\left(\omega + \frac{\Delta}{2} + t\right) + \langle 2\uparrow_+ | c_{0\uparrow}^\dagger | GS \rangle \delta\left(\omega - \frac{\Delta}{2} - t\right) \\ + \langle 1\downarrow_+ | c_{0\uparrow} | GS \rangle \delta\left(\omega + \frac{\Delta}{2} - t\right) + \langle 2\uparrow_- | c_{0\uparrow}^\dagger | GS \rangle \delta\left(\omega - \frac{\Delta}{2} + t\right) \quad (\text{B.34})$$

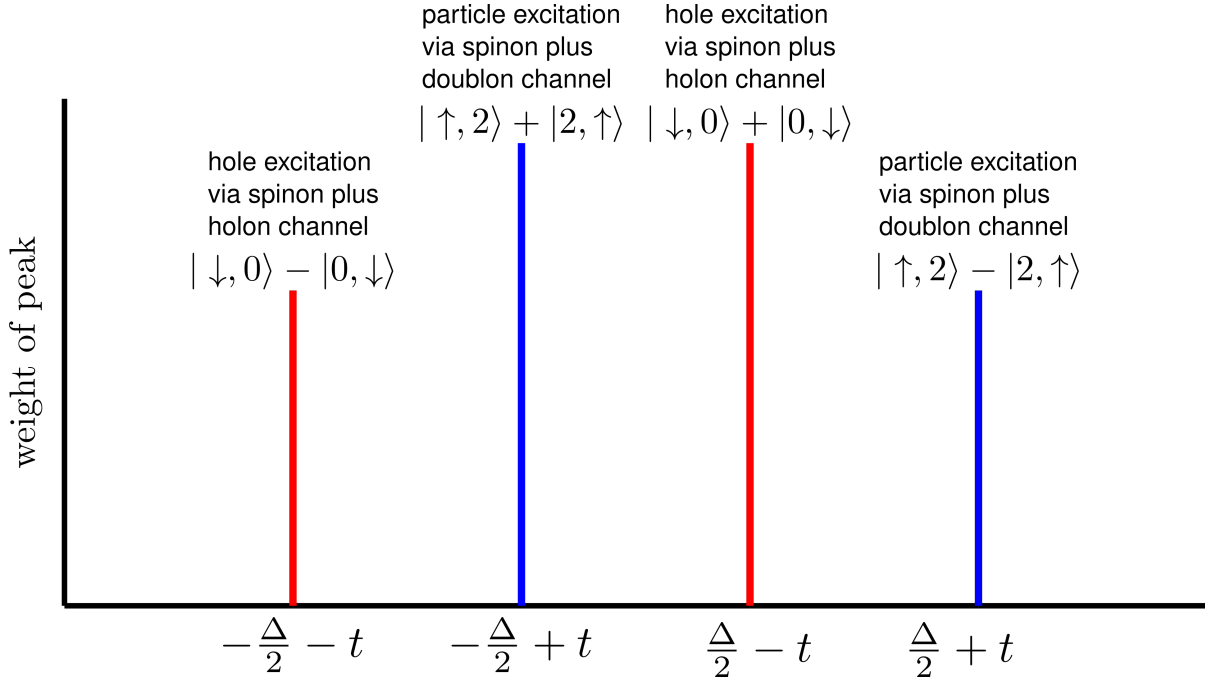


Figure B.1: Position, weight and nature of each of the peaks in the Hubbard dimer site local spectral function

B.6 Relation between single-particle Greens function and the Greens operator ($T = 0$)

The single-particle Greens function is defined as the solution of the equation:

$$(i\partial_t - H(\vec{r})) G(\vec{r}, \vec{r}', t) = \delta(\vec{r} - \vec{r}') \quad (\text{B.35})$$

and is given by the expression

$$G(\vec{r}, \vec{r}', t) = -i\theta(t) \langle \{c(\vec{r}, t) c^\dagger(\vec{r}', 0)\} \rangle \quad (\text{B.36})$$

This solution can be written in the Lehmann-Kallen representation and at $T = 0$ as

$$G(\vec{r}\sigma, \vec{r}'\sigma, \omega) = \sum_n \left[\frac{\langle GS | c(\vec{r}, \sigma) | n \rangle \langle n | c^\dagger(\vec{r}', \sigma) | GS \rangle}{\omega + E_{GS} - E_n} + \frac{\langle GS | c^\dagger(\vec{r}', \sigma) | n \rangle \langle n | c(\vec{r}, \sigma) | GS \rangle}{\omega + E_n - E_{GS}} \right] \quad (\text{B.37})$$

The sum is over the exact eigenstates of the Hamiltonian. In what follows, we will represent $\vec{r}, \sigma \equiv \nu$ and $\vec{r}', \sigma' \equiv \nu'$.

$$\begin{aligned} G(\nu, \nu', \omega) &= \sum_n \left[\frac{\langle GS | c(\nu) | n \rangle \langle n | c^\dagger(\nu') | GS \rangle}{\omega + E_{GS} - E_n} + \frac{\langle GS | c^\dagger(\nu') | n \rangle \langle n | c(\nu) | GS \rangle}{\omega + E_n - E_{GS}} \right] \\ &= \langle GS | c(\nu) \frac{1}{\omega + E_{GS} - H} c^\dagger(\nu') | GS \rangle + \langle GS | c^\dagger(\nu') \frac{1}{\omega + H - E_{GS}} c(\nu) | GS \rangle \end{aligned} \quad (\text{B.38})$$

If we now define a Greens operator

$$\mathcal{G}(\omega, H) = \frac{1}{\omega - (H - E_{GS})} \quad (\text{B.39})$$

we can write the single-particle Greens function as a sum of the matrix elements of this operator:

$$G(\nu, \nu', \omega) = \langle \nu | \mathcal{G}(\omega, H) | \nu' \rangle - \langle \bar{\nu}' | \mathcal{G}(-\omega, H) | \bar{\nu} \rangle = \mathcal{G}(\omega, H)_{\nu, \nu'} - \mathcal{G}(-\omega, H)_{\bar{\nu}, \bar{\nu}} \quad (\text{B.40})$$

where we have defined the states $|\nu\rangle \equiv c^\dagger(\nu) |GS\rangle$ and $|\bar{\nu}\rangle \equiv c(\nu) |GS\rangle$. The two matrix elements can also be represented in their individual spectral representations:

$$\begin{aligned} \mathcal{G}(\omega, H)_{\nu, \nu'} &= \sum_n \frac{\langle GS | c(\nu) | n \rangle \langle n | c^\dagger(\nu') | GS \rangle}{\omega + E_{GS} - E_n} \\ \mathcal{G}(\omega, H)_{\bar{\nu}, \bar{\nu}} &= \sum_n \frac{\langle GS | c^\dagger(\nu') | n \rangle \langle n | c(\nu) | GS \rangle}{\omega + E_{GS} - E_n} \end{aligned} \quad (\text{B.41})$$

B.7 Writing single-particle excitations of ground state in terms of $N = 3, S^z = \frac{1}{2}$ eigenstates

The excited state $c_{0\uparrow}^\dagger |GS\rangle$ can actually be written in terms of the $N = 3, S^z = +\frac{1}{2}$ eigenstates $|3\pm\uparrow\rangle$ defined in table B.1.

$$|3\pm\uparrow\rangle = \frac{1}{\sqrt{2}} (|\uparrow, 2\rangle \pm |2, \uparrow\rangle), \quad H^D |3\pm\uparrow\rangle = \pm t |3\pm\uparrow\rangle \quad (\text{B.42})$$

In terms of these eigenstates, we can write

$$\begin{aligned} c_{0\uparrow}^\dagger |GS\rangle &= c_{0\uparrow}^\dagger [a_1 |SS\rangle + a_2 |CT\rangle] \\ &= a_2 \frac{1}{\sqrt{2}} |\uparrow, 2\rangle - a_1 \frac{1}{\sqrt{2}} |2, \uparrow\rangle \\ &= (x + y) \frac{1}{\sqrt{2}} |\uparrow, 2\rangle + (x - y) \frac{1}{\sqrt{2}} |2, \uparrow\rangle \\ &= x |3+\uparrow\rangle + y |3-\uparrow\rangle \end{aligned} \quad (\text{B.43})$$

where $x + y \equiv a_2$ and $x - y \equiv -a_1$. Similarly, for the other site excitation, we can write

$$\begin{aligned}
c_{1\uparrow}^\dagger |GS\rangle &= c_{1\uparrow}^\dagger [a_1 |SS\rangle + a_2 |CT\rangle] \\
&= a_2 \frac{1}{\sqrt{2}} |2, \uparrow\rangle - a_1 \frac{1}{\sqrt{2}} |\uparrow, 2\rangle \\
&= (x + y) \frac{1}{\sqrt{2}} |2, \uparrow\rangle + (x - y) \frac{1}{\sqrt{2}} |\uparrow, 2\rangle \\
&= x |3+\uparrow\rangle - y |3-\uparrow\rangle
\end{aligned} \tag{B.44}$$

Solving for x and y gives

$$x = \frac{a_2 - a_1}{2}, \quad y = \frac{a_2 + a_1}{2} \tag{B.45}$$

Similarly, we can also write the single-hole excitation $c_{0\uparrow} |GS\rangle$ in terms of the $N = 1, S^z = -\frac{1}{2}$ eigenstates, $|1\pm\downarrow\rangle$:

$$|1\pm\downarrow\rangle = \frac{1}{\sqrt{2}} (|\downarrow, 0\rangle \pm |0, \downarrow\rangle), \quad H^D |1\pm\downarrow\rangle = \mp t |1\pm\downarrow\rangle \tag{B.46}$$

$$\begin{aligned}
c_{0\uparrow} |GS\rangle &= a_1 \frac{1}{\sqrt{2}} |0, \downarrow\rangle + a_2 \frac{1}{\sqrt{2}} |\downarrow, 0\rangle = y |1+\downarrow\rangle + x |1-\downarrow\rangle \\
c_{1\uparrow} |GS\rangle &= a_1 \frac{1}{\sqrt{2}} |\downarrow, 0\rangle + a_2 \frac{1}{\sqrt{2}} |0, \downarrow\rangle = y |1+\downarrow\rangle - x |1-\downarrow\rangle
\end{aligned} \tag{B.47}$$

B.8 Matrix elements of G^{-1} between single-particle momentum excitations, for the Hubbard dimer

$$G^{-1} \equiv \omega + E_{GS} - H_D \tag{B.48}$$

The particle excitation momentum space kets are $|k_0\rangle = \frac{1}{\sqrt{2}} (|0\rangle + |1\rangle)$, $|k_\pi\rangle = \frac{1}{\sqrt{2}} (|0\rangle - |1\rangle)$. Therefore,

$$\begin{aligned}
(G^{-1})_{k_0 k_0} &= \frac{1}{2} (\langle 0| + \langle 1|) (\omega + E_{GS} - H_D) (|0\rangle + |1\rangle) \\
&= \frac{1}{2} (2x \langle +|) (\omega + E_{GS} - H_D) (2x |+>) \\
&= 2x^2 (\omega + E_{GS} - t)
\end{aligned} \tag{B.49}$$

At the final step, we used $\langle +, + \rangle = 1$ and $\langle + | H_D | + \rangle = t$.

B.9 Topological interpretation of the Wilson ratio

From the Friedel sum rule [269], we can relate the phase shift $\delta(0)$ due to scattering (at the Fermi surface) off a local impurity to the number of electrons bound in the potential well produced by that impurity:

$$\tilde{N} = \frac{1}{2\pi i} \text{Tr } \ln S(0) = \int_{\Gamma} dz \partial_z \frac{1}{2\pi i} \text{Tr } \ln S(0) \tag{B.50}$$

From the optical theorem, we can write

$$S = 1 + TG_0 = \frac{G}{G_0} \quad [G = G_0 + G_0TG_0] \quad (\text{B.51})$$

This allows us to write [1]

$$\tilde{N} = \int_{\Gamma} dz \partial_z \frac{1}{2\pi i} \text{Tr} \ln \frac{G}{G_0} \quad (\text{B.52})$$

Since $\text{Tr} \ln \hat{O} = \sum_{\lambda} \ln O_{\lambda} = \ln \prod_{\lambda} O_{\lambda} = \ln \text{Det} \hat{O}$, we get

$$\begin{aligned} \tilde{N} &= \int_{\Gamma} dz \partial_z \frac{1}{2\pi i} \ln \text{Det} \frac{G}{G_0} \\ &= - \int_{\Gamma} dz \partial_z \frac{1}{2\pi i} \ln \frac{\text{Det } G_0}{\text{Det } G} \\ &\equiv - \int_{\Gamma} dz \partial_z \frac{1}{2\pi i} \ln D \\ &= - \int_{\Gamma(D)} \frac{dD}{D} \end{aligned} \quad (\text{B.53})$$

From the work of Seki and Yunoki [124], we know that this quantity is essentially the winding number of the curve $\Gamma(D)$ in the complex plane spanned by the real and imaginary parts of D , and is equal to the change in Luttinger's volume V_L at $T = 0$.

$$\tilde{N} = - \int_{\Gamma(D)} \frac{dD}{D} = -\Delta V_L \quad (\text{B.54})$$

The incoming electrons can have $\sigma = \uparrow, \downarrow$. Since the impurity singlet ground state is rotationally invariant, we have $\delta_{\uparrow} = \delta_{\downarrow} = \delta(0)$.

$$\begin{aligned} \tilde{N} &= \frac{1}{\pi} \sum_{\sigma} \delta_{\sigma}(0) \\ \implies \delta(0) &= \frac{\pi}{2} \tilde{N} = -\frac{\pi}{2} \Delta V_L \end{aligned} \quad (\text{B.55})$$

$$\begin{aligned} R &= 1 + \sin^2 \left(\frac{\pi}{2} \tilde{N} \right) \\ &= 1 + \sin^2 \left(\frac{\pi}{2} \Delta V_L \right) \end{aligned} \quad (\text{B.56})$$

We note that this connection between R and ΔV_L has not been obtained in the existing literature thus far. In the unitary limit, $\delta(0) = \frac{\pi}{2}$, giving $\Delta V_L = -1 = -\tilde{N}$ [303] (i.e., one electronic state from the impurity has been absorbed into the Luttinger volume of the conduction bath), such that $R = 2$ in this limit. In this way, we see that a change in the topological quantum number \tilde{N} causes the well known renormalisation of the Wilson ratio R from its non-interacting value (1) to the value (2) obtained for the local Fermi liquid [238].

Bibliography

- [1] Anirban Mukherjee and Siddhartha Lal. Holographic unitary renormalisation group for correlated electrons-i: a tensor network approach. *Nuclear Physics B*, 960:115170, 2020.
- [2] Anirban Mukherjee and Siddhartha Lal. Holographic unitary renormalisation group for correlated electrons-ii: insights on fermionic criticality. *Nuclear Physics B*, 960:115163, 2020.
- [3] Anirban Mukherjee and Siddhartha Lal. Scaling theory for mott–hubbard transitions: I. $t = 0$ phase diagram of the 1/2-filled hubbard model. *New Journal of Physics*, 22(6):063007, jun 2020.
- [4] Anirban Mukherjee and Siddhartha Lal. Scaling theory for mott–hubbard transitions-II: quantum criticality of the doped mott insulator. *New Journal of Physics*, 22(6):063008, jun 2020.
- [5] Kenji Suzuki and Ryoji Okamoto. General structure of effective interaction in degenerate perturbation theory. *Progress of Theoretical Physics*, 71(6):1221–1238, 1984.
- [6] PW Anderson. A poor man’s derivation of scaling laws for the kondo problem. *Journal of Physics C: Solid State Physics*, 3(12):2436, 1970.
- [7] FDM Haldane. Scaling theory of the asymmetric anderson model. *Physical Review Letters*, 40(6):416, 1978.
- [8] A. C. Hewson. *The Kondo Problem to Heavy Fermions*. Cambridge University Press, 1993.
- [9] Tathagata Chowdhury and Kevin Ingersent. Critical charge fluctuations in a pseudogap anderson model. *Phys. Rev. B*, 91:035118, Jan 2015.
- [10] Rukhsan-Ul-Haq Wani and Vidhyadhiraja N S. Scaling analysis of the extended single impurity anderson model: Renormalization due to valence fluctuations. 10 2017.
- [11] J H Jefferson. a renormalisation group approach to the mixed valence problem. *Journal of Physics C: Solid State Physics*, 10(18):3589–3599, sep 1977.
- [12] Stefan Kehrein. *The flow equation approach to many-particle systems*, volume 217. Springer, 2007.
- [13] S. D Glazek and Kenneth G Wilson. Renormalization of hamiltonians. *Physical Review D*, 48(12):5863, 1993.
- [14] Franz Wegner. Flow-equations for hamiltonians. *Annalen der physik*, 506(2):77–91, 1994.
- [15] Barbara M. Terhal, Michael M. Wolf, and Andrew C. Doherty. Quantum entanglement: A modern perspective. *Physics Today*, 56(4):46–52, 2003.

- [16] Ryszard Horodecki, Paweł Horodecki, Michał Horodecki, and Karol Horodecki. Quantum entanglement. *Reviews of modern physics*, 81(2):865, 2009.
- [17] J. Eisert, M. Cramer, and M. B. Plenio. Colloquium: Area laws for the entanglement entropy. *Rev. Mod. Phys.*, 82:277–306, Feb 2010.
- [18] Nicolas Laflorencie. Quantum entanglement in condensed matter systems. *Physics Reports*, 646:1–59, 2016.
- [19] Bei Zeng, Xie Chen, Duan-Lu Zhou, and Xiao-Gang Wen. *Quantum information meets quantum matter*. Springer, 2019.
- [20] Manuel Erhard, Mario Krenn, and Anton Zeilinger. Advances in high-dimensional quantum entanglement. *Nature Reviews Physics*, 2(7):365–381, Jul 2020.
- [21] X. G. Wen. Topological orders in rigid states. *International Journal of Modern Physics B*, 04(02):239–271, 1990.
- [22] X. G. Wen and Q. Niu. Ground-state degeneracy of the fractional quantum hall states in the presence of a random potential and on high-genus riemann surfaces. *Phys. Rev. B*, 41:9377–9396, May 1990.
- [23] Xiao-Gang Wen. Topological orders and edge excitations in fractional quantum hall states. *Advances in Physics*, 44(5):405–473, 1995.
- [24] Qian Niu, Ds J Thouless, and Yong-Shi Wu. Quantized hall conductance as a topological invariant. *Physical Review B*, 31(6):3372, 1985.
- [25] Saurya Das and S. Shankaranarayanan. How robust is the entanglement entropy-area relation? *Phys. Rev. D*, 73:121701, Jun 2006.
- [26] M. Cramer, J. Eisert, M. B. Plenio, and J. Dreißig. Entanglement-area law for general bosonic harmonic lattice systems. *Phys. Rev. A*, 73:012309, Jan 2006.
- [27] Oskar Vafek and Ashvin Vishwanath. Dirac fermions in solids: From high-tc cuprates and graphene to topological insulators and weyl semimetals. *Annual Review of Condensed Matter Physics*, 5(1):83–112, 2014.
- [28] B. Andrei Bernevig and Taylor L. Hughes. *Topological Insulators and Topological Superconductors*. Princeton University Press, 2013.
- [29] Jérôme Cayssol. Introduction to dirac materials and topological insulators. *Comptes Rendus Physique*, 14(9):760–778, 2013. Topological insulators / Isolants topologiques.
- [30] Roderich Moessner and Joel E. Moore. *Topological Phases of Matter*. Cambridge University Press, 2021.
- [31] Stephan Rachel. Interacting topological insulators: a review. *Reports on Progress in Physics*, 81(11):116501, oct 2018.

- [32] Jinying Wang, Shibin Deng, Zhongfan Liu, and Zhirong Liu. "The rare two-dimensional materials with Dirac cones". *National Science Review*, 2(1):22–39, 01 2015.
- [33] Menghao Wu, Zhijun Wang, Junwei Liu, Wenbin Li, Huahua Fu, Lei Sun, Xin Liu, Minghu Pan, Hongming Weng, Mircea Dincă, Liang Fu, and Ju Li. Conetronics in 2d metal-organic frameworks: double/half dirac cones and quantum anomalous hall effect. *2D Materials*, 4(1):015015, nov 2016.
- [34] Xiaojuan Ni, Huaqing Huang, and Jean-Luc Brédas. Emergence of a two-dimensional topological dirac semimetal phase in a phthalocyanine-based covalent organic framework. *Chemistry of Materials*, 34(7):3178–3184, 2022.
- [35] Shi-Liang Zhu, Baigeng Wang, and L.-M. Duan. Simulation and detection of dirac fermions with cold atoms in an optical lattice. *Phys. Rev. Lett.*, 98:260402, Jun 2007.
- [36] L. Lepori, G. Mussardo, and A. Trombettoni. (3+1) massive dirac fermions with ultracold atoms in frustrated cubic optical lattices. *EPL (Europhysics Letters)*, 92(5):50003, dec 2010.
- [37] O Boada, A Celi, J I Latorre, and M Lewenstein. Dirac equation for cold atoms in artificial curved spacetimes. *New Journal of Physics*, 13(3):035002, mar 2011.
- [38] Yoshihito Kuno, Ikuo Ichinose, and Yoshiro Takahashi. Generalized lattice wilson–dirac fermions in (1 + 1) dimensions for atomic quantum simulation and topological phases. *Scientific Reports*, 8(1):10699, Jul 2018.
- [39] Kenjiro K. Gomes, Warren Mar, Wonhee Ko, Francisco Guinea, and Hari C. Manoharan. Designer dirac fermions and topological phases in molecular graphene. *Nature*, 483(7389):306–310, Mar 2012.
- [40] Xiang Yuan, Cheng Zhang, Yanwen Liu, Awadhesh Narayan, Chaoyu Song, Shoudong Shen, Xing Sui, Jie Xu, Haochi Yu, Zhenghua An, Jun Zhao, Stefano Sanvito, Hugen Yan, and Faxian Xiu. Observation of quasi-two-dimensional dirac fermions in zrte5. *NPG Asia Materials*, 8(11):e325–e325, Nov 2016.
- [41] Matthieu Bellec, Ulrich Kuhl, Gilles Montambaux, and Fabrice Mortessagne. Topological transition of dirac points in a microwave experiment. *Phys. Rev. Lett.*, 110:033902, Jan 2013.
- [42] Guifre Vidal, José Ignacio Latorre, Enrique Rico, and Alexei Kitaev. Entanglement in quantum critical phenomena. *Physical review letters*, 90(22):227902, 2003.
- [43] J. I. Latorre, E. Rico, and G. Vidal. Ground state entanglement in quantum spin chains. 2003.
- [44] J. I. Latorre, C. A. Lütken, E. Rico, and G. Vidal. Fine-grained entanglement loss along renormalization-group flows. *Phys. Rev. A*, 71:034301, Mar 2005.
- [45] Pasquale Calabrese and John Cardy. Entanglement entropy and quantum field theory. *Journal of Statistical Mechanics: Theory and Experiment*, 2004(06):P06002, 2004.
- [46] Michael M Wolf, Frank Verstraete, Matthew B Hastings, and J Ignacio Cirac. Area laws in quantum systems: mutual information and correlations. *Physical review letters*, 100(7):070502, 2008.

- [47] H Casini, C D Fosco, and M Huerta. Entanglement and alpha entropies for a massive dirac field in two dimensions. *Journal of Statistical Mechanics: Theory and Experiment*, 2005(07):P07007–P07007, jul 2005.
- [48] J. L. Cardy, O. A. Castro-Alvaredo, and B. Doyon. Form factors of branch-point twist fields in quantum integrable models and entanglement entropy. *Journal of Statistical Physics*, 130(1):129–168, Jan 2008.
- [49] H Casini and M Huerta. Reduced density matrix and internal dynamics for multicomponent regions. *Classical and Quantum Gravity*, 26(18):185005, sep 2009.
- [50] Benjamin Doyon. Bipartite entanglement entropy in massive two-dimensional quantum field theory. *Phys. Rev. Lett.*, 102:031602, Jan 2009.
- [51] Xiao Chen, William Witczak-Krempa, Thomas Faulkner, and Eduardo Fradkin. Two-cylinder entanglement entropy under a twist. *Journal of Statistical Mechanics: Theory and Experiment*, 2017(4):043104, apr 2017.
- [52] Pablo Bueno and William Witczak-Krempa. Holographic torus entanglement and its renormalization group flow. *Phys. Rev. D*, 95:066007, Mar 2017.
- [53] Max A. Metlitski, Carlos A. Fuertes, and Subir Sachdev. Entanglement entropy in the $o(n)$ model. *Phys. Rev. B*, 80:115122, Sep 2009.
- [54] Raúl E Arias, David D Blanco, and Horacio Casini. Entanglement entropy as a witness of the aharonov-bohm effect in QFT. *Journal of Physics A: Mathematical and Theoretical*, 48(14):145401, mar 2015.
- [55] Seth Whitsitt, William Witczak-Krempa, and Subir Sachdev. Entanglement entropy of large- n wilson-fisher conformal field theory. *Phys. Rev. B*, 95:045148, Jan 2017.
- [56] Wei Zhu, Xiao Chen, Yin-Chen He, and William Witczak-Krempa. Entanglement signatures of emergent dirac fermions: Kagome spin liquid and quantum criticality. *Science Advances*, 4(11):eaat5535, 2018.
- [57] Shijie Hu, W. Zhu, Sebastian Eggert, and Yin-Chen He. Dirac spin liquid on the spin-1/2 triangular heisenberg antiferromagnet. *Phys. Rev. Lett.*, 123:207203, Nov 2019.
- [58] Valentin Crépel, Anna Hackenbroich, Nicolas Regnault, and Benoit Estienne. Universal signatures of dirac fermions in entanglement and charge fluctuations. *Phys. Rev. B*, 103:235108, Jun 2021.
- [59] G.'t Hooft. A planar diagram theory for strong interactions. *Nuclear Physics B*, 72(3):461–473, 1974.
- [60] A.M. Polyakov. Thermal properties of gauge fields and quark liberation. *Physics Letters B*, 72(4):477–480, 1978.
- [61] A.M. Polyakov. *Gauge Fields and Strings (1st ed.)*. Routledge, 1987.

- [62] David J. Gross and Washington Taylor. Two-dimensional qcd is a string theory. *Nuclear Physics B*, 400(1):181–208, 1993.
- [63] Raphael Bousso. The holographic principle. *Rev. Mod. Phys.*, 74:825–874, Aug 2002.
- [64] Jan Zaanen, Yan Liu, Ya-Wen Sun, and Koenraad Schalm. *Holographic Duality in Condensed Matter Physics*. Cambridge University Press, 2015.
- [65] S. A. Hartnoll, A. Lucas, and S. Sachdev. *Holographic Quantum Matter*. The MIT Press, 2018.
- [66] E.T. Akhmedov. A remark on the ads/cft correspondence and the renormalization group flow. *Physics Letters B*, 442(1):152–158, 1998.
- [67] Enrique Álvarez and César Gómez. Geometric holography, the renormalization group and the c-theorem. *Nuclear Physics B*, 541(1):441–460, 1999.
- [68] D. Z. Freedman, S. S. Gubser, K. Pilch, and N. P. Warner. Renormalization group flows from holography–supersymmetry and a c-theorem. 1999.
- [69] M. Petratti and A. Starinets. Rg fixed points in supergravity duals of 4-d field theory and asymptotically ads spaces. *Physics Letters B*, 454(1):77–83, 1999.
- [70] Shamit Kachru, Michael Schulz, and Eva Silverstein. Self-tuning flat domain walls in 5d gravity and string theory. *Phys. Rev. D*, 62:045021, Jul 2000.
- [71] L. Girardello, M. Petrini, M. Petratti, and A. Zaffaroni. The supergravity dual of n=1 super yang–mills theory. *Nuclear Physics B*, 569(1):451–469, 2000.
- [72] Jan De Boer, Erik Verlinde, and Herman Verlinde. On the holographic renormalization group. *Journal of High Energy Physics*, 2000(08):003, 2000.
- [73] Jan de Boer. The holographic renormalization group. *Fortschritte der Physik*, 49(4-6):339–358, 2001.
- [74] Clifford V Johnson, Kenneth J Lovis, and David C Page. Probing some $N = 1$ AdS/CFT RG flows. *Journal of High Energy Physics*, 2001(05):036–036, may 2001.
- [75] Satoshi Yamaguchi. AdS branes corresponding to superconformal defects. *Journal of High Energy Physics*, 2003(06):002–002, jun 2003.
- [76] Jacob D. Bekenstein. Black holes and entropy. *Phys. Rev. D*, 7:2333–2346, Apr 1973.
- [77] S. W. Hawking. Black hole explosions? *Nature*, 248(5443):30–31, Mar 1974.
- [78] S. W. Hawking. Particle creation by black holes. *Communications in Mathematical Physics*, 43(3):199–220, Aug 1975.
- [79] Juan Maldacena. The large-n limit of superconformal field theories and supergravity. *International journal of theoretical physics*, 38(4):1113–1133, 1999.

- [80] S.S. Gubser, I.R. Klebanov, and A.M. Polyakov. Gauge theory correlators from non-critical string theory. *Physics Letters B*, 428(1):105–114, 1998.
- [81] Edward Witten. Anti de sitter space and holography. *arXiv preprint hep-th/9802150*, 2:253–291, 1998.
- [82] Shinsei Ryu and Tadashi Takayanagi. Holographic derivation of entanglement entropy from the anti-de sitter space/conformal field theory correspondence. *Physical review letters*, 96(18):181602, 2006.
- [83] Shinsei Ryu and Tadashi Takayanagi. Aspects of holographic entanglement entropy. *Journal of High Energy Physics*, 2006(08):045, 2006.
- [84] P. K. Kovtun, D. T. Son, and A. O. Starinets. Viscosity in strongly interacting quantum field theories from black hole physics. *Phys. Rev. Lett.*, 94:111601, Mar 2005.
- [85] Kedar Damle and Subir Sachdev. Nonzero-temperature transport near quantum critical points. *Phys. Rev. B*, 56:8714–8733, Oct 1997.
- [86] Sean A. Hartnoll, Pavel K. Kovtun, Markus Müller, and Subir Sachdev. Theory of the nernst effect near quantum phase transitions in condensed matter and in dyonic black holes. *Phys. Rev. B*, 76:144502, Oct 2007.
- [87] Sung-Sik Lee. Non-fermi liquid from a charged black hole: A critical fermi ball. *Phys. Rev. D*, 79:086006, Apr 2009.
- [88] Hong Liu, John McGreevy, and David Vegh. Non-fermi liquids from holography. *Phys. Rev. D*, 83:065029, Mar 2011.
- [89] Thomas Faulkner, Hong Liu, John McGreevy, and David Vegh. Emergent quantum criticality, fermi surfaces, and ads₂. *Phys. Rev. D*, 83:125002, Jun 2011.
- [90] Mihailo Ćubrović, Jan Zaanen, and Koenraad Schalm. String theory, quantum phase transitions, and the emergent fermi liquid. *Science*, 325(5939):439–444, 2009.
- [91] Steven S. Gubser, Silviu S. Pufu, and Fabio D. Rocha. Quantum critical superconductors in string theory and m-theory. *Physics Letters B*, 683(2):201–204, 2010.
- [92] Jerome P. Gauntlett, Julian Sonner, and Toby Wiseman. Holographic superconductivity in m theory. *Phys. Rev. Lett.*, 103:151601, Oct 2009.
- [93] Sean A. Hartnoll, Christopher P. Herzog, and Gary T. Horowitz. Building a holographic superconductor. *Phys. Rev. Lett.*, 101:031601, Jul 2008.
- [94] Sean A Hartnoll, Christopher P Herzog, and Gary T Horowitz. Holographic superconductors. *Journal of High Energy Physics*, 2008(12):015–015, dec 2008.
- [95] RongGen Cai, Li Li, LiFang Li, and RunQiu Yang. Introduction to holographic superconductor models. *Science China Physics, Mechanics & Astronomy*, 58(6):1–46, Jun 2015.

- [96] Chunyan Wang, Dan Zhang, Guoyang Fu, and Jian-Pin Wu. Analytical study of the holographic superconductor from higher derivative theory. *Advances in High Energy Physics*, 2020:5902473, Jan 2020.
- [97] Aristomenis Donos and Jerome P. Gauntlett. Holographic striped phases. *Journal of High Energy Physics*, 2011(8):140, Aug 2011.
- [98] Aristomenis Donos. Striped phases from holography. *Journal of High Energy Physics*, 2013(5):59, May 2013.
- [99] Sera Cremonini, Li Li, and Jie Ren. Holographic fermions in striped phases. *Journal of High Energy Physics*, 2018(12):80, Dec 2018.
- [100] Shamit Kachru, Xiao Liu, and Michael Mulligan. Gravity duals of lifshitz-like fixed points. *Phys. Rev. D*, 78:106005, Nov 2008.
- [101] Mihailo Čubrović, Yan Liu, Koenraad Schalm, Ya-Wen Sun, and Jan Zaanen. Spectral probes of the holographic fermi ground state: Dialing between the electron star and ads dirac hair. *Phys. Rev. D*, 84:086002, Oct 2011.
- [102] T. Senthil, Subir Sachdev, and Matthias Vojta. Fractionalized fermi liquids. *Phys. Rev. Lett.*, 90:216403, May 2003.
- [103] Subir Sachdev. Model of a fermi liquid using gauge-gravity duality. *Phys. Rev. D*, 84:066009, Sep 2011.
- [104] Sean A. "Hartnoll, Diego M. Hofman, and David" Vegh. "Stellar spectroscopy: Fermions and holographic Lifshitz criticality". *JHEP*, "08":096, "2011".
- [105] Hiroaki Matsueda. Multiscale entanglement renormalization ansatz for kondo problem. *arXiv:1208.2872*, 2012.
- [106] Bartłomiej Czech. Einstein equations from varying complexity. *Phys. Rev. Lett.*, 120:031601, Jan 2018.
- [107] Sung-Sik Lee. Background independent holographic description: from matrix field theory to quantum gravity. *Journal of High Energy Physics*, 2012(10):160, Oct 2012.
- [108] Sung-Sik Lee. Quantum renormalization group and holography. *Journal of High Energy Physics*, 2014(1):76, 2014.
- [109] Guifré Vidal. Entanglement renormalization. *Physical review letters*, 99(22):220405, 2007.
- [110] Guifré Vidal. Class of quantum many-body states that can be efficiently simulated. *Physical review letters*, 101(11):110501, 2008.
- [111] Brian Swingle. Entanglement renormalization and holography. *Physical Review D*, 86(6):065007, 2012.

- [112] G. Evenbly and G. Vidal. Scaling of entanglement entropy in the (branching) multiscale entanglement renormalization ansatz. *Phys. Rev. B*, 89:235113, Jun 2014.
- [113] Sung-Sik Lee. Holographic description of quantum field theory. *Nuclear Physics B*, 832(3):567–585, 2010.
- [114] Sung-Sik Lee. Tasi lectures on emergence of supersymmetry, gauge theory and string in condensed matter systems. *arXiv:1009.5127*, 2010.
- [115] Ashley Milsted and Guifre Vidal. Geometric interpretation of the multi-scale entanglement renormalization ansatz. 2018.
- [116] Xiao-Liang Qi. Exact holographic mapping and emergent space-time geometry. *arXiv preprint arXiv:1309.6282*, 2013.
- [117] Ching Hua Lee and Xiao-Liang Qi. Exact holographic mapping in free fermion systems. *Physical Review B*, 93(3):035112, 2016.
- [118] Ki-Seok Kim, Suk Bum Chung, Chanyong Park, and Jae-Ho Han. *Phys. Rev. D*, 99:105012, 2019.
- [119] Ki-Seok Kim, Miok Park, Jaeyoon Cho, and Chanyong Park. Emergent geometric description for a topological phase transition in the kitaev superconductor model. *Phys. Rev. D*, 96:086015, Oct 2017.
- [120] Ki-Seok Kim and Chanyong Park. Emergent geometry from field theory: Wilson’s renormalization group revisited. *Phys. Rev. D*, 93:121702, Jun 2016.
- [121] Anirban Mukherjee and Siddhartha Lal. Superconductivity from repulsion in the doped 2d electronic hubbard model: an entanglement perspective. *Journal of Physics: Condensed Matter*, 34(27):275601, apr 2022.
- [122] Brian Swingle. Entanglement entropy and the fermi surface. *Physical review letters*, 105(5):050502, 2010.
- [123] Masaki Oshikawa. Topological approach to luttinger’s theorem and the fermi surface of a kondo lattice. *Physical Review Letters*, 84(15):3370, 2000.
- [124] Kazuhiro Seki and Seiji Yunoki. Topological interpretation of the luttinger theorem. *Physical Review B*, 96(8):085124, 2017.
- [125] Philipp Gegenwart, Qimiao Si, and Frank Steglich. Quantum criticality in heavy-fermion metals. *Nature Physics*, 4(3):186–197, Mar 2008.
- [126] Anirban Mukherjee and Siddhartha Lal. Superconductivity from repulsion in the doped 2d electronic hubbard model: an entanglement perspective. *Journal of Physics: Condensed Matter*, 34(27):275601, apr 2022.
- [127] J. Custers, P. Gegenwart, H. Wilhelm, K. Neumaier, Y. Tokiwa, O. Trovarelli, C. Geibel, F. Steglich, C. Pépin, and P. Coleman. The break-up of heavy electrons at a quantum critical point. *Nature*, 424(6948):524–527, Jul 2003.

- [128] S. D. Glazek and Kenneth G. Wilson. Renormalization of hamiltonians. *Phys. Rev. D*, 48:5863–5872, Dec 1993.
- [129] S. D. Glazek and Kenneth G. Wilson. Perturbative renormalization group for hamiltonians. *Phys. Rev. D*, 49:4214–4218, Apr 1994.
- [130] Samuel Savitz and Gil Refael. Stable unitary integrators for the numerical implementation of continuous unitary transformations. *Physical Review B*, 96(11):115129, 2017.
- [131] Louk Rademaker and Miguel Ortuno. Explicit local integrals of motion for the many-body localized state. *Physical review letters*, 116(1):010404, 2016.
- [132] Cécile Monthus. Flow towards diagonalization for many-body-localization models: adaptation of the toda matrix differential flow to random quantum spin chains. *Journal of Physics A: Mathematical and Theoretical*, 49(30):305002, 2016.
- [133] Yi-Zhuang You, Xiao-Liang Qi, and Cenke Xu. Entanglement holographic mapping of many-body localized system by spectrum bifurcation renormalization group. *Physical Review B*, 93(10):104205, 2016.
- [134] Ming-Chiang Chung and Ingo Peschel. Density-matrix spectra for two-dimensional quantum systems. *Phys. Rev. B*, 62:4191–4193, Aug 2000.
- [135] Sara Murciano, Paola Ruggiero, and Pasquale Calabrese. Symmetry resolved entanglement in two-dimensional systems via dimensional reduction. *Journal of Statistical Mechanics: Theory and Experiment*, 2020(8):083102, aug 2020.
- [136] Siddhartha Patra, Somnath Basu, and Siddhartha Lal. Unveiling topological order through multipartite entanglement. *Phys. Rev. A*, 105:052428, May 2022.
- [137] Hai-Zhou Lu, Wen-Yu Shan, Wang Yao, Qian Niu, and Shun-Qing Shen. Massive dirac fermions and spin physics in an ultrathin film of topological insulator. *Phys. Rev. B*, 81:115407, Mar 2010.
- [138] Weiyao Zhao, Chi Xuan Trang, Qile Li, Lei Chen, Zengji Yue, Abuduliken Bake, Cheng Tan, Lan Wang, Mitchell Nancarrow, Mark Edmonds, David Cortie, and Xiaolin Wang. Massive dirac fermions and strong shubnikov–de haas oscillations in single crystals of the topological insulator Bi_2Se_3 doped with sm and fe. *Phys. Rev. B*, 104:085153, Aug 2021.
- [139] B. Hunt, J. D. Sanchez-Yamagishi, A. F. Young, M. Yankowitz, B. J. LeRoy, K. Watanabe, T. Taniguchi, P. Moon, M. Koshino, P. Jarillo-Herrero, and R. C. Ashoori. Massive dirac fermions and hofstadter butterfly in a van der waals heterostructure. *Science*, 340(6139):1427–1430, 2013.
- [140] A.G. Abanov and P.B. Wiegmann. Theta-terms in nonlinear sigma-models. *Nuclear Physics B*, 570(3):685–698, 2000.
- [141] Santanu Pal, Anirban Mukherjee, and Siddhartha Lal. Correlated spin liquids in the quantum kagome antiferromagnet at finite field: a renormalization group analysis. *New Journal of Physics*, 21(2):023019, feb 2019.

- [142] Hui Li and F Duncan M Haldane. Entanglement spectrum as a generalization of entanglement entropy: Identification of topological order in non-abelian fractional quantum hall effect states. *Physical review letters*, 101(1):010504, 2008.
- [143] Pasquale Calabrese and Alexandre Lefevre. Entanglement spectrum in one-dimensional systems. *Phys. Rev. A*, 78:032329, Sep 2008.
- [144] JM Luttinger. Fermi surface and some simple equilibrium properties of a system of interacting fermions. *Physical Review*, 119(4):1153, 1960.
- [145] Joaquin Mazdak Luttinger and John Clive Ward. Ground-state energy of a many-fermion system. ii. *Physical Review*, 118(5):1417, 1960.
- [146] Joshuah T Heath and Kevin S Bedell. Necessary and sufficient conditions for the validity of luttinger's theorem. *New Journal of Physics*, 22(6):063011, jun 2020.
- [147] Kenneth G. Wilson. The renormalization group: Critical phenomena and the kondo problem. *Rev. Mod. Phys.*, 47:773–840, Oct 1975.
- [148] H Casini and M Huerta. Entanglement entropy in free quantum field theory. *Journal of Physics A: Mathematical and Theoretical*, 42(50):504007, dec 2009.
- [149] M. Blasone, F. Dell'Anno, S. De Siena, and F. Illuminati. Hierarchies of geometric entanglement. *Phys. Rev. A*, 77:062304, Jun 2008.
- [150] Glen Evenbly and Guifré Vidal. Algorithms for entanglement renormalization. *Physical Review B*, 79(14):144108, 2009.
- [151] Glen Evenbly and Steven R. White. Entanglement renormalization and wavelets. *Phys. Rev. Lett.*, 116:140403, Apr 2016.
- [152] Patrick Hayden, Matthew Headrick, and Alexander Maloney. Holographic mutual information is monogamous. *Phys. Rev. D*, 87:046003, Feb 2013.
- [153] Ning Bao, Sepehr Nezami, Hirosi Ooguri, Bogdan Stoica, James Sully, and Michael Walter. The holographic entropy cone. *Journal of High Energy Physics*, 2015(9):130, Sep 2015.
- [154] Mark Van Raamsdonk. Building up spacetime with quantum entanglement. *General Relativity and Gravitation*, 42(10):2323–2329, 2010.
- [155] Katharine Hyatt, James R Garrison, and Bela Bauer. Extracting entanglement geometry from quantum states. *Physical review letters*, 119(14):140502, 2017.
- [156] Robert C. Myers and Aninda Sinha. Seeing a c-theorem with holography. *Phys. Rev. D*, 82:046006, Aug 2010.
- [157] Robert C. Myers and Aninda Sinha. Holographic c-theorems in arbitrary dimensions. *Journal of High Energy Physics*, 2011(1):125, Jan 2011.

- [158] Chong-Sun Chu and Dimitrios Giataganas. *c*-theorem for anisotropic rg flows from holographic entanglement entropy. *Phys. Rev. D*, 101:046007, Feb 2020.
- [159] ChunJun Cao, Sean M. Carroll, and Spyridon Michalakis. Space from hilbert space: Recovering geometry from bulk entanglement. *Phys. Rev. D*, 95:024031, Jan 2017.
- [160] Sudipto Singha Roy, Silvia N. Santalla, Javier Rodríguez-Laguna, and Germán Sierra. Entanglement as geometry and flow. *Phys. Rev. B*, 101:195134, May 2020.
- [161] Sheng Bau and Alan F. Beardon. The metric dimension of metric spaces. *Computational Methods and Function Theory*, 13(2):295–305, Aug 2013.
- [162] Joseph J. Bisognano and Eyvind H. Wichmann. ”On the duality condition for a Hermitian scalar field”. *Journal of Mathematical Physics*, 16(4):985–1007, 09 2008.
- [163] Joseph J. Bisognano and Eyvind H. Wichmann. ”On the duality condition for quantum fields”. *Journal of Mathematical Physics*, 17(3):303–321, 08 2008.
- [164] David D. Blanco, Horacio Casini, Ling-Yan Hung, and Robert C. Myers. Relative entropy and holography. *Journal of High Energy Physics*, 2013(8):60, Aug 2013.
- [165] Sayan Kar. Geometry of renormalization group flows in theory space. *Phys. Rev. D*, 64:105017, Oct 2001.
- [166] Sayan Kar and Soumitra Sengupta. The raychaudhuri equations: A brief review. *Pramana*, 69(1):49–76, 2007.
- [167] Ingo Peschel. Calculation of reduced density matrices from correlation functions. *Journal of Physics A: Mathematical and General*, 36(14):L205, mar 2003.
- [168] A. Alexandradinata, Taylor L. Hughes, and B. Andrei Bernevig. Trace index and spectral flow in the entanglement spectrum of topological insulators. *Phys. Rev. B*, 84:195103, Nov 2011.
- [169] DJ Thouless, Mahito Kohmoto, MP Nightingale, and M Den Nijs. Quantized hall conductance in a two-dimensional periodic potential. *Physical Review Letters*, 49(6):405, 1982.
- [170] Michael O. Flynn, Long-Hin Tang, Anushya Chandran, and Chris R. Laumann. Momentum space entanglement of interacting fermions, 2022.
- [171] Vijay Balasubramanian, Michael B McDermott, and Mark Van Raamsdonk. Momentum-space entanglement and renormalization in quantum field theory. *Physical Review D*, 86(4):045014, 2012.
- [172] TC.L. Hsu, M.B. McDermott, and M. Van Raamsdonk. Momentum-space entanglement for interacting fermions at finite density. *J. High Energ. Phys.*, 121 (2013), 2013.
- [173] Matheus H. Martins Costa, Jeroen van den Brink, Flavio S. Nogueira, and Gastão I. Krein. Momentum space entanglement from the wilsonian effective action. *Phys. Rev. D*, 106:065024, Sep 2022.

- [174] Siddhartha Patra, Anirban Mukherjee, and Siddhartha Lal. Universal entanglement signatures of quantum liquids as a guide to fermionic criticality. *New Journal of Physics*, 25(6):063002, jun 2023.
- [175] Vijay Balasubramanian and Per Kraus. Spacetime and the holographic renormalization group. *Physical Review Letters*, 83(18):3605, 1999.
- [176] V. Balasubramanian, A. Bernamonti, N. Copland, B. Craps, and F. Galli. Thermalization of mutual and tripartite information in strongly coupled two dimensional conformal field theories. *Phys. Rev. D*, 84:105017, Nov 2011.
- [177] M. Asadi and M. Ali-Akbari. Holographic mutual and tripartite information in a symmetry breaking quench. *Physics Letters B*, 785:409–418, 2018.
- [178] M. Ali-Akbari, M. Asadi, and M. Rahimi. Holographic mutual and tripartite information in a non-conformal background. *arXiv:1907.08917*, 2019.
- [179] N. F. Mott. Metal-insulator transition. *Rev. Mod. Phys.*, 40:677–683, Oct 1968.
- [180] R F Milligan and G A Thomas. The metal-insulator transition. *Annual Review of Physical Chemistry*, 36(1):139–158, 1985.
- [181] Masatoshi Imada, Atsushi Fujimori, and Yoshinori Tokura. Metal-insulator transitions. *Reviews of modern physics*, 70(4):1039, 1998.
- [182] Y Kuramoto and T Watanabe. Theory of momentum-dependent magnetic response in heavy-fermion systems. In *Proceedings of the Yamada Conference XVIII on Superconductivity in Highly Correlated Fermion Systems*, pages 80–83. Elsevier, 1987.
- [183] D. L. Cox and N. Grewe. Transport properties of the anderson lattice. *Zeitschrift für Physik B Condensed Matter*, 71(3):321–340, Sep 1988.
- [184] Walter Metzner and Dieter Vollhardt. Correlated lattice fermions in $d = \infty$ dimensions. *Phys. Rev. Lett.*, 62:324–327, Jan 1989.
- [185] X. Y. Zhang, M. J. Rozenberg, and G. Kotliar. Mott transition in the $d=\infty$ hubbard model at zero temperature. *Phys. Rev. Lett.*, 70:1666–1669, Mar 1993.
- [186] Antoine Georges, Gabriel Kotliar, Werner Krauth, and Marcelo J Rozenberg. Dynamical mean-field theory of strongly correlated fermion systems and the limit of infinite dimensions. *Reviews of Modern Physics*, 68(1):13, 1996.
- [187] O. Parcollet, G. Biroli, and G. Kotliar. Cluster dynamical mean field analysis of the mott transition. *Phys. Rev. Lett.*, 92:226402, Jun 2004.
- [188] Thomas Maier, Mark Jarrell, Thomas Pruschke, and Matthias H. Hettler. Quantum cluster theories. *Rev. Mod. Phys.*, 77:1027–1080, Oct 2005.
- [189] G. Kotliar, S. Y. Savrasov, K. Haule, V. S. Oudovenko, O. Parcollet, and C. A. Marianetti. Electronic structure calculations with dynamical mean-field theory. *Rev. Mod. Phys.*, 78:865–951, Aug 2006.

- [190] Takuma Ohashi, Tsutomu Momoi, Hirokazu Tsunetsugu, and Norio Kawakami. Finite temperature mott transition in hubbard model on anisotropic triangular lattice. *Phys. Rev. Lett.*, 100:076402, Feb 2008.
- [191] N F Mott. The basis of the electron theory of metals, with special reference to the transition metals. *Proceedings of the Physical Society. Section A*, 62(7):416–422, jul 1949.
- [192] Martin C. Gutzwiller. Effect of correlation on the ferromagnetism of transition metals. *Phys. Rev. Lett.*, 10:159–162, Mar 1963.
- [193] Junjiro Kanamori. Electron Correlation and Ferromagnetism of Transition Metals. *Progress of Theoretical Physics*, 30(3):275–289, 09 1963.
- [194] John Hubbard. Electron correlations in narrow energy bands. In *Proceedings of the royal society of london a: mathematical, physical and engineering sciences*, volume 276, pages 238–257. The Royal Society, 1963.
- [195] W. F. Brinkman and T. M. Rice. Application of gutzwiller’s variational method to the metal-insulator transition. *Phys. Rev. B*, 2:4302–4304, Nov 1970.
- [196] David E Logan and Martin R Galpin. Mott insulators and the doping-induced mott transition within DMFT: exact results for the one-band hubbard model. *Journal of Physics: Condensed Matter*, 28(2):025601, dec 2015.
- [197] J. Vučičević, H. Terletska, D. Tanasković, and V. Dobrosavljević. Finite-temperature crossover and the quantum widom line near the mott transition. *Phys. Rev. B*, 88:075143, Aug 2013.
- [198] Hyowon Park, Kristjan Haule, and Gabriel Kotliar. Cluster dynamical mean field theory of the mott transition. *Physical review letters*, 101(18):186403, 2008.
- [199] G. Rohringer, H. Hafermann, A. Toschi, A. A. Katanin, A. E. Antipov, M. I. Katsnelson, A. I. Lichtenstein, A. N. Rubtsov, and K. Held. Diagrammatic routes to nonlocal correlations beyond dynamical mean field theory. *Rev. Mod. Phys.*, 90:025003, May 2018.
- [200] A. I. Lichtenstein and M. I. Katsnelson. Ab initio calculations of quasiparticle band structure in correlated systems: Lda++ approach. *Phys. Rev. B*, 57:6884–6895, Mar 1998.
- [201] K. Held. Electronic structure calculations using dynamical mean field theory. *Advances in Physics*, 56(6):829–926, 2007.
- [202] Karsten Held, Andrey A Katanin, and Alessandro Toschi. Dynamical vertex approximationan introduction. *Progress of Theoretical Physics Supplement*, 176:117–133, 2008.
- [203] Qimiao Si and Gabriel Kotliar. Metallic non-fermi-liquid phases of an extended hubbard model in infinite dimensions. *Phys. Rev. B*, 48:13881–13903, Nov 1993.
- [204] Gabriel Kotliar and Qimiao Si. Quantum chemistry, anomalous dimensions, and the breakdown of fermi liquid theory in strongly correlated systems. *Physica Scripta*, T49:165, 1993.

- [205] H. Terletska, J. Vučičević, D. Tanasković, and V. Dobrosavljević. Quantum critical transport near the mott transition. *Phys. Rev. Lett.*, 107:026401, Jul 2011.
- [206] P. W. Anderson. Localized magnetic states in metals. *Phys. Rev.*, 124:41–53, Oct 1961.
- [207] P. W. Anderson. Local moments and localized states. *Rev. Mod. Phys.*, 50:191–201, Apr 1978.
- [208] Philip W Anderson and Gideon Yuval. Exact results in the kondo problem: equivalence to a classical one-dimensional coulomb gas. *Physical Review Letters*, 23(2):89, 1969.
- [209] Philip W Anderson, G Yuval, and DR Hamann. Exact results in the kondo problem. ii. scaling theory, qualitatively correct solution, and some new results on one-dimensional classical statistical models. *Physical Review B*, 1(11):4464, 1970.
- [210] H. R. Krishna-murthy, J. W. Wilkins, and K. G. Wilson. Renormalization-group approach to the anderson model of dilute magnetic alloys. i. static properties for the symmetric case. *Phys. Rev. B*, 21:1003–1043, Feb 1980.
- [211] N. Andrei. Diagonalization of the kondo hamiltonian. *Phys. Rev. Lett.*, 45:379–382, Aug 1980.
- [212] N Andrei, K Furuya, and J H Lowenstein. Solution of the kondo problem. *Rev. Mod. Phys.*, 55:331, 1983.
- [213] P B Wiegmann. Exact solution of the s-d exchange model (kondo problem). *Journal of Physics C: Solid State Physics*, 14(10):1463–1478, apr 1981.
- [214] A M Tsvelick and P B Wiegmann. Exact results in the theory of magnetic alloys. *Adv. in Phys.*, 32:453, 1983.
- [215] Gabriel Kotliar and Qimiao Si. Toulouse points and non-fermi-liquid states in the mixed-valence regime of the generalized anderson model. *Phys. Rev. B*, 53:12373–12388, May 1996.
- [216] Solomon F. Duki. Solvable limit for the $\text{su}(n)$ kondo model. *Phys. Rev. B*, 83:134423, Apr 2011.
- [217] L. Borda, A. Schiller, and A. Zawadowski. Applicability of bosonization and the anderson-yuval methods at the strong-coupling limit of quantum impurity problems. *Phys. Rev. B*, 78:201301, Nov 2008.
- [218] Simon Streib, Aldo Isidori, and Peter Kopietz. Solution of the anderson impurity model via the functional renormalization group. *Phys. Rev. B*, 87:201107, May 2013.
- [219] Anirban Mukherjee, Abhirup Mukherjee, N. S. Vidhyadhiraja, A. Taraphder, and Siddhartha Lal. Unveiling the kondo cloud: Unitary renormalization-group study of the kondo model. *Phys. Rev. B*, 105:085119, Feb 2022.
- [220] Erik S. Sørensen and Ian Affleck. Scaling theory of the kondo screening cloud. *Phys. Rev. B*, 53:9153–9167, Apr 1996.
- [221] Ian Affleck and Pascal Simon. Detecting the kondo screening cloud around a quantum dot. *Phys. Rev. Lett.*, 86:2854–2857, Mar 2001.

- [222] Pascal Simon and Ian Affleck. Kondo screening cloud effects in mesoscopic devices. *Phys. Rev. B*, 68:115304, Sep 2003.
- [223] C. A. Busser, G. B. Martins, L. C. Ribeiro, E. Vernek, E. V. Anda, and E. Dagotto. *Phys. Rev. B*, 81:045111, 2010.
- [224] L. C. Ribeiro, G. B. Martins, G. Gomez-Silva, and E. V. Anda. *Phys. Rev. B*, 99:085139, 2019.
- [225] D. Goldhaber-Gordon, Hadas Shtrikman, D. Mahalu, David Abusch-Magder, U. Meirav, and M. A. Kastner. Kondo effect in a single-electron transistor. *Nature*, 391(6663):156–159, Jan 1998.
- [226] Sara M. Cronenwett, Tjerk H. Oosterkamp, and Leo P. Kouwenhoven. A tunable kondo effect in quantum dots. *Science*, 281(5376):540–544, July 1998.
- [227] Jörg Schmid, Jürgen Weis, Karl Eberl, and Klaus v. Klitzing. A quantum dot in the limit of strong coupling to reservoirs. *Physica B: Condensed Matter*, 256–258:182–185, 1998.
- [228] Michael Pustilnik and Leonid Glazman. Kondo effect in quantum dots. *Journal of Physics: Condensed Matter*, 16(16):R513, apr 2004.
- [229] Ivan V. Borzenets, Jeongmin Shim, Jason C. H. Chen, Arne Ludwig, Andreas D. Wieck, Seigo Tarucha, H.-S. Sim, and Michihisa Yamamoto. Observation of the kondo screening cloud. *Nature*, 579(7798):210–213, Mar 2020.
- [230] N. Néel, J. Kröger, R. Berndt, T. O. Wehling, A. I. Lichtenstein, and M. I. Katsnelson. Controlling the kondo effect in CoCu_n clusters atom by atom. *Phys. Rev. Lett.*, 101:266803, Dec 2008.
- [231] Aidi Zhao, Qunxiang Li, Lan Chen, Hongjun Xiang, Weihua Wang, Shuan Pan, Bing Wang, Xudong Xiao, Jinlong Yang, J. G. Hou, and Qingshi Zhu. Controlling the kondo effect of an adsorbed magnetic ion through its chemical bonding. *Science*, 309(5740):1542–1544, sep 2005.
- [232] Masahiro Nozaki, Shinsei Ryu, and Tadashi Takayanagi. Holographic geometry of entanglement renormalization in quantum field theories. *Journal of High Energy Physics*, 2012(10):193, 2012.
- [233] Christophe Mora, Cătălin Pașcu Moca, Jan von Delft, and Gergely Zaránd. Fermi-liquid theory for the single-impurity anderson model. *Phys. Rev. B*, 92:075120, Aug 2015.
- [234] Anirban Mukherjee, Siddhartha Patra, and Siddhartha Lal. Fermionic criticality is shaped by fermi surface topology: a case study of the tomonaga-luttinger liquid. *Journal of High Energy Physics*, 04:148, 2021.
- [235] Siddhartha Patra and Siddhartha Lal. Origin of topological order in a cooper-pair insulator. *Phys. Rev. B*, 104:144514, Oct 2021.
- [236] Siddhartha Patra, Abhirup Mukherjee, Anirban Mukherjee, N S Vidhyadhiraja, A Taraphder, and Siddhartha Lal. Frustration shapes multi-channel kondo physics: a star graph perspective. *Journal of Physics: Condensed Matter*, 35(31):315601, may 2023.
- [237] Supplementary Materials are available online.

- [238] P Nozieres. A “fermi-liquid” description of the kondo problem at low temperatures. *Journal of Low Temperature Physics*, 17:31, 1974.
- [239] T.A. Costi and A.C. Hewson. A new approach to the calculation of spectra for strongly correlated systems. *Physica B: Condensed Matter*, 163(1):179–181, 1990.
- [240] Nozières, Ph. Some comments on kondo lattices and the mott transition. *Eur. Phys. J. B*, 6(4):”447–457”, ”” 1998.
- [241] Abner Shimony. Degree of entanglement. *Annals of the New York Academy of Sciences*, 755(1):675–679, 1995.
- [242] Tzu-Chieh Wei and Paul M Goldbart. Geometric measure of entanglement and applications to bipartite and multipartite quantum states. *Physical Review A*, 68(4):042307, 2003.
- [243] Philipp Hauke, Markus Heyl, Luca Tagliacozzo, and Peter Zoller. Measuring multipartite entanglement through dynamic susceptibilities. *Nature Physics*, 12(8):778–782, Aug 2016.
- [244] Goetz Moeller, Qimiao Si, Gabriel Kotliar, Marcelo Rozenberg, and Daniel S. Fisher. Critical behavior near the mott transition in the hubbard model. *Phys. Rev. Lett.*, 74:2082–2085, Mar 1995.
- [245] K. Held, R. Peters, and A. Toschi. Poor man’s understanding of kinks originating from strong electronic correlations. *Phys. Rev. Lett.*, 110:246402, Jun 2013.
- [246] R. Bulla. Zero temperature metal-insulator transition in the infinite-dimensional hubbard model. *Phys. Rev. Lett.*, 83:136–139, Jul 1999.
- [247] Antoine Georges. Strongly correlated electron materials: Dynamical mean-field theory and electronic structure. *AIP Conference Proceedings*, 715(1):3–74, 2004.
- [248] Antoine Georges and Werner Krauth. Physical properties of the half-filled hubbard model in infinite dimensions. *Phys. Rev. B*, 48:7167–7182, Sep 1993.
- [249] Marcelo J. Rozenberg, Goetz Moeller, and Gabriel Kotliar. The metal–insulator transition in the hubbard model at zero temperature ii. *Modern Physics Letters B*, 08(08n09):535–543, 1994.
- [250] Walter Kohn. Theory of the insulating state. *Physical Review*, 133(1A):A171, 1964.
- [251] C. Castellani, C. Di Castro, D. Feinberg, and J. Ranninger. New model hamiltonian for the metal-insulator transition. *Phys. Rev. Lett.*, 43:1957–1960, Dec 1979.
- [252] H. R. Krishnamurthy, C. Jayaprakash, Sanjoy Sarker, and Wolfgang Wenzel. Mott-hubbard metal-insulator transition in nonbipartite lattices. *Phys. Rev. Lett.*, 64:950–953, Feb 1990.
- [253] P. Limelette, A. Georges, D. Jérôme, P. Wzietek, P. Metcalf, and J. M. Honig. Universality and critical behavior at the mott transition. *Science*, 302(5642):89–92, 2003.
- [254] F. Kagawa, K. Miyagawa, and K. Kanoda. Unconventional critical behaviour in a quasi-two-dimensional organic conductor. *Nature*, 436(7050):534–537, Jul 2005.

- [255] Tetsuya Furukawa, Kazuya Miyagawa, Hiromi Taniguchi, Reizo Kato, and Kazushi Kanoda. Quantum criticality of mott transition in organic materials. *Nature Physics*, 11(3):221–224, Mar 2015.
- [256] Heike Eisenlohr, Seung-Sup B. Lee, and Matthias Vojta. Mott quantum criticality in the one-band hubbard model: Dynamical mean-field theory, power-law spectra, and scaling. *Phys. Rev. B*, 100:155152, Oct 2019.
- [257] Satyaki Kundu, Tapas Bar, Rajesh Kumble Nayak, and Bhavtosh Bansal. Critical slowing down at the abrupt mott transition: When the first-order phase transition becomes zeroth order and looks like second order. *Phys. Rev. Lett.*, 124:095703, Mar 2020.
- [258] Nozières, Ph. and Blandin, A. Kondo effect in real metals. *J. Phys. France*, 41(3):”193–211”, 1980.
- [259] Piers Coleman. *Introduction to many-body physics*. Cambridge University Press, 2015. Chapter:18.
- [260] A. C. Hewson. Renormalized perturbation expansions and fermi liquid theory. *Phys. Rev. Lett.*, 70:4007–4010, Jun 1993.
- [261] CM Varma, Z Nussinov, and Wim Van Saarloos. Singular or non-fermi liquids. *Physics Reports*, 361(5-6):267–417, 2002.
- [262] Gabriel Kotliar and Qimiao Si. Quantum chemistry, anomalous dimensions, and the breakdown of fermi liquid theory in strongly correlated systems. *Physica Scripta*, T49A:165–171, jan 1993.
- [263] Jan von Delft, Gergely Zaránd, and Michele Fabrizio. Finite-size bosonization of 2-channel kondo model: A bridge between numerical renormalization group and conformal field theory. *Phys. Rev. Lett.*, 81:196–199, Jul 1998.
- [264] P Coleman, C Pépin, Qimiao Si, and R Ramazashvili. How do fermi liquids get heavy and die? *Journal of Physics: Condensed Matter*, 13(35):R723, aug 2001.
- [265] Qimiao Si, Silvio Rabello, Kevin Ingersent, and J. Lleweilun Smith. Locally critical quantum phase transitions in strongly correlated metals. *Nature*, 413(6858):804–808, Oct 2001.
- [266] Philip W Anderson. Infrared catastrophe in fermi gases with local scattering potentials. *Physical Review Letters*, 18(24):1049, 1967.
- [267] P. W. Anderson. “luttinger-liquid” behavior of the normal metallic state of the 2d hubbard model. *Phys. Rev. Lett.*, 64:1839–1841, Apr 1990.
- [268] J. Friedel. On some electrical and magnetic properties of metallic solid solutions. *Canadian Journal of Physics*, 34(12A):1190–1211, 1956.
- [269] JS Langer and V Ambegaokar. Friedel sum rule for a system of interacting electrons. *Physical Review*, 121(4):1090, 1961.
- [270] David C. Langreth. Friedel sum rule for anderson’s model of localized impurity states. *Phys. Rev.*, 150:516–518, Oct 1966.

- [271] Richard M Martin. Fermi-surface sum rule and its consequences for periodic kondo and mixed-valence systems. *Physical Review Letters*, 48(5):362, 1982.
- [272] Joshua T Heath and Kevin S Bedell. Necessary and sufficient conditions for the validity of luttinger's theorem. *New Journal of Physics*, 22(6):063011, jun 2020.
- [273] Sudeshna Sen, Patrick J. Wong, and Andrew K. Mitchell. The mott transition as a topological phase transition. *Phys. Rev. B*, 102:081110, Aug 2020.
- [274] A. J. Heeger, S. Kivelson, J. R. Schrieffer, and W. P. Su. Solitons in conducting polymers. *Rev. Mod. Phys.*, 60:781–850, Jul 1988.
- [275] M. Stone. Elementary derivation of one-dimensional fermion-number fractionalization. *Phys. Rev. B*, 31:6112–6115, May 1985.
- [276] János K. Asbóth, László Oroszlány, and András Pályi. *A Short Course on Topological Insulators*. Springer International Publishing, 2016.
- [277] Daria Gazizova and J. P. F. LeBlanc. Emergent nearest-neighbor attraction in the fully renormalized interactions of the single-band repulsive hubbard model at weak coupling, arxiv:2307.02360, 2023.
- [278] Z. Iftikhar, S. Jezouin, A. Anthore, U. Gennser, F. D. Parmentier, A. Cavanna, and F. Pierre. Two-channel kondo effect and renormalization flow with macroscopic quantum charge states. *Nature*, 526(7572):233–236, Oct 2015.
- [279] Z. Iftikhar, A. Anthore, A. K. Mitchell, F. D. Parmentier, U. Gennser, A. Ouerghi, A. Cavanna, C. Mora, P. Simon, and F. Pierre. Tunable quantum criticality and super-ballistic transport in a “charge” kondo circuit. *Science*, 360(6395):1315–1320, 2018.
- [280] T. Giamarchi, C. M. Varma, A. E. Ruckenstein, and P. Nozières. Singular low energy properties of an impurity model with finite range interactions. *Phys. Rev. Lett.*, 70:3967–3970, Jun 1993.
- [281] Qimiao Si and G. Kotliar. Fermi-liquid and non-fermi-liquid phases of an extended hubbard model in infinite dimensions. *Phys. Rev. Lett.*, 70:3143–3146, May 1993.
- [282] AE Ruckenstein and CM Varma. A theory of marginal fermi-liquids. *Physica C: Superconductivity*, 185:134–140, 1991.
- [283] J. Vučičević, D. Tanasković, M. J. Rozenberg, and V. Dobrosavljević. Bad-metal behavior reveals mott quantum criticality in doped hubbard models. *Phys. Rev. Lett.*, 114:246402, Jun 2015.
- [284] Michel Ferrero, Lorenzo De Leo, Philippe Lecheminant, and Michele Fabrizio. Strong correlations in a nutshell. *Journal of Physics: Condensed Matter*, 19(43):433201, oct 2007.
- [285] Shiro Sakai, Yukitoshi Motome, and Masatoshi Imada. Evolution of electronic structure of doped mott insulators: Reconstruction of poles and zeros of green's function. *Phys. Rev. Lett.*, 102:056404, Feb 2009.

- [286] Samuel L Braunstein and Carlton M Caves. Statistical distance and the geometry of quantum states. *Physical Review Letters*, 72(22):3439, 1994.
- [287] Thierry Giamarchi. *Quantum physics in one dimension*. Clarendon Oxford, 2004.
- [288] Matthew T Glossop and David E Logan. Single-particle dynamics of the anderson model: a local moment approach. *Journal of Physics: Condensed Matter*, 14(26):6737, jun 2002.
- [289] David E. Logan, Adam P. Tucker, and Martin R. Galpin. Common non-fermi liquid phases in quantum impurity physics. *Phys. Rev. B*, 90:075150, Aug 2014.
- [290] Angela Kopp, Xun Jia, and Sudip Chakravarty. Replacing energy by von neumann entropy in quantum phase transitions. *Annals of Physics*, 322(6):1466–1476, 2007.
- [291] Richard M. Martin, Lucia Reining, and David M. Ceperley. *Interacting Electrons: Theory and Computational Approaches*. Cambridge University Press, 2016.
- [292] Alexandrina Stoyanova. *Delocalized and correlated wave functions for excited states in extended systems*. PhD thesis, University of Groningen, 2006.
- [293] Abhirup Mukherjee, N S Vidhyadhiraja, A Taraphder, and Siddhartha Lal. Kondo frustration via charge fluctuations: a route to mott localisation. *New Journal of Physics*, 25(11):113011, nov 2023.
- [294] A. M. Tsvelick and P. B. Wiegmann. Exact solution of the multichannel kondo problem, scaling, and integrability. *Journal of Statistical Physics*, 38(1):125–147, Jan 1985.
- [295] V. J. Emery and S. Kivelson. Mapping of the two-channel kondo problem to a resonant-level model. *Phys. Rev. B*, 46:10812–10817, Nov 1992.
- [296] CM Varma, P Be Littlewood, S Schmitt-Rink, E Abrahams, and AE Ruckenstein. Phenomenology of the normal state of cu-o high-temperature superconductors. *Physical Review Letters*, 63(18):1996, 1989.
- [297] P. Coleman, L. B. Ioffe, and A. M. Tsvelik. Simple formulation of the two-channel kondo model. *Phys. Rev. B*, 52:6611–6627, Sep 1995.
- [298] D L Cox and M Jarrell. The two-channel kondo route to non-fermi-liquid metals. 8(48):9825–9853, nov 1996.
- [299] P. W. Anderson. Infrared catastrophe in fermi gases with local scattering potentials. *Phys. Rev. Lett.*, 18:1049–1051, Jun 1967.
- [300] Kōsaku Yamada and Kei Yosida. Orthogonality Catastrophe Due to Local Electron Interaction. *Progress of Theoretical Physics*, 59(4):1061–1071, 04 1978.
- [301] Kosaku Yamada and Kei Yosida. Orthogonality catastrophe for a system of interacting electrons. ii. *Progress of Theoretical Physics*, 62(2):363–369, 1979.
- [302] Philip Phillips. Mottness. *Annals of Physics*, 321(7):1634–1650, 2006.
- [303] Richard M Martin. Fermi-surface sum rule and its consequences for periodic kondo and mixed-valence systems. *Physical Review Letters*, 48(5):362, 1982.